UNIVERSITE CATHOLIQUE DE LOUVAIN

UNIVERSITE DE DOUALA

INSTITUTE OF CONDENSED MATTER AND NANOSCIENCES (IMCN) - NANOSCOPIC PHYSICS (NAPS)

The Abdus Salam INTERNATIONAL CENTRE FOR THEORETICAL PHYSICS (ICTP)

UNIT OF ATOMIC MOLECULAR PHYSICS AND OPTICS (PAMO)

CENTRE FOR ATOMIC MOLECULAR PHYSICS AND QUANTUM OPTICS (CEPAMOQ)

Academic Year 2010-2011

Ionization Dynamics of a Model Atom Exposed to a Strong Laser Pulse and Relativistic Calculation of Matrix Elements for Two-Photon Transitions in Hydrogen-Like Ions

Thesis in joint supervision

Presented and Defended November, 17 2010

By

Hugues Merlain TETCHOU NGANSO

Noma (UCL): 5901-05-00

Noma (UD) : 05A2096

In Partial Fulfillment of the Requirements for
The Degree of

Doctor of Philosophy of Université Catholique de Louvain
and
Doctorat/PhD of University of Douala

Speciality**: Atoms and Molecules**

Jury

President:	Prof. P. DEFRANCE	Université Catholique de Louvain, Belgium
Supervisors:	Prof. B. PIRAUX	Université Catholique de Louvain, Belgium
	Prof. M. G. KWATO NJOCK	University of Douala, Cameroon
Examiners:	Prof. Yu. V. POPOV	Moscow State University, Russia
	Prof. H. BACHAU	University of Bordeaux, CNRS, France
	Prof. P. ANTOINE	Université Catholique de Louvain, Belgium
	Prof. G. GASANEO	Universidad Nacional Del Sur, Argentina

Dedication

C'est quoi réussir sa vie?
"Ecouter son coeur, suivre son destin, même si vous vous brûler. Prendre le temps d'aimer ses proches, ses amis. Eviter les conflits inutiles. Etre en paix avec soi-même. Vivre tout simplement." ***J-C. Van Damme***.

TO:

My GOD
My WIFE, My MOTHERS and FATHER
My SISTERS, BROTHERS, Whole FAMILY and in-LAWS
My COUNTRY

"Si tu penses, lecteur... que l'on est en train de te concocter une sorte de roman sentimental, tu fais fausse route. Espères-tu trouver du sentiment, de la poésie, de la rêverie ? Rêves-tu de passion, d'émotion ou de mélodrame ? Modère tes attentes, réduis-les à des proportions plus humbles. C'est quelque chose de réel, de froid et de consistant qui t'attend ; quelque chose d'aussi peu romantique qu'un lundi matin lorsque tous ceux qui ont du travail se réveillent avec la même préoccupation : se lever et se rendre tout de suite au travail." ***Charlotte Brontë (Prologue à 'Shirley')***.

"La plus grave maladie du cerveau, c'est de réfléchir." ***Devise Shadock***.

"S'il n'y a pas de solution, c'est qu'il n'y a pas de problème." ***Devise Shadock***.

"Je voudrais avoir l'ignorance de l'aube." ***William Butler Yeats***.

"Pour qu'il y ait le moins de mécontents possibles, il faut toujours taper sur les mêmes." ***Devise Shadock***.

Acknowledgements

"To Give all, Forgive, Accommodate, Have patience, Contemplate and Choose"
H. M. Tetchou Nganso.

This thesis is not only the product of my own effort, on the contrary many people have contributed directly or indirectly to it. Unfortunately there is not time nor space enough to properly mention and thank everybody who contributed their efforts and advice to my education and to my training, and I hope the understanding of those who do not appear here.

This work has been done jointly at the Institute of Condensed Matter and Nanosciences (IMCN-NAPS) of the Université Catholique de Louvain (UCL, Louvain-la-Neuve, Belgium), at the Abdus Salam International Centre for Theoretical Physics (ICTP, Trieste, Italy) and at the Centre for Atomic Molecular Physics and Quantum Optics (CEPAMOQ) of the University of Douala (Douala, Cameroon). I thank all the scientific and non scientific staff of these institutes for creating the perfect environment to work.

I am highly indebted to Professor M. G. KWATO NJOCK, Co-ordinator of CEPAMOQ, Associate Member of the Abdus Salam ICTP and to Professor B. PIRAUX, President of the Doctoral School of Physics for accepting to co-supervise this research work. They helped me formulate the scope of this study and supervised step by step the evolution of this work despite their numerous occupations. They have served alternately as resources, references, and role-model, both scientifically and otherwise. More than the supervisors of this thesis, they have been friends, who encouraged and supported me during these PhD's years and also enriched my limited knowledge with stimulating discussions on the "*Why-of-How-of-Because*" of the physics. I also thank them for thoroughly proofreading of my manuscript. I would like to take this opportunity to say that I will never forget all their appreciated encouragements, support and advice, without which it would have been very difficult to achieve this personal challenge. Once more, many thanks Moïse and Bernard.

I want to express my deepest gratitude to Professor Yu. V. POPOV for innumerable enlightening and illuminating discussions about many aspects of this thesis. Many thanks for having been always open for discussions, giving me advice and helping in all questions. The success of my thesis in particular would not be possible without his enormous contribution and support. He devoted a great deal of skills and unending attention to this exciting research work and to the preparation of this manuscript. His enthusiasm and insight kept me from making good on my discouragement and anxiety, on my constant threats to quit school and become a goat farmer. Words alone will never be enough to express my gratitude to him. Again thank a lot Yuri.

I would like to thank the members of my defence committee, namely Professor P. DEFRANCE, Professor H. BACHAU, Professor P. ANTOINE, Professor G. GASANEO. They took a special interest in the work carried out in this thesis and critically reviewed what I have written - Many thanks for their valuable insights, criticisms, rich discussions, fruitful suggestions which have been used to improve an earlier version of this thesis.

A special debt of gratitude is due to Professors P. WOAFO and E. NGAMENI for being always open for discussions, giving me advice and encouragement in tough times. I hereby expressed my sincere recognition to them.

I would like to honestly thank the Administrations of the Universities of Douala and Yaounde I in general, their Faculties of Science, and especially CEPAMOQ and all the teachers of the Department of Physics for ensuring my basic training and evolution of this work. All my classmates and colleagues are not forgotten.

I would not have undertaken this research work without the financial support from the International Atomic Energy Agency (IAEA) through the Abdus Salam ICTP-IAEA Sandwich Training Educational Programme (STEP). I seize this advisability to gratefully acknowledge this financial support. I would like to express all my gratitude to the Abdus Salam ICTP, to have given me the privilege to benefit from their equipments and existing documentations to advance my research works. I am greatly indebted to Professor G. DENARDO (ICTP) who has passed away, and the staff of the Office of External Activities (OEA) for their warm hospitality during the periods when this work was performed. Many thanks for all their efforts towards the development of physics in Africa, the co-operation between African research groups and between African at whole with developed countries.

I am most indebted to the Administration of the Université Catholique de Louvain for ensuring a smooth evolution of this work. I am very grateful to the Faculty of Science and to the Faculty of Medicine for having given me the opportunity to work as Assistant Lecturer in Physics. I have learned more from Professors P. DEFRANCE, P. ANTOINE and J. LEGA, and especially for their multiple advices on the teaching content. I heartily thank the cordial

relationships prevailing over the entire staff and the student body of IMCN-NAPS. I cannot forget this warm hospitality during my stay at the Université Catholique de Louvain.

I would particularly like to thank Mme Christian De WAN (Assistante Sociale, Service d'aide, UCL) for the support, the hospitality and her assistance during all the time and especially at the last step of my thesis which contributed both to my work and to my well being.

Let me also address my deep thanks to Mme Nicole COISMAN, Secretary of NAPS pole, Mme Roseline VAN DYCK, Secretary of Doctoral School of Physics and Mathematics and to Marc DAMAN for their administrative and moral supports during the execution of this thesis.

I gratefully acknowledge the Institut de Calcul Intensif et de Stockage de Masse (CISM, UCL) for computing time in their supercomputers. Thanks to Bernard VAN RENTERGHEM and the entire Staffs for their help in solving some of my computational problems.

I also benefited greatly from the rich discussions I had with Professors O. MOTAPON, L. C. OWONO OWONO, J. P. NGUENANG, Doctors E. FOUMOUO, C. BOURI, M. NGOKO, H. NYENGERI, G. J. MADROÑERO PABÓN, R. MBIAKE, S. G. NANA ENGO, M. NSANGOU, G. BEN BOLI, C. P. NANSEU, L. KWUIDA, C. PUEMI SUKAM, L. MBUMBIA and P. T. AMOUGOU, MM ALIOU HAMIDO, MARIUS SILENOU, VALERY MEZOUI NDO.

I would like to express my sincere thanks to my friends B. KWUINDJA, S. FOGUEM, F. TCHATAT, L. TCHASEM, G. YEPNDJO, B. TOGUEM, for their excellent cooperation, their friendly atmosphere and heartiness, their assistance in many problems, their support and encouragements helped me to go ahead. They have been with me during the sad and happy moments.

I wish to thank the Elie KADJI, Jean Baptiste TCHANA, Guy FOKOU, Fernand TCHEUKO, Hilaire NGAMEN, Dominique MALLOUN, Zambo MBALLA, Felix NGALLA, Jean Claude NDOUMA, Stephane TANKOUA families and all the members of Asbl PLACET via ARP of Louvain-la-Neuve for their friendly and fatherly loves during my stay in Belgium.

I want to thank five special families, Mesac NOUNJIO, Hilaire NANA, Daniel SANDJONG, Jean LENGUE and JOUOPNANG. There are not words enough to explain or express all what they have done for me. They have been endlessly loving and patient during the difficult times, and they have been there to celebrate the good times as well. I am grateful for every day I get to spend with them.

Moreover, many thanks to the people, not mentioned by name, who contributed to the successful completion of this thesis.

The biggest debts I owe are to my FATHER, my MOTHERS, my BROTHERS, my SISTERS, my FAMILY and in-LAWS at whole for their constant love

and support. I learned more about the importance of education from them than from anyone else. Your moral support have urged me to look forward despite the numerous odds around and behind.

A special word to my mother in law. Mom!!! Jeanne TCHAPDA, you are on my mind and in my heart each moment of the day, and no one else in all the world could make me feel this way!!!.

As in all my endeavors, the debts I owe to my Wife EMILIENNE NGAMPA cannot be adequately expressed in word. Always remember that there is nothing I will not do for your happiness, and for your happiness, I will give my last breath. As days go by, my love for you grows bigger and bigger. You are everything to me, someone I can count on, someone I believe in, someone I love with all my heart.

And finally, to the uncertainty and hope that guide my life....

Abstract

"Time is the coin of your life. It is the only coin you have, and only you can determine how it will be spent. Be careful lest you let other people spend it for you".

Carl Sandburg.

Part I

The area of atom-light interaction is of growing importance mainly due to unprecedented advances in laser technology and detection systems. One of the most important phenomena in intense laser-atom physics is above-threshold ionization, *i.e.* the ionization of an atom with absorption of a larger number of laser field photons than the minimum necessary for ionization. Since its discovery in 1979 by Agostini *et al.* (Phys. Rev. Lett. **42**, 1127 (1079)), a large body of knowledge has accumulated in the last three decades on the experimental properties and theoretical interpretations of multiphoton ionization and simultaneous generation of higher harmonics of the laser light impinging on the target atom. Besides its intrinsic interest as a source of high-energy electrons in laser-atom interactions, above-threshold ionization plays a key role in other laser-atom phenomena, such as high-order harmonic generation. For this reason it has continued to be actively investigated now for more than three decades (see, *e.g.*, L. F. DiMauro and P. Agostini, Adv. At. Mol. Opt. Phys. **35**, 79 (1995); W. Becker *et al.*, Adv. At. Mol. Opt. Phys. **48**, 35 (2002)).

Nowadays, powerful laser systems are available as table top devices, allowing for the experiments to be performed in a simpler manner than in the past. More precise detection systems have made it possible to observe energy-resolved spectra of ionized electrons with higher accuracy, leading for example, to the observation of the rescattering plateau in above threshold ionization as well as their narrow resonancelike structures appearing at specific intensities.

Also, a large number of known phenomena can be studied in entirely new regimes, using intense few-cycle laser pulses. This new regime led to new features of the known processes to be discovered, as well as to new phenomena. The high laser intensity requires the development of new mathematical and computational tools, as the perturbational techniques break down. New physical models allow for a better understanding of most of the experimental results.

According to the well-established strong-field approximation, the effective potential, the atomic electrons are exposed to, exhibits a time dependent barrier. If the frequency is sufficiently low and the electric field strong enough, an electron can tunnel out, propagate in the external field and possibly return towards the residual ion where it may recombine to generate high-order harmonics or be rescattered to form the high energy parts of the above-threshold ionization spectrum. In these conditions, the atomic structure (except for the ground state) does not play a specific role in the ionization mechanism. This contrasts with recent experimental results obtained by A. Rudenko *et al.* (J. Phys. B: At. Mol. Opt. Phys. **37**, L407 (2004)). Their data show that deep in the tunneling regime, the low-energy parts of the electron spectrum clearly exhibit a fine structure that is unambiguously attributed to a resonant multiphoton process. It is precisely this low-energy part of the spectrum that provides the dominant contribution to the ionization yield for a given photon energy. Moreover, these experimental results for the momentum distribution of the ejected electrons show an interference pattern that cannot be explained by the strong field approximation. This suggests that the Coulomb potential, which is assumed negligible compared to the external field in the strong-field approximation, plays a significant role. Numerical simulation based on the numerical solution of the time-dependent Schrödinger equation in momentum space suggests that low-energy electrons are produced within the Coulomb potential and not at large distance through tunneling (Phys. Rev. Lett. **89**, 113002 (2002)). Upon these conditions, the strong-field approximation is not valid anymore. This explains why the tunneling formula for the total ionization rate gives results that disagree either qualitatively or quantitatively with those obtained by solving the time-dependent Schrödinger equation. From the experimental side, this was confirmed by numerous experiments (M. Uiberacker *et al.* Nature **446**, 627 (2007)) in the literature. The main motivation of the present analysis stems for these discrepancies. It consists to reconsider the mechanism leading to ionization within this energy range and to elucidate the role of the Coulomb potential.

The main objective of this part is to analyze the role of the Coulomb potential in the ionization dynamics of an atom exposed to a strong laser pulse, and particularly in the strong field limit. For that purpose, we have sketched

a mathematical model which goes far beyond the strong-field approximation and developed an efficient scheme to solve numerically the corresponding time-dependent Schrödinger equation in momentum space (in the velocity gauge). In this representation, the Coulomb potential is non-local and characterized by a singular kernel. Our present approach consists in replacing the kernel of the non-local Coulomb potential by a series of N separable potentials, each term supporting one atomic bound state of hydrogen. Thus, the model amounts to solving a system of N coupled 1-dimensional linear Volterra integral equations of the second kind for the total wave function contrary to the complex resolution of 3-dimensional time-dependent Schrödinger equation. Firstly, we dealt with the simple case where only one term in the above series is included; this term supports only the ground state. Our preliminary theoretical results showed a good agreement with the well-known behavior of the high-energy parts of the above-threshold ionization spectrum and exhibited some interesting features that tend to show that only the fast electron ($E \gg 2U_p$) are emitted through tunneling. This is an agreement with the recent experimental results obtained by A. Rudenko *et al.*. Secondly, we introduced more terms in the separable potential in such a way that in the configuration space, more bound states are correctly described. In that case we obtain a system of coupled linear Volterra integral equations that gives valuable information on the actual role of the atomic structure in the ionization dynamics. Finally, a fast and accurate numerical code for solving this system of equations has been implemented. Appropriate physical observables have been calculated and detailed analysis have been given within the framework of our model for well-known physical processes in the high and low-frequency regimes.

Part II

An important number of works in both experimental and theoretical physics may be performed only if spectroscopic constants or physical quantities such as transition rates, scattering amplitudes and cross-sections are known. When investigating the interactions of the electromagnetic field with the inner shell electrons of high Z atoms, for instance two-photon transitions like Rayleigh and Raman scattering, the incident photons energies are in X-ray and γ-ray domains. For this range of energies, accurate analytical formulae which take into account relativistic, retardation and multipole effects are needed. Various theoretical approaches continue to be proposed in the literature.

The main goal of the present work is to derive exact closed-form expressions of relativistic two-photon transition amplitudes in hydrogen-like ions, namely the two-photon absorption, Rayleigh and Raman scattering, within

the framework of covariant second-order perturbation theories. More precisely, we investigate the fully relativistic transition amplitude probabilities from the ground state towards L and M shells for linear polarized photons. The main difficulty experienced in calculating the second-order matrix elements stands in the correct evaluation of the infinite summations embedded implicitly. Such summations are extended over the whole (discrete and continuum) atomic spectrum and are usually evaluated by means of some adequate approximation techniques. The Coulomb Green function method has proven to be a valuable tool to perform these infinite summations over the complete set of states. The main advantage of this method lies in its ability of providing analytical expressions for the high-order perturbation matrix elements and it permits to avoid the explicit integration over the intermediate continuum states. To this aim, the Sturmian expansion of the first-order Dirac-Coulomb Green function is exploited in the evaluation of the fully relativistic treatment of the S-matrix elements describing two-photon bound-bound transition amplitudes in the hydrogen-like ions.

The main task is to construct complete sets of relativistic Sturmian basis associated directly to both the first-order and second-order Dirac-Coulomb equations. In this context, convenient constructions based on coupled first-order Sturm-Liouville equations were proposed by Drake and Goldman (Adv. At. Mol. Phys. **25**, 393 (1988)) and by Grant (Adv. At. Mol. Opt. Phys. **32**, 169 (1994)). Few years later, Szmytkowski (J. Phys. B: At. Mol. Opt. Phys. **30**, 825 (1997)) proved that none of these later functions can form a complete fully relativistic Sturmian set. The motivation of this work stems in part from that point. However, the previous works undertaken by Manakov *et al.* (Phys. Lett. **43A**, 139 (1973)) and Szymanowski *et al.* (Phys. Rev. A **56**, 700 (1997)) were based on a second-order Sturm-Liouville problem arising from the Gell-Mann Feynman equation. Following the genuine method developed by Szmytkowski, we constructed in the similar manner the Sturmian basis set and the Sturmian expansion of Green function of the second-order.

Using these Sturmian expansions of the Dirac-Coulomb Green's functions derived by Szmytkowski and us, we have derived in a rigorous way the explicit expressions of the two-photon absorption, Rayleigh and Raman scattering probability amplitudes. The treatment takes care of the relativistic structure of the atoms according to the Dirac theory and to the fully retarded interaction with the electromagnetic field. A distinctive feature of our tensor treatment is that the expressions derived are quite general and could be applied to any multipole of the two-photon bound-bound transitions. An illustration of our method is undertaken by computing the two-photon absorption transition rates from the ground state towards the excited states of L and M shells

for the lighter elements to the heavier ones. A comparison is made also with the quasirelativistic treatment. The numerical results obtained enable us to draw inferences as to the improvements of our method.

"Demander ne coûte qu'un instant d'embarras. Ne pas demander, c'est d'être embarrassé toute sa vie."
Proverbes Japonais.

Résumé

"Ceux qui ne savent rien en savent toujours autant que ceux qui n'en savent pas plus qu'eux."
Pierre Dac.

Les progrès considérables réalisés dans le développement des lasers de haute intensité ont déclenché une rapide avancée de la physique atomique et de l'optique, notamment dans l'exploration des processus non-linéaires. Dans ce contexte, deux processus physiques rentrent en compétition dans l'interaction d'atomes ou d'ions avec de tels champs électromagnétiques à savoir: (1) la réponse non linéaire de l'atome, en l'occurrence la génération d'harmoniques d'ordre élevé, et (2) le mécanisme d'ionisation (multiphotonique ou par effet tunnel) de l'atome. La présence d'intensités de laser de plus en plus élevées et des sources de rayonnement à longueur d'onde courte nécessite une estimation critique (3) des effets relativistes et du retard dus au rayonnement. Les travaux que nous présentons comportent deux parties principales. La première partie est dédiée à l'étude théorique de la dynamique de l'ionisation d'un atome modèle d'hydrogène exposé à un champ laser intense, et la seconde partie aux calculs relativistes d'amplitudes de transitions à deux photons.

L'approximation du champ fort (SFA) consiste essentiellement à négliger les effets éventuels de la structure atomique (excepté l'état fondamental), mais aussi et surtout à "négliger" la présence du potentiel coulombien dans la dynamique du mécanisme d'émission et de propagation des électrons dans le champ laser. C'est une approximation très efficace amplement utilisée qui a permis d'expliquer de nombreuses structures des spectres observés expérimentalement dans le domaine de l'interaction atome-laser. Des calculs récents de taux d'ionisation, calculs fondés sur la résolution numérique de l'équation de Schrödinger dépendante du temps (ESDT) dans l'espace des configurations donnent des résultats en désaccord avec les taux d'ionisation obtenus dans le cadre de cette approximation, c'est-à-dire en supposant que l'ionisation se fait

par effet tunnel. Par ailleurs, les résultats expérimentaux récents présentés dans la littérature, lesquels montrent clairement entre autre, (a) la présence des structures résonantes dans la région de basses énergies du spectre des électrons émis et (b) des figures d'interférences pour la distribution des moments des électrons émis ne peuvent être expliqués dans le contexte de cette approximation. Ces résultats renforcent l'idée que les électrons émis, du moins ceux de basses énergies, le sont par un autre processus que l'effet tunnel. Dans ces conditions, l'influence du potentiel Coulombien devant celle du champ électrique reste importante même dans la limite des champs forts. Pour analyser le rôle du potentiel Coulombien, nous résolvons directement l'ESDT dans l'espace des moments (dont les avantages sont repris dans le texte). Cette résolution directe de l'ESDT est rendue difficile par la non-localité du potentiel Coulombien et le fait que le noyau présente une singularité. Pour ce faire, nous avons développé un nouveau modèle mathématique qui va au-delà de la SFA et mis sur pied un code numérique efficient qui permettent d'obtenir des informations pertinentes sur le rôle de la structure atomique dans la dynamique d'ionisation. La méthode consiste à substituer le noyau du potentiel Coulombien par une somme de N potentiels séparables, chaque terme de la série supportant un état lié de l'atome d'hydrogène. Ainsi, l'ESDT est transformée en un système linéaire couplé de N équations intégrales de Volterra de second type. Une comparaison détaillée de nos résultats avec d'autres résultats théoriques disponibles est présentée et discutée.

Théoriquement, il est clair que le traitement non-relativiste dipolaire de l'interaction atome-laser n'est plus valable pour les atomes lourds et les ions hautement chargés. Aux limites inhérentes à une telle approche simplifiée, il faut proposer un traitement qui tienne compte simultanément des effets relativiste et du retard. Ceci est le but de cette partie du projet. La méthode que nous proposons est fondée sur la théorie covariante des perturbations. Dans notre contexte, il est question d'évaluer des éléments de matrices du deuxième ordre, contenant la fonction de Green Coulombienne de Dirac. Un calcul direct de telles amplitudes du deuxième ordre est rendu difficile à cause des sommes infinies (qui tiennent compte de tous les états intermédiaires qu'ils soient liés ou du continuum) et intégrations sur des bases complètes. Par conséquent une forme compacte de la fonction de Green doit être utilisée. Pour ce faire, nous avons décomposé cette fonction sur une base de fonctions Sturmiennes complètement relativistes (R. Szmytkowski, J. Phys. B: At. Mol. Opt. Phys. 30, 825 (1997)) et quasirelativistes (que nous avons construites). L'approche tensorielle qui est développée ici diffère de façon significative de celles utilisées dans les travaux antérieurs par le fait que nos expressions sont exactes, générales et peuvent être étendues à des multipolarités quelconques dans les processus à deux photons (absorption, diffusion Rayleigh et Raman etc.). Dans le cas de l'absorption de deux photons, les résultats numériques

pour des transitions de l'état fondamental 1s aux états 2s, 3s et 3d des couches L et M pour un rayonnement laser polarisé linéairement sont présentés et discutés.

Ces travaux ouvrent des perspectives intéressantes qui sont reprises dans les conclusions.

"Bien sûr que l'enfer existe....L'enfer, c'est le désert sinistre où le soleil n'apporte ni chaleur ni lumière, et où l'Habitude nourrit de force le désir sénile. C'est le lieu où le mortel besoin cohabite avec l'immortelle nécessité, et où la nuit devient horrible quand s'élèvent les gémissements de l'un ou les cris d'extase de l'autre. Oui, l'enfer existe, mon garçon, et il n'est guère besoin de creuser pour le trouver...."

Jim Thompson - Nuit de fureur.

List of Figures

2.1 *Schematic diagram of ionization processes. Each process results in a free electron with kinetic energy E_{kin}: (a) one-photon ionization; (b) multiphoton ionization by n photons; (c) above-threshold ionization by $(n + s)$ photons.* 14

2.2 *Photoelectron energy spectra (ATI) from Xe using a* $\lambda = 1064$ nm *with* 130 ps *laser pulses. (a)* $I = 2 \times 10^{12}$ W.cm^{-2}*; (b)* $I = 10^{13}$ W.cm^{-2}*. From Petite et al. [22].* 18

2.3 *Schematic diagram for the Stark shift of the ionization potential versus the laser intensity. At the intensity I_1 five-photon ionization occurs, whereas at the higher light intensity I_2 one photon more is needed for ionization. The ionization threshold is increased by U_p.* 19

2.4 *Schematic diagram showing the two possible strong-field photoionization mechanisms: in (a) tunneling ionization; over-the-barrier ionization is depicted in (b).* 22

2.5 *Temporal variation of the electron velocity $v_x(t)$ for different moment of release. The electron's final velocity v_f shown on the right-hand-side sensitively depend on the instant of release. From Ferenc Krausz and Misha Ivanov [54].* 26

2.6 *ATI spectra calculated from the one-dimensional TDSE and model potential $V(x) = -(1 + x^2)^{1/2}$ for several U_p between* 6 *and* 20 eV*. The classical high energy part is marked by an arrow in each case. From Paulus et al. [57].* 29

2.7 *ATI spectra calculated from our three-dimensional TDSE model. Laser parameters are given in the bottom of graph. Vertical dashed lines mark the positions of the plateau cut-off respectively at $2U_p$ (brown) and $10U_p$ (green).* 30

2.8 *Kinetic energy E_{kin} of the returning electron to the core vs their characteristic phases corresponding to the return time in units of U_p. This dependence indicates that electron wave packets returning along short ($\tau_1 = t_{r_1} - t_0$) and long ($\tau_2 = t_{r_2} - t_0$) trajectories carry the same kinetic energy. From A. de Bohan [55].* 32

2.9 *The time variation of the vector potential and its envelope of laser pulses consisting of very few optical cycles depends on the phase $\phi = 0,\ \pi/2,\ \pi$ of the carrier frequency with respect to the pulse's envelope. Laser parameters are given in the top left of graph.* 41

2.10 *The electric field of laser pulses as a function of time in optical cycle for three values of the carrier phase envelope $\phi = 0,\ \pi/2,\ \pi$. The laser field corresponds to $\omega = 0.057$ a.u. of 4 optical cycle and intensity 3×10^{14} W.cm^{-2}* 42

3.1 *Argand curves of function $F_1(t)$ when the laser field is switched off (left panel) and on (right panel). Our model potential supports only $1s$ state. The peak laser field intensity is $I = 3 \times 10^{14}$ W.cm^{-2}.* 64

3.2 *Argand curves of component $F_1(t)$ when the laser field is switched off (left panel) and on (right panel). Our model potential supports only $1s$, $2s$ and $2p$ states. The peak laser field intensity is $I = 3 \times 10^{14}$ W.cm^{-2}.* 65

3.3 *Argand curves of component $F_2(t)$ when the laser field is switched off (left panel) and on (right panel). Our model potential supports only $1s$, $2s$ and $2p$ states. The peak laser field intensity is $I = 3 \times 10^{14}$ W.cm^{-2}.* 65

3.4 *Argand curve of component $F_3(t)$ when the laser field is switched on. Our model potential supports only $1s$, $2s$ and $2p$ states. The peak laser field intensity is $I = 3 \times 10^{14}$ W.cm^{-2}.* 66

3.5 *Probability of ionization of our model atom initially in the $1s$ state, as a function of the peak field intensity. The total duration of the pulse is 8 optical cycle and the photon energy is 0.6 a.u.. The blue dashed straight line has a slope exactly equal to 1. The vertical brown dashed line delimits the intensity region where one-photon processes dominate. The vertical green dashed line corresponds to an intensity of 3×10^{16} W/cm^2 for which $U_p = \omega$ in a.u.. For larger peak intensities, the interaction of the atom with the field is predominantly non perturbative.* 70

3.6 *Electron energy spectrum resulting from the interaction of our model atom, initially in the* $1s$ *state, with a* 8 *optical cycle pulse. The peak intensity is equal to* 10^{15} W/cm^2 *and the photon energy, to* 1 a.u.. 71

3.7 *Electron energy spectrum for* $\mathcal{E}_0 = 0.04$ a.u. *at resonance (*$\omega = 0.375$ a.u.*) obtained with a perturbative approach. A rectangular* 32*-cycle pulse is used. The dashed vertical lines indicate the positions of the two Autler-Townes peaks, and their centre by the dotted vertical lines. From Girju et al.[17]* 72

3.8 *Electron energy spectrum for* $\mathcal{E}_0 = 0.04$ a.u. *at resonance (*$\omega = 0.375$ a.u.*) obtained from our model atom. The pulse has a trapezoidal shape with a 1 optical cycle linear turn on and off and a 30 optical cycle flat top.* 73

3.9 *Electron energy spectrum for* $\mathcal{E}_0 = 0.04$ a.u. *at resonance (*$\omega = 0.375$ a.u.*) obtained from TDSE in r-space. A trapezoidal* 32*-cycle pulse (up and down ramping over* 1 *cycle) is used. From Girju et al.[17]* 74

3.10 *Electron energy spectrum resulting from the interaction of our model atom, initially in the* $1s$ *state, with a pulse whose peak electric field is equal to* $\mathcal{E}_0 = 0.107$ a.u. *and the frequency equals to* $\omega = 0.375$ a.u.. *The pulse has a trapezoidal shape with a* 2 *optical cycle up and down ramping and a* 36 *optical cycle flat top.* 75

3.11 *Electron energy spectra resulting from the interaction of our model atom, initially in the* $1s$ *state, with laser pulses at resonance* 0.375 a.u. *photon energy. All pulses have the same trapezoidal shape as in Figure 3.10 but various peak field intensities (given in the lower left part of the graphs) are considered. Color curves are drawn to guide the eye.* 76

3.12 *First ATI peak of the electron energy spectra shown in Zoom in linearly scaled electron energy spectra resulting from the interaction of our model atom, initially in the* $1s$ *state, with the same laser pulse as in Figure 3.11. Color curves are drawn to guide the eye.* 77

3.13 *Ground state populations versus time (in optical cycle) for our model atom, interacting with a laser pulse whose frequency is equal to* 0.375 a.u.. *The pulse is turned on and off linearly over* 2 *optical cycles and has a flat top of* 36 *optical cycles. The pulse shape (dashed black line) is shown in arbitrary units. The peak intensity taking the values* 2×10^{14} W/cm^2 *and* 10^{15} W/cm^2 *respectively.* 78

3.14 *Rabi oscillations of the* $1s$ *and* $2p$ *state populations as a function of time. Our model atom which is assumed initially in the* $1s$ *state, interacts with a laser pulse whose frequency is equal to the* $1s$-$2p$ *transition frequency. The pulse is turned on and off linearly over* 2 *optical cycles and has a flat top of* 36 *optical cycles. The pulse shape (dashed black line) is shown in arbitrary units. The peak intensity is equal to* 4×10^{14} W/cm^2. 79

3.15 *Real parts of the complex Floquet energies as a function of the frequency* ω *for a laser peak intensity of* 4×10^{14} W/cm^2 *(upper panel), the corresponding ionization rates (middle panel) and the overlaps between these Floquet states and the "bare" atomic states* $|1s\rangle$ *and* $|2p\rangle$ *(lower panel). The red full circles correspond to a Floquet state that has the largest overlap with the* $|1s\rangle$ *state while the blue open circles correspond to the second largest overlap with the* $|1s\rangle$ *state and the first largest overlap with the* $|2p\rangle$ *state.* 81

3.16 *Electron energy spectrum resulting from the interaction of our model atom initially in the* $|1s\rangle$ *with a laser pulse of* 0.375 a.u. *photon frequency and of* 4×10^{14} W/cm^2 *peak intensity. The laser pulse shape is trapezoidal with a* 2 *cycle linear turn on and off and with a flat top of* 36 *optical cycles. The gray line is the result obtained by solving numerically the time-dependent Schrödinger equation while the black line is the result obtained with our model.* 82

3.17 *Angular distribution of the probability density at the end of the laser pulse, resulting from the interaction of our model atom initially in the* $|1s\rangle$ *with a laser pulse of* 0.375 a.u. *photon frequency and of* 4×10^{14} W/cm^2 *peak intensity. The laser pulse shape is trapezoidal with a* 2 *cycle linear turn on and off and with a flat top of* 36 *optical cycles.* 83

4.1 *Electron probability density as a function of time and* $p_z, p_n = 0$ *(left panel), for the interaction of our model atom with an* 8 *optical cycle pulse and the photon energy* $\omega = 0.057$ a.u. *and the ionization yield (right panel). The pulse intensity varies between* $I = 1.3 \times 10^{14}$ W.cm^{-2} *and* $I = 5 \times 10^{14}$ W.cm^{-2}. *The solid oscillating blue line in the left panel represents* $A(t)$ *and the separable potential supports only* $1s$ *state.* 106

4.2 *Electron probability density as a function of time and* $p_z, p_n = 0$ *(left panel), for the interaction of our model atom with an* 8 *optical cycle pulse and the photon energy* $\omega = 0.057$ a.u. *and the ionization yield (right panel). The pulse intensity varies between* $I = 1.3 \times 10^{14}$ W.cm^{-2} *and* $I = 5 \times 10^{14}$ W.cm^{-2}. *The solid oscillating blue line in the left panel represents* $A(t)$ *and the separable potential supports* $1s$ *and* $2s$ *states.* 107

4.3 *Electron probability density as a function of time and* $p_z, p_n = 0$ *(left panel), for the interaction of our model atom with an* 8 *optical cycle pulse and the photon energy* $\omega = 0.057$ a.u. *and the ionization yield (right panel). The pulse intensity varies between* $I = 1.3 \times 10^{14}$ W.cm^{-2} *and* $I = 5 \times 10^{14}$ W.cm^{-2}. *The solid oscillating blue line in the left panel represents* $A(t)$ *and the separable potential supports* $1s$, $2s$ *and* $2p$ *states.* 108

4.4 *Electron probability density as a function of time and* $p_z, p_n = 0$ *obtained within an exact Coulomb potential (upper panel, from de Bohan [3]) and our* $(1s)$ *potential model (lower panel). The laser peak intensity is* $I = 1.3 \times 10^{14}$ W.cm^{-2} *and other laser parameters as in Figure 4.1. The solid oscillating blue line represents the vector potential* $A(t)$. 109

4.5 *Electron probability density as a function of time and* $p_z, p_n = 0$ *obtained respectively within our* $(1s + 2s)$ *(upper panel) and* $(1s + 2s + 2p)$ *(lower panel) potential models. The laser peak intensity is* $I = 1.3 \times 10^{14}$ W.cm^{-2} *and other laser parameters as in Figure 4.1. The solid oscillating blue line represents the vector potential* $A(t)$. 110

4.6 *Ionization probability density at the end of the pulse obtained within an exact Coulomb potential (upper panel, from de Bohan [3]) and our* $(1s + 2s + 2p)$ *potential model (lower panel). The laser parameters as in Figure 4.7.* 111

4.7 *Ionization probability density* $\mid \Phi_{ion}(p_n = 0, p_z; T_p) \mid^2$ *(is obtained by removing all the bound states of the total wave packets) at the end of the pulse (Left panel) and electron energy spectrum (right panel) for the interaction of our model atom with an* 8 *optical cycle pulse. The laser parameters are* $\omega = 0.057$ a.u., $I = 1.3 \times 10^{14}$ W.cm^{-2}. *Our separable potential supports respectively* $1s$ *state (upper panel),* $1s + 2s$ *states (middle panel) and* $1s + 2s + 2p$ *states (lower panel).* 112

4.8 *Ionization probability density* $\mid \Phi_{ion}(p_n = 0, p_z; T_p) \mid^2$ *(is obtained by removing all the bound states of the total wave packets) at the end of the pulse for different laser peak intensities given to the right of the graphs. The laser field frequency is* $\omega = 0.057$ a.u. *and the pulse duration is* 8 *optical cycle. Our separable potential supports respectively* $1s$ *state (upper panel),* $1s + 2s$ *states (middle panel) and* $1s + 2s + 2p$ *states (lower panel). The vertical dashed lines indicate the value of* p_z *corresponding to* $2U_p$ *and* $10U_p$ *. The spectra are vertically shifted for better visibility.* 113

4.9 *Angular distribution of the ionization probability density* $p_n \mid \Phi_{ion}(p_n, p_z; T_p) \mid^2$ *at the end of the pulse, for the interaction of our model atom with an* 8 *optical cycle pulse. The laser parameters are* $\omega = 0.057$ a.u., $I = 1.3 \times 10^{14}$ W.cm^{-2}. *Our separable potential supports respectively* $1s$ *state (upper panel),* $1s + 2s$ *states (middle panel) and* $1s + 2s + 2p$ *states (lower panel).* 114

4.10 *The same figure as in 4.9 compared to the result obtained with an exact Coulomb potential (upper panel, from de Bohan [3]) and our* $(1s + 2s + 2p)$ *potential model (lower panel). The laser parameters as in 4.9* 115

4.11 *The same figure as in 4.9, for various laser peak intensities: upper panel* $I = 2 \times 10^{14}$ W.cm^{-2}, *middle panel* $I = 3 \times 10^{14}$ W.cm^{-2} *and lower panel* $I = 8 \times 10^{14}$ W.cm^{-2}. *Our separable potential supports* $1s + 2s + 2p$ *states.* 116

4.12 *Probability of ionization of our model atom initially in the* $1s$ *state, as a function of the peak field intensity. The total duration of the pulse is* 8 *optical cycle and the photon energy is* 0.057 a.u.. *The blue solid straight line represents the case where only* $1s$ *state is included in the separable potential, the red solid straight line for* $1s + 2s$*-model potential, the green solid straight line for* $1s + 2s + 2p$*-model potential and the magenta solid straight line for the case of exact Coulomb potential.* 117

4.13 *Ionization probability density* $\mid \Phi_{ion}(p_n = 0, p_z; T_p) \mid^2$ *as function of the electron kinetic energy* E *at the end of the pulse, for a linearly polarized* 4*-optical cycle sine-quare pulse with CEP* $\phi = 0$ *(upper panel) and* $\phi = \pi/2$ *(lower panel). The laser field parameters are given on the graphs. Our separable potential supports* $1s + 2s + 2p$ *states.* 118

4.14 *Ionization probability density* $\mid \Phi_{ion}(p_n = 0, p_z; T_p) \mid^2$ *as function of the electron kinetic energy* E *at the end of the pulse, for a linearly polarized* 4*-optical cycle sine-quare pulse with CEP* $\phi = 0$ *(upper panel) and* $\phi = \pi/2$ *(lower panel). The laser field parameters are given on the graphs. Our separable potential supports* $1s + 2s + 2p$ *states.* 119

4.15 *Ionization probability density* $\mid \Phi_{ion}(p_n = 0, p_z; T_p) \mid^2$ *as function of the electron kinetic energy E at the end of the pulse, for a linearly polarized 2-optical cycle sine-quare pulse with CEP* $\phi = 0$ *(upper panel) and* $\phi = \pi/2$ *(lower panel). The laser field parameters are given on the graphs. Our separable potential supports* $1s + 2s + 2p$ *states.* 120

4.16 *Angular distribution of the ionization probability density* $p_n \mid \Phi_{ion}(p_n, p_z; T_p) \mid^2$ *at the end of the pulse, for the interaction of our model atom with a 4 optical cycle sine-quare pulse with CEP* $\phi = 0$ *(upper panel) and* $\phi = \pi/2$ *(lower panel). The laser parameters are* $\omega = 0.057$ a.u., $I = 5 \times 10^{13}$ W.cm^{-2}. *Our separable potential supports* $1s$ *state.* 121

4.17 *Angular distribution of the ionization probability density* $p_n \mid \Phi_{ion}(p_n, p_z; T_p) \mid^2$ *at the end of the pulse, for the interaction of our model atom with a 4 optical cycle sine-quare pulse with CEP* $\phi = 0$ *(upper panel) and* $\phi = \pi/2$ *(lower panel). The laser parameters are* $\omega = 0.057$ a.u., $I = 5 \times 10^{13}$ W.cm^{-2}. *Our separable potential supports* $1s + 2s$ *states.* 122

4.18 *Angular distribution of the ionization probability density* $p_n \mid \Phi_{ion}(p_n, p_z; T_p) \mid^2$ *at the end of the pulse, for the interaction of our model atom with a 4 optical cycle sine-quare pulse with CEP* $\phi = 0$ *(upper panel) and* $\phi = \pi/2$ *(lower panel). The laser parameters are* $\omega = 0.057$ a.u., $I = 5 \times 10^{13}$ W.cm^{-2}. *Our separable potential supports* $1s + 2s + 2p$ *states.* 123

4.19 *Plot of the vector potential as a function of time (in optical cycle) for different phases* $\phi = 0,\ \pi/2$ *of the carrier frequency with respect to the pulse envelope. Laser parameters are given in the top right of graphs.* 125

4.20 *Electron energy spectrum resulting from the interaction of our model atom, initially in the* $1s$ *state, with a laser pulse. The pulse parameters are as in Figure 3.10.* 126

4.21 *Electron energy spectrum resulting from the interaction of our model atom, initially in the* $1s$ *state, with a laser pulse, compared to the results obtained from the TDSE with B-Spline's and Sturmian's methods in the configuration space. The pulse parameters are as in Figure 3.10.* 127

4.22 *The same figure as in Figure 4.20, but for different values of pulse's duration* $n_c = 10,\ 20,\ 40$ *optical cycle.* 128

4.23 *The same figure as in Figure 4.20, but for different values of laser peak intensities (given in the top right of the graphs).* . . . 128

8.1 *Feynman diagram for the second-order amplitudes of the two photons absorption. The diagram describes processes by which an atomic transition from initial state $|i\rangle$ to final state $|f\rangle$ is accompanied by absorption of two photons $\mathbf{k}_i$ and $\mathbf{k}_f$* 193
8.2 *Feynman diagram for the second-order amplitudes of the two photons scattering. The diagram describes processes by which an atomic transition from initial state $|i\rangle$ to final state $|f\rangle$ is accompanied by absorption of one photon $\mathbf{k}_i$ and by emission of one photon $\mathbf{k}_f$.* 201
8.3 *Feynman diagram for the second-order amplitudes of the two photons scattering. The diagram describes processes by which an atomic transition from initial state $|i\rangle$ to final state $|f\rangle$ is accompanied by emission of one photon $\mathbf{k}_f$ and by absorption of one photon $\mathbf{k}_i$.* 202
8.4 *Raman anti-Stokes scattering.* 202
8.5 *Raman Stokes scattering.* 203
8.6 *Modulus of the matrix elements multiplied by 2π versus the nuclear charge Z for the transition $|\,1^2S\rangle \rightarrow |\,2^2S\rangle$ in relativistic atomic units for several selected hydrogen-like atoms. Left panel: (QR) and (FR1). Right Panel: (QR) and (FR2). Curves are drawn to guide the eye.* 216
8.7 *Left panel: (FR1), (FR2) and (CFR) Modulus of the matrix elements multiplied by 2π versus the nuclear charge Z for the transition $|\,1^2S\rangle \rightarrow |\,2^2S\rangle$ in relativistic atomic units for several selected hydrogen-like atoms. Right panel: Plot of the differences Δ between the quasirelativistic (QR), fully relativistic (FR2) values and exact fully relativistic (FR1) values versus the nuclear charge Z for the selected transition $|\,1^2S\rangle \rightarrow |\,2^2S\rangle$. Curves are drawn to guide the eye.* 216
8.8 *Modulus of the matrix elements multiplied by 2π versus the nuclear charge Z for the transition $|\,1^2S\rangle \rightarrow |\,3^2S\rangle$ in relativistic atomic units for several selected hydrogen-like atoms. Left panel: (QR) and (FR1). Right panel: (QR) and (FR2). Curves are drawn to guide the eye.* 218
8.9 *Left panel: (FR1), (FR2) and (CFR) Modulus of the matrix elements multiplied by 2π versus the nuclear charge Z for the transition $|\,1^2S\rangle \rightarrow |\,3^2S\rangle$ in relativistic atomic units for several selected hydrogen-like atoms. Right panel: Plot of the differences Δ between the quasirelativistic (QR), fully relativistic (FR2) values and exact fully relativistic (FR1) values versus the nuclear charge Z for the selected transition $|\,1^2S\rangle \rightarrow |\,3^2S\rangle$. Curves are drawn to guide the eye.* 218

8.10 *Modulus of the matrix elements multiplied by 2π versus the nuclear charge Z for the transition $\mid 1^2S\rangle \rightarrow \mid 3^2D_{3/2}\rangle$ in relativistic atomic units for several selected hydrogen-like atoms. Left panel: (QR) and (FR1). Right panel: (QR) and (FR2). Curves are drawn to guide the eye.* 220

8.11 *Left panel: (FR1), (FR2) and (CFR) Modulus of the matrix elements multiplied by 2π versus the nuclear charge Z for the transition $\mid 1^2S\rangle \rightarrow \mid 3^2D_{3/2}\rangle$ in relativistic atomic units for several selected hydrogen-like atoms. Right panel: Plot of the differences Δ between the quasirelativistic (QR), fully relativistic (FR2) values and exact fully relativistic (FR1) values versus the nuclear charge Z for the selected transition $\mid 1^2S\rangle \rightarrow \mid 3^2D_{3/2}\rangle$. Curves are drawn to guide the eye.* 220

8.12 *Modulus of the matrix elements multiplied by 2π versus the nuclear charge Z for the transition $\mid 1^2S\rangle \rightarrow \mid 3^2D_{5/2}\rangle$ in relativistic atomic units for several selected hydrogen-like atoms. Left panel: (QR) and (FR1). Right panel: (QR) and (FR2). Curves are drawn to guide the eye.* 222

8.13 *Left panel: (FR1), (FR2) and (CFR) Modulus of the matrix elements multiplied by 2π versus the nuclear charge Z for the transition $\mid 1^2S\rangle \rightarrow \mid 3^2D_{5/2}\rangle$ in relativistic atomic units for several selected hydrogen-like atoms. Right panel: Plot of the differences Δ between the quasirelativistic (QR), fully relativistic (FR2) values and exact fully relativistic (FR1) values versus the nuclear charge Z for the selected transition $\mid 1^2S\rangle \rightarrow \mid 3^2D_{5/2}\rangle$. Curves are drawn to guide the eye.* 222

8.14 *Plot of the contribution of the negative part of the set (CFR) to the exact fully relativistic FR1 values versus the nuclear charge Z for all selected transitions.* 223

8.15 *Ratio $\mathcal{R}_d$ of modulus of the relativistic two-photon transition amplitudes of $\mid 1^2S\rangle \rightarrow \mid 3^2D_{5/2}\rangle$ to $\mid 1^2S\rangle \rightarrow \mid 3^2D_{3/2}\rangle$ for hydrogen-like ions versus the nuclear charge Z. Curves are drawn to guide the eye.* 223

C.1 *Discretization local error ε as a function of stepsize h, calculated for $F_1(t = 10)$ and $\mid \mathcal{C}_{1s}(t = 10) \mid^2$ when the laser field is switched off. The standard block-by-block numerical method is used for this calculation and one observes a convergence in $h^{3/2}$.* 271

C.2 *Discretization local error ε as a function of stepsize h, calculated for $F_1(t = 10)$ and $\mid \mathcal{C}_{1s}(t = 10) \mid^2$ when the laser field is switched off. The adapted block-by-block numerical method is used for this calculation and one observes a convergence in h^2.* . . 272

List of Tables

8.1 *Quantum numbers for the allowed dipole excitation paths for the transition* $|\ 1^2S\rangle \rightarrow |\ 2^2S\rangle$. *Initial state is labelled by index 1, virtual states by superscript prime and final states by index 2.* . 208

8.2 *Modulus of the matrix elements multiplied by* 2π *for the transition* $|\ 1^2S\rangle \rightarrow |\ 2^2S\rangle$ *in relativistic atomic units for several selected hydrogen-like ions. The superscript* (2) *refers to the quasirelativistic approach (QR) and* (1) *to the fully relativistic treatment where a is related to the Sturmian basis sets with the radial quantum number* $-100 \leq n \leq 100$ *(FR1), b to the case* $0 \leq n \leq 100$ *(FR2) and c for* $-100 \leq n \leq -1$ *(CFR). The number in brackets following the entries is the power of* 10 *by which the entry is to be multiplied.* 209

8.3 *Quantum numbers for the allowed dipole excitation paths for the transition* $|\ 1^2S\rangle \rightarrow |\ 3^2S\rangle$. *Initial state is labelled by index 1, virtual states by superscript prime and final states by index 2.* . 210

8.4 *Modulus of the matrix elements multiplied by* 2π *for the transition* $|\ 1^2S\rangle \rightarrow |\ 3^2S\rangle$ *in relativistic atomic units for several selected hydrogen-like ions. The superscript* (2) *refers to the quasirelativistic approach (QR) and* (1) *to the fully relativistic treatment where a is related to the Sturmian basis sets with the radial quantum number* $-100 \leq n \leq 100$ *(FR1), b to the case* $0 \leq n \leq 100$ *(FR2) and c for* $-100 \leq n \leq -1$ *(CFR). The number in brackets following the entries is the power of* 10 *by which the entry is to be multiplied.* 211

8.5 *Quantum numbers for the allowed dipole excitation paths for the transition* $|\ 1^2S\rangle \rightarrow |\ 3^2D_{3/2}\rangle$. *Initial state is labelled by index 1, virtual states by superscript prime and final states by index 2.* . 212

8.6 *Modulus of the matrix elements multiplied by* 2π *for the transition* $|\ 1^2S\rangle \rightarrow |\ 3^2D_{3/2}\rangle$ *in relativistic atomic units for several selected hydrogen-like ions. The superscript* (2) *refers to the quasirelativistic approach (QR) and* (1) *to the fully relativistic treatment where a is related to the Sturmian basis sets with the radial quantum number* $-100 \leq n \leq 100$ *(FR1), b to the case* $0 \leq n \leq 100$ *(FR2) and c for* $-100 \leq n \leq -1$ *(CFR). The number in brackets following the entries is the power of* 10 *by which the entry is to be multiplied.* 213

8.7 *Quantum numbers for the allowed dipole excitation paths for the transition* $|\ 1^2S\rangle \rightarrow |\ 3^2D_{5/2}\rangle$*. Initial state is labeled by index 1, virtual states by superscript prime and final states by index 2.* . 214

8.8 *Modulus of the matrix elements multiplied by* 2π *for the transition* $|\ 1^2S\rangle \rightarrow |\ 3^2D_{5/2}\rangle$ *in relativistic atomic units for several selected hydrogen-like ions. The superscript* (2) *refers to the quasirelativistic approach (QR) and* (1) *to the fully relativistic treatment where a is related to the Sturmian basis sets with the radial quantum number* $-100 \leq n \leq 100$ *(FR1), b to the case* $0 \leq n \leq 100$ *(FR2) and c for* $-100 \leq n \leq -1$ *(CFR). The number in brackets following the entries is the power of* 10 *by which the entry is to be multiplied.* 215

G.1 *Angular integrals for different dipole excitation paths from the initial S state* $|j_1 = 1/2, m_1 = 1/2\rangle$ *to virtual* $P_{j'}$ *states in the first interaction.* 304

G.2 *Angular integrals for different dipole excitation paths from virtual* $P_{j'}$ *states in the second interaction to final* D_j *states.* . . . 305

Contents

Dedication i

Acknowledgements iii

Abstract vii

Résumé xiii

List of Figures xxvi

List of Tables xxviii

Scientific Outputs xxxv

I Ionization Dynamics of a Model Atom Exposed to a Strong Laser Pulse 1

1 General Introduction 3
1.1 Framework and formulation of the problem 3
1.2 Structure of the thesis 6

2 Laser Atom Interaction in Intense Field 9
2.1 Introduction 9
2.2 Strong-field multiphoton processes 10

2.2.1 Electron-field interaction: Stark shifts 10
2.2.2 Multiphoton ionization 13
2.2.3 Above threshold ionization 17
2.2.4 Tunneling ionization 21
2.2.5 Semiclassical modeling of strong field matter interaction 24
2.2.6 High harmonic generation 29
2.3 Strong field calculational techniques 33
2.3.1 Floquet theory 33
2.3.2 Volkov final states 34
2.3.3 Strong field approximations 35
2.3.4 Direct integration of the TDSE 37
2.4 Semi classical model of the laser field 38
2.4.1 Vector-potential pulse envelope 39
2.4.2 Electric-field-vector pulse envelope 40
2.5 The Ehrenfest theorem in velocity and length gauges 40
2.6 Conclusion 43

3 Quasi Analytical Model of the Interaction of the Hydrogen-Like Ions with a Laser Pulse 49
3.1 Introduction 49
3.2 Theoretical formulation of the problem 50
3.3 Construction of separable potentials 51
3.4 Theoretical treatment of the TDSE in momentum space 54
3.4.1 $(1s)$-model potential 55
3.4.2 $(1s + 2s)$-model potential 56
3.4.3 $(1s + 2s + 2p)$-model potential 58
3.5 Calculation of the physical observables 61
3.5.1 Total ionization probability 61
3.5.2 Electron energy spectrum 61
3.6 On the functions $F_j(t)$ 64
3.7 Description of numerical implementation 66
3.8 Validation of the model 68
3.8.1 Ionization yield versus peak field intensity 69
3.8.2 Above-threshold ionization spectrum 69
3.8.3 Rabi oscillations and Autler-Townes duplets 69
3.9 Conclusion 84

4 Detailed Study of the ATI Spectra within our Model Atom 87
4.1 Introduction 87
4.2 Interaction of the model atom with strong low-frequency fields . 88
4.2.1 Probability density as a function of time and p_z 88
4.2.2 Backward and forward electron emission 92

4.2.3 Electron angular distributions . . . 95
4.2.4 Total ionization probability . . . 96
4.2.5 Pulse duration and phase-dependent effects . . . 97
4.3 Resonant interaction of the model atom in the high-frequency regime . . . 100
4.4 Conclusion . . . 102
4.5 Figures . . . 105
4.6 Figures . . . 125

5 Summary and Perspectives 129
5.1 Summary . . . 129
5.2 Outlook . . . 131

II Relativistic Calculation of Matrix Elements for Two-Photon Transitions in Hydrogen-Like Ions 133

6 General Introduction 135
6.1 Motivations and general scope . . . 135
6.2 Outline of the dissertation . . . 140

7 The Relativistic Sturmian Functions 149
7.1 Introduction . . . 149
7.2 The Dirac-Coulomb Sturmian functions . . . 152
7.2.1 Definitions . . . 152
7.2.2 General properties . . . 157
7.2.3 The relativistic hydrogen-like problem . . . 158
7.3 The Quasirelativistic Coulomb Sturmian functions . . . 159
7.3.1 Quasirelativistic Coulomb wave functions . . . 159
7.3.2 Quasirelativistic Coulomb Sturmian . . . 164
7.4 Dirac-Coulomb Green's function representations . . . 166
7.4.1 Fully relativistic treatment . . . 167
7.4.2 Quasirelativistic treatment . . . 170
7.5 The nonrelativistic limit . . . 172
7.5.1 Coulomb Sturmian functions . . . 173
7.5.2 Coulomb Green's functions . . . 175
7.6 Conclusion . . . 176

8 Two-Photon Transition Amplitudes in Hydrogen-Like Ions 183
8.1 Introduction . . . 183
8.2 The covariant formulation of the electromagnetic field . . . 185
8.3 Relativistic formulation of the S-matrix . . . 187
8.3.1 Definition . . . 187

8.3.2 Green's function method . . . 189
8.4 Two-photon absorption transition amplitudes . . . 191
8.4.1 Fully relativistic formulation . . . 193
8.4.2 Quasirelativistic formulation . . . 198
8.5 Other bound-bound scattering processes . . . 200
8.5.1 Raman scattering . . . 201
8.5.2 Rayleigh scattering . . . 206
8.6 Numerical results and discussion . . . 208
8.7 Conclusion . . . 224

9 Summary and Perspectives 229
9.1 Summary . . . 229
9.2 Outlook . . . 230

A System of Units 235
A.1 Nonrelativistic atomic units . . . 235
A.1.1 Physical quantities in atomic units . . . 236
A.1.2 Other physical quantities in atomic units . . . 237
A.2 Relativistic Atomic units . . . 238
A.2.1 Some physical units in relativistic atomic units . . . 238

B The Time-Independent Schrödinger Equation in Momentum Space 239
B.1 The generalized eigenvalue problems . . . 239
B.1.1 Configuration space . . . 239
B.1.2 Momentum space . . . 240
B.2 Analytical solutions to stationary states . . . 241
B.3 The continuum spectrum and scattering theory . . . 243
B.3.1 The continuum states $\varphi_k^{\pm}(\mathbf{p})$ . . . 244
B.3.2 One-state model potential . . . 246
B.3.3 Two-states model potential . . . 246
B.3.4 Three-states model potential . . . 247

C The Numerical Methods for Volterra Integral Equations of the Second Kind 249
C.1 Definitions . . . 249
C.2 On the quadrature methods . . . 250
C.3 The multi-step methods . . . 252
C.3.1 Extended trapezoidal's rule . . . 252
C.3.2 Extended Simpson's rule . . . 253
C.4 Standard block-by-block method . . . 256
C.5 Methods based on more accurate numerical integration . . . 257
C.5.1 Product integration . . . 258

C.5.2 Adapted block-by-block method 259
C.6 Convergence and stability of the approximate solution 262

D Detailed Account of the Intermediate Calculations 273
D.1 Functions $\mathcal{J}_n(x,y)$ and $\mathcal{G}_n(x,y)$ 273
D.2 First derivatives $\frac{\partial}{\partial y}\mathcal{J}_n(x,y)$ and $\frac{\partial}{\partial y}\mathcal{G}_n(x,y)$ 277
D.3 Second derivatives $\frac{\partial^2}{\partial y^2}\mathcal{J}_n(x,y)$ and $\frac{\partial^2}{\partial y^2}\mathcal{G}_n(x,y)$ 279
D.4 Functions $\widetilde{\mathcal{D}}_n(x,y;k)$ and $\widetilde{\mathcal{M}}_n(x,y;k)$ 283
D.5 First derivatives $\frac{\partial}{\partial y}\widetilde{\mathcal{D}}_n(x,y;k)$ and $\frac{\partial}{\partial y}\widetilde{\mathcal{M}}_n(x,y;k)$ 284
D.6 Second derivatives $\frac{\partial^2}{\partial y^2}\widetilde{\mathcal{D}}_n(x,y;k)$ and $\frac{\partial^2}{\partial y^2}\widetilde{\mathcal{M}}_n(x,y;k)$ 284
D.7 Explicit analytical expressions of functions $\mathcal{H}_k^{(i)}(t)$ 285

E Kernel Expressions of the Integral Equations 289
E.1 Recurrence relations 289
E.2 Basic derivatives 290
E.3 Components $K_{ij}(t,\xi)$ of kernels $\mathbf{K}(t,\xi)$ 293
E.4 Kernels $K_i(t,\xi)$ for $\mathcal{C}_{1s}(t)$ 294
E.5 Kernels $\tilde{K}_i(t,\xi)$ for $\mathcal{C}_{2s}(t)$ 294
E.6 Kernels $\bar{K}_i(t,\xi)$ for $\mathcal{C}_{2p}(t)$ 295
E.7 Components of $\mathbf{F}_0(t)$ and free terms of $\mathcal{C}_{js}(t)$ and $\mathcal{C}_{2p}(t)$ 295

F Special Functions and Some Useful Properties 297
F.1 The Whittaker function 297
F.2 The generalized Laguerre polynomials 299

G Angular Integrals and Selection Rules 301
G.1 Angular integrals 301
G.2 Selection rules 305

H Radial Integrals 307
H.1 Radial integrals of the first-order $\widetilde{K}_i(l), i = 1,2,3,4$ 307
H.2 Radial integrals of the second-order $K_i(l), i = 1,2,3,4$ 313

Scientific Outputs

"Il arrive un moment dans ta vie où tu réalises qui est important pour toi, qui ne l'a jamais été, qui ne l'est plus et qui le sera toujours."
Not cited.

Publications

- **H. M. Tetchou Nganso**, Yu. V. Popov, B. Piraux, J. Madroñero and M. G. Kwato Njock.
  Ionization of Atoms by Strong Infrared Fields: Solution of the Time-Dependent Schrödinger Equation in Momentum Space for a Model Based on Separable Potentials.
  Phys. Rev. A ***83****, 013401, 1-13 (2011).*

- **H. M. Tetchou Nganso** and M. G. Kwato Njock.
  Use of Dirac-Coulomb Sturmians of First Order for Relativistic Calculations of Two Photon Bound-Bound Transition Amplitudes in Hydrogen-like Ions.
  J. Phys. B: At. Mol. Opt. Phys. ***40****, 807-836 (2007).*

- **H. M. Tetchou Nganso**, S. Giraud, B. Piraux, Yu. V. Popov and M. G. Kwato Njock.
  On the Role of the Coulomb Potential in Strong Field Atomic Ionization Dynamics.
  *J. Electron. Spectrosc. Rel. Phenom.****161****, 178-181 (2007).*

- J. M. Ngoko Djiokap, **H. M. Tetchou Nganso** and M. G. Kwato Njock.
  Effects of the Electron's Anomaly in Relativistic Laser-Assisted Mott

Scattering.
Phys. Scr. ***75****, 726-733 (2007).*

- S. Giraud, B. Piraux, Yu. V. Popov and **H. M. Tetchou Nganso**.
  Strong Field Atomic Ionization Dynamics: Role of Coulomb Potential Studied by Means of a Model.
  Proc. SPIE Vol. ***6165****, 61650D, 1-8 (2006). Laser Physics and Photonics, Spectroscopy and Molecular Modeling VI, Eds. Vladimir L. Derbov, Leonid A. Melnikov and Lev M. Babkov.*

To be submitted

- **H. M. Tetchou Nganso**, Yu. V. Popov, B. Piraux and M. G. Kwato Njock.
  Ionization of Atoms by Strong Infrared Fields. II. Resonant Interaction of the Model Atom in the High-Frequency Regime.
  Phys. Rev. Lett. (2011).

- **H. M. Tetchou Nganso** and M. G. Kwato Njock.
  Rayleigh and Raman Scattering in the Relativistic Hydrogen-Like Ions: Application of the Sturmian Expansion of the First-Order Dirac-Coulomb Green Function.
  J. Phys. B: At. Mol. Opt. Phys. (2011).

- **H. M. Tetchou Nganso** and M. G. Kwato Njock.
  The Continuum Quasirelativistic Dirac-Coulomb Sturmian Functions.
  J. Phys. A: Math.Theor. (2011).

- B. Piraux, **H. M. Tetchou Nganso**, M. G. Kwato Njock, E. Foumouo, G. Gasaneo and G. Lagmago Kamta.
  The Sturmian Functions and their Applications in Physics.
  Physics Reports. Elsevier Science (in progress).

Conference Proceedings and Preprints

- **H. M. Tetchou Nganso** and M. G. Kwato Njock.
  The Second-Order S-Matrix Element for Two Photon Absorption Processes in Highly Ionized Hydrogen-Like Systems Revisited in the Light

of Dirac-Coulomb Sturmians of the First Order.
The proceedings of the international conference on Optics and Laser Applications in Medicine and Environmental Monitoring for Sustainable Development. 19-24 November 2007, Cape Coast, Ghana.

- **H. M. Tetchou Nganso**, B. Piraux, Yu. V. Popov and M. G. Kwato Njock.
On the Role of the Coulomb Potential in Strong Field Atomic Ionization Dynamics.
*Preprint N° **IC/2006/06** , The Abdus Salam ICTP Publications (2006).*

- J. M. Ngoko Djiokap, **H. M. Tetchou Nganso** and M. G. Kwato Njock.
Effects of the Electron's Anomaly in Relativistic Laser-Assisted Mott Scattering.
*Preprint N° **IC/2006/007**, The Abdus Salam ICTP Publications (2006).*

- **H. M. Tetchou Nganso** and M. G. Kwato Njock.
Use of Dirac-Coulomb Sturmians of First Order for Relativistic Calculations of Two Photon Bound-Bound Transition Amplitudes in Hydrogenic-like Ions.
*Preprint N° **IC/2005/053**, The Abdus Salam ICTP Publications (2005).*

- J. M. Ngoko Djiokap, M. G. Kwato Njock and **H. M. Tetchou Nganso**.
Coulomb Effects in Relativistic Laser-Assisted Mott Scattering.
*Preprint N° **IC/2004/82**, The Abdus Salam ICTP Publications (2004).*

Other Scientific meeting attended

- Université Extras Muros. Coopérer pour un Développement Ciblé des Pays du Sud.
Commission Universitaire pour le Développement: International Auditorium, Belgium, 21-22 October 2010.

- Ph.D. Students' Day.
Université Catholique de Louvain, Louvain-la-Neuve, Belgium, 21 May 2010.

- Sun Application Tuning Seminar.
  University of Namur, Namur, Belgium, 21-23 October 2008.

- 6th Edward Bouchet-Abdus Salam Institute International Conference.
  University of Cape Town, Cape Town, South Africa, 23-26 January 2007.

- Doctoral School Thematic Physics and Astrophysics.
  University of Liege, Liege, Belgium, 25 May 2007.

- The International Conference on Many Particle Spectroscopy of Atoms, Molecules, Clusters and Surfaces.
  University of Roma, Roma, Italy, 22-24 June 2006.

- The X International School for Junior Scientists and Students on Optics, Laser Physics and Biophysics.
  Saratov Fall Meeting 2006, Saratov, Russia, 26-29 September 2006.

- The IX International School for Junior Scientists and Students on Optics, Laser Physics and Biophysics.
  Saratov Fall Meeting 2005, Saratov, Russia, 27-30 September 2005.

- The International Conference on Electron and Photon Impact Ionization and Related Topics (EPIIRT).
  Université Catholique de Louvain, Louvain-la-Neuve, Belgium, 01-03 July 2004.

- Seventh International Workshop on Physics and Modern Applications of Lasers.
  University of Douala, Douala, Cameroon, 6-10 December 2004.

- The UK Forum for International Education and Training (UKFIET): The 7th Oxford International Conference on Education and Development.
  University of Oxford, Oxford, United Kingdom, 9-12 September 2003.

- Sixth International Workshop on Laser Physics and its Applications.
  University of Tunis, Tunis, Tunisia, 05-09 July 2002.

- Winter School on Laser and Applications.
  The Abdus Salam ICTP, Trieste, Italy, 19 Fev-02 March 2001.

- Spring College on Computational Condensed Matter Physics: Numerical Methods in Electronic Structure Theory.
  The Abdus Salam ICTP, Trieste, Italy, 07-25 May 2001.

Part I

Ionization Dynamics of a Model Atom Exposed to a Strong Laser Pulse

Chapter 1

General Introduction

"Difficulties are meant to rouse, not discourage. The human spirit is to grow strong by conflict."
William Ellery Channing.

1.1 Framework and formulation of the problem

The study of the highly non-linear interaction of one-electron atoms with intense infrared laser pulses has stimulated the development of numerous mathematical methods and numerical algorithms to solve the corresponding time-dependent Schrödinger equation (TDSE). The numerical solution of the TDSE by means of spectral and finite difference grid methods [1, 2, 3, 4, 5, 6, 7, 8] has provided fundamental insights into the basic processes that dominate laser-matter physics in this regime, namely above-threshold ionization (ATI) and high-order harmonic generation (HOHG). However, it is very difficult to draw conclusions regarding the actual mechanisms that lead to these two processes because it is always *after* the laser turnoff that the relevant information is extracted from the numerical solution of the TDSE [9]. Nevertheless, by means of a simple model, Keldysh [10] has shown that depending on the field intensity, we can distinguish two regimes where different mechanisms take place: the perturbative regime at relatively low intensity where multiphoton processes are dominant and the tunneling regime in the strong field limit. More precisely, Keldysh has introduced the adiabaticity parameter $\gamma = \frac{\omega}{\mathcal{E}_0}\sqrt{2I_p}$, where $\mathcal{E}_0$ is the field strength, ω the laser frequency and I_p the ionization potential of the atom. For $\gamma >> 1$, the ATI and harmonic generation occur via multiphoton transitions while in the strong field limit, for $\gamma << 1$, tunnel ionisation takes place. In this latter case, the electron can escape from the vicinity of the ion core by tunnelling through the barrier formed by the Coulomb attraction of the core and the time dependent electric field generated by the laser. Once

the electron is released, it is accelerated away from the atom by the laser field (acquiring a kinematic momentum along the direction of laser polarization), and after the field changes sign, it is driven back and forth by the external field. It can therefore experience multiple returns to the nucleus. When the electron gets back to the nucleus, it can be scattered by the ion core (changing the direction of its momentum and producing the observed angular distribution of ATI electrons) or recombine in the ground state of the atom leading to HOHG of the driving field [11, 12, 13]. This picture is the basis of a well known theoretical model, the so-called "strong field approximation" (SFA), sometimes termed Krainov-Faisal-Reiss (KFR) models [14, 15, 16] where it is assumed that the dynamics are governed by the coupling of the ground state with the continuum and that the ejected electron is described by a Volkov state that ignores the presence of the Coulomb potential. This theoretical approach has been immensely successful in predicting and explaining all the main features of a variety of multiphoton processes in particular high-order (the high energy features in the) ATI in strong infrared fields. Although this model describes surprisingly well the essential features of nonresonant ATI, it fails to predict a sufficient number of hot electrons in the case of linear laser light polarization as pointed out by Mohideen *et al.* [17].

The energy spectra of ATI electrons (constituted by a series of peaks separated by the photon energy) [18] can be divided into distinct regions depending on the relation between the ionized electron's energy E_{kin} and the ponderomotive energy U_p (*i.e.*, the average energy of free-electron oscillations in a laser electric field). The two most important spectral regions are the *low-energy part* (extends in energy up to $2U_p$, which corresponds to the maximum instantaneous energy of free-oscillations in the electric field) and the *high-energy part* (plateau or rescattering) which extends up to $\sim 10U_p$. The ATI spectrum of atoms exposed to intense laser pulses normally decreases in magnitude after the first few orders, levels off in a plateau, and then drops to noise level [19]. The structure of the spectrum can be readily explained by a simple classical model, the well-known three-step scenario [19] or "simple-man model": the plateau is formed by photoelectrons (with peaks of nearly equal magnitude) that rescatter from their parent ion before escaping, while those that do not rescatter (the majority) contribute only to low ATI orders [11, 20].

It has been known from some time that the emission of low-energy electrons is strongly enhanced, and often completely dominated, by series of multiphoton resonances between the ground state and excited states Stark shifted by the field [21]. Nowadays, it is possible to reproduce delicate resonant features present in ATI spectra with astonishing precision by solving the TDSE for model atomic potentials [22]. However, no simple picture can be drawn for

the *mechanism leading to electron ejection* according to the fact that the relevant information is extracted after the laser turnoff both theoretically and experimentally. However, a central question arises: *how are electrons emitted in the low-energy part of the photoelectron spectra? are they by a tunnel or multiphoton processes?* far above this simple question emerges the *crucial role of the Coulomb potential.*

In fact, for $\gamma << 1$ and *a fortiori* for $\gamma \approx 1$, it is impossible to make a clear-cut separation between the two mechanisms. Both of them, multiphoton processes and tunnel ionization play a role. This has been confirmed experimentally and by numerical simulations. High-resolution fully differential experimental data on single ionisation of rare gases (He, Ne and Ar) by short laser pulses have been obtained by Rudenko *et al.* [23] . Their data clearly show that deep in the tunneling regime, the low-energy ATI peaks exhibit a fine structure that is unambiguously attributed to a resonant multiphoton process. Similar structures were observed by Maharjan *et al.* [24] for Ar at selected wavelengths in the range from 400 to 800 nm for $\gamma < 1$. Very recent theoretical and experimental studies confirm the importance of the discrete photo-absorption even deep in the tunnelling regime [25]. Furthermore, Potvliege *et al.* [26] explored the importance of the resonant coupling of the field with intermediate excited states in the tunnelling regime and predicted that at $\gamma < 1$ ionization from the ground state can still be significantly affected by multiphoton resonances. From the theoretical point of view, de Bohan [27] have shown that for $\gamma < 1$, the first ATI peaks corresponding to an electron energy smaller than twice ($E_{kin} < 2U_p$) the ponderomotive potential does not result from a tunneling process. This has been demonstrated by carefully analyzing the behaviour of the ionized wave packet both in the momentum and configuration space. It is important to note that it is precisely the low-energy part of the ATI spectrum that provides the dominant contribution to the ionization yield for a given photon energy. These results raise the fundamental question of the actual role of the Coulomb potential in the intensity regime where tunnel ionization is supposed to take place. In order to address this question, we have developed a model calculation which *goes far beyond* the SFA. It is this mathematical model that we present in this part of the thesis.

de Bohan [27] has shown that in the present context, it is more "natural" to solve the TDSE in the momentum space. By using Ehrenfest's theorem she has shown that in the velocity gauge, the canonical momentum of continuum electrons becomes a constant of motion which, in atomic units, is equal to the electron drift velocity. As a result, working in the momentum space, provides direct information on the ionization dynamics and in particular on the time at which the electron is emitted. In our model, we start from the TDSE associated

to the interaction of atomic hydrogen with an intense infrared field in the velocity gauge. The external electric field is supposed to be linearly polarized. In the momentum space, the Coulomb potential is non local. The main idea of the present approach is to substitute the kernel of the non-local Coulomb potential by a sum of N separable potentials, each of them supporting one bound state of atomic hydrogen. This approach which is widely used in nuclear physics for short range potentials, allows to reduce the 3-dimensional TDSE to a system of N coupled 1-dimensional linear Volterra integral equations of the second kind that we solve numerically. The present model presents several advantages. First, it provides a rigorous solution for the electron wave packet. Second, and by contrast with the SFA, more than one bound states may be included in the model, third, the continuum-continuum dipole matrix elements are treated exactly and finally, the theory is fully invariant.

1.2 Structure of the thesis

This first part of the thesis discusses the interaction processes we are concerned with, the theoretical developments and the concrete applications of our approach to a model atom. This part is divided into five Chapters and is organized as follows.

Chapter 2 deals with the details of the laser-matter interaction at the atomic scale and describes the processes we are interested in. We present a state of the art as far as theory is concerned in order to identify specific treatments that already exist. Finally, we outline more formally the context of our method.

The **Chapter 3** describes our theoretical model and its numerical implementation. Validity tests are conducted at high frequencies for a few well-known physical processes.

In the light of the above quasi-analytical method, detailed investigations of the role of the atomic potential and consequently the atomic structure in the regime of strong field tunnelling ionization are given in **Chapter 4**. Also, we investigate effects of pulse duration and carrier-envelope phase (CEP) on angular distribution of photoelectrons and energy distributions, and we reconsider the resonance interaction of our model atom in the high-frequency regime.

Finally, conclusions and future perspectives are given in **Chapter 5**.

Bibliography

[1] E. Huens, B. Piraux, A. Bugacov and M. Gajda, *Phys. Rev. A* **55**, 2132 (1997).

[2] L. A. Collins and A. L. Merts, *Phys. Rev. A* **40**, 4127 (1989).

[3] X. Tang, H. Rudolph and P. Lambropoulos, *Phys. Rev. Lett.* **65**, 3269 (1990).

[4] M. Pont, D. Proulx and R. Shakeshaft, *Phys. Rev. A* **44**, 4486 (1991).

[5] C. Cerjan and K. Kulander, *Comput. Phys. Commun.* **63**, 529 (1991).

[6] E. Cormier, H. Bachau and J. Zhang, *J. Phys. B: At. Mol. Phys.* **26**, 4449 (1993).

[7] K. C. Kulander, *Phys. Rev. A* **35**, 445 (1987).

[8] K. C. Kulander and B. W. Shore, *J. Opt. Soc. Am. B* **7**, 502 (1990).

[9] A. de Bohan, B. Piraux, L. Ponce, R. Taïeb, V. Véniard and A. Maquet, *Phys. Rev. Lett.* **89**, 113002 (2002).

[10] L. V. Keldysh, *Zh. Éksp. Teor. Fiz.* **47**, 1945 (1964)
L. V. Keldysh, *Sov. Phys. JETP* **20**, 1307 (1965) (Engl. Transl.)

[11] P. B. Corkum, *Phys. Rev. Lett.* **71**, 1994 (1993).

[12] M. Lewenstein, Ph. Balcou, M. Yu. Ivanov, A. L'Huillier and P. B. Corkum, *Phys. Rev. A* **49**, 2117 (1994).

[13] M. Lewenstein, K. C. Kulander, K. J. Schafer and P. H. Bucksbaum, *Phys. Rev. A* **51**, 1495 (1995).

[14] F. H. M. Faisal, *J. Phys. B* **6**, L89 (1973).

[15] H. R. Reiss, *Phys. Rev. A* **22**, 1786 (1980).

[16] N. B. Delone and V. P. Krainov, *Multiphoton Processes in Atoms* (Springer Series on Atoms and Plasmas, 1993).

[17] U. Mohideen, M. H. Sher, H. W. K. Tom, G. D. Aumiller, O. R. Wood II, R. R. Freeman and J. Bokor, *Phys. Rev. Lett.* **71**, 509 (1993).

[18] P. Agostini, F. Fabre, G. Petite and N. K. Rahman, *Phys. Rev. Lett.* **42**, 1127 (1979).

[19] W. Becker *et al.*, *Adv. At. Mol. Opt. Phys.* **48**, 35 (2002).

[20] K. C. Kulander, K. J. Shafer and J. L. Krause, *in Super-Intense Laser-Atom Physics*, edited by B. Piraux, A. L'Huillier and K. Rzążewski (Plenum Press, New York, 1993), p. 95.

[21] R. R. Freeman *et al.*, *Phys. Rev. Lett.* **59**, 1092 (1987).

[22] M. J. Nandor *et al.*, *Phys. Rev. A* **60**, R1771 (1999).

[23] A. Rudenko, K. Zrost, C. D. Schröter, V. L. B. de Jesus, B. Feuerstein, R. Moshammer and J. Ullrich, *J. Phys. B: At. Mol. Opt. Phys.* **37**, L407 (2004).

[24] C. M. Maharjan, A. S. Alnaser, I. Litvinyuk, P. Ranitivic and C. L. Cocke, *J. Phys. B: At. Mol. Opt. Phys.* **39**, 1955 (2006).

[25] T. Marchenko, H. G. Muller, K. J. Schafer and M. J. J. Vrakking, *J. Phys. B: At. Mol. Opt. Phys.* **43**, 185001 (2010).

[26] R. M. Potvliege, E. Mese and Svetlana Vučić, *Phys. Rev. A* **81**, 053402 (2010).

[27] A. de Bohan, *Dynamique de l'Interaction Laser-Atome. Moment Canonique et Approximation du Champ Fort*, PhD Thesis, Université Catholique de Louvain, Belgium (2001).

Chapter 2

Laser Atom Interaction in Intense Field

"People are made to be loved and things are made to be used. Chaos in the world is because people are used and things are loved"

Not cited.

2.1 Introduction

There is a tremendous body of work on the theory of light-matter interaction, much of it extremely complex. This Chapter presents the fundamental aspects of the dynamics of atoms exposed to strong laser fields. The presented material is partly guided by several reviews devoted to multiphoton processes in intense laser fields [1, 2, 3, 4]. Their understanding will allow us to interpret the numerical results obtained in the next Chapters of this thesis. Unless otherwise stated, we use both the SI and *a.u.* unit systems throughout this Chapter.

In Section (2.2) we give a brief outline of some atomic processes occurring in the interaction between a laser pulse and the matter in the atomic scale. We restrict ourselves only on the processes that we are concerned in this thesis. Different approaches for the study of aforementioned processes through Schrödinger equation are presented in Section (2.3). After a brief sketch of the semiclassical model of a laser field in Section (2.4), the main results arising from the Ehrenfest theorem in its velocity and length gauges are given in Section (2.5). The chapter ends with a conclusion in Section (2.6).

2.2 Strong-field multiphoton processes

2.2.1 Electron-field interaction: Stark shifts

The classical electromagnetic field *in vacuo* is described by the electric $\mathcal{E}(\mathbf{r},t)$ and magnetic $\mathcal{B}(\mathbf{r},t)$ field vectors, which satisfy Maxwell's equations [5, 6]. They can be generated from scalar and vector potentials $\varphi(\mathbf{r},t)$ and $\mathbf{A}(\mathbf{r},t)$ by

$$\mathcal{E}(\mathbf{r},t) = -\boldsymbol{\nabla}\varphi(\mathbf{r},t) - \frac{1}{c}\frac{\partial}{\partial t}\mathbf{A}(\mathbf{r},t), \qquad \mathcal{B}(\mathbf{r},t) = \boldsymbol{\nabla}\times\mathbf{A}(\mathbf{r},t).$$

The potentials are not completely defined by these equations. In particular, $\mathcal{E}(\mathbf{r},t)$ and $\mathcal{B}(\mathbf{r},t)$ are unaltered by the substitutions, the well known *gauge transformations*

$$\varphi(\mathbf{r},t) \to \varphi(\mathbf{r},t) - \frac{1}{c}\frac{\partial}{\partial t}\chi(\mathbf{r},t), \qquad \mathbf{A}(\mathbf{r},t) \to \mathbf{A}(\mathbf{r},t) + \boldsymbol{\nabla}\chi(\mathbf{r},t),$$

where $\chi(\mathbf{r},t)$ is an arbitrary real differentiable function. Since all observable quantities can be expressed in terms of $\mathcal{E}$ and $\mathcal{B}$, it is a fundamental requirement of any theory formulated in terms of potentials that it is *gauge-invariant*, *i.e.* that the predictions for observable quantities are invariant under such gauge transformations. This property of gauge invariance allow us to impose a further condition on $\mathbf{A}$ and φ, the well-known *Coulomb or radiation gauge or transversality condition*

$$\boldsymbol{\nabla}\cdot\mathbf{A}(\mathbf{r},t) = 0, \quad \varphi(\mathbf{r},t) = 0.$$

A vector field inferred from the latter equation is called a *transverse or radiation field*. From Maxwell's equations without sources one can show that $\mathcal{E}$ satisfies the wave equation

$$\boldsymbol{\nabla}^2\mathcal{E} - \frac{1}{c^2}\frac{\partial^2}{\partial t^2}\mathcal{E} = 0, \tag{2.1}$$

where c is the velocity of the light *in vacuo*. In classical electromagnetism an electron of velocity $\mathbf{v}$ moving in electric and magnetic fields experiences the Lorentz force

$$\mathbf{F} = -e(\mathcal{E} + \mathbf{v}\times\mathcal{B}). \tag{2.2}$$

For an electron in a light atom the ratio v/c is small. This can be inferred from the Bohr model of one-electron atom. In this model, for an orbit with principal quantum number n, the electron velocity is $v = Ze^2/(4\pi\epsilon_0\hbar n)$. The largest value of v is for $n = 1$, $v = Z\alpha c \simeq Zc/137$ where α stands here for the fine structure constant. For a monochromatic radiation field of a given frequency, $\mid \mathcal{B} \mid / \mid \mathcal{E} \mid = 1/c$. It follows that when v/c is very small, the magnetic term

in the Lorentz force for a radiation field is always small in comparison with the electric term. Apart from special circumstances in which the effect of the electric field vanishes, it is a good approximation to neglect the magnetic term in (2.2) and this will be done in what follows.

A monochromatic stationary plane wave solution of equation (2.1) corresponding to the angular frequency ω is

$$\mathcal{E}(\mathbf{r},t) = \mathcal{E}_0 \cos(\mathbf{k}\cdot\mathbf{r} - \omega t + \phi), \tag{2.3}$$

where $\mathbf{k}$ is the propagation vector, ϕ is a real carrier-phase or absolute phase and $\omega = kc$. Starting with equation (2.2) (in which we neglect the magnetic term), one can determine the classical equations of motion of an electron in a plane wave of infinite extent. If the electron is initially at rest at the origin, the problem is in one-dimension along the linearly polarization of the electric field (denoted x -axis for example). Conceptually, the motion is an oscillatory or "quivering" with the electric field, and using Newton's equations one writes

$$F = m\ddot{x}, \quad \ddot{x} = \frac{e}{m}\mathcal{E}_0 \cos(\omega t), \quad \dot{x} = \frac{e}{m}\frac{\mathcal{E}_0}{\omega}\sin(\omega t), \quad x = -\frac{e}{m}\frac{\mathcal{E}_0}{\omega^2}\cos(\omega t). \tag{2.4}$$

From this simplified picture, two results can be drawn. The first is to determine the maximum spatial excursion of an electron in a plane wave by means of equation (2.4). For an intensity of 10^{12} W.cm^{-2}, one finds ~ 0.9 Å. This is almost twice the Bohr radii a_0 - for higher intensities, the maximum excursion can be much larger than the size of an atom, but tiny compared to typical focal dimensions. This guarantees that even electron with a slow initial velocity will not sample a large spatial region of the field. The infinite plane wave approximation is therefore valid.

The ponderomotive energy U_p

From equation (2.4) let us now calculate the time averaged kinetic energy of an electron in a laser field. The calculation of the kinetic energy E_{kin} is straightforward

$$E_{kin} = \frac{e^2\mathcal{E}_0^2}{2m\omega^2}\sin^2(\omega t), \tag{2.5}$$

and the cycle-averaged kinetic energy of a free (or quivering) electron in the field (for non-relativistic velocities) is given by

$$\langle E_{kin}\rangle_t \equiv U_p = \frac{e^2\mathcal{E}_0^2}{4m\omega^2}, \tag{2.6}$$

where $\langle\ \rangle_t$ indicates averaging over an optical period of time. For a relatively weak intensity of 10^{12} W.cm^{-2}, the average kinetic energy of a free electron is

0.06 eV. This is called the *quiver* or *ponderomotive energy* (hereafter denoted by U_p). It gives a scale for how much energy an electron must have to be considered "free". It is worth mentioning that U_p is directly proportional to the intensity and the square of the wavelength and is of great importance as a scale intensity. Equation (2.5) immediately predicts a *maximum kinetic energy of* $2U_p$ *for electrons or photoelectrons.*

Stark shifts

We consider now the effect of a light field on an atom, specifically the response of the atomic energy levels when perturbed by an external light field [7]. To include the light-field in the quantum mechanical Hamiltonian, it is best to formulate the electromagnetic field in terms of potentials, rather than fields.

$$\boldsymbol{\nabla}^2\varphi + \frac{1}{c}\frac{\partial}{\partial t}(\boldsymbol{\nabla}\cdot\mathbf{A}) = 0, \tag{2.7}$$

$$\boldsymbol{\nabla}^2\mathbf{A} - \frac{1}{c^2}\frac{\partial^2}{\partial t^2}\mathbf{A} - \boldsymbol{\nabla}\left(\boldsymbol{\nabla}\cdot\mathbf{A} + \frac{1}{c}\frac{\partial}{\partial t}\varphi\right) = 0 \tag{2.8}$$

There are gauge freedoms associated with $\mathbf{A}$ and φ, and in this derivation, the so-called Coulomb gauge is used although the results are invariant [8]. Thus the potential equation reduces to

$$\boldsymbol{\nabla}^2\mathbf{A} - \frac{1}{c^2}\frac{\partial^2}{\partial t^2}\mathbf{A} = 0. \tag{2.9}$$

Using the Helmholtz theorem to write an arbitrary electric field as the sum of transverse (no divergence) and longitudinal (no curl) components, $\mathcal{E} = \mathcal{E}_\perp + \mathcal{E}_\parallel$ together with $\boldsymbol{\nabla}\times\mathcal{E}_\parallel = 0$ and $-\boldsymbol{\nabla}\times\boldsymbol{\nabla}\varphi = 0$, one easily shows that the vector potential describes transverse electric fields, $\mathcal{E}_\perp = -\partial\mathbf{A}/\partial t$, including plane waves.

The Hamiltonian operator for a spinless particle moving in an electromagnetic field described by a vector potential $\mathbf{A}$ is obtained by replacing the classical momentum operator $\mathbf{p}$ with a quantum momentum operator $\boldsymbol{\Pi}$ that includes the field,

$$\boldsymbol{\Pi} = \mathbf{p} + \frac{e}{c}\mathbf{A}, \qquad e < 0. \tag{2.10}$$

This transforms the Hamiltonian to

$$\begin{aligned} H &= \frac{1}{2m}\boldsymbol{\Pi}^2 + V(r), \\ &= \frac{1}{2m}\left[\mathbf{p}^2 + \frac{e}{c}(\mathbf{p}\cdot\mathbf{A} + \mathbf{A}\cdot\mathbf{p}) + \frac{e^2}{c^2}\mathbf{A}^2\right] + V(r), \end{aligned} \tag{2.11}$$

where $V(r)$ is the electrostatic Coulomb potential. This can be divided into two parts: the field-free hamiltonian H_0 and the laser-atom interaction hamiltonian H_{int}, given respectively by

$$H_0 = \frac{1}{2m}\mathbf{p}^2 + V(r) \text{ and } H_{int} = \frac{e}{2mc}\left(\mathbf{p}\cdot\mathbf{A} + \mathbf{A}\cdot\mathbf{p}\right) + \frac{e^2}{2mc^2}\mathbf{A}^2. \quad (2.12)$$

We can now approach the problem classically, using the vector potential for stationary plane wave polarized along $\mathbf{e}_z$, $\mathbf{A} = (c\mathcal{E}_0/\omega)\cos(\omega t)\mathbf{e}_z$. In the dipole approximation, this leads directly to a simplification of the interaction Hamiltonian in terms of the classical field,

$$H_{int} = \frac{1}{2m}\left[\frac{2\mathcal{E}_0}{\omega}\cos(\omega t)(\mathbf{p}\cdot\mathbf{e}_z) + \frac{ec\mathcal{E}_0^2}{\omega^2}\cos^2(\omega t)\right]. \quad (2.13)$$

The first order correction to energy level vanishes. We can then evaluate the shift of energy levels using perturbation theory in second order. The results in a shift of energy level i by an amount ΔE_i can be written as [9]

$$\Delta E_i = \frac{e^2\mathcal{E}_0^2}{4\omega^2}\left[1 - \sum_{i\neq f}\bar{f}_{fi}\frac{\omega_{fi}^2}{\omega_{fi}^2 - \omega^2}\right]. \quad (2.14)$$

In this expression, the sum is over all final states of the electron, $\hbar\omega_{fi}$ is the difference in energies of initial and final states, and $\bar{f}_{fi}$ is the oscillator strength.

There are two easily evaluated limits that are useful in guiding our thinking about atomic states in intense fields. For *very weakly bound states (e.g. Rydberg states)*, close to the continuum states, $\omega_{fi} \ll \omega$ and in fact the ratio in the summation approaches zero, leading to a simple expression for the energy shift that is the ponderomotive shift. This result is in perfect agreement with our intuition, as weakly bound states are expected to behave much like free electrons. In the opposite extreme, *very deeply bound states* (like the ground state) have energy spacings to other levels that are much larger than a photon, so $\omega_{fi} \gg \omega$. In this case, the sum is dominated by the sum of oscillator strengths which is identically 1 according to the Thomas-Reiche-Kuhn sum rule. This leads to an energy shift that is zero (or very small in magnitude). This simple argument is used to justify the most common assumptions in understanding bound states in an *AC field* - the ground state undergoes basically no shift. *The weakly bound states and the free electron continuum shift by the ponderomotive potential U_p. This has the net effect of increasing the ionization potential I_p by an amount which is about U_p.*

2.2.2 Multiphoton ionization

In recent years, intense laser fields have become available over a frequency range extending from the infrared (IR) to ultraviolet (UV), in the form of short

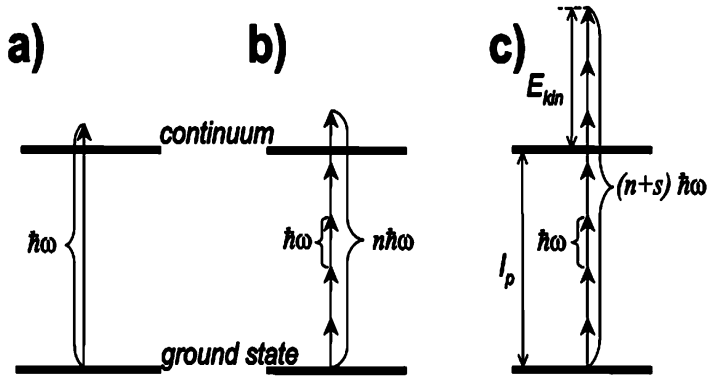

Figure 2.1: *Schematic diagram of ionization processes. Each process results in a free electron with kinetic energy E_{kin}: (a) one-photon ionization; (b) multiphoton ionization by n photons; (c) above-threshold ionization by $(n+s)$ photons.*

pulses yielding intensities of the order of or exceeding the value $I_a = 3.5095 \times 10^{16}$ W.cm^{-2}, corresponding to the atomic unit of electric field strength $\mathcal{E}_a = 5.14221 \times 10^9$ V.cm^{-1}. The "Chirped Pulse Amplification" (CPA) scheme, in which laser pulses are stretched, amplified and then compressed (Strickland and Mourou [10]) has been used to obtain such laser fields. They are strong enough to compete with the Coulomb forces in controlling the electron dynamics in atomic systems. As a result, atoms and molecules in intense laser fields exhibit new properties which have been discovered via the study of multiphoton processes. These modified properties generate new behavior of bulk matter in intense laser field, with wide ranging potential applications such as the study of ultra-fast phenomena, the development of powerful high-frequency (XUV and X-ray) lasers, the investigation of the properties of plasmas and condensed matter under extreme conditions of temperature and pressure, and intense field control of atomic and molecular reactions. The excitation of atoms by intense laser pulses can be divided into two broad regimes determined by the characteristics of the laser pulse relative to the atomic response. The first regime involves relatively weak optical laser fields of long duration ($>$ 1 ns), and the second involves strong fields of short duration (*i.e.* when the duration of the ionizing laser pulse, typically $<$ 1 ps is shorter than the time it takes a photoelectron to leave the interaction volume). These will be referred to as the weak-long (WL) and strong-short (SS) cases respectively.

In the case of atomic excitation by WL pulses, the intensity is presumed to be high enough for multiphoton transitions to occur. However, the intensity is

still low enough for a theoretical description based on perturbations of field-free atomic states to be valid, and the time dependence of the field amplitude does not play an essential role. The SS case is fundamentally different in that the atomic electrons are strongly driven by fields too large to be treated by perturbation theory, and the time dependence of the pulse as it switches on and off must be taken into account.

Perturbation theory

For photon energies much smaller than the ionization potential ($\hbar\omega \ll I_p$), several photons must be absorbed to produce ionization, or even electronic excitation in many cases. The transition from a bound state to a continuum state by absorbing many photons is known as *multiphoton ionization* (MPI). This process is depicted schematically in **Figure** 2.1 (b) and denoted as follows

$$n\hbar\omega + A^q \rightarrow A^{q+1} + e^- \tag{2.15}$$

where q is the charge of the target atomic system A, $\hbar\omega$ is the photon energy and n is an integer. As known, this process was first observed by G. S. Delone and N. B. Voronov in 1965 [11], who detected seven-photon ionization of xenon using a ruby laser. During the same year J. L. Hall and collaborators recorded two-photon ionization of the negative Iodine ion $\mathtt{I}^-$ [12]. Early experiments on MPI at relatively low light intensity ($< 10^{13}$ W.cm^{-2}) were in good agreement with lowest-order perturbation theory (LOPT) [13, 14] where the rate of an n-photon transition can then be calculated using nth order perturbation theory for the atom-field interaction. For an incident photon number flux ϕ_F of frequency ω, the rate is

$$W^{(n)}_{i\rightarrow f} = \left(\frac{2\pi\alpha\phi_F\omega}{e^2}\right)^n \mid T^{(n)}_{i\rightarrow f} \mid^2 [2\pi\delta(\omega_i + n\omega - \omega_f)], \tag{2.16}$$

where

$$T^{(n)}_{i\rightarrow f} = \langle f \mid DG[\omega_i + (n-1)\omega]DG[\omega_i + (n-2)\omega]\cdots DG[\omega_i + \omega]D \mid i\rangle, \tag{2.17}$$

$\mid i\rangle$ is the ith eigenstate of the field-free atomic Hamiltonian, $D = e(\mathbf{e}\cdot\mathbf{r})$, with $\mathbf{e}$ the polarization direction and

$$G(\omega) = \sum_j \frac{\mid j\rangle\langle j \mid}{(\omega - \omega_j + \mathrm{i}\Gamma_j/2)}. \tag{2.18}$$

The sum over j includes an integration over the continuum for all sequences of transitions allowed by angular momentum and parity selection rules. Methods for calculating cross sections and rates in the weak field regime are described

in References [15, 16].

Nonresonant multiphoton ionization

Along the line of the perturbative approach outlined above, one can imagine multiphoton ionization as an extension of single photon ionization, known as the *photoelectric effect*. For most atoms and molecules, having ionization potentials I_p greater than a few electronvolts, single photon ionization requires (UV) light. The result in terms of electron kinetic energy is given by $E_{kin} = \hbar\omega - I_p$. In the following, we keep considering the absorption of many photons by the atom. In the absence of resonances, absorption of multiple photons would take place through virtual states, the lifetime of which is determined from the uncertainty principle and their detuning from the nearest real state. This indicates that multiphoton absorption must be nearly instantaneous for bound states that require a large number of photons to ionize. This implies a requirement for large photon fluxes, or high intensity fields. The resulting electron kinetic energy after multiphoton ionization is then given by $E_{kin} = n\hbar\omega - I_p(I)$, where n is the minimum number of photons to ionize, and I_p now depends on the laser intensity I, because the AC Stark shift can not be neglected at high intensities. The Stark-shifted ionization potential is in good approximation $I_p(I) = I_p + U_p$. The MPI process results in $E_{kin} \leq \hbar\omega$, because we only consider the absorption of the minimum number of photons to ionize. From equation (2.16) one easily proves that the n-photon ionization rate takes the form

$$W_{i\to f}^{(n)} = \sigma_n I^n, \tag{2.19}$$

where σ_n is the generalized n-photon ionization cross section. This highly nonlinear dependence on light intensity was proven experimentally up to $n = 22$ for MPI of He by Nd:YAG laser fields [17]. However this intensity scaling breaks down at a critical intensity. Above this critical value there is no change in the intensity dependence of the ion yield [18]. This is explained in terms of population depletion [19]. For a pulse of a given duration, there is a maximum value of intensity above which no more ionization can occur since all the sample atoms have been ionized. This intensity is known as the *saturation intensity* (I_{sat}). The latter can be lower than the peak intensity of the laser pulse. In order to obtain ionization up to the peak intensity of the laser pulse one requires shorter pulses. Despite the relative simple appearance of equation (2.19), σ_n is quite difficult to calculate since high-order processes are needed to ensure an accurate perturbative description. Further complications occur with the perturbative approach as the intensity of the incident light increases; the atomic states involved can no longer be considered as unperturbed since they shift in a dynamic fashion in pulsed fields due to the strong coupling

with the laser field. The resulting energy shifts are "non-perturbative" and do not fit into the LOPT framework although they can be included by going to higher orders; these perturbed energies have been used to explain many of the effects observed in MPI [20, 21]. Furthermore, more difficulties arise when *near-resonant* and *resonant- behaviour* are investigated since, strictly speaking, perturbation theory is no longer valid; although methods have been developed which can handle these difficulties [15, 16].

Resonant enhanced multiphoton ionization

For multiphoton ionization, ω can be continuously varied because the final state in equation (2.16) lies in the continuum. If ω is tuned so that $\omega_i + m\omega \simeq \omega_j$ for some contributing intermediate state $\mid j\rangle$ in (2.18), then that state lies an integer m photons above the initial state, and the corresponding denominator vanishes (to within the level width Γ_j), producing a strongly peaked resonance. Since it takes $k = n - m$ additional photons for ionization, the process is called m, k *resonant enhanced multiphoton ionization* (REMPI). Measurements of the photoelectron angular distribution are useful in characterizing the resonant intermediate state. The perturbation equation (2.16) indicates that the rate for nonresonant multiphoton ionization scales as ϕ_F^n for a n-photon process. However, this is not the case for REMPI since the resonant transition saturates and (2.16) no longer applies. Then the rate can be controlled either by the m-photon resonant excitation step, or by the number of photons k needed for the ionization step.

2.2.3 Above threshold ionization

The MPI assumption, however, is only realistic for relatively low intensities. In high intensity experiments ($> 10^{13}$ W.cm^{-2}), absorption of photons rarely stops at the minimum required, while the lowest-order perturbation theory is no longer valid because of the strong coupling of the atomic states with the pulsed laser field, which leads to the AC-Stark shift. In this regime of light intensity, electrons can gain more than minimum amount of energy required for ionization. *Rather than forming a single peak, the emitted electron energy spectrum contains a series of peaks separated by the photon energy.* This is called *above threshold ionization*, or ATI and is plotted in **Figure** 2.1 (c). The peaks appear at the energies

$$E_{kin} = (n + s)\hbar\omega - I_p, \tag{2.20}$$

where n is the minimum number of photons needed to exceed I_p, and $s = 0, 1, \cdots$ is called the number of excess photons or above threshold photons carried by the electron. Experimentally ATI was first observed by P. Agostini *et al.*

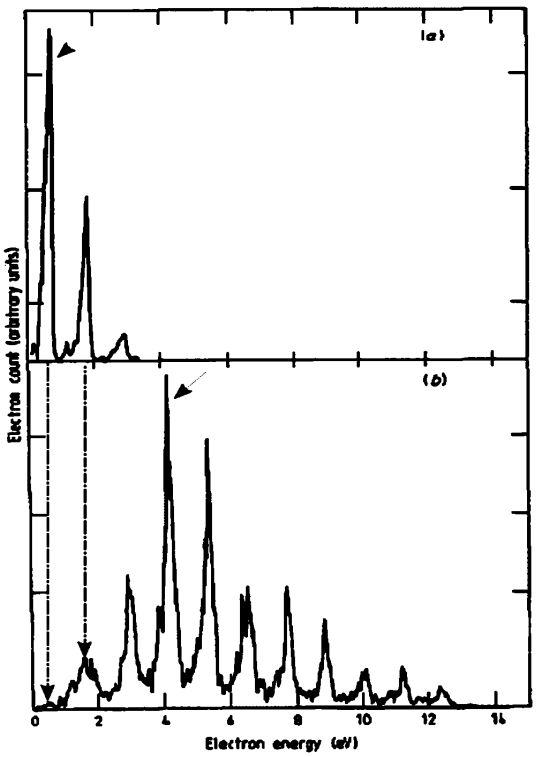

Figure 2.2: *Photoelectron energy spectra (ATI) from Xe using a* $\lambda = 1064$ nm *with* 130 ps *laser pulses. (a)* $I = 2 \times 10^{12}$ W.cm^{-2}*; (b)* $I = 10^{13}$ W.cm^{-2}*. From Petite et al. [22].*

[23]. In the photoelectron energy spectrum of six-photon ionization of Xe at 10^{13} W.cm^{-2} they found a second energy peak separated from the expected first one by the photon energy. An example of ATI spectra of Xe is shown in **Figure** 2.2.

This phenomenon was surprising and misunderstood at first, because how can we admit that the electron, once ionized absorbs again the photons. Indeed, it is easy to show that a free electron, that is to say free from the action of the Coulomb potential, can not emit or absorb photons. After this discovery energy-resolved photoelectron spectra have been studied in detail for different atoms and molecules interacting with lasers at different wavelengths [13, 20, 24, 25, 26]. Despite its obstructions, calculations in the perturbative regime for ATI are given for hydrogen in Reference [26]. This perturbation theory has been shown to be sufficient to account for experimental results in a

certain intensity range [13]. The ionization rate then has a more general form than equation (2.19) $W_{i\to f}^{(n+s)} =\propto I^{n+s}$.

Peak shifting: Long pulse

As the intensity approaches the nonperturbative regime, the AC-Stark shift of the atomic states begins to play a significant role in the structure of the ATI spectrum. The first effect is a shift of the ionization potential, given roughly by the ponderomotive energy U_p. The ionization barrier is boosted by U_p in the laser and the final photoelectron energy is given by

$$E_{kin} = (n+s)\hbar\omega - (I_p + U_p). \tag{2.21}$$

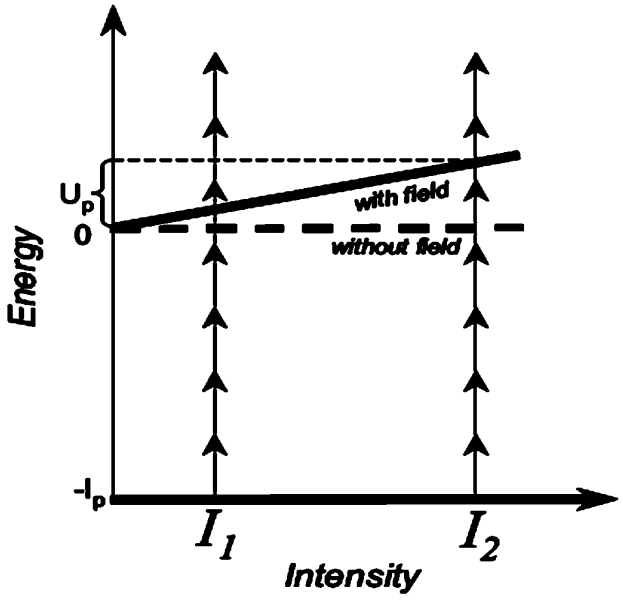

Figure 2.3: *Schematic diagram for the Stark shift of the ionization potential versus the laser intensity. At the intensity I_1 five-photon ionization occurs, whereas at the higher light intensity I_2 one photon more is needed for ionization. The ionization threshold is increased by U_p.*

Figure 2.3 illustrates the mechanism (AC-Stark shift) responsible for the suppression of low-energy peaks in ATI spectra. One can see that ionization by absorption of $n = 5$ photons, which is possible at the laser intensity I_1, is energetically forbidden at I_2. In this case, one more photon is needed to ionize

the atom. However, in experiment, one deals with a smoothly varying intensity in the focus during the laser pulse, so that the corresponding energy peak at I_1 will not completely disappear. **Figure** 2.2 exhibits well this evolution of the main energy peak with increasing laser intensity. More generally, additional photons may then be required in order to extract the electron from the atom; *i.e.* enough to exceed $I_p(I) = I_p + U_p$. If the emitted electron escapes from the focal volume while the laser is still on, it is accelerated by the gradient of the ponderomotive potential. That means, due to the intensity gradient of a focused laser beam, a freed electron experiences a force $-\boldsymbol{\nabla} U_p$. Accelerated by this force in the laser field, the electron regains exactly its ponderomotive energy deficit, which appears due to the ionization potential shift by U_p [27]. In order words, the quiver motion is converted into radial motion, increasing the kinetic energy by U_p and exactly canceling the shift of the continuum. This negates the effect of the Stark shift on the measured electron kinetic energies. This is possible for long laser pulses ($\gg$ 1 ps) (picosecond pulses) when the laser intensity changes slowly compared with the time, the photoelectron needs to leave the focal spot. *As a consequence, the photoelectron peaks appear at the same energy as predicted in equation (2.20).* However, when U_p exceeds the photon energy, *i.e.* $U_p > \hbar\omega$ a remarkable feature of ATI is the suppression of the low-energy peaks in the photoelectron spectra. This effect occurs at increasing laser intensity (see the first two peaks marked with vertical arrows in **Figure** 2.2). In this long pulse limit, no electron is observed with energy less than U_p. This is called *peak shifting* in that the dominant peak in the ATI spectrum moves to higher order as the intensity increases.

Moreover, during the MPI and ATI processes one also needs to account for resonances. If a number s of photons is resonant with an excited state of the system, the ionization rate will be much greater than for purely nonresonant ionization because of the larger cross section of the real intermediate state. This would predict a large photoelectron emission at some E_{kin}^{res} when $s\hbar\omega = E_{res}$. Therefore,

$$E_{kin}^{res} = E_{res} + n\hbar\omega - (I_p + U_p). \tag{2.22}$$

This resonant multiphoton process, or REMPI, has been exploited to perform spectroscopy on one-photon forbidden transitions.

ATI resonance substructure: Short pulse

In the case of sub-picosecond laser pulses ($<$ 1 ps), drastically different photoelectron spectra were observed. The electric field from the laser focus turned off much faster than the electrons could sample its spatial variation. Electrons were no longer able to "slide" down the potential hill - the hill simply disappeared out from under them. There was no time for the photoelectron to

acquire the full amount of energy during the ponderomotive acceleration in the laser field before the end of the pulse. Then the ponderomotive energy was returned to the field and the ATI spectrum becomes much more complicated (*i.e.* peaks become shifted towards lower energies as equation (2.21) would suggest). Such a shift as well as a broadening of the ATI energy peaks with decreasing laser pulse width has been observed experimentally [20]. Additionally, fine structures appear in the photoelectron energy spectrum when sub-picosecond laser pulses are used [21, 28]. The origin of these structures has been attributed to resonant MPI processes (as equation (2.22) would suggest). The latter occur for excited states when AC-Stark shifted into resonance during the laser pulse [28] (electrons from different regions of the focal volume are thus emitted with different ponderomotive shifts, introducing substructure in the spectrum which can be directly associated with AC-Stark shifted resonances). In the long pulse regime the substructures in the ATI electron energy spectrum cannot be resolved due to the ponderomotive acceleration of the photoelectron in the intensity gradient of the focused laser beam.

2.2.4 Tunneling ionization

The preceding discussions use a photon model of the interaction to predict electron kinetic energies. However, at sufficiently high intensity (10^{14}–10^{15} W.cm^{-2}) and low frequency, a *tunneling* mechanism changes the character of the ionization process. Such a light intensity corresponds to an electrical field strength of about $10^8 - 10^9$ V.cm^{-1}. This is already comparable with the strength of the Coulomb field in an atom and is considered as a strong field. In this case perturbation theory is no more valid. A more useful approach is obtained by considering the strong-field photoionization process as tunneling through an effective potential barrier. The latter is formed by the superposition of the atomic potential and the laser electric field as shown in **Figure** 2.4. Such an approach is valid if the oscillation period of the external field is long enough in comparison with the $\ll$ *pseudo time* $\gg$ the electron needs to tunnel through the potential barrier. This quasi-stationary theory was first worked out by Keldysh (1965) [29] and then developed further by many theoreticians [30, 31, 32, 33, 34, 35].

One can then calculate the ionization rate - the rate at which bound electrons can tunnel through the barrier. For this tunneling model the field is entirely classical and the only parameters are the initial state energy (ionization potential) and the strength of the laser field. To determine photoelectron energies from this model, one must consider a *three step process*. First the tunneling ionization of the electron, the acceleration of the electron in the laser field and then accelerated back to the parent ion from which it scatters. Tunneling is the small electron probability that extends past the classical turning point - *all tunneling electrons are "born" with essentially zero kinetic energy.*

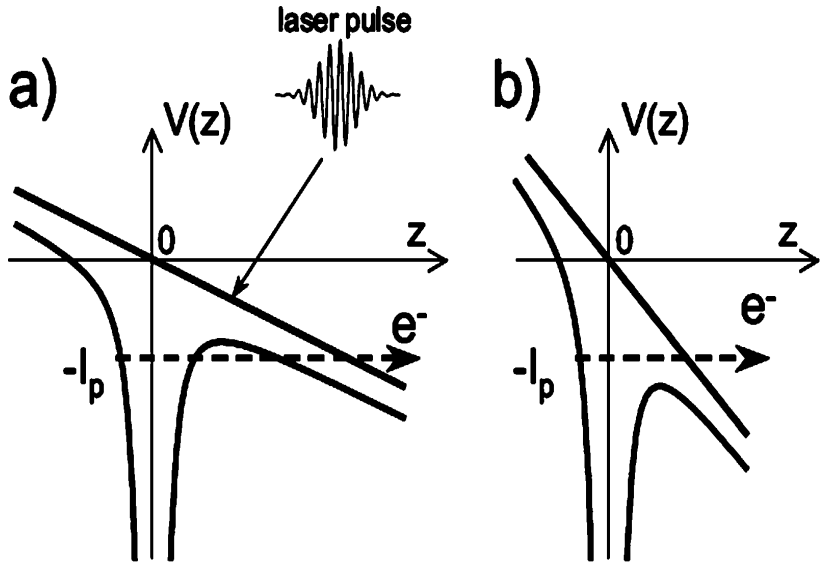

Figure 2.4: *Schematic diagram showing the two possible strong-field photoionization mechanisms: in (a) tunneling ionization; over-the-barrier ionization is depicted in (b).*

The rate of production, however, is highly dependent on the field strength. The stronger the field, the smaller the barrier - the ionization rate is exponential in field strength. Therefore, *most electrons are produced at the peak of the laser field, and no electrons are able to escape at the nodes of the field.* Using a quasi-stationary model in the low-frequency limit first Perelomov, Popov, and Terent'ev [30] and then Amosov, Delone and Krainov [31] have found a tunneling ionization rate (ADK rate) which is given (in the *a.u.*) by

$$W = W_0 \exp\left[-\frac{2(2I_p)^{3/2}}{3\mathcal{E}_0}\right]. \tag{2.23}$$

Here, I_p is the atomic ionization potential, $\mathcal{E}_0$ is the laser field strength and W_0 is a slowly varying function of $\mathcal{E}_0$, I_p and Z, the atomic core charge. The tunneling step determines the number of electrons, while the second step, the acceleration in the field, determines their final kinetic energies. Electrons born at the peak of the field are unable to gain kinetic energy from the field, as after each half-cycle of the field the electron has zero velocity. If an electron were born at the zero crossing of the field, at any half cycle later it would have

a maximum velocity. This results in a characteristic photoelectron spectrum that has an exponential falloff of electron kinetic energy.

An extreme case of tunnel ionization occurs for large amplitude laser fields. As the laser intensity is further increased a critical value of the intensity is eventually reached. Beyond this value the Coulomb potential is so strongly suppressed by the external field that the ground state is no longer bound (leaving a formerly bound electron in the continuum). An electron then just "flows" over the "top" of the barrier. This scenario is shown in **Figure** 2.4 (b). This process is known as *over-the-barrier ionization* (OTBI) and occurs at 1.4×10^{14} W.cm^{-2} for atomic hydrogen. The critical field is obtained by equating the maximum induced by the field in the atomic potential to the binding energy. The critical intensity induced by critical field for OTBI is defined by [2]

$$I_{cOTBI} = \frac{c\epsilon_0 I_p^4}{32Z^2}, \tag{2.24}$$

with c the speed of light and ϵ_0 the dielectric constant of vacuum.

The Keldysh parameter

We have presented three simple, yet very different, models for ionization in high field experiments - MPI, ATI and tunneling. The two formers rely on a photon picture while the latter assumes a classical field. **How does one determine which process is most applicable?** In his pioneering paper describing many effects of high field ionization, Keldysh described an *adiabaticity parameter* γ, now known as the *Keldysh parameter* which has been used as a quantity indicating the transition from multiphoton ionization to the low frequency tunneling limit. *It can be defined as the ratio of the* $\ll$ *mean time* $\gg$ *the electron needs to tunnel through the potential barrier (the tunneling* $\ll$ *pseudo time* $\gg$ *of a bound electron)* [29] *to the period of the laser field oscillation*, which can be expressed as

$$\gamma = \frac{\omega}{\omega_{tunnel}} = \frac{\omega}{e\mathcal{E}_0}\sqrt{2mI_p} = \sqrt{\frac{I_p}{2U_p}}, \tag{2.25}$$

where I_p is the field free atomic ionization potential, U_p is the ponderomotive energy, $\mathcal{E}_0$ is the field amplitude, and m and e are the mass and charge of the electron. For $\gamma > 1$, multiphoton absorption is adequate to describe the ionization process. In contrast, for $\gamma < 1$ the quasistatic tunneling ionization is most appropriate. The transition between the two approaches, multiphoton and tunneling, takes place at $\gamma = 1$. In the intermediate regime with $\gamma \sim 1$ the ionization process has a complicated character and is difficult to model. In fact multiphoton ionization and tunneling are two limiting cases of one ionization

process. Moreover, the formula (2.23) was obtained with a short-range atomic potential, while for real atoms it is rather long-range. Actually, for real atoms the laser field effect on a freed photoelectron is accompanied by the Coulomb force of the ionic core. An analytical solution of such a complex problem is highly complicated [36]. Experiments in optical and infrared wavelength ranges have confirmed qualitatively the exponential dependency of the ionization rate found in (2.23) at $\gamma < 1$ and also at $\gamma \sim 1$ [37, 38, 39, 40].

From equations (2.25) and (2.6) it follows that the Keldysh parameter depends on the frequency and is inversely proportional to the square root of intensity of the field. In contrast to the quite high laser intensities needed to obtain tunneling ionization in the optical region (e.g. $> 10^{14}$ W.cm^{-2} for an 800 nm Ti:Sa laser), microwave tunneling ionization of highly excited Rydberg atoms has been obtained in considerably weaker fields [41, 42].

2.2.5 Semiclassical modeling of strong field matter interaction

Early intense field experiments reported three somewhat surprising observations. The first was an extensive range of high harmonics known as *high harmonic generation* (HHG) [43]. The second was a significant enhancement in the production of *non-sequential double ionization* events (NSDI) [44, 45, 46, 47]. The third surprise was the observation of photoelectrons with kinetic energies much greater than would be expected from a tunneling model. A simple and very satisfying explanation for all three observations came from the *semiclassical model* (which asserts that the release of an electron from the core is by no means the end of the ionization process), the well-known three-step process introduced by Corkum [48], Kulander *et al.* [49], and Schafer *et al.* [50].

The first foundation of the semiclassical model is tunnel ionization or, more generally, optical field ionization. It is often modeled using the Keldysh theory or its refined versions [51, 52, 53]. Once the electronic wave packet appears at the tunnel exit in the other side of the tunneling barrier at x_0, it is pulled or accelerated far away from the parent ion within a small fraction of the electric field oscillation cycle until the field reverses its direction in about a fraction of cycle. More precisely, the emitted electron is then driven by the Lorentz force, and at the usual intensities for tunnel ionization this is dominated by the electric field of the laser initially driving the electron away from the atomic core. Consequently, the Coulomb attraction to the parent ion quickly becomes a small perturbation compared to the laser field. The simplest approximation consists of neglecting the Coulomb field after ionization. This is the main assumption of the strong-field approximation (SFA), a theoretical workhorse in strong-field physics. In the dipole approximation (which will be clearly stated below), for a linearly polarized laser field, the interaction potential energy for

an electron at position $\mathbf{r}$ is (in *a.u.*)

$$V(\mathbf{r},t) = V(\mathbf{r}) + x\mathcal{E}(t), \tag{2.26}$$

where we choose the laser electric field

$$\mathcal{E}(t) = \mathcal{E}_0 f(t)\cos(\omega t + \varphi) \tag{2.27}$$

polarized along the x axis. Here $f(t)$ is a pulse shape, peaked at $t = 0$, *i.e.* $f(0) = 1$.

Setting $V(\mathbf{r}) = 0$ in equation (2.26), the center-of-mass motion of the quantum wave packet is described by

$$\dot{v}_x(t) = -\mathcal{E}(t), \qquad \dot{v}_y(t) = 0, \qquad \dot{v}_z(t) = 0. \tag{2.28}$$

A further essential assumption of the semiclassical model is that the electron appears at the "exit" of the tunneling barrier x_0 with zero velocity $v_x(t_0) = 0$. Then equation (2.28) yields for the electron's velocity [which equals to its kinematic momentum in *a.u.*]

$$v_x(t) = v_x(t_0) + A(t) - A(t_0) = A(t) - A(t_0), \tag{2.29}$$

where the vector potential $A(t)$ can be inferred from $\mathcal{E}(t) = -\mathrm{d}A/\mathrm{d}t$. In the limit of a slowly varying envelope, *i.e.* $\mathrm{d}f/\mathrm{d}t \ll \omega f$, one obtains

$$A(t) \approx -(\mathcal{E}_0/\omega) f(t)\sin(\omega t + \varphi), \tag{2.30}$$

which is valid down to the few-cycle regime. In this limit, equation (2.29) yields

$$v_x(t) \approx \frac{\mathcal{E}_0}{\omega}\left[f(t_0)\sin\phi_0 - f(t)\sin(\omega t + \varphi)\right], \tag{2.31}$$

where $\phi_0 = \omega t_0 + \varphi$ is the phase of the laser field at the instant of ionization. In **Figure** 2.5 the velocity $v_x(t)$ of the electron is plotted for different instants of release. The final momentum is

$$\begin{aligned} v_f &= v_x(t\to\infty) = A(t\to\infty) - A(t_0) && (2.32)\\ &= -A(t_0) \\ &\approx (\mathcal{E}_0/\omega) f(t_0)\sin\phi_0. && (2.33) \end{aligned}$$

Thus further integration gives the electron trajectory

$$x(t) \approx x_0 + \frac{\mathcal{E}_0}{\omega^2}\left[f(t)\cos(\omega t + \varphi) - f(t_0)\left(\cos\phi_0 - \omega(t - t_0)\sin\phi_0\right)\right]. \tag{2.34}$$

The electron motion during these oscillations depends sensitively on the phase of the electric field $\mathcal{E}(t)$ at which ionization has occurred, ϕ_0. Whether the

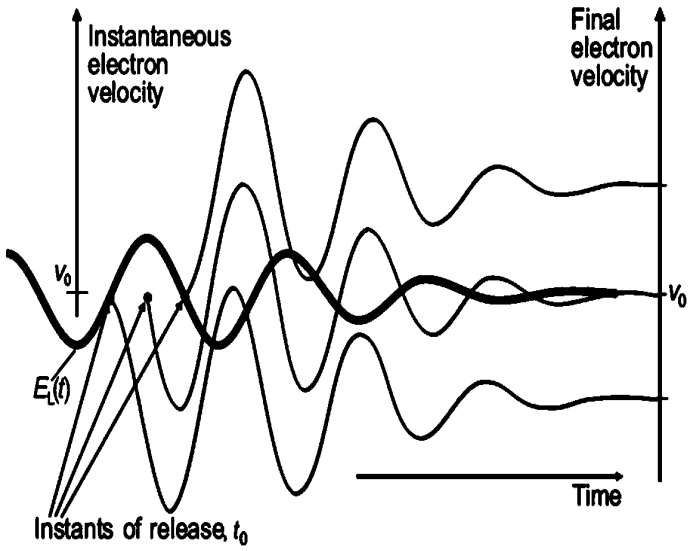

Figure 2.5: *Temporal variation of the electron velocity $v_x(t)$ for different moment of release. The electron's final velocity v_f shown on the right-hand-side sensitively depend on the instant of release. From Ferenc Krausz and Misha Ivanov [54].*

electron comes back to the parent ion or not depends on the initial time t_0 when the motion starts. Analyzing the electron motion along the electric field of the light wave obtained from equation (2.34), one distinguished two types of trajectories corresponding to different range of ϕ_0: - "**Direct**" trajectories, those for which the electron does not return to the vicinity of the parent ion. Here, electrons are released before the peak of the field. The "**direct**" electrons have their canonical moment opposite to the sign of electric field. - "**Indirect**" or **Recolliding** trajectories, those for which the electron, released after the peak of the field, recollides with the core (because they satisfy the condition of return $x(t_r) = 0$). To each order of return corresponds a pair of trajectories, one with *shorter* and one with *longer* travel time $t_r - t_0$. The canonical moment for the **indirect** electrons has the same sign as the electric field. If the electron re-encounters the core, **what can we expect to happen?** Upon return, the electron wave packet may interact with other electrons left behind in their bound states. Many interactions are confined to a fraction of the optical cycle, giving rise to a wealth of subfemtosecond phenomena. **Figure** 15 in the review paper of Ferenc Krausz and Misha Ivanov [54] summarizes the most important

ones namely: The electron can be *re-captured* and return to the ground state with the release of a high energy photon. This process is responsible for the HHG plateau. The electron may also *scatter elastically*, gain more energy from the field, and be detected as a high energy electron. This leads to high-energetic photoelectrons, *viz.* the ATI plateau. Finally, the accelerated electron might *scatter inelastically* with the remaining core, possibly doubly/multiple ionizing and/or inner-shell excitation of the atom. This leads to NSDI. Also in **Figure** 15 of [54], the trajectory $x(t)$ is sketched for an instant of release shortly after the field oscillation peak. In a few-cycle, linearly polarized laser field, ionization is significant only a few times near the strongest field oscillation peaks.

Figure 17 in [54] clearly illustrates trajectories launched shortly after the oscillation peak and returning to the core with maximum kinetic energy, which are responsible for emission of the highest-energy photons (upon recombination) and electrons (upon elastic backscattering). Predictions of this simple classical model including the assumption $v_x(t_0) = 0$ have been checked against full quantum mechanical simulations, with good agreement in the strong-field limit by Armel de Bohan [55, 56].

Elastic backscattering and high-energy electron emission: the cut-off of the ATI plateau

We return to the elastic scattering of the recolliding electron and ask for its drift energy after rescattering. The scattering breaks the phase of the electron's wiggling motion and abruptly changes the direction of the electron velocity. Equation (2.29) yields for the instant just before the recollision (denoted by $t_{r-} = t_r - 0^+$)

$$v_x(t_{r-}) = A(t_r) - A(t_0). \tag{2.35}$$

We assume that the laser field is linearly polarized and the electron is moving along the direction of the laser polarization for $t < t_r$. Upon elastic scattering, the electron changes the direction of its velocity while keeping its absolute value the same:

$$v_x^2(t_{r+}) + v_\perp^2(t_{r+}) = [A(t_r) - A(t_0)]^2, \tag{2.36}$$

where $t_{r+} = t_r + 0^+$, v_x and $v_\perp$ stand for the momentum vector components parallel and perpendicular to the laser polarization. At the end of the laser pulse, these two components become

$$v_f = v_x(t_{r+}) - A(t_r), \qquad v_{\perp,f} = v_\perp(t_{r+}). \tag{2.37}$$

As an example, take a closer look at backscattering. Then $v_\perp = 0$ and the relationship between the momenta before and after the collision is

$$v_x(t_{r+}) = -v_x(t_{r-}) = -A(t_r) + A(t_0). \tag{2.38}$$

At the end of the pulse we then have

$$v_f = -v_x(t_{r-}) - A(t_r) = -2A(t_r) + A(t_0). \tag{2.39}$$

For times $t \geq t_r$, the component of its velocity, along the polarization axis is given by

$$v_x(t) = A(t) + v_x(t_{r+}) - A(t_r) = A(t) - 2A(t_r) + A(t_0). \tag{2.40}$$

The result (2.39) is different from the final momentum $-A(t_0)$ for the case when no collision was present. The backscattered electron's final momentum is sensitive to the values of the vector potential at the moment of ionization and the moment of recollision. The drift energy after rescattering is

$$E_{drift} \equiv E_{kin,rescattering} = \frac{1}{2}\langle v_x(t)\rangle_t^2 = \frac{1}{2}\left[2A(t_r) - A(t_0)\right]^2. \tag{2.41}$$

Comparison of equations (2.41) and (2.42) demonstrates the possibility of additional energy gain by rescattering. The similarity of these equations means that the start and return times for the maximally possible drift energy $E_{drift,max}$ are close to those for the maximal return energy $E_{kin,max}$ [57]. If we are interested in the maxima of the backscattering energy (2.41), the numerical evaluation yields the *cut-off energy* (maximal backscattering energy) $E_{drift,max} = 10.0007\ U_p$ [58]. Below, in **Figure** 2.6 we exhibit results of a numerical solution of the one-dimensional Schrödinger equation which demonstrate that the classical cut-off energy is well obeyed by the calculated high-energy ATI spectra. In **Figure** 2.7 we show additional results from our separable potential model that may aid in the determination of this classical cut-off energy. Detailed comments on this latter graph will be given later in the text.

In a few-cycle laser field the final energy and the number of the highest-energy backscattered electrons is a sensitive probe of the subcycle field evolution. Owing to this sensitivity and the intuitive insight provided by a simple "billiard-ball" model (a reasonable approximation for energetic backscattered electrons, which spend little time near the core) into the underlying physical process, backscattered electrons constitute a reliable tool for determining the carrier envelop (CE) phase. Simultaneous detection of electrons ejected in both directions along the laser polarization offers robustness against laser amplitude noise. This "stereo-ATI" detection scheme was invented by Paulus *et al.* [59] and subsequently used for the first unambiguous determination of the CE phase of few-cycle light [60]. The stereo-ATI technique is about to become a standard diagnostic tool in attosecond laboratories.

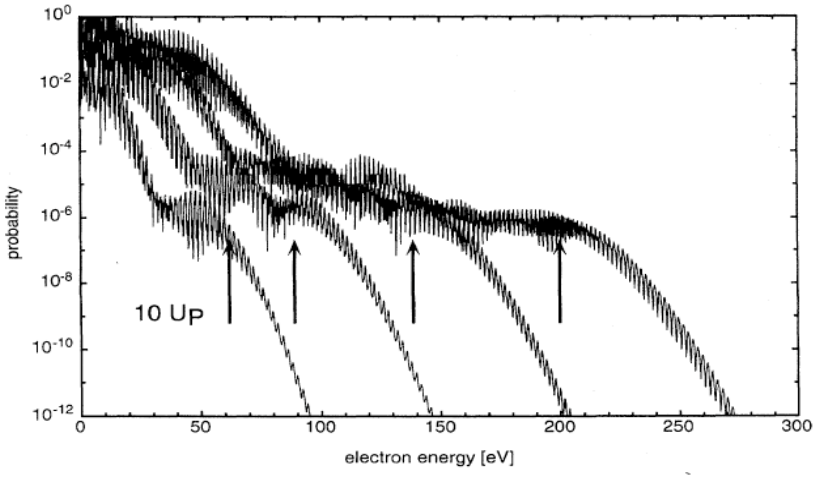

Figure 2.6: *ATI spectra calculated from the one-dimensional TDSE and model potential* $V(x) = -(1+x^2)^{1/2}$ *for several* U_p *between* 6 *and* 20 eV. *The classical high energy part is marked by an arrow in each case. From Paulus et al. [57].*

2.2.6 High harmonic generation

When a strong-short pulse interacts with an atomic gas, the atoms respond in a nonlinear way, emitting coherent radiation at frequencies that are integral multiples of the laser frequency. Due to the inversion symmetry of the atom, only *odd harmonics* of the fundamental are emitted. In the high intensity ($> 10^{13}$ W.cm^{-2}), low frequency regime, the harmonic strengths fall off for the first few orders, followed by a broad plateau of nearly constant conversion efficiency, and then a rather *sharp cut-off* [61].

Plateau and cut-off

In the previous Section, a developed two-step model, which combines quantum and classical aspects of laser-atom physics, accounts for many strong field

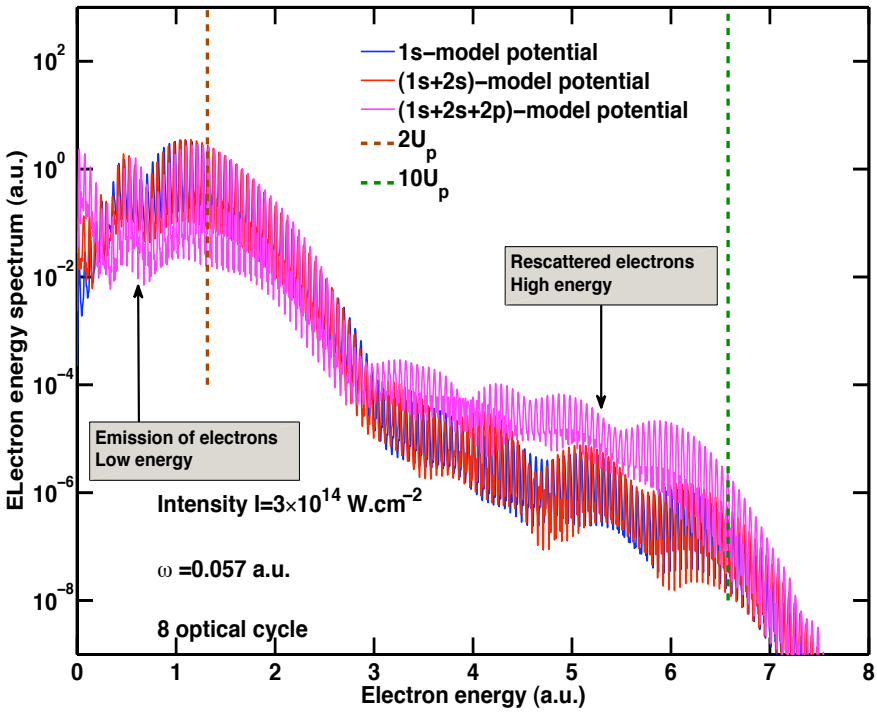

Figure 2.7: *ATI spectra calculated from our three-dimensional TDSE model. Laser parameters are given in the bottom of graph. Vertical dashed lines mark the positions of the plateau cut-off respectively at* $2U_p$ *(brown) and* $10U_p$ *(green).*

phenomena. In this model, depending on the phase at the instant of ionization, ϕ_0, oscillations in the laser field may bring the electron back to its parent ion. In equation (2.31), the first term describes the drift velocity of the electron, which changes the sign near the maximum of the electric field, at $\phi_0 = 0$. Electrons released after the peak of the field, $\phi_0 > 0$, return to the core (see the shaded part of the electron emission probability in **Figure** 20 of [54]). The respective trajectories as a function of the instant of release t_0 or the phase ϕ_0 are given by equation (2.34). The return time t_r can be obtained by setting $x(t_r) = 0$ in equation (2.34) for $t_r > t_0$. The upper panel of this **Figure** 20 shows recolliding electron trajectories along with the energy of the electrons at t_r, in units of U_p (in *a.u.*) in the lower panel. The instantaneous kinetic energy of the electron upon its return to the origin (just before rescattering) is

$$E_{kin,return} = \frac{1}{2}v_x^2(t_{r-}) = \frac{1}{2}\left[A(t_r) - A(t_0)\right]^2. \tag{2.42}$$

The maximum of this energy determines the cut-off of high-harmonic production. If we are interested in the highest possible harmonic, we should try to make the difference between $A(t_r)$ and $A(t_0)$ as big as possible.

Figure 20 of [54] conveys several important messages. First, it shows that the moment of return is uniquely determined by the moment of ionization. Second, the maximum kinetic energy of the returning electron $E_{kin,max}$, reaches about 3.17 U_p, resulting in a cut-off in the harmonic spectrum at the harmonic of order (yielding for the maximum photon energy emitted during recollision) [48]

$$N_{max} \approx (I_p + 3.17\ U_p)/\omega. \tag{2.43}$$

Third, for each recollision energy $E_{kin,return} < E_{kin,max}$, there are two trajectories along which the electron can acquire the same energy by the time it returns to the core. These two sets of trajectories have been termed *short* and *long* trajectories (see **Figure** 2.8). Last but not least, the electron wave packet returning to the core is heavily chirped. As a consequence, its duration is substantially longer ($\sim$ 1 fs) than the duration of the original wave packet released by optical field ionization [62].

Theoretical methods

The theoretical treatment of harmonic generation by an intense laser pulse focused into a gaseous medium has two main aspects. First, the microscopic, single atom response to laser field must be analyzed. The single atom spectra must then be combined to obtain the macroscopic harmonic fields generated from the coherent emission of all the atoms in the laser focus; this is done by using the single-atom polarization fields a source terms in the Maxwell equations. We present here the microscopic aspect of the problem. Calculation of harmonic strengths requires the evaluation of the time-dependent dipole moment of the atom

$$\mathbf{d}(t) = \langle \Psi(t) \mid e\mathbf{R} \mid \Psi(t) \rangle, \tag{2.44}$$

where $\mid \Psi(t) \rangle$ denotes the atomic state vector in the presence of the laser field and $\mathbf{R} = \sum_{i=1}^{N} \mathbf{r}_i$ is the sum of the coordinates $\mathbf{r}_i$ of the N atomic electrons. The power spectrum of the emitted radiation is proportional to the modulus squared of the Fourier transform of the dipole acceleration $\ddot{\mathbf{d}}(t)$. When the atom is driven by a monochromatic field, the emitted harmonic radiation can be simply calculated from the induced dipole moment, which can now be expanded as

$$\mathbf{d}(t) = \sum_q \left[\mathbf{d}(q\omega) \mathrm{e}^{-\mathrm{i}q\omega t} + c.c \right], \tag{2.45}$$

where $c.c$ denotes the complex conjugate, q an odd integral number, and $\mathbf{d}(-q\omega) = [\mathbf{d}(q\omega)]^*$ since $\mathbf{d}(t)$ is real. The rate of emission of photons of

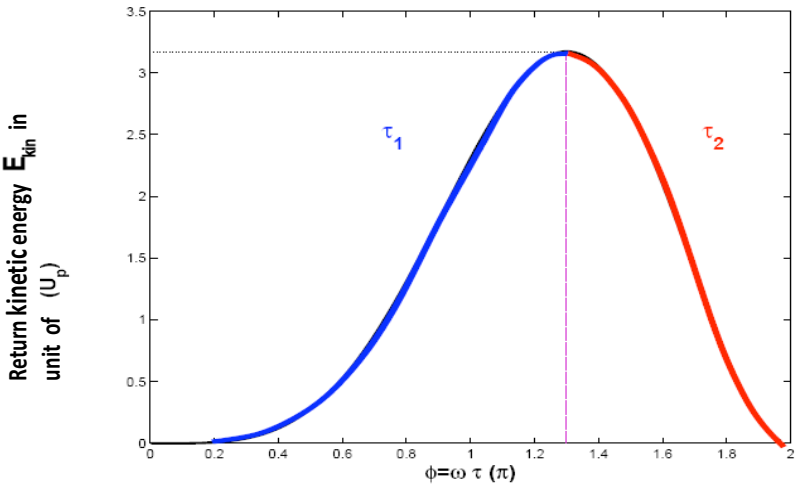

Figure 2.8: *Kinetic energy E_{kin} of the returning electron to the core vs their characteristic phases corresponding to the return time in units of U_p. This dependence indicates that electron wave packets returning along short ($\tau_1 = t_{r_1} - t_0$) and long ($\tau_2 = t_{r_2} - t_0$) trajectories carry the same kinetic energy. From A. de Bohan [55].*

angular frequency $q\omega$ is then proportional to $\mid \mathbf{d}(q\omega) \mid^2$. The induced dipole moment $\mathbf{d}(t)$ can be directly evaluated from the numerical [63] or Floquet [64] solutions of the TDSE. Good agreement with numerical and experimental data is also obtained using some approaches discussed below. In the calculation of harmonic generation, it is important to note that the velocity gauge gives a better result than in the length gauge (experience difficulties linked to background noises). The acceleration gauge is the most accurate in this treatment.

There are a number of oversimplifications in the previously mentioned semiclassical arguments despite its appealing simplicity. The model neglects the effect of the potential which would accelerate the escaping electron wave packet and makes the assumption of zero initial velocity incorrect. Also, the electron trajectories are taken to originate at the ionic core, although in reality, when the electron tunnels out it is 'born' some distance away from the core. However, probably more important than these are quantum effects such as depletion of the ground state and the interference, which the model lacks. These prob-

lems have been addressed and a quantum theory based on a system with a single bound state and a continuum has been formulated which agrees with the semiclassical model [65, 66, 67].

2.3 Strong field calculational techniques

The strong-short pulse regime requires a nonperturbative solution of the TDSE. For the purpose, several approaches have been developed in the literature. Most of the models mentioned below are restricted to a particular parameter domain, for which there has been significantly use in generating qualitative understanding or even in giving precise quantitative results in agreement with experiments. It is not our aim to outline exhaustively all these methods. We describe below the most useful one.

2.3.1 Floquet theory

The excitation and ionization dynamics of an atom in a strong laser field can be determined by turning the problem into a time-independent eigenvalue problem [68, 69]. In the Floquet approach, each bound state of the field-free atom turns into a dressed state associated with a complex quasi-energy, E, the imaginary part of which is related to the rate of ionization from that state, $\Gamma = -2ImE$. From *Floquet's theorem* [19, 70], the eigenfunctions for a perfectly periodic Hamiltonian (in the velocity or the length gauges) of the form

$$H = H_0 + \sum_{n=-\infty}^{+\infty} \mathrm{e}^{-\mathrm{i}n\omega t} \left(H_{int}\right)_n \tag{2.46}$$

can be expressed in the form

$$\mid \Psi(t)\rangle = \mathrm{e}^{-\mathrm{i}Et/\hbar} \mid F(t)\rangle = \mathrm{e}^{-\mathrm{i}Et/\hbar} \sum_{n=-\infty}^{+\infty} \mathrm{e}^{-\mathrm{i}n\omega t} \mid F_n\rangle. \tag{2.47}$$

We can consider this as indicating that the nth harmonic components $\mid F_n\rangle$ represents an electron which has absorbed n photons. Inserting the Floquet vector $\mid F(t)\rangle$ into the TDSE results in an infinite set of coupled *Floquet equations* for the harmonic components. In the velocity gauge, the Floquet equations are

$$\begin{aligned} (E + n\hbar\omega - H_0) \mid F_n\rangle &= V_+ \mid F_{n-1}\rangle + V_- \mid F_{n+1}\rangle, & (2.48)\\ V_+ &= \frac{e}{2mc}\mathbf{A}\cdot\mathbf{p}, & (2.49) \end{aligned}$$

where the time-independent operators V_+ and V_- verify the relation $V_- = V_+^\dagger$. This system of coupled equations is manifestly time independent and has solutions with complex quasi-energies that represent decaying states. Equations

(2.48) have been solved after truncation to a manageable number of terms, using many techniques to provide the eigenvalues E

$$E = E_i + \Delta - \mathrm{i}\frac{\Gamma}{2}, \tag{2.50}$$

where E_i is the initial unperturbed energy of the state, Δ is the AC Stark shift of the state and Γ is the width of the state and represents the ionization rate of that state. The generated rate are found to be very accurate as long as the pulse length of the laser field is not too short. The eigenfunctions provide the amplitudes for the photoelectron energy spectra, and the time-dependent dipole of the state can be related to the photo-emission spectrum of the system. Using such a construction, multiphoton ionization rates and threshold shifts have been obtained [71] and important calculations have been performed by Shakeshaft and co-workers to examine the role of resonances on the ionization rate and photoelectron spectra of atomic hydrogen [64]. The interesting results from this work have been the observation of multiphoton resonance enhancement in MPI and the interpretation of the photoelectron peaks due to these resonances. More recently, and within the non-Hermitian Floquet theory, Potvliege *et al.* [70] have studied in more details the rate of ionization of an atom of helium, argon, and hydrogen exposed to an intense monochromatic laser field and the quasi-energy spectrum of their dressed states for the Keldysh parameter between 1 and 0.6 and wavelenght between 390 and 1300nm. Besides the *ab initio* Floquet calculations, they have also obtained the ionization rate within the strong-field approximation, both in its length gauge (Keldysh) formulation and its velocity gauge (Faisal-Reiss) formulation, as well as within the ω^2-expansion theory of Pont *et al.* [72]. They have also shown that for the same model potential, and except where multiphoton resonances are important, these four different approaches all yield total ionization rates in good quantitative agreement with each other at the intensities and wavelengths considered in their article.

2.3.2 Volkov final states

The Schrödinger equation for a free electron in a plane wave electric field, but outside the range of the atomic potential writes

$$\mathrm{i}\hbar\frac{\partial}{\partial t}\Psi_{\mathbf{p}}^{(V)}(\mathbf{r},t) = \left(\frac{1}{2}\mathbf{p}^2 + H_{int}(t)\right)\Psi_{\mathbf{p}}^{(V)}(\mathbf{r},t) \tag{2.51}$$

is exactly solvable. The solutions, known as *Volkov states*, are plane waves with an oscillating phase, which depends on the vector potential. When the

dipole approximation is valid, these solutions may be written as

$$\Psi_{\mathbf{p}}^{(V)}(\mathbf{r},t) = (2\pi)^{-3/2} \exp\left(\frac{\mathrm{i}}{\hbar}\left[\mathbf{p} - \frac{e}{c}\mathbf{A}(t)\right]\cdot\mathbf{r} - \frac{\mathrm{i}}{\hbar}\int^{t}\frac{1}{2m}\left[\mathbf{p} - \frac{e}{c}\mathbf{A}(t')\right]^2 \mathrm{d}t'\right), \tag{2.52}$$

$$= (2\pi)^{-3/2}\, \mathrm{e}^{\frac{\mathrm{i}}{\hbar}\mathbf{p}} \exp\left(\frac{\mathrm{i}}{\hbar}\phi(\mathbf{p},\mathbf{r},t)\right), \tag{2.53}$$

where the phase $\phi(\mathbf{p},\mathbf{r},t)$ depends on the form of interaction $H_{int}(t)$.
Velocity gauge

$$\phi(\mathbf{p},\mathbf{r},t) = \mathbf{p}\cdot\boldsymbol{\alpha}(t), \tag{2.54}$$

Length gauge

$$\phi(\mathbf{p},\mathbf{r},t) = \mathbf{p}\cdot\boldsymbol{\alpha}(t) - \frac{e}{c}\mathbf{A}(t)\cdot\mathbf{r} - \frac{e^2}{2mc^2}\int_{ti}^{t}\mathbf{A}^2(t')\mathrm{d}t', \tag{2.55}$$

and

$$\boldsymbol{\alpha}(t) = \frac{e}{mc}\int_{ti}^{t}\mathbf{A}(t')\mathrm{d}t' \tag{2.56}$$

corresponding to the *classical excursion amplitude* of a free electron in laser field, and t_i the initial time of interaction. In a linearly polarized field, the electron oscillates along the direction of polarization with an amplitude $\alpha_0 = e\mathcal{E}_0/(m\omega^2) = eA_0/(mc\omega)$. In the strong field regime, this amplitude can greatly exceed the size of a bound state orbital. Volkov states provide a useful tool that can be applied in various strong field approximations.

2.3.3 Strong field approximations

There have been several attempts to solve the TDSE in the strong field limit using approximate, but analytic methods. Such *strong field approximations* (SFA) typically neglect all the bound states of the atom except for the initial state. In the tunneling regime ($\gamma < 1$), and a quasistatic limit ($\omega \to 0$), one can use the ADK theory [31] in which the ionization occurs due to the tunneling through the Coulomb barrier distorted by electric field of the laser. The wave function is constructed as a combination of a bare initial wave function of the electron (close to the nucleus) and a wave function describing a motion of the electron in a quasistatic electric field (far from the nucleus). Following on from this work a wide range of similar non-perturbative calculations have been performed, led predominantly by Faisal [34] and Reiss [35]: these are collectively known as the KFR models. Following Keldysh, the KFR approaches use Volkov states as approximations to the final state of the electron, field-free eigenstates as initial wave functions and connect the states by some

interaction. The system wavefunction is written in terms of the bound states of the atom and Volkov functions, and the evolution of the system is described in terms of a set of coupled, first-order differential equations, whose solution is the time-dependent expansion coefficients of the bound and Volkov states. However, such calculations implicitly neglect the laser-induced shifts and the effect of the ion on the electron as it ionizes and passes out of the region of the atomic potential. Also this approximation is really only valid if the system is not appreciably ionized ($I \ll I_{sat}$). Furthermore, there is an upper limit to the intensity for which this approach is valid because when the ponderomotive energy of the electron is larger than the binding energy of the atom ($U_p \gg I_p$), then the initial state of the atom can no longer be taken as an unperturbated eigenstate. There has been extensive work performed using Keldysh theory as a basis, examining such aspects as the role of the Volkov states on the ATI spectra obtained [73] and the role of the ponderomotive shift on the ATI peak positions [74]. Further extensions to the theory have included the use of an effective multiphoton matrix element that lifts the electron into the continuum with the minimum number of photons and then considers transitions between Volkov states, forming the higher ATI peaks [73] and the role of the Coulomb interaction on the final states [75]. Yet another method consists of writing the electronic continuum-continuum dipole matrix elements in terms corresponding to matrix elements for free electrons plus corrections due to the Coulomb potential [66].

In the latter version of SFA, the amplitude of the electronic wavefunction $b(\mathbf{p})$ corresponding to outgoing momentum $\mathbf{p}$ is given by

$$b(\mathbf{p}) = \mathrm{i} \int_0^{t_F} \mathrm{d}t \; \mathbf{d}\left(\mathbf{p} - e\mathbf{A}(t)/c\right) \mathcal{E}(t) \exp\left[-\mathrm{i}S(t_F, t)/\hbar\right]. \tag{2.57}$$

Here $\mathbf{d}\left(\mathbf{p} - e\mathbf{A}(t)/c\right)$ denotes the dipole matrix element for the transition from the initial bound state to the continuum state in which the electron has the kinetic momentum $\mathbf{p} - e\mathbf{A}(t)/c$, t_F is the switch-off time of the laser pulse, and

$$S(t_F, t) = \int_t^{t_F} \mathrm{d}t' \left[\frac{\left(\mathbf{p} - e\mathbf{A}(t')/c\right)^2}{2m} + I_p\right] \tag{2.58}$$

is a quasiclassical action for an electron which is born in the continuum at t and propagates freely in the laser field. The form of the expression (2.57) is generic to the SFA. However there are limitations to this type of approach and the theory will not be valid when the intermediate resonances play an important role, or when the depletion from the initial state becomes significant.

2.3.4 Direct integration of the TDSE

Methods that have been extensively used to study multiphoton processes are that of the direct numerical integration of the time-dependent Schrödinger equation [19]. The wave functions are obtained by means of finite difference grid method [76] and spectral method [77, 78]. The latter consists of expanding the wave function in a finite basis of L^2-integrable functions. In some cases, the L^2-integrable functions are either Coulomb-Sturmian functions [78] or B-spline functions [79]. The time evolution is obtained by either explicit or implicit time propagators. All these methods are capable of generating numerically exact results for an atom with a single electron in a short pulsed field for a wide range of pulse shapes, wavelengths and intensities. The solutions are time-dependent wave functions for the electrons which can be analyzed to obtain excitation and ionization rates, photoelectron energies, angular distributions, and photoemission yields. A problem generally encountered with these methods is the large and intensive computations needed for integration over a reasonable pulse length. Another crucial problem arises with the production of spurious effects deriving from the size of the basis and the reflections near the edges of the basis. The reasons for this are due to the high velocities that ionizing electrons can gain via continuum-continuum transitions or imparted by quiver motion in high-intense laser field. The freed electron wave packets could then propagate large distance even in small time intervals. As a consequence, the large spatial grids with small spatial separation must be used in integration methods so that we may be able to track the movement of the wave packet. Such large grids substantially enlarge computation time. Also, the discretization of time, used in all integration algorithms, induces a restriction on the size of the temporal step; a large number of small time steps are needed for accurate results. To avoid the excessively long calculation time, various different approaches have been developed. They are grouped into two categories; one-dimensional and approximate three-dimensional calculations. Each has its disadvantages and advantages.

The most straightforward method of reducing the amount of computation time is to reduce the dimensionality of the system. This treatment has been extensively investigated by Eberly *et al.* [80] and several workers [81, 82, 83]. Such calculations have produced many results that have contributed much to the understanding of multiphoton processes. The main disadvantages of this extreme simplification are that effects related to the transverse structure of the beam, the magnetic-field is neglected and the Coulomb potential must be replaced by some smoothed model potential [83]. However, the advantages of one-dimensional calculations are many. They are relatively fast, allowing many calculations to be performed to investigate the effect of a diverse range of parameters (angular frequency, intensity or pulse length) on the multiphoton

ionization processes. It means that realistic pulse lengths and large spatial grids can be used without the concern of producing spurious effects deriving from grid boundary reflections. The ease of the computation allowed the use of one-dimensional calculations for testing other calculational approaches such as Keldysh and Floquet calculations [84, 85].

The one-dimensional calculations are very effective methods for qualitatively investigating atom-laser interactions. To fix our ideas, let us remind that Rae *et al.* [86] compared one-dimensional and three-dimensional models of nine-photon ionization of hydrogen at 800 nm laser wavelength and showed that at 10^{14} W.cm^{-2} the former model predicts 94% ionization whereas the latter model predicts 22% ionization. This has been attributed to over-emphasis of the role of the atomic core. Then this approach can only be viewed as an approximation to three-dimensional calculations, which are, of course, more realistic, but represent a far more formidable computing task (large-scale computation, computer memory). Two routes have been adopted to reduce this load: one is to reduce the size of the calculation by choosing linearly polarized light, so that the system has axial symmetry in the dipole approximation and dimensions considered can be reduced by one. Such three-dimensional calculations have been developed by Kulander and co-workers and they have been exploited to study the effect of bound state resonances on harmonic spectra [87]. Another is to decrease the pulse length, which makes comparison with experiment difficult, and the other involves using absorbing boundary conditions near the edges of the spatial grids, so that any ionized wavepacket is removed and not allowed to reflect. Therefore, the wavefunction does not remain normalized; however, this decrease in the normalization can be used as a measure of the ionization rate. For multi-electron atoms, the theoretical treatments have to limit the calculations to that for a single electron in effective potentials which represent, as well as possible, the influences of the remaining atomic electrons. This *single-active-electron* (SAE) approximation gives generally accurate results for systems with no non-sequential ionization process or no low-lying doubly excited states. In these cases, the excitation or ionization dynamics are dominated by the sequential promotion of a single electron at a time. This approach falls into difficulties when one expects to clarify the effect of the dynamics of one electron on the other, *i.e.* the situation in which non-sequential double-ionization plays a great role.

2.4 Semi classical model of the laser field

Modeling the laser pulse is a difficult choice. We are interested in radiation in the VUV-IR domains and the order of few femtoseconds which requires taking into account the temporal variation of the envelope of the field.

Several technical issues that are especially relevant for few-cycle pulses have been discussed in the literature [88], more precisely two alternative theoretical descriptions of such a pulse have retained the attention. One specifies the electric-field of the laser pulse, while the other starts from its vector potential. Therefore the pulse envelope can be associated with the vector potential or with the electric-field vector. The *zero-net-force condition* ($\int_{-\infty}^{\infty} \mathcal{E}(\zeta)\mathrm{d}\zeta = \mathbf{A}(-\infty) - \mathbf{A}(\infty) = -\mathbf{A}(\infty) = 0$, not only valid for this dipole approximation case, but always satisfied by the general case of spatial-temporal variation of fields) which any real laser pulse has to satisfy is given in details in [88].

2.4.1 Vector-potential pulse envelope

From the point of view of numerical integration of the TDSE, it is more convenient to consider a linearly polarized (along the z axis) few-cycle pulse in the dipole approximation wherein the incident field $\mathcal{E}(t) = (-1/c)\partial\mathbf{A}(t)/\partial t$ is defined through the following extensively used vector potential

$$\mathbf{A}(t) = A_0 f(t) \sin(\omega t + \phi)\, \mathbf{e}_z = A(t)\mathbf{e}_z, \qquad A_0 = \frac{c}{\omega}\sqrt{\frac{I}{I_a}}, \tag{2.59}$$

for $0 \leq t \leq T_p$, and $\mathbf{A}(t) = \mathbf{0}$ outside this interval, where $T_p = n_c T$ is the total pulse duration (alternatively, it is sometimes defined as the full width at half maximum (FWHM) of the electric-field-vector amplitude. Experimentalists usually define the pulse duration τ by the FWHM of the intensity), $T = 2\pi/\omega$ its period, n_c the number of optical cycle and $\mathbf{e}_z$ is the unit vector along the z axis in the laboratory frame, with a peak amplitude of A_0. We consider a sine-square pulse envelope function

$$f(t) = \begin{cases} \sin^2\left(\frac{\pi t}{T_p}\right) & for \quad 0 \leq t \leq T_p \\ 0 & elsewhere, \end{cases} \tag{2.60}$$

that assumes its maximum at $t = T_p/2$. This definition guarantees that the electric field has no static (dc) component because the zero-net-force condition is automatically satisfied, since by (2.59) the vector potential is by definition equal to zero at the beginning and at the end of the pulse, regardless of whether the number of cycles is integer or not. This prevents possible problems related to the gauge invariance. In the precedent equation (2.59), ϕ is the carrier-envelope phase that specifies the delay between the maximum of the envelope and the nearest maximum of the electric field of the carrier wave with frequency ω. For $\phi = 0$, the maxima of electric field and envelope coincide, while for $\phi = \pi/2$ the maximum of the envelope coincides with the zero of the electric field. Therefore, $\phi = 0$ and $\phi = \pi/2$ (modulo π) correspond to cosine and sine

pulses with respect to the maximum of the envelope. Note that both the energy and the duration of the laser pulse do not depend on this phase ϕ. In this work, we set the carrier envelope phase to particular values and consider different femtosecond pulse durations corresponding to integer number n_c of optical cycles, respectively, with peak intensities in the range $10^{12} \leq I \leq 10^{16}$ W.cm^{-2} in order to reflect different physical mechanisms.

2.4.2 Electric-field-vector pulse envelope

A different definition of a few-cycle pulse is considered in this thesis. We define the pulse envelope via the electric-field vector, following [55]

$$\mathcal{E}(t) = \mathcal{E}_0 f(t) \cos(\omega t + \phi)\, \mathbf{e}_z = \mathcal{E}(t)\mathbf{e}_z, \qquad \mathcal{E}_0 = \sqrt{\frac{I}{I_a}}, \tag{2.61}$$

for $0 \leq t \leq T_p$, and $\mathcal{E}(t) = \mathbf{0}$ outside this interval, where $\mathcal{E}_0$ represents the maximum field strength. The pulse envelope is given by

$$f(t) = \begin{cases} \left[1 - \cos^8\left(\frac{\pi t}{T_p}\right)\right] & for \quad 0 \leq t \leq T_p \\ 0 & otherwise. \end{cases} \tag{2.62}$$

Note that while $\mathcal{E}(0) = \mathcal{E}(T_p) = \mathbf{0}$, the vector potential is, in general, different from zero for $t \leq 0$ and $t \geq T_p$. However, if the total pulse duration equals an integer number n_c of laser cycles, we have $\mathbf{A}(0) = \mathbf{A}(T_p)$ so that the integral over the electric field is zero, $\int_0^{T_p} \mathcal{E}(\zeta)\mathrm{d}\zeta = -[\mathbf{A}(T_p) - \mathbf{A}(0)] = \mathbf{0}$, that is, the electric field has no *dc* component as required.

Examples of a linearly polarized few-cycle laser field $(\mathcal{E}(t), \mathbf{A}(t))$ for temporal envelope (2.60) are plotted in **Figures** 2.9 and 2.10, corresponding to intensity $I = 3 \times 10^{14}$ W.cm^{-2}, $T_p = 10.67$ fs and $n_c = 4$ optical cycles.

2.5 The Ehrenfest theorem in velocity and length gauges

Once the gauge in which we work is fixed we can study the time evolution of the average of any operator by the virtue of Ehrenfest's theorem. Let us consider an observable $\mathcal{O}$. The expectation value $\langle\mathcal{O}\rangle$ of this observable in the state Ψ, normalized to unity, is given by $\langle\Psi \mid \mathcal{O} \mid \Psi\rangle$. The rate of change of this expectation value is therefore

$$\frac{\mathrm{d}}{\mathrm{d}t}\langle\mathcal{O}\rangle = (\mathrm{i}\hbar)^{-1}\langle\Psi \mid [\mathcal{O}, H] \mid \Psi\rangle + \langle\Psi \mid \frac{\partial\mathcal{O}}{\partial t} \mid \Psi\rangle, \tag{2.63}$$

where the Hamiltonian H is a Hermitian operator. In particular, if the operator $\mathcal{O}$ does not depend explicitly on time (that is, if $\partial\mathcal{O}/\partial t = 0$) equation (2.63)

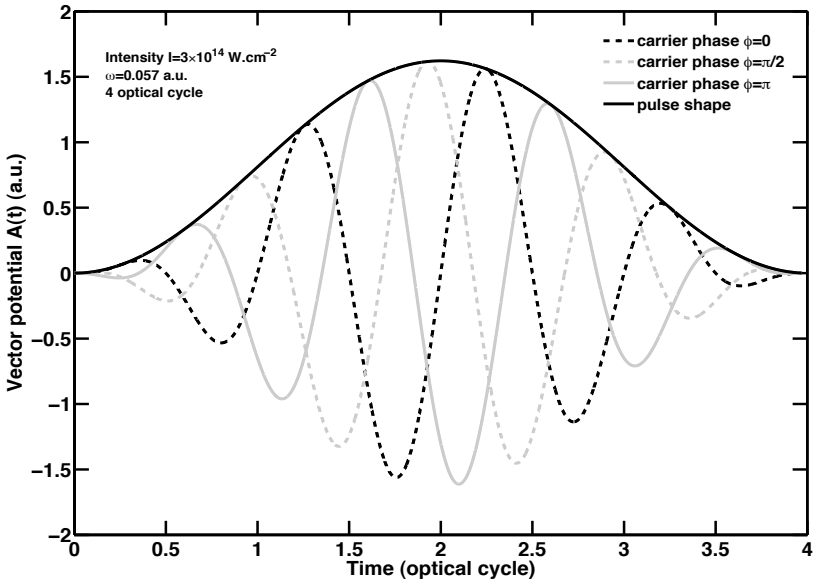

Figure 2.9: *The time variation of the vector potential and its envelope of laser pulses consisting of very few optical cycles depends on the phase* $\phi = 0,\ \pi/2,\ \pi$ *of the carrier frequency with respect to the pulse's envelope. Laser parameters are given in the top left of graph.*

reduces to

$$\frac{\mathrm{d}}{\mathrm{d}t}\langle\mathcal{O}\rangle = (\mathrm{i}\hbar)^{-1}\langle\Psi \mid [\mathcal{O}, H] \mid \Psi\rangle. \tag{2.64}$$

Hence, if $\partial\mathcal{O}/\partial t = 0$ and the operator $\mathcal{O}$ commutes with H, its expectation value does not vary in time, and we can say that *the observable* $\mathcal{O}$ *is a constant of the motion.* As an example of the preceding discussion, we now apply the above result to the particular case of a particle moving in a classical electromagnetic field. Moreover, we choose $\mathcal{O}$ to be the time-independent operator $\mathbf{p}$. We then have: from (2.64)

Velocity gauge:

$$\frac{\mathrm{d}}{\mathrm{d}t}\langle\mathbf{p}\rangle = (\mathrm{i}\hbar)^{-1}\langle\Psi \mid [\mathbf{p}, H] \mid \Psi\rangle = -\langle\boldsymbol{\nabla}V\rangle. \tag{2.65}$$

- The kinematic momentum $\boldsymbol{\pi}(t) \equiv \mathbf{v}(t)$, which is the measurable quantity, is related to the canonical momentum $\mathbf{p}(t)$ through the vector potential $\mathbf{A}(t)$ by $\mathbf{v}(t) = \mathbf{p}(t) + \mathbf{A}(t)$.

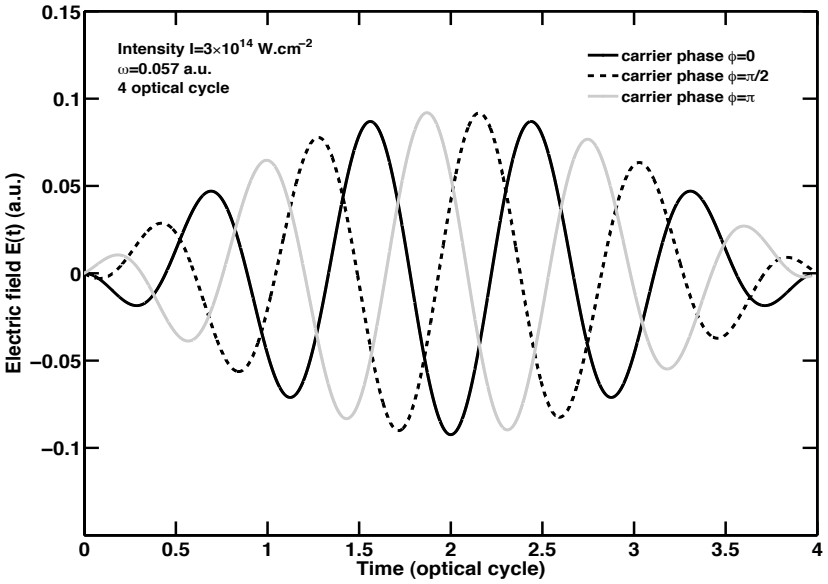

Figure 2.10: *The electric field of laser pulses as a function of time in optical cycle for three values of the carrier phase envelope* $\phi = 0,\ \pi/2,\ \pi$. *The laser field corresponds to* $\omega = 0.057$ a.u. *of* 4 *optical cycle and intensity* 3×10^{14} W.cm^{-2}
.

- The canonical momentum evolution reflects "only" the effect of the gradient of the Coulomb potential on the wave function.

During the laser-atom interaction, the eigenstates of atomic's field-free Hamiltonian $H_0 = \mathbf{p}^2/2 + V(\mathbf{r})$ *do not describe the same physical states than those of standard Hamiltonian with eigenenergy* $\boldsymbol{\pi}^2/2 + V(\mathbf{r})$ *of particles.*

In the velocity form, we see immediately that, if the system Ψ considered is such that $-\langle \boldsymbol{\nabla} V \rangle = 0$, **the canonical momentum p becomes a constant of motion**. In the case of laser-atom interaction, a system satisfying this condition is that of a free particle oscillating in the laser field, a system which we will refer very often in our work.

Length gauge:

$$\frac{\mathrm{d}}{\mathrm{d}t}\langle \mathbf{p} \rangle = (\mathrm{i}\hbar)^{-1} \langle \Psi \mid [\mathbf{p}, H] \mid \Psi \rangle = -\langle \boldsymbol{\nabla} V \rangle - e\mathcal{E}(t). \tag{2.66}$$

- The canonical momentum $\mathbf{p}(t)$ in this form coinciding with the mechanical momentum $\boldsymbol{\pi}(t)$, the role of the Coulomb potential is decoupled from that of the electric field from the perspective of the interpretation in terms of forces.

Here, the atomic's field-free Hamiltonian H_0 corresponds to the eigenenergy of particles, an eigenstate of Hamiltonian H_0 describes the same physical state than the one of standard Hamiltonian. In other words, an eigenstate of Hamiltonian H_0 remains a physical state.

2.6 Conclusion

Some theoretical approaches, namely the lowest order perturbation theory (LOPT), the Floquet theory, the strong field approximations (SFA) and the direct numerical integration of the TDSE for studying laser-atom interactions (for a general review, see Joachain *et al.* [3]) have been presented as well as their advantages and limits. The LOPT is adequate for the study of multiphoton processes only at low intensities (typically lower than $\sim 10^{13}$ W/cm^2). The Floquet method is based on the assumption that the hamiltonian of the atomic system in the laser field is periodic in time. Although this is not true for a realistic laser pulse, it is possible to incorporate pulse shape effects into the Floquet method, which is in fact nonperturbative method. In the strong field limit, the SFA neglects all the bound states of the atom except the initial state. The fundamental idea governing this method assumes that at high intensities, the Coulomb field created by the kernel can be seen as a disturbance in light of the laser electric field. The direct numerical integration of the TDSE, has been proven to be the most practical method [76] for obtaining realistic information about multiphoton processes. This is particularly true when ultrashort laser pulses ($\sim 10^{15}$ s) are involved, as well as when one is interested in the study of ATI and HOHG, which are the two most prominent multiphoton processes of nonperturbative behavior. The Ehrenfest theorem recalled here will be of undeniable utility in the physical interpretation of the results obtained in the following Chapters with our new mathematical model.

As a short conclusion to this Chapter we should mention that the multiphoton ionization process is very complex and no one type of calculation models all the relevant aspects. So although all the above calculational techniques that directly integrate the Schrödinger equation rely on some approximations to make finding the solution easier, they can all provide important insight into the multiphoton ionization process.

Bibliography

[1] L. F. DiMauro and P. Agostini, *Adv. At. Mol. Opt. Phys.* **35**, 79 (1995).

[2] M. Protopapas, C. H. Keitel and P. L. Knight, *Atomic Physics with Super-High Intensity Lasers*, *Rep. Prog. Phys.* **60**, 389 (1997).

[3] C. J. Joachain, M. Dörr and N. Kylstra, *Adv. At. Mol. Opt. Phys.* **42**, 225 (2000).

[4] R. Dörner, Th. Weber, M. Weckenbrock, A. Staudte, M. Hattass, H. Schmidt-Böcking, R. Moshammer and J. Ullrich, *Adv. At. Mol. Opt. Phys.* **48**, 1 (2002).

[5] B. H. Bransden and C. J. Joachain, *Quantum Mechanics* 2nd ed (Pearson Education Ltd, England, 2000).

[6] H. M. Pilkuhn, *Relativistic Quantum Mechanics* (Springer, Berlin, 2003).

[7] N. Delone and V. Krainov, *Physics-Uspekhi* **42**, 669 (1999).

[8] C. K. Au, *J. Phys. B: At. Mol. Phys.* **16**, L563 (1983).

[9] Patrick. J. Randerson, *Fundamental Dynamics in High Intensity Laser Ionization, PhD thesis*, The Ohio State University, USA (2005).

[10] D. Strickland and G. Mourou, *Opt. Commun.* **56**, 219 (1985).

[11] G. S. Voronov and N. B. Delone, *JETP Letters* **1**, 66 (1965).

[12] J. L. Hall, E. J. Robinson and L. M. Branscomb, *Phys. Rev. Lett.* **14**, 1013 (1965).

[13] F. Fabre, G. Petite, P. Agostini and M. Clement, *J. Phys. B* **15**, 1353 (1982).

[14] G. Petite, F. Fabre, P. Agostini, M. Crance and M. Aymar, *Phys. Rev. A* **29**, 2677 (1984).

[15] F. H. M. Faisal, *Theory of Multiphoton Processes* (Plenum, New York, 1987).

[16] P. Lambropoulos, *Adv. At. Mol. Phys.* **12**, 87 (1976).

[17] L. A. Lompre, G. Mainfray, C. Manus and J. Thebault, *Phys. Rev. A* **15**, 1604 (1977).

[18] L. A. Lompre, A. L'Huillier, G. Mainfray and C. Manus, *J. Opt. Soc. Am. B* **2**, 1906 (1985).

[19] K. Burnett, V. C. Reed and P. L. Knight, *J. Phys. B* **26**, 561 (1993).

[20] R. R. Freeman, P. H. Bucksbaum, H. Milchberg, S. Darack, D. Schumacher and M. E. Geusic, *Phys. Rev. Lett.* **59**, 1092 (1987).

[21] P. Agostini, P. Breger, A. L'Huillier, H. G. Muller, G. Petite, A. Antonetti and A. Migus, *Phys. Rev. Lett.* **63**, 2208 (1989a).
P. Agostini, A. Antonetti, P. Breger, M. Crance, A. Migus, H. G. Muller and G. Petite, *J. Phys. B: At. Mol. Opt. Phys.* **22**, 1971 (1989b).

[22] G. Petite, P. Agostini and H. G. Muller, *J. Phys. B* **21**, 4097 (1988).

[23] P. Agostini, F. Fabre, G. Petite and N. K. Rahman, *Phys. Rev. Lett.* **42**, 1127 (1979).

[24] P. Kruit, J. Kimman, H. G. Muller and M. J. Van der Wiel, *Phys. Rev. A* **28**, 248 (1983).

[25] P. Hansch, M. A. Walker and L. D. Woerkom, *Phys. Rev. A* **55**, R2535 (1997).

[26] Y. Gontier and M. Trahin, *J. Phys. B* **13**, 4383 (1980).

[27] P. H. Bucksbaum, R. R. Freeman, M. Bashkansky and T. J. McIlrath, *J. Opt.Soc. Am. B* **4**, 760 (1980).

[28] H. Rottke, B. Wolff, X. Brickwedde, D. Feldmann and K. H. Welge, *Phys. Rev. Lett.* **64**, 404 (1990).

[29] L. V. Keldysh, *Sov. Phys. JETP* **20**, 1307 (1965).

[30] A. M. Perelomov, V. S. Popov and M. V. Terent'ev, *Sov. Phys. JETP* **23**, 924 (1966).

[31] M. V. Ammosov, N. B. Delone and V. P. Krainov, *Sov. Phys. JETP* **64**, 1191 (1986).

[32] A. M. Perelomov, V. S. Popov and M. V. Terent'ev, *Sov. Phys. JETP* **24**, 207 (1967).

[33] V. S. Popov, V. P. Kuznetsov and A. M. Perelomov, *Sov. Phys. JETP* **26**, 222 (1968).

[34] F. H. M. Faisal, *J. Phys. B* **6**, L89 (1973).

[35] H. R. Reiss, *Phys. Rev. A* **22**, 1786 (1980).

[36] N. B. Delone and V. P. Krainov, *Multiphoton Processes in Atoms* (Springer Series on Atoms and Plasmas, 1993).

[37] D. N. Fittinghoff, P. R. Bolton, B. Chang and K. C. Kulander, *Phys. Rev. Lett.* **69**, 2642 (1992).

[38] S. Augst, D. D. Meyerhofer, D. Strickland and S. L. Chin, *J. Opt.Soc. Am. B* **8**, 858 (1991).

[39] G. Gibson, T. S. Luk and C. K. Rhodes, *Phys. Rev. A* **41**, 5049 (1990).

[40] F. A. Ilkov, J. E. Decker and S. L. Chin, *J. Phys. B* **25**, 4005 (1992).

[41] G. E. Bayfield and P. M. Koch, *Phys. Rev. Lett.* **33**, 258 (1974).

[42] T. F. Gallagher, *Phys. Rev. Lett.* **61**, 2304 (1988).

[43] X. F. Li, A. L'Huillier, M. Ferray, L. A. Lompre and G. Mainfray, *Phys. Rev. A* **39**, 5751 (1989).

[44] A. L'Huillier, L. A. Lompre, G. Mainfray and C. Manus, *Phys. Rev. Lett.* **48**, 1814 (1982).

[45] A. L'Huillier, L. A. Lompre, G. Mainfray and C. Manus, *Phys. Rev. A* **27**, 2503 (1983).

[46] B. Walker, E. Mevel, B. Yang, P. Breger, J. P. Chambaret, A. Antonetti, L. F. DiMauro and P. Agostini, *Phys. Rev. A* **48**, R894 (1993).

[47] B. Walker, B. Sheehy, L. F. DiMauro, P. Agostini, K. J. Schafer and K. C. Kulander, *Phys. Rev. Lett.* **73**, 1227 (1994).

[48] P. B. Corkum, *Phys. Rev. Lett.* **71**, 1994 (1993).

[49] K. C. Kulander, K. J. Schafer and J. L. Krause, *in Super-Intense Laser-Atom Physics* edited by B. Piraux, A. L'Huillier and K. Rzazewski, Vol. 316 of NATO Advanced Study Institute Series B: Physics (Plenum, New York 1993), p. 95.

[50] K. J. Schafer, B. Yang, L. F. DiMauro and K. C. Kulander, *Phys. Rev. Lett.* **70**, 1599 (1993).

[51] N. B. Delone and V. P. Krainov, *Atoms in Strong Light Fields* (Springer, Berlin, 1985).

[52] H. R. Reiss, *Prog. Quantum Electron.* **16**, 1 (1992).

[53] A. Becker and F. H. M. Faisal, *J. Phys. B* **38**, R1 (2005).

[54] F. Krausz and M. Ivanov, *Rev. Mod. Phys.* **81**, 163 (2009).

[55] A. de Bohan, *Dynamique de l'Interaction Laser-Atome. Moment Canonique et Approximation du Champ Fort, PhD Thesis*, Université Catholique de Louvain, Belgium (2001).

[56] A. de Bohan, B. Piraux, L. Ponce, R. Taïeb, V. Véniard and A. Maquet, *Phys. Rev. Lett.* **89**, 113002 (2002).

[57] G. G. Paulus, W. Becker and H. Walther, *Phys. Rev. A* **52**, 4043 (1995).

[58] Zhangjin Chen, Anh-Thu Le, Toru Morishita and C. D. Lin, *Phys. Rev. A* **79**, 033409 (2009).

[59] G. G. Paulus, F. Grasbon, H. Walther, P. Villoresi, M. Nisoli, S. Stagira, E. Priori and S. De Silvestri, *Nature* (London) **414**, 182 (2001).

[60] D. Miloševic, G. G. Paulus, D. Bauer and W. Becker, *J. Phys. B* **39**, R203 (2006).

[61] A. L'Huillier, L. A. Lompre, G. Mainfray and C. Manus, *Atoms in Intense Laser Fields*, edited by M. Gavrila (Academic Press, San Diego 1992) pp. 139-205.

[62] H. Niikura, D. M. Villeneuve and P. B. Corkum, *Phys. Rev. Lett.* **94**, 083003 (2005).

[63] J. L. Krause, K. J. Schafer and K. C. Kulander, *Phys. Rev. A* **45**, 4998 (1992).

[64] R. M. Potvliege and R. Shakeshaft, *Phys. Rev. A* **40**, 3061 (1989).

[65] W. Becker, S. Long and J. K. McIver, *Phys. Rev. A* **50**, 1540 (1994).

[66] M. Lewenstein, Ph. Balcou, M. Yu. Ivanov, A. L'Huillier and P. B. Corkum, *Phys. Rev. A* **49**, 2117 (1994).
M. Lewenstein, K. C. Kulander, K. J. Schafer and P. H. Bucksbaum, *Phys. Rev. A* **51**, 1495 (1995).

[67] M. Yu. Kuchiev and V. N. Ostrovsky, *Phys. Rev. A* **60**, 3111 (1999).

[68] J. H. Shirley, *Phys. Rev. B* **138**, 979 (1965).

[69] S. I. Chu, *Adv. Chem. Phys.* **73**, 739 (1989).

[70] R. M. Potvliege, E. Mese and Svetlana Vučić, *Phys. Rev. A* **81**, 053402 (2010).

[71] S. I. Chu, *Adv. At. Mol. Phys.* **21**, 197 (1985).

[72] M. Pont, R. M. Potvliege, R. Shakeshaft and Z.-j. Teng, *Phys. Rev. A* **45**, 8235 (1992).

[73] W. Becker, R. R. Schlicher and M. O. Scully, *J. Phys. B: At. Mol. Phys.* **19**, L785 (1986).

[74] P. W. Milonni and J. R. Ackerhalt, *Phys. Rev. A* **39**, 1139 (1989).

[75] S. Basile, G. Ferrante and F. Trombetta, *J. Phys. B: At. Mol. Opt. Phys.* **21**, L377 (1988).

[76] K. C. Kulander, *Phys. Rev. A* **35**, 445 (1987).

[77] E. Cormier, H. Bachau, and J. Zhang, *J. Phys. B: At. Mol. Phys.* **26**, 4449 (1993).

[78] E. Huens, B. Piraux, A. Bugacov, and M. Gajda, *Phys. Rev. A* **55**, 2132 (1997).

[79] H. Bachau, E. Cormier, P. Decleva, J. E. Hansen F. Martín, *Rep. Prog. Phys.* **64**, 1815 (2001).

[80] J. H. Eberly, Q. Su and J. Javanainen, *Phys. Rev. Lett.* **62**, 881 (1989).

[81] C. V. Reed and K. Burnett, *Phys. Rev. A* **42**, 3152 (1990).

[82] J. Javanainen, J. H. Eberly and Q. Su, *Phys. Rev. A* **38**, 3430 (1988).

[83] Q. Su, J. H. Eberly and J. Javanainen, *Phys. Rev. Lett.* **64**, 862 (1990).

[84] J. Javanainen and J. H. Eberly, *Phys. Rev. A* **39**, 458 (1989).

[85] M. S. Pindzola and M. Dörr, *Phys. Rev. A* **43**, 439 (1991).

[86] S. C. Rae, X. Chen and K. Burnett, *Phys. Rev. A* **50**, 1946 (1994).

[87] K. C. Kulander and B. W. Shore, *J. Opt.Soc. Am. B* **7**, 502 (1990).

[88] D. B. Milošević, G G Paulus and W Becker, *Laser Phys.* **13**, 948 (2003). D. B. Milošević, G G Paulus, D. Bauer and W Becker, *J. Phys. B: At. Mol. Opt. Phys.* **39**, R203 (2006).

Chapter 3

Quasi Analytical Model of the Interaction of the Hydrogen-Like Ions with a Laser Pulse

"It's amazing what can grow with a little inspiration. Provide Youth with creative tools and watch them succeed."
Not cited.

3.1 Introduction

In order to address the fundamental question of the actual role of the Coulomb potential in the intensity regime where tunnel ionization is supposed to take place, we have developed a new model calculation which goes far beyond the SFA. In this Chapter of the thesis we outline our mathematical model that already includes the fundamental assumptions as well as the basic theoretical approximations that are standard and compatible with the application to multiphoton processes in the MPI, ATI and Tunnel ionization regimes. The theoretical description involves treating the laser-atom interaction semiclassically in which the laser field is treated classically, while the atomic system is studied by using quantum mechanics and within the dipole approximation's framework.

This Chapter is organized as follows. In the second Section (3.2), we give a general formulation of the problem. In the next Section (3.3), we give the general framework of the construction of separable potentials. Emphasis is made on the specific cases of one, two and three level energy states. Our new

theoretical treatment of the TDSE in momentum space is described in Section (3.4). We consider separately the case where the first two s-states are included and the case where the $1s$, $2s$ and $2p$ are taken into account. The calculation of various observables at the end of the interaction with the pulse, in particular, the ionization yield and the electron energy spectrum, is given in Section (3.5). Section (3.6) is devoted to a simple illustration of the defined function $F_j(t)$ which contains all the information on the dynamics of the ionization process. In Section (3.7), we describe the numerical implementation of the method used to solve the linear Volterra integral equations of the second kind. Finally, before a short conclusion given in Section (3.9), and in order to validate our model we consider in Section (3.8), various physical situations in which the dynamics are well known. Unless stated, we use atomic units throughout this Chapter.

3.2 Theoretical formulation of the problem

In the momentum-space, the TDSE that governs the dynamics of atomic hydrogen exposed to a laser field, linearly polarized along the unit vector $\mathbf{e}$, reads:

$$\left[\mathrm{i}\frac{\partial}{\partial t} - \frac{1}{2}\mathbf{p}^2 + (\mathbf{p}\cdot\mathbf{e})\left(\frac{\partial}{\partial t}b(t)\right)\right]\Phi(\mathbf{p},t) - \int \frac{\mathrm{d}\mathbf{p}'}{(2\pi)^3} V\left(\mathbf{p},\mathbf{p}'\right)\Phi(\mathbf{p}',t) = 0. \quad (3.1)$$

We normalize the wave packets in the usual way

$$\int \frac{\mathrm{d}\mathbf{p}}{(2\pi)^3} \mid \Phi(\mathbf{p},t) \mid^2 = 1.$$

We work in the dipole approximation and use the velocity form for the laser-atom interaction Hamiltonian where we have set
$b(t) = -(1/c)\int_{-\infty}^{t} \mathrm{d}\tau\ A(\tau)$ for convenience. One can readily obtain this equation from the Fourier transform of its configuration space. The vector potential $\mathbf{A}(t)$ is defined by expressions (2.59)-(2.60) or via the electric-field vector given in equations (2.61)-(2.62) in which we have set $\phi = 0$. The second term of the left-hand-side (LHS) of equation (3.1) is the Coulomb potential which, in the momentum space, is not local. The kernel $V\left(\mathbf{p},\mathbf{p}'\right)$ is given by:

$$V\left(\mathbf{p},\mathbf{p}'\right) = -\frac{4\pi Z}{\mid \mathbf{p}-\mathbf{p}' \mid^2}, \quad (3.2)$$

where Z is the nucleus charge. The TDSE (3.1) is impossible to solve exactly. Here we develop a model which simplifies the resolution of this equation. The calculation consists in replacing this kernel by a sum of separable potentials, each of them supporting one bound state of atomic hydrogen. The derivation of these separable potentials is explained in the following section.

3.3 Construction of separable potentials

We approximate the kernel $V(\mathbf{p},\mathbf{p}')$ of the non-local Coulomb potential as a sum of N symmetric separable potentials [1, 2]:

$$V\left(\mathbf{p},\mathbf{p}'\right) \simeq -\sum_{n=1}^{N} v_n(\mathbf{p}) v_n^*(\mathbf{p}'). \tag{3.3}$$

We demand that this new kernel supports N atomic hydrogen bound eigenstates $|\phi_n\rangle$ of eigenenergy ε_n. This means that :

$$\left(\varepsilon_j - \frac{1}{2}p^2\right)\phi_j(\mathbf{p}) + \sum_{n=1}^{N} a_{jn} v_n(\mathbf{p}) = 0, \tag{3.4}$$

where

$$a_{jn} = \int \frac{\mathrm{d}\mathbf{p}'}{(2\pi)^3} v_n^*(\mathbf{p}')\phi_j(\mathbf{p}'). \tag{3.5}$$

The coefficients a_{jn} are the elements of a $N \times N$ matrix $\mathcal{A}$. Let us define the vector $\mathcal{V}$ consisting of the elements $\{v_n(\mathbf{p})\}$, and vector $\mathbf{\Phi}$ consisting of the elements $\left\{\left(\varepsilon_j - \frac{1}{2}p^2\right)\phi_j(\mathbf{p})\right\}$. In these notations, equation (3.4) writes:

$$\mathbf{\Phi} = -\mathcal{A}\mathcal{V}, \tag{3.6}$$

or, provided that $\mathcal{A}^{-1}$ exists,

$$\mathcal{V} = -\mathcal{A}^{-1}\mathbf{\Phi}. \tag{3.7}$$

We now introduce the symmetric $N \times N$ matrix $\mathbf{\Gamma}$ defined by:

$$\mathbf{\Gamma} = \mathcal{A}\mathcal{A}^T \tag{3.8}$$

where $\mathcal{A}^T$ denotes the transpose matrix of $\mathcal{A}$. The elements of $\mathbf{\Gamma}$ are given by:

$$\gamma_{ij} = -\int \frac{\mathrm{d}\mathbf{p}}{(2\pi)^3}\phi_i^*(\mathbf{p})(\varepsilon_j - \frac{1}{2}p^2)\phi_j(\mathbf{p}) = Z\int \frac{\mathrm{d}\mathbf{r}}{r}\psi_i^*(\mathbf{r})\psi_j(\mathbf{r}), \tag{3.9}$$

where $\psi_j(\mathbf{r})$ is the wave function associated with a Coulomb bound state in the configuration space. This is a general scheme for the factorization of the Coulomb potential. The integrals in (3.9) are well known. They only allow transitions $ns \to ms, np \to mp, nd \to md$, and so on. In addition, it is clear that the matrix $\mathbf{\Gamma}$ is *block-diagonal*, each block being associated with a value of the angular momentum. This and the angular structure of the hydrogen eigenfunctions (B.18) allow us to rewrite the kernel (3.1) in the following way:

$$V\left(\mathbf{p},\mathbf{p}'\right) \simeq -V^{(s)}\left(\mathbf{p},\mathbf{p}'\right) - V^{(p)}\left(\mathbf{p},\mathbf{p}'\right) - V^{(d)}\left(\mathbf{p},\mathbf{p}'\right) - ..... \tag{3.10}$$

with

$$V^{(l)}\left(\mathbf{p},\mathbf{p}'\right)=\sum_{j=1}^{N_l} v_j^{(l)}(p)v_j^{(l)}(p')\langle Y_l(\mathbf{p})\cdot Y_l(\mathbf{p}')\rangle, \tag{3.11}$$

where $\langle Y_l(\mathbf{p})\cdot Y_l(\mathbf{p}')\rangle$ is the scalar product of spherical harmonics, N_l is an integer denoting the number of angular momentum among the N atomic bound energies considered in (3.3). As a result, equation (3.4) takes the form:

$$\left(\varepsilon_j-\frac{1}{2}p^2\right)F_{jl}(p)+\sum_{j'=1}^{N_l} a_{jj'}^{(l)}v_{j'}^{(l)}(p)=0, \tag{3.12}$$

where

$$a_{jj'}^{(l)}=\int_0^\infty \frac{p^2\mathrm{d}p}{(2\pi)^3}F_{jl}(p)v_{j'}^{(l)}(p). \tag{3.13}$$

It determines the form of the potential functions inside a l-block. According to equation (3.7), we have to solve a system of algebraic equations for each l-block. Its solution however is not unique. Let us consider for instance, the following model potential cases.

$(1s)$-model potential

In this simple case where the Coulomb kernel in equation (3.1) supports only the ground state $1s$. We have

$$V^{(s)}\left(\mathbf{p},\mathbf{p}'\right)\simeq v_1^{(s)}(\mathbf{p})v_1^{(s)*}(\mathbf{p}'),\quad v_1^{(s)}(\mathbf{p})=\frac{4\sqrt{\pi}}{p^2+1}. \tag{3.14}$$

$(1s+2s)$-model potential

Let us consider here a model composed by the ground state $1s$ and the first excited state $2s$, namely the $(1s+2s)$ potential whose components are given by:

$$V^{(s)}\left(\mathbf{p},\mathbf{p}'\right)\simeq v_1^{(s)}(\mathbf{p})v_1^{(s)*}(\mathbf{p}')+v_2^{(s)}(\mathbf{p})v_2^{(s)*}(\mathbf{p}'), \tag{3.15}$$

where

$$\begin{aligned} v_1^{(s)}(\mathbf{p}) &= \alpha_{11}\left(\varepsilon_{1s}-\frac{1}{2}p^2\right)\phi_{1s}(\mathbf{p})+\alpha_{12}\left(\varepsilon_{2s}-\frac{1}{2}p^2\right)\phi_{2s}(\mathbf{p}),\\ v_2^{(s)}(\mathbf{p}) &= \alpha_{21}\left(\varepsilon_{1s}-\frac{1}{2}p^2\right)\phi_{1s}(\mathbf{p})+\alpha_{22}\left(\varepsilon_{2s}-\frac{1}{2}p^2\right)\phi_{2s}(\mathbf{p}). \end{aligned} \tag{3.16}$$

The complete normalized eigenfunctions $\phi_{1s}(\mathbf{p})$ and $\phi_{2s}(\mathbf{p})$ are given in Appendix B. From equation (3.8), we obtain the following system of nonlinear

equations:

$$\begin{aligned} a_{11}^2 + a_{12}^2 &= \gamma_{11}, \\ a_{21}^2 + a_{22}^2 &= \gamma_{22}, \\ a_{11}a_{21} + a_{22}a_{12} &= \gamma_{12}, \end{aligned} \tag{3.17}$$

where

$$\gamma_{11} = 1, \quad \gamma_{22} = \frac{1}{4}, \quad \gamma_{12} = \frac{4\sqrt{2}}{27}. \tag{3.18}$$

The general solution takes the form:

$$\alpha_{11} = -\frac{\cos(\kappa - \theta)}{\sqrt{\gamma_{11}}\cos\kappa}, \qquad \alpha_{12} = \frac{\sin\theta}{\sqrt{\gamma_{22}}\cos\kappa}, \tag{3.19}$$

$$\alpha_{21} = \frac{\sin(\kappa - \theta)}{\sqrt{\gamma_{11}}\cos\kappa}, \qquad \alpha_{22} = -\frac{\cos\theta}{\sqrt{\gamma_{22}}\cos\kappa}. \tag{3.20}$$

where θ is an arbitrary angle and κ can take two possible values: $\kappa_1 = \arcsin(\gamma_{12}/\sqrt{\gamma_{11}\gamma_{22}})$ and $\kappa_2 = \pi - \arcsin(\gamma_{12}/\sqrt{\gamma_{11}\gamma_{22}})$. Hence, we clearly see that there are two families of solutions characterized by the two pairs of parameters (κ_1, θ) and (κ_2, θ). Therefore, it is necessary to determine some rules to select the unique potential. We can, for instance, force the l-blocks of matrix $\mathcal{A}^{-1}$ to be triangular. This particular choice fixes the value of θ to zero in equations (3.19)-(3.20). In that case, $\alpha_{11} = -1/\sqrt{\gamma_{11}}$ and $\alpha_{12} = 0$. In turn, $\alpha_{21} = \tan\kappa_1/\sqrt{\gamma}_{11}$ and $\alpha_{22} = -1/(\sqrt{\gamma_{22}}\cos\kappa_1)$. Note that if instead of κ_1 we use κ_2, both coefficients α_{21} and α_{22} change their sign. This however, has no impact because it is only the products $v_j^{(l)}(p)v_j^{(l)}(p')$ that enter the separable potentials. Instead of imposing a triangular structure to the matrix $\mathcal{A}^{-1}$, we could equally well force this matrix to be symmetric, which implies that $\alpha_{12} = \alpha_{21}$ in equations (3.19)-(3.20). Such a rule, however, does not lead to a unique solution. This ambiguity is well known from nuclear physics and has been discussed by Bargmann [3] and Weinberg [4]. In this thesis, we assume matrix $\mathcal{A}^{-1}$ symmetric and write

$$\tan\theta = \frac{\sin\kappa}{(\sqrt{\gamma_{11}/\gamma_{22}} + \cos\kappa)}, \tag{3.21}$$

with $\kappa = \kappa_2$. Note that if we choose the l-blocks of matrix $\mathcal{A}^{-1}$ to be triangular or $\kappa = \kappa_1$ in the last expression of $\tan\theta$, the potential components $v_j^{(l)}(p)$ have not always the same sign. In that case, the corresponding separable potential (3.3) may be positive (repulsive) in contrast to the kernel (3.2) associated with the Coulomb potential. On the other hand it is important to stress that irrespective of the choice of the separable potentials, the wave

function associated with the atomic hydrogen bound state that these separable potentials support is exact. Therefore the previous discussion shows that the unphysical effects we observe in our final results with the wrong choice of the separable potentials are linked to a very bad description of the continuum wave functions. When our model atom contains only the ground state, it is needless to say that the previous argumentation about the choice of a separable potential is irrelevant. This particular case has been treated explicitly in [1, 2].

$(1s + 2s + 2p)$-model potential

We deal here with the case for which the separable potential model has the additional $2p$-excited states. According to the foregoing analysis we obtain for the $2p$ components of the separable potential, the following expression:

$$V^{(p)}\left(\mathbf{p},\mathbf{p}'\right) \simeq v_3^{(p)}(p)v_3^{(p)*}(p')\left(\mathbf{p}\cdot\mathbf{p}'\right), \quad v_3^{(p)}(p) = \frac{\sqrt{8\pi}}{(p^2+1/4)^2}. \tag{3.22}$$

The separable analogue potential now reduces to the form suited for our calculations

$$\begin{aligned} V\left(\mathbf{p},\mathbf{p}'\right) &\simeq -V^{(s)}\left(\mathbf{p},\mathbf{p}'\right) - V^{(p)}\left(\mathbf{p},\mathbf{p}'\right) && (3.23)\\ &\simeq -v_1^{(s)}(\mathbf{p})v_1^{(s)*}(\mathbf{p}') - v_2^{(s)}(\mathbf{p})v_2^{(s)*}(\mathbf{p}') - \frac{4\pi}{3}pp'v_3^{(p)}(p)v_3^{(p)*}(p') \\ &\times \sum_{m=-1}^{+1} Y_{1m}(\mathbf{p})Y_{1m}^*(\mathbf{p}'), && (3.24)\end{aligned}$$

where $Y_{lm}(\mathbf{p})$ ($-l \leq m \leq +l$, l denotes the orbital angular momentum quantum number, m the magnetic quantum number) are the well-known spherical harmonics, and where the components $v_1^{(s)}$ and $v_2^{(s)}$ are given in equation (3.16). The inclusion of higher np-states in the scheme can be performed according to the general procedure outlined above.

3.4 Theoretical treatment of the TDSE in momentum space

In this section, we describe our theoretical method, which is based on a direct solution of the TDSE right in the momentum space where the wave function remains more compact. We focus our attention to a mathematical model that amounts to solving a system of a few coupled one-dimensional linear Volterra integral equations of the second kind for the time-dependence of the total wave function. In what follows, and for the sake of simplicity, we omit the upper and lower scripts s, p in the potential components.

3.4.1 (1s)-model potential

The above scheme leads to the following form of the TDSE for the "(1s)" hydrogen-like atom

$$\left[\mathrm{i}\frac{\partial}{\partial t} - \frac{1}{2}\mathbf{p}^2 + (\mathbf{p}\cdot\mathbf{e})\left(\frac{\partial}{\partial t}b(t)\right)\right]\Phi(\mathbf{p},t) + v_1(\mathbf{p})F_1(t) = 0, \tag{3.25}$$

with the initial condition

$$\Phi(\mathbf{p},0) = \phi_{1s}(\mathbf{p}) = \frac{8\sqrt{\pi}}{(p^2+1)^2}, \tag{3.26}$$

and where we have defined the functions

$$F_1(t) = \int \frac{\mathrm{d}\mathbf{p}}{(2\pi)^3} v_1(\mathbf{p})\Phi(\mathbf{p},t). \tag{3.27}$$

Equation (3.25) can be solved formally. Its solution which satisfies the initial condition reads:

$$\begin{aligned}\Phi(\mathbf{p},t) = \exp\left(-\mathrm{i}\frac{p^2}{2}t + \mathrm{i}b(t)(\mathbf{p}\cdot\mathbf{e})\right)\Big[\Phi(\mathbf{p},0) \\ +\mathrm{i}v_1(\mathbf{p})\int_0^t \mathrm{d}\xi\ F_1(\xi)\exp\left(\mathrm{i}\frac{p^2}{2}\xi - \mathrm{i}b(\xi)(\mathbf{p}\cdot\mathbf{e})\right)\Big].\end{aligned} \tag{3.28}$$

The intrinsic symmetry of the atom naturally leads us to express the wave functions in spherical coordinates. However, in the present case of extremely short and intense laser pulses, the spherical symmetry is broken because the system is now dominated by a strong field. The problem has now a cylindrical symmetry imposed by the linearly polarized field whose direction is chosen to coincide with the z-axis. As a consequence, the wave packets $\Phi(\mathbf{p},t)$ do not depend on quantum number m, but depend only on the longitudinal momentum p_z and transverse momentum $p_\perp = \sqrt{p_x^2 + p_y^2}$. The TDSE provides the wave function which, together with the function $F_1(t)$, contains all information about physical observables.
Substitution of equation (3.28) into (3.27) leads to the time-dependent linear Volterra integral equation

$$F_1(t) = \frac{16}{\pi}\mathcal{J}_3\left(t/2, b(t)\right) + \mathrm{i}\frac{8}{\pi}\int_0^t \mathcal{J}_2\left((t-\xi)/2, b(t)-b(\xi)\right)F_1(\xi)\mathrm{d}\xi, \tag{3.29}$$

where the functions $\mathcal{J}_n(x,y)$ are given in Appendix D. The transition amplitude $\mathcal{C}_{1s}(t)$ for the system to remain in its ground state reads:

$$\begin{aligned}\mathcal{C}_{1s}(t) &= \langle\phi_{1s} \mid \Phi(t)\rangle \\ &= \frac{32}{\pi}\mathcal{J}_4\left(t/2, b(t)\right) + \mathrm{i}\frac{16}{\pi}\int_0^t \mathcal{J}_3\left((t-\xi)/2, b(t)-b(\xi)\right)F_1(\xi)\mathrm{d}\xi.\end{aligned} \tag{3.30}$$

3.4.2 $(1s+2s)$-model potential

In a similar way as above, the TDSE for the "$(1s+2s)$" hydrogen-like atom writes

$$\left[\mathrm{i}\frac{\partial}{\partial t}-\frac{1}{2}\mathbf{p}^2+(\mathbf{p}\cdot\mathbf{e})\left(\frac{\partial}{\partial t}b(t)\right)\right]\Phi(\mathbf{p},t)+v_1(\mathbf{p})F_1(t)+v_2(\mathbf{p})F_2(t)=0, \quad (3.31)$$

where

$$F_j(t)=\int\frac{\mathrm{d}\mathbf{p}}{(2\pi)^3}v_j(\mathbf{p})\Phi(\mathbf{p},t), \quad j=1,2. \quad (3.32)$$

A complete solution of equations (3.31)-(3.32) satisfying (3.26) now writes:

$$\begin{aligned}\Phi(\mathbf{p},t)=\exp\left(-\mathrm{i}\frac{p^2}{2}t+\mathrm{i}b(t)(\mathbf{p}\cdot\mathbf{e})\right)&\left[\Phi(\mathbf{p},0)\right.\\ &+\mathrm{i}v_1(\mathbf{p})\int_0^t\mathrm{d}\xi\ F_1(\xi)\exp\left(\mathrm{i}\frac{p^2}{2}\xi-\mathrm{i}b(\xi)(\mathbf{p}\cdot\mathbf{e})\right)\\ &\left.+\ \mathrm{i}v_2(\mathbf{p})\int_0^t\mathrm{d}\xi\ F_2(\xi)\exp\left(\mathrm{i}\frac{p^2}{2}\xi-\mathrm{i}b(\xi)(\mathbf{p}\cdot\mathbf{e})\right)\right]. \quad (3.33)\end{aligned}$$

Inserting equation (3.33) into (3.32) yields the system of coupled linear Volterra integral equations of the second kind

$$\begin{aligned}F_1(t) &= F_{10}(t)+\int_0^t\sum_{i=1}^{2}K_{1i}(t,\xi)F_i(\xi)\mathrm{d}\xi,\\ F_2(t) &= F_{20}(t)+\int_0^t\sum_{i=1}^{2}K_{2i}(t,\xi)F_i(\xi)\mathrm{d}\xi. \quad (3.34)\end{aligned}$$

Using the vector-matrix notation, the linear system can be written as

$$\mathbf{F}(t)=\mathbf{F}_0(t)+\int_0^t\mathbf{K}(t,\xi)\mathbf{F}(\xi)\mathrm{d}\xi. \quad (3.35)$$

The steps involved in obtaining the solution of the system of equations are formally the same as those for the single equation. For the sake of clarity, it is convenient to define the following functions

$$J_{\mu\nu}(x,y)=\frac{1}{(2\pi)^2\mathrm{i}y}\int_{-\infty}^{\infty}\mathrm{d}p\phi_{\mu s}(\mathbf{p})\phi_{\nu s}(\mathbf{p})\exp(-\mathrm{i}xp^2+\mathrm{i}yp) \quad (\mu,\nu=1,2). \quad (3.36)$$

Clearly $J_{\mu\nu}(0,0)=\delta_{\mu\nu}$. The elements of vector $\mathbf{F}_0(t)$ are given by:

$$\begin{aligned}F_{10}(t) &= \left[\alpha_{11}\left(\varepsilon_1-\frac{\mathrm{i}}{2}\frac{\partial}{\partial x}\right)J_{11}(x,b(t))+\alpha_{12}\left(\varepsilon_2-\frac{\mathrm{i}}{2}\frac{\partial}{\partial x}\right)J_{12}(x,b(t))\right]_{x=t/2},\\ F_{20}(t) &= \left[\alpha_{21}\left(\varepsilon_1-\frac{\mathrm{i}}{2}\frac{\partial}{\partial x}\right)J_{11}(x,b(t))+\alpha_{22}\left(\varepsilon_2-\frac{\mathrm{i}}{2}\frac{\partial}{\partial x}\right)J_{12}(x,b(t))\right]_{x=t/2}. \quad (3.37)\end{aligned}$$

After some manipulations, the elements of the 2×2 symmetric matrix $\mathbf{K}$ are:

$$\begin{aligned}
K_{11}(t,\xi) &= \mathrm{i}\left[\alpha_{11}^2\left(\varepsilon_1 - \frac{\mathrm{i}}{2}\frac{\partial}{\partial x}\right)^2 J_{11}(x,y) + 2\alpha_{11}\alpha_{12}\left(\varepsilon_1 - \frac{\mathrm{i}}{2}\frac{\partial}{\partial x}\right)\right. \\
&\quad \left.\times\left(\varepsilon_2 - \frac{\mathrm{i}}{2}\frac{\partial}{\partial x}\right) J_{12}(x,y) + \alpha_{12}^2\left(\varepsilon_2 - \frac{\mathrm{i}}{2}\frac{\partial}{\partial x}\right)^2 J_{22}(x,y)\right]_{x=(t-\xi)/2}; \\
K_{12}(t,\xi) &= \mathrm{i}\left[\alpha_{11}\alpha_{21}\left(\varepsilon_1 - \frac{\mathrm{i}}{2}\frac{\partial}{\partial x}\right)^2 J_{11}(x,y) + (\alpha_{11}\alpha_{22} + \alpha_{21}\alpha_{12})\left(\varepsilon_1 - \frac{\mathrm{i}}{2}\frac{\partial}{\partial x}\right)\right. \\
&\quad \left.\times\left(\varepsilon_2 - \frac{\mathrm{i}}{2}\frac{\partial}{\partial x}\right) J_{12}(x,y) + \alpha_{12}\alpha_{22}\left(\varepsilon_2 - \frac{\mathrm{i}}{2}\frac{\partial}{\partial x}\right)^2 J_{22}(x,y)\right]_{x=(t-\xi)/2}; \\
K_{22}(t,\xi) &= \mathrm{i}\left[\alpha_{21}^2\left(\varepsilon_1 - \frac{\mathrm{i}}{2}\frac{\partial}{\partial x}\right)^2 J_{11}(x,y) + 2\alpha_{21}\alpha_{22}\left(\varepsilon_1 - \frac{\mathrm{i}}{2}\frac{\partial}{\partial x}\right)\right. \\
&\quad \left.\times\left(\varepsilon_2 - \frac{\mathrm{i}}{2}\frac{\partial}{\partial x}\right) J_{12}(x,y) + \alpha_{22}^2\left(\varepsilon_2 - \frac{\mathrm{i}}{2}\frac{\partial}{\partial x}\right)^2 J_{22}(x,y)\right]_{x=(t-\xi)/2},
\end{aligned} \tag{3.38}$$

with $y = b(t) - b(\xi)$. Applying now (3.33), we easily obtain an expression of the amplitude of probability for the system to be in one of the two bound states ($1s$ or $2s$) as a function of time:

$$\mathcal{C}_{1s}(t) = J_{11}(t/2, b(t)) + \mathrm{i}\int_0^t \mathrm{d}\xi\ K_1(t,\xi)F_1(\xi) + \mathrm{i}\int_0^t \mathrm{d}\xi\ K_2(t,\xi)F_2(\xi); \tag{3.39}$$

$$\begin{aligned}
\mathcal{C}_{2s}(t) &= \langle \phi_{2s} \mid \Phi(t) \rangle \\
&= J_{12}(t/2, b(t)) + \mathrm{i}\int_0^t \mathrm{d}\xi\ \tilde{K}_1(t,\xi)F_1(\xi) + \mathrm{i}\int_0^t \mathrm{d}\xi\ \tilde{K}_2(t,\xi)F_2(\xi),
\end{aligned} \tag{3.40}$$

where:

$$\begin{aligned}
K_1(t,\xi) &= \left[\alpha_{11}\left(\varepsilon_1 - \frac{\mathrm{i}}{2}\frac{\partial}{\partial x}\right) J_{11}(x,y) + \alpha_{12}\left(\varepsilon_2 - \frac{\mathrm{i}}{2}\frac{\partial}{\partial x}\right) J_{12}(x,y)\right]_{x=(t-\xi)/2}, \\
K_2(t,\xi) &= \left[\alpha_{21}\left(\varepsilon_1 - \frac{\mathrm{i}}{2}\frac{\partial}{\partial x}\right) J_{11}(x,y) + \alpha_{22}\left(\varepsilon_2 - \frac{\mathrm{i}}{2}\frac{\partial}{\partial x}\right) J_{12}(x,y)\right]_{x=(t-\xi)/2},
\end{aligned} \tag{3.41}$$

$$\tilde{K}_1(t,\xi) = \left[\alpha_{11}\left(\varepsilon_1 - \frac{\mathrm{i}}{2}\frac{\partial}{\partial x}\right)J_{12}(x,y) + \alpha_{12}\left(\varepsilon_2 - \frac{\mathrm{i}}{2}\frac{\partial}{\partial x}\right)J_{22}(x,y)\right]_{x=(t-\xi)/2},$$
$$\tilde{K}_2(t,\xi) = \left[\alpha_{21}\left(\varepsilon_1 - \frac{\mathrm{i}}{2}\frac{\partial}{\partial x}\right)J_{12}(x,y) + \alpha_{22}\left(\varepsilon_2 - \frac{\mathrm{i}}{2}\frac{\partial}{\partial x}\right)J_{22}(x,y)\right]_{x=(t-\xi)/2}. \tag{3.42}$$

In equations (3.41)-(3.42), the variable $y = b(t) - b(\xi)$.

3.4.3 $(1s+2s+2p)$-model potential

Let us now introduce the $2p$ components of the separable potential in the TDSE. In this condition, the TDSE becomes:

$$\left[\mathrm{i}\frac{\partial}{\partial t} - \frac{1}{2}\mathbf{p}^2 + (\mathbf{p}\cdot\mathbf{e})\left(\frac{\partial}{\partial t}b(t)\right)\right]\Phi(\mathbf{p},t) + v_1(\mathbf{p})F_1(t) + v_2(\mathbf{p})F_2(t) + \frac{4\pi}{3}pv_3(p)\sum_{m=-1}^{1} Y_{1m}(\mathbf{p})\mathbf{F}_{3m}(t) = 0, \tag{3.43}$$

where

$$\mathbf{F}_{3m}(t) = \int \frac{\mathrm{d}\mathbf{p}}{(2\pi)^3}pv_3(p)Y^*_{1m}(\mathbf{p})\Phi(\mathbf{p},t). \tag{3.44}$$

Given the symmetry of the problem, we can write $\mathbf{F}_{3m}(t) = F_3(t)Y^*_{1m}(\mathbf{e})$. This means that

$$F_3(t) = \int \frac{\mathrm{d}\mathbf{p}}{(2\pi)^3}v_3(p)(\mathbf{p}\cdot\mathbf{e})\Phi(\mathbf{p},t) \tag{3.45}$$

and

$$\sum_{m=-1}^{1} Y_{1m}(\mathbf{p})\mathbf{F}_{3m}(t) = \frac{3}{4\pi}\frac{(\mathbf{p}\cdot\mathbf{e})}{p}F_3(t). \tag{3.46}$$

Consequently, the solution of equation (3.43) which verifies (3.26) takes the following form:

$$\begin{aligned}\Phi(\mathbf{p},t) = \exp\left(-\mathrm{i}\frac{p^2}{2}t + \mathrm{i}b(t)(\mathbf{p}\cdot\mathbf{e})\right)\Big[&\Phi(\mathbf{p},0)\\ &+\mathrm{i}v_1(\mathbf{p})\int_0^t \mathrm{d}\xi\ F_1(\xi)\exp\left(\mathrm{i}\frac{p^2}{2}\xi - \mathrm{i}b(\xi)(\mathbf{p}\cdot\mathbf{e})\right)\\ &+\mathrm{i}v_2(\mathbf{p})\int_0^t \mathrm{d}\xi\ F_2(\xi)\exp\left(\mathrm{i}\frac{p^2}{2}\xi - \mathrm{i}b(\xi)(\mathbf{p}\cdot\mathbf{e})\right)\\ &+\mathrm{i}v_3(p)(\mathbf{p}\cdot\mathbf{e})\int_0^t \mathrm{d}\xi\ F_3(\xi)\exp\left(\mathrm{i}\frac{p^2}{2}\xi - \mathrm{i}b(\xi)(\mathbf{p}\cdot\mathbf{e})\right)\Big].\end{aligned} \tag{3.47}$$

As in the previous case, the functions F_j with $j = 1, 2, 3$ are the solution of a system of three coupled time-dependent linear Volterra integral equations

$$\begin{aligned} F_1(t) &= F_{10}(t) + \int_0^t \sum_{i=1}^{3} K_{1i}(t,\xi) F_i(\xi) \mathrm{d}\xi, \\ F_2(t) &= F_{20}(t) + \int_0^t \sum_{i=1}^{3} K_{2i}(t,\xi) F_i(\xi) \mathrm{d}\xi, \\ F_3(t) &= F_{30}(t) + \int_0^t \sum_{i=1}^{3} K_{3i}(t,\xi) F_i(\xi) \mathrm{d}\xi, \end{aligned} \tag{3.48}$$

which can be written in matrix form as follows:

$$\mathbf{F}(t) = \mathbf{F}_0(t) + \int_0^t \mathbf{K}(t,\xi)\mathbf{F}(\xi)\mathrm{d}\xi. \tag{3.49}$$

The new 3×3 symmetric matrix $\mathbf{K}$ includes three new elements and a third element for $\mathbf{F}_0(t)$. Along the same line as before, we introduce three new functions similar to those defined by equation (3.36):

$$\begin{aligned} J_{j3}(x,y) &= \frac{1}{(2\pi)^2 \mathrm{i}y} \int_{-\infty}^{\infty} \mathrm{d}p \phi_{js}(\mathbf{p}) \phi_3(p) \exp(-\mathrm{i}xp^2 + \mathrm{i}yp), \quad j = 1, 2, \\ J_{33}(x,y) &= \frac{1}{(2\pi)^2 \mathrm{i}y} \int_{-\infty}^{\infty} \frac{\mathrm{d}p}{p} \phi_3^2(p) \exp(-\mathrm{i}xp^2 + \mathrm{i}yp), \end{aligned} \tag{3.50}$$

$$\phi_3(p) = \frac{8\pi}{\sqrt{6}} \frac{p}{(p^2 + 1/4)^3}. \tag{3.51}$$

In terms of these functions, the three new elements of matrix $\mathbf{K}$ write:

$$\begin{aligned} K_{13}(t,\xi) = -\sqrt{\frac{3}{\pi}} \frac{\partial}{\partial y} \left(\varepsilon_2 - \frac{\mathrm{i}}{2}\frac{\partial}{\partial x}\right) \Bigg[& \alpha_{11} \left(\varepsilon_1 - \frac{\mathrm{i}}{2}\frac{\partial}{\partial x}\right) J_{13}(x,y) \\ & + \alpha_{12} \left(\varepsilon_2 - \frac{\mathrm{i}}{2}\frac{\partial}{\partial x}\right) J_{23}(x,y) \Bigg]_{x=(t-\xi)/2, y=b(t)-b(\xi)}, \\ K_{23}(t,\xi) = -\sqrt{\frac{3}{\pi}} \frac{\partial}{\partial y} \left(\varepsilon_2 - \frac{\mathrm{i}}{2}\frac{\partial}{\partial x}\right) \Bigg[& \alpha_{21} \left(\varepsilon_1 - \frac{\mathrm{i}}{2}\frac{\partial}{\partial x}\right) J_{13}(x,y) \\ & + \alpha_{22} \left(\varepsilon_2 - \frac{\mathrm{i}}{2}\frac{\partial}{\partial x}\right) J_{23}(x,y) \Bigg]_{x=(t-\xi)/2, y=b(t)-b(\xi)}, \\ K_{33}(t,\xi) = \left[-\mathrm{i}\frac{3}{\pi} \frac{\partial^2}{\partial y^2} \left(\varepsilon_2 - \frac{\mathrm{i}}{2}\frac{\partial}{\partial x}\right)^2 J_{33}(x,y) \right]_{x=(t-\xi)/2, y=b(t)-b(\xi)}. & \end{aligned} \tag{3.52}$$

Similarly, we have:

$$F_{30}(t) = \mathrm{i}\sqrt{\frac{3}{\pi}} \left[\frac{\partial}{\partial y} \left(\varepsilon_2 - \frac{\mathrm{i}}{2}\frac{\partial}{\partial x}\right) J_{13}(x,y) \right]_{x=t/2, y=b(t)}. \tag{3.53}$$

Now, we calculate the population of the $2p$-states. The corresponding amplitude reads

$$\mathcal{C}_{2p,m}(t) = \langle \phi_{2p,m} | \Phi(t) \rangle.$$

As before, we have $\mathcal{C}_{2p,m}(t) = \mathcal{C}_{2p}(t) Y_{1m}(\mathbf{e})$. Thus,

$$\mathcal{C}_{2p}(t) = \int \frac{\mathrm{d}\mathbf{p}}{(2\pi)^3} \phi_3(p) \frac{(\mathbf{p}\cdot\mathbf{e})}{p} \Phi(\mathbf{p}, t). \tag{3.54}$$

Obviously one has:

$$\mathcal{C}_{2p}(t) = \left[-\mathrm{i} \frac{\partial}{\partial y} J_{13}(t/2, y) \right]_{y=b(t)} + \mathrm{i} \int_0^t \mathrm{d}\xi \; \bar{K}_1(t,\xi) F_1(\xi) + \mathrm{i} \int_0^t \mathrm{d}\xi \; \bar{K}_2(t,\xi) F_2(\xi) + \mathrm{i} \int_0^t \mathrm{d}\xi \; \bar{K}_3(t,\xi) F_3(\xi), \tag{3.55}$$

where we have set

$$\begin{aligned}
\bar{K}_1(t,\xi) &= -\mathrm{i} \left[\alpha_{11} \left(\varepsilon_1 - \frac{\mathrm{i}}{2} \frac{\partial}{\partial x} \right) \frac{\partial}{\partial y} J_{13}(x,y) + \alpha_{12} \left(\varepsilon_2 - \frac{\mathrm{i}}{2} \frac{\partial}{\partial x} \right) \frac{\partial}{\partial y} J_{23}(x,y) \right], \\
\bar{K}_2(t,\xi) &= -\mathrm{i} \left[\alpha_{21} \left(\varepsilon_1 - \frac{\mathrm{i}}{2} \frac{\partial}{\partial x} \right) \frac{\partial}{\partial y} J_{13}(x,y) + \alpha_{22} \left(\varepsilon_2 - \frac{\mathrm{i}}{2} \frac{\partial}{\partial x} \right) \frac{\partial}{\partial y} J_{23}(x,y) \right], \\
\bar{K}_3(t,\xi) &= \left[\sqrt{\frac{3}{\pi}} \left(\varepsilon_2 - \frac{\mathrm{i}}{2} \frac{\partial}{\partial x} \right) \frac{\partial^2}{\partial y^2} J_{33}(x,y) \right],
\end{aligned} \tag{3.56}$$

in which $x = (t-\xi)/2, \; y = b(t) - b(\xi)$ after performing all differentiations. Furthermore, we have:

$$\sum_{m=-1}^{+1} \mid \mathcal{C}_{2p,m}(t) \mid^2 = \frac{3}{4\pi} \mid \mathcal{C}_{2p}(t) \mid^2 . \tag{3.57}$$

It is clear that the amplitudes $\mathcal{C}_{1s}(t)$ and $\mathcal{C}_{2s}(t)$ must be calculated with the new wave packet (3.47). This leads to adding new terms in equations (3.39) and (3.40), which include the integrals in $F_3(\xi)$ and the corresponding derivatives of the functions $J_{j3}, \; j = 1, 2$. These new kernel components are respectively given by

$$\begin{aligned}
K_3(t,\xi) &= \left[\mathrm{i} \sqrt{\frac{3}{\pi}} \left(\varepsilon_2 - \frac{\mathrm{i}}{2} \frac{\partial}{\partial x} \right) \frac{\partial}{\partial y} J_{13}(x,y) \right]_{x=(t-\xi)/2, y=b(t)-b(\xi)}, \\
\tilde{K}_3(t,\xi) &= \left[\mathrm{i} \sqrt{\frac{3}{\pi}} \left(\varepsilon_2 - \frac{\mathrm{i}}{2} \frac{\partial}{\partial x} \right) \frac{\partial}{\partial y} J_{23}(x,y) \right]_{x=(t-\xi)/2, y=b(t)-b(\xi)}.
\end{aligned} \tag{3.58}$$

3.5 Calculation of the physical observables

3.5.1 Total ionization probability

The probability of ionization is defined as the amount of population which is in the continuum states [5]. It is given by

$$\begin{aligned} P(t) &= 1 - \sum_{n=1}^{N} \mid \langle \phi_n \mid \Phi(t) \rangle \mid^2, \\ &= 1 - \mid \mathcal{C}_{1s}(t) \mid^2 - \mid \mathcal{C}_{2s}(t) \mid^2 - \sum_{m=-1}^{+1} \mid \mathcal{C}_{2p,m}(t) \mid^2, \end{aligned} \tag{3.59}$$

where N is the total number of bound states, ϕ_n are field-free bound states of the atomic system and $\Phi(t)$ is the evolved wave function in the velocity gauge. The probability of ionization defined above is the probability of being in the continuum if the pulse has been turned off at time t. Although for instance, it is important to know the total ionization probability, other quantities like the energy spectrum and the angular distributions of the ejected electrons are important to calculate. They require to determine the transition amplitude $\mathcal{C}_k(t)$ into the continuum states. A simple way to calculate $\mathcal{C}_k(t)$ is to project the outgoing total wave packet after the interaction with the laser field onto the final continuum states. We first point out that, by contrast to the pure Coulomb potential, our separable potential has a short range. This means that we can use the Lippmann-Schwinger equation to build the continuum state $\varphi^{\pm}(\mathbf{k}, \mathbf{p}) \equiv \varphi_k^{\pm}(\mathbf{p})$ of wave vector $\mathbf{k}$, the free part of which looks like $(2\pi)^{3/2}\delta(\mathbf{k} - \mathbf{p})$ (see Appendix B). The upper scripts + and - refer to an outgoing and an ingoing wave behaviour respectively.

3.5.2 Electron energy spectrum

In addition to the population of the various bound states calculated in the previous section, we show here, how to calculate the energy spectrum of the ejected electron. Following the above considerations, the ionization amplitude writes:

$$\mathcal{C}_k(t) = \langle \varphi^+(\mathbf{k}) \mid \Phi(t) \rangle = \int \frac{\mathrm{d}\mathbf{p}}{(2\pi)^3} \left\{ \varphi^+(\mathbf{k}, \mathbf{p}) \right\}^* \Phi(\mathbf{p}, t). \tag{3.60}$$

It is important to note that the total wave packet $\Phi(\mathbf{p}, t)$ can be decomposed as follows:

$$\Phi(\mathbf{p}, t) = \mathcal{C}_{1s}(t)\phi_{1s}(\mathbf{p}) + \mathcal{C}_{2s}(t)\phi_{2s}(\mathbf{p}) + \mathcal{C}_{2p,m}(t)\phi_{2p,m}(\mathbf{p}) + \int \mathrm{d}\mathbf{k}\mathcal{C}_k(t)\varphi^+(\mathbf{k}, \mathbf{p}). \tag{3.61}$$

After lengthy manipulations, we get from equation (3.60) the three needed expressions

$$\begin{aligned}\mathcal{C}_k^{(1s)}(t) = &\frac{2\sqrt{2}}{\pi}\frac{1}{(\mathbf{k}^2+1)^2}\exp\left(-\mathrm{i}\frac{t}{2}\mathbf{k}^2+\mathrm{i}b(t)(\mathbf{k}\cdot\mathbf{e})\right)\\ &+\frac{\mathrm{i}\sqrt{2}}{\pi}\frac{1}{(\mathbf{k}^2+1)}\int_0^t \mathrm{d}\xi F_1(\xi)\exp\left(-\mathrm{i}\frac{(t-\xi)}{2}\mathbf{k}^2+\mathrm{i}(b(t)-b(\xi))(\mathbf{k}\cdot\mathbf{e})\right)\\ &-\frac{\mathrm{i}16}{\pi}\left\{\tilde{C}_1^+(\mathbf{k})\right\}^*\widetilde{\mathcal{D}}_3\left(\frac{t}{2},b(t);k\right)\\ &+\frac{8}{\pi}\left\{\tilde{C}_1^+(\mathbf{k})\right\}^*\int_0^t \mathrm{d}\xi\widetilde{\mathcal{D}}_2\left(\frac{(t-\xi)}{2},b(t)-b(\xi);k\right)F_1(\xi),\end{aligned} \tag{3.62}$$

with $\left\{\tilde{C}_1^+(\mathbf{k})\right\}$ given by (B.35) - (B.36).

$$\begin{aligned}\mathcal{C}_k^{(1s2s)}(t) = &\frac{1}{(2\pi)^{3/2}}\mathcal{H}_k^{(1)}(t)+\mathrm{i}\tilde{v}_1(\mathbf{k})\mathcal{H}_k^{(3)}(t)+\mathrm{i}\tilde{v}_2(\mathbf{k})\mathcal{H}_k^{(6)}(t)\\ &-\left\{\tilde{C}_1^+(\mathbf{k})\right\}^*\left[\mathcal{H}_k^{(2)}(t)+\mathrm{i}\left(\mathcal{H}_k^{(4)}(t)+\mathcal{H}_k^{(8)}(t)\right)\right]\\ &-\left\{\tilde{C}_2^+(\mathbf{k})\right\}^*\left[\mathcal{H}_k^{(5)}(t)+\mathrm{i}\left(\mathcal{H}_k^{(7)}(t)+\mathcal{H}_k^{(9)}(t)\right)\right],\end{aligned} \tag{3.63}$$

$$\begin{aligned}\mathcal{C}_k^{(1s2s2p)}(t) = &\mathcal{C}_k^{(1s2s)}(t)+\mathrm{i}\tilde{v}_3(k)(\mathbf{k}\cdot\mathbf{e})\mathcal{H}_k^{(11)}(t)-\mathrm{i}\left\{\tilde{C}_1^+(\mathbf{k})\right\}^*\mathcal{H}_k^{(13)}(t)\\ &-\mathrm{i}\left\{\tilde{C}_2^+(\mathbf{k})\right\}^*\mathcal{H}_k^{(14)}(t)-\left\{\tilde{C}_3^+(\mathbf{k})\right\}^*\left[\mathcal{H}_k^{(10)}(t)\right.\\ &\left.+\mathrm{i}\left(\mathcal{H}_k^{(12)}(t)+\mathcal{H}_k^{(15)}(t)+\mathcal{H}_k^{(16)}(t)\right)\right].\end{aligned} \tag{3.64}$$

The functions $\tilde{v}_j(\mathbf{k}) = (2\pi)^{-3/2}v_j(\mathbf{k})$, $j = 1,2,3$ are given by equations (B.38), (B.39) and (B.45) while $\left\{\tilde{C}_j^+(\mathbf{k})\right\}$ are defined by (B.41), (B.43), (B.47) and (B.48). Details of the calculation of the kernels and the free terms encountered in the theory above are outlined in Appendices D and E.

The spectral continuum, namely the energy distribution density $D(E_k,t)$ of the ejected electrons is simply given by

$$\frac{\partial P}{\partial E_k} = D(E_k,t) = \sqrt{2E_k}\int \mathrm{d}\Omega_k \mid \mathcal{C}_k(t)\mid^2, \tag{3.65}$$

with Ω_k denoting the solid angle under which the electron is emitted. The angular distribution for a given energy is

$$\frac{\partial^2 P}{\partial E_k \partial\Omega_k} = \sqrt{2E_k}\mid \mathcal{C}_k(t)\mid^2. \tag{3.66}$$

Obviously, the total ionization yield is also equal to

$$P(t) = \int_0^{+\infty} D(E_k, t) \mathrm{d}E_k. \tag{3.67}$$

It is worth stressing that, our separable (non local) potential can possibly have more bound states than the selected amount. In this case, it is necessary to determine all bound states beforehand. This is done by setting in equation (3.43), $b(t) = 0$ and $|\Phi(t)\rangle = \mathrm{e}^{-\mathrm{i}\varepsilon_s t}|\phi_s\rangle$ ($\varepsilon_s < 0$), and by solving the system of algebraic equations for the values $f_j = \mathrm{e}^{\mathrm{i}\varepsilon_s t} F_j(t)$.

On the gauge invariance

In the momentum space, it is rather subtle to formulate the gauge invariance of equations (3.25), (3.31) or (3.43). Instead, it is more convenient to go back momentarily to the configuration space. As it is in momentum space, each component of the atomic potential is non local and separable. It therefore involves a product of functions $\tilde{v}(\mathbf{r})\tilde{v}^*(\mathbf{r}')$. Within the dipole approximation, the unitary transformation that allows to move from the velocity to the length gauge must be applied to both the functions $\tilde{v}(\mathbf{r})$ and $\tilde{v}^*(\mathbf{r}')$ to guarantee the gauge invariance.

Consider the TDSE, which describes the interaction of an electron with an electromagnetic field and some non-electromagnetic local potential V

$$\left[\mathrm{i}\frac{\partial}{\partial t} - \frac{1}{2}\left(-\mathrm{i}\boldsymbol{\nabla} + \frac{1}{c}\mathbf{A}(\mathbf{r}, t)\right)^2 - U(\mathbf{r}, t) - V(\mathbf{r}, t)\right]\Psi(\mathbf{r}, t) = 0. \tag{3.68}$$

Let us perform now the transformation $\Psi = \exp(-\mathrm{i}/c\ \chi)\Psi'$. It is easy to see that equation (3.68) is unaltered under the well known gauge transformations $(\mathbf{A}', U', \Psi')$. This is the classical gauge invariance in the case of local potentials. In our case formally we can consider $(\mathbf{A}, U = 0)$ like the potentials of an external field and the potential $V = -Z/r$ like "internal" potential. In principle, this particular equation is also gauge invariant in terms of external laser field. Let us remind that in the momentum space

$$Q(\mathbf{r}, t)\Psi(\mathbf{r}, t) \to \int \frac{\mathrm{d}\mathbf{p}'}{(2\pi)^3}\ \widetilde{Q}(\mathbf{p} - \mathbf{p}')\widetilde{\Psi}(\mathbf{p}', t)$$

for any local smooth function Q, and a tilde denotes the Fourier transforms. Let now

$$\widetilde{V}(\mathbf{p} - \mathbf{p}', t) \to \widetilde{v}(\mathbf{p}, t)\widetilde{v}^*(\mathbf{p}', t)$$

or be a sum of such terms. In this case

$$\int \frac{\mathrm{d}\mathbf{p}'}{(2\pi)^3}\ \widetilde{V}(\mathbf{p} - \mathbf{p}')\widetilde{\Psi}(\mathbf{p}', t) \to C(t)\widetilde{v}(\mathbf{p}, t) \tag{3.69}$$

with

$$C(t) = \int \frac{\mathrm{d}\mathbf{p}'}{(2\pi)^3}\ \widetilde{v}^*(\mathbf{p}',t)\widetilde{\Psi}(\mathbf{p}',t).$$

Going back to the coordinate space we obtain for equation (3.68)

$$\left[\mathrm{i}\frac{\partial}{\partial t} - \frac{1}{2}\left(-\mathrm{i}\boldsymbol{\nabla} + \frac{1}{c}\mathbf{A}(\mathbf{r},t)\right)^2 - U(\mathbf{r},t)\right]\Psi(\mathbf{r},t) = C(t)v(\mathbf{r},t),$$

where $C(t)$ now reads

$$C(t) = \int \mathrm{d}\mathbf{r}'\ v^*(\mathbf{r}',t)\Psi(\mathbf{r}',t),$$

which is equivalent to (3.69). We can also obtain the gauge invariance demanding implementation of the condition $v = \exp(-\mathrm{i}/c\ \chi)v'$.

3.6 On the functions $F_j(t)$

The functions $F_j(t)$ contain the whole information on the dynamics. It is therefore interesting to analyze the behaviour of these functions in more details. For the sake of mathematical illustration, we consider here the case for which separable potential sustains only one bound state (*i.e.* $1s$ - state). In this case $v_1(\mathbf{p}) = \left(\varepsilon_1 - \frac{1}{2}p^2\right)\phi_{1s}(\mathbf{p})$. For $t > T_p$ we have from equation (3.25)

$$\left[\mathrm{i}\frac{\partial}{\partial t} - \frac{1}{2}\mathbf{p}^2\right]\Phi(\mathbf{p},t) + \left(\varepsilon_1 - \frac{1}{2}p^2\right)\phi_{1s}(\mathbf{p})F_1(t) = 0. \tag{3.70}$$

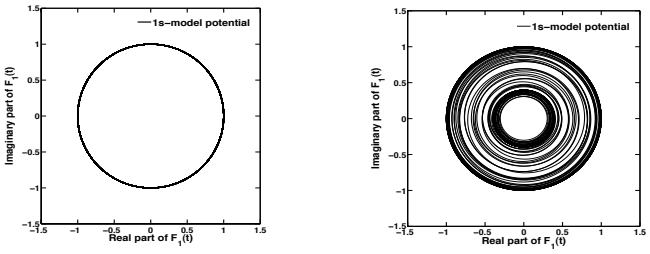

Figure 3.1: *Argand curves of function $F_1(t)$ when the laser field is switched off (left panel) and on (right panel). Our model potential supports only $1s$ state. The peak laser field intensity is $I = 3 \times 10^{14}$ W.cm^{-2}.*

At the same time

$$\Phi(\mathbf{p},t) = \mathcal{C}_{1s}(T_p)\mathrm{e}^{-\mathrm{i}\varepsilon_1 t}\phi_{1s}(\mathbf{p}) + \int \mathrm{d}\mathbf{k}\mathcal{C}_k^{(1s)}(T_p)\mathrm{e}^{-\mathrm{i}tk^2/2}\varphi^-(\mathbf{k},\mathbf{p}). \tag{3.71}$$

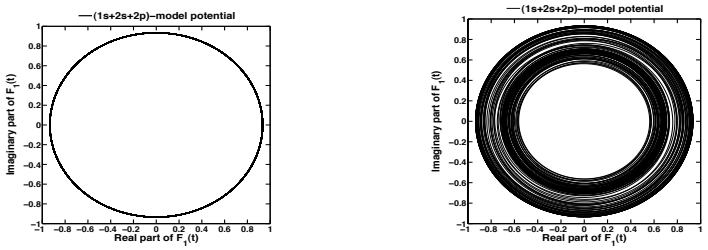

Figure 3.2: *Argand curves of component $F_1(t)$ when the laser field is switched off (left panel) and on (right panel). Our model potential supports only $1s$, $2s$ and $2p$ states. The peak laser field intensity is $I = 3 \times 10^{14}$ W.cm^{-2}.*

Equations (3.70) and (3.71) together yield

$$\left(\varepsilon_1 - \frac{1}{2}p^2\right)\phi_{1s}(\mathbf{p})\left[\mathcal{C}_{1s}(T_p)\mathrm{e}^{-\mathrm{i}\varepsilon_1 t} + F_1(t)\right] + \int \mathrm{d}\mathbf{k}\mathcal{C}_k^{(1s)}(T_p) \times \left(\frac{1}{2}k^2 - \frac{1}{2}p^2\right)\mathrm{e}^{-\mathrm{i}tk^2/2}\varphi^-(\mathbf{k},\mathbf{p}) = 0. \tag{3.72}$$

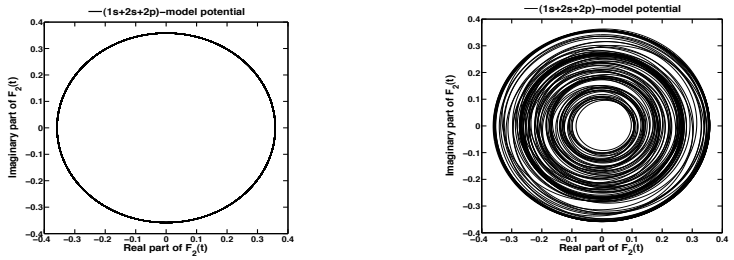

Figure 3.3: *Argand curves of component $F_2(t)$ when the laser field is switched off (left panel) and on (right panel). Our model potential supports only $1s$, $2s$ and $2p$ states. The peak laser field intensity is $I = 3 \times 10^{14}$ W.cm^{-2}.*

On the other hand,

$$\varphi^{\pm}(\mathbf{k},\mathbf{p}) = (2\pi)^{3/2}\delta(\mathbf{k}-\mathbf{p}) - \frac{\left(\varepsilon_1 - \frac{1}{2}p^2\right)\phi_{1s}(\mathbf{p})}{\left(\frac{1}{2}k^2 - \frac{1}{2}p^2 \pm \mathrm{i}0\right)}g^{\pm}(\mathbf{k}), \tag{3.73}$$

with

$$g^{\pm}(\mathbf{k}) = \left(\varepsilon_1 - \frac{1}{2}k^2\right)\phi_{1s}(\mathbf{k}) \Big/ \left[1 + 2\int \frac{\mathrm{d}\mathbf{p}}{(2\pi)^3}\frac{\left(\varepsilon_1 - \frac{1}{2}p^2\right)^2\phi_{1s}^2(\mathbf{p})}{(k^2 - p^2 \pm \mathrm{i}0)}\right]. \tag{3.74}$$

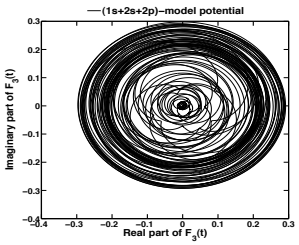

Figure 3.4: *Argand curve of component $F_3(t)$ when the laser field is switched on. Our model potential supports only $1s$, $2s$ and $2p$ states. The peak laser field intensity is $I = 3 \times 10^{14}$ W.cm^{-2}.*

Inserting now (3.73) into (3.72) we obtain

$$F_1(t)_{t>T_p} = -\mathcal{C}_{1s}(T_p)\mathrm{e}^{-\mathrm{i}\varepsilon_1 t} + \int \mathrm{d}\mathbf{k} g^-(\mathbf{k})\mathcal{C}_k^{(1s)}(T_p)\mathrm{e}^{-\mathrm{i}tk^2/2}. \tag{3.75}$$

Because all functions composing the integrand in equation (3.75) are smooth, the integral decreases quickly as a function of time. Consequently,

$$F_1(t)_{t\to\infty} \approx -\mathcal{C}_{1s}(T_p)\mathrm{e}^{-\mathrm{i}\varepsilon_1 t}. \tag{3.76}$$

In the light of this development, we observe that the Argand representation of function $F_1(t)$ at $t > T_p$ is a circle of radius $\mid \mathcal{C}_{1s}(T_p) \mid$. If the field is switch off (*i.e.* $b(t) = 0$), the circle has a unit radius (see **Figure** 3.1). In **Figure** 3.1 to **Figure** 3.4 we show the argand representations of components $F_j(t)$ as a function of time respectively when the laser field is switched off and on with peak intensity $I = 3\times10^{14}$ W.cm^{-2}. As we can see, for qualitative comparison, all these figures almost have the same shape while quantitatively, there exist marked discrepancies between these figures. A close look allows us to remark that when $b(t) = 0$, the empty circle have radius less than 1 if the separable potentials support more than one atomic states. In addition, as soon as laser field is switched on, the circles start to fill in.

3.7 Description of numerical implementation

In this section, we briefly describe the technique implemented to solve numerically the linear Volterra integral equation:

$$f(t) = g(t) + \int_0^t \mathrm{d}y\ K(t,y)f(y), \qquad 0 \le t \le T, \tag{3.77}$$

under the sufficient conditions [6, 7] that guarantee the existence and uniqueness of the continuous solution on $0 \leq t \leq T$. This method which combines a block-by-block integration technique and the Simpson interpolation formula, was developed several years ago by Linz [6]. However, its implementation in the present case, requires to rewrite the kernel $K(t, y)$ as follows:

$$K(t, y) = C_K + \sqrt{t - y}\ K^{(c)}(t, y), \tag{3.78}$$

where $K^{(c)}(t, y)$ is a smooth and continuous function and C_K a constant. As a result, equation (3.77) becomes:

$$f(t) = g(t) + C_K \int_0^t \mathrm{d}y\ f(y) + \int_0^t \mathrm{d}y\ \sqrt{t - y}\ K^{(c)}(t, y) f(y). \tag{3.79}$$

In order to implement the Linz method, we proceed as follows. We first subdivide the time interval $[0, t]$ into equal subintervals $[t_j, t_{j+2}]$ of length $2h$ with $j = 0, ..., N - 2$, N being an even number. Each subinterval $[t_j, t_{j+2}]$ is further subdivided into equal subintervals $[t_{j0}, t_{j2}]$ with $t_{jl} = t_j + lh$, $l = 0, 1, 2$. In each subinterval $[t_j, t_{j+2}]$, we use a three point (t_{j0}, t_{j1} and t_{j2}) Lagrange interpolation to approximate the well-behaved part of the integrand, namely $K^{(c)}(t, y) f(y)$. We then perform the change of variable $y = t_j + uh$ and integrate analytically over u in each subinterval $[t_j, t_{j+2}]$. Thus

$$\begin{aligned} \int_0^{t_i} \mathrm{d}y\ \sqrt{t_i - y}\ K^{(c)}(t_i, y) f(y) &= h \sum_{j=0}^{i-2} \int_{t_j}^{t_{j+2}} \mathrm{d}u\ \sqrt{t_i - (t_j + uh)} \\ &\quad \times K^{(c)}(t_i, t_j + uh) f(t_j + uh), \qquad (3.80) \\ &\approx \sum_{j=0}^{i-2} \sum_{l=0}^{2} \varpi_{jl} K^{(c)}(t_i, t_{jl}) f(t_{jl}), \qquad (3.81) \end{aligned}$$

where the integration weights ϖ_{jl}

$$\varpi_{jl} = h \int_0^2 \mathrm{d}u\ \sqrt{t_i - (t_j + uh)}\ \ell_{jl}(t_j + uh) \tag{3.82}$$

can be found explicitly if the fundamental polynomials ℓ_{jl} (defined in Appendix C) are known. After simple manipulations, we obtain:

$$\begin{aligned} \int_0^{t_i} \mathrm{d}y\ \sqrt{t_i - y}\ K^{(c)}(t_i, y) f(y) \quad &\approx \quad h^{3/2} \sum_{j=0}^{i-2} \Big[\alpha(t_i - t_j) K^{(c)}(t_i, t_j) f(t_j) \\ &+ \quad \beta(t_i - t_j) K^{(c)}(t_i, t_{j+1}) f(t_{j+1}) \\ &+ \quad \gamma(t_i - t_j) K^{(c)}(t_i, t_{j+2}) f(t_{j+2}) \Big], \qquad (3.83) \end{aligned}$$

where the functions α, β and γ are well-defined in Appendix C. The remaining integral in (3.79) can be calculated by means of the well-known Simpson's rule. In order to simplify the notations, we write $F_i \equiv f(t_i)$ and $K^{(c)}(t_i, t_j) \equiv K^{(c)}_{i,j}$. After some manipulations, we obtain the following system of equations to solve for the unknowns F_{2m+1} and F_{2m+2}:

$$\begin{aligned} F_{2m+1} &= g_{2m+1} + hC_K \sum_{i=0}^{2m} \varpi_i F_i + \frac{1}{6} hC_K \left[F_{2m} + 4F_{2m+1/2} + F_{2m+1}\right] \\ &+ h^{3/2} \sum_{l=0}^{m-1} \Big[\alpha(2m+1-2l) K^{(c)}_{2m+1,2l} F_{2l} \\ &+ \beta(2m+1-2l) K^{(c)}_{2m+1,2l+1} F_{2l+1} + \gamma(2m+1-2l) K^{(c)}_{2m+1,2l+2} F_{2l+2}\Big] \\ &+ \left(\frac{1}{2}h\right)^{3/2} \Big[\alpha(2) K^{(c)}_{2m+1,2m} F_{2m} + \beta(2) K^{(c)}_{2m+1,2m+1/2} F_{2m+1/2} \\ &+ \gamma(2) K^{(c)}_{2m+1,2m+1} F_{2m+1}\Big], \end{aligned} \tag{3.84}$$

$$\begin{aligned} F_{2m+2} &= g_{2m+2} + hC_K \sum_{i=0}^{2m} \varpi_i F_i + \frac{1}{3} hC_K \left[F_{2m} + 4F_{2m+1} + F_{2m+2}\right] \\ &+ h^{3/2} \sum_{l=0}^{m-1} \Big[\alpha(2m+2-2l) K^{(c)}_{2m+2,2l} F_{2l} \\ &+ \beta(2m+2-2l) K^{(c)}_{2m+2,2l+1} F_{2l+1} + \gamma(2m+2-2l) K^{(c)}_{2m+2,2l+2} F_{2l+2}\Big] \\ &+ h^{3/2} \Big[\alpha(2) K^{(c)}_{2m+2,2m} F_{2m} + \beta(2) K^{(c)}_{2m+2,2m+1} F_{2m+1} \\ &+ \gamma(2) K^{(c)}_{2m+2,2m+2} F_{2m+2}\Big], \end{aligned} \tag{3.85}$$

where $\varpi_i = \frac{1}{3}\{1, 4, 2, \cdots, 2, 4, 1\}$ and $t_{2m+1/2} = t_{2m} + \frac{1}{2}h$. To deal with the unknown value $F_{2m+1/2}$, we approximate it by quadratic interpolation, using values $F_{2m}, F_{2m+1}, F_{2m+2}$, that is, we write

$$F_{2m+1/2} \simeq \frac{3}{8} F_{2m} + \frac{3}{4} F_{2m+1} - \frac{1}{8} F_{2m+2}.$$

Starting with $F_0 = g_0$, we solve equations (3.84) and (3.85) successively for blocks of values $(F_1, F_2), (F_3, F_4), \cdots$, using a standard BLAS and LAPACK library programs.

3.8 Validation of the model

In order to validate our model and check the pertinence of the present choice of the separable potentials, we consider in this section, several physical situations

where the electron dynamics in strong oscillating fields are well known. In all our calculations, we take into account the three bound states $1s$, $2s$ and $2p$ and assume that the model atom is initially in its ground state. Accurate numerical tools to propagate the exact wave function and to calculate the electron spectra have been performed, using a block-by-block integration technique. The approximation applied in our calculations is the dipole approximation, which is well applicable, as was already mentioned at the end of previous Chapter. The TDSE results are thus fully non perturbative.

3.8.1 Ionization yield versus peak field intensity

We first calculate by means of equations (3.59) and (3.67), the total probability of ionization of our model atom as a function of the peak field intensity. We consider the case of a 8 optical cycle pulse of 0.6 a.u. photon energy. The results are presented in **Figure** 3.5. At low peak field intensity, only one photon is necessary to ionize the atom. According to the lowest order of the perturbation theory, the ionization probability should be proportional to the peak intensity giving a straight line on a *log-log* plot. At low peak intensity, our results for the probability of ionization coincides with the straight dashed line of slope exactly one. For higher intensities, above 3×10^{14} W/cm^2, multiphoton transitions occur before reaching an intensity regime where saturation takes place and non perturbative effects are important. As a matter of fact, non perturbative effects become important when the ponderomotive potential U_p exceeds the photon energy ω. In **Figure** 3.5, the green vertical dashed line indicates the value of the peak intensity, namely 3×10^{16} W/cm^2 that corresponds to $U_p = \omega$.

3.8.2 Above-threshold ionization spectrum

In **Figure** 3.6, we show the spectrum resulting from the interaction of our model atom with a 8 optical cycle pulse of 10^{15} W/cm^2 for the peak intensity and 1 a.u. for the photon energy. The spectrum exhibits several ATI peaks separated by the photon energy as expected in equation (2.21). Among the ATI peaks, the first one is by far the dominant one. It is due to the absorption of a single photon. The satellite peaks on both sides of the first ATI peak result from the fact that the density of probability is proportional to the square of the Fourier transform of the sine square pulse (see equation (2.60)).

3.8.3 Rabi oscillations and Autler-Townes duplets

Now we consider resonant two-photon ionization of atomic hydrogen starting from its ground state. Theoretical models in which two discrete states $\mid a\rangle$ and $\mid b\rangle$ are coupled to the continuum have been treated by many authors. See for example References [8, 9, 10, 11, 12, 13, 14, 15]. In the case where laser

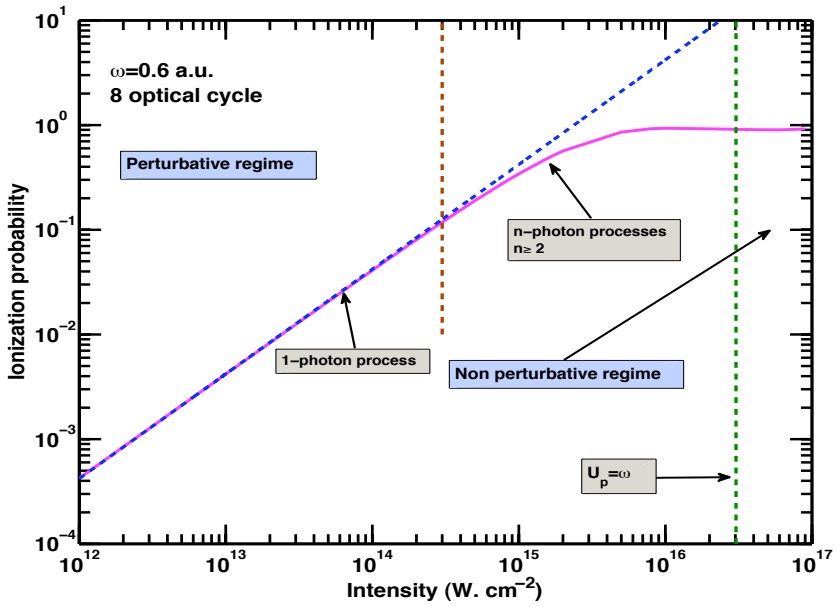

Figure 3.5: *Probability of ionization of our model atom initially in the* $1s$ *state, as a function of the peak field intensity. The total duration of the pulse is* 8 *optical cycle and the photon energy is* 0.6 a.u.. *The blue dashed straight line has a slope exactly equal to* 1. *The vertical brown dashed line delimits the intensity region where one-photon processes dominate. The vertical green dashed line corresponds to an intensity of* 3×10^{16} W/cm^2 *for which* $U_p = \omega$ *in* a.u.. *For larger peak intensities, the interaction of the atom with the field is predominantly non perturbative.*

pulse frequency ω corresponds exactly to the $\mid a\rangle \rightarrow \mid b\rangle$ transition frequency ΔE, the coupling of the external field to the atom is thus resonant. Therefore, Rabi oscillations and the Autler-Townes effect are expected to manifest in the time evolution of the atomic state populations and in the ATI spectrum respectively. The electron energy spectra are found to be profoundly altered by the resonant coupling. The electron spectra display duplets due to the AC Stark splitting of the bound-bound resonance, namely the Autler-Townes [16] effects. In this case where only two states play a significant role, it makes sense to compare the results of our model, both qualitatively and quantitatively to those obtained by solving the TDSE with no approximation on the Coulomb potential.

Girju *et al.* [17] discussed an analytical model, capable of describing the main qualitative features in the photoelectron spectra and compared their model

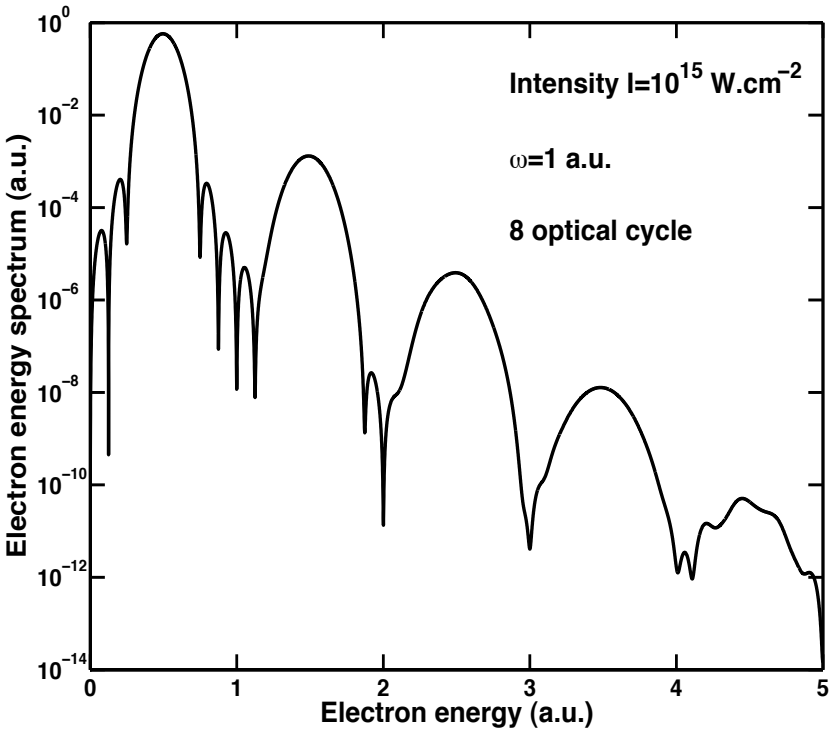

Figure 3.6: *Electron energy spectrum resulting from the interaction of our model atom, initially in the* 1s *state, with a* 8 *optical cycle pulse. The peak intensity is equal to* 10^{15} W/cm^2 *and the photon energy, to* 1 a.u..

results to those obtained from the solution of the TDSE in the configuration space (see **Figures** 3.7 and 3.9 for illustration). **Figure** 3.8 shows our corresponding results. Although all the results are in good qualitative agreement as far as the peak positions are concerned, the relative magnitudes of the two peaks are different in both model calculations and the r-space TDSE. This confirms the observations made in reference [18].

The quantitative disagreement between the model calculations (their and ours) and r-space TDSE results is most likely linked to the description of the continuum states (which differ from pure Coulomb states) in both models: pure plane waves in Girju's model and exact continuum state associated with our model potential in our case. It is known that the plane wave approximation plagues the strong field approach, despite several attempts to include Coulomb effects in the latter [19, 20]. Under several simplifying assumptions [17], It has

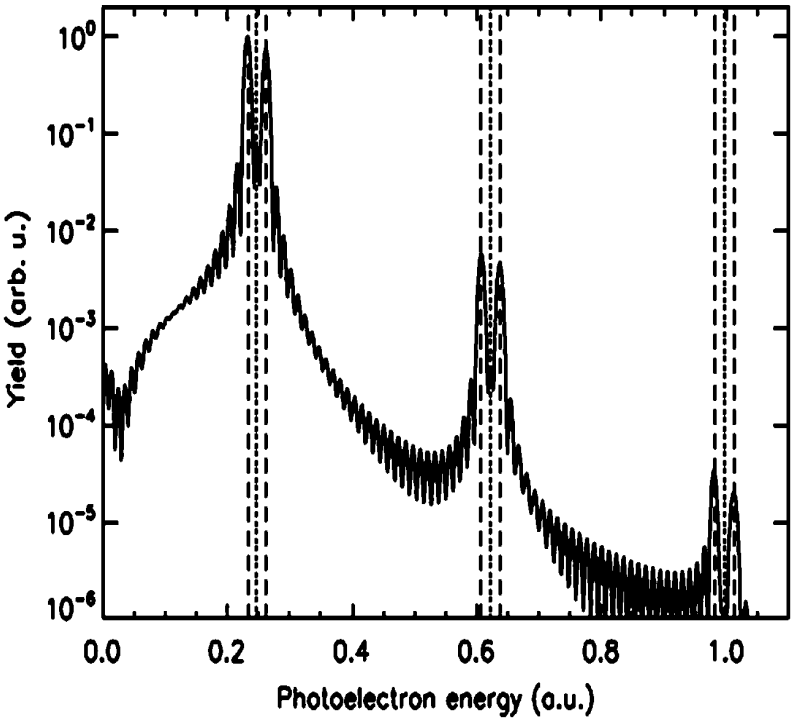

Figure 3.7: *Electron energy spectrum for* $\mathcal{E}_0 = 0.04$ a.u. *at resonance* ($\omega = 0.375$ a.u.*) obtained with a perturbative approach. A rectangular* 32*-cycle pulse is used. The dashed vertical lines indicate the positions of the two Autler-Townes peaks, and their centre by the dotted vertical lines. From Girju et al.[17]*

been shown from a semi-classical Rabi model that, close to resonance and for modest ionization, one may obtain the well-known unperturbed Rabi-flopping dynamics [21] with the generalized Rabi frequency defined as (in a.u.):

$$\Omega(\omega) = \sqrt{\Omega_{Rabi}^2 + \Delta^2(\omega)}, \qquad \Delta(\omega) = E_b - E_a - \omega = \Delta E - \omega, \tag{3.86}$$

where the "*detuning*" Δ is a measure of how far the light is *off* resonance with the transition, ΔE the unperturbed level spacing and the unperturbed Rabi frequency at the resonance given in the length gauge by

$$\Omega_{Rabi} = \mathcal{E}_0 \langle \psi_b \mid \mathbf{d} \cdot \mathbf{e} \mid \psi_a \rangle, \tag{3.87}$$

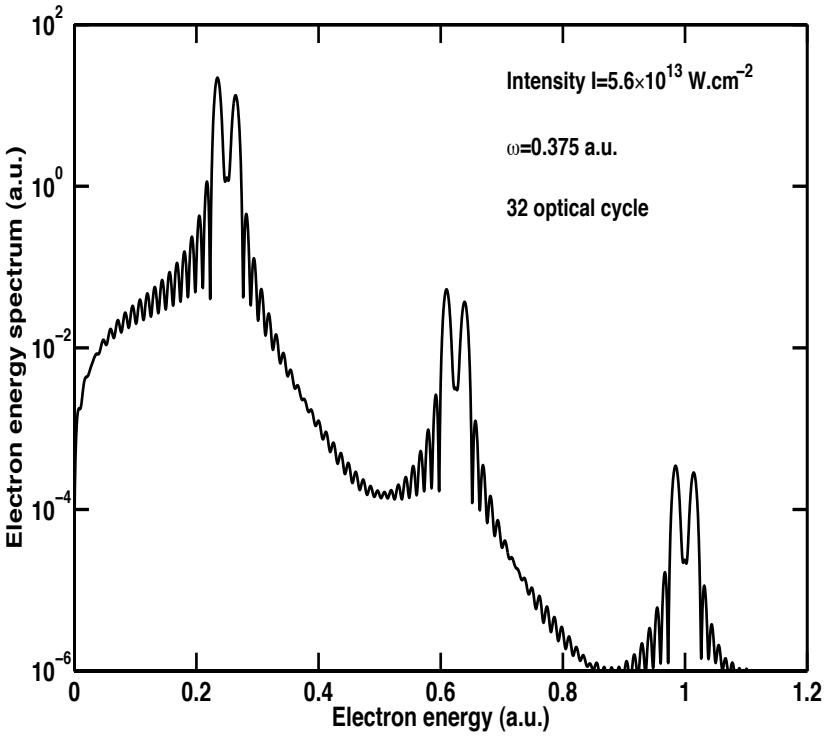

Figure 3.8: *Electron energy spectrum for* $\mathcal{E}_0 = 0.04$ a.u. *at resonance* ($\omega = 0.375$ a.u.*) obtained from our model atom. The pulse has a trapezoidal shape with a 1 optical cycle linear turn on and off and a 30 optical cycle flat top.*

and in the velocity gauge by

$$\Omega_{Rabi} = A_0 \langle \psi_b \mid \boldsymbol{\nabla} \cdot \mathbf{e} \mid \psi_a \rangle, \tag{3.88}$$

with $\mathbf{d}$, $\mathcal{E}_0$ and A_0 denoting the electric dipole operator of a one-electron atom and peak field amplitudes respectively, $\mathbf{e}$ the polarization vector of field.
According to the above simplifying theory, in the weak-field limit and at the resonance $\Delta(\omega) = 0$, series of pair of peaks (a so-called Autler-Townes duplet) are expected at the positions [17]

$$E_{kin} = E_b + n\omega \pm \frac{\Omega_{Rabi}}{2}, \quad n = 1, 2, ... \tag{3.89}$$

in the photoelectron spectra.
It is important to stress out that this perturbative approach works as long

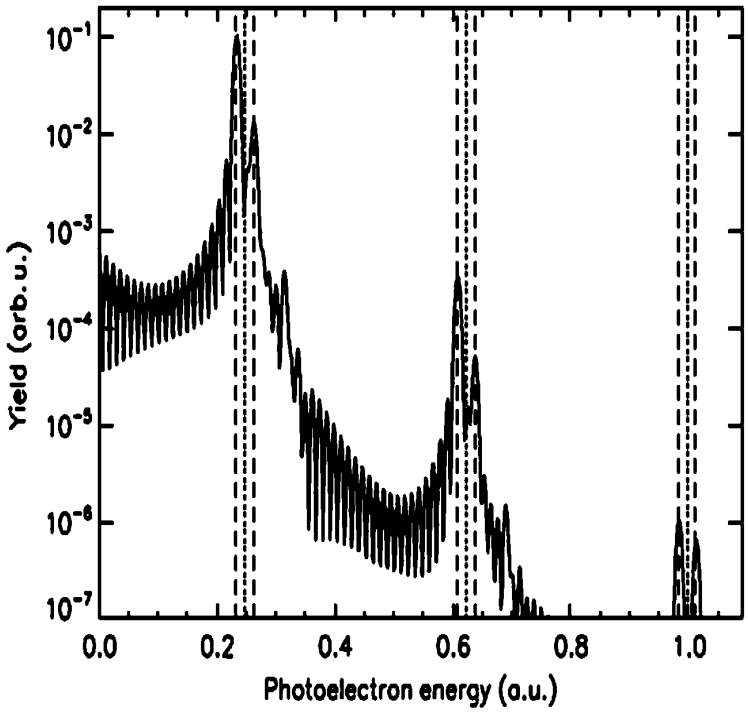

Figure 3.9: *Electron energy spectrum for* $\mathcal{E}_0 = 0.04$ a.u. *at resonance* ($\omega = 0.375$ a.u.*) obtained from TDSE in r-space. A trapezoidal* 32*-cycle pulse (up and down ramping over* 1 *cycle) is used. From Girju et al.[17]*

as ionization and AC Stark effect do not influence the bound state dynamics significantly. Otherwise, they should be taken into account in any theoretical calculations. Let us now consider the case where our model atom interacts with a laser pulse whose frequency of 0.375 a.u. is equal to the $1s$-$2p$ transition frequency ΔE. In such a case, the coupling of the external field to the atom is resonant. We assume that the laser pulse is turned on and off linearly over 2 optical cycles and has a flat top of 36 optical cycles. We calculated $P(t)$ according to equations (3.67) using $D(E_k, t)$ and the populations $\mathcal{C}_{js}(t)$ and $\mathcal{C}_{2p,m}(t)$. For hydrogen-like ions of charge Z (with $Z = 1$ in the present case), the Rabi frequency at resonance is given by

$$\Omega_{Rabi} = \frac{256}{243}\frac{\mathcal{E}_0}{\sqrt{2}Z} = \frac{256}{243}\frac{1}{\sqrt{2}Z}\sqrt{\frac{I}{I_a}}. \tag{3.90}$$

Figure 3.10 shows the electron energy spectrum resulting from our model

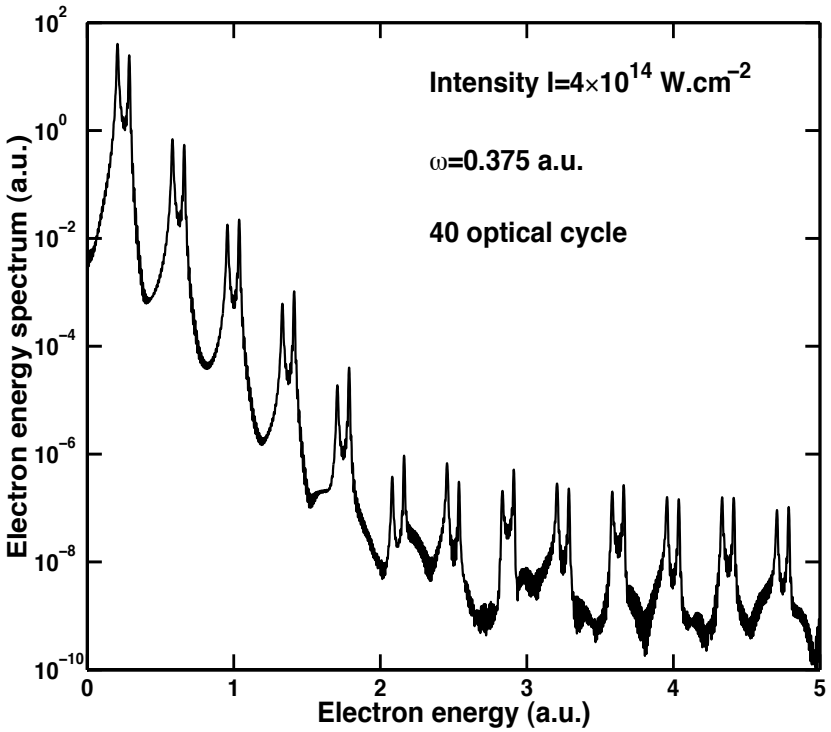

Figure 3.10: *Electron energy spectrum resulting from the interaction of our model atom, initially in the* $1s$ *state, with a pulse whose peak electric field is equal to* $\mathcal{E}_0 = 0.107$ a.u. *and the frequency equals to* $\omega = 0.375$ a.u.. *The pulse has a trapezoidal shape with a* 2 *optical cycle up and down ramping and a* 36 *optical cycle flat top.*

atom, initially in its ground state, and interacting with a pulse whose peak electric field is equal to $\mathcal{E}_0 = 0.107$ a.u. and the frequency equals to $\omega = 0.375$ a.u.. During such a pulse the atom undergoes $\simeq 4.7$ Rabi cycles. The electron energy spectrum exhibits the well-known Autler-Townes duplets (the splitting of each ATI peak) at the positions that was expected in equation (3.89). This Autler-Townes effect is the evidence of the coupling of both the $2s$ and $2p$ state to the continuum.

Let us investigate now in more detail how the electron spectra behave at resonance with the increase of the laser strength, up to $\mathcal{E}_0 = 0.170$ a.u. which corresponds to an intensity 10^{15} W/cm^2. In **Figures** 3.11 and 3.12, we show the first ATI peaks for the same laser parameters as before, but for various peak field intensities. These **Figures** summarize the most important phenom-

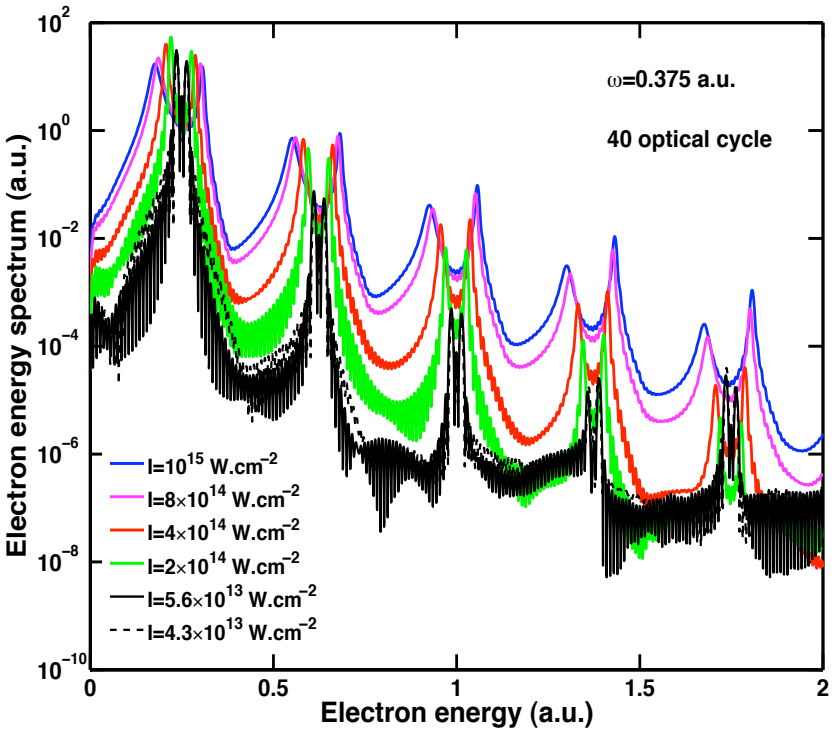

Figure 3.11: *Electron energy spectra resulting from the interaction of our model atom, initially in the* 1s *state, with laser pulses at resonance* 0.375 a.u. *photon energy. All pulses have the same trapezoidal shape as in Figure 3.10 but various peak field intensities (given in the lower left part of the graphs) are considered. Color curves are drawn to guide the eye.*

ena observed. We understand by "resonance" a constant laser frequency of $\omega = 0.375$ a.u., hereafter called as "true" resonance frequency. It is only valid for negligible AC Stark shifts and ionization *i.e.* $\Delta E_{1s,2p} \simeq 0 \simeq \Gamma_{1s,2p}$. It is expected and obvious that the AC Stark effect pushes the system towards a positive detuning $\Delta(\omega) \rightarrow \tilde{\Delta}(\omega) = \Delta E - \omega + \Delta E_{2p} - \Delta E_{1s} > 0$ knowing that the AC Stark shift ΔE_{1s} of the 1s state is negative while the 2p state is shifted upwards by $\Delta E_{2p} \simeq U_p(\omega)$. Thus, as the peak intensity increases, the subpeaks of the Autler-Townes duplets move apart - the separation of the two peaks within the nth Autler-Townes duplet increases. This of course is expected since the dynamic AC Stark effect leads to an increasing Rabi frequency. On the other hand, ionization losses rapidly damp (this is due to the coupling of both the 2s and 2p state to the continuum which is fully taken into

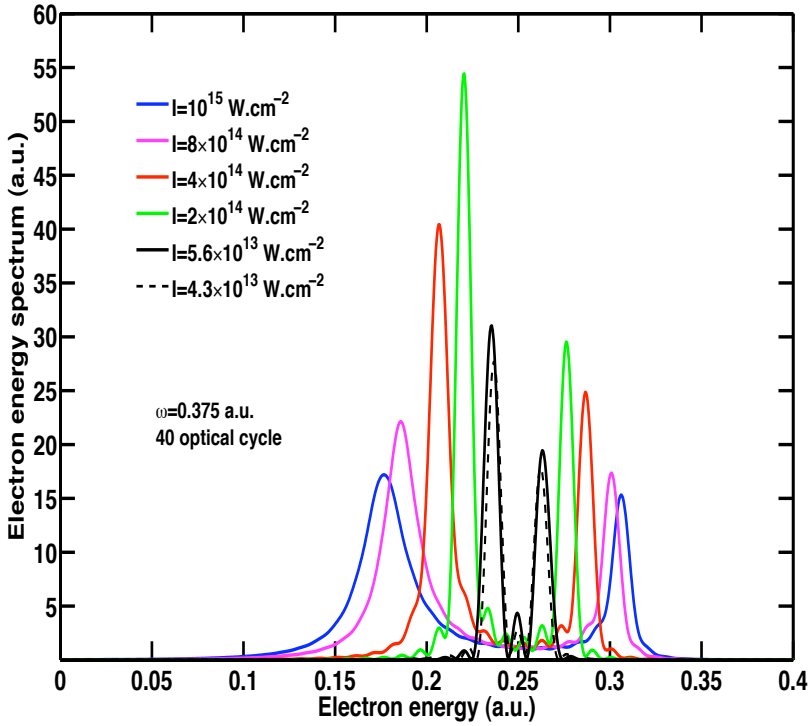

Figure 3.12: *First ATI peak of the electron energy spectra shown in Zoom in linearly scaled electron energy spectra resulting from the interaction of our model atom, initially in the* $1s$ *state, with the same laser pulse as in Figure 3.11. Color curves are drawn to guide the eye.*

account in our model) the ground state probability. *Both AC Stark shifts of all bound and continuum states as well as ionization are implicitly included in the TDSE solution.*

Given the resonant coupling of the $1s$ state to the $2p$ state, we expect Rabi oscillations of the corresponding populations of these "bare" atomic states. When cross examining the bound state populations $\mid \mathcal{C}_{1s}(t) \mid^2$ and $\sum_{m=-1}^{+1} \mid \mathcal{C}_{2p,m}(t) \mid^2$ versus time (in optical cycle) for $\mathcal{E}_0 = 0.076$ a.u., 0.107 a.u. and 0.170 a.u. displayed in **Figures** 3.13 and 3.14 it becomes apparent that the Rabi frequency increases with increasing field strength, whereas ionization leads to losses. The ground state population then decreases due to ionization and therefore does not take again the value 1. In the case of strongly damped oscillation ($I = 10^{15}$ W.cm^{-2}), ionization clearly dominates the bound state dynamics. We have checked that the oscillation frequency of the population

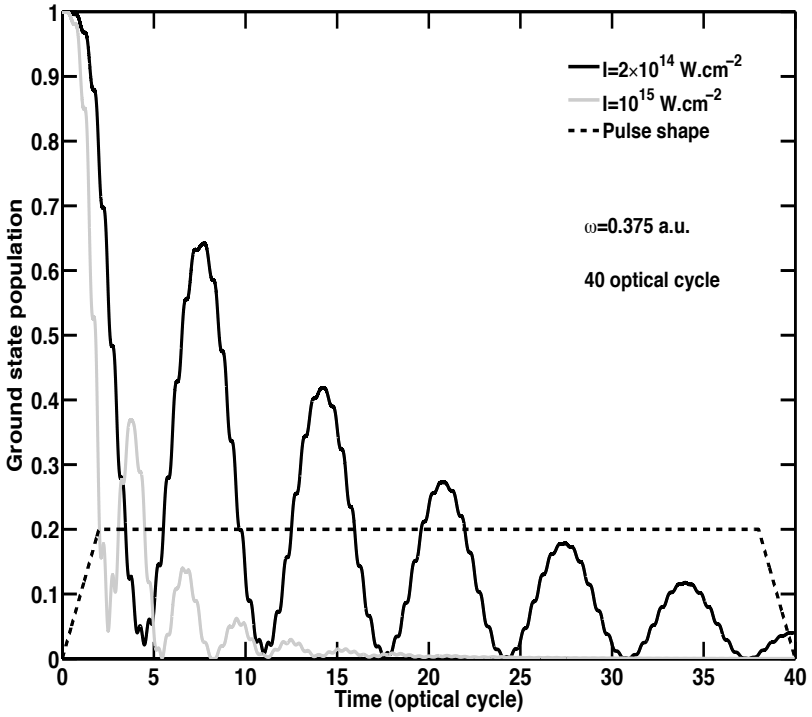

Figure 3.13: *Ground state populations versus time (in optical cycle) for our model atom, interacting with a laser pulse whose frequency is equal to* 0.375 a.u.. *The pulse is turned on and off linearly over* 2 *optical cycles and has a flat top of* 36 *optical cycles. The pulse shape (dashed black line) is shown in arbitrary units. The peak intensity taking the values* 2×10^{14} W/cm^2 *and* 10^{15} W/cm^2 *respectively.*

transfer between the $1s$ and the $2p$ state is exactly equal to the separation of the two subpeaks in an Autler-Townes duplet in the electron energy spectra as long as $\Gamma_{1s,2p} \ll \Omega_{Rabi}$. Clearly, the Rabi oscillations occur during the time the field intensity is constant and equals to the peak intensity. We can therefore estimate the corresponding Rabi frequency. We obtain $\Omega_{\text{Rabi}} = 0.08$ a.u. for the particular case of $\mathcal{E}_0 = 0.107$ a.u.. In the present case, we find from equation (3.90) that $\Omega_{\text{Rabi}} = 0.0795$ a.u. which is in very good agreement with the estimated value.

Let's take a close look at the **Figures** 3.11 and 3.12 once more. Another feature that we observe in the electron energy spectra is that: - the left subpeak

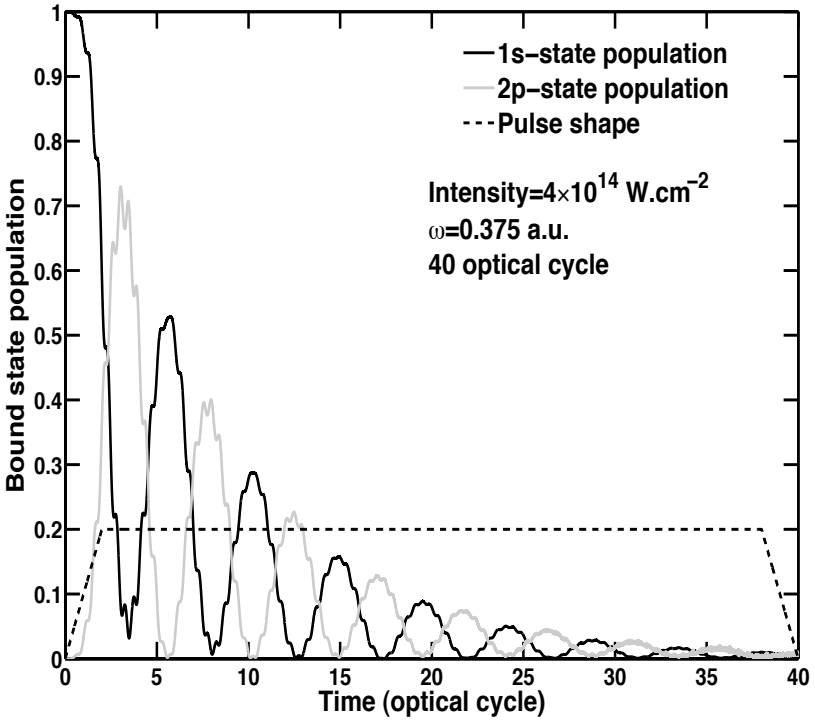

Figure 3.14: *Rabi oscillations of the* $1s$ *and* $2p$ *state populations as a function of time. Our model atom which is assumed initially in the* $1s$ *state, interacts with a laser pulse whose frequency is equal to the* $1s$-$2p$ *transition frequency. The pulse is turned on and off linearly over* 2 *optical cycles and has a flat top of* 36 *optical cycles. The pulse shape (dashed black line) is shown in arbitrary units. The peak intensity is equal to* 4×10^{14} W/cm^2.

of each Autler-Townes duplet gets broader as the field amplitude increases in contrast to the right Autler-Townes-subpeak which remains narrow and shifts less or whose width hardly changes. This effect is clearly depicted in **Figure** 3.12 where the first Autler-Townes doublet is presented on a linear scale for various peak intensities. This latter result has been thoroughly analyzed and confirmed via the Floquet theory [22] in terms of complex Floquet energies, that give the exact AC Stark shifts and ionization rates for laser pulses of infinite duration [17].

Within a quantized field picture in which we assume for the time being that the atom-field interaction is switched off, the dressed state energy spectrum is

made of a ladder of pairs of states $|1s,(n+1)\omega\rangle$ and $|2p,n\omega\rangle$ of the atom-field system. n gives the number of photons involved at each step of the ladder. If the field frequency is exactly on resonance with the atomic transition frequency, these unperturbed dressed states are degenerate in energy. If we now switch on the atom-field interaction, the degeneracy is lifted up leading to pairs of dressed states separated in energy by the Rabi frequency. These dressed states are in fact linear superpositions of the unperturbed $|1s,(n+1)\omega\rangle$ and $|2p,n\omega\rangle$ states. It is the coupling of these dressed states to the atomic continuum that leads to the Autler-Townes effect, *i.e.* to the splitting of each ATI peak into a doublet. The width of the subpeaks of each doublet depends on the coupling strength of the dressed states to the continuum or in other words, on the ionization rate of each of the dressed states. The results presented in **Figures** 3.11 and 3.12 suggest that for each pair of dressed state energy levels, the rate of ionization of the lower state is higher than the one of the upper state. In order to check that this result is not an artefact of the present model, we have performed Floquet calculations in the case of atomic hydrogen. These calculations have been obtained by means of a representation in a basis of Sturmian functions of the Floquet operator associated with the Hamiltonian of atomic hydrogen interacting with a periodic field of fixed frequency ω and intensity I in the velocity gauge [23, 24]. By complex rotating the Hamiltonian, it is possible to identify the resonances of the system with the complex eigenvalues E of the rotated Floquet operator: the energy is given by $\mathcal{R}e(E)$ while the decay rate is $-2\mathcal{I}m(E)$ [23, 24, 25]. The results are presented in **Figure** 3.15 for the same intensity as before, namely 4×10^{14} W/cm^2. This figure is made of three panels. In the upper panel, we show the energy of the relevant Floquet states. The second panel shows the corresponding decay rates and the lower panel, the overlaps of these Floquet states with the bare atomic states. In the three panels, the Floquet states associated with the red full circles exhibit the largest overlap and can be identified with the $|1s\rangle$ state. The blue circles correspond to the second largest overlap with the $|1s\rangle$ state and to the first largest overlap with the $|2p\rangle$ state. Note that above $\omega = 0.415$ a.u., there is a third state whose overlap with the $|1s\rangle$ state becomes relevant (larger than 0.1). This Floquet state indicates that in the pure Coulomb states, the influence of atomic states that are not resonantly coupled to the ground state becomes important. In the upper panel of **Figure** 3.15, we observe an avoided crossing of the Floquet energies at a frequency slightly higher than the transition frequency at 0.375 a.u.. This explains why for $\omega = 0.375$ a.u., the contribution of the bare $|1s\rangle$ and $|2p\rangle$ atomic states to the dressed or Floquet states is not symmetric (see the lower panel of **Figure** 3.15) as it should be exactly at resonance. The energies of the dressed states with larger overlap with the $|1s\rangle$ and $|2p\rangle$ states at $\omega = 0.375$ a.u. are $E_{1s} = -0.5472$ a.u. and $E_{2p} = -0.4716$ a.u.. Due to the periodicity of the Floquet spectrum the Floquet states associated with

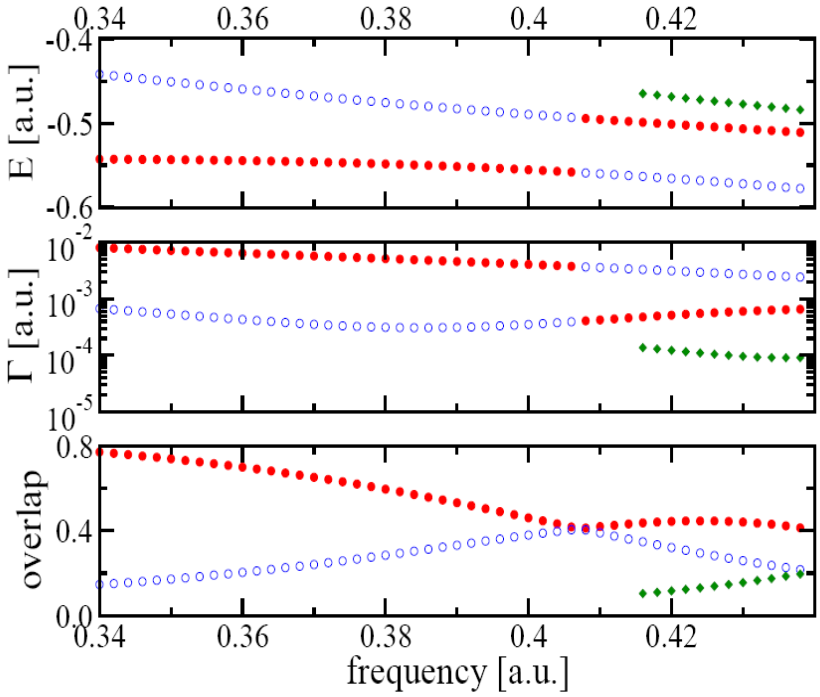

Figure 3.15: *Real parts of the complex Floquet energies as a function of the frequency ω for a laser peak intensity of 4×10^{14} W/cm^2 (upper panel), the corresponding ionization rates (middle panel) and the overlaps between these Floquet states and the "bare" atomic states $|1s\rangle$ and $|2p\rangle$ (lower panel). The red full circles correspond to a Floquet state that has the largest overlap with the $|1s\rangle$ state while the blue open circles correspond to the second largest overlap with the $|1s\rangle$ state and the first largest overlap with the $|2p\rangle$ state.*

the energies E and $E + k\omega$, k some integer number, correspond to the same physical state. The positions of the left and right subpeaks in **Figure** 3.12 are quite close to $E_{1s} + 2\omega = 0.2028$ and $E_{2p} + 2\omega = 0.2784$, respectively. This indicates that the $|1s\rangle$ ($|2p\rangle$) state is more dominant in the left (right) subpeak. Finally, at $\omega = 0.375$ a.u., we see in the second panel that the ionization rates of both Floquet states differ by one order of magnitude. Consequently, it is expected that left subpeak of the Autler-Townes doublet is broader than the right one. These results confirm those of Girju *et al.* [17] and show that in the present physical situation, the predictions of our model are qualitatively

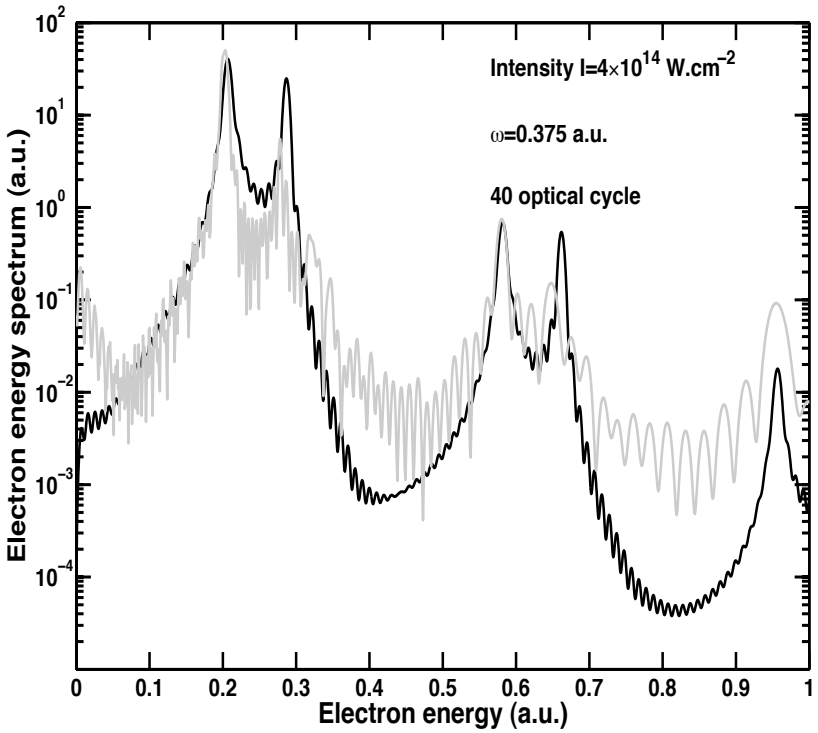

Figure 3.16: *Electron energy spectrum resulting from the interaction of our model atom initially in the* $|1s\rangle$ *with a laser pulse of* 0.375 a.u. *photon frequency and of* 4×10^{14} W/cm^2 *peak intensity. The laser pulse shape is trapezoidal with a* 2 *cycle linear turn on and off and with a flat top of* 36 *optical cycles. The gray line is the result obtained by solving numerically the time-dependent Schrödinger equation while the black line is the result obtained with our model.*

correct. Then, *AC Stark effect and ionization lead to a pronounced shift and broadening of the left Autler-Townes-peak at high intensities.*

In **Figure** 3.16, we compare the first ATI peaks obtained with our model, to those calculated by solving numerically the TDSE for atomic hydrogen [26]. The agreement is quantitatively relatively good as expected since mainly two states, $|1s\rangle$ and $|2p\rangle$ are dominating the dynamics.

Finally in **Figure** 3.17 we present the angular distribution of the ejected electron, namely $p_n \mid \Phi(p_z, p_n) \mid^2$ for laser peak intensity $I = 4 \times 10^{14}$ W/cm^2, obtained in the framework of our separable model potential. The horizontal axis in the plot is the momentum parallel to the laser field polarization and

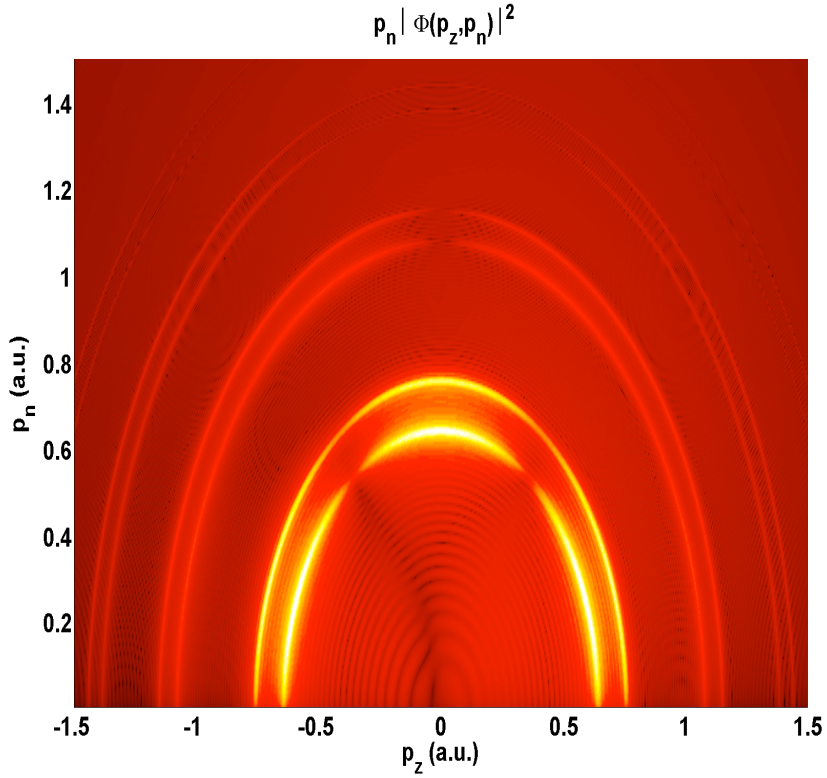

Figure 3.17: *Angular distribution of the probability density at the end of the laser pulse, resulting from the interaction of our model atom initially in the* $|1s\rangle$ *with a laser pulse of* 0.375 a.u. *photon frequency and of* 4×10^{14} W/cm^2 *peak intensity. The laser pulse shape is trapezoidal with a* 2 *cycle linear turn on and off and with a flat top of* 36 *optical cycles.*

the vertical axis is the perpendicular momentum defined by $p_n = \sqrt{p_x^2 + p_y^2}$. The splitting of ATI peaks (the Autler-Townes doublets) clearly appear here as pair of circles in the momentum distribution, each with alternating energy (3.89). It can be seen that the ionization probability is not constant on a given circle, but has maximum and minimum. One sees rings of constant energy which are easily identified with the ATI subpeaks in the energy spectrum (see **Figure** 3.10). As seen from **Figure** 3.17, the first pair of circles corresponding to the first ATI subpeaks are the most pronounced or dominant one, the next pair of circles are still visible and finally the remaining pair of circles become hardly visible.

3.9 Conclusion

In this Chapter, we considered the ionization of atomic hydrogen by an intense infrared pulse. We solved the corresponding TDSE in momentum space when the kernel of the non local Coulomb potential is replaced by a finite sum of separable potentials, each of them supporting one bound state of atomic hydrogen. Such approach bears some resemblance to a spectral method. However, instead of the usual expansion of the solution of the TDSE in terms of a finite set of L^2-integrable functions, it is the potential kernel which is now expanded in terms of separable potentials. The choice of these separable potentials however is not unique and requires attention to avoid any unphysical effects. This approach has significant advantages when it is compared to the well established SFA. By contrast to the SFA, it provides a rigorous solution for the electron wave packet, it includes more than one bound states, it takes fully into account the continuum-continuum transitions and, more important, it is fully gauge invariant. In addition, we have shown that this model allows to reduce the 3-dimensional Schrödinger equation to a small system of coupled 1-dimensional linear Volterra integral equations, the numerical solution of which is relatively easy to obtain. In order to validate the model, we have checked that in the perturbative regime, when the ponderomotive potential is smaller than the laser frequency ($U_p \ll \omega$), the corresponding behaviors of the ionization yield and the ATI spectrum are well reproduced. Furthermore, we have shown that the resonant coupling of the $1s$ to the $2p$ states leads to Rabi oscillations of the corresponding populations at the correct frequency as well as to a Rabi splitting of the ATI peaks.

The main objective of the present contribution is to provide a theoretical tool to understand the actual role of the atomic potential in the intensity regime where tunnel ionization is supposed to take place and where the experimental data for the first ATI peaks are in contradiction with the theoretical predictions based on the SFA model. This problem will be the subject of the next Chapter.

Bibliography

[1] H. M. Tetchou Nganso, S. Giraud, B. Piraux, Yu. V. Popov and M. G. Kwato Njock, *J. Elect. Spect. Rel. Phen.* **161**, 178 (2007).

[2] S. Giraud, B. Piraux, Yu. V. Popov, and H. M. Tetchou Nganso, in *Proc. SPIE "Saratov Fall Meeting - SFM'05: Laser Physics and Photonics, Spectroscopy and Molecular Modelling VI"*, edited by V. L. Derbov, L. A. Melnikov, and L. M. Babkov, **6165**, 61650D-1 (2006).

[3] V. Bargmann, *Rev. Mod. Phys* **21**, 488 (1949).

[4] S. Weinberg, *Phys. Rev.* **131**, 440 (1963).

[5] B. H. Bransden and C. J. Joachain, *Quantum Mechanics*, 2nd edition (Pearson Education Ltd, England 2000).

[6] P. Linz *Analytical and numerical methods for Volterra equations* (SIAM, Philadelphia 1985).

[7] F. de Hoog F and R. Weiss *Implicit Runge-Kutta methods for second kind Volterra integral equations, Numer. Math.* **23** 199 (1975).

[8] B. L. Beers and L. Jr. Armstrong, *Phys. Rev. A* **12**, 2447 (1975).

[9] M. Crance and S. Feneuille, *Phys. Rev. A* **16**, 1587 (1977).

[10] J. R. Ackerhalt, *Phys. Rev. A* **17**, 293 (1978).

[11] P. L. Knight, *J. Phys. B: At. Mol. Phys.* **12**, 3297 (1979).

[12] E. J. Austin, *J. Phys. B: At. Mol. Phys.* **12**, 4045 (1979).

[13] S. Geltman, *J. Phys. B: At. Mol. Phys.* **13**, 115 (1980).

[14] F. H. M. Faisal and J. V. Moloney, *J. Phys. B: At. Mol. Phys.* **14**, 3603 (1981).
F. H. M. Faisal, *Theory of Multiphoton Processes* (Plenum, New York 1087).

[15] M. H. Mittleman, *J. Phys. B: At. Mol. Phys.* **17**, L351 (1984).

[16] S. H. Autler and C. H. Townes, *Phys. Rev.* **100**, 703 (1955).

[17] M. G. Girgu, K. Hristov, O. Kidun, and D. Bauer, *J. Phys. B: At. Mol. Opt. Phys.* **40**, 4165 (2007).

[18] K. J. LaGattuta, *Phys. Rev. A* **47**, 1560 (1993).

[19] O. Smirnova, M. Spanner and M. Ivanov, *J. Phys. B: At. Mol. Opt. Phys.* **39**, S307 (2006).

[20] F. H. M. Faisal and G. Schlegel, *J. Mod. Opt.* **53**, 207 (2006).

[21] M. O. Scully and M. S. Zubairy, *Quantum Optics* (Cambridge University Press, Cambridge 1997) pp 145-92.

[22] R. M. Potvliege, *Comput. Phys. Commun.* **114**, 42 (1998).

[23] R. Potvliege and R. Shakeshaft, *Phys. Rev. A* **38**, 1098 (1988).

[24] A. Buchleitner, D. Delande, and J. C. Gay, *J. Opt. Soc. Am. B* **12**, 505 (1994).

[25] J. Madroñero and A. Buchleitner, *Phys. Rev. A* **77**, 053402 (2008).

[26] J. Madroñero and B. Piraux, *Phys. Rev. A* **80**, 033409 (2009).

Chapter 4

Detailed Study of the ATI Spectra within our Model Atom

"Le tact dans l'audace, c'est de savoir jusqu'où on peut aller trop loin."
Jean Cocteau.

4.1 Introduction

One of the basic questions, which still disturbs a comprehensive understanding of the ionization dynamics, concerns the mechanism of ejection of electron in the low energy pattern (whose energy is less than twice the ponderomotive potential $2U_p$) of the spectrum. For this purpose, we use the formalism developed in the preceding Chapter to conduct a detailed study of ATI spectra in high and low frequency regimes. The influences of laser parameters such as intensity, duration and the absolute phase of the pulse will also be analyzed.

The aim of this Chapter is as follows. Firstly, in the low-frequency regime, we want to analyze the role of the Coulomb potential and consequently the atomic structure in the dynamics of the ionization process, and particularly in the strong field limit by means of our model atom. Now that few-cycle pulses have become available with tunable CEPs, secondly, it is of interest to explore the kinds of CEP-induced effects on angular distribution of photoelectrons and energy distributions that are possible. In particular, analysis of asymmetric photoelectron distributions resulting from ionization by long and few-cycle infrared laser pulses will be discussed. Finally we return to the interesting problem of the emission of highly energetic electrons at resonance in the interaction of our model atom with a strong laser field in high frequency regime. For the sake of convenience, all graphs belonging to this **Chapter** 4 have been given at the end of the Chapter in two new Sections.

4.2 Interaction of the model atom with strong low-frequency fields

Our model actually reproduces all well known features of the ATI spectra as well as the ionization probability. There are however some interesting and unexpected observations requiring a deeper analysis. We discuss these features in the following Sections.

4.2.1 Probability density as a function of time and p_z

It has been shown that in a range of intensity close to the saturation intensity, neither the Keldysh strong-field approximation nor the A. D. K theory was adequate to account for the ionization rate obtained for hydrogen [1]. It is then necessary to define clearly the range of intensities $10^{14} \leq I \leq 10^{15}$ W.cm^{-2} to which we refer.

Definitions

We adopt in this thesis the following definitions.

- According to R. Shakeshaft *et al.* [2], the *saturation intensity* (I_{sat}) is defined as the value for which the ionization is complete in less than a laser period. For hydrogen in its ground state $1s$, the authors found $\mathcal{E}_{sat} \approx 0.159$ a.u. $\Rightarrow I_{sat} \approx 7.9 \times 10^{14}$ W.cm^{-2}. Numerical solution of TDSE has allowed to obtain an ionization of about 90% in the center of the interaction, a half of period after that I_{sat} has been reached [1]. This numerical result is in fairly good agreement with the value $I_{sat} \approx 8 \times 10^{14}$ W.cm^{-2} $\Rightarrow \mathcal{E}_{sat} \approx 0.16$ a.u..
- The classical argument is used to define the *critical intensity* (I_{crit}). When the classical ionization is initiated, the regime of above the barrier is reached and therefore the ionization is significant. Then, the critical intensity is defined as the value for which the ionization above the barrier is reached. Comparing the classical and quantum ionization rates, A. de Bohan [1] defined as the value of this intensity $I_{crit} \approx 5 \times 10^{14}$ W.cm^{-2} $\Rightarrow \mathcal{E}_{crit} \approx 0.11$ a.u..

These two intensity values, which are crucial for our study of ionization mechanism, are now clearly defined for hydrogen. We can now begin to analyze the dynamics of the process by demonstrating the effectiveness of momentum space for its characterization. We are interested in this Section in low frequency regime for which tunneling ionization becomes important. We consider the hydrogen atom initially in its ground state interacting with a Ti: Sapphire laser ($\omega = 0.057$ a.u.) and the duration of the pulse is 8 optical cycles. The temporal shape of the electric field is defined by equations (2.61) and (2.62). The

carrier-envelope phase, ϕ in equation (2.61), has been set to 0 for all numerical calculations since the pulse duration we assume in this Section is more than a few cycles and accordingly there are no notable phase-dependent effects. In this way, the laser intensity remains practically constant over 4 optical cycles. We studied the dynamics of ionization using the new model of the hydrogen atom that we introduced in **Chapter** 3, for peak laser intensities taking values between $I = 1.3 \times 10^{14}$ W.cm^{-2} and $I = 8 \times 10^{14}$ W.cm^{-2}. Under these conditions, the ponderomotive potential U_p varies between 0.285 a.u. and 1.754 a.u., and the Keldysh parameter γ between 0.937 and 0.378. Therefore, one is in a regime where a subtle interplay between multiphoton and tunnel ionizations exists, and the dynamics of the process is not easy to discriminate.

We represent in the left panel of **Figures** 4.1, 4.2 and 4.3, for various peak intensities ($I = 1.3 \times 10^{14}$ W.cm^{-2} to $I = 5 \times 10^{14}$ W.cm^{-2}), the time evolution (in optical cycle) of the component of the probability density along p_z, namely $\mid \Phi(p_n = 0, p_z, t) \mid^2$. In the first time, we restrict the analysis to the electrons having only a canonical momentum along the polarization axis, thus the transverse component p_n is set equal to zero. Together with these graphs, in the right panel, we show the ionization yield $P(t)$ as a function of time (in optical cycle). Although none of the two quantities ($\Phi(p_n = 0, p_z, t)$, $P(t)$) are observable as they are gauge-dependent during the interaction, they ($\mid \Phi(p_n = 0, p_z, t) \mid^2$ which is gauge-independent, $P(t)$) provide however valuable information for a deep understanding of ionization dynamics. We can now describe the main features of these graphs.
Before investigating closer the potential issue, let us first recall the following fundamental relations. In the gauge velocity, the canonical momentum $\mathbf{p}(t)$ is connected to the velocity $\mathbf{v}(t)$ (in a.u.)

$$\mathbf{p}(t) = \mathbf{v}(t) - \mathbf{A}(t) \tag{4.1}$$

where $\mathbf{A}(t) = A(t)\mathbf{e}_z$ is the vector potential associated with the linearly polarized laser field. Moreover, applying Ehrenfest's theorem to continuum states (which are free in relation to the interaction) yields:

$$\frac{\mathrm{d}}{\mathrm{d}t}\langle \mathbf{p} \rangle = -\langle \boldsymbol{\nabla} \boldsymbol{V} \rangle \approx 0. \tag{4.2}$$

For the lowest peak intensity, $I = 1.3 \times 10^{14}$ W.cm^{-2}, the atomic system is very weakly ionized. Part of the probability density shows oscillations whose periodicity matches that of the laser field. By overlaying the vector potential $A(t)$ at this probability density, we find that the maximum density is exactly out of phase (in phase opposition) with the vector potential. This appearance is characteristic of low-frequency regime and is of great interest in terms of

defining the tunnel regime. We can give a straightforward interpretation. *Since we are in the low frequency regime, the ground state must be the only physical bound state playing a role in the interaction, if there is no effective radiative transitions to excited states. This is only true in the strong field approximation, that is to say, in the tunnel model. This distinguishes finally the tunnel regime from multiphoton regime.* Correlatively, at the initial time $t = 0$, the total wavefunction coincides with the ground state of the atom. Therefore, the oscillating fraction of the probability density can be associated with the bound part of the population in the momentum space as the average velocity along the z axis reads

$$\langle v_z(t)\rangle_{bound} \approx 0 \Leftrightarrow \langle p_z(t)\rangle_{bound} \approx -A(t). \tag{4.3}$$

It is important to emphasize at this level that a systematic study of the phase relationship existing between $\langle v_z(t)\rangle$ and $A(t)$ in the case of strong low-frequency field was conducted by de Bohan [1]. This study has highlighted another *"tunnel" criterion.* In good approximation within the framework of strong field model, the average speed along the axis of polarization is proportional to $A(t)$ and the density of states $\Gamma(t)$ injected into the continuum.

$$\langle v_z(t)\rangle = A(t)\Gamma(t), \quad \Gamma(t) = \int \mathrm{d}\mathbf{k} \mid g(\mathbf{k}, t) \mid^2 . \tag{4.4}$$

This approximation is basically related to the tunnel model proposed by Keldysh because it was obtained with the assumption of a single bound state describing the atom and for which all what is linked remains motionless (zero velocity) in average. Interesting conclusion in the light of this study was that: *What distinguishes finally the two regimes of ionization is that the multiphoton ionization can occur at any phase of the electric field, while "tunnel" electrons are emitted significantly to the maxima of the electric field (minima of vector potential $\mathbf{A}(t) = 0$).* Also this "tunnel" criterion allows one to determine clearly the range of intensity for which the strong field regime starts.

After 2 optical cycles, we start to see vertical stripes whose position remains in good approximation constant on the axis p_z as a function of time. These stripes correspond to a fraction of the wavefunction characterized by a constant canonical momentum and which satisfies equation (4.2). On the other hand, the stripes represent ionizing wave packets starting to be ejected after the second laser period and being reinforced after each cycle. They can be associated to electrons of a given energy in the continuum. We verified that energy associated to each stripe $\mathbf{p}^2/2$ corresponds exactly to the kinetic energy of the ejected electron, and hence to the peaks obtained in the ATI spectrum. *The momentum space associated with the velocity form of the interaction is therefore a privileged representation to study the dynamics of ionization.* We want

to stress here that in contrast to the configuration space where the oscillation amplitude of ionized wave packets can exceed α_0 (classical excursion amplitude of a free electron in laser field) as the peak laser intensity increases and experiences the crucial problem of numerical reflections and spurious effects, the probability density remains localized in momentum space. *The appearance of the stripes can therefore be interpreted as the instantaneous signature of the ionization.* It is well known that a *time-frequency* analysis performed for the harmonic spectrum provides access to time of emission of these harmonics. The study of the dynamics of the probability density which is a *time-energy* analysis, is nothing more than an equivalent of the previous method. For the ionized part of the wavefunction, such an analysis is possible since we work in terms of canonical momentum - identical to final kinetic energy (well defined) of electrons. Furthermore, a closer look of the time evolution of $\mid \Phi(p_n = 0, p_z, t) \mid^2$ clearly reveals that, it is possible to have access to ejection times t_{ion} of wave packets in the continuum, and therefore the energies of ionized states with mean canonical momenta along the z given by [1]

$$p_z^{ion} \approx -A(t_{ion}). \tag{4.5}$$

This means that wave packets are indeed ejected with a velocity along z equals zero; they emerge directly from the bound state as it moves along p_z like $-A(t)$, in good agreement with the SFA approach. However, the values taken by the Keldysh parameter γ suggest that multiphoton absorption should remain important. When the peak intensity increases further, the oscillation of the probability density is drastically washed out as the system ionizes quickly and the number of stripes corresponding to higher values of the canonical momentum increases significantly. However, in the case of **Figures** 4.1 and 4.4 (the lower panel) where only the ground state is included in the separable potential, we do not observe clear stripes for small values of component p_z. This contrasts sharply with what one obtains in the case of the exact Coulomb potential (represented in the upper panel of **Figure** 4.4) and those for which more than one component are included in the expansion of the Coulomb potential kernel (see **Figures** 4.2, 4.3 and 4.5). In this case, we observe a gradual onset of stripes in the vicinity of small values of the canonical momentum p_z, and whose the density increases with the number of bound states included in the separable potential. Another important feature highlighted on our curves of the probability density is that, as the intensity of the laser field increases progressively the density of stripes around the small values of p_z drops sharply when the threshold of the strong field's regime is reached ($I = 2 \times 10^{14}$ W.cm^{-2}, $\gamma = 0.755$). Conversely, there is a gradual emergence of bands of stripes for large values of p_z, and especially when the regime of ionization above the barrier is reached.

4.2.2 Backward and forward electron emission

In what follows, we will try to explain the structure of the ATI spectra of electrons emitted by the virtue of dynamics of the probability density. The results in **Figure** 4.7 are displayed on a logarithmic scale in order to reveal the global ATI energy distribution. In the left panel of **Figure** 4.7, we show the ionization probability density

$$\begin{aligned} \mid \Phi_{ion}(p_n = 0, p_z; T_p) \mid^2 = & \mid \Phi(\mathbf{p}, T_p) - \mathcal{C}_{1s}(T_p)\phi_{1s}(\mathbf{p}) - \mathcal{C}_{2s}(T_p)\phi_{2s}(\mathbf{p}) \\ & - \mathcal{C}_{2p,m}(T_p)\phi_{2p,m}(\mathbf{p}) \mid^2 \\ = & \mid \mathcal{C}_k(T_p) \int \mathrm{d}\mathbf{k}\varphi^+(\mathbf{k}, \mathbf{p}) \mid^2 \end{aligned}$$

as a function of the canonical momentum along the polarization axis p_z at the end of the interaction, for the forward ejected electrons $p_z > 0$ and backward ejected electrons $p_z < 0$. The corresponding electron energy distribution density $D(E_k, t)$ is plotted in the right panel of **Figure** 4.7. In **Figure** 4.6 we compare our result to the numerical treatment of TDSE obtained within an exact Coulomb potential for a special case of laser peak intensity $I = 1.3 \times 10^{14}$ W.cm^{-2}. Let us open a parenthesis to say that the choice of this specific case is not as naive, because it poses a crucial problem from the perspective of the strong field approximation. For the laser frequency considered, the Keldysh parameter γ is 0.937. Therefore the criterion of strong field ($\gamma \ll 1$) can not apply *a priori*. We are in an intermediary regime where multiphoton ionization and tunnel ionization coexist. The vertical dashed line indicates in each case, the value of the canonical momentum corresponding to $2U_p$ and $10U_p$. These results share some common features: (1) - The electrons are preferentially emitted along the polarization vector and, in spite of the different numbers of bound states and continuum states taken into account for each wave packets, the observed secondary structures (above $2U_p$) are in qualitative good agreement with those corresponding to the exact Coulomb potential. (2) - The spectrum consists of the ATI peaks separated each another by the energy of a photon ω (how can we visualize them on this graph?) It would be interesting to recall what it corresponds in terms of the dynamical point of view. However, they exhibit some discrepancies below $2U_p$ where the results obtained with our model strongly underestimate ($1s$ and $(1s + 2s)$-model potentials) or overestimate ($(1s + 2s + 2p)$-model potential) what is expected with the exact Coulomb potential, for example the size of the central peaks ATI in the low-energy pattern of the spectrum. Overall we can say that the only major difference with the Coulomb potential is the lack of excited states included in our separable potential. Therefore, one could attribute the existence (or absence) of central peaks to resonances with excited states of the Coulomb potential. Another important difference related to the decrease of

the amplitude of the central peaks, is the value of the ionization probability. Indeed for a laser peak intensity $I = 1.3 \times 10^{14}$ W.cm^{-2}, de Bohan [3] obtained a probability of ionization of about 14% while we get a little less than 1% in the case of the $1s$ model potential and about 2.5% for the case of $(1s+2s+2p)$-model potential.

Now we focus our attention on the ω structure of the spectra. Looking deeper into our graph of the probability density, we realize that the position and the formation of stripes that we have associated with ionization, their p_z's location corresponds to an energy ω. These stripes, we have already stressed only appear after 2-3 optical cycles. It is worth to mention that, even if the task is not easy, all the ATI peaks up to $2U_p$ are already present in the spectrum. Regarding the time evolution of the population of the continuum states, one finds that less than a percent of the wavefunction has been ionized between 1 and 2 optical cycles. This fact explained clearly why we do not observe a structure at that time. When the number of optical cycle increases, the shape of the peak structure is becoming better and better well-defined. We can therefore verify that the structure in ω of spectra of electrons corresponds to the repetition of the same event all periods. On the other hand, the electrons are emitted both forward and backward depending on the sign of the electric field, which justifies from the energetic point of view, the periodicity ω in ATI spectra. Before continuing our analysis, let us stop and try to understand the presence of the first boundary of ATI plateau at $2U_p$.

To do this, let us return once more to movement of the probability density as a function of time and let's look particularly the dominant contributions to the ionization. The spectra of **Figure** 4.7 clearly show that the majority of the ejected electrons have a kinetic energy around $2U_p$, that is $p_z \approx 1.07$ a.u. for the problematic case of the lower peak intensity $I = 1.3 \times 10^{14}$ W.cm^{-2}. The time evolution of the probability density, which behaves as $-\mathbf{A}(t)$ along the polarization axis, allows us to understand the presence of this limit. We have seen that, in the low-frequency regime, the maximum of this probability moves as $-\mathbf{A}(t)$ such that the average velocity of the bound state remains zero. At the moment where the maximum of this probability density reaches the value $-\mathbf{A}_0$, the interaction term becomes maximum in the velocity gauge of the TDSE. An effective transition to the continuum states is possible for a wave packet characterized by a canonical momentum $\mathbf{p}_0 = -\mathbf{A}_0$. Indeed, when the electric field is zero, the potential barrier reduces itself to Coulomb potential, therefore it is not lowered and the tunnel ionization cannot take place. Despite the fact that we have $\gamma < 1$, the dominant regime here is the multiphoton ionization, induced necessarily by the influence of Coulomb potential. The electrons that are ejected with a canonical momentum $\mathbf{p}_0 = -\mathbf{A}_0$, and therefore with a final

kinetic energy

$$E_{kin} = \frac{\mathbf{p}^2}{2} = \frac{\mathbf{A}_0^2}{2} = 2U_p$$

must therefore make an *inelastic collision* with the nucleus and not escape through tunneling. *The momentum transfer necessary for the ionization is induced uniquely by the Coulomb potential. It is thus seen to appear here a first sign of the importance of the presence of the Coulomb potential in the ionization mechanism. This new interpretation of the value of* $2U_p$ *seems more explicit than that given by the classical calculation. This first boundary of ATI plateau at* $2U_p$ *is a characteristic of strong low-frequency field due to the fact that* $\langle v_z(t)\rangle_{bound} \approx 0$.

Let us continue our analysis of these graphs. Regarding the ionization probability density obtained via the Coulomb potential, it is found that photo-electrons with energy less than $2U_p$ are emitted when the vector potential is zero. That is to say when the electric field is maximum, and thus the potential barrier is the lowest. In those circumstances, the tunneling ionization dominates and we do not observe it in our results with the separable potential. How to understand this? the only plausible interpretation seems to be linked to the excited states that can make possible intermediate transitions with less photon followed by a tunnel ionization above the barrier. As shown by the significance difference between the ionization probabilities, this process would be the dominant process during the ionization and therefore would undermine the model of strong field of a single bound state.

Figure 4.8 displays the ATI spectra obtained from our model atom interacting with a laser field for various laser peak intensities between $I = 1.3 \times 10^{14}$ W.cm^{-2} and $I = 8 \times 10^{14}$ W.cm^{-2}, $\omega = 0.057$ a.u. and an 8 optical cycle for pulse duration. The two most prominent features highlighted in this ATI spectra are: (1) The dips in the low-energy part around $p_z = 0$ or below the first cutoff $2U_p$ are gradually filled with the increasing number of atomic bound states included into our separable potential. (2) Moreover, there is a clear asymmetry at high peak intensity. This asymmetry was already visible on the **Figures** 4.1, 4.2 and 4.3. This is surely due to the fact that the time it takes to the system to be ionized is very short.

4.2.3 Electron angular distributions

Photoelectron angular distributions provide detailed information about interferences between different quantum pathways of photoionization. Structures in the low p_z momentum distribution have been intensively studied for atoms experimentally [4, 5] as well as theoretically [6, 7, 8, 9, 10, 11] and originate from the interaction between the outgoing low-energy electron and the long-range asymptotic Coulomb potential. Their number depends on the intensity and the binding energy [10]. We represent in **Figure** 4.9 the angular distribution of electrons ejected after the interaction, given by $p_n \mid \Phi_{ion}(p_n, p_z; T_p) \mid^2$, for our model atom with an 8 optical cycle pulse and photon energy $\omega = 0.057$ a.u.. We also choose to adjust the laser intensity $I = 1.3 \times 10^{14}$ W.cm^{-2}, corresponding to an intermediary ionization regime between the multiphoton and the "tunnel". These figures show the same characteristic than that of the density of probability: the central peaks are much weaker for the benefit of the peaks corresponding to $2U_p$. However, the distribution (p_z, p_n) of electrons ejected presents the structures whose physical origin will be specified below. Since we are in an intermediate regime, the strong field model is valid for analysis. In this context, the ionization mechanism is then described by a dipole transition $1s$-continuum directly followed by a free propagation to the end of the interaction, the periodic repetition of the phenomenon explaining the ATI structure clearly visible on distribution of **Figure** 4.9. The theory of classical dynamics outlined in **Chapter** 2 highlights the contributions of "**direct**" electrons (issued before the maximum of the field) and "**indirect**" electrons (launched after the peak of the field). These two contributions can interfere and give rise to structures in the angular distribution. We believe that this phenomenon is the cause of the sharp structures including the first ATI peak visible in **Figure** 4.9. Theses ATI peaks manifest themselves as ring-like structures. As a common features of these figures, for the laser parameters considered, the momentum distribution presents a symmetric distribution with respect to the transverse axis, clearly displays a number of interference pattern radially as well as angularly in the forward and backward direction at specific momentum position. The low-energy electron momentum distributions present stripes fanning out radially from $p_z = 0$. These stripes are more pronounced in the case of $(1s+2s+2p)$ model potential than in the case of $(1s+2s)$, $1s$ model potential where a lack of structures is more than evident. An other interesting observation is that, the interference lines appear at different angles with respect to the polarization axis. The tendency of these interference lines to be parallel to the polarization axis is more pronounced in the case of the exact treatment of Coulomb potential (see upper panel of **Figure** 4.10) than that of our separable potential (see lower panel of **Figure** 4.10). This difference is another indication of the nature of the dominant ionization regime. Indeed,

the very pronounced rings on our figures can be interpreted as a signature of the multiphoton ionization.
A systematic study of the complex dynamics of ionization in the intermediate regime, has allowed to de Bohan [3] to explain the angular structure of the first ATI peaks (for example $[p_z = \pm 0.5,\ p_n = 0.4]$). From its analysis, we note that the first moment of interaction that the ATI structure appears is beyond 2.5 optical cycle. We also note that all peaks are formed simultaneously, contrary to predictions of the strong field model; which highlights the contribution of multiphoton process in the ionization mechanism. Beyond these first ATI peaks, ring formation is justified entirely by the presence of a tunnel mechanism, with the consecutive (or sequential) creation of the different peaks at the maximum of probability density.
We have seen previously that the regime of strong field starts to occur when the laser peak intensity reaches the value $I = 2 \times 10^{14}$ W.cm^{-2} and is actually reached at the value of $I = 3 \times 10^{14}$ W.cm^{-2}. When the peak intensity increases progressively until the value of $I = 2 \times 10^{14}$ W.cm^{-2}, one sees an intensification of the ring formation around low values of p_z at the same time as formation of stripes in the wings (large values of p_z) (see upper panel in **Figure** 4.11). The first lobe of the distribution - revealed on either side of $p_z = 0$ is less curved on the axis of polarization than that obtained in the exact treatment of Coulomb potential. When the strong field regime is reached for the value $I = 3 \times 10^{14}$ W.cm^{-2}, the rings or interference figures are again clearly distinct, but gradually diminishing progressively as the intensity increases (see middle panel in **Figure** 4.11). For the higher intensity, the difference between **Figure** 4.11 appears to be larger. A closer look finds that the difference is easily understood. In addition to the general difference in the low-energy part, we note that for the highest value of the intensity the electrons tend to be located more at small p_n, reflecting the greater importance of tunneling ionization. At the value $I = 8 \times 10^{14}$ W.cm^{-2}, the system completely ionize at 99%, the regime of ionization over the barrier is reached, therefore the dynamics of ionization can be treated as a classical ionization. The ejection of electrons into the continuum is a direct process in the absence of any barrier and with a relatively insignificant influence of Coulomb potential. A simple observation of this spectrum (see lower panel in **Figure** 4.11) therefore indicates that with increasing intensity, the propagation singularly promotes the ejection along the polarization axis of the laser field, followed by a destruction of interference figures, which is physically understandable.

4.2.4 Total ionization probability

In this Section, we compare the rates of ionization from the ground state $1s$ obtained within the framework of our separable potential to the numerical

treatment of TDSE (in its length form) with exact Coulomb potential, for intensities up to $I = 8 \times 10^{14}$ W.cm^{-2}. The latter approach is accomplished through a very efficient novel explicit method, namely Fatunla's theory [12, 13] which is briefly described in [14]. The behaviour of these ionization probabilities is showed in **Figure** 4.12. The $(1s + 2s + 2p)$-model approach yields rate varying more smoothly than $1s$ and $(1s + 2s)$-model separable potential rates. The curves have almost the same shape. However there exists some discrepancies. Overall they increase as the peak intensity increases. The two approaches are particularly close at low intensity, $I \ll 10^{14}$ W.cm^{-2}, $\gamma = 1.068$ where the dynamics of ionization is purely multiphoton. The agreement gradually deteriorates as the intensity increases. Up to the intensity $I = 2 \times 10^{14}$ W.cm^{-2}, $\gamma = 0.755$ where the strong field starts, our three-levels model potential tends to underestimate the ionization rate but rarely by more than 31% and significantly overestimates ionization probability (1.8 order of magnitude larger than in the exact Coulomb treatment) above this intensity. Above the peak intensity $I = 3 \times 10^{14}$ W.cm^{-2}, $\gamma = 0.616$, where the tunneling dominates the ionization process, as can be seen from **Figure** 4.12, the rate of ionization obtained numerically by solving the TDSE shows a strong resonance features which could probably originate from the interaction of the ground state with moderately excited states. The presence of this structure can be understood through the non-Hermitian Floquet theory where the resonance structures are assigned to particular intermediate states [15, 16, 17, 18]. The lack of sufficient number of bound states included into our separable potential explains why we did not observe such structure in our results. We also note from **Figure** 4.12 that at the highest intensities resonances with the more highly excited states tend to suppress ionization rather than increase it. This reduction is not surprising since in such strong fields many of these excited states are more stable against ionization than the ground state [18], while our model atom is already completely ionized.

4.2.5 Pulse duration and phase-dependent effects

We also investigate here the effects of pulse duration and CEP. The investigation of these effects is timely in view of progress in laser technology. Ultrashort pulses have the advantage that the highest pulse intensity is reached in a time shorter than that which the electron needs to escape from an atom, allowing the use of much higher effective field strengths. The peak electric field of such few-cycle pulses depends on the CEP, which specifies the delay between the maximum of the envelope and the nearest maximum of the electric field of the carrier wave with frequency ω. Since the ionization process depends on the field in a highly nonlinear way, the asymmetry of the field induces an asymmetry in the emission direction of photoelectrons [19, 20, 21, 22, 23, 24, 25].

It is important to point out that the spectrum of the electrons created by ionization exhibits inversion symmetry. Such a symmetry can be caused by an appropriate symmetry of the laser field. However, even in the absence of this symmetry, the theoretically calculated spectrum may display inversion symmetry, if certain approximations are made in the calculation.

Backward and forward electron emission and asymmetry

Here, we present examples of ATI ionization probabilities for our model atom interacting with a linearly polarized few-cycle laser pulse of photon energy $\omega = 0.057$ a.u.. The pulse has sine-square shape and vector potential is given by (2.59) and (2.60). The numerical results are obtained within the framework of the theory presented in **Chapter** 3. We consider the spectra along the polarization axis for backward emission ($p_z < 0$, red curves in the following figures) and forward emission ($p_z > 0$, blue curves). The left-right or backward-forward asymmetry is analyzed as a function of the CEP ϕ, the pulse duration (in optical cycle n_c) and the laser peak intensity I.

For the pulse length of 4 optical cycle and the laser peak intensities $I = 1.3 \times 10^{14}$ W.cm^{-2} and $I = 3 \times 10^{14}$ W.cm^{-2}, results are shown in **Figures** 4.13 and 4.14 for two values of $\phi = 0$ (the upper panel) and $\phi = \pi/2$ (the lower panel). For $\phi = 0$, the spectrum of the direct electrons obeys left-right "quasi" symmetry, which is visible in the low-energy part (less than $2U_p$) of **Figure** 4.13. This left-right symmetry is more pronounced and extended over the $2U_p$ in the case of $I = 3 \times 10^{14}$ W.cm^{-2}. Furthermore, the high-energy rescattered electrons violate this symmetry. Let us recall that, at first sight, it may appear counterintuitive that the electric field (which obey temporal inversion symmetry [21]), which does not exhibit any spatial backward-forward symmetry, produces an electron spectrum that does. Knowing that, it is the electric field that causes ionization, while it is, however, the vector potential that governs the subsequent propagation in the laser field, which in turn, determines the spectrum, and the corresponding vector potential which satisfies the temporal inversion symmetry is backward-forward symmetric. Note that, in the case that the binding potential is accounted for after the electron has been set free, the exact backward-forward symmetry is violated [1, 26] and this is also the case when the symmetry upon time translation of the field breakdown for the short pulse. For $\phi = \pi/2$, both the direct and the rescattered electrons violate the symmetry. An observation of the curves presented in **Figures** 4.13 and 4.14 shows that some of them are smooth, while others show a characteristic oscillatory behaviour. This feature is well explained within a classical model formulated in the Review paper by Milošević [21]. Indeed, these oscillations are the result of constructive or efficient interference between the trajectories

of "direct" electrons, the trajectories of "indirect or rescattered" electrons and also between the two types of electron trajectories.

Figure 4.15 exhibits the analogue of **Figure** 4.13 for a shorter pulse with $n_c = 2$. We see that the left-right asymmetry still exists for the two values of ϕ. Now, the asymmetry is most conspicuous in the presence or absence of oscillations.

We have check that the left-right asymmetry becomes less and less pronounced when the number of optical cycle of field increases. In another word, the left-right asymmetry of the electron spectra reduces with increasing pulse length. Therefore, the spectra in opposite directions become more and more indistinguishable. When concentrating on the high-energy part of all these spectra, we observed the common behaviour that more high-energy electrons are emitted to the left. Another interesting result is that there exists a well-defined cross-over energy where emission to the right becomes more prominent than to the left. It is worth mentioning that the afore-discussed CEP effects can be served as a tool for an accurate determination of the absolute phase by comparing the experimental spectra to the theoretical results. For an accurate determination of the absolute phase, the theoretical results should be subjected to focal averaging. Results similar to those shown here have been obtained in [21, 23].

Momentum distributions and asymmetry

In this part we analyze the angular distribution of emitted electrons for a short interaction of our model atom with a laser field whose parameters are: laser peak intensity is $I = 5 \times 10^{13}$ W.cm^{-2}, the photon energy is given by $\omega = 0.057$ a.u., the duration of pulse is $n_c = 4$ optical cycle and the CEP taking the two values $\phi = 0,\ \pi/2$. In this context, the ponderomotive energy takes the value $U_p = 0.11$ a.u. and the Keldysh parameter $\gamma = 1.51$. Therefore, the multiphoton ionization process is assumed to set in.

Let's start with the case where our separable potential supports only a single $1s$ state. We see on the **Figure** 4.16 (upper panel for $\phi = 0$) that the ejection of electrons in the continuum is symmetrical with respect to $p_z = 0$. In other words, no emission direction along the axis of polarization is privileged and therefore the angular distribution of electrons exhibits a symmetric behaviour. Moreover, when the absolute phase of the field takes the value $\phi = \pi/2$, this electron angular distribution shows a clear asymmetry (see the lower panel of **Figure** 4.16). In this case, the backward emission of electrons is preponderant. This analysis can be easily understood by means of the tem-

poral evolution of the vector potential $\mathbf{A}(t)$ of the laser field and the Ehrenfest theorem. It is well known that, in this regime of frequency and intensity, the electron is launched each time in the continuum when the vector potential is maximum. A glance at the **Figure** 4.19 shows that the vector potential has symmetric extreme values (≈ 0.351 a.u., 0.748 a.u., 1.028 a.u. and their opposites) in the case of $\phi = 0$, while these extremum (≈ 0.490 a.u., 0.609 a.u., 1.064 a.u., -0.226 a.u., -0.871 a.u., -0.956 a.u.) are all different for $\phi = \pi/2$. These extremum values of vector potential help us to clarify the positions of rings and then the momentum p_z in the electron angular distributions.

The above result (valid for $\phi = 0,\ \pi/2$) does not change significantly when adding the second discrete state $2s$ in our separable potential. The remarkable difference with the previous case lies in the preponderance of the electron emission at low moment p_z. This can be understood by the possibility of resonant transitions on the state $2s$. This is depicted on the **Figure** 4.17. The further addition of the discrete state $2p$ in the separable potential leads to a surprising observation. In addition to the resonant transitions on the state $2p$, to the emission of electrons with low moment p_z more and more pronounced, one notes curiously the restoration of symmetry in the backward and forward emissions of electrons, most particulary when $\phi = \pi/2$. This is shown in **Figure** 4.18. How to understand such behavior? In weak field and low-frequency, the following reasons could elucidate the sudden breakdown of this asymmetry. (1) - the threshold ionization in this case is lower down than in the case of $1s$, (2) - the interaction time of the field must be longer in order to ionize the system and therefore requires a large range of the pulse, (3) - the coupling of $2p$ to the continuum is easier than that of the $1s$ state. Therefore the ionization rate of $2p$ is higher than that of $1s$. Also noteworthy is that in the case of very strong low-frequency laser field, the time the system takes to ionize is very short, and thus the range of pulse does not play anymore a role in the ionization process.

4.3 Resonant interaction of the model atom in the high-frequency regime

We return in this last section to the problem of resonant interaction of our model atom with a strong laser field and high frequency. We considered at first the following laser parameters: peak intensity $I = 4 \times 10^{14}$ W.cm^{-2}, $|1s\rangle \rightarrow |2p\rangle$ resonant frequency $\omega = 0.375$ a.u. and $n_c = 40$ optical cycle for the duration of the pulse. The result of the spectrum of electrons emitted obtained through our theory is shown in **Figure** 4.20. This spectrum reveals the surprisingly high-energy electron emission. The coupling of the dressed

states to the continuum states, which is preceded by the lifting of degeneracy clearly explains the presence of Autler-Townes doublets. This spectrum is essentially structured in two main parts, namely a fast decay (large slope) of spectrum in its low energy part followed by a slight decay (low slope) in its high energy part. The latter part is termed hereafter "quasi-plateau." This unexpected and promising behaviour requires a deepest investigation in order to be sure that this result is not an artefact of our model. Thus the following questions arise. Does the "quasi-plateau" varies with the pulse duration? does it depend on the laser peak intensity? does it depend on the laser frequency? does it depend on the pulse shape? does it depend on the atomic parameters? Our current investigations are part of the prospect of researching clear and explicit answers to previous questions. To date, our numerical calculations are running on the supercomputers of the "Institut de Calcul Intensif et de Stockage de Masse (CISM, UCL)".

Before going further, we compared our result to the one obtained by virtue of TDSE with B-Spline's and Sturmian's methods [27, 28]. Let us remember that in **Chapter** 2, we noted some difficulties usually faced by spectral methods and the grid methods. The most recurrent problems are - the reflections near the edges of the basis - the size of the basis - the large and intensive computation times. To refresh our memory, in the configuration space, a box with a size of at least 2010 a.u. is needed to properly describe an electron with energy 5 a.u. with a velocity of about 3 a.u.. So, for an electron with energy about 50 a.u. and velocity 10 a.u., we will need a box of size 6700 a.u.. This calculation is very difficult to achieve with such methods. As illustrated in **Figure** 4.21 we compare ATI spectra obtained with our model, to those calculated by solving numerically the TDSE for atomic hydrogen. These three different approaches yield results in excellent quantitative agreement for the first ATI peaks as expected since mainly two states, $|1s\rangle$ and $|2p\rangle$ are dominating the dynamics at intensity and frequency considered here. However, there exist a discrepancy between these methods at the high energy part of the spectrum. At this stage, the investigations are going on to clarify this point.

In **Figures** 4.22 and 4.23 we present the first results with respect to the pulse duration and the laser peak intensity respectively. We find that the pulse duration shall affect hardly the energy spectrum of electrons emitted, except the size and the shape of the doublets. More precisely, for a given intensity, the doublets are well-resolved or well-pronounced for a long time of interaction. The size of the doublets increases when the pulse duration increases. This behavior is extended over the whole field of spectrum considered and can be easily understood by the fact that, the Rabi oscillations occur during the time the field intensity is constant and equals to the peak intensity; i.e. when the field is in its flat top range. On the other hand, for a given pulse duration, the

shape of the doublets is well-pronounced over all the spectrum, but contrary to the previous case, their sizes behave differently in the second part of the spectrum. The size of doublets decreases in this second part of the spectrum when the intensity increases. This last result could be a signature of the presence of two different processes. Finally, we also point out that the slope of the "quasi-plateau" is weakly affected by the pulse duration and the laser peak intensity.

4.4 Conclusion

In short summary, in this Chapter, our approach to solving the TDSE directly in momentum space, coupled with our separable potential model has allowed us to analyze the dynamics of the ionization process. More precisely, the role played by the Coulomb potential in the underlined process. Unlike the configuration space in which the ionization is defined in terms of the distance of the wave packet relative to the core, the momentum space is therefore a privileged space to study the mechanism of ionization. The canonical momentum that we use in the velocity form of the interaction is linked, for the fraction "ionized" of the probability density, to final kinetic energy of the ejected electron. This global probability density remains localized in the momentum space. The above presented momentum space analysis helps to uncover the actual mechanisms contributing to the dominant part of ATI spectra, up to $2U_p$. At intensities such that the Keldysh parameter γ is close to unity, there is a subtle interplay between the multiphoton ionization and tunnelling ionization. A remarkable stripe obtained in the time dependence of the probability density represents an unambiguous signature of the determinant role of the Coulomb potential. Another advantage of the momentum space analysis is to provide a convenient tool for exploring the transition between the multiphoton and the strong field regimes. We conclude that our numerical results are consistent with the interpretation previously given in [3]. We have also investigated the role of the pulse CEP of a few-cycle infrared pulse on ionized electron momentum and electron energy distributions. We've also showed the emission of very energetic electrons that remains to be elucidated. These promising features should serve as a stimulus for extending our model potential and developing accurate and efficient computational tools adapted to such momentum space methods.

Bibliography

[1] A. de Bohan, B. Piraux, L. Ponce, R. Taïeb, V. Véniard and A. Maquet, *Phys. Rev. Lett.* **89**, 113002 (2002).

[2] R. Shakeshaft, R. Potvliege, M. Dörr and W. E. Cooke, *Phys. Rev. A* **42**, 1656 (1990).

[3] A. de Bohan, *Dynamique de l'Interaction Laser-Atome. Moment Canonique et Approximation du Champ Fort, PhD Thesis*, Université Catholique de Louvain, Belgium (2001).

[4] A. Rudenko, K. Zrost, C. D. Schröter, V. L. B. de Jesus, B. Feuerstein, R. Moshammer and J. Ullrich, *J. Phys. B: At. Mol. Opt. Phys.* **37**, L407 (2004).

[5] C. M. Maharjan, A. S. Alnaser, I. Litvinyuk, P. Ranitovic and C. L. Cocke, *J. Phys. B: At. Mol. Opt. Phys.* **39**, 1955 (2006).

[6] Z. Chen, T. Morishita, A. T. Le, M. Wickenhauser, X. M. Tong and C. D. Lin, *Phys. Rev. A* **74**, 053405 (2006).

[7] D. G. Arbo, S. Yoshida, E. Persson, K. I. Dimitriou and J. Burgdörfer, *Phys. Rev. Lett.* **96**, 143003 (2006).

[8] T. Morishita, Z. Chen, S. Watanabe and C. D. Lin, *Phys. Rev. A* **75**, 023407 (2007).

[9] D. G. Arbo, J. E. Miraglia, M. S. Gravielle, K. Schiessl, E. Persson and J. Burgdörfer, *Phys. Rev. A* **77**, 013401 (2008).

[10] D. G. Arbo, K. I. Dimitriou, E. Persson and J. Burgdörfer, *Phys. Rev. A* **77**, 013406 (2008).

[11] M. Abu-samha, D. Dimitrovski and L. B. Madsen, *J. Phys. B: At. Mol. Opt. Phys.* **41**, 245601 (2008).

[12] S. O. Fatunla, *Math. Comp.* **32**, 1 (1978).

[13] S. O. Fatunla, *Math. Comp.* **34**, 373 (1980).

[14] J. Madroñero and B. Piraux, *Phys. Rev. A* **80**, 033409 (2009).

[15] A. Maquet, Shih-I. Chu and W. P. Reinhardt, *Phys. Rev. A* **27**, 2946 (1983).

[16] Shih-I. Chu and D. A. Telnov, *Phys. Rep.* **390**, 1 (2004).

[17] R. M. Potvliege and R. Shakeshaft, *Adv. At. Mol. Opt. Phys. Suppl.* **1**, 373 (1992).

[18] R. M. Potvliege, E. Mese and Svetlana Vučić, *Phys. Rev. A* **81**, 053402 (2010).

[19] E. Cormier and P. Lambropoulos, *Eur. Phys. J. D.* **2**, 15 (1998).

[20] G. G. Paulus, F. Grasbon, H. Walther, P. Villoresi, M. Nisoli, S. Stagira, E. Priori and S. D. Silvestri, *Nature* (London) **414**,182 (2001).

[21] D. B. Milošević, G. G. Paulus, D. Bauer and W. Becker, *J. Phys. B: At. Mol. Opt. Phys.* **39**, R203 (2006).

[22] D. B. Milošević, G. G. Paulus and W. Becker, *Phys. Rev. Lett.* **89**, 153001 (2002).

[23] S. Chelkowski and A. D. Bandrauk, *Phys. Rev. A* **71**, 053815 (2005).

[24] C. P. J. Martiny and L. B. Madsen, *Phys. Rev. Lett.* **97**, 093001 (2006).

[25] C. P. J. Martiny and L. B. Madsen, *Phys. Rev. A* **76**, 043416 (2007).

[26] A. D. Bandrauk, S. Chelkowski and N. H. Shon, *Phys. Rev. Lett.* **89**, 283903 (2002).

[27] H. Bachau, E. Cormier, P. Decleva, J. E. Hansen F. Martín, *Rep. Prog. Phys.* **64**, 1815 (2001).

[28] E. Huens, B. Piraux, A. Bugacov, and M. Gajda, *Phys. Rev. A* **55**, 2132 (1997).

Figures of Chapter 4

"Au début, il n'y avait rien. Enfin, ni plus ni moins de rien qu'ailleurs."
Devise Shadock.

4.5 Figures

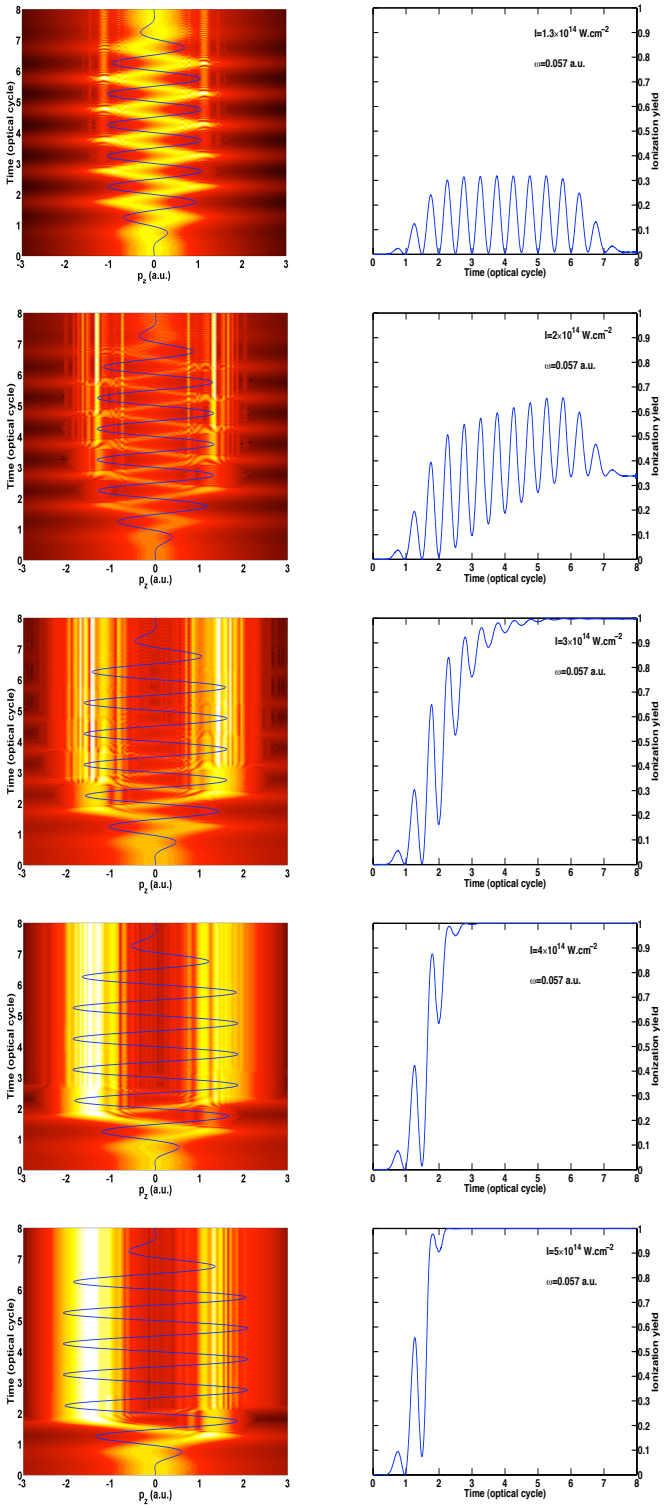

Figure 4.1: *Electron probability density as a function of time and* $p_z, p_n = 0$ *(left panel), for the interaction of our model atom with an* 8 *optical cycle pulse and the photon energy* $\omega = 0.057$ a.u. *and the ionization yield (right panel). The pulse intensity varies between* $I = 1.3 \times 10^{14}$ W.cm^{-2} *and* $I = 5 \times 10^{14}$ W.cm^{-2}. *The solid oscillating blue line in the left panel represents* $A(t)$ *and the separable potential supports only* $1s$ *state.*

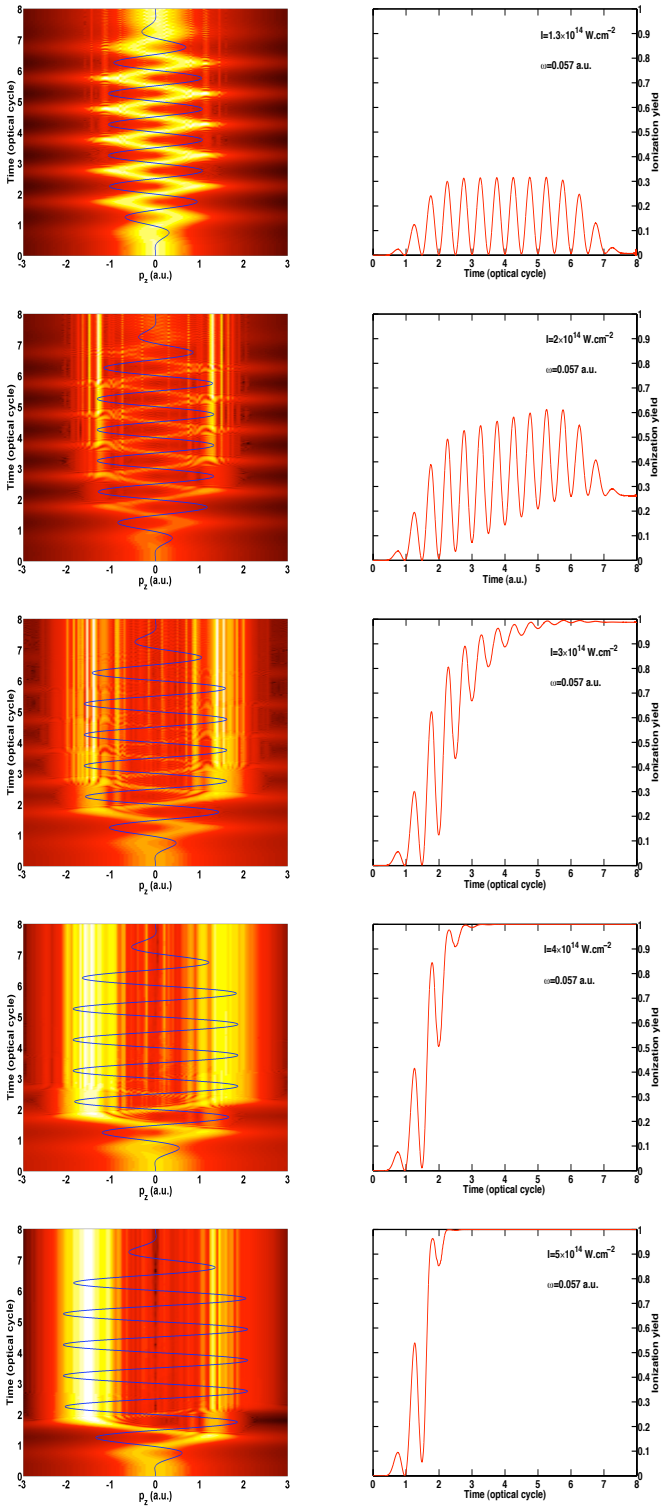

Figure 4.2: *Electron probability density as a function of time and* $p_z, p_n = 0$ *(left panel), for the interaction of our model atom with an* 8 *optical cycle pulse and the photon energy* $\omega = 0.057$ a.u. *and the ionization yield (right panel). The pulse intensity varies between* $I = 1.3 \times 10^{14}$ W.cm^{-2} *and* $I = 5 \times 10^{14}$ W.cm^{-2}. *The solid oscillating blue line in the left panel represents* $A(t)$ *and the separable potential supports* $1s$ *and* $2s$ *states.*

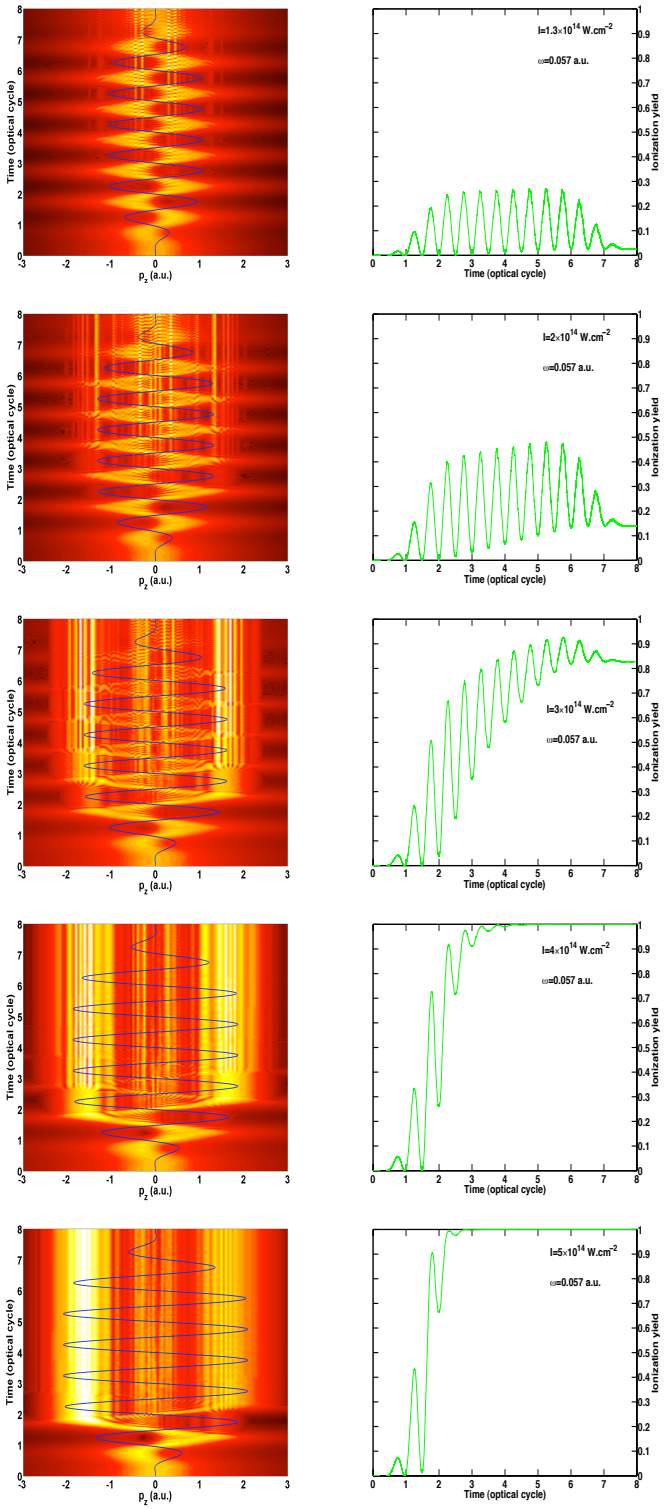

Figure 4.3: *Electron probability density as a function of time and* $p_z, p_n = 0$ *(left panel), for the interaction of our model atom with an* 8 *optical cycle pulse and the photon energy* $\omega = 0.057$ a.u. *and the ionization yield (right panel). The pulse intensity varies between* $I = 1.3 \times 10^{14}$ W.cm^{-2} *and* $I = 5 \times 10^{14}$ W.cm^{-2}. *The solid oscillating blue line in the left panel represents* $A(t)$ *and the separable potential supports* $1s$, $2s$ *and* $2p$ *states.*

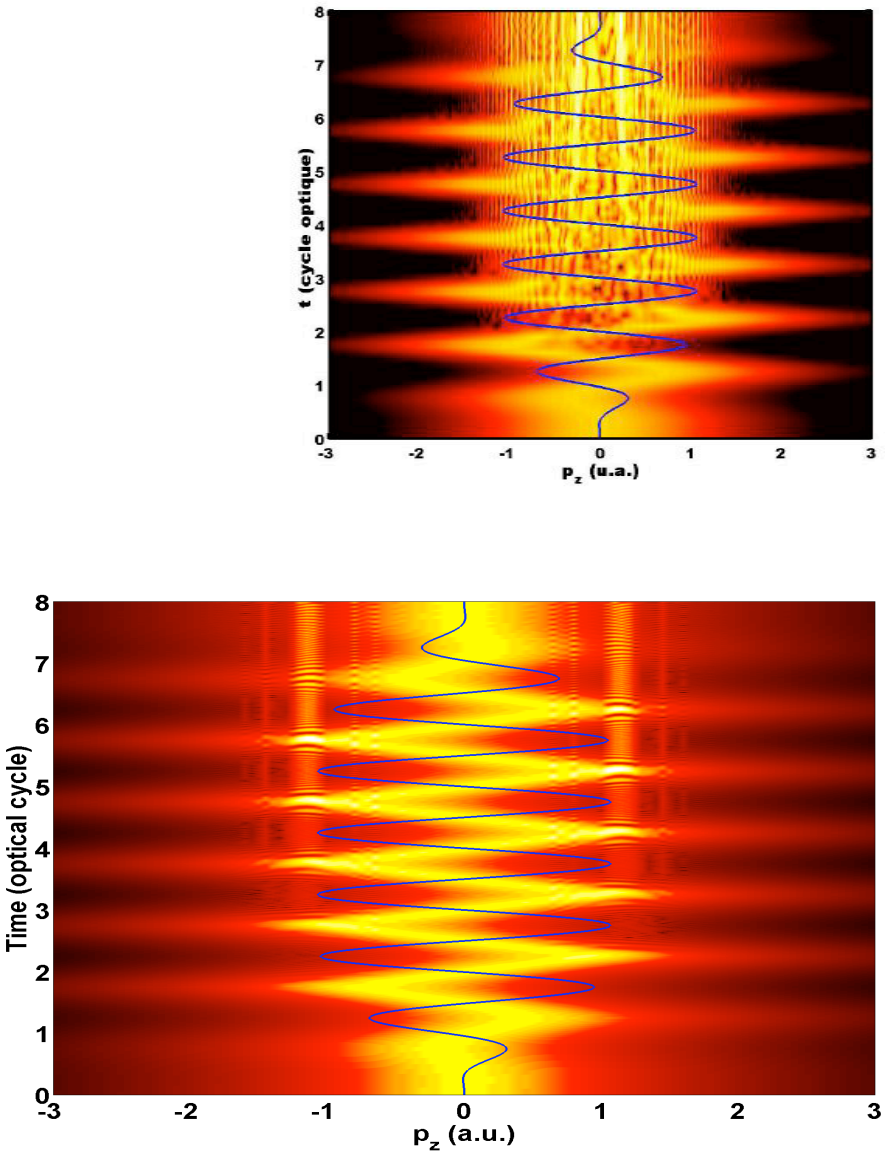

Figure 4.4: *Electron probability density as a function of time and* $p_z, p_n = 0$ *obtained within an exact Coulomb potential (upper panel, from de Bohan [3]) and our* $(1s)$ *potential model (lower panel). The laser peak intensity is* $I = 1.3 \times 10^{14}$ W.cm^{-2} *and other laser parameters as in Figure 4.1. The solid oscillating blue line represents the vector potential* $A(t)$.

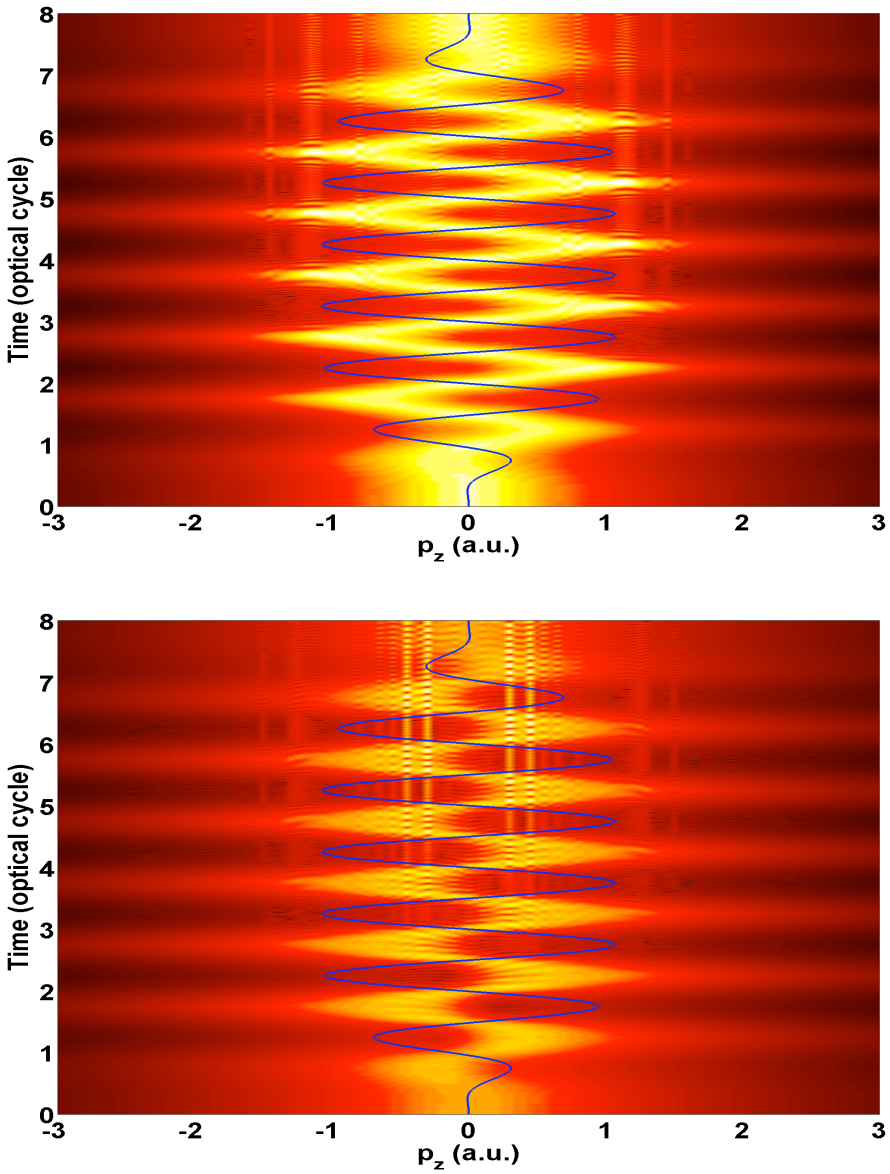

Figure 4.5: *Electron probability density as a function of time and* $p_z, p_n = 0$ *obtained respectively within our* $(1s{+}2s)$ *(upper panel) and* $(1s{+}2s{+}2p)$ *(lower panel) potential models. The laser peak intensity is* $I = 1.3 \times 10^{14}$ W.cm^{-2} *and other laser parameters as in Figure 4.1. The solid oscillating blue line represents the vector potential* $A(t)$.

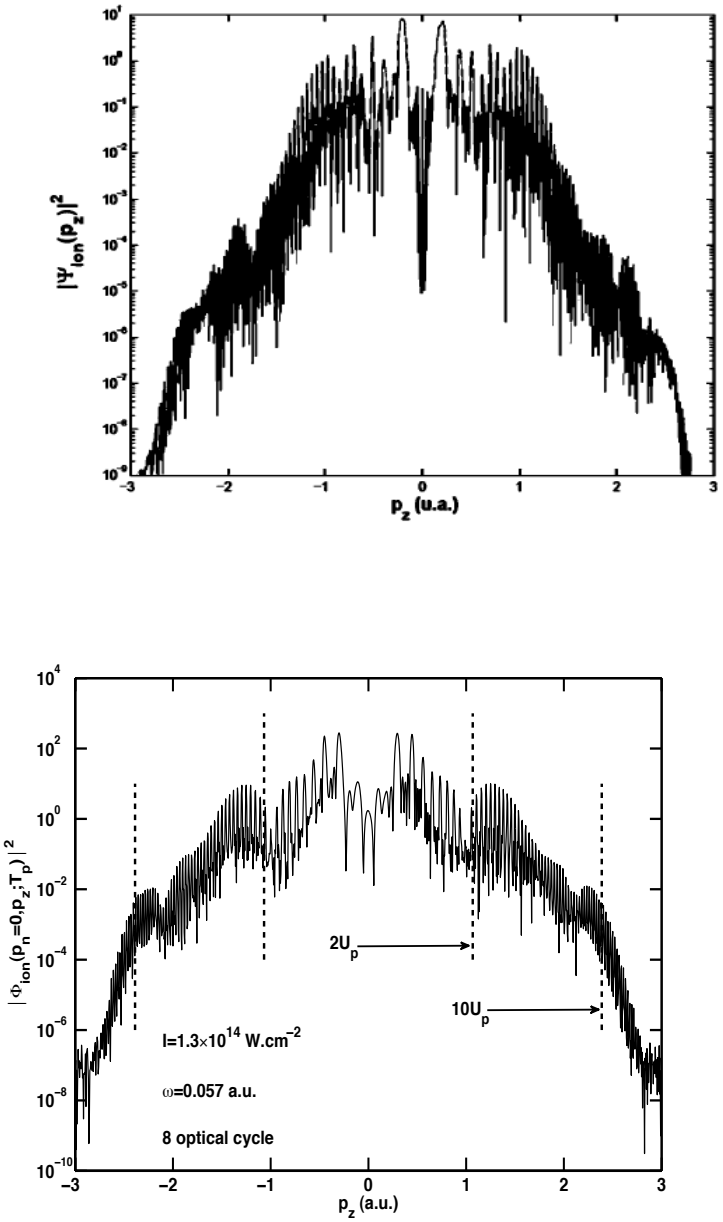

Figure 4.6: *Ionization probability density at the end of the pulse obtained within an exact Coulomb potential (upper panel, from de Bohan [3]) and our* $(1s + 2s + 2p)$ *potential model (lower panel). The laser parameters as in Figure 4.7.*

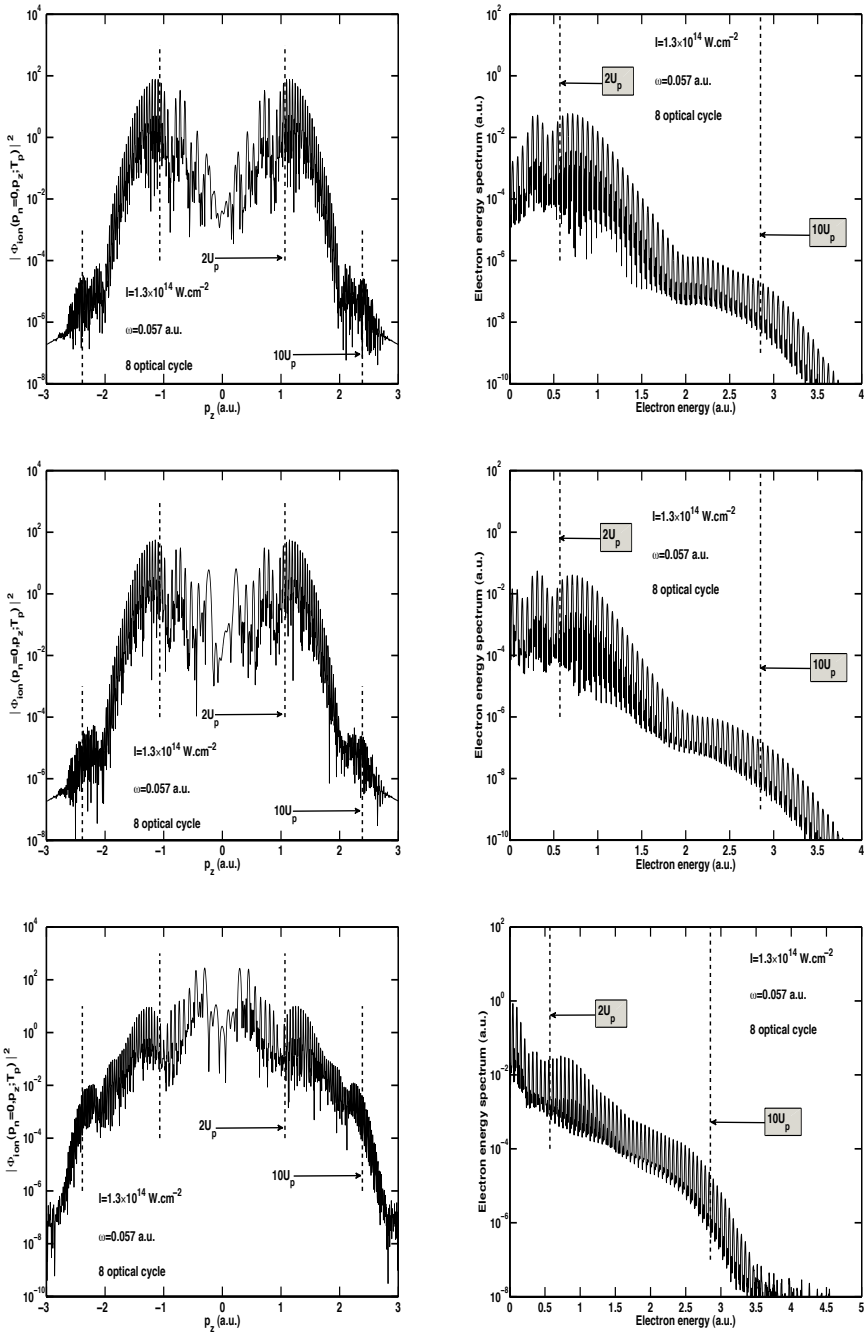

Figure 4.7: *Ionization probability density* $|\ \Phi_{ion}(p_n = 0, p_z; T_p)\ |^2$ *(is obtained by removing all the bound states of the total wave packets) at the end of the pulse (Left panel) and electron energy spectrum (right panel) for the interaction of our model atom with an* 8 *optical cycle pulse. The laser parameters are* $\omega = 0.057$ a.u., $I = 1.3 \times 10^{14}$ W.cm^{-2}. *Our separable potential supports respectively* $1s$ *state (upper panel),* $1s$+$2s$ *states (middle panel) and* $1s$+$2s$+$2p$ *states (lower panel).*

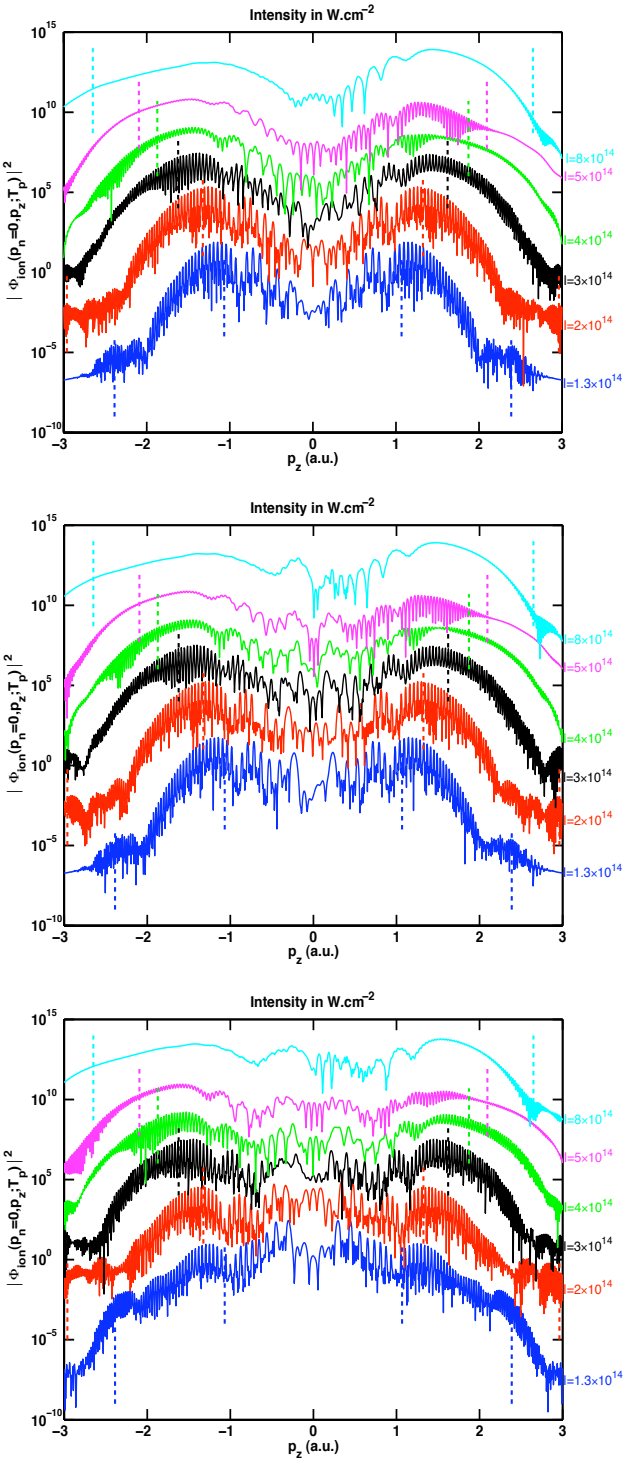

Figure 4.8: *Ionization probability density* $|\ \Phi_{ion}(p_n = 0, p_z; T_p)\ |^2$ *(is obtained by removing all the bound states of the total wave packets) at the end of the pulse for different laser peak intensities given to the right of the graphs. The laser field frequency is* $\omega = 0.057$ a.u. *and the pulse duration is* 8 *optical cycle. Our separable potential supports respectively* $1s$ *state (upper panel),* $1s + 2s$ *states (middle panel) and* $1s + 2s + 2p$ *states (lower panel). The vertical dashed lines indicate the value of* p_z *corresponding to* $2U_p$ *and* $10U_p$ *. The spectra are vertically shifted for better visibility.*

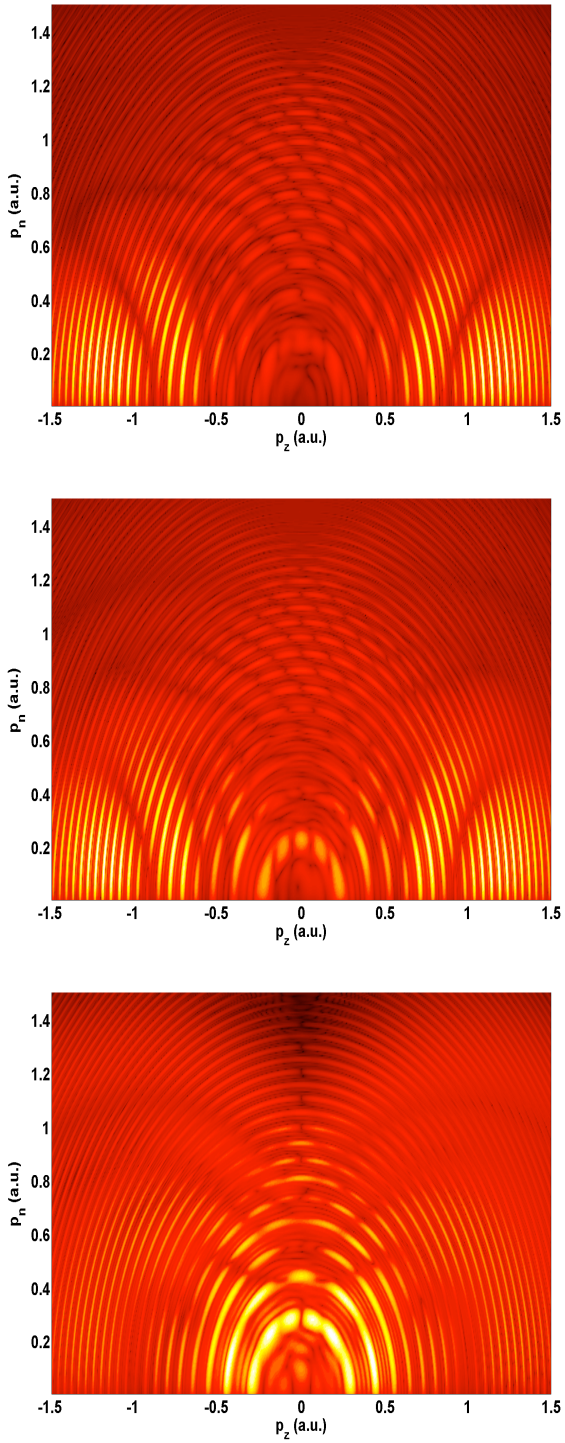

Figure 4.9: *Angular distribution of the ionization probability density* $p_n \mid \Phi_{ion}(p_n, p_z; T_p) \mid^2$ *at the end of the pulse, for the interaction of our model atom with an* 8 *optical cycle pulse. The laser parameters are* $\omega = 0.057$ a.u., $I = 1.3 \times 10^{14}$ W.cm^{-2}. *Our separable potential supports respectively* $1s$ *state (upper panel),* $1s + 2s$ *states (middle panel) and* $1s + 2s + 2p$ *states (lower panel).*

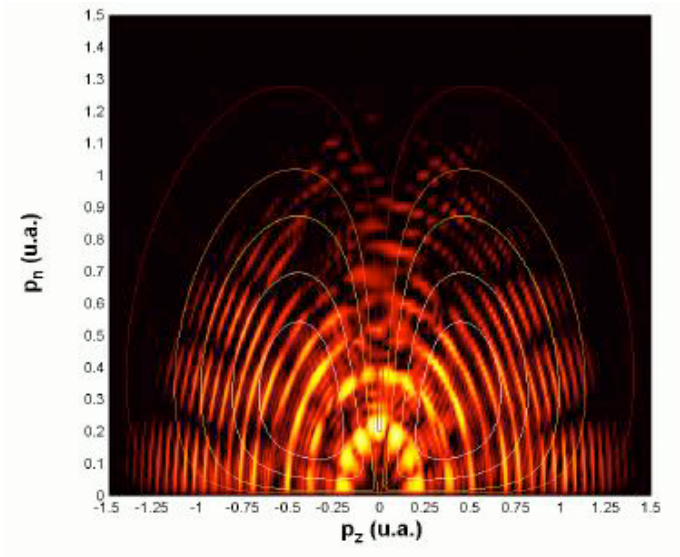

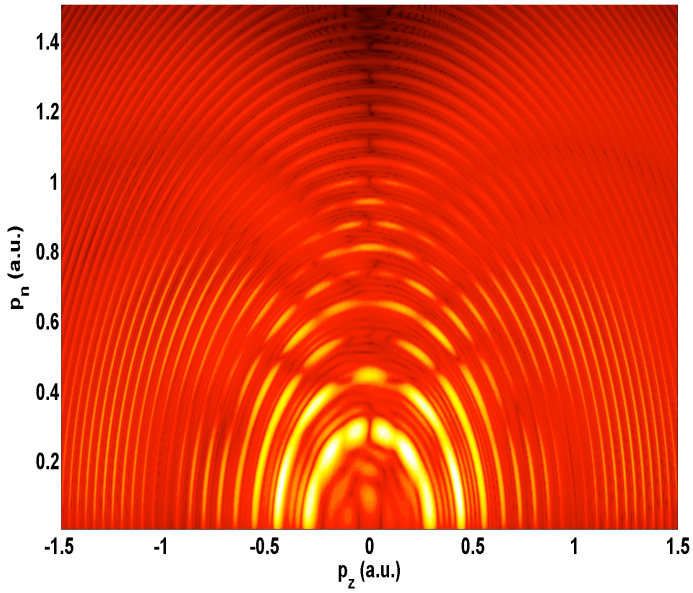

Figure 4.10: *The same figure as in 4.9 compared to the result obtained with an exact Coulomb potential (upper panel, from de Bohan [3]) and our $(1s + 2s + 2p)$ potential model (lower panel). The laser parameters as in 4.9 .*

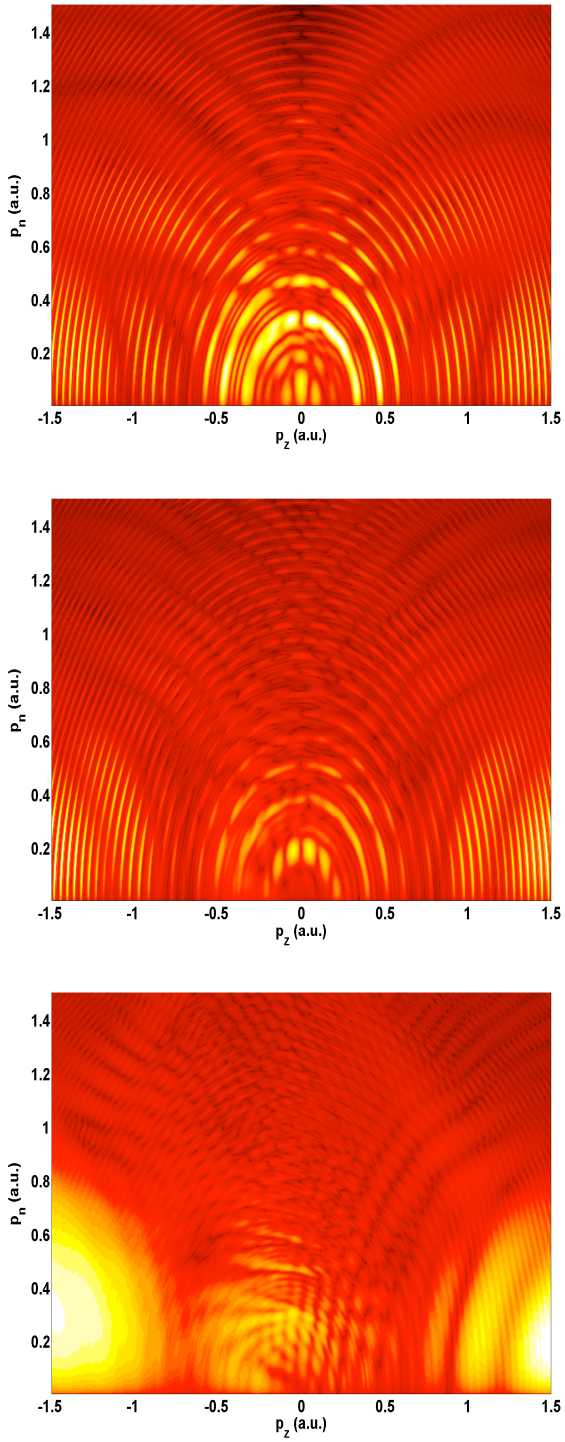

Figure 4.11: *The same figure as in 4.9, for various laser peak intensities: upper panel* $I = 2 \times 10^{14}$ W.cm^{-2}, *middle panel* $I = 3 \times 10^{14}$ W.cm^{-2} *and lower panel* $I = 8 \times 10^{14}$ W.cm^{-2}. *Our separable potential supports* $1s + 2s + 2p$ *states.*

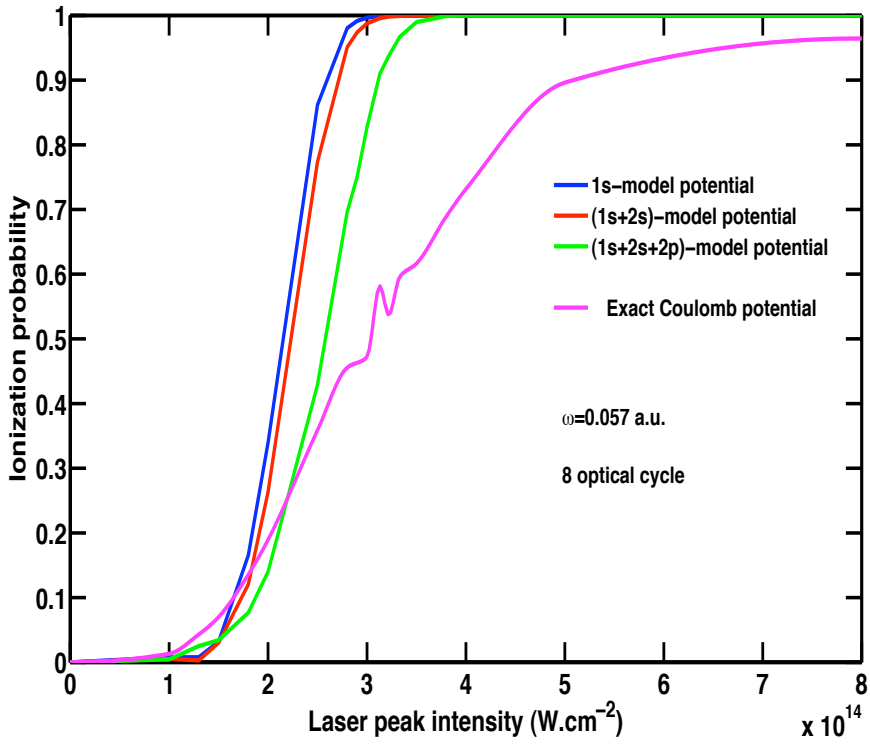

Figure 4.12: *Probability of ionization of our model atom initially in the* $1s$ *state, as a function of the peak field intensity. The total duration of the pulse is* 8 *optical cycle and the photon energy is* 0.057 a.u.. *The blue solid straight line represents the case where only* $1s$ *state is included in the separable potential, the red solid straight line for* $1s + 2s$*-model potential, the green solid straight line for* $1s + 2s + 2p$*-model potential and the magenta solid straight line for the case of exact Coulomb potential.*

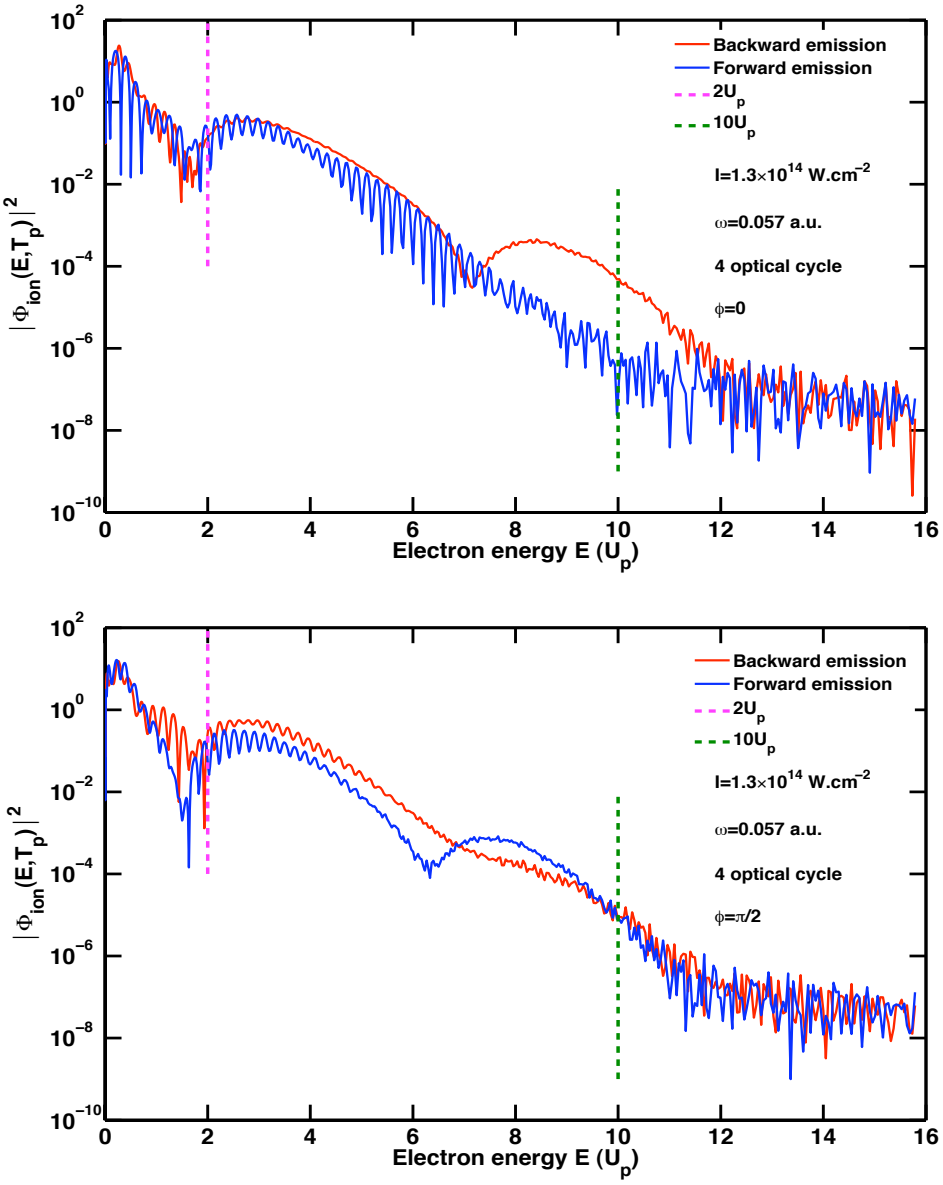

Figure 4.13: *Ionization probability density* $\mid \Phi_{ion}(p_n = 0, p_z; T_p) \mid^2$ *as function of the electron kinetic energy* E *at the end of the pulse, for a linearly polarized* 4*-optical cycle sine-quare pulse with CEP* $\phi = 0$ *(upper panel) and* $\phi = \pi/2$ *(lower panel). The laser field parameters are given on the graphs. Our separable potential supports* $1s + 2s + 2p$ *states.*

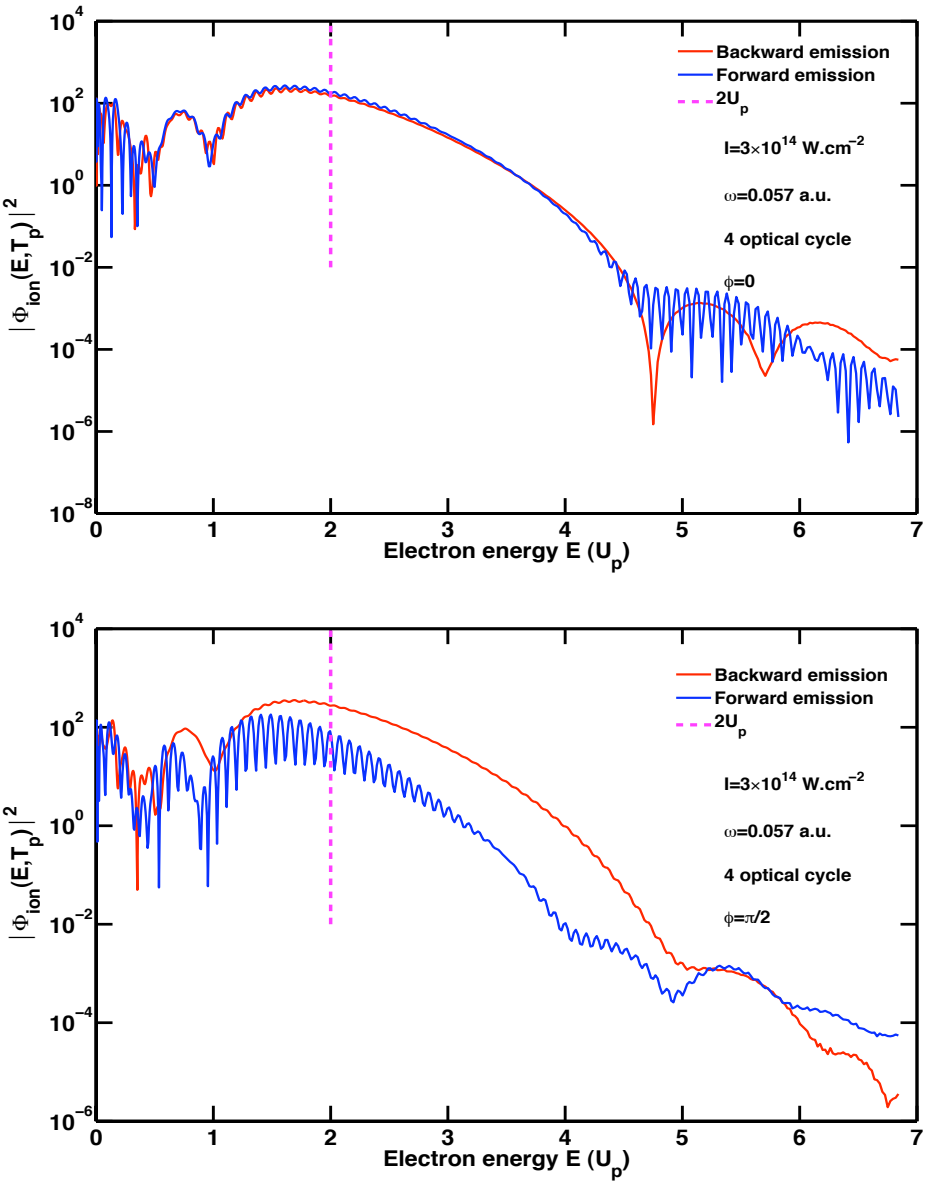

Figure 4.14: *Ionization probability density* $\mid \Phi_{ion}(p_n = 0, p_z; T_p) \mid^2$ *as function of the electron kinetic energy* E *at the end of the pulse, for a linearly polarized* 4*-optical cycle sine-quare pulse with CEP* $\phi = 0$ *(upper panel) and* $\phi = \pi/2$ *(lower panel). The laser field parameters are given on the graphs. Our separable potential supports* $1s + 2s + 2p$ *states.*

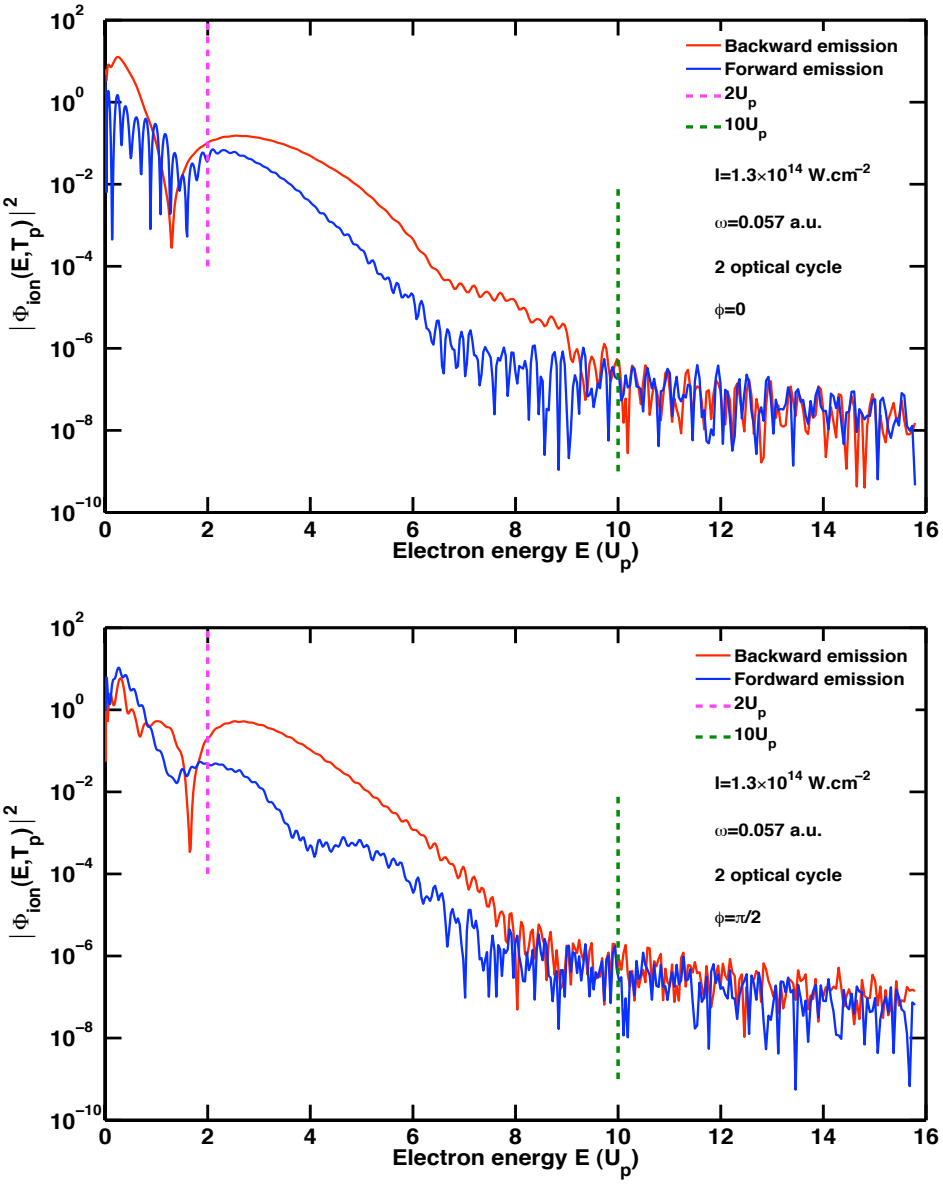

Figure 4.15: *Ionization probability density* $\mid \Phi_{ion}(p_n = 0, p_z; T_p) \mid^2$ *as function of the electron kinetic energy* E *at the end of the pulse, for a linearly polarized* 2*-optical cycle sine-quare pulse with CEP* $\phi = 0$ *(upper panel) and* $\phi = \pi/2$ *(lower panel). The laser field parameters are given on the graphs. Our separable potential supports* $1s + 2s + 2p$ *states.*

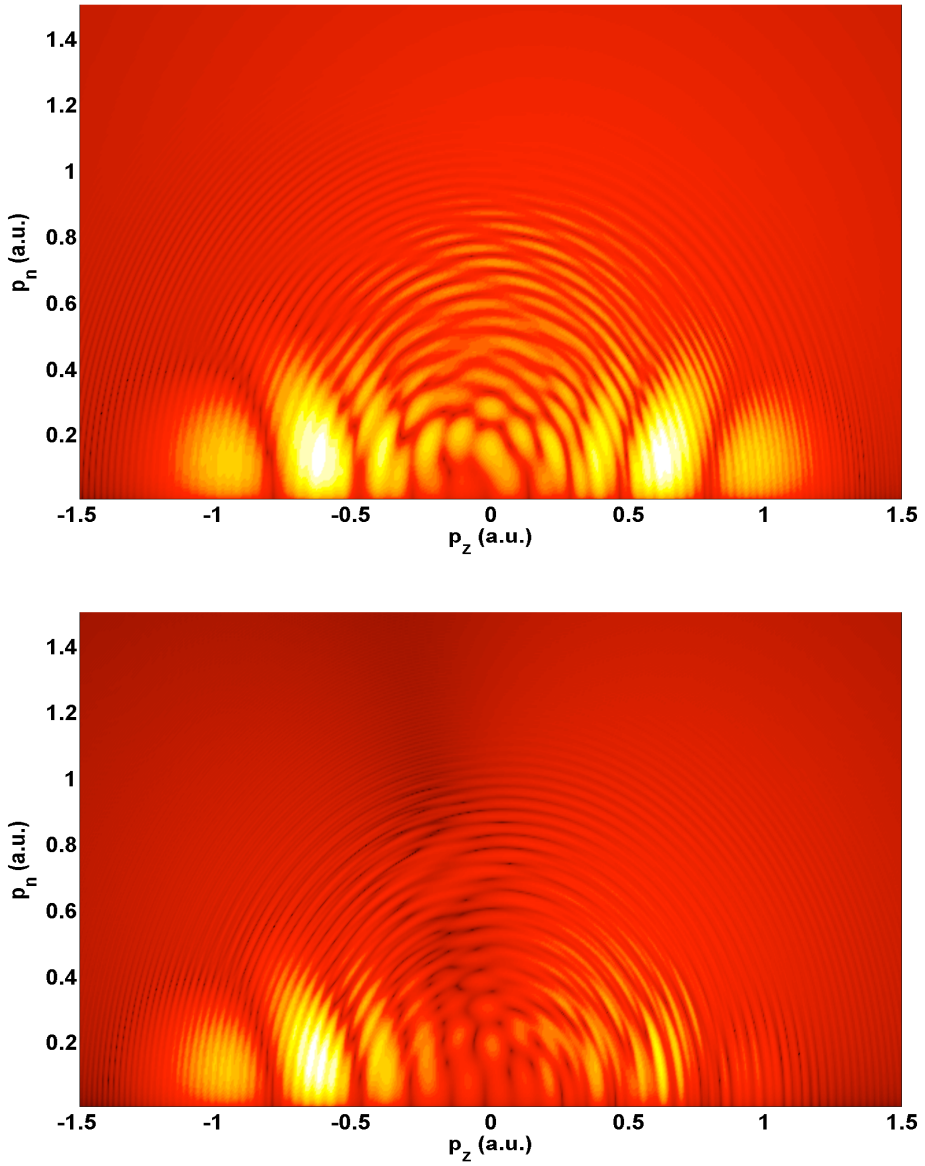

Figure 4.16: *Angular distribution of the ionization probability density* $p_n \mid \Phi_{ion}(p_n, p_z; T_p) \mid^2$ *at the end of the pulse, for the interaction of our model atom with a* 4 *optical cycle sine-quare pulse with CEP* $\phi = 0$ *(upper panel) and* $\phi = \pi/2$ *(lower panel). The laser parameters are* $\omega = 0.057$ a.u., $I = 5 \times 10^{13}$ W.cm^{-2}. *Our separable potential supports* $1s$ *state.*

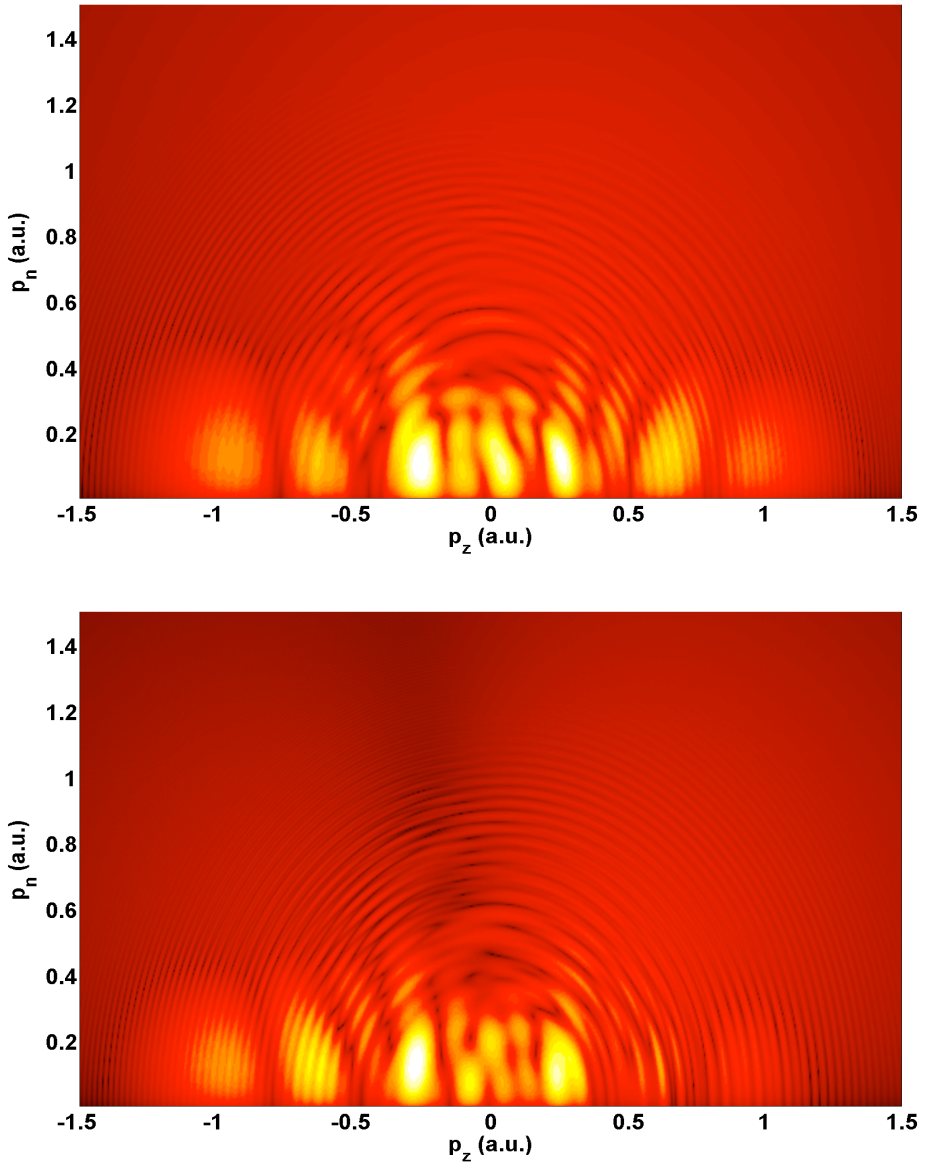

Figure 4.17: *Angular distribution of the ionization probability density* $p_n \mid \Phi_{ion}(p_n, p_z; T_p) \mid^2$ *at the end of the pulse, for the interaction of our model atom with a* 4 *optical cycle sine-quare pulse with CEP* $\phi = 0$ *(upper panel) and* $\phi = \pi/2$ *(lower panel). The laser parameters are* $\omega = 0.057$ a.u., $I = 5 \times 10^{13}$ W.cm^{-2}. *Our separable potential supports* $1s + 2s$ *states.*

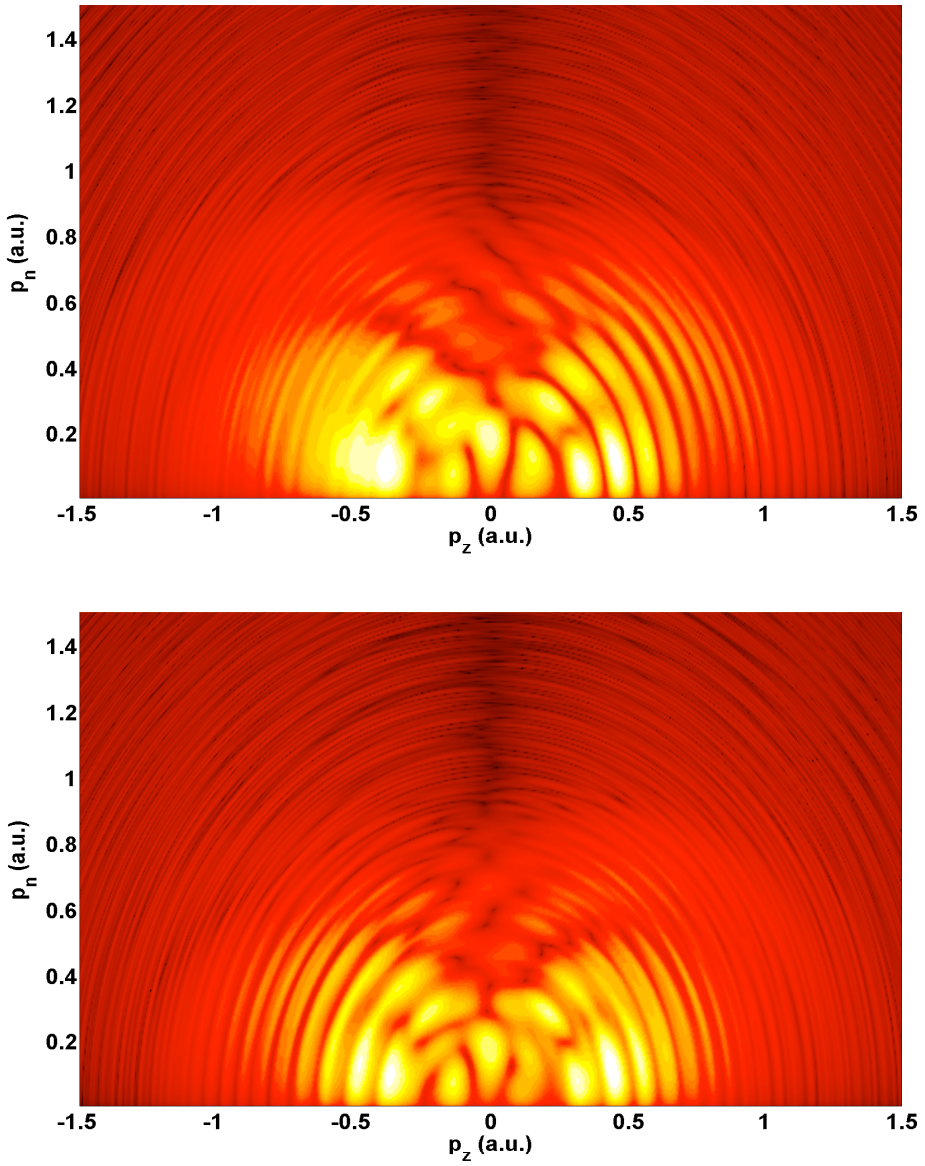

Figure 4.18: *Angular distribution of the ionization probability density* $p_n \mid \Phi_{ion}(p_n, p_z; T_p) \mid^2$ *at the end of the pulse, for the interaction of our model atom with a* 4 *optical cycle sine-quare pulse with CEP* $\phi = 0$ *(upper panel) and* $\phi = \pi/2$ *(lower panel). The laser parameters are* $\omega = 0.057$ a.u., $I = 5 \times 10^{13}$ W.cm^{-2}. *Our separable potential supports* $1s + 2s + 2p$ *states.*

Next Figures of Chapter 4

"Si ça fait mal, c'est que ça fait du bien."
Devise Shadock.

4.6 Figures

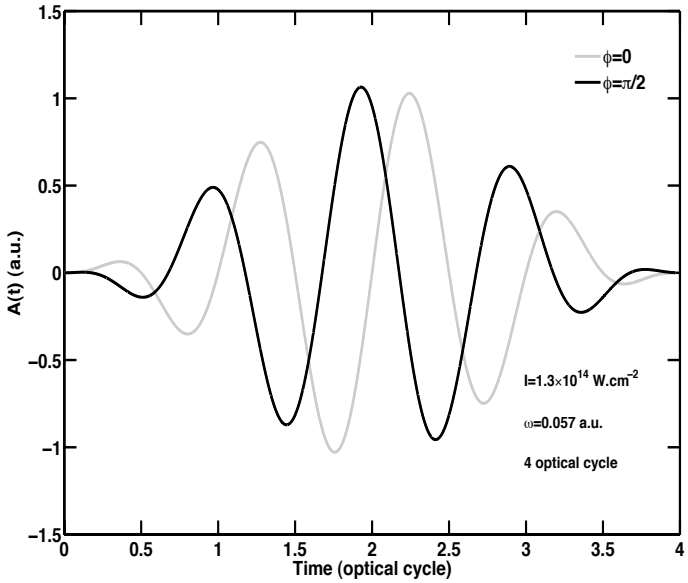

Figure 4.19: *Plot of the vector potential as a function of time (in optical cycle) for different phases $\phi = 0,\ \pi/2$ of the carrier frequency with respect to the pulse envelope. Laser parameters are given in the top right of graphs.*

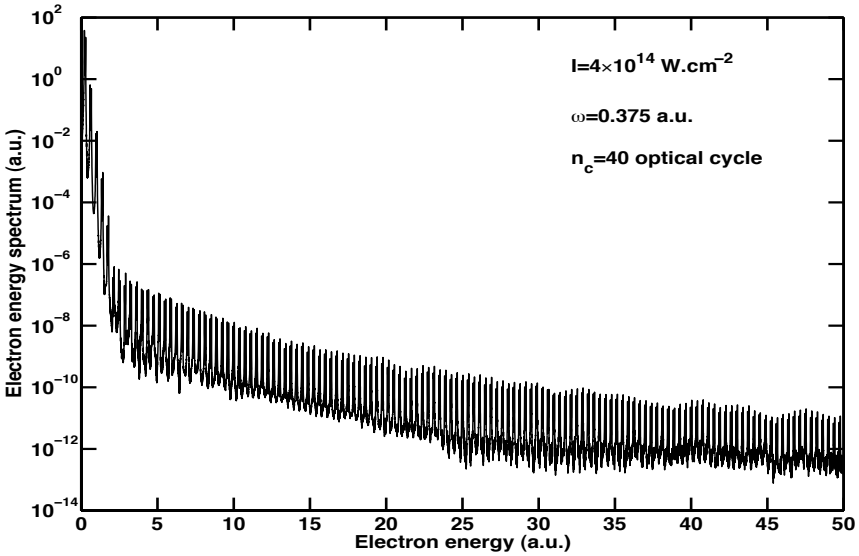

Figure 4.20: *Electron energy spectrum resulting from the interaction of our model atom, initially in the* $1s$ *state, with a laser pulse. The pulse parameters are as in Figure 3.10.*

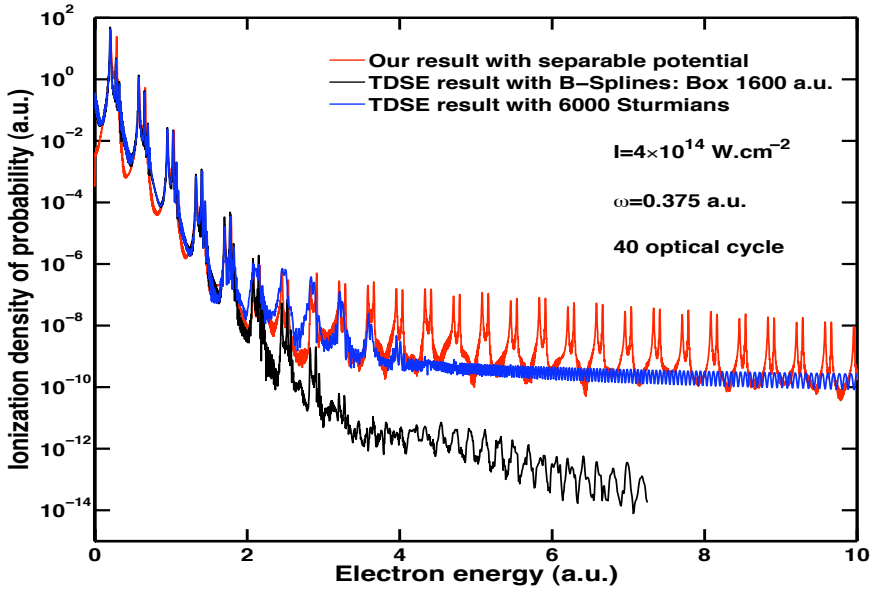

Figure 4.21: *Electron energy spectrum resulting from the interaction of our model atom, initially in the* 1*s state, with a laser pulse, compared to the results obtained from the TDSE with B-Spline's and Sturmian's methods in the configuration space. The pulse parameters are as in Figure 3.10.*

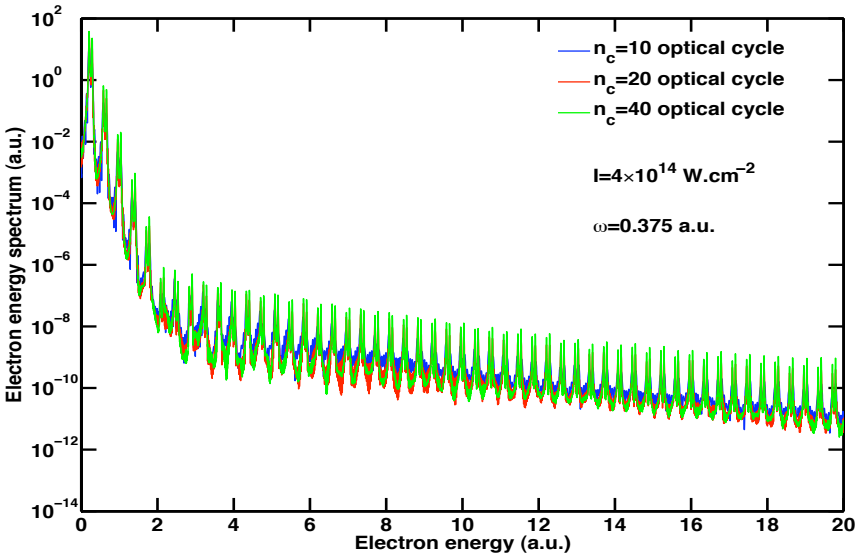

Figure 4.22: *The same figure as in Figure 4.20, but for different values of pulse's duration* $n_c = 10,\ 20,\ 40$ *optical cycle.*

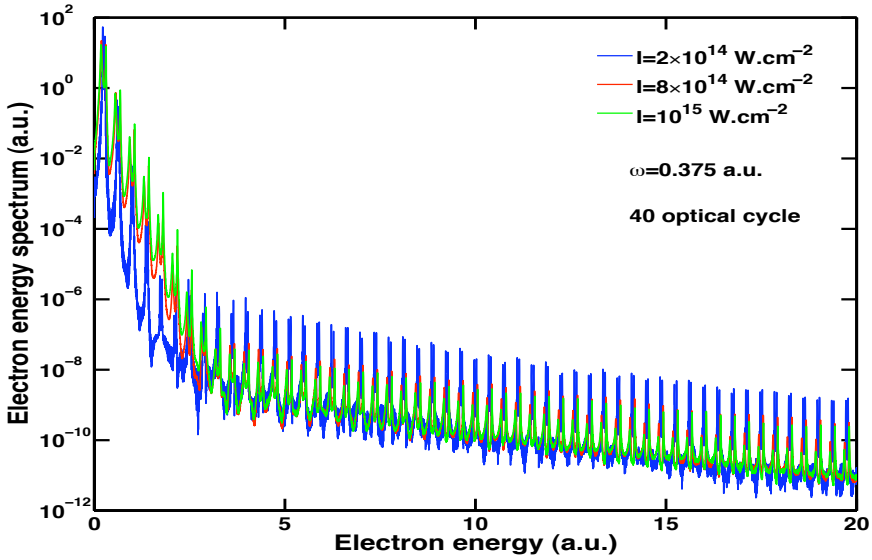

Figure 4.23: *The same figure as in Figure 4.20, but for different values of laser peak intensities (given in the top right of the graphs).*

Chapter 5

Summary and Perspectives

"On peut vivre sa vie de deux façons. Soit comme si rien n'est un miracle, soit comme si tout l'est."
Albert Einstein.

5.1 Summary

A summary of the results of the first part of this thesis has already been given in the general introduction. Here, we intend to focus once again on the benefits of using the momentum space to the analysis of ionization dynamics. It has been shown that the momentum space is, despite the non-locality of the atomic potential, actually well suited to probe the dynamics and the atomic potential effects [1, 2]. It highlights, in fact, a quasi-instantaneous viewing of the process since at the first sight, ionization happens first in terms of moment before being in terms of position. In other word, working in the momentum space, provides direct information on the ionization dynamics and in particular on the time at which the electron is emitted. This finding prompted us to develop a method of solving the time-dependent Schrödinger equation directly in the momentum space. We have adopted the velocity form of the laser-atom interaction. Our model calculation goes far beyond the well-known strong-field approximation [3, 4, 5]. The main idea of our method is to replace the kernel of the non-local Coulomb potential by a finite sum of N separable potentials, each of them supporting one bound state of atomic hydrogen. This approach which is suited for short range potentials, allows to reduce the 3-dimensional time-dependent Schrödinger equation to a system of N coupled 1-dimensional linear Volterra integral equations of the second kind that we solve numerically. Our model presents several advantages.

- it provides a rigorous solution for the electron wave packet,

- by contrast with the strong-field approximation, more than one bound states may be included in the model,
- the continuum-continuum dipole matrix elements are treated exactly,
- the theory is fully gauge invariant.

We have found this approach analytically and numerically attractive because all the physical observables are expressed in a quasi-analytically manner and the global probability density remains localized in the momentum space. Another advantage of the momentum space analysis is to provide a convenient tool for exploring the transition between the multiphoton and the strong field regimes.

By means of the Ehrenfest theorem, we studied the temporal evolution of the probability density, which allowed us to distinguish the two regimes of ionization - multiphoton and strong field regime. In the first, scattering rings are clearly present, meaning that electrons gain energy by collision with the potential, the ionization can occur at any phase of the field, while in the strong field regime, ionization takes place at a specific phase of the field (when the electric field takes its maximum values). Also in this analysis, we have identified the emergence of a series of "stripes" (from the ground state and then remaining constant as time evolves) as a signature of the ionization. Our theoretical model of the momentum space analysis helps to uncover the role of Coulomb potential in the actual mechanisms contributing to the dominant part of ATI spectra, up to $2U_p$. At intensities such that the Keldysh parameter γ is close to unity, there is a subtle interplay between the perturbative regime, where multiphoton processes dominate, and the strong field limit where tunnel ionization is assumed to set in.

Our model also allowed us to study in detail the structure of the ATI spectra, angular distributions of emitted electrons and the influence of laser parameters such as peak intensity, the laser frequency, the absolute phase and pulse duration on these spectra. Remarkable asymmetries have been highlighted in the momentum distribution, electron angular distributions and the ATI spectra.

Another interesting result obtained within the framework of our theoretical model is the emission of highly energetic electrons in the resonant interaction of our atom model with an intense high-frequency laser field. This unexpected and promising behaviour requires a deepest investigation in order to be sure that this result is not an artefact of our model.

5.2 Outlook

One of the main results of this thesis is the application of a finite sum of N separable potentials, each of them supporting one bound state of atomic hydrogen to investigate the ionization of atomic hydrogen by a strong infrared field. Here, we consider only the $1s$, $2s$ and $2p$ states. This method has allowed us to get a deep insight on the mechanism leading to electron ejection, more precisely to the clarification on the role of the Coulomb potential in such a mechanism. Furthermore, the qualitative and quantitative comparisons have been made for various physical situations in which the dynamics are well known. However, our approach can be extended by including more discrete states than previously in the separable potential in order to access to a better comparison with experimental data. Due to the highly efficient method for the computation of the total wave packets the inclusion of additional atomic bound states in the separable potential does not pose analytically and numerically a specific problem. However, this inclusion will increase the system of coupled 1-dimensional linear Volterra integral equations to be solved and will also increase computation time tremendously. As other perspectives, on the one hand, our theoretical model could be perfectly suited for the investigation, qualitatively and quantitatively of the harmonic generation [6, 7]. On the other hand, our approach opens up the possibility for its extension within the Floquet theory [8], which provides a mathematically rigorous description of the interaction of an atom with a monochromatic laser field based on complex dilation analyticity [9, 10, 11]. Also, but not the least, this approach could be easily applied for the study of systems of more than one active electron in the interaction with a strong electromagnetic field. Here, the separable potential model should be reconstructed in order to account for correlations between electrons. It is surely not an easy task these forthcoming works.

Bibliography

[1] A. de Bohan, *Dynamique de l'Interaction Laser-Atome. Moment Canonique et Approximation du Champ Fort, PhD Thesis*, Université Catholique de Louvain, Belgium (2001).

[2] A. de Bohan, B. Piraux, L. Ponce, R. Taïeb, V. Véniard and A. Maquet, *Phys. Rev. Lett.* **89**, 113002 (2002).

[3] F. H. M. Faisal, *J. Phys. B* **6**, L89 (1973).

[4] H. R. Reiss, *Phys. Rev. A* **22**, 1786 (1980).

[5] N. B. Delone and V. P. Krainov, *Multiphoton Processes in Atoms* (Springer Series on Atoms and Plasmas, 1993).

[6] A. de Bohan, Ph. Antoine, D. B. Milošević and B. Piraux, *Phys. Rev. Lett.* **81**, 1837 (1998).

[7] A. de Bohan, Ph. Antoine, D. B. Milošević, G. L. Kamta and B. Piraux, *Laser Phys.* **9**, 175 (1999).

[8] R. M. Potvliege, E. Mese and Svetlana Vučić, *Phys. Rev. A* **81**, 053402 (2010).

[9] A. Maquet, S.-I. Chu and W. P. Reinhardt, *Phys. Rev. A* **27**, 2946 (1983).

[10] R. M. Potvliege and R. Shakeshaft, *Adv. At. Mol. Opt. Phys. Suppl.* **1**, 373 (1992).

[11] S.-I. Chu and D. A. Telnov, *Phys. Rep.* **390**, 1 (2004).

Part II

Relativistic Calculation of Matrix Elements for Two-Photon Transitions in Hydrogen-Like Ions

Chapter 6

General Introduction

Nous (Hommes) devrions nous considérer comme l'instrument que Dieu, la conscience universelle, a choisi pour accomplir une mission parmi les Hommes. Trois principes essentiels gouvernent cette mission:
" Je ne suis pas né pour moi, je suis né pour les autres."
"Chacun de nous n'est qu'une simple passoire dans laquelle les dons sont versés pour passer aux autres."
"Nous adultes de maintenant n'avons pas le droit de mourir sans laisser couler dans la conscience des enfants dont nous avons la charge, les connaissances reçues."
Kange Ewane.

6.1 Motivations and general scope

The interaction of light with matter has been a fundamental topic in the history of quantum theory and as such has been studied now for a century. In spite of its obvious importance from many standpoints, is a subject of wide interest and active research. The recent upsurge of activity in studying the response of quantum systems (atoms, molecules, clusters, solids) subjected to strong electromagnetic radiation is a consequence of the availability of very intense and stable laser systems with high repetition rates in the laboratory. Simultaneously in the field of basic research, it led to the discovery of novel aspects of light-matter interaction at the atomic level. Many high-order processes are possible and competing (*e.g.* above-threshold ionization, tunnelling ionization, multiphoton ionization, high-order harmonic generation, scattering, etc) and, even in nonresonant situations, the atom may absorb a great deal of electromagnetic energy in a rather short time [1, 2]. Most of these concern two-photon processes that were first described by the Kramers-Heisenberg formula [3] which expresses the scattering in terms of an expansion over the

complete set of *intermediate* (or *virtual*) *discrete* and *continuum* states of the atomic or molecular system. When investigating the interactions of the electromagnetic field with the inner shell electrons of high Z atoms, the incident photons energies are in X-ray and γ-ray domains, so that accurate analytical formulae are needed for this range of energies. In this thesis, we shall limit ourselves, to a *fully relativistic treatment* of the S-matrix elements describing *two-photon absorption* (TPA), *Raman and Rayleigh scattering* (RRS) processes in hydrogen-like ions. TPA is one of the most basic radiation-matter interaction mechanisms. It is a very important tool in laser spectroscopy as it makes possible the transition between two states that cannot be connected by electric-dipole interaction. With the advent of lasers, a wide range of TPA applications have been reported in the literature (see [4] and references therein). For example, TPA is being studied for a variety of applications, including three-dimensional (3D) microfabrication, ultra-high-density optical data storage, biological imaging by TPA-excited fluorescence microscopy, and the controlled release of biologically relevant species. The theory of TPA was first developed in 1931 by Göppert-Mayer [5] who considered the interaction between an atom and the radiation field treated as a system of quantized harmonic oscillators and applied second-order perturbation theory to the interaction Hamiltonian in the dipole approximation. This theory allowed the calculation of the transition probabilities for two-photon processes, such as Raman / Rayleigh scattering, two-photon absorption and stimulated or spontaneous two-photon emission [6]. Of these processes, the most interesting from the astrophysical point of view is the spontaneous emission. Her prediction that an atom might absorb two or more photons simultaneously [5] could not be investigated in detail until the construction of the first laser in 1960. As a multiphoton process, TPA is closely related to RRS. In Rayleigh scattering the scattered and incident photons have the same frequency and the process is elastic, whereas in Raman scattering, the frequencies differ and the process is inelastic. In other words, the target atom suffers level transition twice -one associated with the annihilation of the incident photon and the other associated with the creation of the scattered photon. Rayleigh and Raman scattering are important phenomena in the study of solids, liquids and gases [7, 8]. In gases, Rayleigh scattering is a source of extinction in planetary and stellar atmospheres and Raman scattering is a source of emission (in symbiotic stars). Raman scattering may be a useful diagnostic probe of plasma containing sources of ultraviolet radiation because it converts the incident ultraviolet photons into photons of longer wavelength that may be more readily detectable.

Although the conventional perturbation theory offers a well established theoretical framework for calculating transition rates and related quantities in the weak-field regime (for hydrogen, say, below $5 \times 10^{11} W/cm^2$), no treatment

is fully satisfactory for higher intensities, at which new phenomena are actually occurring [9]. Several approaches to perform calculations in the weak-field regime have been proposed in the literature. For instance, the quoted pioneering work by Brown *et al.* [10, 11] who considered Rayleigh scattering from the ground state. Following the method introduced by Brown *et al.* [10, 11] and Dalgarno and Lewis [12], Johnson [13] reduced the calculation of a second-order amplitude to the numerical integration of the inhomogeneous differential equation for the perturbed wave function. This method has been successfully applied to various two-photon problems such as Lamb-shift calculations by Schwartz and Tiemann [14], elastic scattering of photons by Mittleman and Wolf [15], and two-photon ionization by Zernik [16, 17]. Later on Gontier and Trahin [18, 19] succeeded in generalizing it to the cases where the number of photons N involved in the process is greater than 2. Although this method has proven its reliability, it involves elaborate numerical techniques, especially for higher-order calculations ($N > 2$). Sadeghpour and Dalgarno [20] used an inhomogeneous differential equation method to calculate the Rayleigh and Raman scattering cross sections for atomic hydrogen and atomic caesium as functions of wavelength below and above the ionization limits. The Rayleigh scattering cross section has been calculated by Gavrila [21, 22, 23] with a procedure specific to atomic hydrogen that employs an analytic representation of the Coulomb-Green function (hereafter denoted as CGF) implicit in the Kramers-Heisenberg formula in the dipole approximation. This method was extended by Gavrila and Costescu [24, 25] to include *retardation effects*. Costescu *et al.* [26] subsequently extended the result by investigating analytically all *multipole* and retardation effects on Rayleigh scattering of photons from the ground state of hydrogen-like ions. The Kramers-Heisenberg formula has been used by Nussbaumer *et al.* [27] to calculate the Raman cross section for scattering from the $1s$ to the $2s$ state of atomic hydrogen. The probabilities of the two-photon spontaneous decay in the hydrogen atom and hydrogen-like ions were studied since the theoretical formalism was worked out by Göppert-Mayer [5] and the first estimate for the two-photon transition $2s \to 1s$ was obtained by Breit and Teller [28] who found that double photon emission is the most probable radiative decay mode, and is therefore the principal cause of the decay mechanism of the interstellar $2s$ hydrogen atoms. Studies of two-photon decay are important as they test our understanding of the entire structure of an atom, since the amplitude includes contributions from all discrete and continuum states (Schaffer *et al.* [29] and Dunford *et al.* [30]). In the past, most of the studies of two-photon decay have relied on measurement of the *lifetimes* of two-photon emitting states (Marrus and Mohr [31], Dunford *et al.* [32] and Simionovici *et al.* [33]). Declémy *et al.* [34] have performed the calculation of matrix elements for the two-photon absorption with spin-orbit coupling in the framework of quantum-defect theory for alkali atoms. Similar applications may

be found in [35, 36, 37]. Calculations along these lines can also be performed for the so-called Fues potential [38, 39]. For other interesting applications, the reader is referred to [40-52].

The chief difficulty experienced in calculating the second-order amplitudes stands in the correct evaluation of the infinite summations embedded implicitly. Such summations are extended over the *whole atomic spectrum* and are usually evaluated by means of some adequate approximation techniques which we will evoke in the text. But it is well-known that if the atomic system under consideration is hydrogenic, the calculation can be carried out rigorously without approximation. In the previous papers [16-19] it has been shown how a particular technique, introduced by Dalgarno and Lewis [12] and reformulated by Schwartz and Tiemann [14] could be generalized to calculate the sums contained in transition matrix elements built up from the matrix components of the position operator. We present here the *Coulomb Green function method* to perform these infinite summations over the complete set of states. The main advantage of this method lies in its ability of providing analytical expressions for the high-order perturbation matrix elements and it permits to avoid the explicit integration over the intermediate continuum states. Properties of the CGF that are related to the study of the scattering Coulomb T- matrix can be found in the review paper of Chen and Chen [53], which gives a good account of the analytical properties of the coulomb T- matrix and discusses the connection between the various representations of the CGF, and in the articles of Shakeshaft [54, 55]. One of the main reasons for the interest in CGF lies on one hand to the advent of powerful laser sources and the concomitant observation of multiphoton transitions at optical frequencies, and on the other to the fact that it provides useful tools in actual computations of second-order matrix elements and more generally, lowest-order N-photon absorption transition amplitudes from an initial (bound) state towards any other (bound or belonging to a continuum) final state (see, for instance, [56, 57, 58]).

The above-mentioned difficulties have motivated the search for various functional basis sets for representing wave and Green functions of a particular physical system as series or integral expansions or compact representations. The advantages of these methods have been recognized by Vetchinkin and Khristenko [59] and Gavrila [21, 22, 23]. A number of authors have improved the technique and have applied it to the study of many higher-order processes (refer to [60] and [61] for a comprehensive topical review and references therein). After the pioneering findings by Wichmann and Kroll [62] and by Martin and Glauber [63], other authors investigated the problem. We mention in this case the works by Hostler [64-69] and authors of [70-87]. Although in principle any complete set may be used for this purpose, it is well known

that for particular applications, some basis sets are more suitable than others. On physical grounds it is expected, and experience confirms it, that adequate functions may be frequently generated by solving a *Sturm-Liouville problem* [88, 89] consisting of some solvable time-independent model wave equations, with structure reflecting the main physical features of a system considered, plus *appropriate boundary conditions*. Generally, in such problems one chooses energy E as an eigenvalue and functions generated are called "*Energy eigenfunctions*". In some cases, however it may be more profitable to obtain a basis in an alternative procedure by treating the energy E as a fixed parameter and introduce an eigenvalue parameter in some other place in the wave equation. Functions generated in that manner are referred to as "*Sturmian functions*" [90, 91, 92].

The Schrödinger-Coulomb Sturmians [90] proved to be a valuable tool in nonrelativistic atomic physics, namely that, they were used as a variational set for the determination of atomic energy levels, as a basis for a discrete expansion of the Coulomb Green function, as an expansion basis in L^2 techniques of the scattering theory and for atom-laser field interaction processes. Since then it became necessary to build up their relativistic counterparts, which should find numerous applications in relativistic atomic physics. Among a variety of Sturmian basis sets which may be obtained by making different choices of wave equations and eigenvalue parameters, Dirac-Coulomb Sturmian functions are of particular value because of the exceptional role played in atomic physics by the Coulomb problem [90-93]. In this context, the works undertaken by Manakov *et al.* [82, 83, 84] were based on a second-order Sturm-Liouville problem arising from the Gell-Mann-Feynman equation. More convenient constructions based on coupled first-order Sturm-Liouville equations were proposed by Drake and Goldman [42, 43] and by Grant [94-97]. Few years later, Szmytkowski [93] proved that none of these later functions can form a complete fully relativistic Sturmian set. The basis constructed by Drake and Goldman should not be considered as a Sturmian set since it consists of two subsets of functions satisfying different Sturm-Liouville problems contrary to the general theory [88] which stipulated that all Sturmians must be solutions to the same boundary-value problem. In turn, Grant's basis cannot form a complete set since he restricted himself only to solutions of a Sturm-Liouville problem corresponding to a part of the complete spectrum of its eigenvalues. This problem has been overcome by Szmytkowski in his paper [93]. He generalized the ideas of Drake and Goldman and Grant to derive complete sets of Dirac-Coulomb Sturmians associated directly with first-order Sturm-Liouville problems. The utility of this basis was illustrated by computing relativistic static electric dipole polarizabilities for hydrogen-like atoms [93]. The efficiency of this basis has also been proved through some recent relevant applications in the literature. For instance, see

Szmytkowski [98, 99], Szmytkowski and Mielewczyk [100] and Mielewczyk and Szmytkowski [101]. The motivation of this work stems in part from that point.

Using a representation of the *first-order* Dirac-Coulomb Green function in terms of an expansion over the Sturmian basis associated to the *second-order* Dirac equation (also known as Gell-Mann Feynman equation) [35, 36], Szymanowski *et al.* [85, 86] computed two-photon probability amplitudes which take into account *relativistic* and *retardation effects* for transitions in hydrogen-like ions from the ground state towards states in the L and M shells. Owing to the above-mentioned reason concerning the nature of the basis set used, we found necessary to reconsider their calculations. In this thesis, We are going to study the two-photon excitation, namely the two-photon absorption and Raman / Rayleigh scattering of hydrogen-like ions within the framework of *second-order perturbation* theory. More precisely, and for the moment, we are interested in the derivation of the exact fully and quasi relativistic expressions of the probability amplitudes of the above mentioned physical processes. It is worth underlining that our expressions already include all the well-known relativistic , retardation and multipole effects. At the present stage, we did not study the relative importance of these effects. That was not the objective of this work. Their discrimination is analytically complex as shown by the works of Costescu *et al.* [26], Costescu and Spanulescu [102] and Costescu *et al.* [103]. A distinctive feature of our treatment is that we use the representation of the first-order Dirac-Coulomb Green function in terms of an expansion over the Sturmian basis sets constructed by Szmytkowski and us to derive *exact* explicit expressions of the two-photon absorption as well as Rayleigh and Raman scattering probability amplitudes. Moreover our fully relativistic and quasirelativistic treatments based on the *tensor algebra* take into account retardation effects, and, compared to the above method, offer the advantage that our results could be applied to any *multipole* of the two photons. The radial integrals involved in the processes are conveniently solved analytically. This leads to closed-form expressions for the two-photon bound-bound transition amplitudes. As for the angular part of the analysis in both approaches, we have performed in a simple manner the angular integrals obtained through tedious calculations by the authors of [85, 86].

6.2 Outline of the dissertation

This part of dissertation consists of four Chapters, four Appendices, starting in **Chapter 6** with the present General Introduction.

Chapter 7 is devoted to the derivation of the fully and quasirelativistic

radial wave functions. These functions are used later on to determine the two-photon transition rates in hydrogen-like ions. The Coulomb Green's functions play also a similar important role, in particular, if the interaction of atoms with external fields is to be studied. In second-and higher order perturbation theory, for instance, these functions help to carry out the summation over the complete spectrum in a rather efficient way. Although different analytic representations are known for the Green's functions until today, their Sturmian expansions have proven to be very useful in nonrelativistic and relativistic atomic physics, especially for actual two-photon amplitude computations. In this respect, the Coulomb Sturmian basis functions as well as different Coulomb Green's function representations for the first-order Dirac-Coulomb equation and the Gell-Mann Feynman equation have been presented. An account of nonrelativistic limit of these above mentioned functions are also given throughout.

Chapter 8 is dedicated to the derivation of the fully and quasirelativistic S-matrix elements describing two-photon transition amplitude probabilities between hydrogenic bound states. One of the implicit summation methods, based on the Coulomb Green's functions has been exploited for these computations. As an illustration of this method, for linear polarized photons, first numerical results on two-photon absorption transition rates in hydrogen-like ions from the lighter to the heavier elements are given and discussed. The explicit analytical formulae for Rayleigh and Raman scattering processes are clearly derived.

In **Chapter 9** we conclude our work with a short summary, and give a brief outlook of future applications of our approach. In addition, we include four Appendices which contain some details that are relevant to the comprehension of certain analytical derivations. They include a system of units, special functions, angular and radial integrals.

Bibliography

[1] M. Protopapas, C. H. Keitel and P. L. Knight, *Rep. Prog. Phys.* **60**, 389 (1997).

[2] V. Veniard and B. Piraux, *Phys. Rev. A* **41**, 4019 (1990).

[3] H. H. Kramers and W. Heisenberg, *Z. Phys.* **31**, 681 (1925).

[4] Z. Zheng, A. M. Weiner, J. H. Marsh and M. M. Karkhanehchi, *IEEE Photon. Technol. Lett.* **9**, 493 (1997).

[5] M. Göppert-Mayer, *Ann. Phys., Lpz* **9**, 273 (1931).

[6] D. O'Connell, K. J. Kollath, A. J. Duncan and H. Kleinpoppen, *J. Phys. B: At. Mol. Opt. Phys.* **11**, L214 (1975).

[7] H. M. Schmid, *Astron. Astrophys.* **211**, L31 (1989).

[8] H. M. Schmid and H. Schild, *Astron. Astrophys.* **236**, L13 (1990).

[9] F. Trombetta, S. Basile and G. Ferrante, *J. Opt. Soc. Am. B* **7**, 598 (1990).

[10] G. E. Brown, R. E. Peierls and J. B. Woodward, *Proc. R. Soc. A* **227**, 51 (1954).

[11] S. Brenner, G. E. Brown and J. B. Woodward, *Proc. R. Soc. A* **227**, 59 (1954).

[12] A. Dalgarno and J. T. Lewis, *Proc. R. Soc. A* **233**, 70 (1955).

[13] W. R. Johnson, *Phys. Rev. Lett.* **29**, 1123 (1972).

[14] C. Schwartz and J. J. Tiemann, *Ann. Phys.* **6**, 178 (1959).

[15] M. H. Mittleman and F. A. Wolf, *Phys. Rev.* **128**, 2686 (1962).

[16] W. Zernik, *Phys. Rev. A* **135**, 51 (1964).

[17] W. Zernik and R. W. Klopfenstein, *J. Math. Phys.* **6**, 262 (1965).

[18] Y. Gontier and M. Trahin, *Phys. Rev.* **172**, 83 (1968).

[19] Y. Gontier and M. Trahin, *Phys. Rev. A* **4**, 1896 (1971).
Y. Gontier and M. Trahin, *Phys. Rev. A* **14**, 1935 (1976) (erratum).

[20] H. R. Sadeghpour and A. Dalgarno, *J. Phys. B: At. Mol. Opt. Phys.* **25**, 4801 (1992).

[21] M. Gavrila, *Phys. Rev.* **163**, 147 (1967).

[22] M. Gavrila, *Phys. Rev. A* **6**, 1348 (1972).

[23] M. Gavrila, *Phys. Rev. A* **6**, 1360 (1972).

[24] M. Gavrila and A. Costescu, *Phys. Lett. A* **28**, 614 (1969).

[25] M. Gavrila and A. Costescu, *Phys. Rev. A* **2**, 1752 (1970).

[26] A. Costescu, P. M. Bergstrom, Jr. C. Dinu and R. H. Pratt, *Phys. Rev. A* **50**, 1390 (1994).

[27] H. Nussbaumer, H. M. Schmid and M. Vogel, *Astron. Astrophys.* **211**, L27 (1989).

[28] G. Breit and E. Taller, *Astrophys. J.* **91**, 215 (1940).

[29] H. W. Schaffer *et al.,*, *Phys. Rev. A* **59**, 245 (1999).

[30] R. W. Dunford *et al.,*, *Phys. Scr.* **T80**, 143 (1999).

[31] M. Marrus and P. J. Mohr, *Adv. At. Mol. Phys.* **14**, 181 (1978).

[32] R. W. Dunford *et al.,*, *Phys. Rev. A* **48**, 2729 (1993).

[33] A. Simionovici *et al.,*, *Phys. Rev. A* **48**, 1695 (1993).

[34] A. Declémy, A. Rachman, M. Jaouen and G. Laplanche, *Phys. Rev. A* **23**, 1823 (1981).

[35] B. A. Zon, N. L. Manakov and L. P. Rapoport, *Sov. Phys.-Dokl.* **14**, 904 (1970).

[36] B. A. Zon, N. L. Manakov and L. P. Rapoport, *Yad. Fiz.* **15**, 508 (1972). B. A. Zon, N. L. Manakov and L. P. Rapoport, *Sov. J. Nucl. Phys.* **15**, 282 (1972).

[37] Y. Flank and A. Rachman, *Phys. Lett. A* **53**, 247 (1975).

[38] N. L. Manakov and V. D. Ovsiannikov, *J. Phys. B: At. Mol. Phys.* **10**, 569 (1977).

[39] N. L. Manakov, V. D. Ovsiannikov and L. P. Rapoport, *Phys. Rep.* **141**, 319 (1986).

[40] V. Florescu and M. Gavrila, *Phys. Rev. A* **14**, 211 (1976).

[41] R. Sternheimer, *Phys. Rev.* **84**, 244 (1951).

[42] S. P. Goldman and G. W. F. Drake, *Phys. Rev. A* **24**, 183 (1981).

[43] G. W. F. Drake and S. P. Goldman, *Adv. At. Mol. Phys.* **25**, 393 (1988).

[44] Y. B. Bannet and I. Freud, *Phys. Rev. Lett.* **49**, 539 (1982).

[45] Y. B. Bannet and I. Freud, *Phys. Rev. A* **30**, 299 (1984).

[46] S. A. Zapryagaev and N. L. Manakov, *Izv. Akad. Nauk SSSR* **45**, 2336 (1981).

[47] S. A. Zapryagaev, N. L. Manakov and V. G. Palchikov, *Theory of Multiply Charged Ions with One and Two Electrons* (Energoatomizdat, Moscow, 1985) (in Russian).

[48] N. L. Manakov, A. A. Nekipelov and A. G. Faĭnshteĭn, *Yad. Fiz.* **45**, 1091 (1987).
N. L. Manakov, A. A. Nekipelov and A. G. Faĭnshteĭn, *Sov. J. Nucl. Phys.* **45**, 67 (1987) (Engl. transl.).

[49] S. Klarsfeld, *Lett. Nuovo Cimento* **1**, 682 (1969).

[50] S. Klarsfeld, *Lett. Nuovo Cimento* **2**, 548 (1969).

[51] S. Klarsfeld, *Lett. Nuovo Cimento* **3**, 395 (1970).

[52] C. Fronsdal, *Phys. Rev.* **179**, 1513 (1969).

[53] J. C. Y. Chen and A. C. Chen, *Adv. At. Mol. Phys.* **8**, 71 (1972).

[54] R. Shakeshaft, *J. Phys. B: At. Mol. Phys.* **18**, L611 (1985).

[55] R. Shakeshaft, *Phys. Rev. A* **34**, 244 (1986).

[56] H. B. Bebb and A. Gold, *Phys. Rev.* **143**, 1 (1966).

[57] P. Lambropoulos, *Adv. At. Mol. Phys.* **12**, 87 (1976).

[58] F. H. M. Faisal, *Theory of Multiphoton Process* (Plenum, New York, 1987).

[59] S. I. Vetchinkin and S. V. Khristenko, *Chem. Phys. Lett.* **1**, 437 (1967).

[60] A. Maquet, *Phys. Rev. A* **15**, 1088 (1977).

[61] A. Maquet, V. Veniard and T. A. Marian, *J. Phys. B: At. Mol. Opt. Phys.* **31**, 3743 (1998).

[62] E. H. Wichmann and N. M. Kroll, *Phys. Rev.* **101**, 843 (1956).

[63] P. C. Martin and R. J. Glauber, *Phys. Rev.* **109**, 1307 (1958).

[64] L. Hostler and R. H. Pratt, *Phys. Rev. Lett.* **10**, 469 (1963).

[65] L. Hostler, *J. Math. Phys.* **5**, 591 (1964).

[66] L. Hostler, *J. Math. Phys.* **5**, 1235 (1964).

[67] L. Hostler, *J. Math. Phys.* **11**, 2966 (1970).

[68] L. Hostler, *J. Math. Phys.* **24**, 2366 (1983).

[69] L. Hostler, *J. Math. Phys.* **28**, 2984 (1987).

[70] P. J. Mohr, *Ann. Phys., NY* **88**, 26 (1974).

[71] P. J. Mohr, *Ann. Phys., NY* **88**, 52 (1974).

[72] Ya. I. Granovskiĭ, *Zh. Eksp. Teor. Fiz* **56**, 605 (1969).
Ya. I. Granovskiĭ, *Sov. Phys.-JETP* **29**, 333 (1969).

[73] Ya. I. Granovskiĭ and V. I. Nechet, *Teor. Mat. Fiz* **18**, 262 (1974).
Ya. I. Granovskiĭ and V. I. Nechet, *Theor. Math. Phys.* **18**, 185 (1974) (Engl. transl.).

[74] L. I. Komarov and T. S. Romanova, *J. Phys. B: At. Mol. Phys.* **18**, 859 (1985).

[75] A. T. Le, V. H. Le, L. I. Komarov and T. S. Romanova, *J. Phys. B: At. Mol. Opt. Phys.* **27**, 4083 (1994).

[76] A. T. Le, V. H. Le, L. I. Komarov and T. S. Romanova, *J. Phys. B: At. Mol. Opt. Phys.* **29**, 2897 (1996).

[77] P. Indelicato and P. J. Mohr, *J. Math. Phys.* **36**, 714 (1995).

[78] S. A. Zapryagaev and N. L. Manakov, *Yad. Fiz.* **23**, 917 (1976).
S. A. Zapryagaev and N. L. Manakov, *Sov. J. Nucl. Phys.* **23**, 482 (1976).

[79] R. A. Swainson and G. W. F. Drake, *J. Phys. A: Math. Gen.* **24**, 79 (1991).

[80] R. A. Swainson and G. W. F. Drake, *J. Phys. A: Math. Gen.* **24**, 95 (1991).

[81] R. A. Swainson and G. W. F. Drake, *J. Phys. A: Math. Gen.* **24**, 1081 (1991).

[82] N. L. Manakov, L. P. Rapoport and S. A. Zapryagaev, *Phys. Lett.* **43A**, 139 (1973).

[83] N. L. Manakov, L. P. Rapoport and S. A. Zapryagaev, *Phys. Lett.* **48A**, 145 (1974).

[84] N. L. Manakov, L. P. Rapoport and S. A. Zapryagaev, *J. Phys. B: At. Mol. Phys.* **7**, 1076 (1974).

[85] C. Szymanowski, V. Véniard, R. Taïeb and A. Maquet, *Phys. Rev. A* **56**, 700 (1997).

[86] C. Szymanowski, V. Véniard, R. Taïeb and A. Maquet, *Europhys. Lett.* **37**, 391 (1997).

[87] E. Karule, *J. Phys. B: At. Mol. Phys.* **4**, L67 (1971).

[88] P. M. Morse and H. Feshbach, *Methods of Theoretical Physics: Part I* (McGraw-Hill, New York, 1953).

[89] E. C. Titchmarsh, *Eigenfunction Expansion Associated with 2nd Order Differential Equations* vol II (Oxford University Press, Oxford, 1958).

[90] M. Rotenberg, *Adv. At. Mol. Phys.* **6**, 233 (1970).

[91] K. G. Lagmago, *PhD Thesis* IMSP, Université Nationale du Bénin (1999).

[92] S. V. Khristenko, *Teor. Mat. Fiz.* **22**, 31 (1975).

[93] R. Szmytkowski, *J. Phys. B: At. Mol. Opt. Phys.* **30**, 825 (1997).
R. Szmytkowski, *J. Phys. B: At. Mol. Opt. Phys.* **30**, 2747 (1997) (erratum).

[94] I. P. Grant, *Adv. Phys.* **19**, 747 (1970).

[95] I. P. Grant, *J. Phys. B: At. Mol. Phys.* **7**, 1458 (1974).

[96] I. P. Grant, *The Effects of Relativity in Atoms, Molecules and the Solid state* ed S Wilson, I P Grant and B L Gyorffy (Plenum, New York, 1991).

[97] I. P. Grant, *Adv. At. Mol. Opt. Phys.* **32**, 169 (1994).

[98] R. Szmytkowski, *Phys. Rev. A* **65**, 012503 (2001).

[99] R. Szmytkowski, *J. Phys. B: At. Mol. Opt. Phys.* **35**, 1379 (2002).

[100] R. Szmytkowski and K. Mielewczyk, *J. Phys. B: At. Mol. Opt. Phys.* **37**, 3961 (2004).

[101] K. Mielewczyk and R. Szmytkowski, *Phys. Rev. A* **73**, 022511 (2006). K. Mielewczyk and R. Szmytkowski, *Phys. Rev. A* **73**, 039908 (2006) (erratum).

[102] A. Costescu and S. Spanulescu, *Phys. Rev. A* **73**, 022702 (2006).

[103] A. Costescu, S. Spanulescu and C. Stoica, *J. Phys. B: At. Mol. Opt. Phys.* **40**, 2995 (2007).

Chapter 7

The Relativistic Sturmian Functions

"Dans l'adversité, j'aspire au bonheur; dans le bonheur, je redoute l'adversité. Entre ces extrêmes, existe-t-il un point d'équilibre où la vie humaine ne soit pas une épreuve?....."

St Augustin, Confessions, X, 28-29.

7.1 Introduction

In theoretical physics one frequently encountered the situation that a given function, defined over some domain, is expanded in a functional basis. Among a variety of bases used in such expansions, those generated by differential eigenvalue problems are of major importance. Properties of expansions in series of eigenfunctions of differential operators were extensively investigated by generations of mathematicians and mathematical physicists and their results are contained in a vast literature of the subject (cf. Refs.[1, 2, 3, 4, 5, 6] and references therein). In theoretical analysis of atomic and molecular phenomena one frequently uses various functional basis sets for representing wave or Green functions of a particular physical system in forms of series or integral expansions [7]. In principle, it seems to be more natural to use the energy eigenstates as basis sets. However, in some cases, it may be more interesting to use the Sturmian eigenfunctions [8, 9].

The advantages of Sturmian basis sets can be summarized as follows [10, 11]. *(i)* Whereas the discrete energy eigenfunctions must be augmented by the continuum to form a complete set, Sturmian basis sets are complete and square integrable for negative energies. *(ii)* Sturmian functions can be defined to satisfy appropriate physical boundary conditions, e.g., bound-state bound-

ary conditions for bound states and outgoing (incoming) boundary conditions at positives energies. *(iii)* Sturmian functions diagonalize the potential and therefore are superior to energy eigenstates for representing waves in regions where the potential is strongest. In other words, all Sturmian functions with a fixed energy are well localized in the physically relevant region of the potential. For this reason they often provide rapidly convergent expansions of wave functions for complex systems. *(iv)* Superior localization of Sturmian basis sets can be effectively employed to describe dynamic atomic and molecular systems characterized by the electronic states that are initially known to be localized around on particular center of force. This property can be especially useful when describing atomic collisions.

Among a variety of Sturmian basis sets which may be obtained by making different choices of wave equations and eigenvalue parameters, Coulomb Sturmian functions are of particular value because of the exceptional role played in atomic physics by the Coulomb potential. Coulomb Sturmian basis sets [8] have been used successfully for some time in nonrelativistic atomic calculations [12]. The vast range of applicability of the nonrelativistic Sturmians suggests that their relativistic counterparts, namely the Dirac-Coulomb Sturmians, should be equally useful in relativistic atomic physics. Such sets should be useful in the analysis of those atomic processes where the relativity is expected to play an important role. In recent years there has been an increasing interest in developing mathematical tools suitable for the use in relativistic theoretical atomic physics [13, 14]. In this standpoint, searches have been conducted to find a relativistic analog of the Schrödinger-Coulomb Sturmians. The first attempts to define the relativistic Sturmians [9, 15], followed by exemplary applications [16], were based on a Sturm-Liouville problem arising from the Gell-Mann Feynman equation [17, 18, 19]. An ingenious procedure for deriving the discrete Sturmian functions associated with the Gell-Mann Feynman equation (dubbed hereafter as quasirelativistic Sturmian functions) has been proposed by Hostler [18, 19] and has been exploited by Szymanowski *et al.* [20] in deriving an explicit expression for the first-order Dirac-Coulomb Green function.

Later on, more elegant constructions based on coupled first-order Sturm-Liouville equations were proposed by Drake and Goldman [21] and by Grant [22]. Few years after, Szmytkowski [23] found, however, that neither the functions of Drake and Goldman [21] nor those obtained by Grant [22, 24, 25, 26] (which he called L-spinors) form Dirac-Coulomb Sturmian sets. The basis constructed by Drake and Goldman should not be considered as a Sturmian set since it consists of *two* subsets of functions satisfying closely related but *different* Sturm-Liouville problems while in accordance with the general theory

[27] all Sturmians must be solutions to the *same* boundary-value problem. In turn, Grant [22] restricted himself to solutions of the defining Sturm-Liouville problem corresponding to a *part* of the complete spectrum of its eigenvalues. This results in L-spinors that are only a *part* of the Dirac-Coulomb Sturmian basis and do not form a complete set, although a set said to be complete [26] can be obtained from L-spinors using projection operators [23]. The author [23] constructed two sets of Dirac-Coulomb Sturmians in a manner which is a generalization of ideas of Drake and Goldman [21] and Grant [22]. The efficiency of this basis has been proved through some recent relevant applications in the literature. For instance, we mention the works undertaken in Refs. [23, 28, 29, 30] and more recently our works dedicated to relativistic calculations of two-photon bound-bound transition amplitudes in hydrogen-like ions [31]. There exists a considerable literature [32, 33] (and references therein) on relativistic Sturmian basis sets, which will nevertheless help to broaden our understanding of their properties.

In the recent work concerning the use of L-spinors in the context of the Rayleigh-Ritz procedure for Dirac Hamiltonians in atomic and molecular physics, Grant and Quiney [34] claimed to the contrary and recognized to have not previously given a full description of their L-spinors in print. They argued by saying, Szmytkowski's suggestion that the L-spinor basis sets are incomplete is based on the limited published material and that is misleading and clearly wrong. For the sake of clarification, they have set out the theory of L-spinor, and demonstrated their orthonormality and completeness properties [34] by calculating sum over-states expressions in perturbation theory. This is illustrated by way of calculations on the static polarizability of hydrogenic atoms. Their calculations provide strong evidence of the completeness of L-spinors expansions provided the negative-energy states are included [34].

The Coulomb Green's functions for both the second-order Dirac-Coulomb equation and the conventional linear or first-order Dirac-Coulomb equation have been investigated. The results presented here generalize known results for the nonrelativistic Schrödinger-Coulomb Green's function. Sturmian basis sets and the Coulomb Green's function of the Gell-Mann Feynman equation are discussed in detail in the literature cited above. However, our new construction of the second-order Sturmian basis set, inspired from the works by Szmytkowski [23] differs considerably from the previous methods in the literature. In the interest of brevity the reader is referred to work outlined in Ref. [18], for background material. We have investigated further the Whittaker function representation [17, 35, 36] and an analytic Sturmian basis set representation for the Dirac-Coulomb Green function [23, 37, 38, 39]. The advantage of the later representation is that it is effectively an eigenfunction

representation suitable for perturbation calculations where one can avoid the introduction of continuum states, and this without sacrificing completeness.

The structure of this Chapter is as follows. In Section (7.2) the first-order Dirac-Coulomb Sturmian basis sets and some of their relevant properties (orthonormality and closure relations) are discussed. In Section (7.3), we outlined solution to the Gell-Mann Feynman equation, the so-called quasirelativistic Coulomb wave function and reconsider the construction of the Sturmian functions of the second-order with their properties. Armed with the Dirac-Coulomb Sturmian technique, the Dirac-Coulomb Green's function materials are presented in Section (7.4). More precisely, we derive the Sturmian expansions of both the second-order and first-order Dirac-Coulomb Green functions, together with their connections to other type of representations. The Section (7.5) deals with the nonrelativistic limits of Dirac-Coulomb Sturmian and Green's functions. The Chapter ends with conclusions, constituting Section (7.6). The relativistic atomic units (r.a.u.) are used throughout unless otherwise stated.

7.2 The Dirac-Coulomb Sturmian functions

7.2.1 Definitions

Let introduce the 4×4 Dirac matrices in the standard representation

$$\begin{aligned} &\boldsymbol{\alpha} = \begin{pmatrix} 0 & \boldsymbol{\sigma} \\ \boldsymbol{\sigma} & 0 \end{pmatrix} = \beta\boldsymbol{\gamma}, \qquad \beta = \begin{pmatrix} I & 0 \\ 0 & -I \end{pmatrix}, \qquad \boldsymbol{\Sigma} = \begin{pmatrix} \boldsymbol{\sigma} & 0 \\ 0 & \boldsymbol{\sigma} \end{pmatrix}, \\ &\mathcal{I} = \begin{pmatrix} I & 0 \\ 0 & I \end{pmatrix}, \end{aligned} \tag{7.1}$$

and

$$\mathcal{K} = -\beta\left(\boldsymbol{\Sigma}\cdot\boldsymbol{L} + \mathcal{I}\right), \qquad \boldsymbol{L} = -\mathrm{i}\mathbf{r}\wedge\boldsymbol{\nabla}, \qquad \boldsymbol{J} = \boldsymbol{L} + \boldsymbol{\Sigma}/2, \tag{7.2}$$

which stand respectively for the spin-orbit, orbital angular momentum and total angular momentum operators. $\boldsymbol{\sigma} \equiv (\sigma_1, \sigma_2, \sigma_3)$ are the well-known Pauli matrices and I the unit 2×2 matrix.

Following the ideas of Drake and Goldman [21] and Grant [22], Szmytkwoski [23] defined the four component Dirac-Coulomb Sturmian functions as simultaneous eigenfunctions of the operators $\mathcal{K}$ and $J_z = L_z + \frac{1}{2}\Sigma_z$, with the respective eigenvalues κ and m,

$$\Phi_{n\kappa m}(E, \mathbf{r}) = \frac{1}{r}\begin{pmatrix} S_{n\kappa}(\varepsilon, 2\lambda r)\Omega_{\kappa m}(\hat{\boldsymbol{r}}) \\ \mathrm{i}T_{n\kappa}(\varepsilon, 2\lambda r)\Omega_{-\kappa m}(\hat{\boldsymbol{r}}) \end{pmatrix}, \tag{7.3}$$

which are solutions of the boundary-value problem consisting of four coupled

first-order partial differential equations

$$\left[-\mathrm{i}\boldsymbol{\alpha}\cdot\boldsymbol{\nabla}+\beta-E\mathcal{I}-\mathcal{M}_{n\kappa}\frac{\mathcal{Z}}{r}\right]\Phi_{n\kappa m}(E,\mathbf{r})=0, \tag{7.4}$$

augmented by the following boundary conditions imposed at the singular end points

$$r\Phi_{n\kappa m}(E,\mathbf{r})\to 0 \qquad \text{for } r\to 0 \qquad r\Phi_{n\kappa m}(E,\mathbf{r})\to 0 \qquad \text{for } r\to\infty. \tag{7.5}$$

In equation (7.4), $\mathcal{Z}=\alpha Z$, where Z is the charge of the nucleus and α stands for Sommerfeld's fine structure constant. The eigenvalue, namely the angular quantum number κ of the spin-orbit operator $\mathcal{K}$ takes all positive and negative integer values except zero. Depending on the angular momentum coupling, we have

$$j=l-\epsilon/2=\bar{l}+\epsilon/2, \qquad \epsilon=\pm 1, \qquad \kappa=\epsilon\,(j+1/2)\,.$$

In the physical and mathematical literature there are no unique phase conventions for defining the spherical harmonics and the spherical spinors. To avoid any misunderstandings, the spherical spinors $\Omega_{\kappa m}(\hat{\boldsymbol{r}})\equiv\Omega_{jlm}(\hat{\boldsymbol{r}})$ are defined as [29]

$$\Omega_{\kappa m}\left(\hat{\boldsymbol{r}}\right)=\begin{pmatrix} sgn(-\kappa)\sqrt{\frac{\kappa+1/2-m}{2\kappa+1}}Y^{m-1/2}_{|\kappa+1/2|-1/2}\left(\hat{\boldsymbol{r}}\right) \\ \\ \sqrt{\frac{\kappa+1/2+m}{2\kappa+1}}Y^{m+1/2}_{|\kappa+1/2|-1/2}\left(\hat{\boldsymbol{r}}\right)\end{pmatrix}, \tag{7.6}$$

where $\hat{\boldsymbol{r}}=\mathbf{r}/r$ means the angular part of the radius vector $\mathbf{r}$, while the spherical harmonics $Y^m_l\left(\hat{\boldsymbol{r}}\right)$ with $l=0,1,2,...,\ m=-l,-l+1,...,l$, conform to Condon-Shortley phase convention [40]. The following properties of the spherical spinors have proved useful in the course of our calculations

$$\int \mathrm{d}^2\hat{\boldsymbol{r}}\ \Omega^{\dagger}_{\kappa m}\left(\hat{\boldsymbol{r}}\right)\Omega_{\kappa' m'}\left(\hat{\boldsymbol{r}}\right)=\delta_{\kappa\kappa'}\delta_{mm'}, \tag{7.7}$$

$$\left(\boldsymbol{\sigma}\cdot\hat{\boldsymbol{r}}\right)\Omega_{\kappa m}\left(\hat{\boldsymbol{r}}\right)=-\Omega_{-\kappa m}\left(\hat{\boldsymbol{r}}\right), \qquad \left(\boldsymbol{\sigma}\cdot\boldsymbol{L}\right)\Omega_{\pm\kappa m}\left(\hat{\boldsymbol{r}}\right)=-(1\pm\kappa)\Omega_{\pm\kappa m}\left(\hat{\boldsymbol{r}}\right), \tag{7.8}$$

$$\left(\boldsymbol{\alpha}\cdot\boldsymbol{p}\right)=\left(\boldsymbol{\sigma}\cdot\hat{\boldsymbol{r}}\right)\left(-\mathrm{i}\frac{\partial}{\partial r}+\mathrm{i}\frac{\boldsymbol{\sigma}\cdot\boldsymbol{L}}{r}\right). \tag{7.9}$$

The dagger throughout means the hermitian conjugate. This boundary-value problem can be rewritten in the appropriate form

$$\left[\left(\boldsymbol{\alpha}\cdot\hat{\boldsymbol{r}}\right)\left(r^{-1}p_r r-\mathrm{i}r^{-1}\beta\mathcal{K}\right)+\beta-E\mathcal{I}-\mathcal{M}_{n\kappa}\frac{\mathcal{Z}}{r}\right]\Phi_{n\kappa m}(E,\mathbf{r})=0 \tag{7.10}$$

$$r\Phi_{n\kappa m}(E,\mathbf{r})\to 0 \qquad \text{for } r\to 0 \qquad r\Phi_{n\kappa m}(E,\mathbf{r})\to 0 \qquad \text{for } r\to\infty,$$

where $p_r = -\mathrm{i}\partial/\partial r$ is the radial momentum. In equation (7.4) E and $\mathcal{Z}$ are fixed parameters such that $-1 < E < 1$ and $0 < |\mathcal{Z}| < 1$, $\mathcal{M}_{n\kappa}$ is the 4×4 matrix of the form

$$\mathcal{M}_{n\kappa} = \begin{pmatrix} \mu_{n\kappa} I & 0 \\ 0 & \mu_{n\kappa}^{-1} I \end{pmatrix}, \tag{7.11}$$

where $\mu_{n\kappa}$ is an eigenvalue for the problem (7.4) and (7.5). Before going further, we would like to stress out that Szmytkowski [23] has defined another set of Sturmian functions, namely the alternative Dirac-Coulomb Sturmians $\{\bar{\Phi}_{n\kappa m}(E, \mathbf{r})\}$ (not to be confuse with the usual Dirac adjoint notation) associated with the Dirac-Coulomb equation. In applications the latter functions are equally useful as the Sturmians $\{\Phi_{n\kappa m}(E, \mathbf{r})\}$ but their particular value lies in that with their aid one defines a set biorthonormal to the set $\{\Phi_{n\kappa m}(E, \mathbf{r})\}$. After separating the angular part of the problem in the standard way [41], one finds that the radial Sturmians are non-trivial solutions to the Sturm-Liouville problem

$$\begin{pmatrix} \varepsilon/2 - \mu_{n\kappa}\mathcal{Z}/x & -\mathrm{d}/\mathrm{d}x + \kappa/x \\ \mathrm{d}/\mathrm{d}x + \kappa/x & -\varepsilon^{-1}/2 - \mu_{n\kappa}^{-1}\mathcal{Z}/x \end{pmatrix} \begin{pmatrix} S_{n\kappa}(\varepsilon, x) \\ T_{n\kappa}(\varepsilon, x) \end{pmatrix} = 0 \tag{7.12}$$

$$(0 \leq x < \infty) \qquad S_{n\kappa}(0) = 0 \qquad T_{n\kappa}(0) = 0 \tag{7.13}$$

$$S_{n\kappa}(\varepsilon, x) \to 0 \quad \text{for } x \to \infty \qquad T_{n\kappa}(\varepsilon, x) \to 0 \quad \text{for } x \to \infty. \tag{7.14}$$

It has been shown [23] that all eigenvalues of this problem are real and therefore hereafter we may choose the radial components $S_{n\kappa}(\varepsilon, x)$ and $T_{n\kappa}(\varepsilon, x)$ to be real. For the sake of convenience, the argument of the Sturmians has been chosen as $x = 2\lambda r$, where

$$\lambda \equiv \lambda(E) = \sqrt{1 - E^2}, \tag{7.15}$$

rather than r. The notation used in this work emphasizes that the Sturmians depend on the energy parameter E not only through λ but also through the parameter

$$\varepsilon \equiv \varepsilon(E) = \sqrt{\frac{1 - E}{1 + E}}. \tag{7.16}$$

To find the explicit form of the radial Dirac-Coulomb Sturmians and their corresponding eigenvalues we rewrite equation (7.12), after simple differentiation of both equations with respect to x, in the form of a system of two coupled second-order differential equations

$$\left(\frac{\mathrm{d}^2}{\mathrm{d}x^2} - \frac{\gamma_\kappa^2}{x^2} + \frac{\eta_{n\kappa}}{x} - \frac{1}{4}\right) \begin{pmatrix} S_{n\kappa}(\varepsilon, x) \\ T_{n\kappa}(\varepsilon, x) \end{pmatrix} + \frac{\mathcal{C}_{n\kappa}}{x^2} \begin{pmatrix} S_{n\kappa}(\varepsilon, x) \\ T_{n\kappa}(\varepsilon, x) \end{pmatrix} = 0, \tag{7.17}$$

where

$$\gamma_\kappa = \sqrt{\kappa^2 - \mathcal{Z}^2}, \qquad \eta_{n\kappa} = \tfrac{1}{2}\mathcal{Z}\left(\varepsilon^{-1}\mu_{n\kappa} - \varepsilon\mu_{n\kappa}^{-1}\right)$$
$$\mathcal{C}_{n\kappa} = \begin{pmatrix} -\kappa & \mu_{n\kappa}^{-1}\mathcal{Z} \\ -\mu_{n\kappa}\mathcal{Z} & \kappa \end{pmatrix}. \tag{7.18}$$

Owing to the fact that the coupling matrix $\mathcal{C}_{n\kappa}$ does not depend on x, equation (7.17) can be decoupled by a similarity transformation that diagonalizes $\mathcal{C}_{n\kappa}$

$$\mathcal{B}_{n\kappa} = \mathcal{A}_{n\kappa}^{-1}\mathcal{C}_{n\kappa}\mathcal{A}_{n\kappa}. \tag{7.19}$$

The spectral matrix $\mathcal{B}_{n\kappa}$ and the transformation matrix $\mathcal{A}_{n\kappa}$, the latter constructed from unnormalized eigenvectors of $\mathcal{C}_{n\kappa}$, are

$$\mathcal{B}_{n\kappa} = \begin{pmatrix} -\gamma_\kappa & 0 \\ 0 & \gamma_\kappa \end{pmatrix}, \qquad \mathcal{A}_{n\kappa} = \begin{pmatrix} 1 & \mu_{n\kappa}^{-1}\mathcal{Z}^{-1}(\kappa - \gamma_\kappa) \\ \mu_{n\kappa}\mathcal{Z}^{-1}(\kappa - \gamma_\kappa) & 1 \end{pmatrix}. \tag{7.20}$$

The form of the transformation (7.19) implies the following ansatz

$$\begin{pmatrix} F_{n\kappa}(\varepsilon, x) \\ G_{n\kappa}(\varepsilon, x) \end{pmatrix} = \mathcal{A}_{n\kappa}^{-1} \begin{pmatrix} S_{n\kappa}(\varepsilon, x) \\ T_{n\kappa}(\varepsilon, x) \end{pmatrix} \tag{7.21}$$

which is used to rewrite equation (7.17) in the form

$$\left(\frac{\mathrm{d}^2}{\mathrm{d}x^2} - \frac{(\gamma_\kappa \pm 1/2)^2 - 1/4}{x^2} + \frac{\eta_{n\kappa}}{x} - \frac{1}{4}\right) \begin{pmatrix} F_{n\kappa}(\varepsilon, x) \\ G_{n\kappa}(\varepsilon, x) \end{pmatrix} = 0, \tag{7.22}$$

where the upper and lower signs refer respectively to the equation satisfied by $F_{n\kappa}(\varepsilon, x)$ and $G_{n\kappa}(\varepsilon, x)$. These are the well known Whittaker equations [42] and their real and regular solutions satisfying the boundary condition (2.15) at the origin ($x = 0$) are

$$\tilde{S}_{n\kappa}(\varepsilon, x) = \mathcal{N}_{n\kappa}\left[M_{\eta_{n\kappa},\gamma_\kappa - 1/2}(x) + \frac{\eta_{n\kappa}\kappa + \xi_{n\kappa}\gamma_\kappa}{2\gamma_\kappa(2\gamma_\kappa + 1)(\kappa - \gamma_\kappa)} M_{\eta_{n\kappa},\gamma_\kappa + 1/2}(x)\right], \tag{7.23}$$

$$\tilde{T}_{n\kappa}(\varepsilon, x) = \mathcal{N}_{n\kappa}\varepsilon\frac{\kappa + \gamma_\kappa}{\xi_{n\kappa} - \eta_{n\kappa}} \times \left[M_{\eta_{n\kappa},\gamma_\kappa - 1/2}(x) + \frac{\eta_{n\kappa}\kappa + \xi_{n\kappa}\gamma_\kappa}{2\gamma_\kappa(2\gamma_\kappa + 1)(\kappa + \gamma_\kappa)} M_{\eta_{n\kappa},\gamma_\kappa + 1/2}(x)\right], \tag{7.24}$$

where

$$\xi_{n\kappa} = \frac{1}{2}\mathcal{Z}\left(\varepsilon^{-1}\mu_{n\kappa} + \varepsilon\mu_{n\kappa}^{-1}\right), \tag{7.25}$$

$\mathcal{N}_{n\kappa}$ is a real constant, $M_{\eta\gamma}(x)$ is the Whittaker function of the first kind [42]. The tilde indicates that the functions $\tilde{S}_{n\kappa}(\varepsilon, x)$ and $\tilde{T}_{n\kappa}(\varepsilon, x)$ satisfy only the boundary condition at the origin.

From the properties of the Whittaker functions summarized in the Appendix F, it follows that these solutions are asymptotically bounded (i.e. for $x \to \infty$) if the parameters $\eta_{n\kappa}$ and γ_κ verify the quantization condition

$$\eta_{n\kappa} - \gamma_\kappa = |n|, \qquad n = 0, \pm 1, \pm 2, ... \tag{7.26}$$

with n denoting the radial quantum number. In this case the Whittaker functions may be written in terms of the generalized Laguerre polynomials (see equation (F.18)). Before going further, let us determine the explicit expression of the eigenvalue $\mu_{n\kappa}$. Exploiting the quantization condition (7.26) and equation (7.18), with no difficulty one shows that the eigenvalue $\mu_{n\kappa}$ satisfies the following quadratic equation

$$\mathcal{Z}\mu_{n\kappa}^2 - 2\varepsilon(|n| + \gamma_\kappa)\mu_{n\kappa} - \varepsilon^2\mathcal{Z} = 0, \tag{7.27}$$

which admits an infinite discrete eigenvalues given by

$$\mu_{n\kappa} \equiv \mu_{n\kappa}(\varepsilon) = \varepsilon\mathcal{Z}^{-1}\left(|n| + \gamma_\kappa \pm N_{n\kappa}\right), \quad N_{n\kappa} = \sqrt{(|n| + \gamma_\kappa)^2 + \mathcal{Z}^2}, \tag{7.28}$$

where $N_{n\kappa}$ is the so-called *apparent principal quantum number.*

A suitable normalization of the upper and the lower components of the corresponding eigenfunctions respectively gives

$$S_{n\kappa}(\varepsilon, x) = x^{\gamma_\kappa}\mathrm{e}^{-x/2}\left[A_{n\kappa}L_{|n|-1}^{(2\gamma_\kappa)}(x) + B_{n\kappa}L_{|n|}^{(2\gamma_\kappa)}(x)\right], \tag{7.29}$$

$$T_{n\kappa}(\varepsilon, x) = \varepsilon x^{\gamma_\kappa}\mathrm{e}^{-x/2}\left[A_{n\kappa}L_{|n|-1}^{(2\gamma_\kappa)}(x) - B_{n\kappa}L_{|n|}^{(2\gamma_\kappa)}(x)\right], \tag{7.30}$$

$$A_{n\kappa} = \sqrt{\frac{(|n| + 2\gamma_\kappa)\,|n|!}{2\varepsilon N_{n\kappa}(N_{n\kappa} \mp \kappa)\Gamma(|n| + 2\gamma_\kappa)}}, \qquad B_{n\kappa} = \frac{\kappa \mp N_{n\kappa}}{|n| + 2\gamma_\kappa}A_{n\kappa}. \tag{7.31}$$

The following sign convention is adopted in the definitions (7.28) and (7.31): *the upper signs should be chosen for* $n > 0$ *and the lower signs for* $n < 0$*; for* $n = 0$ *one should choose the upper signs if* $\kappa < 0$ *and the lower signs if* $\kappa > 0$.

7.2.2 General properties

Orthogonality and closure relations

The upper and the lower components of the Sturmians obey the following generalized orthonormality relation

$$\int_0^\infty \mathrm{d}x \frac{\mathcal{Z}}{x}\left[\mu_{n\kappa}(\varepsilon)S_{n\kappa}(\varepsilon,x)S_{n'\kappa}(\varepsilon,x) - \mu_{n'\kappa}(\varepsilon)^{-1}T_{n\kappa}(\varepsilon,x)T_{n'\kappa}(\varepsilon,x)\right] = \delta_{nn'}. \tag{7.32}$$

The Dirac-Coulomb Sturmians are complete on the real positive semi-axis $0 \leq x < \infty$. Its radial components satisfy the following closure relation:

$$\frac{\mathcal{Z}}{x'}\sum_{n=-\infty}^{\infty}\begin{pmatrix} S_{n\kappa}(\varepsilon,x) \\ -\mu_{n\kappa}(\varepsilon)^{-1}T_{n\kappa}(\varepsilon,x)\end{pmatrix}\begin{pmatrix} \mu_{n\kappa}(\varepsilon)S_{n\kappa}(\varepsilon,x') & T_{n\kappa}(\varepsilon,x')\end{pmatrix} = \delta(x-x')I, \tag{7.33}$$

with $(0 \leq x, x' < \infty)$. Intuitively, the above completeness of the Dirac-Coulomb Sturmians is expected to hold since equations (7.12)-(7.3) constitute an Hermitian Sturm-Liouville problem.
Defining the diagonal matrices

$$\mathcal{U}_{n\kappa} = \begin{pmatrix} \mu_{n\kappa}(\varepsilon)I & 0 \\ 0 & I\end{pmatrix}, \qquad \mathcal{V}_{n\kappa} = \begin{pmatrix} I & 0 \\ 0 & -\mu_{n\kappa}^{-1}(\varepsilon)I\end{pmatrix}, \tag{7.34}$$

and making use of the formulae (7.32) and (7.33) we obtain the three-dimensional orthonormality relation satisfied by $\{\Phi_{n\kappa m}(E,\mathbf{r})\}$

$$\int \mathrm{d}^3\mathbf{r}\ \frac{\mathcal{Z}}{r}\Phi^\dagger_{n\kappa m}(E,\mathbf{r})\mathcal{U}_{n\kappa}\mathcal{V}_{n'\kappa'}\Phi_{n'\kappa' m'}(E,\mathbf{r}) = \delta_{nn'}\delta_{\kappa\kappa'}\delta_{mm'} \tag{7.35}$$

and the corresponding closure relation

$$\frac{\mathcal{Z}}{r'}\sum_{n\kappa m}\mathcal{V}_{n\kappa}\Phi_{n\kappa m}(E,\mathbf{r})\Phi^\dagger_{n\kappa m}(E,\mathbf{r}')\mathcal{U}_{n\kappa} = \delta(\mathbf{r}-\mathbf{r}')\mathcal{I}. \tag{7.36}$$

The close relationship between the two Sturmian sets $\{\Phi_{n\kappa m}(E,\mathbf{r})\}$ and $\{\bar{\Phi}_{n\kappa m}(E,\mathbf{r})\}$ and their radial components $(S_{n\kappa}(\varepsilon,x)\ T_{n\kappa}(\varepsilon,x))^\top$, $(\bar{S}_{n\kappa}(\varepsilon,x)\ \bar{T}_{n\kappa}(\varepsilon,x))^\top$ expressed in [23] respectively by relations $\bar{\Phi}_{n\kappa m}(E,\mathbf{r}) = \beta\mathcal{V}_{n\kappa}\Phi_{n\kappa m}(E,\mathbf{r})$ and $\bar{S}_{n\kappa}(\varepsilon,x) = S_{n\kappa}(\varepsilon,x), \quad \bar{T}_{n\kappa}(\varepsilon,x) = \mu_{n\kappa}^{-1}(\varepsilon)T_{n\kappa}(\varepsilon,x)$ has an interesting consequence in the sense that they give another path to derive other relevant properties verified by the Dirac-Coulomb Sturmians. With these relations one eventually arrives at the following second type of orthonormality relation [23]

$$\frac{1}{2}\int_0^\infty \mathrm{d}x\left[\varepsilon S_{n\kappa}(\varepsilon,x)S_{n'\kappa}(\varepsilon,x) + \varepsilon^{-1}T_{n\kappa}(\varepsilon,x)T_{n'\kappa}(\varepsilon,x)\right] = \delta_{nn'}, \tag{7.37}$$

and the corresponding closure relation

$$\frac{1}{2}\sum_{n=-\infty}^{\infty}\begin{pmatrix} \varepsilon S_{n\kappa}(\varepsilon,x) \\ \varepsilon^{-1}T_{n\kappa}(\varepsilon,x)\end{pmatrix}\begin{pmatrix} S_{n\kappa}(\varepsilon,x') & T_{n\kappa}(\varepsilon,x')\end{pmatrix} = \delta(x-x')I. \tag{7.38}$$

The corresponding orthonormality and closure relations for the four-component Sturmians $\{\Phi_{n\kappa m}(E,\mathbf{r})\}$ are easily found to be

$$\int \mathrm{d}^3\mathbf{r}\ \Phi^\dagger_{n\kappa m}(E,\mathbf{r})(\mathcal{I}-\beta E)\Phi_{n'\kappa' m'}(E,\mathbf{r}) = \delta_{nn'}\delta_{\kappa\kappa'}\delta_{mm'}, \tag{7.39}$$

$$\sum_{n\kappa m}\Phi_{n\kappa m}(E,\mathbf{r})\Phi^\dagger_{n\kappa m}(E,\mathbf{r}')(\mathcal{I}-\beta E) = \delta(\mathbf{r}-\mathbf{r}')\mathcal{I}. \tag{7.40}$$

Sturmian expansion series of a regular spinor wave function

Equations (7.37)-(7.38) imply that the sets $(S_{n\kappa}(\varepsilon,x)\ T_{n\kappa}(\varepsilon,x))^\top$ is complete over the interval $0 \le x < \infty$ and therefore any sufficiently regular two-component function $(F(x)\ G(x))^\top$ may be uniquely expanded in these sets

$$\begin{pmatrix} F(x) \\ G(x)\end{pmatrix} = \sum_{n=-\infty}^{\infty}\mathcal{C}_{n\kappa}\begin{pmatrix} S_{n\kappa}(\varepsilon,x) \\ T_{n\kappa}(\varepsilon,x)\end{pmatrix} \qquad 0<x<\infty, \tag{7.41}$$

with the expansion coefficients defined by

$$\mathcal{C}_{n\kappa} = \frac{1}{2}\int_0^\infty \mathrm{d}x\left[\varepsilon S_{n\kappa}(\varepsilon,x)F(x) + \varepsilon^{-1}T_{n\kappa}(\varepsilon,x)G(x)\right]. \tag{7.42}$$

Since the sets $\{\Phi_{n\kappa m}(E,\mathbf{r})\}$ is complete, any sufficiently regular four-component spinor function $\Psi(\mathbf{r})$ may be uniquely expanded in the series

$$\Psi(\mathbf{r}) = \sum_{n\kappa m}\mathcal{C}_{n\kappa m}\Phi_{n\kappa m}(E,\mathbf{r}), \tag{7.43}$$

where the expansion coefficients are respectively given by

$$\mathcal{C}_{n\kappa m} = \int \mathrm{d}^3\mathbf{r}\ \Phi^\dagger_{n\kappa m}(E,\mathbf{r})(\mathcal{I}-\beta E)\Psi(\mathbf{r}). \tag{7.44}$$

7.2.3 The relativistic hydrogen-like problem

It is interesting to investigate the particular case $\mu_{n\kappa}(\varepsilon) = 1$. In this special case, the Sturmian problem considered here reduces to the relativistic H-like problem [43, 44], and we thus recover radial eigenfunctions $\{P_{n\kappa}(2\lambda_{n\kappa}r), Q_{n\kappa}(2\lambda_{n\kappa}r)\}$ and eigenvalue energies $E_{n\kappa}$ of bound states of that

problem. The generalized discrete Dirac-Coulomb wave functions of the hydrogen-like atoms, with an infinitely heavy, pointlike, and spinless nucleus of charge Z are

$$\Psi_{n\kappa m}(\mathbf{r}) = \frac{1}{r}\begin{pmatrix} P_{n\kappa}(2\lambda_{n\kappa}r)\Omega_{\kappa m}(\hat{\boldsymbol{r}}) \\ \mathrm{i}Q_{n\kappa}(2\lambda_{n\kappa}r)\Omega_{-\kappa m}(\hat{\boldsymbol{r}}) \end{pmatrix}, \tag{7.45}$$

with

$$P_{n\kappa}(x) = x^{\gamma_\kappa}\mathrm{e}^{-x/2}\left[C_{n\kappa}L^{(2\gamma_\kappa)}_{|n|-1}(x) + D_{n\kappa}L^{(2\gamma_\kappa)}_{|n|}(x)\right], \tag{7.46}$$

$$Q_{n\kappa}(x) = x^{\gamma_\kappa}\mathrm{e}^{-x/2}\left[\tilde{C}_{n\kappa}L^{(2\gamma_\kappa)}_{|n|-1}(x) - \tilde{D}_{n\kappa}L^{(2\gamma_\kappa)}_{|n|}(x)\right], \tag{7.47}$$

where

$$C_{n\kappa} = \sqrt{\frac{\lambda_{n\kappa}\left(1+E_{n\kappa}\right)\left(|n|+2\gamma_\kappa\right)|n|!}{2N_{n\kappa}(N_{n\kappa}\mp\kappa)\Gamma(|n|+2\gamma_\kappa)}}, \tilde{C}_{n\kappa} = \sqrt{\frac{\lambda_{n\kappa}\left(1-E_{n\kappa}\right)\left(|n|+2\gamma_\kappa\right)|n|!}{2N_{n\kappa}(N_{n\kappa}\mp\kappa)\Gamma(|n|+2\gamma_\kappa)}}, \tag{7.48}$$

$$D_{n\kappa} = \frac{\kappa \mp N_{n\kappa}}{|n|+2\gamma_\kappa}C_{n\kappa}, \qquad \tilde{D}_{n\kappa} = \frac{\kappa \mp N_{n\kappa}}{|n|+2\gamma_\kappa}\tilde{C}_{n\kappa}, \tag{7.49}$$

$$E_{n\kappa} = \pm\frac{(|n|+\gamma_\kappa)}{N_{n\kappa}}, \qquad n = 0, \pm1, \pm2... \qquad \lambda_{n\kappa} \equiv \lambda(E_{n\kappa}) = \frac{|\mathcal{Z}|}{N_{n\kappa}} \tag{7.50}$$

In equations (7.48)-(7.50), *the convention that $n \geq 0$ for $Z > 0$ and $n \leq 0$ for $Z < 0$ holds (this convention is unique since for $\kappa < 0$ there is no $n = 0$ state if $Z < 0$ while for $\kappa > 0$ there is no $n = 0$ state if $Z > 0$)* while the corresponding radial functions are normalized according to the formula

$$\int_0^\infty \mathrm{d}r\left[P^2_{n\kappa}(2\lambda_{n\kappa}r) + Q^2_{n\kappa}(2\lambda_{n\kappa}r)\right] = 1. \tag{7.51}$$

Comparing equations (7.29) and (7.30) with equations (7.46)-(7.47), one easily finds that

$$S_{n\kappa}(\varepsilon_{n\kappa}, 2\lambda_{n\kappa}r) = \frac{1}{\lambda_{n\kappa}}P_{n\kappa}(2\lambda_{n\kappa}r), \quad T_{n\kappa}(\varepsilon_{n\kappa}, 2\lambda_{n\kappa}r) = \frac{1}{\lambda_{n\kappa}}Q_{n\kappa}(2\lambda_{n\kappa}r). \tag{7.52}$$

7.3 The Quasirelativistic Coulomb Sturmian functions

7.3.1 Quasirelativistic Coulomb wave functions

In this part, we derive the quasirelativistic Dirac hydrogenic bound states with the aid of the second-order Dirac-Coulomb equation, hereafter dubbed as the Gell-Mann Feynman equation. The solution to this equation is conveniently

derived by introducing an angular operator $\mathcal{L}$ which bears a resemblance to the orbital angular momentum. The angular eigenfunctions of this operator are constructed from the ordinary angular momentum eigenfunctions by applying simple projection operators $\mathcal{P}^+$ [17].

Definition

We start here from the covariant form of the conventional first-order Dirac-Coulomb equation

$$\left[\gamma^\mu p_\mu - \mathcal{I} - \beta U(r)\right] \Psi(\mathbf{r}, t) = 0, \tag{7.53}$$

supplemented by the boundary conditions

$$r\Psi(\mathbf{r}, t) \to 0 \qquad \text{for } r \to 0 \qquad r\Psi(\mathbf{r}, t) \to 0 \qquad \text{for } r \to \infty, \tag{7.54}$$

where $\Psi(\mathbf{r}, t)$ is a bispinor and $U(r)$ the well-known Coulomb potential. The usual sum convention for equal four-indices is applied. It is convenient to determine the bispinor $\Psi(\mathbf{r}, t)$ by applying the projection operator $\mathcal{P}^+$, for positive mass, to a new bispinor $\Phi(\mathbf{r}, t)$ such that

$$\Psi(\mathbf{r}, t) = \mathcal{P}^+ \Phi(\mathbf{r}, t) \qquad \mathcal{P}^+ = \frac{1}{2}\left[\gamma^\nu p_\nu + \mathcal{I} - \beta U(r)\right], \tag{7.55}$$

and equation (7.53) takes the form

$$\frac{1}{2}\left[\gamma^\mu p_\mu - \mathcal{I} - \beta U(r)\right]\left[\gamma^\nu p_\nu + \mathcal{I} - \beta U(r)\right] \Phi(\mathbf{r}, t) = 0. \tag{7.56}$$

After tedious calculations, we find that the new bispinor $\Phi(\mathbf{r}, t)$ now obeys the following covariant form of the second-order Dirac-Coulomb equation

$$\frac{1}{2}\left[p_\mu p^\mu - \mathcal{I} + U(r)^2 + \mathrm{i}(\boldsymbol{\alpha} \cdot \hat{\boldsymbol{r}})\left(\partial_r U(r)\right) - 2\mathrm{i}U(r)\left(\partial_t\right)\right] \Phi(\mathbf{r}, t) = 0, \tag{7.57}$$

augmented by the appropriate boundary conditions

$$r\Phi(\mathbf{r}, t) \to 0 \qquad \text{for } r \to 0 \qquad r\Phi(\mathbf{r}, t) \to 0 \qquad \text{for } r \to \infty. \tag{7.58}$$

The stationary bound states $\Phi(\mathbf{r}, t) = \Phi(\mathbf{r}) \exp(-\mathrm{i}Et)$, solutions to this eigenvalue problem are derived in the light of method proposed by Martin and Glauber [17]. Henceforth, the Gell-Mann Feynman equation reads

$$\begin{aligned} &\frac{1}{2}\left[\mathcal{I}\boldsymbol{\nabla}^2 - \mathrm{i}(\boldsymbol{\alpha} \cdot \hat{\boldsymbol{r}})\mathcal{Z}/r^2 + \left(1 - (E + \mathcal{Z}/r)^2\right)\mathcal{I}\right] \Phi(\mathbf{r}) = 0, \\ &r\Phi(\mathbf{r}) \to 0 \qquad \text{for } r \to 0 \qquad r\Phi(\mathbf{r}) \to 0 \qquad \text{for } r \to \infty. \end{aligned} \tag{7.59}$$

To handle the differential equation (7.59), which involves only one of the Dirac matrices, it is necessary to introduce spherical coordinates and define the Kramers-Dirac operator

$$\mathcal{L} = \mathcal{K}\beta - \mathrm{i}(\boldsymbol{\alpha}\cdot\hat{\boldsymbol{r}})\mathcal{Z}, \quad \mathcal{L}(\mathcal{L}+1) = \boldsymbol{L}^2 - \mathrm{i}(\boldsymbol{\alpha}\cdot\hat{\boldsymbol{r}})\mathcal{Z} - \mathcal{Z}^2, \quad \boldsymbol{L}^2 = \mathcal{K}(\mathcal{K}+\beta), \tag{7.60}$$

in terms of which the Gell-Mann Feynman equation reads

$$\frac{1}{2}\left[-\mathcal{I}\frac{\partial^2}{\partial r^2} + \frac{\mathcal{L}(\mathcal{L}+1)}{r^2} + \left(-\frac{2E\mathcal{Z}}{r} + 1 - E^2\right)\mathcal{I}\right] r\Phi(\mathbf{r}) = 0, \tag{7.61}$$
$$r\Phi(\mathbf{r}) \to 0 \qquad \text{for } r \to 0 \qquad r\Phi(\mathbf{r}) \to 0 \qquad \text{for } r \to \infty.$$

This equation is similar to Schrödinger's. There are, however, certain differences in the centrifugal term and due to the fact that $\Phi(\mathbf{r})$ is a bispinor. The spin-orbit operator $\mathcal{K}$ has several properties, among which its commutativity with $\boldsymbol{\alpha}\cdot\hat{\boldsymbol{r}}$, β, the first-order Dirac Hamiltonian $H_D = -\mathrm{i}\boldsymbol{\alpha}\cdot\boldsymbol{\nabla} + \beta + U(r)\mathcal{I}$ and therefore identifies a *constant of the motion.*

Orthogonality and normalization relations

It remains to investigate the problem of the orthogonality and normalization of the eigenfunctions $\Psi(\mathbf{r})$ and $\Phi(\mathbf{r})$. The orthogonality relation is easily found from the conventional procedure to be

$$\int \mathrm{d}^3\mathbf{r}\ \bar{\Phi}_j(\mathbf{r})\left(E_i + E_j + \frac{2\mathcal{Z}}{r}\right)\Phi_i(\mathbf{r}) = 0, \tag{7.62}$$

for $E_i \neq E_j$, and where we defined the adjoint spinor $\bar{\Phi}(\mathbf{r}) = \Phi(\mathbf{r})^\dagger\beta$. The normalization of $\Phi_i(\mathbf{r})$ is most conveniently chosen to agree with the normalization of the first-order wave function $\Psi_i(\mathbf{r})$, that is, so that

$$\int \mathrm{d}^3\mathbf{r}\ \Psi_i(\mathbf{r})^\dagger\Psi_i(\mathbf{r}) = \int \mathrm{d}^3\mathbf{r}\ \bar{\Phi}_i(\mathbf{r})\left(E_i + \frac{\mathcal{Z}}{r}\right)\mathcal{P}^+\Phi_i(\mathbf{r}) = 1. \tag{7.63}$$

We turn to considering the quasi-eigenproblem (7.61). That means we shall seek the normalized wave function $\Phi(\mathbf{r})$. In this approximating method, one has to normalize the wave function in the sense

$$\int \mathrm{d}^3\mathbf{r}\ \bar{\Phi}(\mathbf{r})\Phi(\mathbf{r}) = 1. \tag{7.64}$$

The energy eigenfunctions

For the purpose of constructing eigenvectors $\mathcal{Y}_{jlm}(\hat{\boldsymbol{r}})$ of $\mathcal{L}$ and $\mathcal{K}$ in the standard representation, it is convenient to determine the angular eigenvectors of $\mathcal{K}$ and β for which their corresponding eigenvalues κ and ± 1 have the same and opposite sign. In view of equation (7.60) we infer that in the absence of the Coulomb field ($\mathcal{Z} = 0$), each eigenvector of $\mathcal{K}$ and β is also an eigenvector of $\mathcal{L}$ and $\mathcal{K}$. Moreover, for nonvanishing Coulomb field, however, $\mathcal{L}$ and β do not commute and each of the two eigenvectors of $\mathcal{L}$ is a linear combination of the two eigenvectors of β. Since $\mathcal{L}$ is defined such that $\mathcal{L}^2 = \mathcal{K}^2 - \mathcal{Z}^2$, its real eigenvalues Λ are

$$\Lambda = \bar{\epsilon}\gamma_\kappa \qquad \bar{\epsilon} = \pm 1, \tag{7.65}$$

and the corresponding unnormalized angular eigenfunctions $\mathcal{Y}_{jlm}(\hat{\boldsymbol{r}})$ are easily found to be

$$\begin{gathered}\mathcal{L}\mathcal{Y}_{jlm}(\hat{\boldsymbol{r}}) = \Lambda\mathcal{Y}_{jlm}(\hat{\boldsymbol{r}}), \quad \mathcal{Y}_{jlm}(\hat{\boldsymbol{r}}) = \begin{pmatrix} a_1\Omega_{jlm}(\hat{\boldsymbol{r}}) \\ \mathrm{i}a_2\Omega_{j\bar{l}m}(\hat{\boldsymbol{r}}) \end{pmatrix}, \\ \frac{a_2}{a_1} = \frac{\mathcal{Z}}{\kappa + \bar{\epsilon}\gamma_\kappa} = \frac{\kappa - \bar{\epsilon}\gamma_\kappa}{\mathcal{Z}},\end{gathered} \tag{7.66}$$

where a_1 and a_2 are nonzero constants of normalization. In what precedes, we choose the angular eigenfunctions $\mathcal{Y}_{jlm}(\hat{\boldsymbol{r}})$ corresponding to the eigenvalue $+1$ for β. We seek $\Phi(\mathbf{r})$ in the form

$$\Phi(\mathbf{r}) = G_{\bar{\epsilon}}(r)\mathcal{Y}_{jlm}(\hat{\boldsymbol{r}}). \tag{7.67}$$

It is readily found from equation (7.61) that $G_{\bar{\epsilon}}(r)$ is solution to the differential equation

$$\begin{gathered}\frac{1}{2}\left[-\frac{\mathrm{d}^2}{\mathrm{d}r^2} + 1 - E^2 - \frac{2E\mathcal{Z}}{r} + \frac{\gamma_\kappa(\gamma_\kappa + \bar{\epsilon})}{r^2}\right] rG_{\bar{\epsilon}}(r) = 0, \\ rG_{\bar{\epsilon}}(r) \to 0 \qquad \text{for } r \to 0 \qquad rG_{\bar{\epsilon}}(r) \to 0 \qquad \text{for } r \to \infty.\end{gathered} \tag{7.68}$$

The pair of uncoupled equations for $\bar{\epsilon} = \pm 1$ replaces the coupled first-order equations of the usual treatment of the Dirac-Coulomb equation. The solutions to these equations may also be taken to be eigenfunctions of $\mathcal{K}$ and J_z, since $\mathcal{L}$, $\mathcal{K}$, and J_z all commute with one another and thus constitutes a system of commuting operators. Now, introducing the following parameter and reduced units for length x and energy η

$$\zeta = \gamma_\kappa + (\bar{\epsilon} + 1)/2, \qquad \eta = \mathcal{Z}E/\lambda, \tag{7.69}$$

we easily find that the second-order radial equation (7.68) reduces to the boundary eigenvalue problem

$$\left[\mathrm{d}^2/\mathrm{d}x^2 - \left((\zeta - 1/2)^2 - 1/4\right)/x^2 + \eta/x - 1/4\right] xG_{\bar{\epsilon}}(x) = 0, \tag{7.70}$$

$$(0 < x < \infty), \quad xG_{\bar{\epsilon}}(x) \to 0 \qquad \text{for } x \to 0 \qquad xG_{\bar{\epsilon}}(x) \to 0 \qquad \text{for } x \to \infty.$$

Equation (7.70) is the Whittaker equation considered in the Appendix F and its bounded solutions are well-known. It stems from relation (F.18) that the corresponding unnormalized radial eigenfunctions are

$$G_{\bar{\epsilon}}(x) = \bar{A}_{\bar{\epsilon}} x^{\zeta-1} e^{-x/2} L_{\eta-\zeta}^{(2\zeta-1)}(x), \tag{7.71}$$

with $\bar{A}_{\bar{\epsilon}}$ denoting the normalization factor and the parameters η and ζ satisfying the quantization condition

$$\eta - \zeta = \bar{n} \quad \text{or} \quad \eta - \gamma_\kappa = n, \quad n = \bar{n} + (\bar{\epsilon} + 1)/2, \quad \bar{n} = 0, 1, 2, ... \tag{7.72}$$

where n is the radial quantum number. Equation (7.64) implies that the angular eigenfunctions of the operator $\mathcal{L}$ must satisfy the following orthogonality relation

$$\int \mathrm{d}^2\hat{\boldsymbol{r}}\; \bar{\mathcal{Y}}_{j'l'm'}(\hat{\boldsymbol{r}})\, \mathcal{Y}_{jlm}(\hat{\boldsymbol{r}}) = \delta_{j'j}\delta_{l'l}\delta_{m'm}, \tag{7.73}$$

while the radial eigenfunctions obey the normalization relation

$$\int_0^\infty \mathrm{d}r\, |G_{\bar{\epsilon}}(r)|^2\, r^2 = 1. \tag{7.74}$$

Carrying out the product of harmonic bispinors under the angular integral in equation (7.73), and exploiting the orthogonality of spherical spinors, the angular eigenfunctions of the operator $\mathcal{L}$ are easily found to be [17, 20]

$$\mathcal{Y}_{jlm}(\hat{\boldsymbol{r}}) = \sqrt{\frac{\kappa + \epsilon\gamma_\kappa}{2\epsilon\gamma_\kappa}} \begin{pmatrix} \Omega_{jlm}(\hat{\boldsymbol{r}}) \\ \mathrm{i}\tilde{\beta}\Omega_{j\bar{l}m}(\hat{\boldsymbol{r}}) \end{pmatrix}, \quad \tilde{\beta} = \mathcal{Z}/(\kappa + \epsilon\gamma_\kappa) = (\kappa - \epsilon\gamma_\kappa)/\mathcal{Z}. \tag{7.75}$$

($\frac{\Lambda}{\kappa} > 0$, i.e., $\epsilon = \bar{\epsilon}$). Switching our attention to the above normalization condition (7.74), and combining equations (F.21) and (F.25) leads to the desired quasirelativistic or Dirac-Coulomb scalar wave function [20, 45] in closed-form suitable for our purpose

$$\Phi_{njlm}(\mathbf{r}) = G_{n\epsilon}(r)\mathcal{Y}_{jlm}(\hat{\boldsymbol{r}}) = \Phi_{n\epsilon}(r) \begin{pmatrix} \Omega_{jlm}(\hat{\boldsymbol{r}}) \\ \mathrm{i}\tilde{\beta}\Omega_{j\bar{l}m}(\hat{\boldsymbol{r}}) \end{pmatrix}, \tag{7.76}$$

$$\Phi_{n\epsilon}(r) = \sqrt{\frac{\bar{n}!(|\kappa| + \gamma_\kappa)(2\lambda)^{2\zeta+1}}{4\eta\gamma_\kappa\Gamma(\bar{n} + 2\zeta)}}\, r^{\zeta-1}\mathrm{e}^{-\lambda r} L_{\bar{n}}^{(2\zeta-1)}(2\lambda r). \tag{7.77}$$

7.3.2 Quasirelativistic Coulomb Sturmian

Definition

Many authors [9, 15, 17, 20, 21, 46, 47] have investigated the problem of constructing discrete Sturmian basis sets associated to the second-order Dirac-Coulomb problems for representing wave or Green functions and discussed some of their relevant properties. In this Section, we reconsider the construction of discrete basis sets associated to the Gell-Mann Feynman equation and present some of their relevant properties. It is worth underlining that, our method follows the genuine treatment developed by Szmytkowski [23] and therefore differs from the previous works encountered in the literature. The Dirac conjugation or adjoint spinor $\bar{\Phi}$ is used throughout. We define the discret quasirelativistic Sturmians as simultaneous eigenfunctions of the operators $\mathcal{L}$, $\mathcal{K}$ and J_z

$$\Phi_{\mu jlm}(E, \mathbf{r}) = \frac{1}{r} S_{\mu\epsilon}(2\lambda r) \mathcal{Y}_{jlm}(\hat{\boldsymbol{r}}), \tag{7.78}$$

satisfying the second-order boundary-value problem

$$\frac{1}{2}\left[\mathcal{I}\partial^2/\partial r^2 - \mathcal{L}(\mathcal{L}+1)/r^2 + \left(\mu 2E\mathcal{Z}/r - 1 + E^2\right)\mathcal{I}\right] r\Phi_{\mu jlm}(E, \mathbf{r}) = 0, \tag{7.79}$$

$$r\Phi_{\mu jlm}(E, \mathbf{r}) \to 0 \qquad \text{for} \qquad r \to 0 \qquad \text{and} \qquad r \to \infty.$$

In this equation μ is an eigenvalue for the problem and E and $\mathcal{Z}$ are fixed real parameters such that equation $0 < |\mathcal{Z}| < 1$ and $0 \leq |E| < 1$ is verified. The spherical bispinors $\mathcal{Y}_{jlm}(\hat{\boldsymbol{r}})$, the angular eigenfunctions of the Kramers-Dirac operator $\mathcal{L}$ have been explicitly determined in the precedent Subsection. Introducing the parameters λ, η, ζ as defined in equations (7.15) and (7.69) and the new parameter,

$$\xi_\mu = \mu\eta \tag{7.80}$$

we easily find that the second-order radial Sturmians $\{S_{\mu\epsilon}(x)\}$ are non-trivial solutions of the Sturm-Liouville problem

$$\left[\mathrm{d}^2/\mathrm{d}x^2 - \left((\zeta - 1/2)^2 - 1/4\right)/x^2 + \xi_\mu/x - 1/4\right] S_{\mu\epsilon}(x) = 0 \tag{7.81}$$

$$(0 \leq x < \infty), \quad S_{\mu\epsilon}(x) \to 0 \qquad \text{for} \qquad x \to 0 \qquad \text{and} \qquad x \to \infty,$$

which may be obtained in the standard way after substitution of the functions in equation (7.78) into equation (7.79). The problem defined in equation (7.81) is similar to that of Ref. [23] and therefore its solutions may be derived in the similar manner.

Suitably normalized the regular and bounded radial solutions satisfying the boundary conditions at the origin and at infinity are given by

$$S_{\mu_n\epsilon}(2\lambda r) = \sqrt{\frac{(\xi_{\mu_n}-\zeta)!}{\mathcal{Z}\Gamma\left(\xi_{\mu_n}+\zeta\right)}}(2\lambda r)^{\zeta}e^{-\lambda r}L^{(2\zeta-1)}_{\xi_{\mu_n}-\zeta}\left(2\lambda r\right). \tag{7.82}$$

Because of the boundary condition at infinity, the following quantization relation must be valid

$$\mu_n\frac{\mathcal{Z}E}{\lambda}-\zeta=\bar{n} \quad \text{or} \quad \mu_n\frac{\mathcal{Z}E}{\lambda}-\gamma_\kappa=n, \quad n=\bar{n}+(\epsilon+1)/2. \tag{7.83}$$

($\epsilon=\pm1$, $\bar{n}=0,1,2,.....$). It should be noted that for $\mu_n=1$, we retrieve the eigenenergies $E_{n\kappa}$ and the desired quasirelativistic or Dirac scalar wave function previously derived in Subsection (7.3.1).

Orthogonality and closure relations

The following properties may be inferred from equations (7.78)-(7.81)

(a) μ_n are non-degenerate real eigenvalues; thus we choose $S_{\mu_n\epsilon}(x)$ to be real.

(b) The Sturmians are normalized in the sense

$$\int_0^\infty \mathrm{d}x\frac{\mathcal{Z}}{x}S_{\mu_n\epsilon}\left(x\right)S_{\mu_{n'}\epsilon}\left(x\right)=\delta_{nn'}, \tag{7.84}$$

$$\int \mathrm{d}^3\mathbf{r}\ \frac{\mathcal{Z}}{r}\bar{\Phi}_{\mu_njlm}(E,\mathbf{r})\Phi_{\mu_{n'}j'l'm'}(E,\mathbf{r})=\delta_{nn'}\delta_{jj'}\delta_{ll'}\delta_{mm'}. \tag{7.85}$$

(c) They are complete over the interval $0\leq x<\infty$ and the corresponding closure relations are valid

$$\frac{\mathcal{Z}}{x'}\sum_{n=0}^{\infty}S_{\mu_n\epsilon}(x)S_{\mu_n\epsilon}(x')=\delta(x-x'), \tag{7.86}$$

$$\frac{\mathcal{Z}}{r'}\sum_{njlm}\Phi_{\mu_njlm}(E,\mathbf{r})\Phi^{\dagger}_{\mu_njlm}(E,\mathbf{r}')=\delta(\mathbf{r}-\mathbf{r}')I. \tag{7.87}$$

The Sturmian representation

Any sufficiently regular spinor function $\Psi(\mathbf{r})$ defined in $\mathcal{R}^3$ can be expanded over the set $\{\Phi_{\mu_njlm}(E,\mathbf{r})\}$. One has

$$\Psi(\mathbf{r})=\sum_{njlm}\mathcal{C}_{njlm}\Phi_{\mu_njlm}(E,\mathbf{r}) \tag{7.88}$$

where the expansion coefficients $\mathcal{C}_{njlm}$ are obtained with the aid of equation (7.85)

$$\mathcal{C}_{njlm}=\int \mathrm{d}^3\mathbf{r}\ \frac{\mathcal{Z}}{r}\bar{\Phi}_{\mu_njlm}(E,\mathbf{r})\Psi(\mathbf{r}). \tag{7.89}$$

7.4 Dirac-Coulomb Green's function representations

The solution of a number of problems of atomic and nuclear physics frequently encounters a difficulty connected with the need for taking into account the influence of the external Coulomb field on the particle in the virtual state. The simplest processes of this type are processes of second-order perturbation theory in the quantized external field (electromagnetic or weak) occurring in the field of a nucleus with charge Z. The development of methods for calculating the compound matrix elements of perturbation theory on the basis of solutions of the Dirac equation with a Coulomb potential is motivated by the study of processes of interaction of atoms or ions with large Z in an external field and the calculation of the spectral characteristics of multiply charged ions, with perturbation theory used to take the interactions between electrons into account, and by a number of other problems of atomic and nuclear physics. In this regard, the reader can refer to the work on high-Z atomic quantum electrodynamical (QED) calculations undertaken by Hylton and Snyderman [48] (and references therein). There are various ways to consider the action of the Coulomb field on an electron in a virtual state; they include *(1)* method based on a group theoretical approach [49], *(2)* direct summation of the matrix elements over a complete set of intermediate states, solution of a system of inhomogenious differential equations [50], and *(3)* the CGF method. The latter is of particular interest. In the two-photon bound-bound transition amplitudes in hydrogen-like ions considered in this thesis, all possible virtual intermediate excited states for the electron appear in perturbation theory calculations and are incorporated into the Green function sum over all bound and continuum energy electron states in the strong Coulomb field from the nucleus. The sums over intermediate states, for a fixed angular momentum, can be written in terms of the radial Green's function of the unperturbed system, and in the case where the unperturbed system is described by the Dirac-Coulomb Hamiltonian, the radial Green's function can be expressed in terms of known linear combination of Whittaker functions [35, 51, 52], in terms of integral representations [38, 48], in the form of a series in generalized Laguerre polynomials analogous to the expansion of the quadratic Dirac equation in terms of Sturmian functions [53], and finally is expanded over a Sturmian basis sets [23, 53, 54] associated with the conventional linear Dirac equation. Sturmian expansions of the radial CGF have been widely used for both nonrelativistic and relativistic analytical calculations. The interested reader is referred, for instance, to the review in Ref. [55] and to articles [56, 57, 58]. The use of the CGF is especially convenient in the calculation of multiphoton processes in the perturbative regime and for the analysis of QED effects in the interaction of hydrogen-like ions with electromagnetic fields. The great interest in hydrogen as a model system is based on the fact that QED matrix elements can be

expressed in closed form simplifying quantitative evaluations and permitting analytical estimations of limiting cases.

Up to the present time only a few explicit calculations involving the Dirac CGF have been presented. A finite sum approximation to the Green function is necessary for practical numerical computer implementation of the perturbation theory. Numerical results obtained through the use of compact representations [59] are very scarce and, besides early QED corrections calculations [17, 35], recent applications have chiefly been related to the computation of the dipole polarizability of the ground state (see, for instance, Szmytkowski [23], Zon *et al.* [37], Swainson and Drake [38], Zapryagaev and Manakov [60], Manakov *et al.* [61], Le Anh thu *et al.* [62]), and more recent applications are sketched in [20, 28, 29, 30, 32] and for a very recent derivation, see Tetchou and Kwato [31].

The level of complexity is much higher than in the nonrelativistic case, as the CGF associated to the first-order Dirac equation is a 4×4 matrix solution of an inhomogeneous system of differential equations.

7.4.1 Fully relativistic treatment

The Dirac-Coulomb Green function satisfies the inhomogeneous differential equation [23, 38, 48, 53, 63, 64, 65]

$$\left[(\boldsymbol{\alpha}\cdot\hat{\boldsymbol{r}})\left(r^{-1}p_r r - \mathrm{i}r^{-1}\beta\mathcal{K}\right) + \beta - E\mathcal{I} - \frac{\mathcal{Z}}{r}\mathcal{I}\right] G_E^{(1)}(\mathbf{r},\mathbf{r}') = \delta(\mathbf{r}-\mathbf{r}')\mathcal{I}, \quad (7.90)$$

$$rG_E^{(1)}(\mathbf{r},\mathbf{r}') \to 0 \qquad \text{for } r \to 0 \qquad rG_E^{(1)}(\mathbf{r},\mathbf{r}') \to 0 \qquad \text{for } r \to \infty.$$

Here $\mathbf{r}'$ is fixed, $|E| < 1$ and $0 \leq |\mathcal{Z}| < 1$. It has also been defined as a 4×4 matrix, solution of an inhomogeneous system of differential equations

$$\begin{pmatrix} 1 - E - \mathcal{Z}/r & (\boldsymbol{\sigma}\cdot\hat{\boldsymbol{r}})\left(r^{-1}p_r r + \mathrm{i}\mathcal{K}/r\right) \\ (\boldsymbol{\sigma}\cdot\hat{\boldsymbol{r}})\left(r^{-1}p_r r - \mathrm{i}\mathcal{K}/r\right) & -1 - E - \mathcal{Z}/r \end{pmatrix} G_E^{(1)}(\mathbf{r},\mathbf{r}') = \delta(\mathbf{r}-\mathbf{r}')\mathcal{I}, \quad (7.91)$$

$$rG_E^{(1)}(\mathbf{r},\mathbf{r}') \to 0 \qquad \text{for } r \to 0 \qquad rG_E^{(1)}(\mathbf{r},\mathbf{r}') \to 0 \qquad \text{for } r \to \infty.$$

Since the Dirac-Coulomb Sturmians $\{\Phi_{n\kappa m}(E,\mathbf{r})\}$ are a complete set and satisfy the same boundary conditions as the Dirac-Coulomb Green function, a solution to equation (7.90) is in the form

$$G_E^{(1)}(\mathbf{r},\mathbf{r}') = \sum_{n\kappa m} \Phi_{n\kappa m}(E,\mathbf{r})\Theta^{\dagger}_{n\kappa m}(E,\mathbf{r}'), \quad (7.92)$$

where the expansion coefficients $\Theta^{\dagger}_{n\kappa m}(E,\mathbf{r}')$ are four-component spinors which are to be determined. Equations (7.90), (7.92) together with equation (7.4)

easily yield

$$\sum_{n\kappa m}(\mu_{n\kappa}-1)\frac{\mathcal{Z}}{r}\mathcal{V}_{n\kappa}\Phi_{n\kappa m}(E,\mathbf{r})\Theta^{\dagger}_{n\kappa m}(E,\mathbf{r}')=\delta(\mathbf{r}-\mathbf{r}')\mathcal{I}. \tag{7.93}$$

Premultiplying both sides of the latter equation by $\Phi^{\dagger}_{n'\kappa'm'}(E,\mathbf{r})\mathcal{U}_{n'\kappa'}$, integrating over $\mathcal{R}^3$ and utilizing the orthonormality relation (7.35) we obtain

$$\Theta^{\dagger}_{n\kappa m}(E,\mathbf{r}')=\frac{1}{(\mu_{n\kappa}-1)}\Phi^{\dagger}_{n\kappa m}(E,\mathbf{r}')\mathcal{U}_{n\kappa} \tag{7.94}$$

and therefore

$$G^{(1)}_{E}(\mathbf{r},\mathbf{r}')=\sum_{n\kappa m}\frac{1}{(\mu_{n\kappa}-1)}\Phi_{n\kappa m}(E,\mathbf{r})\Phi^{\dagger}_{n\kappa m}(E,\mathbf{r}')\mathcal{U}_{n\kappa}. \tag{7.95}$$

Equation (7.95) is the Sturmian expansion of the Dirac-Coulomb Green function $G^{(1)}_{E}(\mathbf{r},\mathbf{r}')$. This expression (7.95) easily transforms to the form

$$G^{(1)}_{E}(\mathbf{r},\mathbf{r}')=\sum_{n\kappa m}\frac{1}{(\mu_{n\kappa}-1)}\mathcal{U}_{n\kappa}\Phi_{n\kappa m}(E,\mathbf{r})\Phi^{\dagger}_{n\kappa m}(E,\mathbf{r}'). \tag{7.96}$$

Since $G^{(1)}_{E}(\mathbf{r},\mathbf{r}')$ is the Green function of the Hermitian operator, it possesses a symmetry property

$$G^{(1)}_{E}(\mathbf{r},\mathbf{r}')=G^{(1)\dagger}_{E}(\mathbf{r}',\mathbf{r}).$$

At first sight it is not obvious that the expression (7.95) satisfies this relation. To show that this is the case we utilize equation (7.96).

By expanding the Dirac-Coulomb Green function over the complete set of spin angular eigenfunctions of $\mathcal{K}$ and J_z and separate off the angular part to the radial one, we have the partial-wave-expansion of the form

$$G^{(1)}_{E}(\mathbf{r},\mathbf{r}')=\sum_{\kappa m}\frac{1}{rr'}\begin{pmatrix} g^{(11)}_{\kappa}\Omega_{\kappa m}(\hat{\boldsymbol{r}})\Omega^{\dagger}_{\kappa m}(\hat{\boldsymbol{r}}') & -\mathrm{i}g^{(12)}_{\kappa}\Omega_{\kappa m}(\hat{\boldsymbol{r}})\Omega^{\dagger}_{-\kappa m}(\hat{\boldsymbol{r}}') \\ \mathrm{i}g^{(21)}_{\kappa}\Omega_{-\kappa m}(\hat{\boldsymbol{r}})\Omega^{\dagger}_{\kappa m}(\hat{\boldsymbol{r}}') & g^{(22)}_{\kappa}\Omega_{-\kappa m}(\hat{\boldsymbol{r}})\Omega^{\dagger}_{-\kappa m}(\hat{\boldsymbol{r}}') \end{pmatrix}, \tag{7.97}$$

Sturmian expansions of the four radial coefficients $g^{(ij)}_{\kappa}\equiv g^{(i,j)}_{\kappa}(E;r,r')$, $i,j=1,2$, can be directly inferred from expansions (7.95), (7.96) and the well-known properties of alternative Sturmian basis sets [23]. Thus after very lengthy manipulations one finds the following results given in the Sturmian and Whittaker

function representations

$$
\begin{aligned}
g_\kappa^{(11)}(E;r,r') &= \sum_{n=-\infty}^{\infty} \tilde{\theta}_n S_{n\kappa}(\varepsilon,2\lambda r) S_{n\kappa}(\varepsilon,2\lambda r') \\
&= \sum_{n=-\infty}^{\infty} \bar{\alpha}_n \bar{S}_{n\kappa}(\varepsilon,2\lambda r) \bar{S}_{n\kappa}(\varepsilon,2\lambda r') \\
&= \frac{1}{(rr')^{1/2}} \frac{\Gamma(\gamma_\kappa-\nu)}{4(1-E)\Gamma(2\gamma_\kappa+1)} \left[(\kappa+\nu/E) W_{\nu-1/2,\gamma_\kappa}(2\lambda r_>)\right. \\
&\left. + W_{\nu+1/2,\gamma_\kappa}(2\lambda r_>)\right] \\
&\times \left[(\gamma_\kappa-\nu) M_{\nu-1/2,\gamma_\kappa}(2\lambda r_<) - (\kappa-\nu/E) M_{\nu+1/2,\gamma_\kappa}(2\lambda r_<)\right]
\end{aligned}
\tag{7.98}
$$

$$
\begin{aligned}
g_\kappa^{(12)}(E;r,r') &= \sum_{n=-\infty}^{\infty} \tilde{\alpha}_n S_{n\kappa}(\varepsilon,2\lambda r) T_{n\kappa}(\varepsilon,2\lambda r') \\
&= \sum_{n=-\infty}^{\infty} \bar{\theta}_n \bar{S}_{n\kappa}(\varepsilon,2\lambda r) \bar{T}_{n\kappa}(\varepsilon,2\lambda r') \\
&= \frac{1}{(rr')^{1/2}} \frac{\varepsilon\Gamma(\gamma_\kappa-\nu)}{4(1-E)\Gamma(2\gamma_\kappa+1)} \left[(\kappa+\nu/E) W_{\nu-1/2,\gamma_\kappa}(2\lambda r_>)\right. \\
&\left. - W_{\nu+1/2,\gamma_\kappa}(2\lambda r_>)\right] \\
&\times \left[(\gamma_\kappa-\nu) M_{\nu-1/2,\gamma_\kappa}(2\lambda r_<) - (\kappa-\nu/E) M_{\nu+1/2,\gamma_\kappa}(2\lambda r_<)\right]
\end{aligned}
\tag{7.99}
$$

$$
\begin{aligned}
g_\kappa^{(21)}(E;r,r') &= \sum_{n=-\infty}^{\infty} \tilde{\theta}_n T_{n\kappa}(\varepsilon,2\lambda r) S_{n\kappa}(\varepsilon,2\lambda r') \\
&= \sum_{n=-\infty}^{\infty} \bar{\alpha}_n \bar{T}_{n\kappa}(\varepsilon,2\lambda r) \bar{S}_{n\kappa}(\varepsilon,2\lambda r') \\
&= \frac{1}{(rr')^{1/2}} \frac{\varepsilon\Gamma(\gamma_\kappa-\nu)}{4(1-E)\Gamma(2\gamma_\kappa+1)} \left[(\kappa+\nu/E) W_{\nu-1/2,\gamma_\kappa}(2\lambda r_>)\right. \\
&\left. + W_{\nu+1/2,\gamma_\kappa}(2\lambda r_>)\right] \\
&\times \left[(\gamma_\kappa-\nu) M_{\nu-1/2,\gamma_\kappa}(2\lambda r_<) + (\kappa-\nu/E) M_{\nu+1/2,\gamma_\kappa}(2\lambda r_<)\right]
\end{aligned}
\tag{7.100}
$$

$$
\begin{aligned}
g_{\kappa}^{(22)}(E;r,r') &= \sum_{n=-\infty}^{\infty} \tilde{\alpha}_n T_{n\kappa}(\varepsilon, 2\lambda r) T_{n\kappa}(\varepsilon, 2\lambda r') \\
&= \sum_{n=-\infty}^{\infty} \bar{\theta}_n \bar{T}_{n\kappa}(\varepsilon, 2\lambda r) \bar{T}_{n\kappa}(\varepsilon, 2\lambda r') \\
&= \frac{1}{(rr')^{1/2}} \frac{\varepsilon^2 \Gamma(\gamma_\kappa - \nu)}{4(1-E)\Gamma(2\gamma_\kappa + 1)} \left[(\kappa + \nu/E) W_{\nu-1/2,\gamma_\kappa}(2\lambda r_>) \right. \\
&\left. - W_{\nu+1/2,\gamma_\kappa}(2\lambda r_>) \right] \\
&\times \left[(\gamma_\kappa - \nu) M_{\nu-1/2,\gamma_\kappa}(2\lambda r_<) + (\kappa - \nu/E) M_{\nu+1/2,\gamma_\kappa}(2\lambda r_<) \right]
\end{aligned}
\tag{7.101}
$$

where

$$
\nu = \mathcal{Z}E/\lambda, \quad \tilde{\theta}_n = \frac{\mu_{n\kappa}(\varepsilon)}{\mu_{n\kappa}(\varepsilon) - 1}, \quad \tilde{\alpha}_n = \tilde{\theta}_n - 1, \quad \bar{\alpha}_n = \frac{1}{1 - \bar{\mu}_{n\kappa}(\varepsilon)}, \tag{7.102}
$$

$$
\bar{\theta}_n = \frac{1}{\bar{\mu}_{n\kappa}(\varepsilon)} \bar{\alpha}_n, \quad \bar{\mu}_{n\kappa}(\varepsilon) = \mu_{n\kappa}^{-1}(\varepsilon) = -\varepsilon^{-1} \mathcal{Z}^{-1} \left(|n| + \gamma_\kappa \mp N_{n\kappa} \right), \tag{7.103}
$$

$r_<(r_>) = inf(r,r')(sup(r,r'))$, $M_{\eta\gamma}$ and $W_{\eta\gamma}$ are respectively Whittaker functions of the first and second kind, respectively regular and irregular at the origin, λ and ε given respectively by equations (7.15) and (7.16), $\mu_{n\kappa}(\varepsilon)$ by equation (7.28). Two equivalent symmetric forms of the Sturmian representation of radial Dirac-Coulomb Green function are available in Ref. [23]. But it should be pointed out, however, that in applications the seemingly non-symmetric Sturmian expansions given above may be superior to the symmetric one. They lead to the factorization of the second-order matrix elements (considered in **Chapter** 8 of this thesis) rather than the symmetric analog. It is interesting to consider expansion (7.95) as function of the parameter E and to investigate the location of their poles in the interval $-1 < E < 1$. It is clear that such singularities occur at energies that are solutions of the equations $\mu_{n\kappa}(\varepsilon) = 1$, hence, upon utilizing the definition (7.28), one finds $E = E_{n\kappa}$, thus recovering energies of bound states of the relativistic H-like problem given in equation (7.50).

7.4.2 Quasirelativistic treatment

The Green's function, $G_E^{(1)}(\mathbf{r}, \mathbf{r}')$ (which is defined here in a slight difference with that of the preceding case) of the first-order Dirac equation is easily found by applying the projection operator

$$
\mathcal{P}^+ = \frac{1}{2} \left[\mathcal{I} + \beta E + \mathrm{i}\beta(\boldsymbol{\alpha} \cdot \hat{\boldsymbol{r}}) \left(\frac{\partial}{\partial r} + \frac{\mathcal{L} + \mathcal{I}}{r} \right) \right] \tag{7.104}
$$

to the corresponding function $G_E^{(2)}(\mathbf{r},\mathbf{r}')$ of the second-order equation. The latter is the inhomogeneous counterpart of equation (7.79) in which we set $\mu = 1$

$$\frac{1}{2}\left[\mathcal{I}\partial^2/\partial r^2 - \mathcal{L}(\mathcal{L}+1)/r^2 + \left(2E\mathcal{Z}/r - 1 + E^2\right)\mathcal{I}\right] rG_E^{(2)}(\mathbf{r},\mathbf{r}')r' = -rr'\delta(\mathbf{r}-\mathbf{r}')\mathcal{I}, \qquad (7.105)$$

$$rG_E^{(2)}(\mathbf{r},\mathbf{r}') \to 0 \quad \text{for } r \to 0 \quad rG_E^{(2)}(\mathbf{r},\mathbf{r}') \to 0 \quad \text{for } r \to \infty.$$

Here again $\mathbf{r}'$ is fixed, $|E| < 1$ and $0 \leq |\mathcal{Z}| < 1$. The introduction of the function $G_E^{(2)}(\mathbf{r},\mathbf{r}')$ is convenient because it satisfies a second-order equation in which the angular variables are separated and the radial equation can be solved with a product of Whittaker functions $M_{\alpha\beta}(r_<)$ and $W_{\alpha\beta}(r_>)$ (Ref. [17]). After lengthy calculations, and using the so-called Hille-Hardy expansion [66], Szymanowski *et al.* [20] and Zon *et al.* [37] obtained the Sturmian expansion of the Green function $G_E^{(2)}(\mathbf{r},\mathbf{r}')$ over the discrete Sturmian basis set of the second-order defined in equation (7.82). This representation made it possible to calculate analytically electromagnetic susceptibilities and other effects in static fields for the ground state of a hydrogen-like atom [15].
Following the ideas of Szmytkowski [23], we easily derived the Sturmian expansions of $G_E^{(2)}(\mathbf{r},\mathbf{r}')$ directly from his spectral method rather than solving a radial differential equation. Since the Sturmian functions $\{\Phi_{\mu_n jlm}(E,\mathbf{r})\}$ form a complete set and satisfy the same boundary conditions as the Green function, we may seek a solution to equation (7.105) in the form

$$G_E^{(2)}(\mathbf{r},\mathbf{r}') = \sum_{njlm} \Phi_{\mu_n jlm}(E,\mathbf{r})\bar{\Theta}_{\mu_n jlm}(E,\mathbf{r}'), \qquad (7.106)$$

where the expansion coefficients $\bar{\Theta}_{\mu_n jlm}(E,\mathbf{r}')$ are bispinors which are given by

$$\bar{\Theta}_{\mu_n jlm}(E,\mathbf{r}') = \frac{1}{(\mu_n - 1)E}\bar{\Phi}_{\mu_n jlm}(E,\mathbf{r}') \quad \bar{\Phi}_{\mu_n jlm}(E,\mathbf{r}') = \Phi^\dagger_{\mu_n jlm}(E,\mathbf{r}')\beta. \qquad (7.107)$$

Hence the Sturmian expansion of the Green function of the second-order

$$G_E^{(2)}(\mathbf{r},\mathbf{r}') = \sum_{njlm} \frac{1}{(\mu_n - 1)E}\Phi_{\mu_n jlm}(E,\mathbf{r})\bar{\Phi}_{\mu_n jlm}(E,\mathbf{r}'). \qquad (7.108)$$

It is convenient to separate off the angular part of the Green-function. Using the explicit form of the Sturmians we arrive at the following partial-wave expansion

$$G_E^{(2)}(\mathbf{r},\mathbf{r}') = \sum_{jlm} \frac{1}{rr'}\mathrm{g}_{jl}(E;r,r')\mathcal{Y}_{jlm}(\hat{\boldsymbol{r}})\bar{\mathcal{Y}}_{jlm}(\hat{\boldsymbol{r}}'), \qquad (7.109)$$

where

$$\mathrm{g}_{jl}(E;r,r') = \frac{\mathcal{Z}}{\lambda}\sum_{n}\frac{1}{n-\eta+\zeta}S_{\mu_n\epsilon}(2\lambda r)S_{\mu_n\epsilon}(2\lambda r'). \tag{7.110}$$

(with $\eta \equiv \nu$ given in equation (7.102)). As mentioned previously the poles of the Green function, i.e. $\mu_n = 1$, occur at energies given by $E = E_{n\kappa}$.
The action of the projection operator on $G_E^{(2)}(\mathbf{r},\mathbf{r}')$ clearly displays the dependence of $G_E^{(1)}(\mathbf{r},\mathbf{r}')$ on the elements of the Sturmian basis as

$$G_E^{(1)}(\mathbf{r},\mathbf{r}') = \sum_{njlm}\begin{pmatrix} g^{(11)}\Omega_{jlm}(\hat{\boldsymbol{r}})\Omega^{\dagger}_{jlm}(\hat{\boldsymbol{r}}') & \mathrm{i}g^{(12)}\Omega_{jlm}(\hat{\boldsymbol{r}})\Omega^{\dagger}_{j\bar{l}m}(\hat{\boldsymbol{r}}') \\ \mathrm{i}g^{(21)}\Omega_{j\bar{l}m}(\hat{\boldsymbol{r}})\Omega^{\dagger}_{jlm}(\hat{\boldsymbol{r}}') & -g^{(22)}\Omega_{j\bar{l}m}(\hat{\boldsymbol{r}})\Omega^{\dagger}_{j\bar{l}m}(\hat{\boldsymbol{r}}') \end{pmatrix}, \tag{7.111}$$

where the four radial coefficients $g^{(ij)} \equiv g^{(ij)}(E;r,r')$, $i,j = 1,2$, are [20, 54]

$$g^{(11)} = \frac{\mathcal{Z}^2}{4\epsilon\gamma_\kappa\,(n-\eta+\zeta)}\left[\left(-\frac{E(\kappa+\epsilon\gamma_\kappa)}{\eta(1-E)} - 1 + \frac{n+\zeta-\epsilon\gamma_\kappa}{\lambda r}\right)S_n(r) - \sqrt{(n+1)(n+2\zeta)}\,\frac{1}{\lambda r}S_{n+1}(r)\right]S_n(r'), \tag{7.112}$$

$$g^{(21)} = \frac{\mathcal{Z}(\kappa+\epsilon\gamma_\kappa)}{4\epsilon\gamma_\kappa\,(n-\eta+\zeta)}\left[\left(-\frac{E(\kappa-\epsilon\gamma_\kappa)}{\eta(1+E)} - 1 + \frac{n+\zeta-\epsilon\gamma_\kappa}{\lambda r}\right)S_n(r) - \sqrt{(n+1)(n+2\zeta)}\,\frac{1}{\lambda r}S_{n+1}(r)\right]S_n(r'), \tag{7.113}$$

$$g^{(12)} = \tilde{\beta}g^{(11)} \qquad g^{(22)} = \tilde{\beta}g^{(21)} \qquad S_n(r) = \frac{1}{r}S_{\mu_n\epsilon}(2\lambda r). \tag{7.114}$$

This expression is basically equivalent to those proposed by Szmytkowski [23], Zon *et al.* [37] and Swainson and Drake [38]. It has been used to compute fully relativistic two-photon transition amplitudes in high-Z hydrogenic ions [20, 31].

7.5 The nonrelativistic limit

This Section deals with nonrelativistic limits of relativistic Coulomb Sturmian and Green's functions derived above. Throughout this Section λ stands for the nonrelativistic limit of the same quantity defined in equation (7.15) and the energy parameter E is assumed to be positive. In a nonrelativistic theory, all velocities of the system are small in magnitude compared to c, the speed

of light. Mathematically, the nonrelativistic limit of a relativistic theory is therefore described by the limit $\alpha Z \to 0$, which removes the relativistic bound on the propagation speed of signals. However, in general, we cannot simply set $\alpha Z \to 0$ in the Dirac-Coulomb equation. It seems reasonable to subtract the rest mass energy from the Dirac operator before taking the nonrelativistic limit.

7.5.1 Coulomb Sturmian functions

The quantity λ and the eigenvalues $\mu_{n\kappa}(\varepsilon)$ have the following nonrelativistic limits (in (a.u.))

$$\lambda = \begin{cases} Z/(n+l) & n \geq 1,\ \kappa = +l > 0,\ Z > 0 \\ Z/(n+l+1) & n \geq 0,\ \kappa = -l-1 < 0,\ Z > 0 \end{cases}, \tag{7.115}$$

$$\mu_{nl}(\varepsilon) = \begin{cases} 0 & n \leq 0,\ \kappa = +l > 0,\ Z < 0 \\ (\lambda/Z)(n+l) & n \geq 1,\ \kappa = +l > 0,\ Z > 0 \end{cases}, \tag{7.116}$$

$$\mu_{n,-l-1}(\varepsilon) = \begin{cases} 0 & n \geq -1,\ \kappa = -l-1 < 0,\ Z < 0 \\ (\lambda/Z)(n+l+1) & n \geq 0,\ \kappa = -l-1 < 0,\ Z > 0 \end{cases} \tag{7.117}$$

and the limits of the upper components $S_{n\kappa}(\varepsilon, x) \equiv S_{n\kappa}(x)$ of the radial Sturmians are

$$S_{nl}(x) = \sqrt{\frac{(n-1)!}{Z(n+2l)!}} x^{l+1} \mathrm{e}^{-x/2} L_{n-1}^{(2l+1)}(x) \qquad n \geq 1, \tag{7.118}$$

$$S_{n,-l-1}(x) = -\sqrt{\frac{n!}{Z(n+2l+1)!}} x^{l+1} \mathrm{e}^{-x/2} L_{n}^{(2l+1)}(x) \qquad n \geq 0. \tag{7.119}$$

Thus in the nonrelativistic limit, the eigenvalues $\mu_{n+1,l}(\varepsilon)$ and $\mu_{n,-l-1}(\varepsilon)$ are identical while the functions $S_{n+1,l}(x)$ and $S_{n,-l-1}(x)$ differ only by a phase factor, which is due to the choice made for the phase in equations (7.29) and (7.30). Notice that, in this limit, the lower component $T_{n\kappa}(\varepsilon, x) \equiv T_{n\kappa}(x)$ of the radial Sturmians vanishes. Since $\tilde{n} = n + |\kappa|$, it follows that $S_{n\kappa}(x) \to S_{\tilde{n}l}(x)$ ($\tilde{n} \geq l+1$) for both signs of κ in the nonrelativistic limit.

It is necessary to point out that, in the nonrelativistic limit for the quasirelativistic treatment, the two parameters λ and η recover the well known energy parameter and principal quantum number

$$\begin{aligned} &E \to 1 + \alpha^2 E_c, \quad \lambda \to \sqrt{-2E_c}, \quad \eta \to \frac{Z}{\sqrt{-2E_c}}, \\ &\zeta \to |\kappa| + \frac{\epsilon+1}{2}, \quad |\kappa| = l + \frac{1-\epsilon}{2}, \end{aligned} \tag{7.120}$$

where E_c denotes the nonrelativistic energy, $E_c < 0$. Thus the eigenvalues μ_n for the problem read

$$\mu_n = \frac{\lambda}{Z}\left(n + |\kappa|\right). \tag{7.121}$$

Under this condition the reader will find no difficulty in verifying that the second-order radial Sturmians $\{S_{\mu_n\epsilon}(x)\}$ given in equation (7.82) agrees with the results obtained in equations (7.118)-(7.119).

These radial Schrödinger-Coulomb Sturmians are normalized non-trivial solutions of the Sturm-Liouville problem

$$\left[-\frac{1}{2}\frac{\mathrm{d}^2}{\mathrm{d}r^2} + \frac{l(l+1)}{2r^2} - \mu_{\tilde{n}l}\frac{Z}{r} + \frac{\lambda^2}{2}\right] S_{\tilde{n}l}(r) = 0 \quad (0 \le r < \infty), \tag{7.122}$$

$$S_{\tilde{n}l}(r) \to r^{l+1} \quad \text{for } r \to 0 \quad S_{\tilde{n}l}(r) \quad \text{bounded} \quad \text{for } r \to \infty. \tag{7.123}$$

These functions are orthonormal with respect to the weight function $-Z/r$ so that

$$\int_0^\infty \mathrm{d}r\ S_{\tilde{n}l}(r)\left(-\frac{Z}{r}\right) S_{\tilde{n}l}(r) = -\delta_{\tilde{n}\tilde{n}'}. \tag{7.124}$$

They form a complete orthonormal set on the interval $(0, \infty)$ and the corresponding closure relation

$$\sum_{\tilde{n}=l+1}\left(-\frac{Z}{r}\right) S_{\tilde{n}l}(r) S_{\tilde{n}l}(r') = -\delta(r - r') \tag{7.125}$$

is satisfied.

Pont and Skakeshaft [68] defined their nonrelativistic Coulomb Sturmians

$$S^\kappa_{\tilde{n},l}(r) = N^\kappa_{\tilde{n},l} r^{l+1} \mathrm{e}^{-\kappa r} L^{(2l+1)}_{\tilde{n}-l-1}(2\kappa r), \quad N^\kappa_{\tilde{n},l} = \sqrt{\frac{\kappa}{\tilde{n}}}(2\kappa)^{l+1}\left[\frac{(\tilde{n}-l-1)!}{(\tilde{n}+l)!}\right]^{1/2}, \tag{7.126}$$

with $\kappa = \sqrt{-2E_c}$ as solutions of the Sturm-Liouville problem

$$\left[-\frac{1}{2}\frac{\mathrm{d}^2}{\mathrm{d}r^2} + \frac{l(l+1)}{2r^2} - \frac{Z}{r} + \frac{\kappa^2}{2}\right] S^\kappa_{\tilde{n},l}(r) = 0, \tag{7.127}$$

with the associated boundary conditions $S^\kappa_{\tilde{n},l}(0) = 0$, $S^\kappa_{\tilde{n},l}(\infty) = 0$. Here $Z = \kappa\tilde{n}$ is an eigenvalue for the problem. Such Sturmians are normalized according to

$$\int_0^\infty \mathrm{d}r\ S^\kappa_{\tilde{n},l}(r) S^\kappa_{\tilde{n},l}(r) = 1. \tag{7.128}$$

These Sturmian functions obey the following orthogonality and closure relations

$$\int_0^\infty \mathrm{d}r\ S^\kappa_{\tilde{n}',l}(r)\frac{1}{r}S^\kappa_{\tilde{n},l}(r) = \frac{\kappa}{\tilde{n}}\delta_{\tilde{n}'\tilde{n}} \qquad \sum_{\tilde{n}=l+1}\frac{\tilde{n}}{\kappa}|S^\kappa_{\tilde{n},l}\rangle\langle S^\kappa_{\tilde{n},l}|\frac{1}{r} = I. \tag{7.129}$$

The above nonrelativistic Coulomb Sturmian functions are related by the relation

$$S_{\tilde{n}l} = \sqrt{\frac{\tilde{n}}{Z\kappa}}S^\kappa_{\tilde{n},l}.$$

7.5.2 Coulomb Green's functions

This is achieved by performing the partial wave expansion

$$G_E(\mathbf{r},\mathbf{r}') = \sum_{l=0}^{\infty}\sum_{m_l=-l}^{l} g_l(E;r,r')Y_l^{m_l}(\hat{\boldsymbol{r}})Y_l^{m_l}(\hat{\boldsymbol{r}}')^*, \tag{7.130}$$

where g_l is the radial component of the CGF for angular momentum l. In the nonrelativistic limit ($\alpha Z \to 0$), equations (7.115)-(7.117) hold and the components $g_\kappa^{(ij)}(E;r,r')$ of the radial Dirac-Coulomb Green function reduce to the nonvanishing identical components $g_l^{(11)}(E;r,r')$, $g_{-l-1}^{(11)}(E;r,r')$ which may be transformed in the following well-known expressions

$$g_l(E;r,r') = -\frac{Z}{\lambda}\sum_{\tilde{n}=l+1}\frac{\widetilde{S}_{\tilde{n}l}(r)\widetilde{S}_{\tilde{n}l}(r')}{\tilde{n}-Z/\lambda}, \tag{7.131}$$

$$= -\frac{1}{\lambda r r'}\frac{\Gamma(l+1-Z/\lambda)}{\Gamma(2l+2)}M_{Z/\lambda,l+1/2}(2\lambda r_<)W_{Z/\lambda,l+1/2}(2\lambda r_>), \tag{7.132}$$

where

$$\widetilde{S}_{\tilde{n}l}(r) = \sqrt{\frac{(\tilde{n}-l-1)!(2\lambda)^2}{Z(\tilde{n}+l)!}}(2\lambda r)^l\exp(-\lambda r)L^{(2l+1)}_{\tilde{n}-l-1}(2\lambda r).$$

We see from (7.131) that the Green's function has poles at $Z/\lambda = \tilde{n}$, corresponding in the E plane to the poles $E_{\tilde{n}} = -Z^2/(2\tilde{n}^2)$, which determine the spectrum of the hydrogen-like atom. It is easy to verify that the residues of the function $G_E(\mathbf{r},\mathbf{r}')$ at these poles are equal to the products of the eigenfunctions of the bound states of the Coulomb field. These limits agree well with the corresponding expressions derived previously in the nonrelativistic theory [8, 38].

7.6 Conclusion

A relativistic Sturmian discrete basis set representations for the Dirac-Coulomb Green functions, previously studied by Szymanowski *et al.* [20], Szmytkowski [23] and Zapryagaev *et al.* [39], are investigated for application to relativistic calculations of two-photon bound-bound transition amplitudes in hydrogen-like ions. These pseudoeigenfunction representations follow both from exact identities starting from the Whittaker function representation or by solving the inhomogeneous system of coupled first-order and second-order differential equations. They eliminate the radial ordering problem of the former representation, and so are particularly useful for numerical as well as analytical calculations of the second-order perturbation theory Feynman diagrams with one electron Green function. The discret Dirac-Coulomb Sturmians defined by Szmytkowski [23] are closely related to the L spinors presented by Grant and Quiney [34], although there are major differences. L spinors involve paired *two*-component basis sets for large and small components, whereas Szmytkowski deals only with *four*-component objects. The orthogonality and completeness properties of L spinors have been connected to those of Coulomb Sturmians by examining the nonrelativistic limiting behavior as $\alpha Z \to 0$ [34].

Bibliography

[1] B. M. Levitan, *Eigenfunction Expansions Associated with Second-Order Differential Equations* (Nauka, Moscow, 1950) (in Russian).

[2] R. Courant and D. Hilbert, *Methods of Mathematical Physics* Vol I (Wiley-Interscience, New York, 1953).

[3] E. C. Titchmarsh, *Eigenfunction Expansions Associated with Second-Order Differential Equations* Part I 2nd ed. (Clarendon, Oxford, 1962).

[4] E. C. Titchmarsh, *Eigenfunction Expansions Associated with Second-Order Differential Equations* Part II (Clarendon, Oxford, 1958).

[5] B. M. Levitan and I. S. Sargsjan, *Introduction to Spectral Theory. Self-adjoint Ordinary Differential Operators* (Nauka, Moscow, 1970) (in Russia).

[6] B. M. Levitan and I. S. Sargsjan, *Sturm-Liouville and Dirac Operators* (Nauka, Moscow, 1988) (in Russia).

[7] B. Klahn, *Adv. Quantum Chem.* **13**, 155 (1981).

[8] M. Rotenberg, *Adv. At. Mol. Phys.* **6**, 233 (1970).
M. Rotenberg, *Ann. Phys.* **19**, 262 (1962).

[9] S. V. Khristenko, *Teor. Mat. Fiz.* **22**, 31 (1975) (Engl. transl. Theor. Math. Phys. **22**, 21 (1975)).

[10] R. Shakeshaft, *J. Phys. B: At. Mol. Phys.* **18**, L611 (1985).
R. Shakeshaft, *Phys. Rev. A* **34**, 244 (1986).
R. Shakeshaft, *Phys. Rev. A* **34**, 5119 (1986).

[11] S. Yu. Ovchinnikov and J. H. Macek, *Phys. Rev. A* **55**, 3605 (1997).

[12] A. Maquet, *Phys. Rev. A.* **15**, 1088 (1977).

[13] P. Pyykkö, *Relativistic Theory of Atoms and Molecules. A Bibliography* (Springer, Berlin, 1986), p 1916.

[14] P. Pyykkö, *Relativistic Theory of Atoms and Molecules. II. A Bibliography* (Springer, Berlin, 1993), p 1986.

[15] N. L. Manakov, L. P. Rapoport and S. A. Zapryagaev, *Phys. Lett.* **43A**, 139 (1973).
N. L. Manakov, L. P. Rapoport and S. A. Zapryagaev, *Phys. Lett.* **48A**, 145 (1974).

N. L. Manakov, L. P. Rapoport and S. A. Zapryagaev, *J. Phys. B: At. Mol. Phys.* **7**, 1076 (1974).

[16] N. L. Manakov and S. A. Zapryagaev, *Phys. Lett.* **58A**, 23 (1976).
S. A. Zapryagaev and N. L. Manakov, *Yad. Fiz.* **23**, 917 (1976) (Sov. J. Nucl. Phys. **23**, 482 (1976)).
N. L. Manakov, S. I. Marmo and A. G. Fainshtein, *Teor. Mat. Fiz.* **59**, 49 (1984) (Engl. transl. Theor. Math. Phys. **59**, 351 (1984)).

[17] P. C. Martin and R. J. Glauber, *Phys. Rev.* **109**, 1307 (1958).

[18] L. Hostler, *J. Math. Phys.* **24**, 2366 (1983).

[19] L. Hostler, *J. Math. Phys.* **28**, 2984 (1987).

[20] C. Szymanowski, V. Véniard, R. Taïeb and A. Maquet, *Phys. Rev. A* **56**, 700 (1997).
C. Szymanowski, V. Véniard, R. Taïeb and A. Maquet, *Europhys. Lett.* **37**, 391 (1997).

[21] G. W. F. Drake and S. P. Goldman, *Adv. At. Mol. Phys.* **25**, 393 (1988).

[22] I. P. Grant, *The Effects of Relativity in Atoms, Molecules and the Solid state* ed. S. Wilson, I. P. Grant and B. L. Gyorffy (Plenum, New York, 1991), p 17.

[23] R. Szmytkowski, *J. Phys. B: At. Mol. Opt. Phys.* **30**, 825 (1997).
R. Szmytkowski, *J. Phys. B: At. Mol. Opt. Phys.* **30**, 2747 (1997) (Erratum).

[24] I. P. Grant, in *Relativistic, Quantum Electrodynamic and Weak Interaction Effects in Atoms* ed. P. J. Mohr, W. R. Johnson and J. Sucher, *AIP Conf. Proc.* **189** (AIP, New York, 1989), p 235.

[25] I. P. Grant, *Adv. At. Mol. Opt. Phys.* **32**, 169 (1994).

[26] I. P. Grant, *Relativistic Atomic Structure in Atomic, Molecular and Optical Physics Handbook* ed. Gordon W. F. Drake (AIP, New York, 1996), p 258.

[27] P. M. Morse and H. Feshbach, *Methods of Theoretical Physics* Part I (New York, McGraw-Hill, 1953), Chap 6.

[28] R. Szmytkowski, *Phys. Rev. A* **65**, 012503 (2001).
R. Szmytkowski, *J. Phys. B: At. Mol. Opt. Phys.* **35**, 1379 (2002).

[29] R. Szmytkowski and K. Mielewczyk, *J. Phys. B: At. Mol. Opt. Phys.* **37**, 3961 (2004).

[30] K. Mielewczyk and R. Szmytkowski, *Phys. Rev. A* **73**, 022511 (2006).
K. Mielewczyk and R. Szmytkowski, *Phys. Rev. A* **73**, 039908 (2006) (Erratum).

[31] H. M. Tetchou Nganso and M. G. Kwato Njock, *J. Phys. B: At. Mol. Opt. Phys.* **40**, 807 (2007).

[32] R. Szmytkowski, *J. Phys. A: Math. Gen.* **33**, 427 (2000).

[33] J. Avery and F. Antonsen, *J. Math. Chem.* **24**, 175 (1998).

[34] I. P. Grant and H. M. Quiney, *Phys. Rev. A* **62**, 022508 (2000).

[35] E. H. Wichman and N. M. Kroll, *Phys. Rev.* **101**, 843 (1956)

[36] G. E. Brown and G. W. Schaeffer, *Proc. R. Soc. London A* **233**, 527 (1956).

[37] B. A. Zon, N. L. Manakov and L. P. Rapoport, *Sov. J. Nucl. Phys.* **15**, 282 (1972) (Yad. Fiz. **15**, 508 (1972) in Russian).

[38] R. A. Swainson and G. W. F. Drake, *J. Phys. A: Math. Gen.* **24**, 95 (1991).
R. A. Swainson and G. W. F. Drake, *J. Phys. A: Math. Gen.* **24**, 1801 (1991).
R. A. Swainson and G. W. F. Drake, *J. Phys. A: Math. Gen.* **24**, 79 (1991).

[39] S. A. Zapryagaev, N. L. Manakov and V. G. Pal'chikov, *Opt. Spektrosk.* **52**, 414 (1982) (Opt. Spectrosc. **52**, 248 (1982)).
S. A. Zapryagaev, N. L. Manakov and V. G. Pal'chikov, *Theory of Multiply Charged Ions with One ant Two Electrons* (Energoatomizdat, Moscow, 1985) (in Russia).

[40] E. U. Condon and G. H. Shortley, *The Theory of Atomic Spectra* (Cambridge University Press, England, 1935).

[41] J. J. Sakurai, *Advanced Quantum Mechanics* (Addison-Wesley, MA, Reading, 1967), section 3.8.

[42] W. Magnus, F. Oberhettinger and R. P. Soni, *Formulas and Theorems for the Special Functions of Mathematical Physics* 3rd edn (Springer, Berlin, 1966).

[43] H. A. Bethe and E. E. Salpeter, *Quantum Mechanics of One and Two-Electron Atoms* (Springer-Verlag, Berlin, 1957).

[44] W. Greiner, *Relativistic Quantum Mechanics* (Springer-Verlag, New York, 1994).

[45] M. G. Kwato Njock, S. G. Nana Engo, L. C. Owono Owono, G. Lagmago and B. Oumarou, *Phys. Lett. A* **187**, 191 (1994).
M. G. Kwato Njock, B. Oumarou, L. C. Owono, J. D. Kenmogne, S. G. Nana Engo and M. Onana Boyomo, *Phys. Lett. A* **184**, 352 (1994).
S. G. Nana Engo, M. G. Kwato Njock, L. C. Owono Owono, B. Oumarou, G. K. Lagmago and O. Motapon, *Phys. Rev. A* **56**, 2624 (1997).

[46] S. P. Goldman and G. W. F. Drake, *Phys. Rev. A* **24**, 183 (1981).

[47] I. P. Grant, *Adv. Phys.* **19**, 747 (1970).
I. P. Grant, *J. Phys. B: At. Mol. Phys.* **7**, 1458 (1974).

[48] D. J. Hylton and N. J. Snyderman, *Phys. Rev. A* **55**, 2651 (1997).

[49] C. Fronsdal, *Phys. Rev.* **179**, 1513 (1969).

[50] G. E. Brown, R. E. Peierls and J. B. Woodward, *Proc. Roy. Soc. A* **227**, 51 (1954).

[51] P. J. Mohr, *Ann. Phys.* (N.Y) **88**, 26 (1974).

[52] E. T. Whittaker and G. N. Watson, *A Course of Modern Analysis* (Cambridge University, Cambridge, 1927).

[53] D. J. Hylton, *J. Math. Phys.* 25, 1125 (1984).

[54] A. Maquet, V. Véniard and T. A. Marian, *J. Phys. B: At. Mol. Opt. Phys.* **31**, 3743 (1998).

[55] N. L. Manakov, V. D. Ovsiannikov and L. P. Rapoport, *Phys. Rep.* **141**, 319 (1986).

[56] A. A. Krylovetsky, N. L. Manakov and S. I. Marno, *Laser Phys.* **7**, 817 (1997).

[57] V. L. Yakhontov and M. Ya. Amusia, *Phys. Rev. A* **55**, 1952 (1997).

[58] D. B. Milošević, F. Ehlotzky and B. Piraux, *J. Phys. B: At. Mol. Opt. Phys.* **30**, 4347 (1997).

[59] N. L. Manakov, A. Maquet, S. I. Marno and C. Szymanowski, *Phys. Lett. A* **237**, 234 (1998).

[60] S. A. Zapryagaev and N. L. Manakov, *Izv. Akad. Nauk.* 45, 2336 (1976).

[61] N. L. Manakov, A. A. Nekipelov and A. G. Fainshtein, *Sov. J. Nucl. Phys.* **45**, 677 (1987) (Yad. Fis. **45**, 1091 (1987) in Russian).

[62] Le Anh Thu, Le Van Hoang, L. J. Komarov and T. S. Rachman, *J. Phys. B: At. Mol. Opt. Phys.* **27**, 4083 (1994).
Le Anh Thu, Le Van Hoang, L. J. Komarov and T. S. Rachman, *J. Phys. B: At. Mol. Opt. Phys.* **29**, 2897 (1996).

[63] P. Indelicato and P. J. Mohr, *J. Math. Phys.* **36**, 714 (1995).

[64] H. M. Quiney, *The Effects of Relativity in Atoms, Molecules and the Solid State* ed. S. Wilson, I. P. Grant and B. L. Gyorffy (Plenum, New York, 1991), p 83.

[65] R. Nyden Hill, *Hydrogenic Wave Functions in Springer Handbook of Atomic, Molecular and Optical Physics* ed. Gordon W. F. Drake (Springer, 2006), Part A, p 153.

[66] H. Buchholz, *The Confluent Hypergeometric Function* ed. by B. D. Coleman, Springer Tracts in Natural Philosophy (Springer, Berlin, 1969), Vol 15.

[67] I. P. Grant, *J. Phys. B: At. Mol. Phys.* **19**, 3187 (1986).

[68] M. Pont and R. Shakeshaft, *Phys. Rev. A* **44**, R4110 (1991).

Chapter 8

Two-Photon Transition Amplitudes in Hydrogen-Like Ions

"With ordinary talent and extraordinary perseverance, all things are attainable. Victory becomes, to some degree, a state of mind. Knowing ourselves superior to the anxieties, troubles, and worries which obsess us, we are superior to them"
H. M. Tetchou Nganso.

8.1 Introduction

Multiphoton absorption belongs to those phenomena which have first been predicted theoretically. At the middle of 1920-s, Schrödinger [1] and Dirac [2] developed the *first-order perturbation* theory and applied it to *one-photon absorption* processes. Moreover, Dirac also discussed the applications for the *second-order perturbation* theory. He applied this theory to the electron scattering which is a *two-photon* process. This latter process is regarded as having two steps: the first photon initiates a transition to a virtual state and the second photon brings about a transition to the final state of the target atom. In another word, the two photons simultaneously transfer their energy to the atom. Since the 1930-s, when *two-photon absorption* was first described by Göpper-Mayer [3], it became clear that *higher-order perturbation* theory revealed *multiphoton processes* which have received considerable attention as fundamental components of the interaction of light with matter. She also noticed that the second-order perturbation theory allows to describe another -different from the scattering -process of two-photon absorption as well as *Raman / Rayleigh scattering* and *stimulated or spontaneous two-photon emission.*

In theory, generally, perturbation methods are employed in order to describe multiphoton processes (*e.g.,* excitation and ionization). A characteristic of the second-order perturbation theory is the summation of matrix elements over all *intermediates states* with discrete eigenvalues and the integration over intermediate states in the continuum [4]. This problem is so complicated that one can seldom evaluate it without making some gross approximation. There exist several different methods which avoid the difficult problem of explicit summation, in particular when a large number of intermediate states becomes important and has to be taken into account. Already in first theoretical works, these sums had been calculated by means of *implicit summation methods* [5, 6] which convert the summation into the solving of a relevant differential equation. Although one of the implicit methods - *the differential equation method* - had been implemented firstly, yet another powerful *Green's function method* [7, 8] became widespread. This latter method has been successfully used in many multiphoton processes and in high-order processes of perturbation theory. The Green's function method replaces the summation over the *complete atomic spectrum* by the calculation of a relevant *Green's function.* The method of Kelsey and Macek [9] is a simple reformulation of the method of implicit summation. The *direct summation method* [10] in which only one or a few dominant states in the summation over all intermediate states is or are retained, and the remaining states are estimated by introducing the notion of mean level energy [11]. In the *pseudostate summation technique* [12], the intermediate states are replaced by a finite set of pseudostates which are expanded in terms of a basis which is discrete and complete. Thus, the infinite summation over both discrete and continuum states is replaced by a finite sum over the pseudostates. The energy spectrum of the pseudostates contains both negative and positive values representing both the bound states and the continuum states adequately. The problem of gauge invariance in multiphoton transitions was illustrated by calculating the two-photon transition rates in hydrogen atoms in various gauges [13, 14]. These explicit calculations demonstrated that the gauge invariance can be maintained only by using a complete set of intermediate states. This clearly indicates the need for an accurate evaluation of the sum of the contributions from various virtual states.

For hydrogen-like ions, the relevant Coulomb Green functions are known analytically today in many forms, especially in terms of various special functions from mathematical physics. Despite a formal equivalence of these forms, there are large differences by the accuracy and in the efficiency by actual computations of the two -and multi -photon cross sections / transition probability amplitudes. For instance, an *integral representation* (Klarsfeld [15]) of the Coulomb Green's functions is the slowest, while a *product representation* (La-

planche *et al.* [16]) allows already a faster computation. Furthermore, an expansion of the Coulomb Green's function on a *Sturmian basis* seems to be most efficient in the matrix element calculation (Karule and Pratt [17]).

In this Chapter, we consider the two-photon excitation, namely the two-photon absorption and Raman / Rayleigh scattering of hydrogen-like ions within the framework of second-order perturbation theory, based on the first and second-order Dirac-Coulomb equations. In Section (8.2), we start with a brief concept of the classical electromagnetic field. To obtain the transition probabilities, a Green function approach is applied in Section (8.3) to perform the summation over the *complete hydrogen spectrum* appropriately. Using such an approach in Section (8.4), amplitude probabilities for the aforementioned two-photon absorption of the $1s$ ground state of hydrogen-like ions are calculated for nuclear charges in the range $Z = 1, \ldots, 100$ in order to account both the *relativistic effects* as well as those effects which arise from the higher multipoles in the decomposition of the radiation field, *i.e.* the so-called *retardation effects* in the process underlined. This Section, later, provides a comparison of the two-photon absorption amplitudes from the quasi and fully relativistic theories (as obtained in the dipole approximation). Section (8.5) is devoted to Raman and Rayleigh scattering, where we have derived their new exact relativistic analytical formulae. Numerical results and discussion are given in Section (8.6). Finally, a few conclusions are given in Section (8.7).

8.2 The covariant formulation of the electromagnetic field

The classical electromagnetic field *in vacuo* is described by electric and magnetic field vectors $\mathcal{E}(\mathbf{r}, t)$ and $\mathcal{B}(\mathbf{r}, t)$, which satisfy the well known Maxwell's equations [18, 19]. These equations can be written more concisely in a covariant form if we introduce the antisymmetric field tensor $F_{\mu\nu} = (\mathcal{E}, \mathcal{B})$ as

$$\partial^\nu F_{\mu\nu} = 0, \tag{8.1}$$

$$\partial_\lambda F_{\mu\nu} + \partial_\nu F_{\lambda\mu} + \partial_\mu F_{\nu\lambda} = 0, \tag{8.2}$$

$$F_{\mu\nu} = \partial_\mu A_\nu - \partial_\nu A_\mu, \tag{8.3}$$

where $\partial_\mu = \partial/\partial x^\mu$, the electromagnetic four-vector potential $A^\mu = (\phi, \mathbf{A})$ is generated from scalar and vector potentials $\phi(\mathbf{r}, t)$ and $\mathbf{A}(\mathbf{r}, t)$. In terms of the potentials, equation (8.2) is satisfied identically while equation (8.1) gives the field equation for the four-vector potential

$$\partial_\mu(\partial^\nu A_\nu) - \Box A_\mu = 0, \tag{8.4}$$

with $\Box$ denoting the familiar D'Alembertian operator. These equations are invariant under the gauge transformation

$$A_\mu \to A'_\mu = A_\mu + \partial_\mu \chi \tag{8.5}$$

where χ is an arbitrary space-time function. This substitution can be used to simplify the field equation (8.4). Starting from potentials A_μ in an arbitrary gauge, we can always perform a gauge transformation (8.5) in such a way that the subsidiary condition

$$\partial^\mu A_\mu \equiv \partial_\mu A^\mu = 0, \qquad \Box\chi = 0 \tag{8.6}$$

is satisfied. Equation (8.6) is known as the *Lorentz condition.* Therefore equation (8.4) reduces to the inhomogeneous wave equation

$$\Box A_\mu = 0, \tag{8.7}$$

which enables us to expand the *unquantized* free electromagnetic field A_μ in a complete set of solutions of the wave equation

$$A_\mu(x) = A^{(a)}_\mu(x) + A^{(e)}_\mu(x), \tag{8.8}$$

where

$$A^{(a)}_\mu(x) = \sum_{\lambda,\mathbf{k}} \sqrt{\frac{2\pi}{\omega}} \varepsilon^{(\lambda)}_\mu(\mathbf{k}) \mathrm{e}^{-\mathrm{i}kx}, \quad A^{(e)}_\mu(x) = \sum_{\lambda,\mathbf{k}} \sqrt{\frac{2\pi}{\omega}} \varepsilon^{(\lambda)}_\mu(\mathbf{k}) \mathrm{e}^{+\mathrm{i}kx}, \tag{8.9}$$

and $kx = \omega t - \mathbf{k}\cdot\mathbf{r}$, respectively represent the time-dependent potential, corresponding to the absorption and emission of a photon with the frequency ω. The summation in this equation is over wave vector $\mathbf{k}$ allowed by the periodic boundary conditions, and $k^0 = \omega = |\mathbf{k}|$. The summation over λ, from $\lambda = 0$ to $\lambda = 3$, corresponds to the fact that for the four-vector field $A_\mu(x)$ there exist, for each $\mathbf{k}$, four linearly independent polarization states. These are described by the *polarization vectors* $\varepsilon^{(\lambda)}_\mu(\mathbf{k})$, $\lambda = 0, \ldots, 3$, which we choose to be real, and which satisfy the orthonormality and completeness relations

$$\varepsilon^{(0)}_\mu(\mathbf{k}) = e^{(0)}_\mu \equiv (1,0,0,0), \tag{8.10}$$

$$\varepsilon^{(\lambda)}_\mu(\mathbf{k}) = (0, \hat{\boldsymbol{e}}_r(\mathbf{k})) \qquad r = 1,2,3, \tag{8.11}$$

where $\hat{\boldsymbol{e}}_1(\mathbf{k})$ and $\hat{\boldsymbol{e}}_2(\mathbf{k})$ are mutually orthogonal unit vectors which are also orthogonal to $\mathbf{k}$, and

$$\hat{\boldsymbol{e}}_3(\mathbf{k}) = \mathbf{k}/|\mathbf{k}|, \tag{8.12}$$

i.e.

$$\mathbf{k} \cdot \hat{\boldsymbol{e}}_r(\mathbf{k}) = 0 \qquad r = 1, 2; \qquad \hat{\boldsymbol{e}}_r(\mathbf{k}) \cdot \hat{\boldsymbol{e}}_s(\mathbf{k}) = \delta_{rs} \qquad r, s = 1, 2, 3. \tag{8.13}$$

Then $\varepsilon_\mu^{(1)}$ and $\varepsilon_\mu^{(2)}$ are called *transverse*, $\varepsilon_\mu^{(3)}$ *longitudinal* polarizations, and $\varepsilon_\mu^{(0)}$ *scalar* or *time-like* polarization. For many purposes one only requires the usual general properties of the polarization vectors which are given in textbook on Quantum Field Theory [20]. However a specific choice of polarization vectors (cf. equations (8.10) and (8.11)) in one given frame of reference often facilitates the interpretation. In our treatment, we deal with the property given in equation (8.11).

8.3 Relativistic formulation of the S-matrix

We turn in to considering the realistic and much more interesting case of fields in interaction, in which particles can be scattered, created and destroyed. In essence this requires solving the coupled non-linear field equations for given conditions. This is an extremely difficult problem which has only been solved in perturbation theory, *i.e.* the Hamiltonian of the system is divided into that of the free fields plus an interaction term. The latter is treated as a perturbation which is justifiable if the interaction is sufficiently weak. Note that the perturbative treatment presented here is certainly valid in view of the expected intensities of the currently developed X-ray sources as compared to typical electric field strength intensities in heavier atoms. For quantum electrodynamics, where the coupling of photons and electrons is measured by the small dimensionless fine structure constant α, this approach is outstandingly successful, not only in calculating processes in lowest order of perturbation theory but also in calculating higher-order corrections [20]. The perturbation series solution, known as the S-matrix expansion is of great importance since it contains the complete information about all interaction processes in a form suitable for extracting the transition amplitude for a specific process to any order of perturbation theory. A systematic procedure for doing this has been developed using the language of the second-quantized Dirac theory. In this Section we show that the results rigorously derived from quantum field theory can be obtained more quickly by relying on a more intuitive method, due to R. P. Feynman.

8.3.1 Definition

The Dirac S-matrix is derived here, starting from the standard premises of S-matrix theory and proceeding to a fully covariant formulation at the earliest opportunity. This not only gives a concise and rigorous derivation of the result

but it also serves to verify that there is no limitation in any sense to a perturbation theory. The results are fully equivalent to those of Bjorken and Drell [21], Landau and Lifshitz [22], Akhiezer and Berestetskii [23], Bialynicki-Birula and Bialynicka-Birula [24] and Schwabl [25] but are derived more generally and are extended also to the time-reversed form of the S-matrix.

The fundamental definition of the S-matrix is [26]

$$\mathcal{S}_{fi} = \lim_{t\to+\infty} \left(\Psi_f, \Phi_i^{(+)}\right), \qquad \lim_{t\to-\infty} \Phi_i^{(+)} = \Psi_i \tag{8.14}$$

for the direct (or post) form (involving the retarded Green's function) or

$$\mathcal{S}_{fi} = \lim_{t\to-\infty} \left(\Phi_f^{(-)}, \Psi_i\right), \qquad \lim_{t\to+\infty} \Phi_f^{(-)} = \Psi_f \tag{8.15}$$

for the time-reversed (or prior) form (involving the advanced Green's function). In these expressions, Φ represents a state in full interaction with all potentials in the problem, whereas Ψ is a state lacking only the potential causing the transition. Equation (8.14) which will be considered later in the text gives the amplitude that a completely interacting state that starts in the distant or remote past as a pure noninteracting initial state Ψ_i will be in some different noninteracting final state Ψ_f in the far future at asymptotic positive time. The superscripts $(\pm)$ on Φ denote the two different boundary conditions given by the second elements of equations (8.14) and (8.15). Since the noninteracting states Ψ is presumed to be elements of a complete orthonormal set of states, then equations (8.14) and (8.15) can be rewritten as

$$\mathcal{S}_{fi} - \delta_{fi} = \lim_{t\to+\infty} \left(\Psi_f, \Phi_i^{(+)}\right) - \lim_{t\to-\infty} \left(\Psi_f, \Phi_i^{(+)}\right), \tag{8.16}$$

$$\mathcal{S}_{fi} - \delta_{fi} = \lim_{t\to-\infty} \left(\Phi_f^{(-)}, \Psi_i\right) - \lim_{t\to+\infty} \left(\Phi_f^{(-)}, \Psi_i\right). \tag{8.17}$$

These expressions are entirely general and can be converted to general Lorentz covariant forms after somewhat considerations [26] as the surface integral in four-space

$$\mathcal{S}_{fi} - \delta_{fi} = \int_\Sigma \mathrm{d}\sigma_\mu \bar{\Psi}_f \; \gamma^\mu \; \Phi_i^{(+)} \qquad \Sigma \to \infty, \tag{8.18}$$

$$\mathcal{S}_{fi} - \delta_{fi} = -\int_\Sigma \mathrm{d}\sigma_\mu \bar{\Phi}_f^{(-)} \; \gamma^\mu \; \Psi_i \qquad \Sigma \to \infty, \tag{8.19}$$

respectively in which the concept of the Dirac adjoint has been used. Σ is a closed surface in the four-space. By the virtue of divergence theorem these

results can be transformed into integrals over the volume enclosed by Σ as

$$\mathcal{S}_{fi} - \delta_{fi} = \int \mathrm{d}^4x \; \partial_\mu \left(\bar{\Psi}_f \; \gamma^\mu \; \Phi_i^{(+)} \right), \tag{8.20}$$

$$\mathcal{S}_{fi} - \delta_{fi} = - \int \mathrm{d}^4x \; \partial_\mu \left(\bar{\Phi}_f^{(-)} \; \gamma^\mu \; \Psi_i \right). \tag{8.21}$$

For further simplification let us consider an hydrogen-like atom placed in an external homogeneous field. The covariant form of the time-dependent Dirac-Coulomb equation describing the dynamics of an atomic electron is

$$\left[\mathrm{i}\gamma^\mu \partial_\mu - \mathcal{I} - \beta U(r) \right] \Phi(x) = -e\gamma^\mu A_\mu(x) \Phi(x) \tag{8.22}$$

for the fully interacting state Φ and

$$\left[\mathrm{i}\gamma^\mu \partial_\mu - \mathcal{I} - \beta U(r) \right] \Psi(x) = 0 \tag{8.23}$$

for the noninteracting state Ψ. From the well-known adjoint equations verified by the adjoint states $\bar{\Phi}$ and $\bar{\Psi}$, together with equations (8.22) and (8.23) we easily obtain

$$\partial_\mu \left(\bar{\Psi}_f \; \gamma^\mu \; \Phi_i^{(+)} \right) = -\mathrm{i} \bar{\Psi}_f V \Phi_i^{(+)}, \qquad \partial_\mu \left(\bar{\Phi}_f^{(-)} \; \gamma^\mu \; \Psi_i \right) = \mathrm{i} \bar{\Phi}_f^{(-)} V \Psi_i, \tag{8.24}$$

which then put equations (8.20) and (8.21) respectively into the final forms

$$\mathcal{S}_{fi} - \delta_{fi} = -\mathrm{i} \int \mathrm{d}^4x \; \bar{\Psi}_f(x) V(x) \Phi_i^{(+)}(x), \tag{8.25}$$

$$\mathcal{S}_{fi} - \delta_{fi} = -\mathrm{i} \int \mathrm{d}^4x \; \bar{\Phi}_f^{(-)}(x) V(x) \Psi_i(x), \tag{8.26}$$

where $V(x) = -e\gamma^\mu A_\mu(x)$ is the *minimal coupling* to the electromagnetic field. The basic practical problem in the application of this S-matrix is the presence of a state that contains the full effects of both the binding potential and the applied electromagnetic field described by the four-vector potential A_μ. Up to date, no exact closed-form solution is known for Φ which contains both potentials. In what follows this problem will be solved by using the well-known standard technique of Green's functions.

8.3.2 Green's function method

We argued that it is too difficult to tackle equation (8.22) directly. Instead of solving this equation directly, one usually solves the unit source problem (compared to the known Poisson's equation), the covariant inhomogeneous four dimensional equation

$$\left[\mathrm{i}\gamma^\mu \partial_\mu - \mathcal{I} - \beta U(r) \right] K(x, x') = \delta^{(4)}(x - x') \mathcal{I}, \tag{8.27}$$

where the function $K(x, x')$ represents the relativistic Green's function subjected to Feynman boundary conditions described in details in Ref. [21]. Once the solution to this simpler problem is known, the solution to the more general problem (8.22) can be written immediately because of the superposition principle.

A formal solution for Φ is given by the integral equation [27, 28]

$$\Phi(x) = \Psi(x) + \int \mathrm{d}^4x' K(x, x') V(x') \Phi(x'), \tag{8.28}$$

as can be easily verified by direct substitution into equation (8.22). So, even if we obtain an explicit form of $K(x, x')$, we cannot write the above exact solution in a closed form. However, if a perturbation expansion in powers of e can be justified, we can obtain an approximate solution to (8.22) accurate to any desired power of e by the familiar iteration method

$$\begin{aligned}\Phi(x) = \Psi(x) &+ \int \mathrm{d}^4x' K(x, x') V(x') \Psi(x') \\ &+ \int \mathrm{d}^4x' \mathrm{d}^4x'' K(x, x') V(x') K(x', x'') V(x'') \Psi(x') + \ldots\end{aligned} \tag{8.29}$$

Inserting this equation into equation (8.25), one has

$$\begin{aligned}\mathcal{S}_{fi} - \delta_{fi} = &-\mathrm{i} \int \mathrm{d}^4x \; \bar{\Psi}_f(x) V(x) \Psi_i(x) \\ &- \mathrm{i} \int \mathrm{d}^4x \mathrm{d}^4x' \; \bar{\Psi}_f(x) V(x) K(x, x') V(x') \Psi_i(x') + \ldots\end{aligned} \tag{8.30}$$

In a conventional perturbation expansion, the quantity considered to be the perturbation appears linearly in the first term, quadratically in the second term, and so on. Each term in the expansion gives rise to a Feynman diagram which can be interpreted as amplitude of a physical process. An obvious application of this result can be easily found in the study of multiphoton ionization / excitation processes at moderate laser intensities (see, for instance, Bebb and Gold [29], Lambropoulos [30], Faisal [31], Maquet [32], Maquet *et al.* [33] and references therein.) Within the framework of atom-radiation interactions under consideration, the second-order perturbative matrix element corresponds essentially to the two-photon transition amplitudes

$$\mathcal{S}_{fi} = -\mathrm{i} \int \mathrm{d}^4x \mathrm{d}^4x' \; \bar{\Psi}_f(x) V(x) K(x, x') V(x') \Psi_i(x'). \tag{8.31}$$

The next task is to obtain an explicit integral or spectral representation of $K(x, x')$. First, because of translational invariance (in both space and time)

it is clear that $K(x,x')$ is a function of $x-x'$ only. We solve (8.27) using the well-known relation [20, 23, 24, 34, 35]

$$K(x,x') = \frac{1}{2\pi \mathrm{i}} \int_{-\infty}^{+\infty} \mathrm{d}E \sum_n \frac{\Psi_n(\mathbf{r})\bar{\Psi}_n(\mathbf{r}')}{E_n - E(1+\mathrm{i}0)} \exp\left[-\mathrm{i}E(t-t')\right] \tag{8.32}$$

where i0 is a small positive number defining the usual Feynman contour in the complex E-plane.

Apart from the usual integration over the spatial coordinates, the evaluation of the transition amplitude in equation (8.31) also requires a *summation* over the *whole* spectrum of the hydrogen or ion. Obviously, this summation includes the sum over all discrete states as well as an integration over the continuum. In particular, the second part, *i.e.* the integration over the continuum, is rather difficult to carry out in practice since it implies the computation of *free-free* electronic transitions. An alternative to carrying out the summation over the spectrum explicitly in the transition amplitude is given by a change in the sequence of summation and integration. Then, the summation over the complete hydrogen spectrum can be replaced by the (retarded) Dirac-Coulomb Green function $G_E(\mathbf{r},\mathbf{r}')$ (with energy parameter E) which satisfies the well-known inhomogeneous differential equation given in Section (7.4) of **Chapter** 7.

$$K(x,x') = \frac{1}{2\pi \mathrm{i}} \int_{-\infty}^{+\infty} \mathrm{d}E \left[-\mathrm{i}G_E(\mathbf{r},\mathbf{r}')\beta\right] \exp\left[-\mathrm{i}E(t-t')\right]. \tag{8.33}$$

Using the above spectral expansion for $K(x,x')$, the two-photon transition amplitudes (8.31) can be rewritten in the following form

$$\mathcal{S}_{fi} = \frac{\mathrm{i}}{2\pi} \int \mathrm{d}E \mathrm{d}^4x \mathrm{d}^4x' \; \bar{\Psi}_f(x) V(x) G_E(\mathbf{r},\mathbf{r}') \exp\left[-\mathrm{i}E(t-t')\right] \beta V(x') \Psi_i(x'). \tag{8.34}$$

Based on the Dirac Hamiltonian with a hydrogen potential, H_D, a radial-angular representation of the relativistic Dirac-Coulomb Green function was given earlier in Section (7.4). In the evaluation of matrix elements, such a representation allows for analytic integration over all angles using the techniques of Racah algebra, while the radial integration often has to be carried out numerically. This equation will be used as the fundamental relation on which everything will be based for all further development or application in the text. We shall proceed to discuss processes that involve second-order matrix elements.

8.4 Two-photon absorption transition amplitudes

Inner-shell electrons have the largest binding energy amongst other electrons in atom. One may expect, therefore that the relativistic effects become im-

portant in the processes involving the inner-shell electrons in heavy atoms or ions. From the theoretical point of view, it clearly appears that the usual non-relativistic dipole treatment of the atom-field interaction is no longer valid for heavy atoms and multiply charged ions. More precisely, the question about a treatment taking full care of relativistic, retardation and multipole effects has to be addressed. This is the aim of this contribution.

In addition to photon scattering there are other electron two-photon relativistic processes for which an accurate analysis of photon-polarization effects is interesting and for which experimental investigations have begun during recent years. One is the measurement of the spectral and angular distributions of photons emitted during the two-photon decay of metastable states in H and He, and in hydrogen-and helium-like highly charged ions (see Ali *et al.* [36], Derevianko and Johnson [37], and references therein). Others are multi-photon processes in the strong electric field of VUV lasers, including two and multi-photon excitation and ionization of inner atomic shells which are now becoming more likely to be carried out in the future, including case studies on medium-Z and high-Z hydrogen-like ions (see, *e.g.,* Xenakis *et al.* [38] and Kornberg *et al.* [39]). With increasing charge (and intensity of the light), of course, relativistic effects will become important, and these have been investigated in the past for the two-photon excitation and decay (Goldman and Drake [40], Szymanowski *et al.* [41], Santos *et al.* [43]) as well as ionization (Koval *et al.* [44]) of hydrogen-like ions. Relativistic and screening effects in two-photon decay rates in atomic inner-shell have also been studied by Tong *et al.* [45]. In this contribution, we reconsider (in a refined treatment) the problem of the importance of the fully and quasi relativistic treatments (taking into account the relativistic, retardation and multipole effects) in two-photon excitation of hydrogen-like ions by linearly polarized photons.

Our primary concerns is the two-photon absorption by bound atomic electrons, but with simple modifications the results presented are also valid for other two-photon processes, such as for Raman and Rayleigh scattering. The method followed consists in writing the matrix elements in terms of generalized Green functions expanded over the first-order Dirac-Coulomb Sturmians [46] to derive *exact analytical formulae* for two-photon absorption as well as Raman and Rayleigh scattering. Previous approaches used Sturmian basis associated with the Gell-Mann-Feynman equation[41, 42]. On the other hand, a significant distinctive feature of our *fully relativistic treatment* based on the *tensor algebra* is that the expressions derived are quite general and could be applied to any multipole of the two photons. We pay particular attention to the specific case of several selected transitions from the ground state $\mid 1^2S\rangle$ towards the L and M shells ($\mid 2^2S\rangle$, $\mid 3^2S\rangle$, $\mid 3^2D_{3/2}\rangle$ and $\mid 3^2D_{5/2}\rangle$) in the *dipole-approximation* transition.

8.4.1 Fully relativistic formulation

Feynman's diagram representation

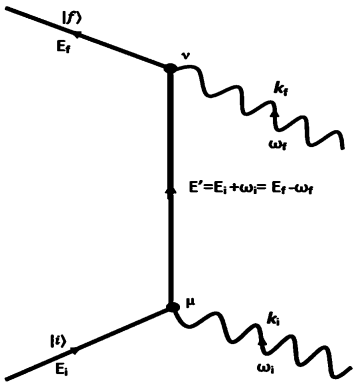

Figure 8.1: *Feynman diagram for the second-order amplitudes of the two photons absorption. The diagram describes processes by which an atomic transition from initial state $|i\rangle$ to final state $|f\rangle$ is accompanied by absorption of two photons* $\mathbf{k}_i$ *and* $\mathbf{k}_f$.

Method and calculations

In what follows, we choose to label all the parameters and quantum numbers associated to initial state with index 1, the final state with 2 and the intermediate or virtual states with the quoted primed sign. Equation (8.34) displays the two-photon transition amplitude in terms of the relativistic wave and Green functions of hydrogen-like ions. We now specialize this result to the description of absorption from the atoms and ions, and present explicit forms for the two-photon amplitudes in terms of reduced (radial) matrix elements, which then simplify by the virtue of Wigner-Eckart theorem. In lowest nonvanishing order in the fine-structure constant α the transition amplitude for such a process may be rewritten as

$$\mathcal{S}_{fi}^{(1)} = \mathrm{i}\frac{1}{2\pi}\int \mathrm{d}E'\mathrm{d}^4x_1\mathrm{d}^4x_2\bar{\Psi}_f(x_2)V^{(a)}(x_2)G_{E'}^{(1)}(\mathbf{r}_2,\mathbf{r}_1)\exp\left[-\mathrm{i}E'(t_2-t_1)\right] \times \beta V^{(a)}(x_1)\Psi_i(x_1). \tag{8.35}$$

For the sake of simplicity, here, we restrict our treatment to the case that both photons will have equal momentum or wavevectors $\mathbf{k}_1 = \mathbf{k}_2 = \mathbf{k}$. Of course, the case of equal photon momenta $\mathbf{k}$ corresponds to the most frequent

experimental set-up of the two-photon ionization/excitation of atoms and ions using, for instance, lasers or synchrotron radiation sources.

On substituting the unperturbed Dirac hydrogenic bound states $\Psi_p(x_l) = \Psi_p(\mathbf{r}_l)\exp(-\mathrm{i}E_p t_l)$ (with $p = i, l = 1$ and $p = f, l = 2$) and the four potential $A_\mu^{(a)}(x_l) = A_\mu^{(a)}(\mathbf{r}_l)\exp(-\mathrm{i}\omega t_l)$, and making use of the well-known Dirac delta function, the time integration guarantees energy conservation at the two vertices of Feynman's diagrams related to the process under consideration, namely that $E' = E_i + \omega = E_f - \omega$. Proceeding further by the energy integration, the amplitude $\mathcal{S}_{fi}^{(1)}$ then reduces to the remaining twofold three-dimensional integral over the spatial components.

$$\begin{aligned}\mathcal{S}_{fi}^{(1)} &= 2\mathrm{i}\pi\alpha\delta(2\omega + E_i - E_f) \\ &\quad\times \int \mathrm{d}^3\mathbf{r}_1\mathrm{d}^3\mathbf{r}_2\Psi_f^\dagger(\mathbf{r}_2)\tilde{V}^{(a)}(\mathbf{r}_2)G_{E'}^{(1)}(\mathbf{r}_2,\mathbf{r}_1)\tilde{V}^{(a)}(\mathbf{r}_1)\Psi_i(\mathbf{r}_1),\end{aligned} \tag{8.36}$$

where the transition operator $\tilde{V}^{(a)} = \boldsymbol{\alpha}\cdot\boldsymbol{A}^{(a)}$ with $\boldsymbol{\alpha}$ denoting the standard Dirac matrix and $\boldsymbol{A}^{(a)} = A_0(\omega)\hat{\boldsymbol{e}}\exp(\mathrm{i}\mathbf{k}\cdot\mathbf{r})$ is the vector potential for the absorption process, with $\hat{\boldsymbol{e}}$ the polarization vector, and $A_0(\omega) = \sqrt{2\pi/\omega}$ represents the moduli of the four potential normalized to one photon with energy ω in the normalization unit volume. The first-order retarded Dirac-Coulomb Green function $G_{E'}^{(1)}(\mathbf{r}_2,\mathbf{r}_1)$ with energy parameter E' is given by its radial-angular representation (7.97).

Multipole expansion of the photon wave

For further evaluation of this amplitude, we need first to write the multipole expansion of the transition operator $\tilde{V}^{(a)}$. For the sake of simplicity, we have taken the orientation of the quantization axis $\hat{\boldsymbol{e}}_z$ along the photon momenta direction $\mathbf{k}$. This situation is useful in calculating the influence of retardation. The exponential term of the interaction can be expanded in the manner [47]

$$\exp(\mathrm{i}\mathbf{k}\cdot\mathbf{r}) = \sum_{l_p=0}^{\infty}\mathrm{i}^{l_p}[l_p]j_{l_p}(kr)C_0^{l_p}(\hat{\boldsymbol{r}}), \tag{8.37}$$

where $[l_p] = 2l_p + 1$, and $C_0^{l_p}(\hat{\boldsymbol{r}})$ is given in equation (G.2); l_p is the angular momentum quantum number of the photon and $j_{l_p}(kr)$ the well-known spherical Bessel function [47]. We consider a *linearly polarized* electromagnetic field along the $\hat{\boldsymbol{e}}_x$ direction and introduce the spherical covariant basis $\{\hat{\boldsymbol{e}}_q, q = \pm1, 0\}$

$$\hat{\boldsymbol{e}}_x = \frac{1}{\sqrt{2}}(\hat{\boldsymbol{e}}_{-1} - \hat{\boldsymbol{e}}_1), \qquad \hat{\boldsymbol{e}}_0 = \hat{\boldsymbol{e}}_z, \qquad \hat{\boldsymbol{e}}^q\cdot\hat{\boldsymbol{e}}_p = \delta_{qp}. \tag{8.38}$$

Inserting equation (8.38) into equation (8.36), one has

$$\mathcal{S}_{fi}^{(1)} = -\mathrm{i}\pi\alpha\delta(2\omega + E_i - E_f) \times \left[\mathcal{S}_{fi}^{(1)}(1,1) - \mathcal{S}_{fi}^{(1)}(1,-1) - \mathcal{S}_{fi}^{(1)}(-1,1) + \mathcal{S}_{fi}^{(1)}(-1,-1)\right], \tag{8.39}$$

where

$$\mathcal{S}_{fi}^{(1)}(q',q) = -\int \mathrm{d}^3\mathbf{r}_1\mathrm{d}^3\mathbf{r}_2\Psi_f^\dagger(\mathbf{r}_2)\tilde{V}_{q'}^{(a)}(\mathbf{r}_2)G_{E'}^{(1)}(\mathbf{r}_2,\mathbf{r}_1)\tilde{V}_q^{(a)}(\mathbf{r}_1)\Psi_i(\mathbf{r}_1), \tag{8.40}$$

with $\tilde{V}_q^{(a)} = \boldsymbol{\alpha}\cdot\boldsymbol{A}_q^{(a)}$ and $\boldsymbol{A}_q^{(a)} = A_0(\omega)\hat{\boldsymbol{e}}_q\exp(\mathrm{i}\mathbf{k}\cdot\mathbf{r})$ the vector potential written in the covariant basis in closed-form needed as follows

$$\tilde{V}_q^{(a)} = \sum_{L=1}^{\infty}(-1)^{L+q}[L]^{1/2}\sum_{l_p=L-1}^{L+1}A_0(\omega)\mathrm{i}^{l_p}[l_p]j_{l_p}(\omega r)\begin{pmatrix} l_p & 1 & L \\ 0 & -q & q\end{pmatrix}\left(C_0^{l_p}\alpha_q^1\right)_q^L, \tag{8.41}$$

where we set

$$\left(C_0^{l_p}\alpha_q^1\right)_q^L = \begin{pmatrix} 0 & \left(C_0^{l_p}\sigma_q^1\right)_q^L \\ \left(C_0^{l_p}\sigma_q^1\right)_q^L & 0\end{pmatrix}, \qquad l_p = L\pm 1. \tag{8.42}$$

L=l_p, $l_p \pm 1$, stands for the total momentum of the photon. The case $l_p = L$ is excluded according to selection rules presented in Appendix G (see equation (G.23)). Employing the well-known Dirac hydrogenic wave functions and the Dirac-Coulomb Green functions of the first-order $G_E^{(1)}(\mathbf{r},\mathbf{r}')$ outlined in (7.97)-(7.102), equation (8.40) gives rise, after few operations, to the generalized expression of the transition amplitude

$$\mathcal{S}_{fi}^{(1)}(q',q) = \sum_{\kappa' m' n'}\tilde{R}_f^{(1)}(q')\tilde{T}_i^{(1)}(q), \tag{8.43}$$

where

$$\tilde{T}_i^{(1)}(q) = \sum_{L=1}^{\infty}(-1)^{L+q}[L]^{1/2}\sum_{l_{1p}=L\pm1}A_0(\omega)\mathrm{i}^{l_{1p}}[l_{1p}]\begin{pmatrix} l_{1p} & 1 & L \\ 0 & -q & q\end{pmatrix} \times \left[\tilde{\theta}_{n'}\tilde{K}_1(l_{1p})\tilde{I}_1^q(l_{1p}) - \tilde{\alpha}_{n'}\tilde{K}_2(l_{1p})\tilde{I}_2^q(l_{1p})\right], \tag{8.44}$$

$$\tilde{R}_f^{(1)}(q') = \sum_{L'=1}^{\infty}(-1)^{L'+q'}[L']^{1/2}\sum_{l_{2p}=L'\pm1}A_0(\omega)\mathrm{i}^{l_{2p}}[l_{2p}]\begin{pmatrix} l_{2p} & 1 & L' \\ 0 & -q' & q'\end{pmatrix} \times \left[\tilde{K}_3(l_{2p})\tilde{I}_3^{q'}(l_{2p}) - \tilde{K}_4(l_{2p})\tilde{I}_4^{q'}(l_{2p})\right], \tag{8.45}$$

the angular and radial integrals are respectively given by

$$\tilde{I}_1^q(l_{1p}) = \int \mathrm{d}\hat{\boldsymbol{r}}\Omega^\dagger_{\kappa'm'}(\hat{\boldsymbol{r}})(C_0^{l_{1p}}\sigma_q^1)^L_q\Omega_{-\kappa_1 m_1}(\hat{\boldsymbol{r}}), \tag{8.46}$$

$$\tilde{I}_2^q(l_{1p}) = \int \mathrm{d}\hat{\boldsymbol{r}}\Omega^\dagger_{-\kappa'm'}(\hat{\boldsymbol{r}})(C_0^{l_{1p}}\sigma_q^1)^L_q\Omega_{\kappa_1 m_1}(\hat{\boldsymbol{r}}), \tag{8.47}$$

$$\tilde{I}_3^{q'}(l_{2p}) = \int \mathrm{d}\hat{\boldsymbol{r}}\Omega^\dagger_{\kappa_2 m_2}(\hat{\boldsymbol{r}})(C_0^{l_{2p}}\sigma_{q'}^1)^{L'}_{q'}\Omega_{-\kappa' m'}(\hat{\boldsymbol{r}}), \tag{8.48}$$

$$\tilde{I}_4^{q'}(l_{2p}) = \int \mathrm{d}\hat{\boldsymbol{r}}\Omega^\dagger_{-\kappa_2 m_2}(\hat{\boldsymbol{r}})(C_0^{l_{2p}}\sigma_{q'}^1)^{L'}_{q'}\Omega_{\kappa' m'}(\hat{\boldsymbol{r}}), \tag{8.49}$$

$$\tilde{K}_1(l_{1p}) = \int_0^\infty \mathrm{d}r\, S_{n'\kappa'}(\varepsilon', 2\lambda' r)\; j_{l_{1p}}(\omega r) Q_{n_1\kappa_1}(2\lambda_1 r), \tag{8.50}$$

$$\tilde{K}_2(l_{1p}) = \int_0^\infty \mathrm{d}r\, T_{n'\kappa'}(\varepsilon', 2\lambda' r)\; j_{l_{1p}}(\omega r) P_{n_1\kappa_1}(2\lambda_1 r), \tag{8.51}$$

$$\tilde{K}_3(l_{2p}) = \int_0^\infty \mathrm{d}r\, T_{n'\kappa'}(\varepsilon', 2\lambda' r)\; j_{l_{2p}}(\omega r) P_{n_2\kappa_2}(2\lambda_2 r), \tag{8.52}$$

$$\tilde{K}_4(l_{2p}) = \int_0^\infty \mathrm{d}r\, S_{n'\kappa'}(\varepsilon', 2\lambda' r)\; j_{l_{2p}}(\omega r) Q_{n_2\kappa_2}(2\lambda_2 r). \tag{8.53}$$

The angular and radial integrals given above are calculated explicitly in the Appendices G and H, respectively. Upon utilizing the explicit expressions of angular integrals obtained from equation (G.6) in Appendix G, we get standard formulae for the transition amplitude $\mathcal{S}_{fi}^{(1)}(q', q)$ in a suitable notation for our needs

$$\begin{aligned}
\tilde{T}_i^{(1)}(q) = &\sum_{L=1}^{\infty} \frac{\mathrm{i}^{L-1} A_0(\omega)}{\sqrt{2L(L+1)}} \\
&\times (-1)^{m'+1/2}[j_1, j']^{1/2} \begin{pmatrix} j' & L & j_1 \\ 1/2 & 0 & -1/2 \end{pmatrix} \begin{pmatrix} j' & L & j_1 \\ -m' & q & m_1 \end{pmatrix} \\
&\times \Big[(L+1) \Big\{ \tilde{\theta}_{n'}(\kappa' - \kappa_1 - L)\tilde{K}_1(L-1) + \tilde{\alpha}_{n'}(\kappa' - \kappa_1 + L)\tilde{K}_2(L-1) \Big\} \\
&- L \Big\{ \tilde{\theta}_{n'}(\kappa' - \kappa_1 + L + 1)\tilde{K}_1(L+1) + \tilde{\alpha}_{n'}(\kappa' - \kappa_1 - L - 1)\tilde{K}_2(L+1) \Big\} \Big],
\end{aligned} \tag{8.54}$$

$$\tilde{R}_f^{(1)}(q') = \sum_{L'=1}^{\infty} \frac{\mathrm{i}^{L'-1} A_0(\omega)}{\sqrt{2L'(L'+1)}}$$
$$\times (-1)^{m_2+1/2}[j', j_2]^{1/2} \begin{pmatrix} j_2 & L' & j' \\ 1/2 & 0 & -1/2 \end{pmatrix} \begin{pmatrix} j_2 & L' & j' \\ -m_2 & q' & m' \end{pmatrix}$$
$$\times \Big[(L'+1) \Big\{ (\kappa_2 - \kappa' - L') \tilde{K}_3(L'-1) + (\kappa_2 - \kappa' + L') \tilde{K}_4(L'-1) \Big\}$$
$$-L' \Big\{ (\kappa_2 - \kappa' + L' + 1) \tilde{K}_3(L'+1) + (\kappa_2 - \kappa' - L' - 1) \tilde{K}_4(L'+1) \Big\} \Big] . \tag{8.55}$$

The transition amplitude $\mathcal{S}_{fi}^{(1)}(q', q)$, refers to two circularly polarized photons for all multipolarities.

Electric dipole approximation

The transition amplitude (8.39) describes the full interaction between the electron and photon fields. With the explicit summation over the multipoles of the photon field or the transition operator (8.41), it includes the so-called *retardation effects* contributions. In practice, however, the contributions from the higher multipoles decrease very rapidly with L (this is no longer valid if ω and Z are in the same order of magnitude) and may therefore be neglected; in fact, the computation of these contributions also become rather tedious because of difficulties with a stable procedure for the above one-dimensional radial integrals. In many cases, therefore, it seems justified to restrict the summation in (8.43) to just the (dominant) *electric dipole* term with $L = 1$ and $l_p = L \pm 1$. *The dipole approximation considered here differs from the well-known long-wavelength approximation due to the fact that the Bessel's functions are into the radial integrals and not the first terms of their expansion series.* For the two-photon excitation, this condition is well satisfied. For the general form (8.43) of the excitation amplitude, the electric dipole approximation is obtained by taking $L = L' = 1$ and $l_{1p}, l_{2p} = 0, 2$ which - owing to the dipole selection rules -then also restricts the summation over κ', m'. Apart from the electric-dipole field, of course, this approximation neglects the contribution from all higher multipoles. For K-shell excitation with (completely) *circularly polarized* light, for instance, the final-state electron can only escape to the M-shell, *i.e.* in the $|\, 3^2D_{3/2}\rangle$ and $|\, 3^2D_{5/2}\rangle$) states while for the *linearly polarized* light, the electron escapes to the L and M -shells, *i.e.* in the final states $|\, 2^2S\rangle$, $|\, 3^2S\rangle$, $|\, 3^2D_{3/2}\rangle$ and $|\, 3^2D_{5/2}\rangle$. And, as seen from equation (8.39), the dipole transition amplitude $\mathcal{S}_{fi}^{(1)}$ is then indeed defined by substituting $\mathcal{S}_{fi}^{(1)}(q', q)$ into

equation (8.39). Equations (8.54) and (8.55) then reduce to

$$\tilde{T}_i^{(1)}(q) = \frac{A_0(\omega)}{2}(-1)^{m'+1/2}[j_1, j']^{1/2} \begin{pmatrix} j' & 1 & j_1 \\ 1/2 & 0 & -1/2 \end{pmatrix} \begin{pmatrix} j' & 1 & j_1 \\ -m' & q & m_1 \end{pmatrix} \times \Big[2 \Big\{ \tilde{\theta}_{n'}(\kappa' - \kappa_1 - 1)\tilde{K}_1(0) + \tilde{\alpha}_{n'}(\kappa' - \kappa_1 + 1)\tilde{K}_2(0) \Big\} - \Big\{ \tilde{\theta}_{n'}(\kappa' - \kappa_1 + 2)\tilde{K}_1(2) + \tilde{\alpha}_{n'}(\kappa' - \kappa_1 - 2)\tilde{K}_2(2) \Big\} \Big], \tag{8.56}$$

$$\tilde{R}_f^{(1)}(q') = \frac{A_0(\omega)}{2}(-1)^{m_2+1/2}[j', j_2]^{1/2} \begin{pmatrix} j_2 & 1 & j' \\ 1/2 & 0 & -1/2 \end{pmatrix} \begin{pmatrix} j_2 & 1 & j' \\ -m_2 & q' & m' \end{pmatrix} \times \Big[2 \Big\{ (\kappa_2 - \kappa' - 1)\tilde{K}_3(0) + (\kappa_2 - \kappa' + 1)\tilde{K}_4(0) \Big\} - \Big\{ (\kappa_2 - \kappa' + 2)\tilde{K}_3(2) + (\kappa_2 - \kappa' - 2)\tilde{K}_4(2) \Big\} \Big]. \tag{8.57}$$

8.4.2 Quasirelativistic formulation

Details

We determine here the two-photon transition amplitudes related to the same process using the quasirelativistic Dirac-Coulomb functions and the expansion of the Green's function over the Sturmian basis set of the second-order outlined in **Chapter** 7, derived respectively in equations (7.76)-(7.77) and (7.111)-(7.114). We follow up the method described previously. The matrix element of the second-order reads

$$\mathcal{S}_{fi}^{(2)} = -\frac{\mathrm{i}}{2\pi} \int \mathrm{d}E' \mathrm{d}^4x_1 \mathrm{d}^4x_2 \bar{\Phi}_f(x_2) V^{(a)}(x_2) G_{E'}^{(1)}(\mathbf{r}_2, \mathbf{r}_1) \exp\left[-\mathrm{i}E'(t_2 - t_1)\right] \times V^{(a)}(x_1)\Phi_i(x_1). \tag{8.58}$$

It is easy to show that

$$\mathcal{S}_{fi}^{(2)} = -\mathrm{i}\pi\alpha\delta(2\omega + E_i - E_f) \sum_{q'q=\pm 1} q'q \; \mathcal{S}_{fi}^{(2)}(q', q), \tag{8.59}$$

where

$$\mathcal{S}_{fi}^{(2)}(q', q) = \int \mathrm{d}^3\mathbf{r}_1 \mathrm{d}^3\mathbf{r}_2 \Phi_f^\dagger(\mathbf{r}_2) \tilde{V}_{q'}^{(a)}(\mathbf{r}_2) G_{E'}^{(1)}(\mathbf{r}_2, \mathbf{r}_1) \beta \tilde{V}_q^{(a)}(\mathbf{r}_1) \Phi_i(\mathbf{r}_1). \tag{8.60}$$

In complete analogy with the procedure described previously, the generalized formula for the transition amplitude is found to be

$$\mathcal{S}_{fi}^{(2)}(q', q) = \sum_{j'l'm'n'} R_f^{(2)}(q') T_i^{(2)}(q), \tag{8.61}$$

where after some considerable algebra one has

$$T_i^{(2)}(q) = \sum_{L=1}^{\infty} \frac{\mathrm{i}^{L-1} A_0(\omega)}{\sqrt{2L(L+1)}} \times (-1)^{m'+1/2} [j_1, j']^{1/2} \begin{pmatrix} j' & L & j_1 \\ 1/2 & 0 & -1/2 \end{pmatrix} \begin{pmatrix} j' & L & j_1 \\ -m' & q & m_1 \end{pmatrix} \times \Big[(L+1) \Big\{ (\tilde{\beta}_1 + \tilde{\beta}')(\kappa' - \kappa_1) - L(\tilde{\beta}_1 - \tilde{\beta}') \Big\} K_1(L-1) - L \Big\{ (\tilde{\beta}_1 + \tilde{\beta}')(\kappa' - \kappa_1) + (L+1)(\tilde{\beta}_1 - \tilde{\beta}') \Big\} K_1(L+1) \Big], \quad (8.62)$$

$$R_f^{(2)}(q') = \sum_{L'=1}^{\infty} -\frac{\mathrm{i}^{L'-1} A_0(\omega)}{\sqrt{2L'(L'+1)}} \times (-1)^{m_2+1/2} [j', j_2]^{1/2} \begin{pmatrix} j_2 & L' & j' \\ 1/2 & 0 & -1/2 \end{pmatrix} \begin{pmatrix} j_2 & L' & j' \\ -m_2 & q' & m' \end{pmatrix} \times \big[(L'+1) \big\{ (\kappa_2 - \kappa' - L') K_3(L'-1) + (\kappa_2 - \kappa' + L') K_4(L'-1) \big\} - L' \big\{ (\kappa_2 - \kappa' + L' + 1) K_3(L'+1) + (\kappa_2 - \kappa' - L' - 1) K_4(L'+1) \big\} \big]. \quad (8.63)$$

In the dipole approximation, i.e. $L = L' = 1$, these formulae become

$$T_i^{(2)}(q) = \frac{A_0(\omega)}{2} (-1)^{m'+1/2} [j_1, j']^{1/2} \begin{pmatrix} j' & 1 & j_1 \\ 1/2 & 0 & -1/2 \end{pmatrix} \begin{pmatrix} j' & 1 & j_1 \\ -m' & q & m_1 \end{pmatrix} \times \Big[2 \Big\{ (\tilde{\beta}_1 + \tilde{\beta}')(\kappa' - \kappa_1) - (\tilde{\beta}_1 - \tilde{\beta}') \Big\} K_1(0) - \Big\{ (\tilde{\beta}_1 + \tilde{\beta}')(\kappa' - \kappa_1) + 2(\tilde{\beta}_1 - \tilde{\beta}') \Big\} K_1(2) \Big], \quad (8.64)$$

$$R_f^{(2)}(q') = -\frac{A_0(\omega)}{2} (-1)^{m_2+1/2} [j', j_2]^{1/2} \begin{pmatrix} j_2 & 1 & j' \\ 1/2 & 0 & -1/2 \end{pmatrix} \begin{pmatrix} j_2 & 1 & j' \\ -m_2 & q' & m' \end{pmatrix} \times \big[2 \big\{ (\kappa_2 - \kappa' - 1) K_3(0) + (\kappa_2 - \kappa' + 1) K_4(0) \big\} - \big\{ (\kappa_2 - \kappa' + 2) K_3(2) + (\kappa_2 - \kappa' - 2) K_4(2) \big\} \big]. \quad (8.65)$$

The new radial integrals involved in the above equations are given by

$$K_1(l_{1p}) = K_2(l_{1p}) = \int_0^{\infty} \mathrm{d}r \; r^2 S_{n'}(2\lambda' r) \; j_{l_{1p}}(\omega r) \Phi_{n_1 \epsilon_1}(r), \quad (8.66)$$

$$K_3(l_{2p}) = \int_0^{\infty} \mathrm{d}r \; r^2 \Phi_{n_2 \epsilon_2}(r) \; j_{l_{2p}}(\omega r) g_d(r), \quad (8.67)$$

$$K_4(l_{2p}) = \tilde{\beta}_2 \int_0^{\infty} \mathrm{d}r \; r^2 \Phi_{n_2 \epsilon_2}(r) \; j_{l_{2p}}(\omega r) g_u(r), \quad (8.68)$$

where the upper (g_u) and lower (g_d) radial components of the virtual bispinor are given in [41]. These radial integrals are conveniently derived in Appendix H. Having determined $\mathcal{S}_{fi}^{(2)}(q', q)$, we deduce the relevant matrix element $\mathcal{S}_{fi}^{(2)}$ in the form needed.

8.5 Other bound-bound scattering processes

When light encounters molecules in the air, the predominant mode of scattering is elastic scattering, called Rayleigh scattering since the energies (frequencies) and wavelengths of the scattered photons are not substantially changed. This effect was first modeled successfully by Lord Rayleigh, from whom it gets its name. This scattering is responsible for the blue color of the Earth's sky; it increases with the fourth power of the frequency and is more effective at short wavelengths. It is also possible for the incident photons to interact with the molecules in such a way that energy is either gained (anti-Stokes, see **Figure** 8.4) or lost (Stokes, see **Figure** 8.5) so that the scattered photons are shifted in frequency. Such inelastic scattering is called Raman scattering. In 1922, the Indian physicist C. V. Raman published his work on the "Molecular Diffraction of Light," the first of a series of investigations with his collaborators which ultimately led to his discovery (on 28 February 1928) of the radiation effect which bears his name. The Raman effect was first reported by C. V. Raman and K. S. Krishnan, and independently by Grigory Landsberg and Leonid Mandelstam, in 1928. Raman received the Nobel Prize in 1930 for his work on the scattering of light. The American Chemical Society and the Indian Association for the Cultivation of Science designated the discovery of the Raman Effect as an International Historic Chemical Landmark in Calcutta, India, on December 15, 1998 in recognition of its significance as a tool for analyzing the composition of liquids, gases, and solids.
In quantum mechanics, the RRS processes are described by a second-order time-dependent perturbation theory, where the target atom or molecule suffers level transition twice, one associated with the annihilation of the incident photon and the other associated with the creation of the scattered photon. Due to the development of high intensity X-ray and γ-ray sources, Rayleigh scattering both above and below the photoeffect threshold energy has become a standard tool for studying the structure and properties of various materials involving intermediate and high atomic numbers. When considering the interactions of the electromagnetic field with the inner shell electrons of high Z atoms, the incident photons energies are in X- and γ-ray domains, so that accurate analytical formulae are needed for this range of energies. The Rayleigh scattering is also of great interest for the investigation of scattering processes from the atomic ground state [49], nanometric powders [50], amorphous materials and

dilute media [51], flames, ionized gases and plasma [52, 53], optical properties of fibres [54] and many other fields. Also, various theoretical approaches continue to be proposed in the literature: Holstein [55] analyzes the structure of the hydrogen atom and the nonrelativistic limit for Compton and Rayleigh scattering, both with the effective interactions approach and the nonrelativistic quantum electrodynamics. Costescu *et al* [56] derive the right analytical expressions of the nonrelativistic K-shell Rayleigh scattering amplitudes and cross-sections by using the Coulomb Green's function method.

Feynman's diagrams representations

There are two Feynman diagrams (cf. **Figures** 8.2 and 8.3) describing the second-order amplitudes of the Rayleigh and Raman scattering processes.

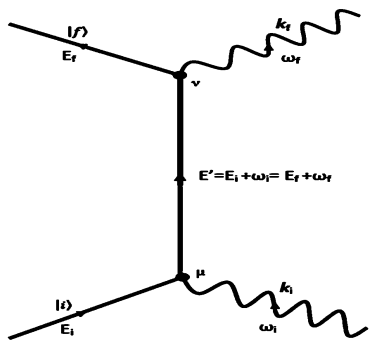

Figure 8.2: *Feynman diagram for the second-order amplitudes of the two photons scattering. The diagram describes processes by which an atomic transition from initial state $|i\rangle$ to final state $|f\rangle$ is accompanied by absorption of one photon $\mathbf{k}_i$ and by emission of one photon $\mathbf{k}_f$.*

8.5.1 Raman scattering

Explicit analytical formulae

In this subsection we present our analytical results [57] of calculations of the Raman and Rayleigh scattering amplitudes for bound-bound transitions in hydrogen-like ions based on the tensor formalism. To accomplish this aim, we also use the fully relativistic Dirac-Coulomb functions and the Sturmian expansions of the Dirac-Coulomb Green function. In terms of matrix elements,

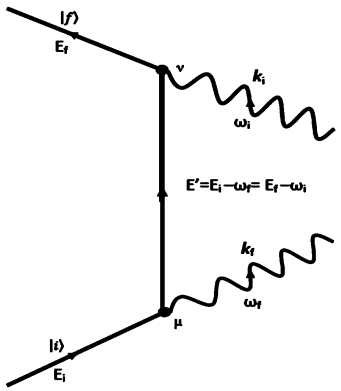

Figure 8.3: *Feynman diagram for the second-order amplitudes of the two photons scattering. The diagram describes processes by which an atomic transition from initial state $|i\rangle$ to final state $|f\rangle$ is accompanied by emission of one photon $\mathbf{k}_f$ and by absorption of one photon $\mathbf{k}_i$.*

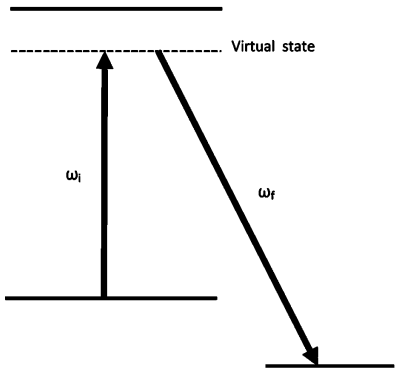

Figure 8.4: *Raman anti-Stokes scattering.*

and after integrating over the time, the Raman scattering amplitude is given as

$$S^{(1)}_{Ram} = S^{(1)}_{fi}(\mathbf{k}_f,\, \mathbf{k}_i) + A^{(1)}_{fi}(\mathbf{k}_i,\, \mathbf{k}_f), \tag{8.69}$$

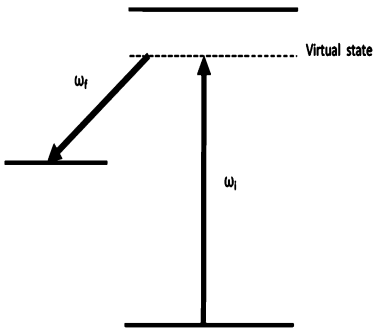

Figure 8.5: *Raman Stokes scattering.*

where

$$S_{fi}^{(1)}(\mathbf{k}_f,\,\mathbf{k}_i) = 2\mathrm{i}\pi\alpha\delta(\omega_i - \omega_f + E_i - E_f)\int \mathrm{d}^3\mathbf{r}_1\mathrm{d}^3\mathbf{r}_2\Psi_f^\dagger(\mathbf{r}_2)\tilde{V}^{(e)}(\mathbf{r}_2,\,\mathbf{k}_f) \times \tilde{G}_{E'}^{(1)}(\mathbf{r}_2,\mathbf{r}_1)\tilde{V}^{(a)}(\mathbf{r}_1,\,\mathbf{k}_i)\Psi_i(\mathbf{r}_1), \tag{8.70}$$

and

$$A_{fi}^{(1)}(\mathbf{k}_i,\,\mathbf{k}_f) = 2\mathrm{i}\pi\alpha\delta(\omega_i - \omega_f + E_i - E_f)\int \mathrm{d}^3\mathbf{r}_1\mathrm{d}^3\mathbf{r}_2\Psi_f^\dagger(\mathbf{r}_2)\tilde{V}^{(a)}(\mathbf{r}_2,\,\mathbf{k}_i) \times \tilde{G}_{E'}^{(1)}(\mathbf{r}_2,\mathbf{r}_1)\tilde{V}^{(e)}(\mathbf{r}_1,\,\mathbf{k}_f)\Psi_i(\mathbf{r}_1). \tag{8.71}$$

In equations (8.70) and (8.71) the transition operator is written in the more appropriate notation to display the incoming and outgoing photon.

$$\tilde{V}^{(a)}(\mathbf{r}_1,\,\mathbf{k}_i) = \boldsymbol{\alpha}\cdot\boldsymbol{A}^{(a)}(\mathbf{r}_1,\,\mathbf{k}_i), \qquad \boldsymbol{A}^{(a)}(\mathbf{r}_1,\,\mathbf{k}_i) = A_0(\omega_i)\hat{\boldsymbol{e}}\exp(\mathrm{i}\mathbf{k}_i\cdot\mathbf{r}_1), \tag{8.72}$$

$$\tilde{V}^{(e)}(\mathbf{r}_2,\,\mathbf{k}_f) = \boldsymbol{\alpha}\cdot\boldsymbol{A}^{(e)}(\mathbf{r}_2,\,\mathbf{k}_f), \qquad \boldsymbol{A}^{(e)}(\mathbf{r}_2,\,\mathbf{k}_f) = A_0(\omega_f)\hat{\boldsymbol{e}}\exp(-\mathrm{i}\mathbf{k}_f\cdot\mathbf{r}_2). \tag{8.73}$$

Dealing with the case of linearly polarized electromagnetic field along the $\hat{\boldsymbol{e}}_x$ direction, equations (8.70) and (8.71) simplify to the following expressions:

$$S_{fi}^{(1)}(\mathbf{k}_f,\,\mathbf{k}_i) = -\mathrm{i}\pi\alpha\delta(\omega_i-\omega_f+E_i-E_f) \times\left[\bar{S}_{fi}^{(1)}(1,1)-\bar{S}_{fi}^{(1)}(1,-1)-\bar{S}_{fi}^{(1)}(-1,1)+\bar{S}_{fi}^{(1)}(-1,-1)\right], \tag{8.74}$$

$$A_{fi}^{(1)}(\mathbf{k}_i,\,\mathbf{k}_f) = -\mathrm{i}\pi\alpha\delta(\omega_i-\omega_f+E_i-E_f) \times\left[A_{fi}^{(1)}(1,1)-A_{fi}^{(1)}(1,-1)-A_{fi}^{(1)}(-1,1)+A_{fi}^{(1)}(-1,-1)\right]. \tag{8.75}$$

Here,

$$\bar{S}_{fi}^{(1)}(q',q) = -\int \mathrm{d}^3\mathbf{r}_1\mathrm{d}^3\mathbf{r}_2\Psi_f^{\dagger}(\mathbf{r}_2)\tilde{V}_{q'}^{(e)}(\mathbf{r}_2,\,\mathbf{k}_f)\tilde{G}_{E'}^{(1)}(\mathbf{r}_2,\mathbf{r}_1)\tilde{V}_q^{(a)}(\mathbf{r}_1,\,\mathbf{k}_i)\Psi_i(\mathbf{r}_1), \tag{8.76}$$

$$A_{fi}^{(1)}(q',q) = -\int \mathrm{d}^3\mathbf{r}_1\mathrm{d}^3\mathbf{r}_2\Psi_f^{\dagger}(\mathbf{r}_2)\tilde{V}_{q'}^{(a)}(\mathbf{r}_2,\,\mathbf{k}_i)\tilde{G}_{E'}^{(1)}(\mathbf{r}_2,\mathbf{r}_1)\tilde{V}_q^{(e)}(\mathbf{r}_1,\,\mathbf{k}_f)\Psi_i(\mathbf{r}_1), \tag{8.77}$$

and $\tilde{V}_q^{(e)}$, $\tilde{V}_q^{(a)}$ take the similar forms in spherical covariant basis. Following the same line of calculations as in the preceding subsections, equations (8.76) and (8.77) may be reduced respectively in the standard way after simple manipulations to

$$\bar{S}_{fi}^{(1)}(q',q) = \sum_{\kappa',m',n'} \bar{R}_f^{(1)}(q')\bar{T}_i^{(1)}(q), \quad A_{fi}^{(1)}(q',q) = \sum_{\kappa',m',n'} \hat{R}_f^{(1)}(q')\hat{T}_i^{(1)}(q). \tag{8.78}$$

It may be easily verified that in equation (8.78) the expressions $\bar{T}_i^{(1)}(q)$, $\bar{R}_f^{(1)}(q')$, $\hat{T}_i^{(1)}(q)$, and $\hat{R}_f^{(1)}(q')$ are formally similar to the corresponding terms $\tilde{T}_i^{(1)}(q)$ and $\tilde{R}_f^{(1)}(q')$ given in equations (8.54) and (8.55) respectively. Thus, one may deduce the following expressions

$$\begin{aligned}\bar{T}_i^{(1)}(q) = &\sum_{L=1}^{\infty}\frac{\mathrm{i}^{L-1}A_0(\omega_i)}{\sqrt{2L(L+1)}} \\ &\times(-1)^{m'+1/2}[j_1,j']^{1/2}\begin{pmatrix} j' & L & j_1 \\ 1/2 & 0 & -1/2\end{pmatrix}\begin{pmatrix} j' & L & j_1 \\ -m' & q & m_1\end{pmatrix} \\ &\times\Big[(L+1)\left\{\tilde{\theta}_{n'}(\kappa'-\kappa_1-L)\bar{K}_1(L-1)+\tilde{\alpha}_{n'}(\kappa'-\kappa_1+L)\bar{K}_2(L-1)\right\} \\ &-L\left\{\tilde{\theta}_{n'}(\kappa'-\kappa_1+L+1)\bar{K}_1\,(L+1)+\tilde{\alpha}_{n'}(\kappa'-\kappa_1-L-1)\bar{K}_2(L+1)\right\}\Big],\end{aligned} \tag{8.79}$$

$$\bar{R}_f^{(1)}(q') = \sum_{L'=1}^{\infty} \frac{\mathrm{i}^{L'-1} A_0(\omega_f)}{\sqrt{2L'(L'+1)}}$$
$$\times (-1)^{m_2+1/2} [j', j_2]^{1/2} \begin{pmatrix} j_2 & L' & j' \\ 1/2 & 0 & -1/2 \end{pmatrix} \begin{pmatrix} j_2 & L' & j' \\ -m_2 & q' & m' \end{pmatrix}$$
$$\times \left[(L'+1) \left\{ (\kappa_2 - \kappa' - L') \bar{K}_3(L'-1) + (\kappa_2 - \kappa' + L') \bar{K}_4(L'-1) \right\} \right.$$
$$\left. -L' \left\{ (\kappa_2 - \kappa' + L' + 1) \bar{K}_3\,(L'+1) + (\kappa_2 - \kappa' - L' - 1) \bar{K}_4(L'+1) \right\} \right], \tag{8.80}$$

$$\hat{T}_i^{(1)}(q) = \sum_{L=1}^{\infty} \frac{\mathrm{i}^{L-1} A_0(\omega_f)}{\sqrt{2L(L+1)}}$$
$$\times (-1)^{m'+1/2} [j_1, j']^{1/2} \begin{pmatrix} j' & L & j_1 \\ 1/2 & 0 & -1/2 \end{pmatrix} \begin{pmatrix} j' & L & j_1 \\ -m' & q & m_1 \end{pmatrix}$$
$$\times \left[(L+1) \left\{ \tilde{\theta}_{n'} (\kappa' - \kappa_1 - L) \hat{K}_1(L-1) + \tilde{\alpha}_{n'} (\kappa' - \kappa_1 + L) \hat{K}_2(L-1) \right\} \right.$$
$$\left. -L \left\{ \tilde{\theta}_{n'} (\kappa' - \kappa_1 + L + 1) \hat{K}_1(L+1) + \tilde{\alpha}_{n'} (\kappa' - \kappa_1 - L - 1) \hat{K}_2(L+1) \right\} \right], \tag{8.81}$$

$$\hat{R}_f^{(1)}(q') = \sum_{L'=1}^{\infty} \frac{\mathrm{i}^{L'-1} A_0(\omega_i)}{\sqrt{2L'(L'+1)}}$$
$$\times (-1)^{m_2+1/2} [j', j_2]^{1/2} \begin{pmatrix} j_2 & L' & j' \\ 1/2 & 0 & -1/2 \end{pmatrix} \begin{pmatrix} j_2 & L' & j' \\ -m_2 & q' & m' \end{pmatrix}$$
$$\times \left[(L'+1) \left\{ (\kappa_2 - \kappa' - L') \hat{K}_3(L'-1) + (\kappa_2 - \kappa' + L') \hat{K}_4(L'-1) \right\} \right.$$
$$\left. -L' \left\{ (\kappa_2 - \kappa' + L' + 1) \hat{K}_3(L'+1) + (\kappa_2 - \kappa' - L' - 1) \hat{K}_4(L'+1) \right\} \right]. \tag{8.82}$$

We emphasize that the radial integrals appearing in the right-hand side of these equations are readily deduced from those of the preceding cases. For the sake of brevity, their explicit expressions are omitted here. Henceforth we choose to underline below appropriate indications for their formulae. $\bar{K}_1(l_{1p})$ and $\bar{K}_2(l_{1p})$ are inferred respectively from their corresponding expressions given in equations (8.50) and (8.51) where we replace ω by ω_i. Similarly $\bar{K}_3(l_{2p})$ and $\bar{K}_4(l_{2p})$ are inferred respectively from their equivalent terms in equations (8.52) and (8.53) where we substitute ω to ω_f. The analogous relations for $\hat{K}_1(l_{1p})$ and $\hat{K}_2(l_{1p})$ are obtained from $\bar{K}_1(l_{1p})$ and $\bar{K}_2(l_{1p})$ by replacing ω_i by ω_f respectively. Also $\hat{K}_3(l_{2p})$ and $\hat{K}_4(l_{2p})$ are obtained directly from $\bar{K}_3(l_{2p})$

and $\bar{K}_4(l_{2p})$ where we substitute ω_f by ω_i. It is interesting to investigate here the case of dipole approximation, i.e. $L = L' = 1$. Thus, the above expressions take the following simple forms

$$\begin{aligned}\bar{T}_i^{(1)}(q) = \frac{A_0(\omega_i)}{2}(-1)^{m'+1/2}[j_1, j']^{1/2} \begin{pmatrix} j' & 1 & j_1 \\ 1/2 & 0 & -1/2 \end{pmatrix} \begin{pmatrix} j' & 1 & j_1 \\ -m' & q & m_1 \end{pmatrix} \\ \times \Big[2\Big\{\tilde{\theta}_{n'}(\kappa' - \kappa_1 - 1)\bar{K}_1(0) + \tilde{\alpha}_{n'}(\kappa' - \kappa_1 + 1)\bar{K}_2(0)\Big\} \\ - \Big\{\tilde{\theta}_{n'}(\kappa' - \kappa_1 + 2)\bar{K}_1(2) + \tilde{\alpha}_{n'}(\kappa' - \kappa_1 - 2)\bar{K}_2(2)\Big\}\Big], \end{aligned} \tag{8.83}$$

$$\begin{aligned}\bar{R}_f^{(1)}(q') = \frac{A_0(\omega_f)}{2}(-1)^{m_2+1/2}[j', j_2]^{1/2} \begin{pmatrix} j_2 & 1 & j' \\ 1/2 & 0 & -1/2 \end{pmatrix} \begin{pmatrix} j_2 & 1 & j' \\ -m_2 & q' & m' \end{pmatrix} \\ \times \big[2\big\{(\kappa_2 - \kappa' - 1)\bar{K}_3(0) + (\kappa_2 - \kappa' + 1)\bar{K}_4(0)\big\} \\ - \big\{(\kappa_2 - \kappa' + 2)\bar{K}_3(2) + (\kappa_2 - \kappa' - 2)\bar{K}_4(2)\big\}\big], \end{aligned} \tag{8.84}$$

$$\begin{aligned}\hat{T}_i^{(1)}(q) = \frac{A_0(\omega_f)}{2}(-1)^{m'+1/2}[j_1, j']^{1/2} \begin{pmatrix} j' & 1 & j_1 \\ 1/2 & 0 & -1/2 \end{pmatrix} \begin{pmatrix} j' & 1 & j_1 \\ -m' & q & m_1 \end{pmatrix} \\ \times \Big[2\Big\{\tilde{\theta}_{n'}(\kappa' - \kappa_1 - 1)\hat{K}_1(0) + \tilde{\alpha}_{n'}(\kappa' - \kappa_1 + 1)\hat{K}_2(0)\Big\} \\ - \Big\{\tilde{\theta}_{n'}(\kappa' - \kappa_1 + 2)\hat{K}_1(2) + \tilde{\alpha}_{n'}(\kappa' - \kappa_1 - 2)\hat{K}_2(2)\Big\}\Big], \end{aligned} \tag{8.85}$$

$$\begin{aligned}\hat{R}_f^{(1)}(q') = \frac{A_0(\omega_i)}{2}(-1)^{m_2+1/2}[j', j_2]^{1/2} \begin{pmatrix} j_2 & 1 & j' \\ 1/2 & 0 & -1/2 \end{pmatrix} \begin{pmatrix} j_2 & 1 & j' \\ -m_2 & q' & m' \end{pmatrix} \\ \times \Big[2\Big\{(\kappa_2 - \kappa' - 1)\hat{K}_3(0) + (\kappa_2 - \kappa' + 1)\hat{K}_4(0)\Big\} \\ - \Big\{(\kappa_2 - \kappa' + 2)\hat{K}_3(2) + (\kappa_2 - \kappa' - 2)\hat{K}_4(2)\Big\}\Big]. \end{aligned} \tag{8.86}$$

On substituting these equations into equation (8.69) we derive the Raman scattering amplitude $S_{Ram}^{(1)}$ in a closed analytical expression suitable to our purpose.

8.5.2 Rayleigh scattering

Explicit analytical formulae

Besides the Raman scattering process already discussed, we now proceed to consider the Rayleigh scattering process. It is obvious that the matrix elements

in this case are easily found to be

$$S^{(1)}_{Ray} = \tilde{S}^{(1)}_{fi}(\mathbf{k}_f, \mathbf{k}_i) + \tilde{A}^{(1)}_{fi}(\mathbf{k}_i, \mathbf{k}_f), \tag{8.87}$$

where the amplitudes $\tilde{S}^{(1)}_{fi}(\mathbf{k}_f, \mathbf{k}_i)$ and $\tilde{A}^{(1)}_{fi}(\mathbf{k}_i, \mathbf{k}_f)$ are deduced from $S^{(1)}_{fi}(\mathbf{k}_f, \mathbf{k}_i)$ and $A^{(1)}_{fi}(\mathbf{k}_i, \mathbf{k}_f)$ by setting $\omega_i = \omega_f = \omega$ in equations (8.70) and (8.71). On transforming equations (8.69)-(8.86) we arrive at the desired closed expression for the Rayleigh scattering amplitude.

8.6 Numerical results and discussion

Case of transition $|1\ ^2S\rangle \rightarrow |2\ ^2S\rangle$

Table 8.1: *Quantum numbers for the allowed dipole excitation paths for the transition* $|\ 1^2S\rangle \rightarrow |\ 2^2S\rangle$. *Initial state is labelled by index 1, virtual states by superscript prime and final states by index 2.*

$\|n_1, j_1, l_1, m_1; \epsilon_1, \kappa_1\rangle$	$\|n', j', l', m'; \epsilon', \kappa'\rangle$	$\|n_2, j_2, l_2, m_2; \epsilon_2, \kappa_2\rangle$	q	q'
$\|0, 1/2, 0, 1/2; -1, -1\rangle$	$\|n', 3/2, 1, 3/2; -1, -2\rangle$	$\|1, 1/2, 0, 1/2; -1, -1\rangle$	1	-1
$\|0, 1/2, 0, 1/2; -1, -1\rangle$	$\|n', 3/2, 1, -1/2; -1, -2\rangle$	$\|1, 1/2, 0, 1/2; -1, -1\rangle$	-1	1
$\|0, 1/2, 0, 1/2; -1, -1\rangle$	$\|n', 1/2, 1, -1/2; 1, 1\rangle$	$\|1, 1/2, 0, 1/2; -1, -1\rangle$	-1	1

In this part, an application of the Sturmian expansion of the Dirac-Coulomb Green functions is illustrated by computing the two-photon probability amplitudes for the selected transitions from the ground state $|\ 1^2S\rangle$ towards $|\ 2^2S\rangle$, $|\ 3^2S\rangle$, $|\ 3^2D_{3/2}\rangle$ and $|\ 3^2D_{5/2}\rangle$ states. For this purpose, we use both the complete set of relativistic Sturmian functions of the first-order and the second-order Sturmian functions associated with the Dirac and Gell-Mann-Feynman equations respectively. We consider a hydrogen-like ion with an infinitely heavy point-like and spinless nucleus exposed to an electromagnetic field polarized along the x-axis. We assume the atom in its ground state. The eigenvalues and eigenfunctions for the atomic states involved in the process are clearly given in Appendix H.

Table 8.2: *Modulus of the matrix elements multiplied by* 2π *for the transition* $|\ 1^2S\rangle \rightarrow |\ 2^2S\rangle$ *in relativistic atomic units for several selected hydrogen-like ions. The superscript* (2) *refers to the quasirelativistic approach (QR) and* (1) *to the fully relativistic treatment where a is related to the Sturmian basis sets with the radial quantum number* $-100 \leq n \leq 100$ *(FR1),* b *to the case* $0 \leq n \leq 100$ *(FR2) and c for* $-100 \leq n \leq -1$ *(CFR). The number in brackets following the entries is the power of* 10 *by which the entry is to be multiplied.*

Z	$2\pi \mid S_{fi}^{(2)} \mid$	$2\pi \mid S_{fi}^{(1)a} \mid$	$2\pi \mid S_{fi}^{(1)b} \mid$	$2\pi \mid S_{fi}^{(1)c} \mid$
1	1.7471002126(+4)	5.0053421923(+4)	3.9611937538(+4)	1.0441484385(+4)
2	4.3688327543(+3)	12.5121781485(+3)	9.9016404168(+3)	2.6104526035(+3)
3	1.9425052184(+3)	5.5600959111(+3)	4.3997334925(+3)	1.1603624186(+3)
4	1.0932907294(+3)	3.1268670609(+3)	2.4740660099(+3)	0.6528010510(+3)
5	0.7002259009(+3)	2.0006296335(+3)	1.5827569960(+3)	0.4178726376(+3)
7	0.3579658274(+3)	1.0199601018(+3)	0.8066510058(+3)	0.2133090960(+3)
10	1.7614125132(+2)	4.9897892201(+2)	3.9434426724(+2)	1.0463465477(+2)
15	0.7909171749(+2)	2.2089402531(+2)	1.7426658065(+2)	0.4662744466(+2)
20	0.4512818578(+2)	1.2356260784(+2)	0.9723790125(+2)	0.2632470659(+2)
25	2.9412175765(+1)	7.8510177299(+1)	6.1582983322(+1)	1.6927193977(+1)
30	2.0879707459(+1)	5.4035220749(+1)	4.2213122615(+1)	1.1822098133(+1)
35	1.5739863829(+1)	3.9275441348(+1)	3.0531859107(+1)	0.8743582241(+1)
40	1.2409216471(+1)	2.9693512702(+1)	2.2948342635(+1)	0.6745170067(+1)
45	1.0131409946(+1)	2.3121800483(+1)	1.7747109397(+1)	0.5374691086(+1)
50	0.8508188828(+1)	1.8418607455(+1)	1.4024629076(+1)	0.4393978379(+1)
55	0.7313734828(+1)	1.4936170613(+1)	1.1268276120(+1)	0.3667894493(+1)
60	0.6412347302(+1)	1.2284754231(+1)	0.9169632732(+1)	0.3115121499(+1)
65	0.5718603612(+1)	1.0218443425(+1)	0.7534106400(+1)	0.2684337025(+1)
70	0.5176686893(+1)	0.8575834457(+1)	0.6233993277(+1)	0.2341841179(+1)
75	0.4749039306(+1)	0.7247409712(+1)	0.5182660411(+1)	0.2064749302(+1)
80	0.4409848833(+1)	0.6156706333(+1)	0.4319645028(+1)	0.1837061305(+1)
85	0.4141187561(+1)	0.5248991548(+1)	0.3601695729(+1)	0.1647295819(+1)
90	0.3930692989(+1)	0.4484205170(+1)	0.2997192391(+1)	0.1487012778(+1)
95	0.3770223148(+1)	0.3832418737(+1)	0.2482560433(+1)	0.1349858305(+1)
100	0.3655225562(+1)	0.3270824039(+1)	0.2039899972(+1)	0.1230924067(+1)

Case of transition $|1\ ^2S\rangle \rightarrow |3\ ^2S\rangle$

For the sake of assessing the effectiveness of the quasirelativistic (QR) approach, we use in this Section the corresponding formulae derived above to compute numerical values of the two-photon absorption probability amplitudes for the process from the ground state towards states in the L and M shells

Table 8.3: *Quantum numbers for the allowed dipole excitation paths for the transition* $|\,1^2S\rangle \rightarrow |\,3^2S\rangle$. *Initial state is labelled by index 1, virtual states by superscript prime and final states by index 2.*

$\|n_1, j_1, l_1, m_1; \epsilon_1, \kappa_1\rangle$	$\|n', j', l', m'; \epsilon', \kappa'\rangle$	$\|n_2, j_2, l_2, m_2; \epsilon_2, \kappa_2\rangle$	q	q'
$\|0, 1/2, 0, 1/2; -1, -1\rangle$	$\|n', 3/2, 1, 3/2; -1, -2\rangle$	$\|2, 1/2, 0, 1/2; -1, -1\rangle$	1	-1
$\|0, 1/2, 0, 1/2; -1, -1\rangle$	$\|n', 3/2, 1, -1/2; -1, -2\rangle$	$\|2, 1/2, 0, 1/2; -1, -1\rangle$	-1	1
$\|0, 1/2, 0, 1/2; -1, -1\rangle$	$\|n', 1/2, 1, -1/2; 1, 1\rangle$	$\|2, 1/2, 0, 1/2; -1, -1\rangle$	-1	1

for hydrogen-like ions with the nuclear charge up to 100. The illustrative application carried out in this part enables us to draw a comparison of the level of achievement in accounting for relativistic effects in the quasirelativistic procedure. Accurate numerical computations of the transition amplitudes have been performed, using 201 Sturmian functions (i.e. the radial quantum number takes the values $-100 \leq n \leq 100$) to obtain converged values up to 10 significant digits in the exact fully relativistic scheme. In the quasirelativistic approach, 101 Sturmian functions (i.e. $0 \leq n \leq 100$) have been used. It is important to stress out that already from n=40 Sturmian functions we observed a convergence of the results on the sum of intermediary states. The corresponding dipole excitation paths for the transitions under consideration are listed in **Tables** 8.1, 8.3, 8.5, 8.7.

Table 8.4: *Modulus of the matrix elements multiplied by* 2π *for the transition* $|\ 1^2S\rangle \rightarrow |\ 3^2S\rangle$ *in relativistic atomic units for several selected hydrogen-like ions. The superscript* (2) *refers to the quasirelativistic approach (QR) and* (1) *to the fully relativistic treatment where a is related to the Sturmian basis sets with the radial quantum number* $-100 \leq n \leq 100$ *(FR1),* b *to the case* $0 \leq n \leq 100$ *(FR2) and c for* $-100 \leq n \leq -1$ *(CFR). The number in brackets following the entries is the power of* 10 *by which the entry is to be multiplied.*

Z	$2\pi \mid S_{fi}^{(2)} \mid$	$2\pi \mid S_{fi}^{(1)a} \mid$	$2\pi \mid S_{fi}^{(1)b} \mid$	$2\pi \mid S_{fi}^{(1)c} \mid$
1	0.8669001366(+4)	2.8294796436(+4)	3.5331958628(+4)	0.7037162193(+4)
2	2.1676587542(+3)	7.0721154581(+3)	8.8311330169(+3)	1.7590175588(+3)
3	0.9637064319(+3)	3.1419894405(+3)	3.9235727774(+3)	0.7815833369(+3)
4	0.5423231347(+3)	1.7664454398(+3)	2.2059267630(+3)	0.4394813232(+3)
5	0.3472828828(+3)	1.1297651895(+3)	1.4109021126(+3)	0.2811369230(+3)
7	0.1774519631(+3)	0.5753772694(+3)	0.7186359643(+3)	0.1432586949(+3)
10	0.8722940079(+2)	2.8085945631(+2)	3.5087007938(+2)	0.7001062307(+2)
15	0.3907168021(+2)	1.2365692908(+2)	1.5456932258(+2)	0.3091239349(+2)
20	0.2221687289(+2)	0.6863869578(+2)	0.8586579745(+2)	0.1722710166(+2)
25	1.4415943248(+1)	4.3176033847(+1)	5.4067791245(+1)	1.0891757399(+1)
30	1.0178873620(+1)	2.9347578991(+1)	3.6796831495(+1)	0.7449252504(+1)
35	0.7624556684(+1)	2.1012723482(+1)	2.6385109078(+1)	0.5372385596(+1)
40	0.5967238299(+1)	1.5606475688(+1)	1.9629694493(+1)	0.4023218805(+1)
45	0.4831548516(+1)	1.1903477270(+1)	1.5000459124(+1)	0.3096981854(+1)
50	0.4019793075(+1)	0.9258357677(+1)	1.1691503290(+1)	0.2433145613(+1)
55	0.3419823558(+1)	0.7304985776(+1)	0.9245610442(+1)	0.1940624666(+1)
60	0.2964185787(+1)	0.5823109811(+1)	0.7387719573(+1)	0.1564609762(+1)
65	0.2610345282(+1)	0.4673797271(+1)	0.5944308161(+1)	0.1270510889(+1)
70	0.2330421429(+1)	0.3765909614(+1)	0.4801528262(+1)	0.1035618648(+1)
75	0.2105545668(+1)	0.3037663431(+1)	0.3882180880(+1)	0.0844517449(+1)
80	0.1922613061(+1)	0.2445991060(+1)	0.3132429231(+1)	0.0686438171(+1)
85	0.1772341715(+1)	0.1960147302(+1)	0.2513813733(+1)	0.0553666431(+1)
90	0.1648085113(+1)	0.1557732184(+1)	0.1998283320(+1)	0.0440551137(+1)
95	0.1545106178(+1)	0.1222142345(+1)	0.1565009814(+1)	0.0342867469(+1)
100	0.1460167257(+1)	0.0940896857(+1)	0.1198292794(+1)	0.0257395937(+1)

Case of transition $|1\ ^2S\rangle \rightarrow |3\ ^2D_{3/2}\rangle$

For each two-photon resonant matrix element the photon frequency and the intermediate energy vary according to $\omega = (E_2 - E_1)/2$ and $E' = (E_2 + E_1)/2$. The modulus of the matrix elements for the selected transition are displayed in **Tables** 8.2, 8.4, 8.6, 8.8. In columns $2-4$ of these tables are listed respectively

Table 8.5: *Quantum numbers for the allowed dipole excitation paths for the transition* $|\,1^2S\rangle \rightarrow |\,3^2D_{3/2}\rangle$. *Initial state is labelled by index 1, virtual states by superscript prime and final states by index 2.*

$\|n_1, j_1, l_1, m_1; \epsilon_1, \kappa_1\rangle$	$\|n', j', l', m'; \epsilon', \kappa'\rangle$	$\|n_2, j_2, l_2, m_2; \epsilon_2, \kappa_2\rangle$	q	q'
$\|0, 1/2, 0, 1/2; -1, -1\rangle$	$\|n', 3/2, 1, 3/2; -1, -2\rangle$	$\|1, 3/2, 2, 1/2; 1, 2\rangle$	1	-1
$\|0, 1/2, 0, 1/2; -1, -1\rangle$	$\|n', 3/2, 1, -1/2; -1, -2\rangle$	$\|1, 3/2, 2, 1/2; 1, 2\rangle$	-1	1
$\|0, 1/2, 0, 1/2; -1, -1\rangle$	$\|n', 3/2, 1, -1/2; -1, -2\rangle$	$\|1, 3/2, 2, -3/2; 1, 2\rangle$	-1	-1
$\|0, 1/2, 0, 1/2; -1, -1\rangle$	$\|n', 1/2, 1, -1/2; 1, 1\rangle$	$\|1, 3/2, 2, 1/2; 1, 2\rangle$	-1	1
$\|0, 1/2, 0, 1/2; -1, -1\rangle$	$\|n', 1/2, 1, -1/2; 1, 1\rangle$	$\|1, 3/2, 2, -3/2; 1, 2\rangle$	-1	-1

the quasirelativistic results ($n \geq 0$), the exact fully relativistic (FR1) results, the fully relativistic results with $n \geq 0$ (FR2) and the contribution of the negative part ($n < 0$) of the spectrum, hereafter denoted as the correction to the fully relativistic results (CFR). When cross examining these tables together with **Figures** 8.6, 8.8, 8.10, 8.12 and the left panel of **Figures** 8.7, 8.9, 8.11, 8.13, it becomes apparent that the modulus of the matrix elements regularly decreases as the nuclear charge Z increases. This observation is in agreement with the usual qualitative arguments regarding the influence of the relativity which is to significantly lower the magnitude of the amplitudes when considering higher Z and, correlatively, higher frequencies. Seeking how closely QR and FR2 results agree with FR1 values, let

$$\Delta = \left| \frac{S_{fi}^{(P)} - S_{fi}^{(FR1)}}{S_{fi}^{(FR1)}} \right|,$$

be a measure of the difference between the $P = FR2,\ QR$ results with the fully relativistic FR1 values taken as the reference. Plots of Δ against Z are displayed in the right panel of **Figures** 8.7, 8.9, 8.11, 8.13.

Table 8.6: *Modulus of the matrix elements multiplied by* 2π *for the transition* $|\ 1^2S\rangle \rightarrow |\ 3^2D_{3/2}\rangle$ *in relativistic atomic units for several selected hydrogen-like ions. The superscript* (2) *refers to the quasirelativistic approach (QR) and* (1) *to the fully relativistic treatment where a is related to the Sturmian basis sets with the radial quantum number* $-100 \leq n \leq 100$ *(FR1),* b *to the case* $0 \leq n \leq 100$ *(FR2) and c for* $-100 \leq n \leq -1$ *(CFR). The number in brackets following the entries is the power of* 10 *by which the entry is to be multiplied.*

Z	$2\pi \mid S_{fi}^{(2)} \mid$	$2\pi \mid S_{fi}^{(1)a} \mid$	$2\pi \mid S_{fi}^{(1)b} \mid$	$2\pi \mid S_{fi}^{(1)c} \mid$
1	0.5205036251(+4)	0.2629098800(+4)	0.2585916400(+4)	0.4318248002(+2)
2	1.3012670304(+3)	0.6572682252(+3)	0.6464723191(+3)	1.0795821147(+1)
3	0.5783468056(+3)	0.2921154419(+3)	0.2873149374(+3)	0.4800504496(+1)
4	0.3253468056(+3)	0.1643116389(+3)	0.1616101486(+3)	0.2701490331(+1)
5	0.2082116542(+3)	0.1051567172(+3)	0.1034267704(+3)	0.1729946739(+1)
7	0.1062356484(+3)	0.0536476173(+3)	0.0527636402(+3)	0.0883977107(+1)
10	0.5206090583(+2)	0.2628328405(+2)	0.2584872761(+2)	0.0434556445(+1)
15	0.2314413158(+2)	0.1167673193(+2)	0.1148206054(+2)	0.0194671392(+1)
20	0.1302329847(+2)	0.0656401074(+2)	0.0645329674(+2)	0.0110714002(+1)
25	0.8338842154(+1)	0.4197078978(+1)	0.4125222690(+1)	0.7185628863(−1)
30	0.5794248371(+1)	0.2910833442(+1)	0.2860082393(+1)	0.5075104922(−1)
35	0.4259993768(+1)	0.2134736987(+1)	0.2096709055(+1)	0.3802793178(−1)
40	0.3264265664(+1)	0.1630467037(+1)	0.1600694257(+1)	0.2977278000(−1)
45	0.2581668205(+1)	0.1284167067(+1)	0.1260051440(+1)	0.2411562629(−1)
50	0.2093490857(+1)	0.1035866673(+1)	0.1015795170(+1)	0.2007150296(−1)
55	0.1732388044(+1)	0.0851538378(+1)	0.0834456872(+1)	0.1708150640(−1)
60	0.1457848857(+1)	0.0710706660(+1)	0.0695897375(+1)	0.1480928536(−1)
65	0.1244322249(+1)	0.0600449197(+1)	0.0587406686(+1)	0.1304251100(−1)
70	0.1075051193(+1)	0.0512281484(+1)	0.0500639784(+1)	0.1164169996(−1)
75	0.0938682401(+1)	0.0440442994(+1)	0.0429930942(+1)	0.1051205170(−1)
80	0.0827311511(+1)	0.0380907754(+1)	0.0371320577(+1)	0.9587177806(−2)
85	0.0735310728(+1)	0.0330789103(+1)	0.0321969807(+1)	0.8819296134(−2)
90	0.0658603341(+1)	0.0287968395(+1)	0.0279795305(+1)	0.8173089546(−2)
95	0.0594205560(+1)	0.0250855624(+1)	0.0243233914(+1)	0.7621709724(−2)
100	0.0539938007(+1)	0.0218229931(+1)	0.0211085874(+1)	0.7144057398(−2)

Case of transition $|1\ ^2S\rangle \rightarrow |3\ ^2D_{5/2}\rangle$

Switching our attention to **Figures** 8.7 and 8.9 (the right panel) which display plots of the differences Δ against the nuclear charge Z, one sees that they have almost the same shape but exhibit a marked discrepancy. For QR approach, the magnitude of Δ for both transition regularly decreases as Z increases whereas

Table 8.7: *Quantum numbers for the allowed dipole excitation paths for the transition* $|\ 1^2S\rangle \rightarrow |\ 3^2D_{5/2}\rangle$. *Initial state is labeled by index 1, virtual states by superscript prime and final states by index 2.*

$\|n_1, j_1, l_1, m_1; \epsilon_1, \kappa_1\rangle$	$\|n', j', l', m'; \epsilon', \kappa'\rangle$	$\|n_2, j_2, l_2, m_2; \epsilon_2, \kappa_2\rangle$	q	q'
$\|0, 1/2, 0, 1/2; -1, -1\rangle$	$\|n', 3/2, 1, 3/2; -1, -2\rangle$	$\|0, 5/2, 2, 5/2; -1, -3\rangle$	1	1
$\|0, 1/2, 0, 1/2; -1, -1\rangle$	$\|n', 3/2, 1, 3/2; -1, -2\rangle$	$\|0, 5/2, 2, 1/2; -1, -3\rangle$	1	-1
$\|0, 1/2, 0, 1/2; -1, -1\rangle$	$\|n', 3/2, 1, -1/2; -1, -2\rangle$	$\|0, 5/2, 2, 1/2; -1, -3\rangle$	-1	1
$\|0, 1/2, 0, 1/2; -1, -1\rangle$	$\|n', 3/2, 1, -1/2; -1, -2\rangle$	$\|0, 5/2, 2, -3/2; -1, -3\rangle$	-1	-1

their FR2 counterparts slightly increase. **Figure** 8.14 clearly shows the CFR contributions to the exact fully relativistic treatment (FR1). As can be seen in this figure, CFR contributes to the amount lying between 20.9% and 37.6% in FR1 with increasing Z, and thus cannot be neglected. The aforementioned differences are related to the fact that FR2 does not account for the negative part ($n < 0$) of the spectrum whereas the quasirelativistic treatment suffers for the second-order approximation made on the relativistic discrete Dirac-Coulomb wave functions to describe the atomic states and the quasirelativistic Coulomb Green functions. When considering transitions leading up to the D state, we have evaluated two different matrix elements due to the fine structure of the level.

Table 8.8: *Modulus of the matrix elements multiplied by* 2π *for the transition* $|\ 1^2S\rangle \rightarrow |\ 3^2D_{5/2}\rangle$ *in relativistic atomic units for several selected hydrogen-like ions. The superscript* (2) *refers to the quasirelativistic approach (QR) and* (1) *to the fully relativistic treatment where a is related to the Sturmian basis sets with the radial quantum number* $-100 \leq n \leq 100$ *(FR1),* b *to the case* $0 \leq n \leq 100$ *(FR2) and c for* $-100 \leq n \leq -1$ *(CFR). The number in brackets following the entries is the power of* 10 *by which the entry is to be multiplied.*

Z	$2\pi \mid S_{fi}^{(2)} \mid$	$2\pi \mid S_{fi}^{(1)a} \mid$	$2\pi \mid S_{fi}^{(1)b} \mid$	$2\pi \mid S_{fi}^{(1)c} \mid$
1	2.8287188100(+4)	2.8286739216(+4)	2.8286764682(+4)	0.2546662514(−1)
2	7.0712992656(+3)	7.0708503913(+3)	7.0708758570(+3)	0.2546563148(−1)
3	3.1424309483(+3)	3.1419820906(+3)	3.1420075546(+3)	0.2546397507(−1)
4	1.7673270201(+3)	1.7668781855(+3)	1.7669036471(+3)	0.2546165544(−1)
5	1.1308503258(+3)	1.1304015209(+3)	1.1304269796(+3)	0.2545867194(−1)
7	0.5766392737(+3)	0.5761905480(+3)	0.5762159987(+3)	0.2545070971(−1)
10	0.2822145264(+3)	0.2817659690(+3)	0.2817914027(+3)	0.2543375993(−1)
15	0.1250593819(+3)	0.1246112369(+3)	0.1246366290(+3)	0.2539204250(−1)
20	0.7005464431(+2)	0.6960707686(+2)	0.6963241008(+2)	0.2533321911(−1)
25	0.4459482354(+2)	0.4414799869(+2)	0.4417325555(+2)	0.2525685992(−1)
30	0.3076427497(+2)	0.3031835774(+2)	0.3034352014(+2)	0.2516239617(−1)
35	0.2242433583(+2)	0.2197949108(+2)	0.2200454018(+2)	0.2504910716(−1)
40	0.1701081028(+2)	0.1656720245(+2)	0.1659211856(+2)	0.2491610286(−1)
45	0.1329870152(+2)	0.1285649436(+2)	0.1288125666(+2)	0.2476230151(−1)
50	0.1064280863(+2)	0.1020216464(+2)	0.1022675104(+2)	0.2458640075(−1)
55	0.8677073414(+1)	0.8238153097(+1)	0.8262539937(+1)	0.2438684036(−1)
60	0.7181261789(+1)	0.6744222497(+1)	0.6768384251(+1)	0.2416175420(−1)
65	0.6016422693(+1)	0.5581416984(+1)	0.5605325892(+1)	0.2390890739(−1)
70	0.5091371560(+1)	0.4658544739(+1)	0.4682170353(+1)	0.2362561349(−1)
75	0.4344254853(+1)	0.3913741333(+1)	0.3937049957(+1)	0.2330862340(−1)
80	0.3731910868(+1)	0.3303828700(+1)	0.3326782674(+1)	0.2295397350(−1)
85	0.3223474404(+1)	0.2797916910(+1)	0.2820473683(+1)	0.2255677334(−1)
90	0.2796395547(+1)	0.2373418229(+1)	0.2395529129(+1)	0.2211090042(−1)
95	0.2433885205(+1)	0.2013484658(+1)	0.2035093204(+1)	0.2160854633(−1)
100	0.2123233199(+1)	0.1705311826(+1)	0.1726351339(+1)	0.2103951394(−1)

Tables 8.6 and 8.8 clearly display the outputs of our computations. The following main points can be drawn out. With increasing Z the magnitude of the matrix element is lowered as expected. In contrast, it does not affect the matrix element in the same way as is found in the previous cases. Comparing QR values with their FR2 and FR1 correspondents, our analysis reveals

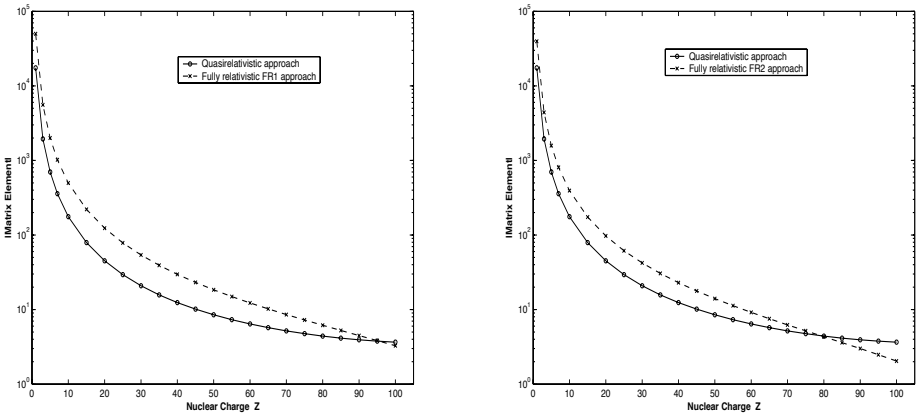

Figure 8.6: *Modulus of the matrix elements multiplied by* 2π *versus the nuclear charge* Z *for the transition* $|\ 1^2S\rangle \rightarrow |\ 2^2S\rangle$ *in relativistic atomic units for several selected hydrogen-like atoms. Left panel: (QR) and (FR1). Right Panel: (QR) and (FR2). Curves are drawn to guide the eye.*

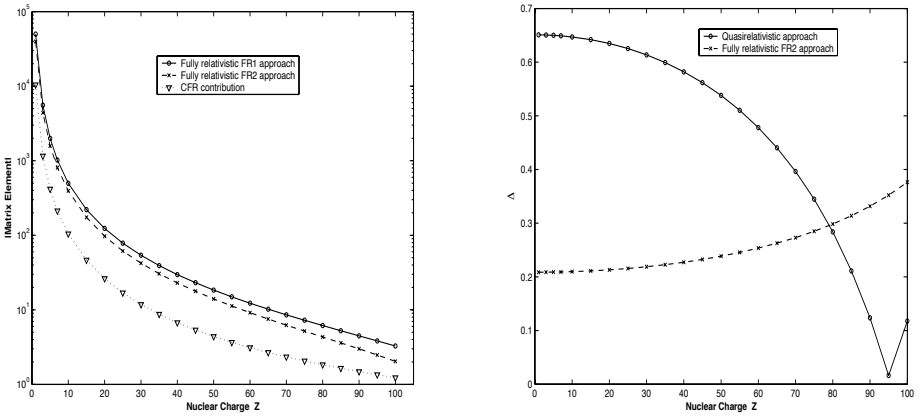

Figure 8.7: *Left panel: (FR1), (FR2) and (CFR) Modulus of the matrix elements multiplied by* 2π *versus the nuclear charge* Z *for the transition* $|\ 1^2S\rangle \rightarrow |\ 2^2S\rangle$ *in relativistic atomic units for several selected hydrogen-like atoms. Right panel: Plot of the differences* Δ *between the quasirelativistic (QR), fully relativistic (FR2) values and exact fully relativistic (FR1) values versus the nuclear charge* Z *for the selected transition* $|\ 1^2S\rangle \rightarrow |\ 2^2S\rangle$*. Curves are drawn to guide the eye.*

that the accuracy of QR results decreases from the lightest elements to the heavier ones. While for smaller Z, a substantial improvement is observed on

the transition (1) | $3^2D_{5/2}\rangle$, the discrepancies are more pronounced for higher nuclear charge in the latter (2) | $3^2D_{3/2}\rangle$ transition. One also sees that for this type of transition (1), the FR2 values agree with reference data within a percentage error very close to the zero value for Z up to 30 and slightly grows up for high-Z elements. The same tendency is observed for the last case (2) with, however the difference Δ lying between 1.64% and 3.27% in FR1 with increasing Z. These are depicted in the right panel of **Figures** 8.11, 8.13 and the **Figure** 8.14.

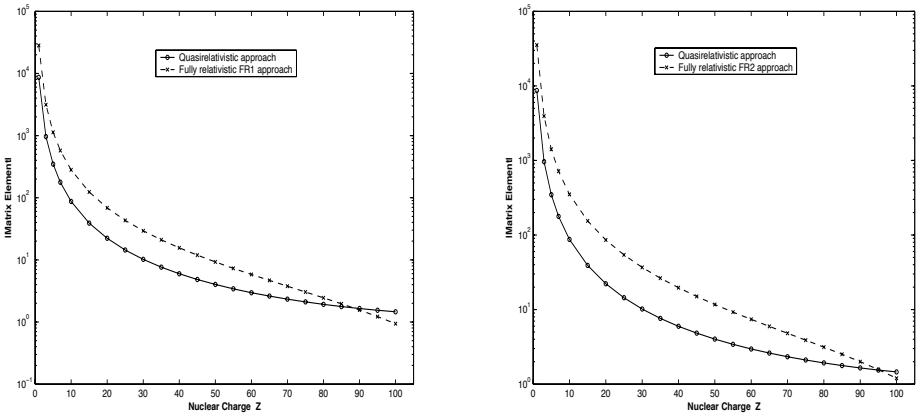

Figure 8.8: *Modulus of the matrix elements multiplied by* 2π *versus the nuclear charge* Z *for the transition* $|\ 1^2S\rangle \rightarrow |\ 3^2S\rangle$ *in relativistic atomic units for several selected hydrogen-like atoms. Left panel: (QR) and (FR1). Right panel: (QR) and (FR2). Curves are drawn to guide the eye.*

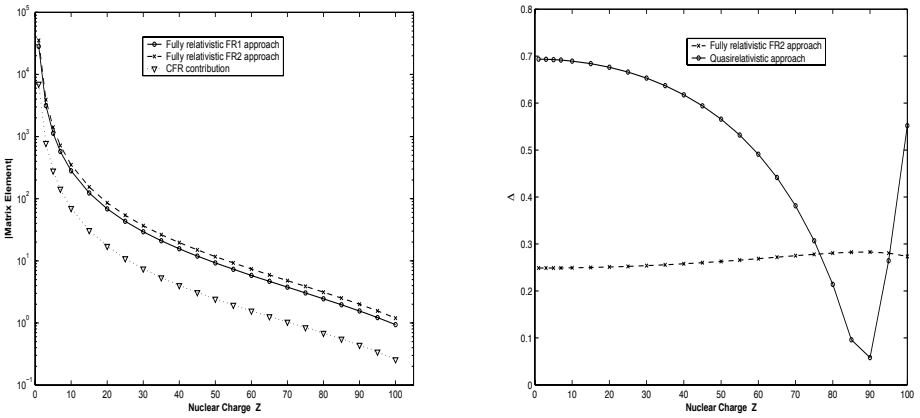

Figure 8.9: *Left panel: (FR1), (FR2) and (CFR) Modulus of the matrix elements multiplied by* 2π *versus the nuclear charge* Z *for the transition* $|\ 1^2S\rangle \rightarrow |\ 3^2S\rangle$ *in relativistic atomic units for several selected hydrogen-like atoms. Right panel: Plot of the differences* Δ *between the quasirelativistic (QR), fully relativistic (FR2) values and exact fully relativistic (FR1) values versus the nuclear charge* Z *for the selected transition* $|\ 1^2S\rangle \rightarrow |\ 3^2S\rangle$*. Curves are drawn to guide the eye.*

Figure 8.15 displays the ratios $\mathcal{R}_d$ of the $|\ 1^2S\rangle \rightarrow |\ 3^2D_{5/2}\rangle$ two-photon absorption amplitude to the $|\ 1^2S\rangle \rightarrow |\ 3^2D_{3/2}\rangle$ two-photon absorption ampli-

tude, for relativistic calculations. Comparing our fully relativistic calculations with the quasirelativistic results for hydrogen-like ions, we found that, there exist approximatively the scale factor 2.0 between the fully relativistic (FR1, FR2) ratios and the quasirelativistic (QR) ratio.

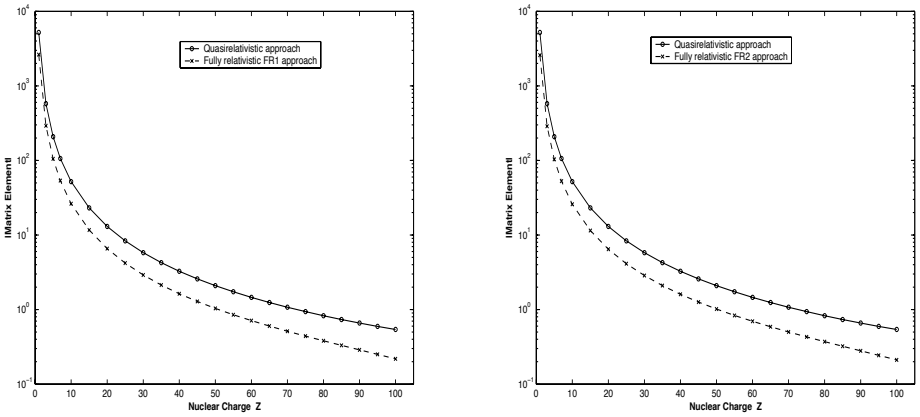

Figure 8.10: *Modulus of the matrix elements multiplied by* 2π *versus the nuclear charge* Z *for the transition* $\mid 1^2S\rangle \rightarrow \mid 3^2D_{3/2}\rangle$ *in relativistic atomic units for several selected hydrogen-like atoms. Left panel: (QR) and (FR1). Right panel: (QR) and (FR2). Curves are drawn to guide the eye.*

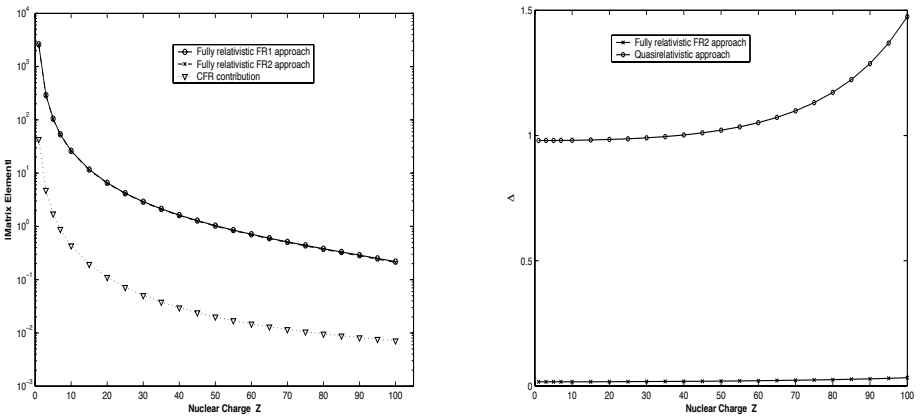

Figure 8.11: *Left panel: (FR1), (FR2) and (CFR) Modulus of the matrix elements multiplied by* 2π *versus the nuclear charge* Z *for the transition* $\mid 1^2S\rangle \rightarrow \mid 3^2D_{3/2}\rangle$ *in relativistic atomic units for several selected hydrogen-like atoms. Right panel: Plot of the differences* Δ *between the quasirelativistic (QR), fully relativistic (FR2) values and exact fully relativistic (FR1) values versus the nuclear charge* Z *for the selected transition* $\mid 1^2S\rangle \rightarrow \mid 3^2D_{3/2}\rangle$. *Curves are drawn to guide the eye.*

As the $\mid 3^2D_{3/2}\rangle$ wave function is more localized than the $\mid 3^2D_{5/2}\rangle$ wave function, the overlap with the $\mid 1^2S\rangle$ wave function is larger for the $\mid 3^2D_{3/2}\rangle$

state than for the $|\, 3^2D_{5/2}\rangle$ state. Thus, the ratio $\mathcal{R}_d$ is getting smaller as the nuclear charge increases as shown in **Figure** 8.15.

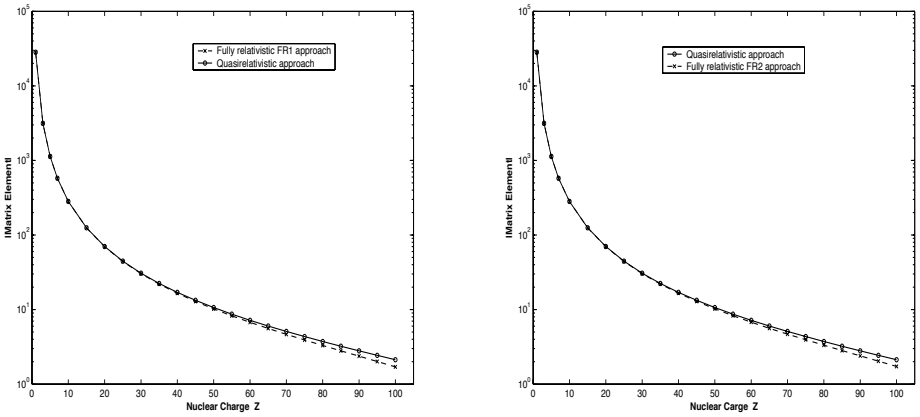

Figure 8.12: *Modulus of the matrix elements multiplied by* 2π *versus the nuclear charge* Z *for the transition* $|\ 1^2S\rangle \rightarrow |\ 3^2D_{5/2}\rangle$ *in relativistic atomic units for several selected hydrogen-like atoms. Left panel: (QR) and (FR1). Right panel: (QR) and (FR2). Curves are drawn to guide the eye.*

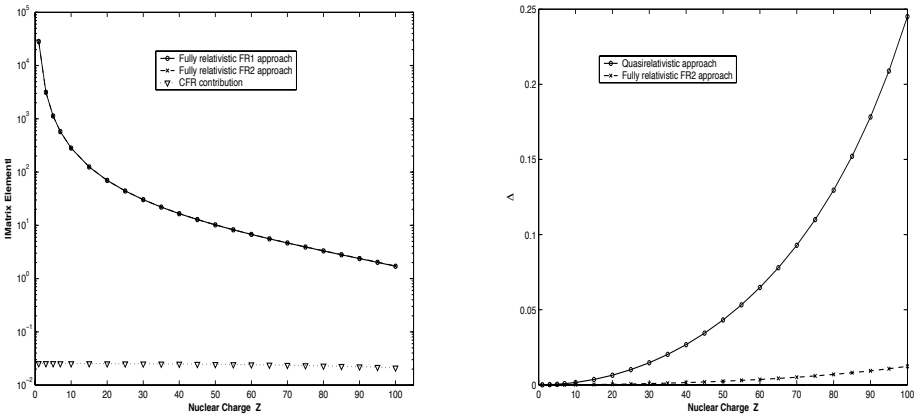

Figure 8.13: *Left panel: (FR1), (FR2) and (CFR) Modulus of the matrix elements multiplied by* 2π *versus the nuclear charge* Z *for the transition* $|\ 1^2S\rangle \rightarrow |\ 3^2D_{5/2}\rangle$ *in relativistic atomic units for several selected hydrogen-like atoms. Right panel: Plot of the differences* Δ *between the quasirelativistic (QR), fully relativistic (FR2) values and exact fully relativistic (FR1) values versus the nuclear charge* Z *for the selected transition* $|\ 1^2S\rangle \rightarrow |\ 3^2D_{5/2}\rangle$. *Curves are drawn to guide the eye.*

From the above observations, it becomes evident that QR and FR2 approaches are less adequate for the description of relativistic features related to

the two-photon bound-bound transitions amplitudes in hydrogen-like ions.

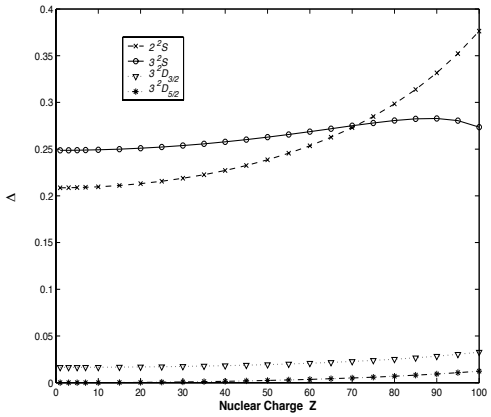

Figure 8.14: *Plot of the contribution of the negative part of the set (CFR) to the exact fully relativistic FR1 values versus the nuclear charge Z for all selected transitions.*

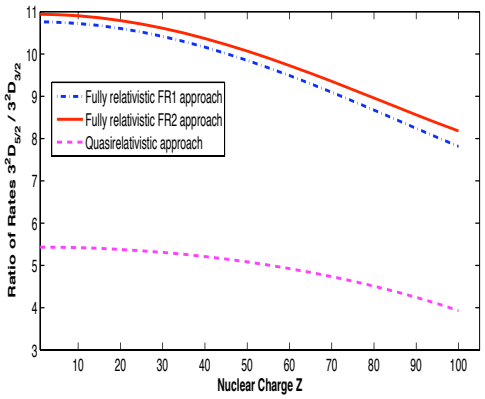

Figure 8.15: *Ratio $\mathcal{R}_d$ of modulus of the relativistic two-photon transition amplitudes of $|\ 1^2S\rangle \rightarrow |\ 3^2D_{5/2}\rangle$ to $|\ 1^2S\rangle \rightarrow |\ 3^2D_{3/2}\rangle$ for hydrogen-like ions versus the nuclear charge Z. Curves are drawn to guide the eye.*

It then clearly appears that the FR1 procedure is needed for a correct treatment of the above process where relativistic effects show up strongly. We may then see in our complete relativistic derivations given above a useful tool to deal with in analytical treatments in which consistent inclusion of relativistic effects is in order.

8.7 Conclusion

In this Chapter, we have performed the derivation of the fully and quasirelativistic S-matrix elements describing two-photon transition amplitude probabilities between hydrogenic bound states. The computation takes advantage of the use of an expansion over a Sturmian basis of the first and second-order Dirac Coulomb Green functions. An interesting outcome of the work is to demonstrate the tractability of relativistic calculations for multiphoton amplitudes, using the properties of Sturmian functions. The analytical formulae obtained are quite general and well suited to account for the influence of relativistic, retardation and multipole effects onto the two-photon excitation of hydrogen-like ions by linearly polarized photons as well as Rayleigh and Raman scattering. This opens interesting perspectives regarding the possibility to address the difficult problem of the simulation of the response of heavy atoms or ions in the presence of an intense, high frequency, radiation field.

The results of our original calculations show that, for two-photon bound-bound transitions, relativistic contributions are indeed significant. The influence of relativity is to decrease the magnitude of the transition matrix element in two-photon processes originating from the ground state and ending in the L and M shells. Such an influence is opposite to the one observed in the case of single-photon bound-free transitions, where according to Ron *et al.* [58] relativistic effects tend to increase the cross sections.

From the numerical values obtained above, it is clear that these amplitude transitions are affected by relativistic effects which become increasingly important for higher nuclear charges, and the FR procedures are superior to QR. Also, we are inclined to believe that for a proper treatment, FR1 method must be used.

Bibliography

[1] E. Schrödinger, *Annalen der Physik* **81**, 109 (1926).

[2] P. A. M. Dirac, *Proc. R. Soc. London Ser. A.* **112**, 661 (1926).

[3] M. Göpper-Mayer, *Ann. Phys., Lpz* **9**, 273 (1931).

[4] P. Lambropoulos, P. Maragakis and J. Zhang, *Phys. Rep.* **305**, 203 (1998).

[5] G. E. Brown, R. E. Peierls and J. B. Woodward, *Proc. Roy. Soc. A* **227**, 51 (1954).

[6] C. Schwartz, *Ann. Phys.* **6**, 156 (1959).
C. Schwartz and J. J. Tiemann, *Ann. Phys.* **6**, 178 (1959).

[7] B. A. Zon and N. L. Manakov, *Zh. Eksp. Teor. Fiz.* **60**, 1264 (1971).
B. A. Zon and N. L. Manakov, *Zh. Eksp. Teor. Fiz.* **61**, 968 (1971).

[8] V. A. Davidkin, B. A. Zon, N. L. Manakov and L. P. Rapaport, *Zh. Eksp. Teor. Fiz.* **60**, 124 (1971).

[9] E. J. Kelsey and J. Macek, *J. Math. Phys.* **17**, 1182 (1976).

[10] H. B. Bebb, *J. Math. Phys.* **7**, 955 (1966).

[11] H. A. Bethe and E. E. Salpeter, *Quantum Mechanics of One and Two-Electron Atoms* (Springer-Verlag, Berlin, 1957).

[12] R. Kundliya, V. Prasad and M. Mohan, *J. Phys. B: At. Mol. Opt. Phys.* **33**, 5263 (2000).

[13] A. Quattropani, F. Bassani and S. Carillo, *Phys. Rev. A* **25**, 3079 (1982).

[14] P. Koval, *PhD Thesis,* University of Kassel, Germany (2004).

[15] S. Klarsfeld, *Lett. Nuovo Cimento* **1**, 682 (1969).
S. Klarsfeld, *Lett. Nuovo Cimento* **2**, 548 (1969).

[16] G. Laplanche, A. Durrieu, Y. Flank, M. Jaouen and A. Rachman, *J. Phys. B: At. Mol. Phys.* **9**, 1263 (1976).

[17] E. Karule and R. H. Pratt, *J. Phys. B: At. Mol. Phys.* **24**, 1585 (1991).

[18] B. H. Bransden and C. J. Joachain, *Quantum Mechanics* 2nd ed (Pearson Education Ltd, England, 2000).

[19] H. M. Pilkuhn, *Relativistic Quantum Mechanics* (Springer, Berlin, 2003).

[20] F. Mandl and G. Shaw, *Quantum Field Theory* (John Wiley and Sons, New York, 1984).

[21] J. D. Bjorken and S. D. Drell, *Relativistic Quantum Mechanics* (McGraw-Hill, New York 1964).

[22] L. D. Landau and E. M. Lifshitz, *Physique Théorique. Tome IV, Electrodynamique Quantique* ed Librairie du Globe (Mir, Paris, 1989).

[23] A. I. Akhiezer and V. B. Berestetskii, *Quantum Electrodynamics* (Interscience Publishers, New York, 1965).

[24] I. Bialynicki-Birula and Z. Bialynicka-Birula, *Quantum Electrodynamics* (Pergamon Press, Oxford, 1975).

[25] F. Schwabl, *Advanced Quantum Mechanics* (Springer-Verlag, Berlin, Heidelberg, 1999).

[26] H. R. Reiss, *J. Opt. Soc. Am. B.* **7**, 574 (1990).
H. R. Reiss, *The Effects of Relativity in Atoms, Molecules and the Solid state* ed. C. A. Nicolaides, M. Nayfeh and C. Clark (Plenum, New York, 1990).

[27] P. M. Morse and H. Feshbach, *Methods of Theoretical Physics* Part I (McGraw-Hill, New York, 1953).

[28] E. C. Titchmarsh, *Eigenfunction Expansion Associated with 2nd Order Differential Equations* Vol II (Oxford University Press, Oxford, 1958).

[29] H. B. Bebb and A. Gold, *Phys. Rev.* **143**, 1 (1966).

[30] P. Lambropoulos, *Adv. At. Mol. Phys.* **12**, 87 (1976).

[31] F. H. M. Faisal, *Theory of Multiphoton Process* (Plenum, New York, 1987).

[32] A. Maquet, *Phys. Rev. A* **15**, 1088 (1977).

[33] A. Maquet, V. Veniard and T. A. Marian, *J. Phys. B: At. Mol. Opt. Phys.* **31**, 3743 (1998).

[34] I. P. Grant, *Relativistic Atomic Structure in Springer Handbook of Atomic, Molecular and Optical Physics* ed. Gordon W. F. Drake (Springer, 2006), part B, Chap 22.

[35] L. M. Labzowsky and A. V. Shonin, *Phys. Rev. A* **69**, 012503 (2004).

[36] R. Ali *et al.*, *Phys. Rev. A* **55**, 994 (1997).

[37] A. Derevianko and W. R. Johnson, *Phys. Rev. A* **56**, 1288 (1997).

[38] D. Xenakis, O. Faucher, D. Charalambidis and C. Fotakis, *J. Phys. B: At. Mol. Opt. Phys.* **29**, L457 (1996).

[39] M. A. Kornberg, A. L. Godunov, S. I. Ortiz, D. L. Ederer, J. H. McGuire and L. Young, *J. Synchrotron. Radiat.* **9**, 298 (2002).

[40] S. P. Goldman and G. W. Drake, *Phys. Rev. A* **24**, 183 (1981).

[41] C. Szymanowski, V. Véniard, R. Taïeb and A. Maquet *Phys. Rev. A* **56**, 700 (1997).

[42] P. Martin and R. J. Glauber, *Phys. Rev.* **109**, 1307 (1958).

[43] J. P. Santos, P. Patte, F. Parente and P. Indelicato, *Eur. J. Phys. D* **13**, 27 (2001).

[44] P. Koval, S. Fritzsche and A. Surzhykov, *J. Phys. B: At. Mol. Opt. Phys.* **36**, 873 (2003).

[45] X-M. Tong, J-M. Li, L. Kissel and R. H. Pratt, *Phys. Rev. A* **42**, 1442 (1990).

[46] R. Szmytkowski, *J. Phys. B: At. Mol. Opt. Phys.* **30**, 825 (1997).
R. Szmytkowski, *J. Phys. B: At. Mol. Opt. Phys.* **30**, 2747 (1997) (erratum).

[47] A. Messiah, *Quantum Mechanics* Vol I (New York, Walter de Gruyter, 1990).
A. Messiah, *Quantum Mechanics* 2nd edn. (Wiley, New York, 1970).

[48] L. D. Landau and E. M. Lifshitz, *Course of Theoretical Physics. Quantum Mechanics* (New York, Wiley, 1986).

[49] A. N. Hopersky, A. M. Nadolinsky and V. A. Yavna, *J. Exp. Theor. Phys.* **101**, 597 (2005).
A. N. Hopersky, I. D. Petrov, A. M. Nadolinsky, V. A. Yavna and R. V. Koneev, *J. Phys. B: At. Mol. Opt. Phys.* **37**, 3313 (2004).

[50] J. Lorimier, F. Bernard, J-C. Niepce, N. Guigue-Millot, O. Isnard and J-F. Bérar, *J. Appl. Cryst.* **36**, 301 (2003).

[51] R. P. Hugtemburg, P. Muthuvelu and D. A. Bradley, *Phys. Med. Biol.* **47**, 3407 (2002).

[52] S. P. Kearney, R. W. Schefer, S. J. Beresh and T. W. Grasser, *Appl. Optics* **44**, 1548 (2005).

[53] S. A. Kaiser, J. H. Frank and M. B. Long, *Appl. Optics* **44**, 6557 (2005).

[54] W. Zhi, R. Guobin, L. Shuqin and J. Shuisheng, *Opt. Express* **11**, 39 (2003).

[55] B. R. Holstein, *Am. J. Phys.* **72**, 333 (2004).

[56] A. Costescu, S. Spanulescu and C. Stoica, *J. Phys. B: At. Mol. Opt. Phys.* **40**, 2995 (2007).

[57] H. M. Tetchou Nganso and M. G. Kwato Njock, *J. Phys. B: At. Mol. Opt. Phys.* **40**, 807 (2007).

[58] A. Ron, I. B. Goldberg, J. Stein, S. T. Mason, R. H. Pratt and R. Y. Yin, *Phys. Rev. A* **50**, 1312 (1994).

Chapter 9

Summary and Perspectives

"En essayant continuellement, on finit par réussir.
Donc: plus ça rate, plus on a de chances que ça marche."
Devise Shadock.

At the end of our work, it is important to summarize the main stages that were crossed as well as to draw out the points that we found relevant in our investigations. Naturally, some outlooks are also in order.

9.1 Summary

In this part of the thesis we have studied the two-photon transition processes in atomic systems. We considered the excitation, Rayleigh and Raman scattering on the basis of Dirac-Coulomb equation and Gell-Mann Feynman equation, which was treated by means of the second-order perturbation theory. To achieve this purpose we have used a tensorial method for the accurate quantum treatment of the processes underlined. Our approach combines efficient theoretical methods and accurate computing techniques and allows for an exact fully relativistic description of both, two-photon absorption, Rayleigh and Raman scattering. The infinite summation over the whole atomic spectrum, which arises in second-order perturbation theory, has been calculated by means of a *Green's function method*. This method requires the computation of analytical expressions of Coulomb Green's functions for the hydrogenic atom. Previous works by Zapryagaev, Manakov, and Pal'chikov [1], Szmytkowski [2], Szymanowski *et al.* [3] (and many other authors in the literature) showed the viability of the relativistic Sturmian basis set representation for the Dirac-Coulomb Green's function for problems with a single Green's function. Details on the derivation of explicit analytical expressions of quasirelativistic and relativistic Coulomb-Sturmian functions are outlined with some of their important properties. Sturmian expansions of the radial Coulomb Green's functions have

been widely used for both nonrelativistic and relativistic analytical calculations. The use of this representation is especially convenient in the calculation of multiphoton processes in the perturbative regime and for the analysis of quantum electrodynamical effects in the interaction of hydrogen-like ions with electromagnetic fields. In concrete calculations some other different representations of this function are often used: the coordinate representation [4], the impulse or momentum representation [5], the coordinate representation in the expansion in power series of the Laguerre polynomial [6]. However, the use of all the above-mentioned representations always leads to an enormous number of calculations of multi-dimensional integrals of special functions. This circumstance strongly decreases the efficiency of the application of analytical methods in perturbation theory with the use of the Dirac-Coulomb Green's function. In order to *improve the efficiency* of the Coulomb Green's function, the advantages of a Sturmian basis set have been explored and used. The Sturmian basis set, which enables us to reduce complicated calculations of the matrix elements, also allows to use the one-dimensional integration for the radial matrix elements calculation. The usage of the one-dimensional functions in the radial integrals certainly *increase the speed* of calculation of the radial matrix elements.

By the virtue of this Green's function, we undertook within the dipole approximation a systematic study of the two-photon absorption, in their relativistic and quasirelativistic viewpoints in hydrogen-like ions from its ground state $|\, 1\,{}^2S\rangle$ towards the L and M shells in order to draw inferences as to the improvements of our method. It is worth mentioning here that, the formulae derived are general and suited to account for any multipole of the two photons. They have also led to closed-form and compact expressions obtained in terms of special hypergeometric functions from which numerical evaluation is most convenient. Concluding, fully relativistic (FR) treatment yields more accurate results than the quasirelativistic (QR) approximations, resulting in a *general decrease* of the two-photon absorption amplitudes [7].

9.2 Outlook

In principle, the Green's function can be used in all the problems which require a summation over the whole atomic spectrum. One can mention here few possible tasks for the Green's functions.

- Rayleigh, Raman and Compton scattering amplitudes of two-photons.
- Calculation of two-photon decay rates.
- Extension of the previous calculations to complex (many-electron) atoms. Construction of Sturmian expansion of an atomic many-electron Green's

function.

Starting from fully relativistic second-order S-matrix elements, we obtain Rayleigh and Raman scattering amplitudes. In the same line, right expression of the fully relativistic K-shell Compton scattering amplitudes and cross sections can be easily obtained. These calculations include higher multipoles as well as retardation and relativistic contributions. However, the relative contributions of these corrections are not given explicitly in the present formulae. We seek to elucidate the nature of higher multipole and retardation contributions in Rayleigh, Raman and Compton scattering of photons from the ground state of hydrogen-like ions. By retardation contributions we mean the evaluation of multipoles beyond their long-wavelength limit. For low photon energies, we will evaluate these contributions simultaneously for all multipoles, for fixed orders in $(k\alpha Z)^2/4$ (where k is the photon energy divided by the relativistic ground state energy), and in terms of $\hbar\omega = k(\alpha Z)^2/2$ and $(\alpha Z)^2$, which characterize the magnitude of relativistic corrections. At $k = 2$ all these parameters are the same, while for $k > 2(< 2)$ multipole and retardation (relativistic) parameters are larger. However, in order to achieve a better understanding of higher multipole contributions and retardation effects in Rayleigh and Raman scattering, we wish to obtain simple formulae which make clear the energy and charge dependence of the amplitudes $S^{(1)}_{Ray}$ and $S^{(1)}_{Ram}$ and how they depend on k and on αZ. A comparison of our numerical results obtained from these formulae with those calculated by Kissel *et al.* [8], Florescu *et al.* [9] and Costescu *et al.* [10] will be given. This will be discussed in a subsequent paper to be submitted soon [11].

For the second task, we wish to present a relativistic calculation of two-photon decay rates in atomic inner shells within the framework of our tensorial formalism by using the Sturmian expansion of Green's function. By comparing our relativistic two-photon decay rates for Mo, Ag, and Xe with results for a series of hydrogen-like ions and existing nonrelativistic results and available experimental data [12, 13, 14, 15], we attempt to identify and clarify the nature of the relativistic effects and atomic screening effects. It has been argued that [15]: (1) the relativistic effects reduce the two-photon decay rates compared with the nonrelatvistic results. Such relativistic effects become more important as the atomic number Z increases; (2) screening effects reduce the atomic two-photon decay rates compared with the corresponding hydrogen-like ions. These effects become smaller as the atomic number Z increases. These transitions, which test external field quantum electrodynamics, have become accessible to experimental measurement. Consistency between theory and experiment has not yet been achieved. With improvements in experimental technique, especially of the coincident measurement technique, one can measure two-photon decay rates in the X-ray region.

For the latter task, we could extend the precedent processes to complex many-electron atoms. Also we could reinvestigate the effects (excitation, ionization) which arise in many-electron atomic inner-shells [16, 17]. Since the relativistic effects are fundamental effects and they are important for heavy hydrogen-like ions, the many-electron inner-shells could be investigated on the basis of the Dirac equation within the framework of an atomic model, namely a *single-active-electron* (SAE) approximation. The SAE approximation assumes that only one electron changes its energy during the atomic process. All the other electrons are frozen, do not change their states and only create a mean-field for the *active electron*. This picture significantly simplifies the calculations because the whole theory remains an one-electronic theory. In order to perform a computation, one must only specify the mean-field and the initial state of the active electron. These problems can be solved if one considers the structure of many-electron atom. An accurate SAE calculation of two-photon processes is realized if one efficiently derives a central-field wave function and a central-field Green's function for many-electron atoms. While calculation of the former is a relatively familiar routine task, to the best of our knowledge, less attempt has been made so far to explore the latter in the literature. Recently, Peter Koval in his works [18] derived a Dirac-central-field Green's function by means of a numerical algorithm, which is the extension on the relativistic framework of the numerical algorithm originally invented by McGuire [19]. Unfortunately, the slowness of his program limits the range of the problems which can be efficiently solved by exploring the advantages of an appropriate Sturmian basis set to expand the central-field Green's function. All these mentioned tasks will be the focus of our forthcoming works.

Let us say as a final word the belief that the material contained in the present thesis may help in other research activities related to what was developed over. It is therefore our hope that this work will stimulate furthers.

Bibliography

[1] S. A. Zapryagaev, N. L. Manakov and V. G. Pal'chikov, *Opt. Spektrosk.* **52**, 414 (1982) [Opt. Spectrosc. **52**, 248 (1982)].
S. A. Zapryagaev, N. L. Manakov and V. G. Pal'chikov, *Theory of Multiply Charged Ions with One and Two Electrons* (Energoatomizdat, Moscow, 1985) (in Russian).

[2] R. Szmytkowski, *J. Phys. B: At. Mol. Opt. Phys.* **30**, 825 (1997).
R. Szmytkowski, *J. Phys. B: At. Mol. Opt. Phys.* **30**, 2747 (1997) (Erratum).

[3] C. Szymanowski, V. Véniard, R. Taïeb and A. Maquet, *Phys. Rev. A* **56**, 700 (1997).
C. Szymanowski, V. Véniard, R. Taïeb and A. Maquet, *Europhys. Lett.* **37**, 391 (1997).

[4] P. C. Martin and R. J. Glauber, *Phys. Rev. A* **109**, 1307 (1958).

[5] N. L. Manakov, L. P. Rapoport and S. A. Zapryagaev, *Phys. Lett.* **43A**, 139 (1973).

[6] B. A. Zon, N. L. Manakov and L. P. Rapoport, *Yad. Fiz.* **15**, 508 (1972).

[7] H. M. Tetchou Nganso and M. G. Kwato Njock, *J. Phys. B: At. Mol. Opt. Phys.* **40**, 807 (2007).

[8] Lynn Kissel, R. H. Pratt and S. C. Roy, *Phys. Rev. A* **22**, 1970 (1980).

[9] Viorica Florescu, M. Marinescu and R. H. Pratt, *Phys. Rev. A* **42**, 3844 (1990).

[10] A. Costescu, P. M. Jr. Bergstrom, C. Dinu and R. H. Pratt, *Phys. Rev. A* **50**, 1390 (1994).

[11] H. M. Tetchou Nganso and M. G. Kwato Njock, *Rayleigh and Raman Scattering in the Relativistic Hydrogen-Like Ions: Application of the Sturmian Expansion of the First-Order Dirac-Coulomb Green Function*, to be submitted to *J. Phys. B: At. Mol. Opt. Phys.*

[12] X. Mu and B. Crasemann, *Phys. Rev. A* **38**, 4585 (1988).
X. Mu and B. Crasemann, *Phys. Rev. Lett.* **57**, 3039 (1986).

[13] Y. Bannett and I. Freund, *Phys. Rev. Lett.* **40**, 539 (1982).
Y. Bannett and I. Freund, *Phys. Rev. A* **30**, 299 (1984).

[14] Ying-Jian Wu and Jia-Ming Li, *J. Phys. B* **21**, 1509 (1988).

[15] Xiao-Min Tong and Jia-Ming Li, *Phys. Rev. A* **42**, 1442 (1990).

[16] P. Koval, *Ph.D. Thesis*, University of Kassel, Kassel (2004).

[17] P. Koval, S. Fritzsche and A. Surzhykov, *J. Phys. B: At. Mol. Opt. Phys.* **37**, 375 (2004).
P. Koval, S. Fritzsche and A. Surzhykov, *J. Phys. B: At. Mol. Opt. Phys.* **36**, 873 (2003).

[18] P. Koval and S. Fritzsche, *Comput. Phys. Commun.* **152**, 191 (2003).

[19] E. J. McGuire, *Phys. Rev. A* **23**, 186 (1981).

Appendix A

System of Units

Mostly in physics, the basis equations are written with all physical constants in a given physical system of units for mass, length, time, and charge. This base units is also known as *International System of Units (SI)* or rationalized *M.K.S.A units*. However, many authors working with microscopic phenomena prefer to use *Gaussian units*, *Heaviside-Lorentz* (H-L) *units*, etc. It is common and useful to use *dimensionless units* in derivations and problem solving. This serves to save time and make equations more transparent by eliminating the physical constants which tend to clutter the equations. In contrast to the popular belief, once you have developed the knack of placing the constant back into the final answers, dimensional analysis is still possible. After a change of units, the new value for a physical quantity is obtained from the value in the old units by multiplication with a *conversion factor*.

A.1 Nonrelativistic atomic units

In the nonrelativistic atomic phenomena, for instance, the system of units for the hydrogen atom in the Bohr model, usually called *atomic units (a.u.)* are often used. We recall below some important physical constants in terms of SI base units and their conversion factors [1] .

[1] Peter J. Mohr and Barry N. Taylor, CODATA Recommended values of the Fundamental Physical Constants, *Journal of Physical and Chemical Reference Data*, (2002); Peter J. Mohr and Barry N. Taylor, Rev. Mod. Phys. **77**, 1 (2005)

A.1.1 Physical quantities in atomic units

Quantity	Conversion factor or Unit	Meaning	Values in SI units
Angular moment	$\hbar = h/2\pi$	Reduced Planck constant	1.05457×10^{-34} J.s
Mass	m	Electron rest mass	9.10938×10^{-31} kg
Charge	e	Elementary charge	1.60218×10^{-19} C

We can combine the physical constants $\hbar$ and c (the speed of light in vacuum) into a dimensionless quantity,

$$\alpha = \frac{e^2}{4\pi\epsilon_0\hbar c} = \frac{1}{137.03599911}$$

which is called Sommerfeld's fine structure constant. Because this quantity is dimensionless, it has the same numerical value with respect to all systems of units. The below physical constants, the electric permittivity ϵ_0 and magnetic permeability μ_0 of vacuum

$$\epsilon_0 = 8.85419 \times 10^{-12} \text{ F/m} \qquad \mu_0 = 4\pi \times 10^{-7} \text{ H/m}$$

are useful. In summary, the basis of the atomic units has

$$\hbar = m = e = 1 \text{ a.u.} \qquad \text{and} \qquad \alpha = 1/c.$$

We obtain immediately that $c = 137.03599911$ a.u. is the velocity of light in atomic units. In the Gaussian system, $4\pi\epsilon_0 = 1$, while $\mu_0\epsilon_0 c^2 = 1$ in the SI system. This value is often combined with atomic units for the sake of simplicity. From these values, we can therefore compute the value of the following physical constant in atomic units.

A.1.2 Other physical quantities in atomic units

Quantity	Conversion factor or Unit	Meaning	Values in SI units
Length	$a_0 = 4\pi\epsilon_0\hbar^2/me^2$	Bohr radius	5.29177×10^{-11} m
Velocity	$v_0 = a_0 E_h/\hbar$	Bohr velocity	2.18769×10^{6} m/s
Time	$\tau_0 = a_0/v_0 = \hbar/E_h$	Time to complete a Bohr orbit	2.41888×10^{-17} s
Hartree Energy	$E_h = e^2/4\pi\epsilon_0 a_0$	Twice the ionization energy	4.35974×10^{-18} J 27.2114 eV
Electric field	$\mathcal{E}_a = E_h/ea_0$	Field felt by electron on a_0	5.14221×10^{11} V/m
Intensity	$I_a = E_h^2/8\pi\hbar\alpha a_0^2$	Intensity of radiation corresponding to $\mathcal{E}_a$	3.5095×10^{20} W/m^2

Another often used energy units in atomic physics are the electron volt, 1 eV $= 1.60218 \times 10^{-19}$ J approximately and the Rydberg constant $hcR_\infty = E_h/2$.

A.2 Relativistic Atomic units

We introduce here the relativistic counterparts *(r.a.u.)* of the above atomic units that should be equally useful in relativistic atomic physics. With these units, the basis of our *relativistic atomic units* has

$$\hbar = m = c = 1 \qquad \text{and} \qquad \alpha = e^2.$$

Remark that, the fine structure constant α play a key role as it serves as conversion factor between the two system of units.

A.2.1 Some physical units in relativistic atomic units

Quantity	Scaling factor between *r.a.u.* and *a.u.*	Meaning	Values in SI units
Length	$\tilde{a}_0 = \alpha a_0$	Compton wavelength	3.86159×10^{-13} m
Velocity	c	Speed of light in vacuum	2.99792×10^{8} m/s
Time	$\tilde{\tau}_0 = \alpha^2 \tau_0$	Time to complete an orbit of radius $\tilde{a}_0$	1.288089×10^{-21} s
Energy	$\tilde{E}_h = E_h/\alpha^2$	Electron rest mass energy	0.818710×10^{-13} J 0.5109989 MeV
Electric field	$\tilde{\mathcal{E}}_a = \mathcal{E}_a/\alpha^3$	Field felt by electron on $\tilde{a}_0$	1.323286×10^{18} V/m
Intensity	$\tilde{I}_a = I_a/\alpha^6$	Intensity of radiation corresponding to $\mathcal{E}_a$	2.324057×10^{33} W/m^2

We stress out that, the conventional *relativistic units (r.u.)* also known as *natural units (n.u.)* differ from our relativistic atomic units in the sense that mass is measured as rest energy. Thus

$$\hbar = c = 1 \qquad \text{and} \qquad \alpha = e^2.$$

Appendix B

The Time-Independent Schrödinger Equation in Momentum Space

This Appendix summarizes the solutions of the one-electron nonrelativistic Schrödinger equation for the Coulomb potential. The spectrum of the hydrogen atom is a part of basic teachings in atomic physics. Thus it was the subject of accurate analytical developments that are unnecessary to recall in this context. The following paragraphs are justified by the simple fact that we are committed to the description of this reference system in atomic physics in the momentum space rather than the position space. We recall the nature of the problem and the tool used to solve it. We are making these reminders of structure for showing how the approximation made is incorrect to describe properly the Coulomb continuum states.

B.1 The generalized eigenvalue problems

B.1.1 Configuration space

The concept of the wave function has been introduced in quantum mechanics to describe the properties of a physical system, and we saw that in the position representation the wave function Ψ of a particle is a function of its space coordinates $\mathbf{r}$ and of the time t. Clearly, in order to make progress we need a method of determining wave functions systematically. The well-known celebrated *time-dependent Schrödinger wave equation* for a particle moving in a potential, which was proposed by E. Schrödinger in 1926 reads in atomic units

$$\mathrm{i}\frac{\partial}{\partial t}\Psi(\mathbf{r},t) = H\Psi(\mathbf{r},t) \qquad H = -\frac{1}{2}\boldsymbol{\nabla}^2 + V(\mathbf{r},t), \tag{B.1}$$

where the Hamiltonian operator H of the particle is composed by the kinetic energy operator and the potential energy operator $V(\mathbf{r},t)$. Let us now consider the particular case such that the potential energy V of the particle does not depend on the time. The Hamiltonian operator $H=-(1/2)\boldsymbol{\nabla}^2+V(\mathbf{r})$ is then also time-independent, and the time-dependent Schrödinger equation (B.1) simplifies considerably. Indeed, we easily show that it admits particular solutions of the form $\Psi(\mathbf{r},t)=\psi(\mathbf{r})\exp(-\mathrm{i}Et)$ which are products of functions of $\mathbf{r}$ and t separately. The general solution of (B.1) can be expressed as a sum of such separable solutions. Equation

$$\left(-\frac{1}{2}\boldsymbol{\nabla}^2+V(\mathbf{r})\right)\psi(\mathbf{r})=E\psi(\mathbf{r}), \tag{B.2}$$

which must be satisfied by the function $\psi(\mathbf{r})$, is called the *time-independent Schrödinger equation*. In contrast to the time-dependent Schrödinger equation (B.1), which describes the time development of the wave function $\Psi(\mathbf{r},t)$, we straightforward see that equation (B.2) can be written in the form of the eigenvalue equation

$$H\psi(\mathbf{r})=E\psi(\mathbf{r}), \tag{B.3}$$

where it is understood that the energy eigenfunctions $\psi(\mathbf{r})$ correspond to the energy eigenvalues E. When we wish to emphasize this fact we shall add a subscript E to the eigenfunction $\psi(\mathbf{r})$, thus writing $\psi_E(\mathbf{r})\equiv\psi(\mathbf{r})$. This spatial factor $\psi(\mathbf{r})$ is called a *time-independent Schrödinger wave function*. We are interested in the equivalent form of the latter in momentum space.

B.1.2 Momentum space

In quantum mechanics, one defined the momentum space wave function $\Phi(\mathbf{p},t)$ of a particle as the Fourier transform of its configuration space wave function $\Psi(\mathbf{r},t)$, and we saw that $\Phi(\mathbf{p},t)$ plays in momentum space the role assigned to the wave function $\Psi(\mathbf{r},t)$ in configuration space. Since the configuration space wave function $\Psi(\mathbf{r},t)$ satisfies the time-dependent Schrödinger equation (B.1), we can readily obtain the corresponding time-dependent Schrödinger equation for the momentum space wave function $\Phi(\mathbf{p},t)$. We can transform (B.1) in momentum space by writing first

$$\mathrm{i}\frac{\partial}{\partial t}\left[\int \mathrm{e}^{-\mathrm{i}\mathbf{p}\cdot\mathbf{r}}\Psi(\mathbf{r},t)\mathrm{d}\mathbf{r}\right]=\int \mathrm{e}^{-\mathrm{i}\mathbf{p}\cdot\mathbf{r}}\left[\frac{\mathbf{p}^2}{2}+V(\mathbf{r},t)\right]\Psi(\mathbf{r},t)\mathrm{d}\mathbf{r}, \tag{B.4}$$

which, upon using $\Phi(\mathbf{p},t)=\int \mathrm{e}^{-\mathrm{i}\mathbf{p}\cdot\mathbf{r}}\Psi(\mathbf{r},t)\mathrm{d}\mathbf{r}$, and the convolution theorem for Fourier transforms, becomes

$$\mathrm{i}\frac{\partial}{\partial t}\Phi(\mathbf{p},t)=\frac{\mathbf{p}^2}{2}\Phi(\mathbf{p},t)+\int\frac{\mathrm{d}\mathbf{p}'}{(2\pi)^3}V(\mathbf{p}-\mathbf{p}',t)\Phi(\mathbf{p}',t), \tag{B.5}$$

where

$$V(\mathbf{p}-\mathbf{p}',t)=\int \mathrm{e}^{-\mathrm{i}(\mathbf{p}-\mathbf{p}')\cdot\mathbf{r}}V(\mathbf{r},t)\mathrm{d}\mathbf{r}. \tag{B.6}$$

Equation (B.5) is the *time-dependent Schrödinger equation for the momentum space wave function*. Because of the integral on the right this equation is generally more complicated than the corresponding time-dependent Schrödinger equation (B.1) in configuration space. This explains why the configuration space Schrödinger equation is used in most applications. If the potential energy V is time-independent, the time-dependent Schrödinger equation (B.5) admits particular solutions of the separable form $\Phi(\mathbf{p},t)=\phi(\mathbf{p})\exp(-\mathrm{i}Et)$ corresponding to precise values of the total energy E. These separable solutions are clearly the Fourier transforms of the stationary states $\Psi(\mathbf{r},t)=\psi(\mathbf{r})\exp(-\mathrm{i}Et)$ given above, so that the time-independent wave functions $\psi(\mathbf{r})$ and $\phi(\mathbf{p})$ are related by the Fourier transformation

$$\phi(\mathbf{p})=\int \mathrm{e}^{-\mathrm{i}\mathbf{p}\cdot\mathbf{r}}\psi(\mathbf{r})\mathrm{d}\mathbf{r}, \tag{B.7}$$

$$\psi(\mathbf{r})=\int \frac{\mathrm{d}\mathbf{p}}{(2\pi)^3}\mathrm{e}^{\mathrm{i}\mathbf{p}\cdot\mathbf{r}}\phi(\mathbf{p}). \tag{B.8}$$

Upon substitution of equations (B.7) and (B.8) into the Schrödinger equation (B.5), we find that the wave function $\phi(\mathbf{p})$ must satisfy the *generalized time-independent Schrödinger eigenvalue equation*

$$\frac{\mathbf{p}^2}{2}\phi(\mathbf{p})+\int \frac{\mathrm{d}\mathbf{p}'}{(2\pi)^3}V(\mathbf{p}-\mathbf{p}')\phi(\mathbf{p}')=E\phi(\mathbf{p}), \tag{B.9}$$

where

$$V(\mathbf{p}-\mathbf{p}')=\int \mathrm{e}^{-\mathrm{i}(\mathbf{p}-\mathbf{p}')\cdot\mathbf{r}}V(\mathbf{r})\mathrm{d}\mathbf{r}. \tag{B.10}$$

The equation (B.9) is an *integral equation*, and hence is generally more difficult to solve than the corresponding time-independent Schrödinger equation (B.2) in configuration space.

B.2 Analytical solutions to stationary states

r-representation

Let us now consider the nonrelativistic motion of a spinless particle in a central potential, *e.g.* a hydrogen-like ions containing a nuclear charge Z and an electron interacting by means of the Coulomb potential $V(\mathbf{r})=V(r)=-Z/r$. Since $V(r)$ is spherically symmetric, we have seen that the full eigenfunctions of the discrete spectrum for hydrogenic atoms may be written as

$$\psi_{nlm}(\mathbf{r})=R_{nl}(r)Y_{lm}(\theta_r,\phi_r) \tag{B.11}$$

where the spherical harmonics $Y_{lm}(\theta_r, \phi_r)$[1] ($-l \leq m \leq +l$, l denotes the orbital angular momentum quantum number, m the magnetic quantum number) provide the angular part of the wave functions and $R_{nl}(r)$ ($n \geq l+1$ represents the principal quantum number) are solutions of the radial equation

$$\left(\frac{\mathrm{d}^2}{\mathrm{d}r^2} + \frac{2}{r}\frac{\mathrm{d}}{\mathrm{d}r} - \frac{l(l+1)}{r^2} + 2(E - V(r))\right) R_{nl}(r) = 0. \tag{B.12}$$

The properly normalized bound state solutions corresponding to energy eigenvalues $E_n = -Z^2/2n^2$ are

$$R_{nl}(r) = \frac{2Z}{n^2}\sqrt{\frac{Z(n-l-1)!}{(n+l)!}}\left(\frac{2Zr}{n}\right)^l \exp(-Zr/n) L_{n-l-1}^{(2l+1)}(2Zr/n), \tag{B.13}$$

where $L_{n-l-1}^{(2l+1)}$ is the generalized Laguerre polynomial[1]. The complete normalized hydrogenic wave functions corresponding to the first two shells K ($1s$) and L ($2s2p$) are given by

$$\psi_{1s}(\mathbf{r}) = 2Z^{3/2}\exp(-Zr)Y_{00}(\theta_r, \phi_r), \tag{B.14}$$

$$\psi_{2s}(\mathbf{r}) = (Z/2)^{3/2}(2 - Zr)\exp(-Zr/2)Y_{00}(\theta_r, \phi_r), \tag{B.15}$$

$$\psi_{2p,m}(\mathbf{r}) = \frac{1}{\sqrt{3}}(Z/2)^{3/2} Zr \exp(-Zr/2)Y_{1m}(\theta_r, \phi_r). \tag{B.16}$$

p-representation

The integral form of equation (B.9) is due to non-locality of the potential in the momentum space. A condition of linearization of equation (B.9) would be to impose that its kernel (the potential) tends "in the sense of distributions" towards the Dirac delta function: $V(\mathbf{p}-\mathbf{p}') = V(\mathbf{p})\delta(\mathbf{p}-\mathbf{p}')$. In atomic physics, and particularly in the description of a hydrogenic atom, the Fourier transforms of the potentials commonly used do not satisfy this condition. The Coulomb potential $V(r)$ describing exactly the hydrogenic system is no exception to the rule. Indeed its Fourier transform reads:

$$V(\mid \mathbf{p} - \mathbf{p}' \mid) = -\frac{4\pi Z}{(\mathbf{p} - \mathbf{p}')^2}. \tag{B.17}$$

The nature of the central potential $V(r)$ in the representation of positions implies that its Fourier transform depends only on modulus of momentum transfer $q = \mid \mathbf{p} - \mathbf{p}' \mid$. It is, of this fact, very simple to prove that the dual

[1] A. R. Edmonds, *Angular Momentum in Quantum Mechanics* (Princeton University Press, Princeton, 1960); I. S. Gradshteyn and I. M. Ryzhik, *Table of Integrals, Series and Products* 7th ed. (Academic Press, Boston, 2007)

solution $\phi(\mathbf{p})$ can also be written with the spherical coordinates (p, θ_p, ϕ_p) corresponding to the momentum $\mathbf{p}$:

$$\phi_{nlm}(\mathbf{p}) = F_{nl}(p) Y_{lm}(\theta_p, \phi_p), \tag{B.18}$$

where the properly normalized radial functions associated with E_n are[2]

$$\begin{aligned} F_{nl}(p) = 2^{2l+2} n^2 l! \sqrt{\frac{2(2\pi)^3 (n-l-1)!}{\pi Z^3 (n+l)!}} \left(\frac{np}{Z}\right)^l \\ \times \frac{Z^{2l+4}}{(n^2p^2+Z^2)^{l+2}} \mathbb{C}_{n-l-1}^{l+1} \left(\frac{n^2p^2-Z^2}{n^2p^2+Z^2}\right), \end{aligned} \tag{B.19}$$

where $\mathbb{C}_{n-l-1}^{l+1}$ denotes the Gegenbauer polynomial[2]. The corresponding K $(1s)$ and L $(2s2p)$ complete normalized eigenfunctions in momentum space are

$$\phi_{1s}(\mathbf{p}) = \frac{16\pi\sqrt{Z^5}}{(p^2+Z^2)^2} Y_{00}(\theta_p, \phi_p), \tag{B.20}$$

$$\phi_{2s}(\mathbf{p}) = \frac{64\pi\sqrt{2Z^5}(4p^2-Z^2)}{(4p^2+Z^2)^3} Y_{00}(\theta_p, \phi_p), \tag{B.21}$$

$$\phi_{2p,m}(\mathbf{p}) = 128\pi\sqrt{\frac{8}{3Z^3}} \frac{Z^5 p}{(4p^2+Z^2)^3} Y_{1m}(\theta_p, \phi_p), \tag{B.22}$$

which can also straightforwardly be inferred from equations (B.14)-(B.16) by the virtue of (B.7). The F_{nl} satisfies the second kind homogeneous integral equation of Fredholm

$$\left(\frac{\mathbf{p}^2}{2} - E\right) F_{nl}(p) = \frac{Z}{\pi p} \int_0^\infty \mathrm{Q}_l \left(\frac{p^2-p'^2}{2pp'}\right) F_{nl}(p') p' \mathrm{d}p', \tag{B.23}$$

which can be obtained by inserting (B.17) and (B.18) in (B.9). Here Q_l is the Legendre function of the second kind, which is clearly defined and studied in Armelle de Bohan's thesis[3].

B.3 The continuum spectrum and scattering theory

The continuum spectrum of a hydrogenic system is a stationary scattering state by the attractive Coulomb potential, it almost a Lapallisade... This means, however, that we can treat the problem of the determination of these states in the context of scattering theory.

[2] R. Nyden Hill, *Hydrogenic Wave Functions in Springer Handbook of Atomic, Molecular and Optical Physics* ed. Gordon W. F. Drake (Springer, 2006), Part A, p 153.

[3] Armelle de Bohan, *PhD Thesis*, Université Catholique de Louvain, Louvain-la-Neuve, Belgium, 2001.

B.3.1 The continuum states $\varphi_k^{\pm}(\mathbf{p})$

The *Lippmann-Schwinger* equation allows the determination of the continuum eigenstates associated with our separable Coulomb potential model. This equation can be obtained by the following method[4] : We write the total Hamiltonian of the atomic system as

$$H = H_0 + V, \tag{B.24}$$

where H_0 stands for the kinetic energy operator and V the operator associated with Coulomb potential. The general theory is based on the fact that the free-Hamiltonian H_0 possesses a continuum energy spectrum $E = k^2/2$ and a well-known eigenstates basis - the plane waves $\Phi_k^0(\mathbf{r})$ "normalized" in such a way that $\Phi_k^0(\mathbf{r}) = (2\pi)^{-3/2} \exp(\mathrm{i}\mathbf{k}\cdot\mathbf{r})$. More generally, one uses Dirac's bra and ket convention $\mid \mathbf{k}\rangle \equiv\mid \Phi_k^0\rangle$, $\Phi_k^0(\mathbf{r}) \equiv \langle \mathbf{r} \mid \mathbf{k}\rangle$. We then have the orthogonality and the closure relations

$$\begin{aligned} \langle \Phi_{k'}^0 \mid \Phi_k^0\rangle \equiv \langle \mathbf{k}' \mid \mathbf{k}\rangle &= \delta(\mathbf{k}-\mathbf{k}'), \\ \int \mathrm{d}\mathbf{k} \mid \mathbf{k}\rangle\langle \mathbf{k} \mid &= \mathcal{I}. \end{aligned}$$

We note that with this choice of "normalization" the orthogonality and closure relations are very simple in momentum (or rather wave vector) space. Therefore in the momentum space, the following relations have been chosen

Normalization

$$\langle \mathbf{p} \mid \Phi_k^0\rangle = (2\pi)^{3/2}\delta(\mathbf{p}-\mathbf{k}), \tag{B.25}$$

and

Closure relation

$$\int \frac{\mathrm{d}\mathbf{p}}{(2\pi)^3} \mid \mathbf{p}\rangle\langle \mathbf{p} \mid = \mathcal{I}, \tag{B.26}$$

where $\mathcal{I}$ stands for unit operator.

Lippmann-Schwinger integral equation

Let us denote by E and $\mid \varphi_k\rangle$ the energy eigenvalue and eigenvector of H. They are solutions to the eigenvalue equation

$$(E - H_0 - V) \mid \varphi_k\rangle = 0. \tag{B.27}$$

[4]The *Lippmann-Schwinger* equation sketched is not strictly speaking rigorous, because it holds only for short-range potential and is no longer valid in the case of long-range pure Coulomb potential.

If one consider a particular eigenstate $\mid \Phi_k^0\rangle$ of H_0 associated with energy E, one has $(E - H_0) \mid \Phi_k^0\rangle = 0$, and it is then possible to write $\mid \varphi_k\rangle = \mid \Phi_k^0\rangle + \mid \chi_k\rangle$ such that $\mid \chi_k\rangle$ satisfies the equation

$$(E - H_0) \mid \chi_k\rangle = V \mid \varphi_k\rangle. \tag{B.28}$$

The solution to equation (B.28) is easily determined by multiplying both side of this equation by the inverse operator $(E - H_0)^{-1}$ in which we have inserted the prescription $\pm \mathrm{i}\epsilon$ to account correctly the singularity of this operator. We thus obtained two possible determinations

$$\mid \chi_k^{\pm}\rangle = \frac{1}{(E - H_0 \pm \mathrm{i}\epsilon)} V \mid \varphi_k^{\pm}\rangle. \tag{B.29}$$

Now, according to the closure relation (B.26) and the fact that $\chi_k^{\pm}(\mathbf{p}) = \langle \mathbf{p} \mid \chi_k^{\pm}\rangle$, we find that the continuum states must satisfy the Lippmann-Schwinger integral equation[5]

$$\varphi_k^{\pm}(\mathbf{p}) = (2\pi)^{3/2}\delta(\mathbf{p} - \mathbf{k}) + \chi_k^{\pm}(\mathbf{p}), \tag{B.30}$$

$$\chi_k^{\pm}(\mathbf{p}) = \frac{2}{(k \pm \mathrm{i}\epsilon)^2 - p^2} \int \frac{\mathrm{d}\mathbf{p}'}{(2\pi)^3} V(\mathbf{p} - \mathbf{p}')\varphi_k^{\pm}(\mathbf{p}'). \tag{B.31}$$

It is worth noting that, each prescription $(\pm)$ is associated to a complete basis set - if one adds the discrete spectrum of eigenstates of H. Choosing the positive prescription corresponds to choose a set of *outgoing* waves. In what follows below we restrict ourselves to this choice. On the other hand, for the Coulombian potential, Guth *et al.*[6] have determined exact expression of Coulombian wave in momentum space, by Fourier transformation of the spatial representation of this latter. They have obtained the following relation that is to be understand in the sense of distributions:

$$\varphi_k^{+}(\mathbf{p}) = -\frac{1}{2\pi^2} \lim_{\epsilon \to 0} \frac{\mathrm{d}}{\mathrm{d}\epsilon} \left\{ \frac{\left[p^2 - (k + \mathrm{i}\epsilon)^2\right]^{-\mathrm{i}Z/k}}{\left[(\mathbf{p} - \mathbf{k})^2 + \epsilon^2\right]^{1-\mathrm{i}Z/k}} \right\}. \tag{B.32}$$

It is essential to recall that, a more comprehensive approach based on group theory allows to obtain the eigenstates of discrete and continuous spectra of hydrogen[7] Also, it is interesting to note[8] that the equivalence between equations (B.30), (B.31) and (B.32) can not be established exactly in the case of

[5] B. A. Lippmann and J. Schwinger, *Phys. Rev.* **79**, 469 (1950); H. A. Bethe and E. E. Salpeter, *Quantum Mechanics of One-and Two-Electron Atoms* (Springer-Verlag, 1957).

[6] E. Guth and C. J. Mullin, *Phys. Rev.* **83**, 667 (1951).

[7] J.-P. Antoine, *Ann. Soc. Sc. Bruxelles* **80 II**, 169 (1966).

[8] J. C. Y. Chen and A. C. Chen, *Adv. At. Mol. Phys.* **8**, 71 (1972); J. D. Dollard, *J. Maths. Phys.* **5**, 729 (1964).

the Coulomb potential due to the infinite range of this latter (in configuration space) which is not compatible with the use of the incident plane wave as scattering asymptotic state (and hence with approach of Lippmann and Schwinger). This ambiguity has been lifted by Dollard[8] by defining the correct asymptotic Hamiltonian in the Coulomb case that does not coincide with the free Hamiltonian $\mathbf{p}^2/2$. The asymptotic states are plane waves "distorted" by a logarithmic Coulomb phase.

This remark is important compared to the analysis of the strong field approximation[3]. Indeed, equation (B.31) corresponds to the expression used by M. Lewenstein to define the continuum states. The asymptotic behavior attributed to these states is defined within the meaning of Lippmann and Schwinger, and no to the correct sense proposed by Dollard. Nevertheless, the equivalence between plane wave and plane wave "distorted" partially exists within the approximation $Z/k \ll 1$[5] which allows to extract the Dirac delta function $\delta(\mathbf{p}-\mathbf{k})$ from equation (B.32). We can conclude, according to these reminders, that this expression is only valid in the approximation of great moments for the pure Coulomb potential. The extraction of the plane wave, for low moments, is strictly speaking not possible for the continuum states of hydrogen.

B.3.2 One-state model potential

We now focus our attention on the simple case for which our separable Coulomb potential contains only the ground state $\mid 1s\rangle$. We perform the substitution below for the Coulomb kernel in equation (B.31)

$$V(\mathbf{p}-\mathbf{p}') \simeq -v_1(\mathbf{p})v_1(\mathbf{p}') \qquad v_1(\mathbf{p}) = \frac{4\sqrt{\pi}}{p^2+1}. \tag{B.33}$$

From this result and equation (B.30), we see that the continuum wave function $\varphi_k^+(\mathbf{p})$ reduces to

$$\varphi_k^+(\mathbf{p}) = (2\pi)^{3/2}\delta(\mathbf{p}-\mathbf{k}) - \frac{2}{(k+\mathrm{i}\epsilon)^2-p^2}v_1(\mathbf{p})\tilde{C}_1^+(\mathbf{k}), \tag{B.34}$$

$$C_1^+(\mathbf{k}) = \int \frac{\mathrm{d}\mathbf{p}'}{(2\pi)^3}v_1(\mathbf{p}')\varphi_k^+(\mathbf{p}'), \qquad \tilde{C}_1^+(\mathbf{k}) = \frac{1}{(2\pi)^{3/2}}C_1^+(\mathbf{k}). \tag{B.35}$$

Inserting (B.34) inside equation (B.35) and upon integration, we find the coefficient

$$C_1^+(\mathbf{k}) = \frac{v_1(\mathbf{k})}{\tilde{b}_{11}(k)} \qquad \tilde{b}_{11}(k) = 1 + \frac{4}{(k+\mathrm{i})^2}. \tag{B.36}$$

B.3.3 Two-states model potential

As a second interesting example, let us consider the case for which our separable Coulomb potential supports the ground state and the first excited state $\mid 1s2s\rangle$.

As in the precedent case, we perform

$$V(\mathbf{p}-\mathbf{p}') \simeq -\left[v_1(\mathbf{p})v_1(\mathbf{p}') + v_2(\mathbf{p})v_2(\mathbf{p}')\right], \tag{B.37}$$

where $v_1(\mathbf{p})$ and $v_2(\mathbf{p})$ are the well-known components given in Chapter 3.

$$v_1(\mathbf{p}) = \frac{4\sqrt{\pi}}{p^2+1}\tilde{a}_{22} - \frac{4\sqrt{2\pi}(4p^2-1)}{(4p^2+1)^2}\tilde{a}_{12}, \tag{B.38}$$

$$v_2(\mathbf{p}) = -\frac{4\sqrt{\pi}}{p^2+1}\tilde{a}_{12} + \frac{4\sqrt{2\pi}(4p^2-1)}{(4p^2+1)^2}\tilde{a}_{11}. \tag{B.39}$$

Putting back equation (B.37) into equation (B.30) yields the continuum wave function

$$\varphi_k^+(\mathbf{p}) = (2\pi)^{3/2}\delta(\mathbf{p}-\mathbf{k}) - \frac{2}{(k+\mathrm{i}\epsilon)^2-p^2}\left[v_1(\mathbf{p})\tilde{C}_1^+(\mathbf{k}) + v_2(\mathbf{p})\tilde{C}_2^+(\mathbf{k})\right] \tag{B.40}$$

$$C_j^+(\mathbf{k}) = \int \frac{\mathrm{d}\mathbf{p}'}{(2\pi)^3} v_j(\mathbf{p}')\varphi_k^+(\mathbf{p}'), j=1,2. \qquad \tilde{C}_j^+(\mathbf{k}) = \frac{1}{(2\pi)^{3/2}}C_j^+(\mathbf{k}). \tag{B.41}$$

In the light of these implicit equations, one obtains after somewhat calculations the coefficients

$$C_1^+(\mathbf{k}) = \frac{1}{\widetilde{\Delta}}\left(\tilde{b}_{22}(k)v_1(\mathbf{k}) - \tilde{b}_{12}(k)v_2(\mathbf{k})\right), \tag{B.42}$$

$$C_2^+(\mathbf{k}) = \frac{1}{\widetilde{\Delta}}\left(-\tilde{b}_{12}(k)v_1(\mathbf{k}) + \tilde{b}_{11}(k)v_2(\mathbf{k})\right), \tag{B.43}$$

with $\widetilde{\Delta} = \tilde{b}_{11}(k)\tilde{b}_{22}(k) - \tilde{b}_{12}^2(k)$ and

$$\tilde{b}_{11}(k) = 1 + 4\tilde{a}_{22}^2\frac{1}{(k+\mathrm{i})^2} + 2\tilde{a}_{12}^2\frac{4k^2-1}{(2k+\mathrm{i})^4} - \frac{16\sqrt{2}}{9}\tilde{a}_{12}\tilde{a}_{22}\frac{4k-\mathrm{i}}{(k+\mathrm{i})(2k+\mathrm{i})^2},$$

$$\tilde{b}_{12}(k) = -4\tilde{a}_{12}\tilde{a}_{22}\frac{1}{(k+\mathrm{i})^2} - 2\tilde{a}_{12}\tilde{a}_{11}\frac{4k^2-1}{(2k+\mathrm{i})^4} + \frac{8\sqrt{2}}{9}\left(\tilde{a}_{11}\tilde{a}_{22} + \tilde{a}_{12}^2\right) \times \frac{4k-\mathrm{i}}{(k+\mathrm{i})(2k+\mathrm{i})^2},$$

$$\tilde{b}_{22}(k) = 1 + 4\tilde{a}_{12}^2\frac{1}{(k+\mathrm{i})^2} + 2\tilde{a}_{11}^2\frac{4k^2-1}{(2k+\mathrm{i})^4} - \frac{16\sqrt{2}}{9}\tilde{a}_{11}\tilde{a}_{12}\frac{4k-\mathrm{i}}{(k+\mathrm{i})(2k+\mathrm{i})^2}.$$

B.3.4 Three-states model potential

In the remaining subsection of this Appendix we shall deal with the case for which our Coulomb potential analogous has additional $2p$-excited state, *e.g.* $|\, 1s2s2p\rangle$. The foregoing analysis can be extended in this more realistic case.

In the same manner as in the previous cases, we easily decompose the Coulomb potential in the form

$$V(\mathbf{p}-\mathbf{p}') \simeq -\left[v_1(\mathbf{p})v_1(\mathbf{p}') + v_2(\mathbf{p})v_2(\mathbf{p}') + \frac{4\pi}{3}pp'v_3(p)v_3(p') \times \sum_{m=-1}^{+1} Y_{1m}(\theta_p,\phi_p)Y_{1m}^*(\theta_{p'},\phi_{p'})\right], \tag{B.44}$$

$$v_3(p) = \frac{16\sqrt{8\pi}}{(4p^2+1)^2}. \tag{B.45}$$

Using this expression in (B.30) and after some tremendous calculations, the continuous wave function can be put in the form

$$\varphi_k^+(\mathbf{p}) = (2\pi)^{3/2}\delta(\mathbf{p}-\mathbf{k}) - \frac{2}{(k+\mathrm{i}\epsilon)^2-p^2}\left[v_1(\mathbf{p})\tilde{C}_1^+(\mathbf{k}) + v_2(\mathbf{p})\tilde{C}_2^+(\mathbf{k}) + v_3(p)(\mathbf{p}\cdot\hat{\boldsymbol{e}})\tilde{C}_3^+(\mathbf{k})\right], \tag{B.46}$$

where $\hat{\boldsymbol{e}}$ denotes the unit vector associated to the laser polarization axis and the new coefficient $\tilde{C}_3^+(\mathbf{k})$ writes

$$C_3^+(\mathbf{k}) = \int \frac{\mathrm{d}\mathbf{p}'}{(2\pi)^3}v_3(\mathbf{p}')(\mathbf{p}'\cdot\hat{\boldsymbol{e}})\varphi_k^+(\mathbf{p}'), \qquad \tilde{C}_3^+(\mathbf{k}) = \frac{1}{(2\pi)^{3/2}}C_3^+(\mathbf{k}). \tag{B.47}$$

We focus our attention here only on the new coefficients involved in this 3-states model. The previous coefficients $\tilde{b}_{11}(k)$, $\tilde{b}_{12}(k)$, $\tilde{b}_{22}(k)$, $C_j^+(\mathbf{k}), j=1,2$ are given above respectively in the 2-states model. Substituting (B.46) into (B.41), (B.47) and combining these three equations we find that

$$C_3^+(\mathbf{k}) = \frac{1}{\tilde{b}_{33}(k)}v_3(k)(\mathbf{k}\cdot\hat{\boldsymbol{e}}) \qquad \tilde{b}_{33}(k) = 1 + \frac{8}{3}\frac{4k^2-1+\mathrm{i}8k}{(2k+\mathrm{i})^4}, \tag{B.48}$$

and the remaining coefficients $\tilde{b}_{ij}(k)=0$. With the expressions (B.34), (B.40) and (B.46) at our disposal we are now ready to carry out the energy spectrum of ejected electron into the continuum.

Appendix C

The Numerical Methods for Volterra Integral Equations of the Second Kind

C.1 Definitions

In practice, few of the Volterra integral equations encountered in physics can be solved explicitly. Generally it is often necessary to resort to numerical methods to solve these integral equations. Among many alternatives available in the literature, we will pay attention here on the underlying ideas on which these methods are based. In order to bring out the essential ideas clearly and to avoid unnecessary complications, we consider the *nonlinear* equation

$$f(t) = g(t) + \int_0^t \mathrm{d}y K(t, y, f(y)), \qquad 0 \leq t \leq T, \tag{C.1}$$

under the conditions

1. $g(t)$ is a continuous function in $0 \leq t \leq T$,
2. the kernel $K(t, y, v)$ is continuous in $0 \leq y \leq t \leq T, -\infty < v < \infty$,
3. the kernel satisfies the Lipschitz condition

$$\mid K(t, y, v_1) - K(t, y, v_2) \mid \leq L \mid v_1 - v_2 \mid, \tag{C.2}$$

for all $0 \leq y \leq t \leq T$, and all v_1, v_2. L is a constant independent of y and t.

These conditions are sufficient to guarantee that (C.1) has a unique continuous solution on $0 \leq t \leq T$. The analysis of the numerical methods will make use of these assumptions, and strictly speaking, holds only when they are

satisfied. For certain types of kernels it may actually be necessary to modify the procedures, as we shall see below. However, additional smoothness conditions will be imposed in the subsequent analysis. The simplest and most completely understood Volterra equation is the *linear* equation of the second kind, obtained when the kernel $K(t, y, f(y))$ in (C.1) factorizes into two parts $K(t, y)f(y)$. It should be noted that although the analysis is presented only for the scalar equation (C.1), the generalization to a system of Volterra integral equations of the second kind follows immediately. We begin our discussion here by presenting a rather simple and intuitively reasonable quadrature methods for standard numerical integration techniques.

C.2 On the quadrature methods

In this part we give some basic techniques for the numerical evaluation of

$$I = \int_a^b \mathrm{d}t\phi(t), \tag{C.3}$$

where $\phi(t)$ is given either as a continuous differentiable function or discretely. It is always assumed that I exists and is finite. One requires good techniques to satisfy two important criteria: (i) the technique should give results of high accuracy (ii) the technique should require only a small number of function evaluations. A further desirable feature of a technique is that it should give some measure of the error in the computational result although this may not always be possible.

Let us briefly summarize the way in which the usual interpolatory integration rules are constructed. To evaluate (C.3) numerically, we first replace ϕ by some approximation $\widetilde{\phi}$, then compute

$$\tilde{I} = \int_a^b \mathrm{d}t\widetilde{\phi}(t). \tag{C.4}$$

The approximation $\widetilde{\phi}$ is chosen in such a way that the integral for $\tilde{I}$ can be evaluated explicitly. Usually $\widetilde{\phi}$ can be some piecewise polynomial approximation to ϕ. In the following, we only describe a general scheme which includes both the trapezoidal and Simpson's rule.
Giving an interval $[a, b]$, we subdivide it into n equal subintervals of width (step-length) h, using $a = t_0 < t_1 < t_2 \cdot \cdot < t_n = b, \quad t_i = a + ih$. In each subinterval we introduce a further subdivision, with points $t_i \leq t_{i0} \leq t_{i1} < \cdots < t_{im} \leq t_{i+1}$. Equation (C.3) can be rewritten as

$$\tilde{I} = \sum_{i=0}^{n-1} \int_{t_{im}}^{t_{(i+1)m}} \mathrm{d}t\widetilde{\phi}(t) = h \sum_{i=0}^{n-1} \int_0^m \mathrm{d}u\widetilde{\phi}(t_{im} + uh), \tag{C.5}$$

where we have made the ansatz $t = t_{im} + uh$ (u not necessarily integral). The function ϕ can be approximated by a polynomial of degree m in each subinterval $[t_i, t_{i+1}]$, using a m-point interpolatory quadrature formula on the points $t_{ij}, j = 0, \cdots, m$, with $t_{im} = t_i + imh$ and $t_{ij} = t_{im} + u_j h$. We write in this context

$$\begin{aligned}\widetilde{\phi}(t_{im} + uh) &= \sum_{j=0}^{m} \ell_{ij}(u)\phi(t_{im} + u_j h) + R_m(t_{im} + uh), \\ &= \sum_{j=0}^{m} \ell_{ij}(u)\phi(t_{im} + jh) + R_m(t_{im} + uh), \end{aligned} \tag{C.6}$$

because interpolation is made on the equally spaced abscissas, *i.e.* $u_j = j$, and where the ℓ_{ij} are the fundamental polynomials defined as

$$\begin{aligned}\ell_{ij}(u) &= \frac{\prod_m(u)}{(u - u_j)\prod'_m(u_j)} \\ &= \frac{(u - u_0)\cdots(u - u_{j-1})(u - u_{j+1})\cdots(u - u_m)}{(u_j - u_0)\cdots(u_j - u_{j-1})(u_j - u_{j+1})\cdots(u_j - u_m)}, \end{aligned} \tag{C.7}$$

and $\ell_{ij}(u_k) = \delta_{kj}$. $\mid R_m(t_{im}+uh) \mid \leq \frac{(b-a)^{m+1}}{(m+1)!} \max_{a\leq t\leq b} \mid \phi^{(m+1)}(t) \mid$ represents the remainder in Lagrange interpolation formula.

Inserting this into (C.5), we have immediately that

$$\tilde{I} = h \sum_{i=0}^{n-1} \sum_{j=0}^{m} \varpi_{ij}\phi(t_{im} + jh), \tag{C.8}$$

$$\varpi_{ij} = \int_0^m \ell_{ij}(u)\mathrm{d}u. \tag{C.9}$$

If the fundamental polynomials (C.7) are known, then the integration weights ϖ_{ij} can be found explicitly.

From equations (C.3) and (C.4) we immediately get that

$$\mid I - \tilde{I} \mid \leq (b - a) \max_{a\leq t\leq b} \mid \phi(t) - \widetilde{\phi}(t) \mid, \tag{C.10}$$

so that error bounds and orders of convergence for integration follow from standard results of approximation theory. Before going further, let give below the two well-known familiar cases:
a *piecewise linear approximation* (case of $m = 1$) to a smooth function ϕ, yields $\mid \phi(t) - \widetilde{\phi}(t) \mid = \mathrm{O}(h^2)$, so that the composite *extended trapezoidal rule* is of the second order

$$\tilde{I} = \frac{h}{2} \sum_{i=0}^{n-1} (\phi_i + \phi_{i+1}) - \frac{(b - a)}{12} h^2 \phi^{(2)}(\xi), \tag{C.11}$$

where we have set $\phi(t_i) = \phi_i$, $a \leq \xi \leq b$ and $\phi^{(2)}$ denotes de second derivative, and
the Simpson's rule, which is based on a *piecewise quadratic interpolation* (for $m = 2$) to a smooth function ϕ, is at least third order. This is well known for the standard Simpson's rule, where an $\mathrm{O}(h^3)$ approximation of the integrand yields an integration method whose order is four. The *extended Simpson's rule* writes

$$\tilde{I} = \frac{h}{3}\sum_{i=0}^{n-1}(\phi_{2i} + 4\phi_{2i+1} + \phi_{2i+2}) - \frac{(b-a)}{180}h^4\phi^{(4)}(\xi). \tag{C.12}$$

We stress out that, Simpson's rule can be applied only when n *is even.* For *odd* n some adjustment has to be made. One way is to apply the so-called *three-eighths rule* ($\frac{3}{8}$th-rule) over four adjacent points and the *extended Simpson's rule* over the rest of the interval. The *Simpson's* $\frac{3}{8}$ *rule* needs four points for basic rule,

$$\begin{aligned}\int_{t_{2i}}^{t_{2i+3}} \mathrm{d}t\widetilde{\phi}(t) &= \frac{3}{8}h\left(\phi_{2i} + 3\phi_{2i+1} + 3\phi_{2i+2} + \phi_{2i+3}\right) \\ &\quad - \frac{3}{80}h^5\phi^{(4)}(\xi), \quad t_{2i} \leq \xi \leq t_{2i+3}, \quad h = \frac{t_{2i+3} - t_{2i}}{3}.\end{aligned} \tag{C.13}$$

Therefore, the extended Simpson's rule in conjunction with Simpson's $\frac{3}{8}$ rule can be often exploited to calculate integral (C.3) in which $a = t_0 < t_1 < t_2 \cdots < t_{2n+1} = b$ is divided into two part $[t_0, t_{2n-2}] \bigcup [t_{2n-2}, t_{2n+1}]$. Thus

$$\begin{aligned}\tilde{I} &= \frac{h}{3}\sum_{i=0}^{n-2}(\phi_{2i} + 4\phi_{2i+1} + \phi_{2i+2}) - \frac{(n-1)}{90}h^5\phi^{(4)}(\xi_1) \\ &\quad + \frac{3}{8}h\left(\phi_{2n-2} + 3\phi_{2n-1} + 3\phi_{2n} + \phi_{2n+1}\right) - \frac{3}{80}h^5\phi^{(4)}(\xi_2),\end{aligned} \tag{C.14}$$

with $a < \xi_1 < t_{2n-2}$, $t_{2n-2} < \xi_2 < t_{2n+1}$, $h = (b-a)/(2n+1)$. There exist many types of quadratures clearly exposed in the specialized books in the literature [1] .

C.3 The multi-step methods

C.3.1 Extended trapezoidal's rule

Intuitively, one can compute an approximate solution to (C.1) by the following simple process. For a given stepsize $h > 0$, suppose that we know the solution

[1] M. Abramowitz and I. A. Stegun, eds. *Handbook of Mathematical Functions, NBS Applied Mathematical Series* (National Bureau of Standards, Washington DC, 1966); William H. Press *et al.*, *Numerical Recipes, The Art of Scientific Computing* (University Press, Cambridge, 1989)

at points $t_i = ih, i = 0, 1, 2, \cdots, n-1$. An approximate value F_n of $f(t_n)$ can then be computed by replacing the integral on the right side of (C.1) by a numerical integration rule using values of the integrand at t_i and solving the resulting equation for F_n. Since $F_0 = g(0)$, the approximate solution can be computed in this step-by-step fashion by

$$F_n = g(t_n) + \frac{h}{2}\left[K(t_n, t_0, F_0) + 2\sum_{i=1}^{n-1} K(t_n, t_i, F_i) + K(t_n, t_n, F_n)\right], \quad \text{(C.15)}$$

$n = 1, 2, 3, \cdots$. The unknown F_n is defined by (C.15) implicitly, but for sufficiently small h the equation has a unique solution, obtained by using some iterative technique to within a desired accuracy. In the linear case one solves it directly for F_n as

$$\left(1 - \frac{1}{2}hK(t_n, t_n)\right) F_n = g(t_n) + \frac{1}{2}h\left[K(t_n, t_0)F_0 + 2\sum_{i=1}^{n-1} K(t_n, t_i)F_i\right]. \quad \text{(C.16)}$$

The trapezoidal method is quite simple but the results are of relatively low accuracy. In view of the conjecture made in a book by Linz [2] -*that in general, if the integral in (C.1) is approximated by a numerical integration having a certain order of accuracy, then the approximate solution computed this way has the same order of accuracy*-then for more accurate methods better integration rules must be used.

C.3.2 Extended Simpson's rule

Because of the stepwise way of computing the solution, we must rely largely on integration rules with constant stepsize h. It is of course possible to vary the stepsize during the computation, for example, by some adaptive approach. Using an integration rule to replace the integral (C.1), we obtain the numerical equations

$$F_n = g(t_n) + h\sum_{i=0}^{n} \varpi_{ni} K(t_n, t_i, F_i), \quad n = r, r+1, ... \quad \text{(C.17)}$$

where r is some fixed integer. This equation has a unique solution for all sufficiently small h if the weigths ϖ_{ni} are uniformly bounded. Also note that equation (C.17) holds only for $n \geq r$. This reflects the fact that higher order integration rules require a minimum number of points. The values of

[2] P. Linz, *Analytical and numerical methods for Volterra equations* (SIAM, Philadelphia, 1985); W. Ledermann, *Handbook of applied mathematics Vol III: Numerical methods,* ed. R. F. Churchhouse (University College Cardiff, John Wiley and Sons (1981))

$F_1, F_2, ..., F_{r-1}$ cannot be obtained by (C.17) and they must be computed by some other methods. In the linear case, equation (C.17) reduces to

$$[1 - h\varpi_{nn}K(t_n, t_n)]\, F_n = g(t_n) + h\sum_{i=0}^{n-1} \varpi_{ni}K(t_n, t_i)F_i. \tag{C.18}$$

Within the restriction of constant stepsize we have the choice of using either Newton-Cotes or Gregory type integration rules. The Newton-Cotes type formulae introduce a slight complication, since these rules involve some restriction on the number of points. For example, we have seen that Simpson's *rule* can be applied only when n is even. For odd n some adjustment has to be made. One way is to apply the so-called *three-eighths rule* over four adjacent points and the Simpson's rule over the rest of the interval. In the case where the three-eighths rule is used on the points t_0, t_1, t_2, t_3, the process is known as *Simpson's method 1*, whereas the second form, dubbed as *Simpson's method 2*, is valid when the three-eighths rule is used at the upper end on the points $t_{n-3}, t_{n-2}, t_{n-1}, t_n$. The starting values F_0, F_1 are required for both forms of Simpson's method. Intuitively there seems to be little difference between the two methods, but Simpson's method 2 is preferable for computational purposes. In this case, one obtains respectively for nonlinear and linear equations

n is even: Extended Simpson's rule

$$\begin{aligned} F_n = g(t_n) + \frac{1}{3}h\,[&K(t_n, t_0, F_0) + 4K(t_n, t_1, F_1) \\ &+ \sum_{i=2}^{n-2} (2K(t_n, t_i, F_i) + 4K(t_n, t_{i+1}, F_{i+1})) + K(t_n, t_n, F_n)\Bigg], \end{aligned} \tag{C.19}$$

or

$$\begin{aligned} \left(1 - \frac{1}{3}hK(t_n, t_n)\right) F_n = g(t_n) + \frac{1}{3}h\,[&K(t_n, t_0)F_0 + 4K(t_n, t_1)F_1 \\ &+ \sum_{i=2}^{n-2} (2K(t_n, t_i)F_i + 4K(t_n, t_{i+1})F_{i+1})\Bigg], \end{aligned} \tag{C.20}$$

n is odd: Extended Simpson's rule+$\frac{3}{8}$th rule

$$
\begin{aligned}
F_n = g(t_n) + \frac{1}{3}h\,[&K(t_n,t_0,F_0) + 4K(t_n,t_1,F_1) \\
&+ \sum_{i=2}^{n-5}\left(2K(t_n,t_i,F_i) + 4K(t_n,t_{i+1},F_{i+1})\right) + K(t_n,t_{n-3},F_{n-3})\Bigg] \\
&+ \frac{3}{8}h\,[K(t_n,t_{n-3},F_{n-3}) + 3K(t_n,t_{n-2},F_{n-2}) + 3K(t_n,t_{n-1},F_{n-1}) \\
&+K(t_n,t_n,F_n)]\,, \qquad \text{(C.21)}
\end{aligned}
$$

or

$$
\begin{aligned}
\left(1 - \frac{3}{8}hK(t_n,t_n)\right)F_n = g(t_n) + \frac{1}{3}h\,[&K(t_n,t_0)F_0 + 4K(t_n,t_1)F_1 \\
&+ \sum_{i=2}^{n-5}\left(2K(t_n,t_i)F_i + 4K(t_n,t_{i+1})F_{i+1}\right) \\
&+K(t_n,t_{n-3})F_{n-3}] \\
&+ \frac{3}{8}h\,[K(t_n,t_{n-3})F_{n-3} + 3K(t_n,t_{n-2})F_{n-2} \\
&+3K(t_n,t_{n-1})F_{n-1}]\,, \qquad \text{(C.22)}
\end{aligned}
$$

with i even. It is worth noting to mention that, in equations (C.19)-(C.22), F_0 and F_1 are assumed to be known or are determined by another procedure. Often, the *Day's starting procedure* [2] is used to compute the first three values F_1, F_2, F_3, and F_0 given by $g(0)$.

Day's formulae or Day's starting procedure

$$
\begin{aligned}
F_1 &= g(t_1) + \frac{1}{6}h\left[K(t_1,t_0)g(t_0) + 4K(t_1,t_{1/2})F_{13} + K(t_1,t_1)F_{12}\right], \\
F_2 &= g(t_2) + \frac{1}{3}h\,[K(t_2,t_0)g(t_0) + 4K(t_2,t_1)F_1 + K(t_2,t_2)F_{21}]\,, \\
F_3 &= g(t_3) + \frac{3}{8}h\,[K(t_3,t_0)g(t_0) + 3K(t_3,t_1)F_1 + 3K(t_3,t_2)F_2 \\
&\quad +K(t_3,t_3)F_{31}]\,,
\end{aligned}
$$

where

$$
\begin{aligned}
F_{11} &= g(t_1) + hK(t_1, t_0)g(t_0), \\
F_{12} &= g(t_1) + \frac{1}{2}h\left[K(t_1, t_0)g(t_0) + K(t_1, t_1)F_{11}\right], \\
F_{13} &= g(t_{1/2}) + \frac{1}{4}h\left[K(t_{1/2}, t_0)g(t_0) + K(t_{1/2}, t_{1/2})\left(\frac{1}{2}g(t_0) + \frac{1}{2}F_{12}\right)\right], \\
F_{21} &= g(t_2) + 2hK(t_2, t_1)F_1, \\
F_{31} &= g(t_3) + \frac{3}{2}h\left[K(t_3, t_1)F_1 + K(t_3, t_2)F_2\right].
\end{aligned}
$$

C.4 Standard block-by-block method

The multi-step methods (except the trapezoidal method) still have the problems that: - several different formulas have to be combined (leading to the possibility of numerical instability) and - more starting values are required which have to be obtained in some other way. The *block-by-block methods* described in this part are convenient because they eliminate these difficulties. They not only give starting values but provides a convenient and efficient way for solving the equation over the whole interval. As in the previous multi-step methods, the block-by-block methods are based on the quadrature techniques. Let us assume and decide to use Simpson's rule as the numerical integration formula. The method consists to simultaneously compute the approximate solution F_{2m+1} and F_{2m+2} for $m = 0, 1, 2, \cdots$ with the well-known initial value $F_0 = g_0$. In what follows, and for simplicity, we adopt the notation $F(t_j) \equiv F_j$. Thus

$$
\begin{aligned}
F_{2m+1} &= g_{2m+1} + \int_0^{t_{2m}} \mathrm{d}yK(t_{2m+1}, y, f(y)) + \int_{t_{2m}}^{t_{2m+1}} \mathrm{d}yK(t_{2m+1}, y, f(y)), \\
F_{2m+2} &= g_{2m+2} + \int_0^{t_{2m}} \mathrm{d}yK(t_{2m+2}, y, f(y)) + \int_{t_{2m}}^{t_{2m+2}} \mathrm{d}yK(t_{2m+2}, y, f(y)).
\end{aligned}
$$

The integrals over the intervals $[0, t_{2m}]$ and $[t_{2m}, t_{2m+2}]$ are computed by using standard Simpson's quadrature method. The remaining integral over $[t_{2m}, t_{2m+1}]$ is evaluated via a Simpson's quadrature with intermediate point

$t_{2m+1/2}$. We then have

$$\begin{aligned} F_{2m+1} &= g_{2m+1} + h\sum_{i=0}^{2m} \varpi_{2m+1,i} K(t_{2m+1}, t_i, F_i) \\ &\quad + h\sum_{r=0}^{2} \widetilde{\varpi}_{2m+1,r} K(t_{2m+1}, t_{2m+r/2}, F_{2m+r/2}), \\ F_{2m+2} &= g_{2m+2} + h\sum_{i=0}^{2m} \varpi_{2m+2,i} K(t_{2m+2}, t_i, F_i) \\ &\quad + h\sum_{r=2m}^{2m+2} \widetilde{\varpi}_{2m+2,r} K(t_{2m+2}, t_r, F_r). \end{aligned}$$

The computation of the approximate solution is given by the general process

$$\begin{aligned} F_{2m+1} &= g_{2m+1} + h\sum_{i=0}^{2m} \varpi_{2m+1,i} K(t_{2m+1}, t_i, F_i) + \frac{1}{6}h\left[K(t_{2m+1}, t_{2m}, F_{2m})\right. \\ &\quad \left. +4K(t_{2m+1}, t_{2m+1/2}, F_{2m+1/2}) + K(t_{2m+1}, t_{2m+1}, F_{2m+1})\right], \\ F_{2m+2} &= g_{2m+2} + h\sum_{i=0}^{2m} \varpi_{2m+2,i} K(t_{2m+2}, t_i, F_i) + \frac{1}{3}h\left[K(t_{2m+2}, t_{2m}, F_{2m})\right. \\ &\quad \left. +4K(t_{2m+2}, t_{2m+1}, F_{2m+1}) + K(t_{2m+2}, t_{2m+2}, F_{2m+2})\right], \end{aligned} \tag{C.23}$$

where $\varpi_{ni} = \frac{1}{3}\{1, 4, 2, \cdots, 2, 4, 1\}, i = 0, 1, 2, \cdots, 2m$ and $t_{2m+1/2} = t_{2m} + \frac{1}{2}h$. To deal with the unknown value $F_{2m+1/2}$ we approximate it by quadratic interpolation, using values $F_{2m}, F_{2m+1}, F_{2m+2}$, that is, we replace

$$F_{2m+1/2} \simeq \frac{3}{8}F_{2m} + \frac{3}{4}F_{2m+1} - \frac{1}{8}F_{2m+2}.$$

At each step, equation (C.23) have to be solved simultaneously for the unknowns F_{2m+1} and F_{2m+2}, so that we obtain a block of unknowns at a time. The case of linear integral equations is directly inferred from (C.23). The system of equations thus obtained can be easily solved via special LAPACK routines.

C.5 Methods based on more accurate numerical integration

The methods previously described were developed under the assumption that all functions involved in the integral equations were well-behaved; more precisely, we assumed that the kernel $K(t, y, f(y))$ and $g(t)$ were continuous. In

many practical situations such conditions are not satisfied. One often encounters the situations where the kernel or some of its lower derivatives are unbounded. In that case, new methods are needed. The previous methods can therefore be adapted to these more complicated conditions if we use more powerful numerical integration techniques, namely *product integration* which is briefly described here. In the interest of clarity and conciseness we will make our treatment somewhat more descriptive and less rigorous than that in Linz's book [2]. We consider the equation

$$f(t) = g(t) + \int_0^t \mathrm{d}y \; p(t,y) K^{(c)}(t,y,f(y)), \qquad 0 \leq t \leq T, \tag{C.24}$$

where we assume that

1. $g(t)$ and $K^{(c)}(t,y,f)$ are continuous functions in the region of interest $0 \leq t \leq T$,

2. the well-behaved part of the kernel satisfies a Lipschitz condition of the form

$$\mid K^{(c)}(t,y,v_1) - K^{(c)}(t,y,v_2) \mid \leq L \mid v_1 - v_2 \mid . \tag{C.25}$$

Since $K^{(c)}(t,y,f)$ is assumed to be smooth, all of the singular properties of the full kernel must be included in the term $p(t,y)$. However, some restrictions must be put on $p(t,y)$. We assume here that all necessary conditions are verified such that a unique continuous solution exists for equation (C.24).

C.5.1 Product integration

The standard numerical integration rules, such as the trapezoidal and Simpson's methods, are constructed under the assumption that the integrand is at least bounded. When this is not the case such methods may not work. Even if the integrand is continuous, a great deal of accuracy is lost if higher derivatives fail to exist. Special methods are needed to handle such cases efficiently. One of the most powerful ways to deal with poorly behaved integrands is product integration. Let us briefly describe the way in which the method is constructed. In the same line as in Section (C.2), instead of approximating the whole integrand by a piecewise polynomial, we only approximate the well-behaved part. We write the integral as

$$I = \int_a^b \mathrm{d}t \; p(t)\psi(t),$$

where $\psi(t)$ is assumed to be continuous and generally smooth. Thus, whatever singularities or poor behavior the integrand has are included in $p(t)$. Then, one approximates ψ by a function $\widetilde{\psi}$ and compute

$$\tilde{I} = \int_a^b \mathrm{d}t \; p(t)\widetilde{\psi}(t).$$

So, the integral of the form $\int t^i p(t)\mathrm{d}t$ must be evaluated either explicitly or by an efficient numerical technique if we use piecewise polynomial approximations. It follows immediately from standard results of approximation theory that

$$\mid I - \tilde{I} \mid \leq \max_{a \leq t \leq b} \mid \psi(t) - \widetilde{\psi}(t) \mid \int_a^b \mathrm{d}t \;\; \mid p(t) \mid,$$

is the error bounds and orders of convergence for product integration. Now, we can find the explicit form of product integration formula, which depends of course on the method of approximation we use to construct $\widetilde{\psi}(t)$. Reasoning as in the Section (C.2) we straightforwardly obtain

$$\tilde{I} = h \sum_{i=0}^{n-1} \sum_{j=0}^{m} \widetilde{\varpi}_{ij} \psi(t_{im} + jh), \tag{C.26}$$

$$\widetilde{\varpi}_{ij} = \int_0^m p(u)\ell_{ij}(u)\mathrm{d}u. \tag{C.27}$$

The fundamental polynomials ℓ_{ij} are defined in (C.7).

C.5.2 Adapted block-by-block method

It is fairly obvious that we have in hand a way of constructing highly accurate numerical methods to tackle equation (C.1). For the sake of simplicity, we restrict ourselves in the particular case of linear Volterra integral equations of the second kind. Exploiting product integration formulae based on approximating integrands by polynomials of degree two. three, etc., one obtains methods which are of the general form

$$F_n = g_n + \sum_{j=0}^{n} \widetilde{\varpi}_{nj} K(t_n, t_j) F_j, \tag{C.28}$$

where the weights $\widetilde{\varpi}_{nj}$ are readily found. Here we only describe a general scheme of *product block-by-block method* based on quadratic interpolation. One proceeds exactly as in the derivation of equations (C.23), using product integration instead of regular integration. Since the full kernel $K(t, y)$ has the

singular properties that must be included in the term $p(t,y)$, we make the following decomposition

$$K(t,y) = C_K + p(t,y)K^{(c)}(t,y), \tag{C.29}$$

where $K^{(c)}(t,y)$ is assumed to be smooth and C_K a constant. Thus equation (C.1) reads

$$f(t) = g(t) + C_K \int_0^t \mathrm{d}y\ f(y) + \int_0^t \mathrm{d}y\ p(t,y)K^{(c)}(t,y)f(y). \tag{C.30}$$

The latter equation can be numerically solved in the light of combination of product block-by-block integration technique and Simpson's rule. We first subdivide the time interval $[0,t]$ into equal subintervals $[t_j, t_{j+2}]$ of length $2h$ with $j = 0, ..., n-2$, n being an even number. We show that

$$\int_0^{t_i} \mathrm{d}y\ p(t_i,y)K^{(c)}(t_i,y)f(y) = \sum_{j=0}^{i-2} \int_{t_j}^{t_{j+2}} \mathrm{d}y\ p(t_i,y)K^{(c)}(t_i,y)f(y), \tag{C.31}$$

where $j = 0, 2, 4, \cdots, i-2$ and i is even. Each subinterval $[t_j, t_{j+2}]$ is further subdivided into equal subintervals $[t_{j0}, t_{j1}, t_{j2}, ..., t_{jm}]$ with $t_{jl} = t_j + lh$, $l = 0, 1, 2, ..., m$. In each subinterval $[t_j, t_{j+2}]$, we use Lagrange interpolation on the points t_{jl} to approximate the well-behaved part of the integrand, namely $K^{(c)}(t,y)f(y)$ by a polynomial of degree m.

$$\int_0^{t_i} \mathrm{d}y\ p(t_i,y)K^{(c)}(t_i,y)f(y) = \sum_{j=0}^{i-2} \int_{t_j}^{t_{j+2}} \mathrm{d}y\ p(t_i,y) \sum_{l=0}^{m} \ell_{jl}(y)K^{(c)}(t_i,t_{jl})f(t_{jl}), \tag{C.32}$$

We then perform the change of variable $y = t_j + uh$ and integrate analytically over u in each subinterval $[t_j, t_{j+2}]$.

$$\int_0^{t_i} \mathrm{d}y\ p(t_i,y)K^{(c)}(t_i,y)f(y) = \sum_{j=0}^{i-2} \sum_{l=0}^{m} \widetilde{\varpi}_{jl} K^{(c)}(t_i,t_{jl})f(t_{jl}), \tag{C.33}$$

$$\begin{aligned} \widetilde{\varpi}_{jl} &= \int_{t_j}^{t_{j+2}} \mathrm{d}y\ p(t_i,y)\ell_{jl}(y) \\ &= h \int_0^2 \mathrm{d}u\ p(t_i, t_j + uh)\ell_{jl}(t_j + uh). \end{aligned} \tag{C.34}$$

In the case of our interest, a piecewise polynomial of degree $m = 2$ is used. One obtains after some manipulations the results

$$\int_0^{t_i} \mathrm{d}y\ p(t_i, y)K^{(c)}(t_i, y)f(y) = \sum_{j=0}^{i-2} \Big[\alpha(t_i, t_j, h)K^{(c)}(t_i, t_j)f(t_j) + \beta(t_i, t_j, h)K^{(c)}(t_i, t_{j+1})f(t_{j+1}) + \gamma(t_i, t_j, h)K^{(c)}(t_i, t_{j+2})f(t_{j+2})\Big], \tag{C.35}$$

where the functions α, β and γ are defined by

$$\alpha(x, y, z) = \frac{1}{2}z\int_0^2 (1-u)(2-u)p(x, y+uz)\mathrm{d}u, \tag{C.36}$$

$$\beta(x, y, z) = z\int_0^2 u(2-u)p(x, y+uz)\mathrm{d}u, \tag{C.37}$$

$$\gamma(x, y, z) = \frac{1}{2}z\int_0^2 u(u-1)p(x, y+uz)\mathrm{d}u. \tag{C.38}$$

In this thesis we deal with the particular case of $p(t, y) = \sqrt{t-y}$ in (C.24), a case which is of some practical importance. Equation (C.35) can be rewritten in the forms

$$\int_0^{t_i} \mathrm{d}y\ \sqrt{t_i - y}K^{(c)}(t_i, y)f(y) = h^{3/2}\sum_{j=0}^{i-2} \Big[\alpha(i-j)K^{(c)}(t_i, t_j)f(t_j) + \beta(i-j)K^{(c)}(t_i, t_{j+1})f(t_{j+1}) + \gamma(i-j)K^{(c)}(t_i, t_{j+2})f(t_{j+2})\Big], \tag{C.39}$$

where the functions α, β and γ take the forms

$$\alpha(k) = \frac{1}{2}\int_0^2 (1-u)(2-u)\sqrt{k-u}\mathrm{d}u, \tag{C.40}$$

$$\beta(k) = \int_0^2 u(2-u)\sqrt{k-u}\mathrm{d}u, \tag{C.41}$$

$$\gamma(k) = \frac{1}{2}\int_0^2 u(1-u)\sqrt{k-u}\mathrm{d}u. \tag{C.42}$$

The remaining integral in (C.30) can be treated by exploiting the well-known classical Simpson's quadrature technique. Gathering all these above expressions, and after tedious manipulations we obtain a system of equations for

unknowns F_{2m+1} and F_{2m+2}.

$$
\begin{aligned}
F_{2m+1} &= g_{2m+1} + hC_K \sum_{i=0}^{2m} \varpi_{2m+1,i} F_i + \frac{1}{6} hC_K \left[F_{2m} + 4F_{2m+1/2} + F_{2m+1} \right] \\
&+ h^{3/2} \sum_{l=0}^{m-1} \Big[\alpha(2m+1-2l) K^{(c)}_{2m+1,2l} F_{2l} \\
&+ \beta(2m+1-2l) K^{(c)}_{2m+1,2l+1} F_{2l+1} + \gamma(2m+1-2l) K^{(c)}_{2m+1,2l+2} F_{2l+2} \Big] \\
&+ \left(\frac{1}{2} h \right)^{3/2} \Big[\alpha(2) K^{(c)}_{2m+1,2m} F_{2m} + \beta(2) K^{(c)}_{2m+1,2m+1/2} F_{2m+1/2} \\
&+ \gamma(2) K^{(c)}_{2m+1,2m+1} F_{2m+1} \Big], \qquad \text{(C.43)} \\
F_{2m+2} &= g_{2m+2} + hC_K \sum_{i=0}^{2m} \varpi_{2m+2,i} F_i + \frac{1}{3} hC_K \left[F_{2m} + 4F_{2m+1} + F_{2m+2} \right] \\
&+ h^{3/2} \sum_{l=0}^{m-1} \Big[\alpha(2m+2-2l) K^{(c)}_{2m+2,2l} F_{2l} \\
&+ \beta(2m+2-2l) K^{(c)}_{2m+2,2l+1} F_{2l+1} + \gamma(2m+2-2l) K^{(c)}_{2m+2,2l+2} F_{2l+2} \Big] \\
&+ h^{3/2} \Big[\alpha(2) K^{(c)}_{2m+2,2m} F_{2m} + \beta(2) K^{(c)}_{2m+2,2m+1} F_{2m+1} \\
&+ \gamma(2) K^{(c)}_{2m+2,2m+2} F_{2m+2} \Big], \qquad \text{(C.44)}
\end{aligned}
$$

where for the sake of brevity, we used the simplified notation $K(t_i, t_j) \equiv K_{i,j}$. Starting with $F_0 = g_0$, we solve (C.43) and (C.44) successively for blocks of values $(F_1, F_2), (F_3, F_4), \cdots$, using standard BLAS and LAPACK library programs.

C.6 Convergence and stability of the approximate solution

The question of convergence and stability for methods discussed in the previous Sections are concerned in the following. Emphasis is given to block-by-block methods. These methods determine an approximate solution only at the error at the points t_i; thus one can talk only at the error at these points. In practice this is usually adequate. We start by giving the useful definitions and theorems [2] (for details and proof, report on the cited reference book).
The *discretization error* is defined as a set of values

$$\varepsilon_i = F_i - f(t_i), \quad i = 0, 1, 2, \cdots \qquad \text{(C.45)}$$

We are interested in the behavior of this discretization error as a function of the stepsize h. For any particular value of h the interval $[0, T]$ is divided into N parts in such a way that $Nh = T$. Therefore, as $h \to 0$, N goes to infinity in such a way that $Nh = T$. This implies that h can take on only certain *admissible* values, namely such that $h \leq T$ and T/h is an integer.

Definition 1. A method of the form (C.17) is said to be a *convergent approximation method* if

$$\lim_{h \to 0} \left(\max_{0 \leq i \leq N} \mid \varepsilon_i \mid \right) = 0. \tag{C.46}$$

Definition 2. If, for all admissible h, there exists a number $M < \infty$, independent of h, such that

$$\max_{0 \leq i \leq N} \mid \varepsilon_i \mid \leq M h^p, \tag{C.47}$$

and if p is the largest number for which such an inequality holds, then p is called the *order of convergence* of the method. The order of convergence is, not surprisingly, closely connected with the accuracy of the numerical integration employed.

Definition 3. Let f be the solution of equation (C.1). Then the function

$$\begin{aligned} \delta(h, t_n) &= f(t_n) - F_n \\ &= \int_0^{t_n} \mathrm{d}y K(t_n, y, f(y)) - h \sum_{i=0}^{n} \varpi_{ni} K(t_n, t_i, F_i) \end{aligned} \tag{C.48}$$

is the *local consistency error* for (C.1).

Definition 4. Let $\mathcal{C}$ be a class of equations of the form (C.1). If for every equation in $\mathcal{C}$

$$\lim_{h \to 0} \left(\max_{0 \leq n \leq N} \mid \delta(h, t_n) \mid \right) = 0, \tag{C.49}$$

then the approximation method (C.17) is said to be *consistent* with (C.1) for the class of equations $\mathcal{C}$. If for every equation in $\mathcal{C}$, there exist a constant c (independent of h, but generally dependent on K and f) such that

$$\max_{0 \leq n \leq N} \mid \delta(h, t_n) \mid \leq c h^p, \tag{C.50}$$

then the method is said to be *consistent of order* p in $\mathcal{C}$.

Theorem 1. Let the sequence $\xi_0, \xi_1, \cdots$ satisfy

$$\mid \xi_n \mid \leq A \sum_{i=0}^{n-1} \mid \xi_i \mid + B_n, \quad n = r, r+1, \cdots, \tag{C.51}$$

where

$$A > 0, \quad \mid B_n \mid \leq B, \quad \sum_{i=0}^{r-1} \mid \xi_i \mid \leq \eta. \tag{C.52}$$

Then

$$\mid \xi_n \mid \leq (1+A)^{n-r}(B + A\eta), \quad \eta = r, r+1, \cdots. \tag{C.53}$$

Theorem 2. Consider the approximate solution of (C.1) by (C.18) and assume that

1. the solution $f(t)$ of (C.1) and the kernel $K(t, y, f)$ are such that the approximate method is consistent of order p with (C.1),
2. the weights satisfy $\sup_{n,i} \mid \varpi_{ni} \mid \leq W < \infty$,
3. the starting errors $F_i - f(t_i), i = 0, 1, \cdots, r-1$ go to zero as $h \to 0$. Since r is fixed, this implies that $\lim_{h \to 0} \sum_{i=0}^{r-1} \mid F_i - f(t_i) \mid = 0$.
   Then the method is a convergent approximation method. Also, in the absence of starting errors, the order of convergence is at least p.

The proof of this main convergence theorem leads to a further conclusion that [2]: *the effect of the starting errors is attenuated by a factor of h, showing that these methods are relatively insensitive to the starting errors. In fact, one needs only that*

$$\mid F_i - f(t_i) \mid = \mathcal{O}(h^{p-1}), \quad i = 0, 1, \cdots, r-1 \tag{C.54}$$

to achieve an order of convergence p for a method whose order of consistency is p. From these theorems, it has been shown that for sufficiently smooth K and f, Simpson's methods are consistent of order 4. Consequently, in the absence of starting errors, they have order of convergence 4.

While the potential efficiency of a method is linked to its order of convergence, one frequently wants to have a better idea of how the error behaves. More precisely, it is the question of the growth of the error. The term "*stability*" is used with many different meanings in the literature. Some authors make stability essentially synonymous with convergence. An appropriate definition of the term shows that, rather generally, *consistency and stability imply convergence.* Since all reasonable methods for Volterra integral equations of the second kind are convergent if they are consistent, we will not use the above definition. We are concerned with the cases where, for fixed h, the error can grow rapidly with t, while the solution itself does not grow very fast at all, such that the method has poor accuracy even though it is of high order. We therefore use the term *numerical instability* for such a phenomenon, which is well-known

in the solution of ordinary differential equations and also occurs with Volterra equations. The most general way of analyzing numerical stability is outlined in this Section. For the sake of simplicity we consider only the linear case. The nonlinear case can be treated in the same manner, yielding similar conclusions.

Putting $t = t_n$ in (C.1) and subtracting from (C.18), one gets for $n = r, r+1, \cdots$, the equation defining the error

$$\varepsilon_n = h \sum_{i=0}^{n} \varpi_{ni} K(t_n, t_i) \varepsilon_i - \delta(h, t_n), \quad n = r, r+1, \cdots. \tag{C.55}$$

The starting errors $\varepsilon_0 = \eta_0, \varepsilon_1 = \eta_1, \cdots, \varepsilon_{r-1} = \eta_{r-1}$ are determined by the starting methods used. The overall error, defined by equation (C.55), arises from two sources: one contribution coming from the propagation of the starting errors and a second one due to the consistency error. They behave quite differently and must be separated for further discussion.

Let denote ε_n^C the *accumulated consistency error* and ε_n^S the *accumulated starting error*, respectively solutions of

$$\begin{aligned} &\varepsilon_n^C = h \sum_{i=0}^{n} \varpi_{ni} K(t_n, t_i) \varepsilon_i^C - \delta(h, t_n), \quad n = r, r+1, \cdots, \\ &\varepsilon_0^C = \varepsilon_1^C = \cdots = \varepsilon_{r-1}^C = 0, \end{aligned} \tag{C.56}$$

and

$$\begin{aligned} &\varepsilon_n^S = h \sum_{i=0}^{n} \varpi_{ni} K(t_n, t_i) \varepsilon_i^S, \quad n = r, r+1, \cdots, \\ &\varepsilon_0^S = \eta_n, \quad n = 0, 1, \cdots, r-1, \end{aligned} \tag{C.57}$$

such that their sum is the discretization error

$$\varepsilon_n = \varepsilon_n^C + \varepsilon_n^S,$$

and is a solution of (C.55). In what follows we define precisely what is meant by saying that the error varies smoothly.

Definition 5. For each admissible h, let $\xi_0(h), \xi_1(h), \cdots, \xi_N(h)$ be a sequence of numbers. This set of sequences has an *expansion of order* p if there exists a continuum function $\chi(t)$ such that, for $n = 0, 1, \cdots, N$,

$$\xi_n(h) = h^p \chi(t_n) + \mathcal{O}(h^q), \quad q > p. \tag{C.58}$$

If the discretization error has an expansion, then it varies smoothly from point to point in the sense that the scaled quantity ε_n / h^p tends to a limit which

is a continuous function. From this definition, we say that the *local consistency error has an expansion of order* p (for a given problem) if there exists a continuous function $Q(t)$ such that

$$\delta(h, t_n) = h^p Q(t_n) + \mathcal{O}(h^q), \quad q > p. \tag{C.59}$$

Theorem 3. Consider the linear equation

$$f(t) = g(t) + \int_0^t \mathrm{d}y K(t, y) f(y).$$

If the local consistency error has an expansion of the form (C.59), then the accumulated consistency error also has an expansion. In particular,

$$\varepsilon_n^C = h^p e(t_n) + \mathcal{O}(h^P), \tag{C.60}$$

where $P = \min(q, p+1)$ and $e(t)$ is the solution of

$$e(t) = -Q(t) + \int_0^t \mathrm{d}y K(t, y) e(y), \tag{C.61}$$

provided that all functions involved in equation (C.61) are sufficiently smooth so that the method in question is consistent for (C.61) with order at least one.

It is possible to show that for the multi-step methods suggested above and indeed all standard numerical integration rules, the local consistency error has an expansion. Thus, in general, the accumulated consistency error behaves smoothly. The accumulated starting error, however, does not always behave as nicely and ε_n^S may exhibit oscillations of magnitude $\mathcal{O}(\varepsilon_n^S)$. Whether or not this occurs seems to depend on the pattern in the weights ϖ_{ni}.

Definition 6. A method of type (C.18) is said to have a *repetition factor* ρ if ρ is the smallest integer such that

$$\varpi_{n+\rho,i} = \varpi_{ni}, \tag{C.62}$$

for $i = 0, 1, 2, \cdots, n-q$, where q is an integer independent of n.

Following this definition the trapezoidal method and Simpson's method 2 *have a repetition factor of* 1*, while Simpson's method* 1 *has repetition factor* 2.

Theorem 4. Consider the numerical method (C.17) under the assumptions

1. the method has repetition factor 1,
2. the method is convergent with at least order 1 for equations (C.64) below,
3. the starting errors $\eta_i = \mid F_i - f(t_i) \mid$ can be written as

$$\eta_i = \gamma_i h^p + \mathcal{O}(h^{p+1}), \quad i = 0, 1, 2, \cdots, r-1$$

Then the accumulated starting error ε_n^S has an asymptotic expansion of the form

$$\varepsilon_n^S = h^{p+1} \sum_{i=0}^{r-1} \gamma_i C_j(t_n) + \mathcal{O}(h^{p+2}), \tag{C.63}$$

where $C_j(t)$ is the solution of

$$C_j(t) = V_j K(t, t_j) + \int_0^t \mathrm{d}y K(t, y) C_j(y), \quad j = 0, 1, \cdots, r-1, \tag{C.64}$$

and the $V_j = \varpi_{nj}$ are constants (since the method has repetition factor 1, the weights $\varpi_{nj}, j = 0, 1, \cdots, r-1$ are independent of n, provided $n \geq r + q$).

It follows from the proof of this theorem that for methods having a repetition factor of 1 both the accumulated consistency error and the accumulated starting error have an asymptotic expansion and therefore the total error behaves in a systematic way. *For methods with repetition factor larger than one this is not necessarily so and significant oscillations may appear.*

Next, we consider the question of stability. According to Noble [8] a finite difference method for (C.1) is numerically stable if the leading term in the asymptotic expansion of the error satisfies an equation whose kernel is the same as that of the linearized form of (C.1). For additional discussions of this concept see also Kobayasi [9] and Linz [2]. One starts with the following definition

Definition 7. A method is said to be *numerically stable* with respect to an error component ε_n if that error has an expansion of the form

$$\varepsilon_n = h^p e(t_n) + \mathcal{O}(h^q), \quad q > p > 0, \tag{C.65}$$

with $e(t)$ satisfying an equation

$$e(t) = Q(t) + \int_0^t \mathrm{d}y K(t, y) e(y), \tag{C.66}$$

for some $Q(t)$.

In the light of this definition and the previous one it is easy to prove that the trapezoidal method and Simpson's method 2 *are stable with respect to the*

[8] B. Noble, *Instability when solving Volterra integral equations of the second kind by multistep methods. Lecture Notes in Mathematics*, No.**109**, 23 (Springer, Berlin-Heidelberg-New-York, 1975)

[9] M. Kobayasi, *On the numerical solution of Volterra integral equations of the second kind by linear multi-step methods. Rep. Stat. Appl. Res.*, JUSE.**13**, 1 (1966)

accumulated consistency error ε_n^C *as well as the accumulated starting error* ε_n^S. *Simpson's method* 1 *is stable with respect to* ε_n^C, *but not necessary with respect to* ε_n^S. One infers from **Theorem 3** that all standard methods are stable with respect to ε_n^C. **Theorem 4** exhibits the same thing for ε_n^S, provided the method has repetition factor 1. The remaining question is the stability with respect to ε_n^S of methods having a repetition factor larger than one. It has been clearly shown that, the general result is that such methods have a tendency to show unstable error growth. *The conclusion is then that Simpson's method* 1 *can show unstable error growth and therefore numerically instable. In practice this method should be avoided.*

Another view of stability.

According to the previous discussion, a method is called numerically stable if the dominant error term satisfies an integral equation having the same kernel as the original equation. We give here another definition of this notion. Let us consider the equation

$$f(t) = 1 - \lambda \int_0^t \mathrm{d}y \; f(y), \tag{C.67}$$

which has the solution $f(t) = \mathrm{e}^{-\lambda t}$. The solution decays exponentially for $\lambda > 0$. It is therefore reasonable to require that the approximate solution should have the same behavior.

Definition 8. Let $F_n(h)$ denote the approximate solution of (C.67) computed by (C.17), with $\lambda > 0$, arbitrary starting values $F_0, F_1, \cdots, F_{r-1}$, and fixed h. The method (C.17) is said to be ***A-stable*** in the interval $[0, h_0]$ if for all $0 < h < h_0$

$$\lim_{n\to\infty} F_n(h) = 0 \quad \textit{for } h \textit{ fixed.} \tag{C.68}$$

If, in addition,

$$\lim_{h\to\infty} F_n(h) = 0 \quad \textit{for } n \textit{ fixed,} \tag{C.69}$$

the method is called ***stiffly A-stable***.

The use of **Definition 8** to define stability has many advantages. The approximate solution usually reduces to a linear difference equation with constant coefficients and hence its behavior is governed by the roots of the characteristic polynomials. It is then a simple computational matter to find the interval of stability. In practice, it is common to consider not only real values of λ, but to take λ in the complex plane with $Re(\lambda) > 0$. Numerical root-finding methods can then be used to find the regions of stability in the complex plane.

Having mastered the precedent useful concepts, we are now well armed to illustrate them with the application to the question of convergence and stability

of the block-by-block methods. Going through the usual procedure we find that the errors satisfy the equations

$$\varepsilon_{2m+1} = h\sum_{i=0}^{2m} \varpi_i K(t_{2m+1}, t_i)\varepsilon_i + h\left[c_{2m}\varepsilon_{2m} + c_{2m+1}\varepsilon_{2m+1} + c_{2m+2}\varepsilon_{2m+2} + \mathcal{R}_{2m+1}\right], \tag{C.70}$$

$$\varepsilon_{2m+2} = h\sum_{i=0}^{2m} \varpi_i K(t_{2m+2}, t_i)\varepsilon_i + h\left[d_{2m}\varepsilon_{2m} + d_{2m+1}\varepsilon_{2m+1} + d_{2m+2}\varepsilon_{2m+2} + \mathcal{R}_{2m+2}\right], \tag{C.71}$$

where the expression for c_i and d_i are obvious and

$$\mathcal{R}_{2m+1} = h\sum_{i=0}^{2m} \varpi_i K(t_{2m+1}, t_i)f(t_i) + h\left[c_{2m}f(t_{2m}) + c_{2m+1}f(t_{2m+1}) + c_{2m+2}f(t_{2m+2})\right] - \int_0^{t_{2m+1}} \mathrm{d}t K(t_{2m+1}, t)f(t), \tag{C.72}$$

$$\mathcal{R}_{2m+2} = h\sum_{i=0}^{2m} \varpi_i K(t_{2m+2}, t_i)f(t_i) + h\left[d_{2m}f(t_{2m}) + d_{2m+1}f(t_{2m+1}) + d_{2m+2}f(t_{2m+2})\right] - \int_0^{t_{2m+2}} \mathrm{d}t K(t_{2m+2}, t)f(t). \tag{C.73}$$

An analysis shows that for sufficiently smooth K and f the terms $\mathcal{R}_{2m+1}$ and $\mathcal{R}_{2m+2}$ which reduce to

$$\mathcal{R}_{2m+1} = \frac{1}{180}h^5 \sum_{j=0}^{m-1} \frac{\mathrm{d}^4}{\mathrm{d}y^4}\left[K(t_{2m+1}, t_{2j})f(t_{2j})\right] - \frac{1}{96}h^4 K(t_{2m+1}, t_{2m+1/2})f^{(3)}(t_{2m+1/2}) + \mathcal{O}(h^5), \tag{C.74}$$

$$\mathcal{R}_{2m+2} = \frac{1}{180}h^5 \sum_{j=0}^{m} \frac{\mathrm{d}^4}{\mathrm{d}y^4}\left[K(t_{2m+2}, t_{2j})f(t_{2j})\right] + \mathcal{O}(h^5), \tag{C.75}$$

are of order h^4, so that, applying **Theorem 1** we find that

$$\max_{0\le i\le N} \mid \varepsilon_i \mid = \mathcal{O}(h^4), \tag{C.76}$$

showing that the *method has order of convergence four.*

To obtain error expansions we consider equations (C.70) and (C.71). Then, after tedious manipulations, we obtain the system

$$x(t) = \mathcal{R}_1(t) + \frac{1}{3}\int_0^t \mathrm{d}y K(t,y)x(y) + \frac{2}{3}\int_0^t \mathrm{d}y K(t,y)z(y), \tag{C.77}$$

$$z(t) = \mathcal{R}_2(t) + \frac{1}{3}\int_0^t \mathrm{d}y K(t,y)x(y) + \frac{2}{3}\int_0^t \mathrm{d}y K(t,y)z(y), \tag{C.78}$$

where

$$\mathcal{R}_2(t) = \frac{1}{180}\int_0^t \frac{\mathrm{d}^4}{\mathrm{d}y^4}\left[K(t,y)f(y)\right]\mathrm{d}y,$$

$$\mathcal{R}_1(t) = \mathcal{R}_2(t) - \frac{1}{96}K(t,t)f^{(3)}(t).$$

Discretizing equations (C.77) and (C.78) by the rectangular rule and compared with (C.70) and (C.71), one finds that

$$\varepsilon_{2m+1} = h^4 x(t_{2m+1}) + \mathcal{O}(h^5), \tag{C.79}$$

$$\varepsilon_{2m+2} = h^4 y(t_{2m+2}) + \mathcal{O}(h^5). \tag{C.80}$$

Owing to the fact that $x(t)$ and $z(t)$ are generally not the same, there does not exist an asymptotic expansion for the error at all points. But there is a separate expansion for the even and odd-numbered points. Although the lack of a unique expansion for the error, the method can be considered stable with respect to the consistency error (there are, of course, no starting errors). This is showed by subtracting (C.77) from (C.78)

$$z(t) = x(t) + \mathcal{R}_2(t) - \mathcal{R}_1(t).$$

Putting this into (C.77) yields

$$x(t) = \mathcal{R}_1(t) + \frac{2}{3}\int_0^t \mathrm{d}y K(t,y)\left[\mathcal{R}_2(y) - \mathcal{R}_1(y)\right] + \int_0^t \mathrm{d}y K(t,y)x(y).$$

The equation for $x(t)$ then satisfies the stability criterion given in equation (C.66). A similar argument can be made for $z(t)$, so that the method can be considered stable according to **Definition 7**. If **Definition 8** is used as the stability criterion, then the method is stable for all values of h, that is, it is *A-stable*.

The equation

$$\varepsilon_{2m+2} - \varepsilon_{2m+1} = \mathcal{O}(h^4), \tag{C.81}$$

indicates that there exist oscillations of the order of magnitude as the error itself. This may be considered a minor drawback of the method, although it

is easily eliminated by retaining, say, only the results at the even-numbered points. The basic framework established in this Appendix allows for a great many variations. A considerable amount of work has been done on this topic and it is not our intention to review all of it here.
Note that when solving Volterra integral equations the bulk of the computations comes from approximating integrals of the form $\int_0^{t_j} \mathrm{d}y K(t_j, y) f(y)$ by sums. To compare the efficiency of the multi-step methods with block-by-block methods, the number $N_K \equiv N_K(h, T)$ of necessary evaluations of kernel $K(t, y)$ can serve as measure for the amount of work required.
Multi-step methods:

1. *Simpson's method*: $N_K \approx \frac{1}{2}N^2 = \frac{1}{2}\left(\frac{T}{h}\right)^2$,

2. *Extended Simpson's rule + $\frac{3}{8}$th rule*: $N_K \approx \frac{1}{2}N^2 + \frac{3}{2}N = \frac{1}{2}\left(\frac{T}{h}\right)^2 + \frac{3}{2}\left(\frac{T}{h}\right)$,

Implicit methods:

1. *Block-by-block methods*: $N_K \approx \frac{1}{2}N^2 + 2N = \frac{1}{2}\left(\frac{T}{h}\right)^2 + 2\left(\frac{T}{h}\right)$.

As for an illustration of the methods used in our calculations, we represent the discretization local error for function $F(t_i)$ and ground state population $\mid \mathcal{C}_{1s}(t_i) \mid^2$ without laser interaction, with respect to the stepsize h. In

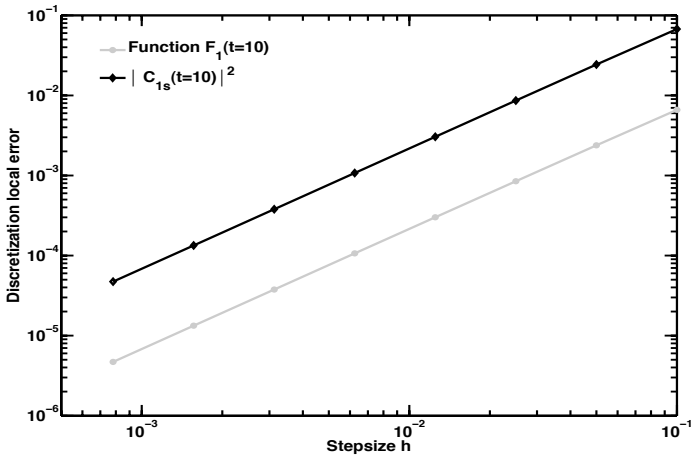

Figure C.1: *Discretization local error ε as a function of stepsize h, calculated for $F_1(t = 10)$ and $\mid \mathcal{C}_{1s}(t = 10) \mid^2$ when the laser field is switched off. The standard block-by-block numerical method is used for this calculation and one observes a convergence in $h^{3/2}$.*

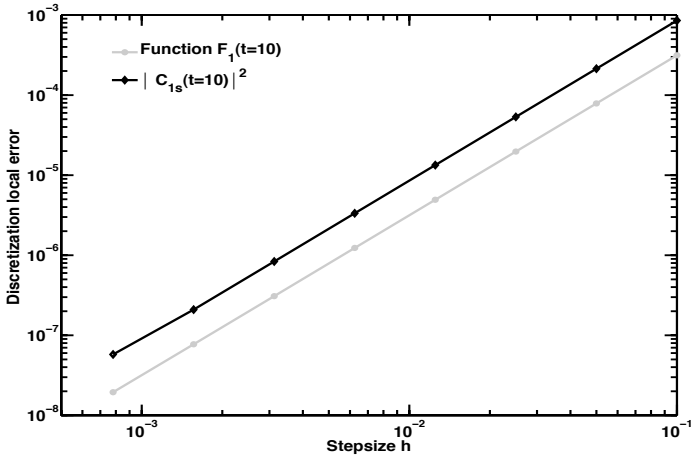

Figure C.2: *Discretization local error ε as a function of stepsize h, calculated for $F_1(t = 10)$ and $\mid \mathcal{C}_{1s}(t = 10) \mid^2$ when the laser field is switched off. The adapted block-by-block numerical method is used for this calculation and one observes a convergence in h^2.*

Figures C.1 and C.2 we displayed the discretization local errors ε as a function of stepsize h. While the block-by-block method is convergent of order 4, we observed in our calculations a convergence in $h^{3/2}$. The failure of expectation of this order of convergence has guided our thinking. After a deep analysis of the kernels, we have found the source of this problem, namely that the full kernel $K(t, y)$ has the singular properties that must be included in the term $p(t, y) = \sqrt{t - y}$. This fact clearly explains the decomposition made in equation (C.29). In this respect, the discretization local error obtained via the adapted block-by-block method exhibits a convergence in h^2 and allows us to gain approximately 3 order of magnitude for a stepsize $h = 0.01$. Let us also point out that, the constant of majoration of local error is about 25 times less than that of standard block-by-block.

Appendix D

Detailed Account of the Intermediate Calculations

This Appendix is devoted to the exact analytical expressions of integrals encountered, which have been used for computation of physical observables investigated in this thesis.

D.1 Functions $\mathcal{J}_n(x,y)$ and $\mathcal{G}_n(x,y)$

Basic integrals

To achieve this purpose we find necessary to define the basic integrals

$$I_\gamma^{(n)}(x,y) = \int_{-\infty}^{+\infty} \mathrm{d}p \frac{p}{(p^2+\gamma)^n} exp\left(-\mathrm{i}xp^2 + \mathrm{i}yp\right), \tag{D.1}$$

$$\mathcal{K}_\gamma^{(n)}(x,y) = \frac{1}{\mathrm{i}2y} I_\gamma^{(n)}(x,y) = \frac{1}{\mathrm{i}2y} \frac{(-1)^{n-1}}{(n-1)!} \frac{\partial^{(n-1)}}{\partial\gamma^{(n-1)}} I_\gamma(x,y), \tag{D.2}$$

from which all integrals can be calculated analytically. Thus, for $n=1$, $I_\gamma^{(1)}(x,y) \equiv I_\gamma(x,y)$; $\gamma = 1$, $\mathcal{K}_1^{(n)}(x,y) \equiv \mathcal{J}_n(x,y)$;
$\gamma = 1/4$, $\mathcal{K}_{1/4}^{(n)}(x,y) \equiv \mathcal{G}_n(x,y)$. Before going further, let us set

$$z_1 = \sqrt{\gamma x}\mathrm{e}^{\mathrm{i}\pi/4} - \frac{y}{2\sqrt{x}}\mathrm{e}^{-\mathrm{i}\pi/4}, \qquad z_2 = \sqrt{\gamma x}\mathrm{e}^{\mathrm{i}\pi/4} + \frac{y}{2\sqrt{x}}\mathrm{e}^{-\mathrm{i}\pi/4},$$

$$\tilde{z} = \sqrt{\gamma x}\mathrm{e}^{\mathrm{i}\pi/4}, \qquad \theta_\gamma = \gamma x - \frac{y^2}{4x}.$$

We obtains the following results:

$$\begin{aligned}\mathcal{K}_\gamma^{(1)}(x,y) &= \frac{\pi}{4}\mathrm{e}^{\mathrm{i}\gamma x}\left[\frac{R_- - R_+}{y}\right] \quad y \neq 0,\\ &= \frac{\pi}{4}\mathrm{e}^{\mathrm{i}\gamma x}\left[-2\sqrt{\gamma}erfc(\tilde{z}) + \frac{2}{\sqrt{\pi x}}\mathrm{e}^{-\mathrm{i}(\gamma x+\pi/4)}\right] \quad y = 0,\\ &= -\frac{\pi}{2}\sqrt{\gamma} \qquad x = 0. \end{aligned} \tag{D.3}$$

where $R_-(x,y,\gamma) \equiv R_- = \mathrm{e}^{-\sqrt{\gamma}y}erfc(z_1)$, $R_+(x,y,\gamma) \equiv R_+ = \mathrm{e}^{\sqrt{\gamma}y}erfc(z_2)$.

$$\mathcal{K}_\gamma^{(1)}(x,y) = -\frac{\pi}{2}\sqrt{\gamma} + \sqrt{2x}\mathcal{K}_\gamma^{(c1)}(x,y). \tag{D.4}$$

Here,

$$erfc(z) = 1 - \frac{2z}{\sqrt{\pi}}\int_0^1 \mathrm{e}^{-z^2t^2}\mathrm{d}t$$

is one of definitions of the complementary Error function.

$$\begin{aligned}\mathcal{K}_\gamma^{(2)}(x,y) &= \frac{\pi}{8\sqrt{\gamma}}\mathrm{e}^{\mathrm{i}\gamma x}\left[A_\gamma R_- + B_\gamma R_+\right] \quad y \neq 0,\\ &= \frac{\pi}{8\sqrt{\gamma}}\mathrm{e}^{\mathrm{i}\gamma x}\left[D_\gamma erfc(\tilde{z}) - E_\gamma \mathrm{e}^{-\mathrm{i}(\gamma x-\pi/4)}\right] \quad y = 0,\\ &= \frac{\pi}{4\sqrt{\gamma}} \qquad x = 0. \end{aligned} \tag{D.5}$$

$$\begin{aligned} A_\gamma &= 1 - \frac{\mathrm{i}x}{y}2\sqrt{\gamma}, \qquad B_\gamma = 1 + \frac{\mathrm{i}x}{y}2\sqrt{\gamma},\\ D_\gamma &= 2(1 + \mathrm{i}2\gamma x), \qquad E_\gamma = 4\sqrt{\frac{\gamma x}{\pi}}. \end{aligned}$$

$$\mathcal{K}_\gamma^{(2)}(x,y) = \frac{\pi}{4\sqrt{\gamma}} + \sqrt{2x}\mathcal{K}_\gamma^{(c2)}(x,y). \tag{D.6}$$

$$\begin{aligned}\mathcal{K}_\gamma^{(3)}(x,y) &= \frac{\pi}{32}\frac{1}{\gamma\sqrt{\gamma}}\mathrm{e}^{\mathrm{i}\gamma x}\left[A_\gamma R_- + B_\gamma R_+ + C_\gamma \mathrm{e}^{-\mathrm{i}(\theta_\gamma-\pi/4)}\right] \quad y \neq 0,\\ &= \frac{\pi}{32}\frac{1}{\gamma\sqrt{\gamma}}\mathrm{e}^{\mathrm{i}\gamma x}\left[D_\gamma erfc(\tilde{z}) + E_\gamma \mathrm{e}^{-\mathrm{i}(\gamma x-\pi/4)}\right] \quad y = 0,\\ &= \frac{\pi}{16\gamma\sqrt{\gamma}} \qquad x = 0. \end{aligned} \tag{D.7}$$

$$
\begin{aligned}
A_\gamma &= 1+\sqrt{\gamma}y-4\gamma\sqrt{\gamma}\frac{x^2}{y}-\mathrm{i}4\gamma x,\\
B_\gamma &= 1-\sqrt{\gamma}y+4\gamma\sqrt{\gamma}\frac{x^2}{y}-\mathrm{i}4\gamma x,\\
C_\gamma &= 4\sqrt{\frac{\gamma x}{\pi}},\quad D_\gamma = 2(1+4\gamma^2x^2-\mathrm{i}4\gamma x),\quad E_\gamma=(1+\mathrm{i}2\gamma x)C_\gamma.
\end{aligned}
$$

$$
\mathcal{K}_\gamma^{(3)}(x,y)=\frac{\pi}{16\gamma\sqrt{\gamma}}+\sqrt{2x}\mathcal{K}_\gamma^{(c3)}(x,y). \tag{D.8}
$$

$$
\begin{aligned}
\mathcal{K}_\gamma^{(4)}(x,y) &= \frac{\pi}{192}\frac{1}{\gamma^2\sqrt{\gamma}}\mathrm{e}^{\mathrm{i}\gamma x}\left[A_\gamma R_- + B_\gamma R_+ + C_\gamma \mathrm{e}^{-\mathrm{i}(\theta_\gamma-\pi/4)}\right] \quad y\neq 0,\\
&= \frac{\pi}{192}\frac{1}{\gamma^2\sqrt{\gamma}}\mathrm{e}^{\mathrm{i}\gamma x}\left[D_\gamma erfc(\tilde{z}) + E_\gamma \mathrm{e}^{-\mathrm{i}(\gamma x-\pi/4)}\right] \quad y=0,\\
&= \frac{\pi}{32\gamma^2\sqrt{\gamma}} \qquad x=0.
\end{aligned} \tag{D.9}
$$

$$
\begin{aligned}
A_\gamma &= 3+3\sqrt{\gamma}y+\gamma y^2-12\gamma^2x^2+\mathrm{i}\left[-6\gamma x-6\gamma\sqrt{\gamma}xy+8\gamma^2\sqrt{\gamma}\frac{x^3}{y}\right],\\
B_\gamma &= 3-3\sqrt{\gamma}y+\gamma y^2-12\gamma^2x^2+\mathrm{i}\left[-6\gamma x+6\gamma\sqrt{\gamma}xy-8\gamma^2\sqrt{\gamma}\frac{x^3}{y}\right],\\
C_\gamma &= (3-\mathrm{i}4\gamma x)\,4\sqrt{\frac{\gamma x}{\pi}},\\
D_\gamma &= 6-24\gamma^2x^2+\mathrm{i}\left[-12\gamma x-16\gamma^3x^3\right],\\
E_\gamma &= \left(3+4\gamma^2x^2-\mathrm{i}4\gamma x\right)4\sqrt{\frac{\gamma x}{\pi}}.
\end{aligned}
$$

$$
\mathcal{K}_\gamma^{(4)}(x,y)=\frac{\pi}{32\gamma^2\sqrt{\gamma}}+\sqrt{2x}\mathcal{K}_\gamma^{(c4)}(x,y). \tag{D.10}
$$

$$
\begin{aligned}
\mathcal{K}_\gamma^{(5)}(x,y) &= \frac{\pi}{96}\frac{1}{16\gamma^3\sqrt{\gamma}}\mathrm{e}^{\mathrm{i}\gamma x}\left[A_\gamma R_- + B_\gamma R_+ + C_\gamma \mathrm{e}^{-\mathrm{i}(\theta_\gamma-\pi/4)}\right] \quad y\neq 0,\\
&= \frac{\pi}{96}\frac{1}{16\gamma^3\sqrt{\gamma}}\mathrm{e}^{\mathrm{i}\gamma x}\left[D_\gamma erfc(\tilde{z}) + E_\gamma \mathrm{e}^{-\mathrm{i}(\gamma x-\pi/4)}\right] \quad y=0,\\
&= \frac{5\pi}{512\gamma^3\sqrt{\gamma}} \qquad x=0.
\end{aligned} \tag{D.11}
$$

$$
\begin{aligned}
A_\gamma &= \gamma\sqrt{\gamma}y^3 + 6\gamma y^2 + 15\sqrt{\gamma}y + 15 - 24\gamma^2\sqrt{\gamma}yx^2 - 24\gamma^2x^2 \\
&\quad + 16\gamma^3\sqrt{\gamma}\frac{x^4}{y} + \mathrm{i}\left[-8\gamma^2y^2x - 24\gamma\sqrt{\gamma}yx + 32\gamma^3x^3 - 24\gamma x\right], \\
B_\gamma &= -\gamma\sqrt{\gamma}y^3 + 6\gamma y^2 - 15\sqrt{\gamma}y + 15 + 24\gamma^2\sqrt{\gamma}yx^2 - 24\gamma^2x^2 \\
&\quad - 16\gamma^3\sqrt{\gamma}\frac{x^4}{y} + \mathrm{i}\left[-8\gamma^2y^2x + 24\gamma\sqrt{\gamma}yx + 32\gamma^3x^3 - 24\gamma x\right], \\
C_\gamma &= \left(\gamma y^2 - 12\gamma^2x^2 + 15 - \mathrm{i}14\gamma x\right)4\sqrt{\frac{\gamma x}{\pi}}, \\
D_\gamma &= 30 - 48\gamma^2x^2 - 32\gamma^4x^4 + \mathrm{i}\left[64\gamma^3x^3 - 48\gamma x\right], \\
E_\gamma &= \left(15 - 12\gamma^2x^2 + \mathrm{i}\left[-8\gamma^3x^3 - 14\gamma x\right]\right)4\sqrt{\frac{\gamma x}{\pi}}.
\end{aligned}
$$

$$
\mathcal{K}_\gamma^{(5)}(x,y) = \frac{5\pi}{512\gamma^3\sqrt{\gamma}} + \sqrt{2x}\mathcal{K}_\gamma^{(c5)}(x,y). \tag{D.12}
$$

$$
\begin{aligned}
\mathcal{K}_\gamma^{(6)}(x,y) &= \frac{\pi}{480}\frac{1}{32\gamma^4\sqrt{\gamma}}\mathrm{e}^{\mathrm{i}\gamma x}\left[A_\gamma R_- + B_\gamma R_+ + C_\gamma\mathrm{e}^{-\mathrm{i}(\theta_\gamma - \pi/4)}\right] \quad y \neq 0, \\
&= \frac{\pi}{480}\frac{1}{32\gamma^4\sqrt{\gamma}}\mathrm{e}^{\mathrm{i}\gamma x}\left[D_\gamma erfc(\tilde{z}) + E_\gamma\mathrm{e}^{-\mathrm{i}(\gamma x - \pi/4)}\right] \quad y = 0, \\
&= \frac{7\pi}{512\gamma^4\sqrt{\gamma}} \qquad x = 0.
\end{aligned} \tag{D.13}
$$

$$
\begin{aligned}
A_\gamma &= \big(\gamma^2y^4 + 10\gamma\sqrt{\gamma}y^3 + 45\gamma y^2 - 40\gamma^3y^2x^2 - 120\gamma^2\sqrt{\gamma}yx^2 \\
&\quad + 105\sqrt{\gamma}y + 80\gamma^4x^4 - 120\gamma^2x^2 + 105 + \mathrm{i}\left[-10\gamma^2\sqrt{\gamma}xy^3\right. \\
&\quad - 60\gamma^2xy^2 + 80\gamma^3\sqrt{\gamma}x^3y - 150\gamma\sqrt{\gamma}xy + 80\gamma^3x^3 - 150\gamma x \\
&\quad \left.-32\gamma^4\sqrt{\gamma}\frac{x^5}{y}\right]\Big), \\
B_\gamma &= \big(\gamma^2y^4 - 10\gamma\sqrt{\gamma}y^3 + 45\gamma y^2 - 40\gamma^3y^2x^2 + 120\gamma^2\sqrt{\gamma}yx^2 \\
&\quad - 105\sqrt{\gamma}y + 80\gamma^4x^4 - 120\gamma^2x^2 + 105 + \mathrm{i}\left[10\gamma^2\sqrt{\gamma}xy^3\right. \\
&\quad - 60\gamma^2xy^2 - 80\gamma^3\sqrt{\gamma}x^3y + 150\gamma\sqrt{\gamma}xy + 80\gamma^3x^3 - 150\gamma x \\
&\quad \left.+32\gamma^4\sqrt{\gamma}\frac{x^5}{y}\right]\Big), \\
C_\gamma &= \left(10\gamma y^2 - 48\gamma^2x^2 + 105 + \mathrm{i}\left[32\gamma^3x^3 - 80\gamma x - 8\gamma^2y^2x\right]\right)4\sqrt{\frac{\gamma x}{\pi}}, \\
D_\gamma &= 210 - 240\gamma^2x^2 + 160\gamma^4x^4 + \mathrm{i}\left[-300\gamma x + 160\gamma^3x^3 + 64\gamma^5x^5\right], \\
E_\gamma &= \left(105 - 48\gamma^2x^2 - 16\gamma^4x^4 + \mathrm{i}\left[-80\gamma x + 32\gamma^3x^3\right]\right)4\sqrt{\frac{\gamma x}{\pi}}.
\end{aligned}
$$

$$\mathcal{K}_\gamma^{(6)}(x,y) = \frac{7\pi}{512\gamma^4\sqrt{\gamma}} + \sqrt{2x}\mathcal{K}_\gamma^{(c6)}(x,y). \tag{D.14}$$

D.2 First derivatives $\frac{\partial}{\partial y}\mathcal{J}_n(x,y)$ and $\frac{\partial}{\partial y}\mathcal{G}_n(x,y)$

After simple derivations we obtain the following results:

$$\begin{aligned}\frac{\partial}{\partial y}\mathcal{K}_\gamma^{(1)}(x,y) &= \frac{\pi}{4}\mathrm{e}^{\mathrm{i}\gamma x}\left[A_\gamma R_- + B_\gamma R_+ + C_\gamma \mathrm{e}^{-\mathrm{i}(\theta_\gamma+\pi/4)}\right] \quad y\neq 0,\\ &= 0 \quad y=0,\\ &= 0 \qquad x=0.\end{aligned} \tag{D.15}$$

$$A_\gamma = -\frac{1}{y^2} - \frac{\sqrt{\gamma}}{y}, \quad B_\gamma = \frac{1}{y^2} - \frac{\sqrt{\gamma}}{y}, \quad C_\gamma = \frac{1}{xy}2\sqrt{\frac{x}{\pi}}.$$

$$\frac{\partial}{\partial y}\mathcal{K}_\gamma^{(1)}(x,y) = \sqrt{2x}\frac{\partial}{\partial y}\mathcal{K}_\gamma^{(c1)}(x,y). \tag{D.16}$$

$$\begin{aligned}\frac{\partial}{\partial y}\mathcal{K}_\gamma^{(2)}(x,y) &= \frac{\pi}{8}\mathrm{e}^{\mathrm{i}\gamma x}\left[A_\gamma R_- + B_\gamma R_+ + C_\gamma \mathrm{e}^{-\mathrm{i}(\theta_\gamma+\pi/4)}\right] \quad y\neq 0,\\ &= 0 \quad y=0,\\ &= 0 \qquad x=0.\end{aligned} \tag{D.17}$$

$$A_\gamma = -1 + \mathrm{i}\left(\frac{2x}{y^2} + \sqrt{\gamma}\frac{2x}{y}\right), \quad B_\gamma = 1 + \mathrm{i}\left(-\frac{2x}{y^2} + \sqrt{\gamma}\frac{2x}{y}\right),$$
$$C_\gamma = -\mathrm{i}\frac{1}{y}4\sqrt{\frac{x}{\pi}}.$$

$$\frac{\partial}{\partial y}\mathcal{K}_\gamma^{(2)}(x,y) = \sqrt{2x}\frac{\partial}{\partial y}\mathcal{K}_\gamma^{(c2)}(x,y). \tag{D.18}$$

$$\begin{aligned}\frac{\partial}{\partial y}\mathcal{K}_\gamma^{(3)}(x,y) &= \frac{\pi}{8}\mathrm{e}^{\mathrm{i}\gamma x}\left[A_\gamma R_- + B_\gamma R_+ + C_\gamma \mathrm{e}^{-\mathrm{i}(\theta_\gamma+\pi/4)}\right] \quad y\neq 0,\\ &= 0 \quad y=0,\\ &= 0 \qquad x=0.\end{aligned} \tag{D.19}$$

$$A_\gamma = \frac{x^2}{y^2} + \sqrt{\gamma}\frac{x^2}{y} - \frac{1}{4\sqrt{\gamma}}y + \mathrm{i}x, \quad B_\gamma = -\frac{x^2}{y^2} + \sqrt{\gamma}\frac{x^2}{y} - \frac{1}{4\sqrt{\gamma}}y - \mathrm{i}x,$$
$$C_\gamma = -\frac{x}{y}2\sqrt{\frac{x}{\pi}}.$$

$$\frac{\partial}{\partial y}\mathcal{K}_\gamma^{(3)}(x,y) = \sqrt{2x}\frac{\partial}{\partial y}\mathcal{K}_\gamma^{(c3)}(x,y). \tag{D.20}$$

$$\begin{aligned}\frac{\partial}{\partial y}\mathcal{K}_\gamma^{(4)}(x,y) &= \frac{\pi}{24}\mathrm{e}^{\mathrm{i}\gamma x}\left[A_\gamma R_- + B_\gamma R_+ + C_\gamma \mathrm{e}^{-\mathrm{i}(\theta_\gamma+\pi/4)}\right] \quad y\neq 0,\\ &= 0 \quad y=0,\\ &= 0 \qquad x=0.\end{aligned} \tag{D.21}$$

$$\begin{aligned}A_\gamma &= \frac{3}{2}x^2 - \frac{1}{8\gamma}y^2 - \frac{1}{8\gamma\sqrt{\gamma}}y + \mathrm{i}\left(\frac{3}{4\sqrt{\gamma}}xy - \frac{x^3}{y^2} - \sqrt{\gamma}\frac{x^3}{y}\right),\\ B_\gamma &= -\frac{3}{2}x^2 + \frac{1}{8\gamma}y^2 - \frac{1}{8\gamma\sqrt{\gamma}}y + \mathrm{i}\left(\frac{3}{4\sqrt{\gamma}}xy + \frac{x^3}{y^2} - \sqrt{\gamma}\frac{x^3}{y}\right),\\ C_\gamma &= \mathrm{i}\left(-\frac{1}{4\gamma}y + \frac{x^2}{y}\right)2\sqrt{\frac{x}{\pi}}.\end{aligned}$$

$$\frac{\partial}{\partial y}\mathcal{K}_\gamma^{(4)}(x,y) = \sqrt{2x}\frac{\partial}{\partial y}\mathcal{K}_\gamma^{(c4)}(x,y). \tag{D.22}$$

$$\begin{aligned}\frac{\partial}{\partial y}\mathcal{K}_\gamma^{(5)}(x,y) &= \frac{\pi}{96}\mathrm{e}^{\mathrm{i}\gamma x}\left[A_\gamma R_- + B_\gamma R_+ + C_\gamma \mathrm{e}^{-\mathrm{i}(\theta_\gamma+\pi/4)}\right] \quad y\neq 0,\\ &= 0 \quad y=0,\\ &= 0 \qquad x=0.\end{aligned} \tag{D.23}$$

$$\begin{aligned}A_\gamma &= -\frac{x^4}{y^2} - \sqrt{\gamma}\frac{x^4}{y} + \frac{3}{2\sqrt{\gamma}}x^2y - \frac{1}{16\gamma\sqrt{\gamma}}y^3 - \frac{3}{16\gamma^2}y^2\\ &\quad - \frac{3}{16\gamma^2\sqrt{\gamma}}y + \mathrm{i}\left[-2x^3 + \frac{1}{2\gamma}xy^2 + \frac{1}{2\gamma\sqrt{\gamma}}xy\right],\\ B_\gamma &= \frac{x^4}{y^2} - \sqrt{\gamma}\frac{x^4}{y} + \frac{3}{2\sqrt{\gamma}}x^2y - \frac{1}{16\gamma\sqrt{\gamma}}y^3 + \frac{3}{16\gamma^2}y^2\\ &\quad - \frac{3}{16\gamma^2\sqrt{\gamma}}y + \mathrm{i}\left[2x^3 - \frac{1}{2\gamma}xy^2 + \frac{1}{2\gamma\sqrt{\gamma}}xy\right],\\ C_\gamma &= \left(\frac{x^3}{y} - \frac{3}{4\gamma}xy - \mathrm{i}\frac{3}{8\gamma^2}y\right)2\sqrt{\frac{x}{\pi}}.\end{aligned}$$

$$\frac{\partial}{\partial y}\mathcal{K}_\gamma^{(5)}(x,y) = \sqrt{2x}\frac{\partial}{\partial y}\mathcal{K}_\gamma^{(c5)}(x,y). \tag{D.24}$$

$$\begin{aligned}\frac{\partial}{\partial y}\mathcal{K}_\gamma^{(6)}(x,y) &= \frac{\pi}{480}\mathrm{e}^{\mathrm{i}\gamma x}\left[A_\gamma R_- + B_\gamma R_+ + C_\gamma \mathrm{e}^{-\mathrm{i}(\theta_\gamma+\pi/4)}\right] \quad y\neq 0,\\ &= 0 \quad y=0,\\ &= 0 \qquad x=0.\end{aligned} \tag{D.25}$$

$$\begin{aligned}A_\gamma &= -\frac{1}{32\gamma^2}y^4 - \frac{3}{16\gamma^2\sqrt{\gamma}}y^3 - \frac{15}{32\gamma^3}y^2 - \frac{15}{32\gamma^3\sqrt{\gamma}}y\\ &\quad + \frac{5}{4\gamma}x^2y^2 + \frac{5}{4\gamma\sqrt{\gamma}}x^2y - \frac{5}{2}x^4 + \mathrm{i}\left[\frac{x^5}{y^2} + \sqrt{\gamma}\frac{x^5}{y}\right.\\ &\quad \left. + \frac{5}{16\gamma\sqrt{\gamma}}xy^3 + \frac{15}{16\gamma^2}xy^2 - \frac{5}{2\sqrt{\gamma}}x^3y + \frac{15}{16\gamma^2\sqrt{\gamma}}xy\right],\\ B_\gamma &= \frac{1}{32\gamma^2}y^4 - \frac{3}{16\gamma^2\sqrt{\gamma}}y^3 + \frac{15}{32\gamma^3}y^2 - \frac{15}{32\gamma^3\sqrt{\gamma}}y\\ &\quad - \frac{5}{4\gamma}x^2y^2 + \frac{5}{4\gamma\sqrt{\gamma}}x^2y + \frac{5}{2}x^4 + \mathrm{i}\left[-\frac{x^5}{y^2} + \sqrt{\gamma}\frac{x^5}{y}\right.\\ &\quad \left. + \frac{5}{16\gamma\sqrt{\gamma}}xy^3 - \frac{15}{16\gamma^2}xy^2 - \frac{5}{2\sqrt{\gamma}}x^3y + \frac{15}{16\gamma^2\sqrt{\gamma}}xy\right],\\ C_\gamma &= \left(-\frac{5}{4\gamma^2}xy + \mathrm{i}\left[-\frac{x^4}{y} - \frac{1}{16\gamma^2}y^3 + \frac{3}{2\gamma}x^2y - \frac{15}{16\gamma^3}y\right]\right)\\ &\quad \times 2\sqrt{\frac{x}{\pi}}.\end{aligned}$$

$$\frac{\partial}{\partial y}\mathcal{K}_\gamma^{(6)}(x,y) = \sqrt{2x}\frac{\partial}{\partial y}\mathcal{K}_\gamma^{(c6)}(x,y). \tag{D.26}$$

D.3 Second derivatives $\frac{\partial^2}{\partial y^2}\mathcal{J}_n(x,y)$ and $\frac{\partial^2}{\partial y^2}\mathcal{G}_n(x,y)$

From the above expressions, we deduce the following:

$$\begin{aligned}\frac{\partial^2}{\partial y^2}\mathcal{K}_\gamma^{(1)}(x,y) &= \frac{\pi}{4}\mathrm{e}^{\mathrm{i}\gamma x}\left[A_\gamma R_- + B_\gamma R_+ + C_\gamma \mathrm{e}^{-\mathrm{i}(\theta_\gamma+\pi/4)}\right] \quad y\neq 0,\\ &= \frac{\pi}{4}\mathrm{e}^{\mathrm{i}\gamma x}\left[D_\gamma erfc(\tilde{z}) + E_\gamma \mathrm{e}^{-\mathrm{i}(\gamma x+\pi/4)}\right] \quad y=0,\\ &= -\frac{\pi}{6}\gamma\sqrt{\gamma} \qquad x=0.\end{aligned} \tag{D.27}$$

$$
\begin{aligned}
A_\gamma &= \frac{2}{y^3} + \sqrt{\gamma}\frac{2}{y^2} + \gamma\frac{1}{y},\\
B_\gamma &= -\frac{2}{y^3} + \sqrt{\gamma}\frac{2}{y^2} - \gamma\frac{1}{y},\\
C_\gamma &= \left(-\frac{2}{xy^2} + \mathrm{i}\frac{1}{2x^2}\right) 2\sqrt{\frac{x}{\pi}},\\
D_\gamma &= -\frac{2}{3}\gamma\sqrt{\gamma},\\
E_\gamma &= \left(\frac{1}{3x}\gamma + \mathrm{i}\frac{1}{6x^2}\right) 2\sqrt{\frac{x}{\pi}}.
\end{aligned}
$$

$$
\frac{\partial^2}{\partial y^2}\mathcal{K}_\gamma^{(1)}(x,y) = -\frac{\pi}{6}\gamma\sqrt{\gamma} + \sqrt{2x}\frac{\partial^2}{\partial y^2}\mathcal{K}_\gamma^{(c1)}(x,y). \tag{D.28}
$$

$$
\begin{aligned}
\frac{\partial^2}{\partial y^2}\mathcal{K}_\gamma^{(2)}(x,y) &= \frac{\pi}{8}\mathrm{e}^{\mathrm{i}\gamma x}\left[A_\gamma R_- + B_\gamma R_+ + C_\gamma \mathrm{e}^{-\mathrm{i}(\theta_\gamma+\pi/4)}\right] \quad y \neq 0,\\
&= \frac{\pi}{8}\mathrm{e}^{\mathrm{i}\gamma x}\left[D_\gamma erfc(\tilde{z}) + E_\gamma \mathrm{e}^{-\mathrm{i}(\gamma x+\pi/4)}\right] \quad y = 0,\\
&= \frac{\sqrt{\gamma}\pi}{4} \qquad x = 0.
\end{aligned} \tag{D.29}
$$

$$
\begin{aligned}
A_\gamma &= \sqrt{\gamma} - \mathrm{i}\left[\frac{4x}{y^3} + \sqrt{\gamma}\frac{4x}{y^2} + \gamma\frac{2x}{y}\right],\\
B_\gamma &= \sqrt{\gamma} - \mathrm{i}\left[-\frac{4x}{y^3} + \sqrt{\gamma}\frac{4x}{y^2} - \gamma\frac{2x}{y}\right],\\
C_\gamma &= \mathrm{i}\frac{8}{y^2}\sqrt{\frac{x}{\pi}},\\
D_\gamma &= 2\sqrt{\gamma} + \mathrm{i}\frac{4}{3}\gamma\sqrt{\gamma}x,\\
E_\gamma &= \left(-\frac{2}{3x} - \mathrm{i}\frac{2}{3}\gamma\right) 2\sqrt{\frac{x}{\pi}}.
\end{aligned}
$$

$$
\frac{\partial^2}{\partial y^2}\mathcal{K}_\gamma^{(2)}(x,y) = \frac{\sqrt{\gamma}\pi}{4} + \sqrt{2x}\frac{\partial^2}{\partial y^2}\mathcal{K}_\gamma^{(c2)}(x,y). \tag{D.30}
$$

$$
\begin{aligned}
\frac{\partial^2}{\partial y^2}\mathcal{K}_\gamma^{(3)}(x,y) &= \frac{\pi}{8}\mathrm{e}^{\mathrm{i}\gamma x}\left[A_\gamma R_- + B_\gamma R_+ + C_\gamma \mathrm{e}^{-\mathrm{i}(\theta_\gamma+\pi/4)}\right] \quad y \neq 0,\\
&= \frac{\pi}{8}\mathrm{e}^{\mathrm{i}\gamma x}\left[D_\gamma erfc(\tilde{z}) + E_\gamma \mathrm{e}^{-\mathrm{i}(\gamma x+\pi/4)}\right] \quad y = 0,\\
&= -\frac{\pi}{16\sqrt{\gamma}} \qquad x = 0.
\end{aligned} \tag{D.31}
$$

$$
\begin{aligned}
A_\gamma &= -\frac{2x^2}{y^3} - \sqrt{\gamma}\frac{2x^2}{y^2} - \gamma\frac{x^2}{y} + \frac{1}{4}y - \frac{1}{4\sqrt{\gamma}} - \mathrm{i}\sqrt{\gamma}x,\\
B_\gamma &= \frac{2x^2}{y^3} - \sqrt{\gamma}\frac{2x^2}{y^2} + \gamma\frac{x^2}{y} - \frac{1}{4}y - \frac{1}{4\sqrt{\gamma}} - \mathrm{i}\sqrt{\gamma}x,\\
C_\gamma &= \left(\frac{2x}{y^2} + \mathrm{i}\frac{1}{2}\right) 2\sqrt{\frac{x}{\pi}},\\
D_\gamma &= -\frac{1}{2\sqrt{\gamma}} + \frac{2}{3}\gamma\sqrt{\gamma}x^2 - \mathrm{i}2\sqrt{\gamma}x,\\
E_\gamma &= \left(-\frac{1}{3}\gamma x + \mathrm{i}\frac{5}{6}\right) 2\sqrt{\frac{x}{\pi}}.
\end{aligned}
$$

$$
\frac{\partial^2}{\partial y^2}\mathcal{K}_\gamma^{(3)}(x,y) = -\frac{\pi}{16\sqrt{\gamma}} + \sqrt{2x}\frac{\partial^2}{\partial y^2}\mathcal{K}_\gamma^{(c3)}(x,y). \tag{D.32}
$$

$$
\begin{aligned}
\frac{\partial^2}{\partial y^2}\mathcal{K}_\gamma^{(4)}(x,y) &= \frac{\pi}{24}\mathrm{e}^{\mathrm{i}\gamma x}\left[A_\gamma R_- + B_\gamma R_+ + C_\gamma \mathrm{e}^{-\mathrm{i}(\theta_\gamma+\pi/4)}\right] \quad y \neq 0,\\
&= \frac{\pi}{24}\mathrm{e}^{\mathrm{i}\gamma x}\left[D_\gamma erfc(\tilde{z}) + E_\gamma \mathrm{e}^{-\mathrm{i}(\gamma x+\pi/4)}\right] \quad y = 0,\\
&= -\frac{\pi}{96\gamma\sqrt{\gamma}} \qquad x = 0.
\end{aligned} \tag{D.33}
$$

$$
\begin{aligned}
A_\gamma &= \frac{1}{8\sqrt{\gamma}}y^2 - \frac{1}{8\gamma}y - \sqrt{\gamma}\frac{3}{2}x^2 - \frac{1}{8\gamma\sqrt{\gamma}}\\
&\quad + \mathrm{i}\left[\frac{2x^3}{y^3} + \sqrt{\gamma}\frac{2x^3}{y^2} + \gamma\frac{x^3}{y} - \frac{3}{4}xy + \frac{3}{4\sqrt{\gamma}}x\right],\\
B_\gamma &= \frac{1}{8\sqrt{\gamma}}y^2 + \frac{1}{8\gamma}y - \sqrt{\gamma}\frac{3}{2}x^2 - \frac{1}{8\gamma\sqrt{\gamma}}\\
&\quad + \mathrm{i}\left[-\frac{2x^3}{y^3} + \sqrt{\gamma}\frac{2x^3}{y^2} - \gamma\frac{x^3}{y} + \frac{3}{4}xy + \frac{3}{4\sqrt{\gamma}}x\right],\\
C_\gamma &= \left(x + \mathrm{i}\left[-\frac{1}{4\gamma} - \frac{2x^2}{y^2}\right]\right) 2\sqrt{\frac{x}{\pi}},\\
D_\gamma &= -\frac{1}{4\gamma\sqrt{\gamma}} - 3\sqrt{\gamma}x^2 + \mathrm{i}\left[\frac{3}{2\sqrt{\gamma}}x - \frac{2}{3}\gamma\sqrt{\gamma}x^3\right],\\
E_\gamma &= \left(\frac{4}{3}x + \mathrm{i}\left[\frac{1}{3}\gamma x^2 - \frac{1}{4\gamma}\right]\right) 2\sqrt{\frac{x}{\pi}}.
\end{aligned}
$$

$$
\frac{\partial^2}{\partial y^2}\mathcal{K}_\gamma^{(4)}(x,y) = -\frac{\pi}{96\gamma\sqrt{\gamma}} + \sqrt{2x}\frac{\partial^2}{\partial y^2}\mathcal{K}_\gamma^{(c4)}(x,y). \tag{D.34}
$$

$$\begin{aligned}\frac{\partial^2}{\partial y^2}\mathcal{K}_\gamma^{(5)}(x,y) &= \frac{\pi}{96}\mathrm{e}^{\mathrm{i}\gamma x}\left[A_\gamma R_- + B_\gamma R_+ + C_\gamma \mathrm{e}^{-\mathrm{i}(\theta_\gamma+\pi/4)}\right] \quad y\neq 0,\\ &= \frac{\pi}{96}\mathrm{e}^{\mathrm{i}\gamma x}\left[D_\gamma erfc(\tilde{z}) + E_\gamma \mathrm{e}^{-\mathrm{i}(\gamma x+\pi/4)}\right] \quad y=0,\\ &= -\frac{\pi}{256\gamma^2\sqrt{\gamma}} \qquad x=0. \end{aligned} \tag{D.35}$$

$$\begin{aligned}A_\gamma &= \frac{2x^4}{y^3}+\sqrt{\gamma}\frac{2x^4}{y^2}+\gamma\frac{x^4}{y}-\frac{3}{2}x^2y+\frac{3}{2\sqrt{\gamma}}x^2+\frac{1}{16\gamma}y^3\\ &\quad -\frac{3}{16\gamma^2}y-\frac{3}{16\gamma^2\sqrt{\gamma}}+\mathrm{i}\left[-\frac{1}{2\sqrt{\gamma}}xy^2+\frac{1}{2\gamma}xy+2\sqrt{\gamma}x^3\right.\\ &\quad \left.+\frac{1}{2\gamma\sqrt{\gamma}}x\right],\\ B_\gamma &= -\frac{2x^4}{y^3}+\sqrt{\gamma}\frac{2x^4}{y^2}-\gamma\frac{x^4}{y}+\frac{3}{2}x^2y+\frac{3}{2\sqrt{\gamma}}x^2-\frac{1}{16\gamma}y^3\\ &\quad +\frac{3}{16\gamma^2}y-\frac{3}{16\gamma^2\sqrt{\gamma}}+\mathrm{i}\left[-\frac{1}{2\sqrt{\gamma}}xy^2-\frac{1}{2\gamma}xy+2\sqrt{\gamma}x^3\right.\\ &\quad \left.+\frac{1}{2\gamma\sqrt{\gamma}}x\right],\\ C_\gamma &= \left(-\frac{2x^3}{y^2}-\frac{3}{4\gamma}x+\mathrm{i}\left[-\frac{3}{2}x^2+\frac{1}{8\gamma}y^2-\frac{3}{8\gamma^2}\right]\right)2\sqrt{\frac{x}{\pi}},\\ D_\gamma &= -\frac{2}{3}\gamma\sqrt{\gamma}x^4+\frac{3}{\sqrt{\gamma}}x^2-\frac{3}{8\gamma^2\sqrt{\gamma}}+\mathrm{i}\left[4\sqrt{\gamma}x^3+\frac{1}{\gamma\sqrt{\gamma}}x\right],\\ E_\gamma &= \left(\frac{1}{3}\gamma x^3-\frac{3}{4\gamma}x+\mathrm{i}\left[-\frac{11}{6}x^2-\frac{3}{8\gamma^2}\right]\right)2\sqrt{\frac{x}{\pi}}.\end{aligned}$$

$$\frac{\partial^2}{\partial y^2}\mathcal{K}_\gamma^{(5)}(x,y) = -\frac{\pi}{256\gamma^2\sqrt{\gamma}}+\sqrt{2x}\frac{\partial^2}{\partial y^2}\mathcal{K}_\gamma^{(\mathrm{c}5)}(x,y). \tag{D.36}$$

$$\begin{aligned}\frac{\partial^2}{\partial y^2}\mathcal{K}_\gamma^{(6)}(x,y) &= \frac{\pi}{480}\mathrm{e}^{\mathrm{i}\gamma x}\left[A_\gamma R_- + B_\gamma R_+ + C_\gamma \mathrm{e}^{-\mathrm{i}(\theta_\gamma+\pi/4)}\right] \quad y\neq 0,\\ &= \frac{\pi}{480}\mathrm{e}^{\mathrm{i}\gamma x}\left[D_\gamma erfc(\tilde{z}) + E_\gamma \mathrm{e}^{-\mathrm{i}(\gamma x+\pi/4)}\right] \quad y=0,\\ &= -\frac{\pi}{512\gamma^3\sqrt{\gamma}} \qquad x=0. \end{aligned} \tag{D.37}$$

$$
\begin{aligned}
A_\gamma &= \frac{1}{32\gamma\sqrt{\gamma}}y^4 + \frac{1}{16\gamma^2}y^3 - \frac{3}{32\gamma^2\sqrt{\gamma}}y^2 - \frac{15}{32\gamma^3}y - \frac{5}{4\sqrt{\gamma}}x^2y^2 \\
&+ \frac{5}{4\gamma}x^2y + \frac{5}{2}\sqrt{\gamma}x^4 + \frac{5}{4\gamma\sqrt{\gamma}}x^2 - \frac{15}{32\gamma^3\sqrt{\gamma}} + \mathrm{i}\left[-\frac{2x^5}{y^3} - \sqrt{\gamma}\frac{2x^5}{y^2}\right. \\
&\left.-\gamma\frac{x^5}{y} - \frac{5}{16\gamma}xy^3 + \frac{5}{2}x^3y + \frac{15}{16\gamma^2}xy - \frac{5}{2\sqrt{\gamma}}x^3 + \frac{15}{16\gamma^2\sqrt{\gamma}}x\right], \\
B_\gamma &= \frac{1}{32\gamma\sqrt{\gamma}}y^4 - \frac{1}{16\gamma^2}y^3 - \frac{3}{32\gamma^2\sqrt{\gamma}}y^2 + \frac{15}{32\gamma^3}y - \frac{5}{4\sqrt{\gamma}}x^2y^2 \\
&- \frac{5}{4\gamma}x^2y + \frac{5}{2}\sqrt{\gamma}x^4 + \frac{5}{4\gamma\sqrt{\gamma}}x^2 - \frac{15}{32\gamma^3\sqrt{\gamma}} + \mathrm{i}\left[\frac{2x^5}{y^3} - \sqrt{\gamma}\frac{2x^5}{y^2}\right. \\
&\left.+\gamma\frac{x^5}{y} + \frac{5}{16\gamma}xy^3 - \frac{5}{2}x^3y - \frac{15}{16\gamma^2}xy - \frac{5}{2\sqrt{\gamma}}x^3 + \frac{15}{16\gamma^2\sqrt{\gamma}}x\right], \\
C_\gamma &= \left(\frac{1}{2\gamma}xy^2 - 2x^3 - \frac{5}{4\gamma^2}x + \mathrm{i}\left[\frac{2x^4}{y^2} + \frac{1}{8\gamma^2}y^2 + \frac{3}{2\gamma}x^2 - \frac{15}{16\gamma^3}\right]\right) \\
&\times 2\sqrt{\frac{x}{\pi}}, \\
D_\gamma &= 5\sqrt{\gamma}x^4 + \frac{5}{2\gamma\sqrt{\gamma}}x^2 - \frac{15}{16\gamma^3\sqrt{\gamma}} + \mathrm{i}\left[\frac{2}{3}\gamma\sqrt{\gamma}x^5 - \frac{5}{\sqrt{\gamma}}x^3\right. \\
&\left.+\frac{15}{8\gamma^2\sqrt{\gamma}}x\right], \\
E_\gamma &= \left(-\frac{7}{3}x^3 - \frac{5}{4\gamma^2}x + \mathrm{i}\left[-\frac{1}{3}\gamma x^4 + \frac{3}{2\gamma}x^2 - \frac{15}{16\gamma^3}\right]\right) 2\sqrt{\frac{x}{\pi}}.
\end{aligned}
$$

$$
\frac{\partial^2}{\partial y^2}\mathcal{K}_\gamma^{(6)}(x,y) = -\frac{\pi}{512\gamma^3\sqrt{\gamma}} + \sqrt{2x}\frac{\partial^2}{\partial y^2}\mathcal{K}_\gamma^{(c6)}(x,y). \tag{D.38}
$$

D.4 Functions $\widetilde{\mathcal{D}}_n(x,y;k)$ and $\widetilde{\mathcal{M}}_n(x,y;k)$

We define the following basic functions

Basic integrals

$$
\widetilde{\mathcal{K}}_\gamma^{(n)}(x,y;k) = \frac{1}{y}\int_{-\infty}^{+\infty}\mathrm{d}p\frac{p}{(p^2+\gamma)^n(p^2-k^2-\mathrm{i}\epsilon)}exp\left(-\mathrm{i}xp^2+\mathrm{i}yp\right) \tag{D.39}
$$

$$
= \frac{1}{y}\frac{(-1)^n}{(n-1)!}\frac{\partial^{(n-1)}}{\partial\gamma^{(n-1)}}\left\{\frac{1}{\gamma-\beta}\left[I_\gamma(x,y) - I_\beta(x,y)\right]\right\} \tag{D.40}
$$

with $\beta = -k^2 + \mathrm{i}\epsilon$. Then, for $\gamma = 1$ $\widetilde{\mathcal{K}}_1^{(n)}(x,y;k) \equiv \widetilde{\mathcal{D}}_n(x,y;k)$, and for $\gamma = 1/4$ $\widetilde{\mathcal{K}}_{1/4}^{(n)}(x,y;k) \equiv \widetilde{\mathcal{M}}_n(x,y;k)$.

$$\widetilde{\mathcal{K}}_\gamma^{(1)}(x,y;k) = -\frac{1}{\gamma+k^2}\left[\frac{I_\gamma(x,y)-I_\beta(x,y)}{y}\right]. \tag{D.41}$$

We show without difficulty the recurrence relation

$$\widetilde{\mathcal{K}}_\gamma^{(n)}(x,y;k) = \frac{1}{\gamma+k^2}\left[\widetilde{\mathcal{K}}_\gamma^{(n-1)}(x,y;k) - 2\mathrm{i}\mathcal{K}_\gamma^{(n)}(x,y)\right] \quad n \geq 2, \tag{D.42}$$

from which we deduce the remaining necessary expressions.

D.5 First derivatives $\frac{\partial}{\partial y}\widetilde{\mathcal{D}}_n(x,y;k)$ and $\frac{\partial}{\partial y}\widetilde{\mathcal{M}}_n(x,y;k)$

Using,

$$\frac{\partial}{\partial y}\widetilde{\mathcal{K}}_\gamma^{(1)}(x,y;k) = -\frac{1}{\gamma+k^2}\frac{\partial}{\partial y}\left[\frac{I_\gamma(x,y)-I_\beta(x,y)}{y}\right], \tag{D.43}$$

and for $n \geq 2$

$$\frac{\partial}{\partial y}\widetilde{\mathcal{K}}_\gamma^{(n)}(x,y;k) = \frac{1}{\gamma+k^2}\left[\frac{\partial}{\partial y}\widetilde{\mathcal{K}}_\gamma^{(n-1)}(x,y;k) - 2\mathrm{i}\frac{\partial}{\partial y}\mathcal{K}_\gamma^{(n)}(x,y)\right], \tag{D.44}$$

we easily recover the needed expressions.

D.6 Second derivatives $\frac{\partial^2}{\partial y^2}\widetilde{\mathcal{D}}_n(x,y;k)$ and $\frac{\partial^2}{\partial y^2}\widetilde{\mathcal{M}}_n(x,y;k)$

These expressions can be obtained from the previous one by using the relations below

$$\frac{\partial^2}{\partial y^2}\widetilde{\mathcal{K}}_\gamma^{(1)}(x,y;k) = -\frac{1}{\gamma+k^2}\frac{\partial^2}{\partial y^2}\left[\frac{I_\gamma(x,y)-I_\beta(x,y)}{y}\right], \tag{D.45}$$

and for $n \geq 2$

$$\frac{\partial^2}{\partial y^2}\widetilde{\mathcal{K}}_\gamma^{(n)}(x,y;k) = \frac{1}{\gamma+k^2}\left[\frac{\partial^2}{\partial y^2}\widetilde{\mathcal{K}}_\gamma^{(n-1)}(x,y;k) - 2\mathrm{i}\frac{\partial^2}{\partial y^2}\mathcal{K}_\gamma^{(n)}(x,y)\right]. \tag{D.46}$$

D.7 Explicit analytical expressions of functions $\mathcal{H}_k^{(i)}(t)$

Guided by the above results, we then give the following terms $\mathcal{H}_k^{(i)}(t)$ in their closed-form expressions suited for the computation of physical observables considered in this thesis.

$$\mathcal{H}_k^{(1)}(t) = \Phi(\boldsymbol{k},0)\exp\left(-\mathrm{i}\frac{t}{2}\boldsymbol{k}^2 + \mathrm{i}b(t)(\boldsymbol{k}\cdot\hat{\boldsymbol{e}})\right). \tag{D.47}$$

$$\begin{aligned}\mathcal{H}_k^{(2)}(t) = {}& \mathrm{i}\frac{448\sqrt{2}}{27\pi}\tilde{a}_{12}\left[\widetilde{\mathcal{D}}_1(x,y;k) - \widetilde{\mathcal{M}}_1(x,y;k)\right] \\ & + \mathrm{i}\frac{80\sqrt{2}}{9\pi}\tilde{a}_{12}\widetilde{\mathcal{D}}_2(x,y;k) + \mathrm{i}\frac{16}{\pi}\tilde{a}_{22}\widetilde{\mathcal{D}}_3(x,y;k) \\ & + \mathrm{i}\frac{32\sqrt{2}}{9\pi}\tilde{a}_{12}\widetilde{\mathcal{M}}_2(x,y;k),\end{aligned} \tag{D.48}$$

with $x = t/2$ and $y = b(t)$.

$$\mathcal{H}_k^{(3)}(t) = \int_0^t \mathrm{d}\zeta F_1(\zeta)\exp\left(-\mathrm{i}\frac{(t-\zeta)}{2}\boldsymbol{k}^2 + \mathrm{i}(b(t)-b(\zeta))(\boldsymbol{k}\cdot\hat{\boldsymbol{e}})\right). \tag{D.49}$$

$$\begin{aligned}\mathcal{H}_k^{(4)}(t) = {}& \mathrm{i}\frac{8}{\pi}\tilde{a}_{22}^2\int_0^t \mathrm{d}\zeta\widetilde{\mathcal{D}}_2(x,y;k)F_1(\zeta) \\ & + \mathrm{i}\frac{1}{\pi}\tilde{a}_{12}^2\int_0^t \mathrm{d}\zeta\left[\frac{1}{4}\widetilde{\mathcal{M}}_4(x,y;k) - \widetilde{\mathcal{M}}_3(x,y;k) + \widetilde{\mathcal{M}}_2(x,y;k)\right] \\ & \times F_1(\zeta) \\ & + \mathrm{i}\frac{80\sqrt{2}}{9\pi}\tilde{a}_{12}\tilde{a}_{22}\int_0^t \mathrm{d}\zeta\left[\widetilde{\mathcal{D}}_1(x,y;k) - \widetilde{\mathcal{M}}_1(x,y;k)\right. \\ & \left. + \frac{3}{10}\widetilde{\mathcal{M}}_2(x,y;k)\right]F_1(\zeta)\end{aligned} \tag{D.50}$$

where $x = (t-\zeta)/2$ and $y = b(t) - b(\zeta)$.

$$\begin{aligned}\mathcal{H}_k^{(5)}(t) = {}& -\mathrm{i}\frac{448\sqrt{2}}{27\pi}\tilde{a}_{11}\left[\widetilde{\mathcal{D}}_1(x,y;k) - \widetilde{\mathcal{M}}_1(x,y;k)\right] \\ & - \mathrm{i}\frac{80\sqrt{2}}{9\pi}\tilde{a}_{11}\widetilde{\mathcal{D}}_2(x,y;k) - \mathrm{i}\frac{16}{\pi}\tilde{a}_{12}\widetilde{\mathcal{D}}_3(x,y;k) \\ & - \mathrm{i}\frac{32\sqrt{2}}{9\pi}\tilde{a}_{11}\widetilde{\mathcal{M}}_2(x,y;k),\end{aligned} \tag{D.51}$$

with $x = t/2$ and $y = b(t)$.

$$\mathcal{H}_k^{(6)}(t) = \int_0^t \mathrm{d}\zeta F_2(\zeta) \exp\left(-\mathrm{i}\frac{(t-\zeta)}{2}\boldsymbol{k}^2 + \mathrm{i}(b(t)-b(\zeta))(\boldsymbol{k}\cdot\hat{\boldsymbol{e}})\right). \tag{D.52}$$

$$\begin{aligned}\mathcal{H}_k^{(7)}(t) = {} & \mathrm{i}\frac{8}{\pi}\tilde{a}_{12}^2 \int_0^t \mathrm{d}\zeta \widetilde{\mathcal{D}}_2(x,y;k) F_2(\zeta) \\ & + \mathrm{i}\frac{1}{\pi}\tilde{a}_{11}^2 \int_0^t \mathrm{d}\zeta \left[\frac{1}{4}\widetilde{\mathcal{M}}_4(x,y;k) - \widetilde{\mathcal{M}}_3(x,y;k) + \widetilde{\mathcal{M}}_2(x,y;k)\right] \\ & \times F_2(\zeta) \\ & + \mathrm{i}\frac{80\sqrt{2}}{9\pi}\tilde{a}_{11}\tilde{a}_{12} \int_0^t \mathrm{d}\zeta \left[\widetilde{\mathcal{D}}_1(x,y;k) - \widetilde{\mathcal{M}}_1(x,y;k)\right. \\ & \left. + \frac{3}{10}\widetilde{\mathcal{M}}_2(x,y;k)\right] F_2(\zeta)\end{aligned} \tag{D.53}$$

where $x = (t-\zeta)/2$ and $y = b(t) - b(\zeta)$.

$$\begin{aligned}\mathcal{H}_k^{(8)}(t) = {} & -\mathrm{i}\frac{8}{\pi}\tilde{a}_{12}\tilde{a}_{22} \int_0^t \mathrm{d}\zeta \widetilde{\mathcal{D}}_2(x,y;k) F_2(\zeta) \\ & - \mathrm{i}\frac{1}{\pi}\tilde{a}_{12}\tilde{a}_{11} \int_0^t \mathrm{d}\zeta \left[\frac{1}{4}\widetilde{\mathcal{M}}_4(x,y;k) - \widetilde{\mathcal{M}}_3(x,y;k) + \widetilde{\mathcal{M}}_2(x,y;k)\right] \\ & \times F_2(\zeta) \\ & - \mathrm{i}\frac{40\sqrt{2}}{9\pi}(\tilde{a}_{11}\tilde{a}_{22} + \tilde{a}_{12}^2) \int_0^t \mathrm{d}\zeta \left[\widetilde{\mathcal{D}}_1(x,y;k) - \widetilde{\mathcal{M}}_1(x,y;k)\right. \\ & \left. + \frac{3}{10}\widetilde{\mathcal{M}}_2(x,y;k)\right] F_2(\zeta)\end{aligned} \tag{D.54}$$

where $x = (t-\zeta)/2$ and $y = b(t) - b(\zeta)$.

$$\begin{aligned}\mathcal{H}_k^{(9)}(t) = {} & -\mathrm{i}\frac{8}{\pi}\tilde{a}_{12}\tilde{a}_{22} \int_0^t \mathrm{d}\zeta \widetilde{\mathcal{D}}_2(x,y;k) F_1(\zeta) \\ & - \mathrm{i}\frac{1}{\pi}\tilde{a}_{12}\tilde{a}_{11} \int_0^t \mathrm{d}\zeta \left[\frac{1}{4}\widetilde{\mathcal{M}}_4(x,y;k) - \widetilde{\mathcal{M}}_3(x,y;k) + \widetilde{\mathcal{M}}_2(x,y;k)\right] \\ & \times F_1(\zeta) \\ & - \mathrm{i}\frac{40\sqrt{2}}{9\pi}(\tilde{a}_{11}\tilde{a}_{22} + \tilde{a}_{12}^2) \int_0^t \mathrm{d}\zeta \left[\widetilde{\mathcal{D}}_1(x,y;k) - \widetilde{\mathcal{M}}_1(x,y;k)\right. \\ & \left. + \frac{3}{10}\widetilde{\mathcal{M}}_2(x,y;k)\right] F_1(\zeta)\end{aligned} \tag{D.55}$$

where $x = (t-\zeta)/2$ and $y = b(t) - b(\zeta)$.

$$\mathcal{H}_k^{(10)}(t) = \frac{1024\sqrt{2}}{27\pi}\frac{\partial}{\partial y}\left[\widetilde{\mathcal{D}}_1(x,y;k) - \widetilde{\mathcal{M}}_1(x,y;k)\right] + \frac{128\sqrt{2}}{9\pi}\frac{\partial}{\partial y}\left[\widetilde{\mathcal{D}}_2(x,y;k) + \widetilde{\mathcal{M}}_2(x,y;k)\right] \tag{D.56}$$

where $x = t/2$ and $y = b(t)$.

$$\mathcal{H}_k^{(11)}(t) = \int_0^t \mathrm{d}\zeta F_3(\zeta)\exp\left(-\mathrm{i}\frac{(t-\zeta)}{2}\boldsymbol{k}^2 + \mathrm{i}(b(t)-b(\zeta))(\boldsymbol{k}\cdot\hat{\boldsymbol{e}})\right). \tag{D.57}$$

$$\mathcal{H}_k^{(12)}(t) = -\mathrm{i}\frac{4}{\pi}\int_0^t \mathrm{d}\zeta \frac{\partial^2}{\partial y^2}\widetilde{\mathcal{M}}_4(x,y;k)F_3(\zeta) \tag{D.58}$$

with $x = (t-\zeta)/2$ and $y = b(t) - b(\zeta)$.

$$\mathcal{H}_k^{(13)}(t) = \frac{64\sqrt{2}}{\pi}\tilde{a}_{22}\int_0^t \mathrm{d}\zeta\frac{\partial}{\partial y}\left[\frac{1}{9}\left\{\widetilde{\mathcal{D}}_1(x,y;k) - \widetilde{\mathcal{M}}_1(x,y;k)\right\} + \frac{1}{12}\widetilde{\mathcal{M}}_2(x,y;k)\right]F_3(\zeta) + \frac{1}{\pi}\tilde{a}_{12}\int_0^t \mathrm{d}\zeta\frac{\partial}{\partial y}\left[\widetilde{\mathcal{M}}_4(x,y;k) - 2\widetilde{\mathcal{M}}_3(x,y;k)\right]F_3(\zeta) \tag{D.59}$$

with $x = (t-\zeta)/2$ and $y = b(t) - b(\zeta)$.

$$\mathcal{H}_k^{(14)}(t) = -\frac{64\sqrt{2}}{\pi}\tilde{a}_{12}\int_0^t \mathrm{d}\zeta\frac{\partial}{\partial y}\left[\frac{1}{9}\left\{\widetilde{\mathcal{D}}_1(x,y;k) - \widetilde{\mathcal{M}}_1(x,y;k)\right\} + \frac{1}{12}\widetilde{\mathcal{M}}_2(x,y;k)\right]F_3(\zeta) - \frac{1}{\pi}\tilde{a}_{11}\int_0^t \mathrm{d}\zeta\frac{\partial}{\partial y}\left[\widetilde{\mathcal{M}}_4(x,y;k) - 2\widetilde{\mathcal{M}}_3(x,y;k)\right]F_3(\zeta) \tag{D.60}$$

with $x = (t-\zeta)/2$ and $y = b(t) - b(\zeta)$.

$$\mathcal{H}_k^{(15)}(t) = \frac{64\sqrt{2}}{\pi}\tilde{a}_{22}\int_0^t \mathrm{d}\zeta\frac{\partial}{\partial y}\left[\frac{1}{9}\left\{\widetilde{\mathcal{D}}_1(x,y;k) - \widetilde{\mathcal{M}}_1(x,y;k)\right\} + \frac{1}{12}\widetilde{\mathcal{M}}_2(x,y;k)\right]F_1(\zeta) + \frac{1}{\pi}\tilde{a}_{12}\int_0^t \mathrm{d}\zeta\frac{\partial}{\partial y}\left[\widetilde{\mathcal{M}}_4(x,y;k) - 2\widetilde{\mathcal{M}}_3(x,y;k)\right]F_1(\zeta) \tag{D.61}$$

with $x = (t-\zeta)/2$ and $y = b(t) - b(\zeta)$.

$$\begin{aligned}\mathcal{H}_k^{(16)}(t) = -\frac{64\sqrt{2}}{\pi}\tilde{a}_{12}\int_0^t \mathrm{d}\zeta \frac{\partial}{\partial y}\Bigg[\frac{1}{9}\left\{\widetilde{\mathcal{D}}_1(x,y;k) - \widetilde{\mathcal{M}}_1(x,y;k)\right\} \\ +\frac{1}{12}\widetilde{\mathcal{M}}_2(x,y;k)\Bigg] F_2(\zeta) - \frac{1}{\pi}\tilde{a}_{11}\int_0^t \mathrm{d}\zeta \frac{\partial}{\partial y}\Big[\widetilde{\mathcal{M}}_4(x,y;k) \\ -2\widetilde{\mathcal{M}}_3(x,y;k)\Big] F_2(\zeta)\end{aligned} \tag{D.62}$$

with $x = (t-\zeta)/2$ and $y = b(t) - b(\zeta)$.

Appendix E

Kernel Expressions of the Integral Equations

The purpose of this Appendix is to give the kernel components of the integral equations in the closed-form expressions suited for the computation of transition amplitude probabilities and others physical observables considered in this thesis. In this Appendix we also show that all principal functions $J_{\mu\nu}$, J_{j3} and J_{33} entering the systems of linear Volterra integral equations can be expressed by means of one analytical function $I_\gamma(x,y) \equiv I(x,y;\gamma)$ and its derivatives with respect to γ.

E.1 Recurrence relations

We first define the expression

$$\int_{-\infty}^{\infty} \frac{p\ \mathrm{d}p}{(p^2+\gamma)^{n+1}(p^2+\beta)^{m+1}}\ \exp\left(-\mathrm{i}xp^2+\mathrm{i}yp\right) = \frac{(-1)^{n+m}}{n!m!}\ \frac{\partial^{(n+m)}}{\partial\gamma^n\partial\beta^m}\frac{1}{(\beta-\gamma)} \times \left[I(x,y;\gamma)-I(x,y;\beta)\right].$$

The recurrence relation below is also useful

$$\left(-\frac{\gamma}{2}-\frac{\mathrm{i}}{2}\frac{\partial}{\partial x}\right)^m I^{(n+1)}(x,y;\gamma) = \left(-\frac{1}{2}\right)^m I^{(n+1-m)}(x,y;\gamma), \quad n \geq m.$$

Taking into account the following equation

$$\frac{\partial R_\pm}{\partial\gamma} = \pm\frac{y}{2\sqrt{\gamma}}\ R_\pm - \sqrt{\frac{x}{\pi\gamma}}\ \exp\left[\mathrm{i}(\pi/4-x\gamma+y^2/4x)\right],$$

it is straightforward to show that

$$\begin{aligned}\frac{\partial I}{\partial\gamma} &= \mathrm{i}xI - \frac{\mathrm{i}\pi y}{4\sqrt{\gamma}}\,\exp(\mathrm{i}x\gamma)\,[R_- + R_+],\\ \frac{\partial^2 I}{\partial\gamma^2} &= \left(2\mathrm{i}x - \frac{1}{2\gamma}\right)\,\frac{\partial I}{\partial\gamma} + \left(x^2 + \frac{\mathrm{i}x}{2\gamma} + \frac{y^2}{4\gamma}\right) I + \frac{y\sqrt{\pi x}}{2\gamma}\,\exp[\mathrm{i}(3\pi/4 + y^2/2x)],\end{aligned}$$

and to generalize these results to the $(n+1)$th derivative of I. We obtain

$$\frac{\partial^{n+1} I}{\partial\gamma^{n+1}} = a_n\,\frac{\partial I}{\partial\gamma} + b_n\,I + c_n,$$

with

$$a_{n+1} = a_n a_1 + \frac{\partial a_n}{\partial\gamma} + b_n,\;\; b_{n+1} = a_n b_1 + \frac{\partial b_n}{\partial\gamma},\;\; c_{n+1} = a_n c_1 + \frac{\partial c_n}{\partial\gamma},\;\; n = 1, 2, ...$$

and

$$a_1 = \left(2ix - \frac{1}{2\gamma}\right),\;\; b_1 = \left(x^2 + \frac{ix}{2\gamma} + \frac{y^2}{4\gamma}\right),\;\; c_1 = \frac{y\sqrt{\pi x}}{2\gamma}\,\exp[i(3\pi/4 + y^2/2x)].$$

It is interesting to mention the following inequality

$$\left|\frac{\partial^n}{\partial\gamma^n} I(x,y;\gamma)\right| \le 2n! \int_0^\infty \frac{p\;\mathrm{d}p}{(p^2+\gamma)^{n+1}} = \frac{(n-1)!}{\gamma^n}, \quad n \ge 1,$$

which is valid for any values of the variables x and y. This equation shows that already the first derivative of I with respect to the parameter γ is bounded and has no singularities. Clearly, these expressions are free of singularities and have a behavior that does not raise any numerical difficulty.

E.2 Basic derivatives

$$\begin{aligned} J_{11}(x,y) &= -\frac{16}{\pi\mathrm{i}y}\left[\frac{1}{3!}\frac{\partial^3}{\partial\gamma^3} I(x,y;\gamma)\right]_{\gamma=1},\\ \left(\varepsilon_1 - \frac{\mathrm{i}}{2}\frac{\partial}{\partial x}\right) J_{11}(x,y) &= -\frac{8}{\pi\mathrm{i}y}\left[\frac{1}{2!}\frac{\partial^2}{\partial\gamma^2} I(x,y;\gamma)\right]_{\gamma=1},\\ \left(\varepsilon_1 - \frac{\mathrm{i}}{2}\frac{\partial}{\partial x}\right)^2 J_{11}(x,y) &= -\frac{4}{\pi\mathrm{i}y}\left[\frac{1}{1!}\frac{\partial}{\partial\gamma} I(x,y;\gamma)\right]_{\gamma=1}. \end{aligned} \tag{E.1}$$

$$
\begin{aligned}
J_{12}(x,y) &= \frac{4\sqrt{2}}{\pi \mathrm{i} y}\left[\left(\frac{\partial^2}{\partial\beta\partial\gamma}+\frac{1}{2\cdot 2!}\frac{\partial^3}{\partial\beta^2\partial\gamma}\right)\right.\\
&\quad\left.\times\frac{1}{(\beta-\gamma)}\left(I(x,y;\gamma)-I(x,y;\beta)\right)\right]_{\gamma=1,\beta=1/4},\\
\left(\varepsilon_1-\frac{\mathrm{i}}{2}\frac{\partial}{\partial x}\right)J_{12}(x,y) &= \frac{2\sqrt{2}}{\pi \mathrm{i} y}\left[\left(\frac{\partial}{\partial\beta}+\frac{1}{2\cdot 2!}\frac{\partial^2}{\partial\beta^2}\right)\right.\\
&\quad\left.\times\frac{1}{(\beta-\gamma)}\left(I(x,y;\gamma)-I(x,y;\beta)\right)\right]_{\gamma=1,\beta=1/4},\\
\left(\varepsilon_2-\frac{\mathrm{i}}{2}\frac{\partial}{\partial x}\right)J_{12}(x,y) &= \frac{2\sqrt{2}}{\pi \mathrm{i} y}\left[\left(\frac{\partial}{\partial\gamma}+\frac{1}{2}\frac{\partial^2}{\partial\beta\partial\gamma}\right)\right.\\
&\quad\left.\times\frac{1}{(\beta-\gamma)}\left(I(x,y;\gamma)-I(x,y;\beta)\right)\right]_{\gamma=1,\beta=1/4},\\
\left(\varepsilon_1-\frac{\mathrm{i}}{2}\frac{\partial}{\partial x}\right)\left(\varepsilon_2-\frac{\mathrm{i}}{2}\frac{\partial}{\partial x}\right)J_{12}(x,y) &= \frac{\sqrt{2}}{\pi \mathrm{i} y}\left[\left(1+\frac{1}{2}\frac{\partial}{\partial\beta}\right)\right.\\
&\quad\left.\times\frac{1}{(\beta-\gamma)}\left(I(x,y;\gamma)-I(x,y;\beta)\right)\right]_{\gamma=1,\beta=1/4}.
\end{aligned}
\tag{E.2}
$$

$$
\begin{aligned}
J_{13}(x,y) &= -\frac{8}{\sqrt{6\pi}\ \mathrm{i} y}\frac{\partial^3}{\partial\beta^2\partial\gamma}\\
&\quad\times\left[\frac{1}{(\beta-\gamma)}\left(I(x,y;\gamma)-I(x,y;\beta)\right)\right]_{\gamma=1,\beta=1/4},\\
\left(\varepsilon_1-\frac{\mathrm{i}}{2}\frac{\partial}{\partial x}\right)J_{13}(x,y) &= -\frac{4}{\sqrt{6\pi}\ \mathrm{i} y}\frac{\partial^2}{\partial\beta^2}\\
&\quad\times\left[\frac{1}{(\beta-\gamma)}\left(I(x,y;\gamma)-I(x,y;\beta)\right)\right]_{\gamma=1,\beta=1/4},\\
\left(\varepsilon_2-\frac{\mathrm{i}}{2}\frac{\partial}{\partial x}\right)J_{13}(x,y) &= -\frac{8}{\sqrt{6\pi}\ \mathrm{i} y}\frac{\partial^2}{\partial\beta\partial\gamma}\\
&\quad\times\left[\frac{1}{(\beta-\gamma)}\left(I(x,y;\gamma)-I(x,y;\beta)\right)\right]_{\gamma=1,\beta=1/4},\\
\left(\varepsilon_1-\frac{\mathrm{i}}{2}\frac{\partial}{\partial x}\right)\left(\varepsilon_2-\frac{\mathrm{i}}{2}\frac{\partial}{\partial x}\right)J_{13}(x,y) &= -\frac{4}{\sqrt{6\pi}\ \mathrm{i} y}\frac{\partial}{\partial\beta}\\
&\quad\times\left[\frac{1}{(\beta-\gamma)}\left(I(x,y;\gamma)-I(x,y;\beta)\right)\right]_{\gamma=1,\beta=1/4}.
\end{aligned}
\tag{E.3}
$$

$$
\begin{aligned}
J_{22}(x,y) &= -\frac{2}{\pi \mathrm{i} y}\left[\left(\frac{1}{3!}\frac{\partial^3}{\partial\beta^3}+\frac{1}{4!}\frac{\partial^4}{\partial\beta^4}+\frac{1}{4\cdot 5!}\frac{\partial^5}{\partial\beta^5}\right) I(x,y;\beta)\right]_{\beta=1/4},\\
\left(\varepsilon_2-\frac{\mathrm{i}}{2}\frac{\partial}{\partial x}\right) J_{22}(x,y) &= -\frac{1}{\pi \mathrm{i} y}\left[\left(\frac{1}{2!}\frac{\partial^2}{\partial\beta^2}+\frac{1}{3!}\frac{\partial^3}{\partial\beta^3}+\frac{1}{4\cdot 4!}\frac{\partial^4}{\partial\beta^4}\right) I(x,y;\beta)\right]_{\beta=1/4},\\
\left(\varepsilon_2-\frac{\mathrm{i}}{2}\frac{\partial}{\partial x}\right)^2 J_{22}(x,y) &= -\frac{1}{2\pi \mathrm{i} y}\left[\left(\frac{1}{1!}\frac{\partial}{\partial\beta}+\frac{1}{2!}\frac{\partial^2}{\partial\beta^2}+\frac{1}{4\cdot 3!}\frac{\partial^3}{\partial\beta^3}\right) I(x,y;\beta)\right]_{\beta=1/4}.
\end{aligned}
\tag{E.4}
$$

$$
\begin{aligned}
J_{23}(x,y) &= \frac{4}{\sqrt{3\pi}\ \mathrm{i} y}\left[\left(\frac{1}{4!}\frac{\partial^4}{\partial\beta^4}+\frac{1}{2\cdot 5!}\frac{\partial^5}{\partial\beta^5}\right) I(x,y;\beta)\right]_{\beta=1/4},\\
\left(\varepsilon_2-\frac{\mathrm{i}}{2}\frac{\partial}{\partial x}\right) J_{23}(x,y) &= \frac{2}{\sqrt{3\pi}\ \mathrm{i} y}\left[\left(\frac{1}{3!}\frac{\partial^3}{\partial\beta^3}+\frac{1}{2\cdot 4!}\frac{\partial^4}{\partial\beta^4}\right) I(x,y;\beta)\right]_{\beta=1/4},\\
\left(\varepsilon_2-\frac{\mathrm{i}}{2}\frac{\partial}{\partial x}\right)^2 J_{23}(x,y) &= \frac{1}{\sqrt{3\pi}\ \mathrm{i} y}\left[\left(\frac{1}{2!}\frac{\partial^2}{\partial\beta^2}+\frac{1}{2\cdot 3!}\frac{\partial^3}{\partial\beta^3}\right) I(x,y;\beta)\right]_{\beta=1/4}.
\end{aligned}
\tag{E.5}
$$

$$
\begin{aligned}
J_{33}(x,y) &= -\frac{16}{\mathrm{i} y}\left[\frac{1}{6!}\frac{\partial^5}{\partial\beta^5} I(x,y;\beta)\right]_{\beta=1/4},\\
\left(\varepsilon_2-\frac{\mathrm{i}}{2}\frac{\partial}{\partial x}\right) J_{33}(x,y) &= -\frac{4}{3\ \mathrm{i} y}\left[\frac{1}{4!}\frac{\partial^4}{\partial\beta^4} I(x,y;\beta)\right]_{\beta=1/4},\\
\left(\varepsilon_2-\frac{\mathrm{i}}{2}\frac{\partial}{\partial x}\right)^2 J_{33}(x,y) &= -\frac{2}{3\ \mathrm{i} y}\left[\frac{1}{3!}\frac{\partial^3}{\partial\beta^3} I(x,y;\beta)\right]_{\beta=1/4}.
\end{aligned}
\tag{E.6}
$$

In the light of the above expressions and after some developments, we obtain the following results:

E.3 Components $K_{ij}(t,\xi)$ of kernels $\mathbf{K}(t,\xi)$

Setting $x = (t-\xi)/2$ and $y = b(t) - b(\xi)$, one has:

$$
\begin{aligned}
K_{11}(t,\xi) &= \mathrm{i}\frac{80\sqrt{2}}{9\pi}\tilde{a}_{12}\tilde{a}_{22}\left[\mathcal{J}_1(x,y) - \mathcal{G}_1(x,y)\right] \\
&\quad + \mathrm{i}\frac{8}{\pi}\tilde{a}_{22}^2\mathcal{J}_2(x,y) + \mathrm{i}\left(\frac{1}{\pi}\tilde{a}_{12}^2 + \frac{8\sqrt{2}}{3\pi}\tilde{a}_{12}\tilde{a}_{22}\right) \\
&\quad \times \mathcal{G}_2(x,y) - \mathrm{i}\frac{1}{\pi}\tilde{a}_{12}^2\mathcal{G}_3(x,y) + \mathrm{i}\frac{1}{4\pi}\tilde{a}_{12}^2\mathcal{G}_4(x,y), \qquad \text{(E.7)} \\
K_{12}(t,\xi) &= -\mathrm{i}\frac{40\sqrt{2}}{9\pi}(\tilde{a}_{11}\tilde{a}_{22} + \tilde{a}_{12}^2)\left[\mathcal{J}_1(x,y) - \mathcal{G}_1(x,y)\right] \\
&\quad - \mathrm{i}\frac{8}{\pi}\tilde{a}_{12}\tilde{a}_{22}\mathcal{J}_2(x,y) - \mathrm{i}\left(\frac{1}{\pi}\tilde{a}_{11}\tilde{a}_{12} + \frac{4\sqrt{2}}{3\pi}\left\{\tilde{a}_{11}\tilde{a}_{22} + \tilde{a}_{12}^2\right\}\right) \\
&\quad \times \mathcal{G}_2(x,y) + \mathrm{i}\frac{1}{\pi}\tilde{a}_{11}\tilde{a}_{12}\mathcal{G}_3(x,y) - \mathrm{i}\frac{1}{4\pi}\tilde{a}_{11}\tilde{a}_{12}\mathcal{G}_4(x,y), \qquad \text{(E.8)} \\
K_{13}(t,\xi) &= \frac{32\sqrt{2}}{\pi}\tilde{a}_{22}\frac{\partial}{\partial y}\left(\frac{2}{9}[\mathcal{J}_1(x,y) - \mathcal{G}_1(x,y)] + \frac{1}{6}\mathcal{G}_2(x,y)\right) \\
&\quad + \frac{1}{\pi}\tilde{a}_{12}\frac{\partial}{\partial y}\left[\mathcal{G}_4(x,y) - 2\mathcal{G}_3(x,y)\right], \qquad \text{(E.9)} \\
K_{22}(t,\xi) &= \mathrm{i}\frac{80\sqrt{2}}{9\pi}\tilde{a}_{11}\tilde{a}_{12}\left[\mathcal{J}_1(x,y) - \mathcal{G}_1(x,y)\right] \\
&\quad + \mathrm{i}\frac{8}{\pi}\tilde{a}_{12}^2\mathcal{J}_2(x,y) + \mathrm{i}\left(\frac{1}{\pi}\tilde{a}_{11}^2 + \frac{8\sqrt{2}}{3\pi}\tilde{a}_{11}\tilde{a}_{12}\right) \\
&\quad \times \mathcal{G}_2(x,y) - \mathrm{i}\frac{1}{\pi}\tilde{a}_{11}^2\mathcal{G}_3(x,y) + \mathrm{i}\frac{1}{4\pi}\tilde{a}_{11}^2\mathcal{G}_4(x,y), \qquad \text{(E.10)} \\
K_{23}(t,\xi) &= -\frac{32\sqrt{2}}{\pi}\tilde{a}_{12}\frac{\partial}{\partial y}\left(\frac{2}{9}[\mathcal{J}_1(x,y) - \mathcal{G}_1(x,y)] + \frac{1}{6}\mathcal{G}_2(x,y)\right) \\
&\quad - \frac{1}{\pi}\tilde{a}_{11}\frac{\partial}{\partial y}\left[\mathcal{G}_4(x,y) - 2\mathcal{G}_3(x,y)\right], \qquad \text{(E.11)} \\
K_{33}(t,\xi) &= -\mathrm{i}\frac{4}{\pi}\frac{\partial^2}{\partial y^2}\mathcal{G}_4(x,y). \qquad \text{(E.12)}
\end{aligned}
$$

E.4 Kernels $K_i(t,\xi)$ for $\mathcal{C}_{1s}(t)$

Putting $x = (t-\xi)/2$ and $y = b(t) - b(\xi)$, one gets:

$$\begin{aligned}
K_1(t,\xi) &= \frac{448\sqrt{2}}{27\pi}\tilde{a}_{12}\left[\mathcal{J}_1(x,y) - \mathcal{G}_1(x,y)\right] + \frac{80\sqrt{2}}{9\pi}\tilde{a}_{12}\mathcal{J}_2(x,y) \\
&\quad + \frac{16}{\pi}\tilde{a}_{22}\mathcal{J}_3(x,y) + \frac{32\sqrt{2}}{9\pi}\tilde{a}_{12}\mathcal{G}_2(x,y), \qquad \text{(E.13)} \\
K_2(t,\xi) &= -\frac{448\sqrt{2}}{27\pi}\tilde{a}_{11}\left[\mathcal{J}_1(x,y) - \mathcal{G}_1(x,y)\right] - \frac{80\sqrt{2}}{9\pi}\tilde{a}_{11}\mathcal{J}_2(x,y) \\
&\quad - \frac{16}{\pi}\tilde{a}_{12}\mathcal{J}_3(x,y) - \frac{32\sqrt{2}}{9\pi}\tilde{a}_{11}\mathcal{G}_2(x,y), \qquad \text{(E.14)} \\
K_3(t,\xi) &= -\mathrm{i}\frac{1024\sqrt{2}}{27\pi}\frac{\partial}{\partial y}\left[\mathcal{J}_1(x,y) - \mathcal{G}_1(x,y)\right] - \mathrm{i}\frac{128\sqrt{2}}{9\pi}\frac{\partial}{\partial y}\left[\mathcal{J}_2(x,y)\right. \\
&\quad \left. + \mathcal{G}_2(x,y)\right]. \qquad \text{(E.15)}
\end{aligned}$$

E.5 Kernels $\tilde{K}_i(t,\xi)$ for $\mathcal{C}_{2s}(t)$

One has:

$$\begin{aligned}
\tilde{K}_1(t,\xi) &= \frac{320\sqrt{2}}{27\pi}\tilde{a}_{22}\left[\mathcal{J}_1(x,y) - \mathcal{G}_1(x,y)\right] + \frac{80\sqrt{2}}{9\pi}\tilde{a}_{22}\mathcal{G}_2(x,y) \\
&\quad - \left(\frac{2}{\pi}\tilde{a}_{12} + \frac{8\sqrt{2}}{3\pi}\tilde{a}_{22}\right)\mathcal{G}_3(x,y) + \frac{2}{\pi}\tilde{a}_{12}\mathcal{G}_4(x,y) \\
&\quad - \frac{1}{2\pi}\tilde{a}_{12}\mathcal{G}_5(x,y), \qquad \text{(E.16)} \\
\tilde{K}_2(t,\xi) &= -\frac{320\sqrt{2}}{27\pi}\tilde{a}_{12}\left[\mathcal{J}_1(x,y) - \mathcal{G}_1(x,y)\right] - \frac{80\sqrt{2}}{9\pi}\tilde{a}_{12}\mathcal{G}_2(x,y) \\
&\quad + \left(\frac{2}{\pi}\tilde{a}_{11} + \frac{8\sqrt{2}}{3\pi}\tilde{a}_{12}\right)\mathcal{G}_3(x,y) - \frac{2}{\pi}\tilde{a}_{11}\mathcal{G}_4(x,y) \\
&\quad + \frac{1}{2\pi}\tilde{a}_{11}\mathcal{G}_5(x,y), \qquad \text{(E.17)} \\
\tilde{K}_3(t,\xi) &= -\mathrm{i}\frac{2}{\pi}\frac{\partial}{\partial y}\left[2\mathcal{G}_4(x,y) - \mathcal{G}_5(x,y)\right], \qquad \text{(E.18)}
\end{aligned}$$

where $x = (t-\xi)/2$ and $y = b(t) - b(\xi)$.

E.6 Kernels $\bar{K}_i(t,\xi)$ for $\mathcal{C}_{2p}(t)$

One obtains:

$$\bar{K}_1(t,\xi) = \mathrm{i}\frac{256\sqrt{2}}{3\pi}\tilde{a}_{22}\left[\frac{1}{9}\frac{\partial}{\partial y}\left[\mathcal{J}_1(x,y)-\mathcal{G}_1(x,y)\right]+\frac{1}{4}\frac{\partial}{\partial y}\left\{\frac{1}{3}\mathcal{G}_2(x,y)\right.\right.$$
$$\left.\left.-\frac{1}{4}\mathcal{G}_3(x,y)\right\}\right]+\mathrm{i}\frac{1}{\pi}\tilde{a}_{12}\frac{\partial}{\partial y}\left[2\mathcal{G}_4(x,y)-\mathcal{G}_5(x,y)\right], \tag{E.19}$$

$$\bar{K}_2(t,\xi) = -\mathrm{i}\frac{256\sqrt{2}}{3\pi}\tilde{a}_{12}\left[\frac{1}{9}\frac{\partial}{\partial y}\left[\mathcal{J}_1(x,y)-\mathcal{G}_1(x,y)\right]+\frac{1}{4}\frac{\partial}{\partial y}\left\{\frac{1}{3}\mathcal{G}_2(x,y)\right.\right.$$
$$\left.\left.-\frac{1}{4}\mathcal{G}_3(x,y)\right\}\right]-\mathrm{i}\frac{1}{\pi}\tilde{a}_{11}\frac{\partial}{\partial y}\left[2\mathcal{G}_4(x,y)-\mathcal{G}_5(x,y)\right], \tag{E.20}$$

$$\bar{K}_3(t,\xi) = -\frac{4}{\pi}\frac{\partial^2}{\partial y^2}\mathcal{G}_5(x,y), \tag{E.21}$$

with $x=(t-\xi)/2$ and $y=b(t)-b(\xi)$.

E.7 Components of $\mathbf{F}_0(t)$ and free terms of $\mathcal{C}_{js}(t)$ and $\mathcal{C}_{2p}(t)$

Simple calculations easily lead to

$$F_{10}(t) = \frac{448\sqrt{2}}{27\pi}\tilde{a}_{12}\left[\mathcal{J}_1(x,y)-\mathcal{G}_1(x,y)\right]+\frac{80\sqrt{2}}{9\pi}\tilde{a}_{12}\mathcal{J}_2(x,y)$$
$$+\frac{16}{\pi}\tilde{a}_{22}\mathcal{J}_3(x,y)+\frac{32\sqrt{2}}{9\pi}\tilde{a}_{12}\mathcal{G}_2(x,y), \tag{E.22}$$

$$F_{20}(t) = -\frac{448\sqrt{2}}{27\pi}\tilde{a}_{11}\left[\mathcal{J}_1(x,y)-\mathcal{G}_1(x,y)\right]-\frac{80\sqrt{2}}{9\pi}\tilde{a}_{11}\mathcal{J}_2(x,y)$$
$$-\frac{16}{\pi}\tilde{a}_{12}\mathcal{J}_3(x,y)-\frac{32\sqrt{2}}{9\pi}\tilde{a}_{11}\mathcal{G}_2(x,y), \tag{E.23}$$

$$F_{30}(t) = -\mathrm{i}\frac{1024\sqrt{2}}{27\pi}\frac{\partial}{\partial y}\left[\mathcal{J}_1(x,y)-\mathcal{G}_1(x,y)\right]-\mathrm{i}\frac{128\sqrt{2}}{9\pi}\frac{\partial}{\partial y}\left[\mathcal{J}_2(x,y)\right.$$
$$\left.+\mathcal{G}_2(x,y)\right], \tag{E.24}$$

$$J_{11}(x,y) = \frac{32}{\pi}\mathcal{J}_4(x,y), \tag{E.25}$$

$$\begin{aligned} J_{12}(x,y) = \frac{64\sqrt{2}}{27\pi}\left[32\left[\mathcal{J}_1(x,y) - \mathcal{G}_1(x,y)\right] + 10\mathcal{J}_2(x,y)\right. \\ \left. +14\mathcal{G}_2(x,y) - 3\mathcal{G}_3(x,y)\right], \end{aligned} \tag{E.26}$$

$$\begin{aligned} \left[-\mathrm{i}\frac{\partial}{\partial y}J_{13}(t/2,y)\right]_{y=b(t)} = \mathrm{i}\frac{512\sqrt{2}}{9\pi}\left[\frac{4}{3}\frac{\partial}{\partial y}\left[\mathcal{J}_1(x,y) - \mathcal{G}_1(x,y)\right] + \frac{\partial}{\partial y}\left[\frac{1}{3}\mathcal{J}_2(x,y)\right.\right. \\ \left.\left. +\frac{2}{3}\mathcal{G}_2(x,y) - \frac{1}{4}\mathcal{G}_3(x,y)\right]\right], \end{aligned} \tag{E.27}$$

where $x = t/2$ and $y = b(t)$.

Appendix F

Special Functions and Some Useful Properties

This Appendix contains a brief list without further discussion of definitions, formulae and some important properties of the special functions which appear in the solutions discussed above in this thesis. Derivations, and many additional formulae, can be found in the standard reference works listed in the bibliography [1] [2] .

F.1 The Whittaker function

In this part we summarize those properties of the Whittaker function of the first kind, $M_{\eta\gamma}(z)$, which have been useful in studying properties of the Sturmian functions as well as in the derivation of the Dirac-Coulomb wave functions. A more comprehensive treatment of the Whittaker function may be found in Refs. [2].
The function $M_{\eta\gamma}(z)$ is defined in terms of the confluent hypergeometric function

$$M_{\eta\gamma}(z) = z^{\gamma+1/2}\mathrm{e}^{-z/2}\ {}_1F_1\left(\gamma+\frac{1}{2}-\eta; 2\gamma+1; z\right), \tag{F.1}$$

[1] M. Abramowitz and I. A. Stegun, eds. *Handbook of Mathematical Functions, NBS Applied Mathematical Series* (National Bureau of Standards, Washington DC, 1966); I. S. Gradshteyn and I. M. Ryzhik, *Table of Integrals, Series and Products* 7th ed. (Academic Press, Boston, 2007)

[2] W. Magnus, F. Oberhettinger and R. P. Soni, *Formulas and Theorems for the Special Functions of Mathematical Physics* 3rd edn (Springer, Berlin, 1966); H. Buchholz, *The Confluent Hypergeometric Function* ed. by B. D. Coleman, Springer Tracts in Natural Philosophy (Springer, Berlin, 1969), Vol 15

where

$$ {}_1F_1(a;b;z) = \sum_{n=0}^{\infty} \frac{(a)_n}{(b)_n} \frac{z^n}{n!}, \quad (c)_n = \frac{\Gamma(n+c)}{\Gamma(c)}, |z| < 1. \tag{F.2} $$

The series (F.2) for ${}_1F_1(a;b;z)$ converges for all finite z if b is not a negative integer or zero. It reduces to a polynomial of degree n in z if $a = -n$ where n is a positive integer and b is not a negative integer or zero.
The function $M_{\eta\gamma}(z)$ is a regular solution of the Whittaker differential equation

$$ \left[\frac{\mathrm{d}^2}{\mathrm{d}z^2} - \frac{\gamma^2 - \frac{1}{4}}{z^2} + \frac{\eta}{z} - \frac{1}{4} \right] M_{\eta\gamma}(z) = 0. \tag{F.3} $$

In the vicinity of the regular singular point $z = 0$ the function $M_{\eta\gamma}(z)$ behaves as

$$ M_{\eta\gamma}(z) \longrightarrow z^{\gamma+1/2} \left(1 - \frac{\eta}{2\gamma+1} z \right) \qquad \text{for} \qquad z \to 0. \tag{F.4} $$

For large values of the argument the function $M_{\eta\gamma}(z)$ has the asymptotic expansion

$$ \begin{aligned} M_{\eta\gamma}(z) &\longrightarrow z^{\gamma+1/2} \mathrm{e}^{-z/2} \\ &\times \left[\frac{\Gamma(2\gamma+1)}{\Gamma(\gamma+\frac{1}{2}+\eta)} (-z)^{-\gamma-\frac{1}{2}+\eta} + \frac{\Gamma(2\gamma+1)}{\Gamma(\gamma+\frac{1}{2}-\eta)} (z)^{-\gamma-\frac{1}{2}-\eta} \mathrm{e}^{z} \right] \end{aligned} \tag{F.5} $$

valid provided $|arg(-z)| < \pi$ and $|argz| < \pi$. This restriction is satisfied if we define

$$ -z = \mathrm{e}^{\mathrm{i}\pi\Delta(z)} z, \quad \Delta(z) = \begin{cases} -1 & \text{for } 0 < argz < \pi \\ +1 & \text{for } -\pi < argz < 0. \end{cases} \tag{F.6} $$

It follows from the relation (F.1), the definition (F.2) and the Kummer identity

$$ {}_1F_1(a;b;z) = \mathrm{e}^{z} \; {}_1F_1(b-a;b;-z) \tag{F.7} $$

that

$$ M_{\eta\gamma}(z) = \mathrm{e}^{-\mathrm{i}\pi(\gamma+1/2)\Delta(z)} M_{-\eta\gamma}(-z). \tag{F.8} $$

The following recurrence relations hold

$$ M_{\eta,\gamma+1/2}(z) = (2\gamma+1) z^{-1/2} M_{\eta-1/2,\gamma}(z) - (2\gamma+1) z^{-1/2} M_{\eta+1/2,\gamma}(z), \tag{F.9} $$

$$ M_{\eta,\gamma-1/2}(z) = \frac{\gamma-\eta}{2\gamma} z^{-1/2} M_{\eta-1/2,\gamma}(z) + \frac{\gamma+\eta}{2\gamma} z^{-1/2} M_{\eta+1/2,\gamma}(z). \tag{F.10} $$

The Whittaker function of the second kind $W_{\eta\gamma}(z)$ is an irregular solution to (F.3). It is related to $M_{\eta\gamma}(z)$ via

$$ W_{\eta\gamma}(z) = \frac{\Gamma(2\gamma)}{\Gamma(\gamma-\eta+1/2)} M_{\eta,-\gamma}(z) + \frac{\Gamma(-2\gamma)}{\Gamma(-\gamma-\eta+1/2)} M_{\eta,\gamma}(z). \tag{F.11} $$

They obey the following product

$$M_{\eta\gamma}(z_1)W_{\eta\gamma}(z_2) = \frac{\Gamma(2\gamma+1)}{\Gamma(1/2-\eta+\gamma)} \times (z_1 z_2)^{\gamma+1/2}\mathrm{e}^{-(z_1+z_2)/2}\sum_{n=0}^{\infty}\frac{n!L_n^{(2\gamma)}(z_1)L_n^{(2\gamma)}(z_2)}{(n+\gamma-\eta+1/2)\Gamma(n+2\gamma+1)}. \tag{F.12}$$

F.2 The generalized Laguerre polynomials

Different definitions of the Laguerre polynomials are in use in the literature which may lead to confusion. Therefore, in this part we define the generalized Laguerre polynomials (adopted from above References) used in this thesis and summarize those of their properties that were useful in the present work.

The Laguerre polynomials $L_n^{(\alpha)}(z)$ are the polynomial solutions of the differential equation

$$\left[z\frac{\mathrm{d}^2}{\mathrm{d}z^2} + (\alpha+1-z)\frac{\mathrm{d}}{\mathrm{d}z} + n\right] L_n^{(\alpha)}(z) = 0. \tag{F.13}$$

They are given explicitly by

$$L_n^{(\alpha)}(z) = \sum_{k=0}^{n}\frac{\Gamma(\alpha+n+1)}{k!(n-k)!\Gamma(\alpha+k+1)}(-z)^k. \tag{F.14}$$

The $L_n^{(\alpha)}$ are sometimes called generalized Laguerre polynomials, because $L_n^{(0)}$, which is often denoted by L_n, is the polynomial introduced by Laguerre. This Laguerre polynomial differs from the ≪associated Laguerre function≫ for which the symbol L_q^p (with p and q both integers) is often used in the physics literature. The relation between the two is

$$\left[L_q^p(z)\right]_{physics} = (-1)^{p+q}q!L_{q-p}^{(p)}(z). \tag{F.15}$$

They are defined in terms of the generating function in the following way

$$G^{(\alpha)}(z,t) = \frac{\exp[-zt/(1-t)]}{(1-t)^{\alpha+1}} = \sum_{n=0}^{\infty}L_n^{(\alpha)}(z)t^n. \tag{F.16}$$

A variety of special functions may be expressed in terms of the confluent hypergeometric function and the regular Whittaker function of the first kind. In this work we have used the relations

$$L_n^{(\alpha)}(z) = \frac{\Gamma(n+\alpha+1)}{n!\Gamma(\alpha+1)}\ {}_1F_1(-n;\alpha+1;z), \tag{F.17}$$

$$L_n^{(\alpha)}(z) = \frac{\Gamma(n+\alpha+1)}{n!\Gamma(\alpha+1)}z^{-(\alpha+1)/2}\mathrm{e}^{z/2}M_{n+(\alpha+1)/2,\alpha/2}(z). \tag{F.18}$$

The functions

$$\phi_n^{(\alpha)}(z) = \sqrt{\frac{n!}{\Gamma(n+\alpha+1)}} z^{\alpha/2} \mathrm{e}^{-z/2} L_n^{(\alpha)}(z) \tag{F.19}$$

form a complete orthonormal set on the interval $[0, \infty[$ and the corresponding closure relation is

$$\sum_{n=0}^{\infty} \phi_n^{(\alpha)}(z)\phi_n^{(\alpha)}(z') = z^{\alpha/2} z'^{\alpha/2} \mathrm{e}^{-(z+z')/2} \times \sum_{n=0}^{\infty} \frac{n!}{\Gamma(n+\alpha+1)} L_n^{(\alpha)}(z) L_n^{(\alpha)}(z') = \delta(z-z'). \tag{F.20}$$

The following recursion relations

$$L_n^{(\alpha)}(z) = L_n^{(\alpha+1)}(z) - L_{n-1}^{(\alpha+1)}(z), \tag{F.21}$$

$$zL_n^{(\alpha+1)}(z) = (n+\alpha+1)L_n^{(\alpha)}(z) - (n+1)L_{n+1}^{(\alpha)}(z), \tag{F.22}$$

$$(n+1)L_{n+1}^{(\alpha)}(z) - (2n+\alpha+1-z)L_n^{(\alpha)}(z) + (n+\alpha)L_{n-1}^{(\alpha)}(z) = 0, \tag{F.23}$$

and the differentiation formula

$$z\frac{\mathrm{d}}{\mathrm{d}z} L_n^{(\alpha)}(z) = nL_n^{(\alpha)}(z) - (n+\alpha)L_{n-1}^{(\alpha)}(z) \tag{F.24}$$

are valid. The orthonormality relation is

$$\int_0^{\infty} \mathrm{d}z \; z^{\alpha} \mathrm{e}^{-z} L_m^{(\alpha)}(z) L_n^{(\alpha)}(z) = \frac{\Gamma(n+\alpha+1)}{n!} \delta_{mn}. \tag{F.25}$$

Other useful integration formulae include

$$\int_0^{\infty} \mathrm{d}z \; z^{\alpha-1} \mathrm{e}^{-z} L_m^{(\alpha)}(z) L_n^{(\alpha)}(z) = \frac{\Gamma(\nu+\alpha+1)}{\alpha \nu!}, \quad \nu = min(m,n), \tag{F.26}$$

$$\int_0^{\infty} \mathrm{d}z \; z^{\gamma} \mathrm{e}^{-z} L_n^{(\alpha)}(z) = \frac{\Gamma(\gamma+1)\Gamma(n+\alpha-\gamma)}{\Gamma(\alpha-\gamma)n!}, \tag{F.27}$$

$$\int_0^{\infty} \mathrm{d}z \; z^{\alpha+1} \mathrm{e}^{-z} L_m^{(\alpha)}(z) L_n^{(\alpha)}(z) = \frac{\Gamma(n+\alpha+1)}{n!} \left[-n\delta_{n,m+1} + (2n+\alpha+1)\delta_{nm} - (n+\alpha+1)\delta_{n,m-1} \right]. \tag{F.28}$$

The Christoffel-Darboux formula is

$$\sum_{k=0}^{n} \frac{k!}{\Gamma(k+\alpha+1)} L_k^{(\alpha)}(z) L_k^{(\alpha)}(z') = \frac{(n+1)!}{(z-z')\Gamma(n+\alpha+1)} \times \left[L_n^{(\alpha)}(z) L_{n+1}^{(\alpha)}(z') - L_{n+1}^{(\alpha)}(z) L_n^{(\alpha)}(z') \right]. \tag{F.29}$$

Appendix G

Angular Integrals and Selection Rules

This Appendix deals with the angular integrals $\tilde{I}^q(l)$ ($q = \pm 1 \equiv \pm$) used in the calculation of second-order amplitude transitions. The selection rules corresponding to two-photon excitation are also investigated.

G.1 Angular integrals

They are defined as [1][2][3]

$$\begin{aligned}\tilde{I}^q(l) &= \langle l_2 s_2 j_2 m_2| \left(C^l \sigma^1\right)^L_q |l_1 s_1 j_1 m_1\rangle \\ &= (-1)^{j_2 - m_2} \begin{pmatrix} j_2 & L & j_1 \\ -m_2 & q & m_1 \end{pmatrix} \langle l_2 s_2 j_2 \| \left(C^l \sigma^1\right)^L \| l_1 s_1 j_1 \rangle \,. \end{aligned} \tag{G.1}$$

It should be noted that

$$C^l_m(\hat{\boldsymbol{r}}) = \sqrt{\frac{4\pi}{2l+1}} Y^l_m(\hat{\boldsymbol{r}}) \qquad \hat{\boldsymbol{r}} = (\theta, \phi), \tag{G.2}$$

with $Y^l_m(\hat{\boldsymbol{r}})$ denoting the spherical harmonics which are components of an irreducible tensor of rank l. The reduced matrix element $\langle l_2 s_2 j_2 \| \left(C^l \sigma^1\right)^L \| l_1 s_1 j_1 \rangle$

[1] E. U. Condon and G. H. Shortley, *The Theory of Atomic Spectra* (Cambridge University Press, England, 1935)

[2] D. M. Brink and G. R. Satchler, *Angular Momentum* 2nd edn (Clarendon Press, Oxford, 1968)

[3] A. R. Edmonds, *Angular Momentum in Quantum Mechanics* 3rd edn (University Press, Princeton, 1974)

is well-known. Using formulae relating $3j$ and $9j$ symbols [3], one readily obtains for the case $s_1 = s_2 = 1/2$ under consideration

$$\tilde{I}^q(l) = (-1)^{m_2+1/2}\sqrt{[j_1, j_2]}a_L \begin{pmatrix} j_2 & L & j_1 \\ -m_2 & q & m_1 \end{pmatrix} \begin{pmatrix} j_2 & j_1 & L \\ 1/2 & -1/2 & 0 \end{pmatrix}, \tag{G.3}$$

with

$$a_L = \begin{cases} \frac{\kappa_1+\kappa_2+l}{\sqrt{l(2l+1)}} & \text{if } \; l = L+1 \\ \frac{\kappa_1-\kappa_2}{\sqrt{l(l+1)}} & \text{if } \; l = L \\ \frac{\kappa_1+\kappa_2-l-1}{\sqrt{(l+1)(2l+1)}} & \text{if } \; l = L-1 \end{cases}, \tag{G.4}$$

$$j_i = l_i - \epsilon_i/2 = \bar{l}_i + \epsilon_i/2, \qquad \kappa_i = \epsilon_i(j_i + 1/2), \qquad \epsilon_i = \pm 1, \quad i = 1, 2. \tag{G.5}$$

and

$$l_1 + l_2 + l \text{ must be an even integer,}$$

or equivalently

$j_1 + j_2 + l$ must be an even integer if $\kappa_1\kappa_2 < 0$ or an odd integer if $\kappa_1\kappa_2 > 0$.

On the other hand angular integrals involved in this thesis are also related to spin orbital states with $\bar{l}$, instead of l. To obtain such integrals, one has to change κ into $-\kappa$ in the above equations. Thus, we find in standard notation

$$\left\langle l_2 \frac{1}{2} j_2 m_2 \middle| \left(C^l \sigma^1\right)^L_q \middle| \bar{l}_1 \frac{1}{2} j_1 m_1 \right\rangle = (-1)^{m_2+1/2}\sqrt{[j_1, j_2]}a'_L \begin{pmatrix} j_2 & L & j_1 \\ -m_2 & q & m_1 \end{pmatrix} \times \begin{pmatrix} j_2 & L & j_1 \\ 1/2 & 0 & -1/2 \end{pmatrix}, \tag{G.6}$$

$$a'_L = \begin{cases} \frac{\kappa_2-\kappa_1+l}{\sqrt{l(2l+1)}} & \text{if } \; l = L+1 \\ -\frac{\kappa_1+\kappa_2}{\sqrt{l(l+1)}} & \text{if } \; l = L \\ \frac{\kappa_2-\kappa_1-l-1}{\sqrt{(l+1)(2l+1)}} & \text{if } \; l = L-1 \end{cases}, \tag{G.7}$$

$$\bar{l}_1 + l_2 + l \text{ must be an even integer,}$$

$j_1 + j_2 + l$ must be an even integer if $\kappa_1\kappa_2 > 0$ or an odd integer if $\kappa_1\kappa_2 < 0$.

The angular integrals obtained by Szymanowski *et al.* [4] ,

$$I_1(l_{1p}) = \sqrt{4\pi}\langle j'l'm' \mid Y_{l_{1p},0}[-\hat{\boldsymbol{e}}_x \cdot \hat{\boldsymbol{e}}_r] \mid j_1 l_1 m_1\rangle, \tag{G.8}$$

$$I_2(l_{1p}) = \sqrt{4\pi}\langle j'l'm' \mid Y_{l_{1p},0}\,[-\mathrm{i}\boldsymbol{\sigma} \cdot (\hat{\boldsymbol{e}}_x \wedge \hat{\boldsymbol{e}}_r)] \mid j_1 l_1 m_1\rangle, \tag{G.9}$$

[4] C. Szymanowski, V. Véniard, R. Taïeb and A. Maquet, *Phys. Rev. A* **56**, 700 (1997)

may be derived in a simple manner from our method. Combining the above equations, one gets

$$I_1(l_{1p}) = \frac{1}{2\sqrt{2}} \sum_L (-1)^{L+1} [L,\, l_{1p}]^{1/2} \begin{pmatrix} l_{1p} & 1 & L \\ 0 & -1 & 1 \end{pmatrix} \times \left[(-1)^{l_{1p}-L-1} \left\{ \tilde{I}_1^-(l_{1p}) + \tilde{I}_2^-(l_{1p}) \right\} - \left\{ \tilde{I}_1^+(l_{1p}) + \tilde{I}_2^+(l_{1p}) \right\} \right], \quad \text{(G.10)}$$

$$I_2(l_{1p}) = \frac{1}{2\sqrt{2}} \sum_L (-1)^{L+1} [L,\, l_{1p}]^{1/2} \begin{pmatrix} l_{1p} & 1 & L \\ 0 & -1 & 1 \end{pmatrix} \times \left[(-1)^{l_{1p}-L-1} \left\{ \tilde{I}_1^-(l_{1p}) - \tilde{I}_2^-(l_{1p}) \right\} - \left\{ \tilde{I}_1^+(l_{1p}) - \tilde{I}_2^+(l_{1p}) \right\} \right], \quad \text{(G.11)}$$

with the constraint that

$$l_{1p} + L + 1 \quad \text{(G.12)}$$

must be an even integer.

It is clear that there are close similarities between $I_1(l_{1p})$ and $I_3(l_{2p})$ and between $I_2(l_{1p})$ and $I_4(l_{2p})$. Thus, one readily finds

$$I_3(l_{2p}) = \frac{1}{2\sqrt{2}} \sum_{L'} (-1)^{L'+1} [L',\, l_{2p}]^{1/2} \begin{pmatrix} l_{2p} & 1 & L' \\ 0 & -1 & 1 \end{pmatrix} \times \left[(-1)^{l_{2p}-L'-1} \left\{ \tilde{I}_3^-(l_{2p}) + \tilde{I}_4^-(l_{2p}) \right\} - \left\{ \tilde{I}_3^+(l_{2p}) + \tilde{I}_4^+(l_{2p}) \right\} \right], \quad \text{(G.13)}$$

$$I_4(l_{2p}) = \frac{1}{2\sqrt{2}} \sum_{L'} (-1)^{L'+1} [L',\, l_{2p}]^{1/2} \begin{pmatrix} l_{2p} & 1 & L' \\ 0 & -1 & 1 \end{pmatrix} \times \left[(-1)^{l_{2p}-L'-1} \left\{ \tilde{I}_3^-(l_{2p}) - \tilde{I}_4^-(l_{2p}) \right\} - \left\{ \tilde{I}_3^+(l_{2p}) - \tilde{I}_4^+(l_{2p}) \right\} \right], \quad \text{(G.14)}$$

with the constraint that

$$l_{2p} + L + 1 \quad \text{(G.15)}$$

must be an even integer.

In the particular case of dipole approximation, *i.e.* $L = 1$, $L' = 1$ and owing to equations (G.6), (G.7) and (G.23), we have the following formulae

$$I_1(0) = -\frac{1}{\sqrt{2}}(-1)^{m'+1/2}[j_1, j']^{1/2} \begin{pmatrix} j' & 1 & j_1 \\ 1/2 & 0 & -1/2 \end{pmatrix} \left[\begin{pmatrix} j' & 1 & j_1 \\ -m' & -1 & m_1 \end{pmatrix} - \begin{pmatrix} j' & 1 & j_1 \\ -m' & 1 & m_1 \end{pmatrix} \right], \tag{G.16}$$

$$I_1(2) = -\frac{1}{\sqrt{5}} I_1(0), \qquad I_2(0) = (\kappa_1 - \kappa') I_1(0), \qquad I_2(2) = \left(\frac{\kappa_1 - \kappa'}{2\sqrt{5}} \right) I_1(0), \tag{G.17}$$

$$I_3(0) = -\frac{1}{\sqrt{2}}(-1)^{m_2+1/2}[j', j_2]^{1/2} \begin{pmatrix} j_2 & 1 & j' \\ 1/2 & 0 & -1/2 \end{pmatrix} \left[\begin{pmatrix} j_2 & 1 & j' \\ -m_2 & -1 & m' \end{pmatrix} - \begin{pmatrix} j_2 & 1 & j' \\ -m_2 & 1 & m' \end{pmatrix} \right], \tag{G.18}$$

$$I_3(2) = -\frac{1}{\sqrt{5}} I_3(0), \qquad I_4(0) = (\kappa' - \kappa_2) I_3(0), \qquad I_4(2) = \left(\frac{\kappa' - \kappa_2}{2\sqrt{5}} \right) I_3(0). \tag{G.19}$$

For transitions from the ground level considered in this work, we have evaluated these angular integrals by means of Clebsch-Gordan Coefficients tabulated in [2] [3]. The numerical results obtained agree with those of Szymanowski *et al.* displayed in **Tables** IX and X, except a sign in the values of $I_3(0)$ and $I_4(0)$ for the case of three particular virtual excitation paths as shown in **Table** G.2. In these tables our results take also into account the contribution of two new terms related to $l_{1p} = 2$ and $l_{2p} = 2$ according to the selection rules.

Table G.1: *Angular integrals for different dipole excitation paths from the initial S state $|j_1 = 1/2, m_1 = 1/2\rangle$ to virtual $P_{j'}$ states in the first interaction.*

Virtual state $\|j', m'\rangle$	$I_1(0)$	$I_1(2)$	$I_2(0)$	$I_2(2)$
$\|3/2, 3/2\rangle$	$1/\sqrt{6}$	$-1/\sqrt{30}$	$1/\sqrt{6}$	$1/2\sqrt{30}$
$\|3/2, -1/2\rangle$	$-1/3\sqrt{2}$	$1/3\sqrt{10}$	$-1/3\sqrt{2}$	$-1/6\sqrt{10}$
$\|1/2, -1/2\rangle$	$1/3$	$-1/3\sqrt{5}$	$-2/3$	$-1/3\sqrt{5}$

Table G.2: *Angular integrals for different dipole excitation paths from virtual $P_{j'}$ states in the second interaction to final D_j states.*

Virtual state $\|j', m'\rangle$	Final state $\|j_2, m_2\rangle$	$I_3(0)$	$I_3(2)$	$I_4(0)$	$I_4(2)$
$\|3/2, 3/2\rangle$	$\|5/2, 5/2\rangle$	$1/\sqrt{5}$	$-1/5$	$1/\sqrt{5}$	$1/10$
$\|3/2, 3/2\rangle$	$\|5/2, 1/2\rangle$	$-1/5\sqrt{2}$	$1/5\sqrt{10}$	$-1/5\sqrt{2}$	$-1/10\sqrt{10}$
$\|3/2, -1/2\rangle$	$\|5/2, 1/2\rangle$	$\sqrt{3/2}/5$	$-\sqrt{3/10}/5$	$\sqrt{3/2}/5$	$\sqrt{3/10}/10$
$\|3/2, -1/2\rangle$	$\|5/2, -3/2\rangle$	$\sqrt{3}/5$	$-\sqrt{3/5}/5$	$\sqrt{3}/5$	$\sqrt{3/5}/10$
$\|3/2, 3/2\rangle$	$\|3/2, 1/2\rangle$	$1/5\sqrt{3}$	$-1/5\sqrt{15}$	$-4/5\sqrt{3}$	$-2/5\sqrt{15}$
$\|3/2, -1/2\rangle$	$\|3/2, 1/2\rangle$	$2/15$	$-2/15\sqrt{5}$	$-8/15$	$-4/15\sqrt{5}$
$\|3/2, -1/2\rangle$	$\|3/2, -3/2\rangle$	$-1/5\sqrt{3}$	$1/5\sqrt{15}$	$4/5\sqrt{3}$	$2/5\sqrt{15}$
$\|1/2, -1/2\rangle$	$\|3/2, 1/2\rangle$	$1/3\sqrt{2}$	$-1/3\sqrt{10}$	$-1/3\sqrt{2}$	$-1/6\sqrt{10}$
$\|1/2, -1/2\rangle$	$\|3/2, -3/2\rangle$	$1/\sqrt{6}$	$-1/\sqrt{30}$	$-1/\sqrt{6}$	$-1/2\sqrt{30}$

G.2 Selection rules

Selection rules may be deduced in a straightforward manner from the previous treatment of angular integrals $\tilde{I}_k^q(l)$. We outline here the following rules as a result of both first and second interactions. The first interaction of the electromagnetic field leads to the constraints

$\bar{l}_1 + l' + l_{1p}$ and $l_1 + \bar{l}' + l_{1p}$ must be even integers or equivalently,
$j' + j_1 + l_{1p}$ must be an even integer if $\kappa'\kappa_1 > 0$ or an odd integer if $\kappa'\kappa_1 < 0$,

$$|L - j_1| \le j' \le L + j_1, \quad m' = m_1 + q, \qquad q = \pm 1, \tag{G.20}$$

and owing to the fact that $l_{1p} + L + 1$ must be an even integer (cf. equation (G.12)), the case $l_{1p} = L$ is forbidden. The second interaction leads to the same relations in which quantum numbers have been changed. We have

$\bar{l}_2 + l' + l_{2p}$ and $l_2 + \bar{l}' + l_{2p}$ must be even integers or equivalently,
$j' + j_2 + l_{2p}$ must be an even integer if $\kappa'\kappa_2 > 0$ or an odd integer if $\kappa'\kappa_2 < 0$,

$$\left|L' - j'\right| \le j_2 \le L' + j', \quad m_2 = m' + q', \;\; q' = \pm 1, \tag{G.21}$$

and with the fact that $l_{2p} + L' + 1$ must be an even integer (cf. equation (G.15)), the case $l_{2p} = L'$ is excluded. With simply manipulation of the above equations, we finally quote the selection rules for multipole transitions in the forms:

$$
\begin{gathered}
j', j_1, L \text{ and } j_2, j', L' \text{ form each a triangle;} \\
m' = m_1 + q,\ m_2 = m' + q',\ (q, q' = \pm 1), \\
l_{1p} + L + 1 \text{ and } l_{2p} + L' + 1 \text{ must be an even integer,}
\end{gathered}
$$

or equivalently

$$
\begin{gathered}
j' + j_1 + L \text{ must be an even (or odd) integer if } \kappa'\kappa_1 < 0 \text{ (or } \kappa'\kappa_1 > 0), \\
j' + j_2 + L' \text{ must be an even (or odd) integer if } \kappa'\kappa_2 < 0 \text{ (or } \kappa'\kappa_2 > 0).
\end{gathered}
$$

In the particular case of the dipole transitions, *i.e.* $L = 1$ and $L' = 1$, it is easy to get the following selection rules

$$
\begin{array}{lllll}
\Delta_1 l = l' - l_1 = \pm 1, & \Delta_1 j = j' - j_1 = \pm 1, & (\kappa'\kappa_1 > 0), & 0 & (\kappa'\kappa_1 < 0), \\
\Delta_2 l = l_2 - l' = \pm 1, & \Delta_2 j = j_2 - j' = \pm 1, & (\kappa'\kappa_2 > 0), & 0 & (\kappa'\kappa_2 < 0), \\
& \Delta_1 m = m' - m_1 = \pm 1, & l_{1p} = 0, 2, & & \\
& \Delta_2 m = m_2 - m' = \pm 1, & l_{2p} = 0, 2, & &
\end{array}
\tag{G.22}
$$

which can be generalized in the suitable form

$$
\begin{aligned}
\Delta l = l_2 - l_1 &= 0, \pm 2, \\
\Delta j = j_2 - j_1 &= 0, \pm 1, \pm 2, \\
\Delta m = m_2 - m_1 &= 0, \pm 2, \\
l_{1p} &= 0, 2, \\
l_{2p} &= 0, 2
\end{aligned}
\tag{G.23}
$$

Applying these selection rules to the fundamental level, we recover all the virtual and final states mentioned in the **Tables** IX and X of Ref.[4].

Appendix H

Radial Integrals

The purpose of this Appendix is to derive the radial integrals in the closed-form expressions needed for the computation of transition amplitude probabilities for two-photon excitation considered in this thesis.

We recall that [1]

$$\int_0^\infty \mathrm{d}t\; t^\varrho \mathrm{e}^{-st}\; j_l(kt) L_n^{(\alpha)}(t) = k^l \frac{\Gamma(\alpha+n+1)}{n!\Gamma(\alpha+1)} J_n(\tilde{\varrho}), \tag{H.1}$$

where we define

$$J_n(\tilde{\varrho}) = \sum_{p=0}^{\infty} J_n^{(p)}(\tilde{\varrho}), \tag{H.2}$$

$$J_n^{(p)}(\tilde{\varrho}) = k^{2p} C_p^l \frac{\Gamma(\tilde{\varrho}+1)}{s^{\tilde{\varrho}+1}}\; {}_2F_1\left(-n, \tilde{\varrho}+1, \alpha+1, 1/s\right), \tag{H.3}$$

and set

$$C_p^l = \frac{(-1/2)^p}{p!(2p+2l+1)!!} \qquad \tilde{\varrho} = \varrho + l + 2p.$$

This result, combined with the functional relation (F.23) are exploited in the calculations of the following radial integrals.

H.1 Radial integrals of the first-order $\widetilde{K}_i(l), i = 1, 2, 3, 4$

Transition $|1\ {}^2S\rangle \to |2\ {}^2S\rangle$

We first consider the case of

$$\widetilde{K}_1(l_{1p}) = \int_0^\infty \mathrm{d}r\; S_{n'\kappa'}(\varepsilon', 2\lambda' r)\; j_{l_{1p}}(\omega r) Q_{n_1\kappa_1}(2\lambda_1 r), \tag{H.4}$$

[1] I. S. Gradshteyn and I. M. Ryzhik, *Table of Integrals, Series and Products* 7th ed. (Academic Press, Boston, 2007)

where $S_{n'\kappa'}$ and $Q_{n_1\kappa_1}$ are the well-known radial functions previously defined in equations (7.29) and (7.47) respectively. For the $1S$ atomic ground state, characterized by the quantum numbers $n_1 = 0$, $j_1 = 1/2$, $l_1 = 0$, $m_1 = \pm 1/2$, $\epsilon_1 = -1$, $\kappa_1 = -1$, the formulae are

$$E_1 = \gamma_1, \quad \lambda_1 = \mathcal{Z}, \quad \gamma_1 = \sqrt{1 - \mathcal{Z}^2},$$
$$\Psi_{0,-1,m_1}(\boldsymbol{r}) = \frac{1}{r} \begin{pmatrix} P_{0,-1}(2\lambda_1 r)\Omega_{-1,m_1}(\hat{\boldsymbol{r}}) \\ \mathrm{i}Q_{0,-1}(2\lambda_1 r)\Omega_{1,m_1}(\hat{\boldsymbol{r}}) \end{pmatrix},$$

where the radial functions are given by

$$P_{0,-1}(2\lambda_1 r) = -\sqrt{\frac{\mathcal{Z}(1+\gamma_1)}{\Gamma(1+2\gamma_1)}}\,(2\mathcal{Z}r)^{\gamma_1}\exp(-\mathcal{Z}r),$$
$$Q_{0,-1}(2\lambda_1 r) = \sqrt{\frac{\mathcal{Z}(1-\gamma_1)}{\Gamma(1+2\gamma_1)}}\,(2\mathcal{Z}r)^{\gamma_1}\exp(-\mathcal{Z}r).$$

Substituting these radial components into equation (H.4), one obtains after few operations, the following explicit form

$$\widetilde{K}_1(l_{1p}) = G_{n'}^{(\pm)}(l_{1p})\left[n' J_{n'-1}(\tilde{\varrho}_1) + (\kappa' \mp N_{n'\kappa'}) J_{n'}(\tilde{\varrho}_1)\right] \tag{H.5}$$

where

$$G_{n'}^{(\pm)}(l_{1p}) = \frac{k^{l_{1p}}}{2\Gamma(2\gamma'+1)}\left(\frac{\lambda_1}{\lambda'}\right)^{\gamma_1+1} \times \sqrt{\frac{\mathcal{Z}\Gamma(n'+2\gamma'+1)}{2(\gamma_1+1)\Gamma(2\gamma_1+1)\varepsilon' N_{n'\kappa'}(N_{n'\kappa'} \mp \kappa')n'!}} \tag{H.6}$$

with

$$s_1 = (\lambda_1 + \lambda')/2\lambda' \qquad k = \omega/2\lambda' \qquad \varrho_1 = \gamma_1 + \gamma'.$$

Note that in the above equations (H.5) and (H.6) and in what follows, the upper sign or upper subscript should be chosen $n' > 0$ and the lower one for $n' < 0$. Next, the case of

$$\widetilde{K}_2(l_{1p}) = \int_0^\infty \mathrm{d}r\; T_{n'\kappa'}(\varepsilon', 2\lambda' r)\; j_{l_{1p}}(\omega r) P_{n_1\kappa_1}(2\lambda_1 r). \tag{H.7}$$

It is clear that this expression can be obtained from the expression of $\widetilde{K}_1(l_{1p})$. Hence, we get

$$\widetilde{K}_2(l_{1p}) = -\frac{(1+E_1)\varepsilon'}{\lambda_1} G_{n'}^{(\pm)}(l_{1p})\left[n' J_{n'-1}(\tilde{\varrho}_1) - (\kappa' \mp N_{n'\kappa'}) J_{n'}(\tilde{\varrho}_1)\right]. \tag{H.8}$$

As for the remaining radial integrals $\widetilde{K}_3(l_{2p})$ and $\widetilde{K}_4(l_{2p})$, it is easy to show that they may be deduced respectively from $\widetilde{K}_2(l_{1p})$ and $\widetilde{K}_1(l_{1p})$ by changing all the initial parameters (subscripts 1) to the final parameters (subscripts 2), the primed parameters remain unchanged.

$$\widetilde{K}_3(l_{2p}) = \int_0^\infty \mathrm{d}r\ T_{n'\kappa'}(\varepsilon', 2\lambda' r)\ j_{l_{2p}}(\omega r) P_{n_2\kappa_2}(2\lambda_2 r). \tag{H.9}$$

The formulae for the $2S$ excited state, with the quantum numbers $n_2 = 1,\ j_2 = 1/2,\ l_2 = 0,\ m_2 = \pm 1/2,\ \epsilon_2 = -1,\ \kappa_2 = -1$, are

$$E_2 = \sqrt{(1+\gamma_2)/2},\ \ \lambda_2 = \sqrt{(1-\gamma_2)/2},\ \ \gamma_2 = \sqrt{1-\mathcal{Z}^2},$$
$$\Psi_{1,-1,m_2}(\boldsymbol{r}) = \frac{1}{r}\begin{pmatrix} P_{1,-1}(2\lambda_2 r)\Omega_{-1,m_2}(\hat{\boldsymbol{r}}) \\ \mathrm{i}Q_{1,-1}(2\lambda_2 r)\Omega_{1,m_2}(\hat{\boldsymbol{r}}) \end{pmatrix},$$

where the radial components are given by

$$\begin{aligned} P_{1,-1}(2\lambda_2 r) &= -\sqrt{\frac{\mathcal{Z}(1+2E_2)(1+E_2)}{2\Gamma(3+2\gamma_2)}}\left(\frac{\mathcal{Z}r}{E_2}\right)^{\gamma_2}\exp\left(-\mathcal{Z}r/2E_2\right) \\ &\quad\times\left[2E_2(2E_2-1) - \mathcal{Z}r/E_2\right], \\ Q_{1,-1}(2\lambda_2 r) &= \sqrt{\frac{\mathcal{Z}(1+2E_2)(1-E_2)}{2\Gamma(3+2\gamma_2)}}\left(\frac{\mathcal{Z}r}{E_2}\right)^{\gamma_2}\exp\left(-\mathcal{Z}r/2E_2\right) \\ &\quad\times\left[(2E_2+2)(2E_2-1) - \mathcal{Z}r/E_2\right]. \end{aligned}$$

After some calculations, one obtains

$$\begin{aligned} \widetilde{K}_3(l_{2p}) = -\frac{(1+E_2)\varepsilon'}{\lambda_2}\widetilde{G}^{(\pm)}_{n'}(l_{2p})\,&\Big[2E_2(2E_2-1) \\ &\times\left\{n' J_{n'-1}(\tilde{\varrho}_2) - (\kappa' \mp N_{n'\kappa'})J_{n'}(\tilde{\varrho}_2)\right\} \\ &-\frac{\lambda_2}{\lambda'}\left\{n' J_{n'-1}(\tilde{\varrho}_2+1) - (\kappa' \mp N_{n'\kappa'})J_{n'}(\tilde{\varrho}_2+1)\right\}\Big], \end{aligned} \tag{H.10}$$

where

$$\begin{aligned} \widetilde{G}^{(\pm)}_{n'}(l_{2p}) = \frac{k^{l_{2p}}}{4\Gamma(2\gamma'+1)}&\left(\frac{\lambda_2}{\lambda'}\right)^{\gamma_2+1} \\ &\times\sqrt{\frac{\mathcal{Z}(1+2E_2)\Gamma(n'+2\gamma'+1)}{(1+E_2)\Gamma(2\gamma_2+3)\varepsilon' N_{n'\kappa'}(N_{n'\kappa'} \mp \kappa')n'!}}, \end{aligned} \tag{H.11}$$

with

$$s_2 = (\lambda_2 + \lambda')/2\lambda' \qquad \varrho_2 = \gamma_2 + \gamma'.$$

The radial integral

$$\widetilde{K}_4(l_{2p}) = \int_0^\infty \mathrm{d}r\ S_{n'\kappa'}(\varepsilon', 2\lambda' r)\ j_{l_{2p}}(\omega r) Q_{n_2\kappa_2}(2\lambda_2 r), \tag{H.12}$$

is straightforwardly deduced

$$\begin{aligned}\widetilde{K}_4(l_{2p}) = \widetilde{G}^{(\pm)}_{n'}(l_{2p}) \Big[& (2E_2+2)(2E_2-1)\left\{ n' J_{n'-1}(\tilde{\varrho}_2) + (\kappa' \mp N_{n'\kappa'}) J_{n'}(\tilde{\varrho}_2) \right\} \\ & - \frac{\lambda_2}{\lambda'} \left\{ n' J_{n'-1}(\tilde{\varrho}_2+1) + (\kappa' \mp N_{n'\kappa'}) J_{n'}(\tilde{\varrho}_2+1) \right\} \Big].\end{aligned} \tag{H.13}$$

It is worth to mention that the radial integrals $\widetilde{K}_1(l_{1p})$ and $\widetilde{K}_2(l_{1p})$ remain unchanged for all four transitions considered. In what follows, we only restrict ourself to integrals $\widetilde{K}_3(l_{2p})$ and $\widetilde{K}_4(l_{2p})$ which vary with transition. After some tremendous manipulations we obtain the following results

Transition $|1\ ^2S\rangle \to |3\ ^2S\rangle$

The formulae for the $3S$ excited state, with the quantum numbers $n_2 = 2,\ j_2 = 1/2,\ l_2 = 0,\ m_2 = \pm 1/2,\ \epsilon_2 = -1,\ \kappa_2 = -1$, are

$$\begin{aligned} E_2 = (\gamma_2+2)/\sqrt{4\gamma_2+5},\ \ \lambda_2 = \mathcal{Z}/\sqrt{4\gamma_2+5},\ \ \gamma_2 = \sqrt{1-\mathcal{Z}^2}, \\ \Psi_{2,-1,m_2}(\boldsymbol{r}) = \frac{1}{r} \begin{pmatrix} P_{2,-1}(2\lambda_2 r)\Omega_{-1,m_2}(\hat{\boldsymbol{r}}) \\ \mathrm{i} Q_{2,-1}(2\lambda_2 r)\Omega_{1,m_2}(\hat{\boldsymbol{r}}) \end{pmatrix}, \end{aligned}$$

with

$$\begin{aligned} P_{2,-1}(2\lambda_2 r) = & \sqrt{\frac{2\mathcal{Z}E_2(1+\gamma_2)(1+E_2)}{\Gamma(2+2\gamma_2)(4\gamma_2+5)(\gamma_2+E_2+2)}}\,(2\lambda_2 r)^{\gamma_2} \exp(-\lambda_2 r) \\ & \times \left[(2\gamma_2+1)\left(\frac{1}{2} - \frac{\gamma_2+2}{2E_2}\right) + 2\mathcal{Z}r - \frac{(\gamma_2+E_2+2)(1-E_2^2)}{E_2(\gamma_2+1)} r^2 \right], \\ Q_{2,-1}(2\lambda_2 r) = & \sqrt{\frac{2\mathcal{Z}E_2(1+\gamma_2)(1-E_2)}{\Gamma(2+2\gamma_2)(4\gamma_2+5)(\gamma_2+E_2+2)}}\,(2\lambda_2 r)^{\gamma_2} \exp(-\lambda_2 r) \\ & \times \left[(2\gamma_2+1)\left(\frac{3}{2} - \frac{\gamma_2+2}{2E_2}\right) + 2\mathcal{Z}\left(1 + \frac{2E_2}{\gamma_2+2}\right) r \right. \\ & \left. - \frac{(\gamma_2+E_2+2)(1-E_2^2)}{E_2(\gamma_2+1)} r^2 \right]. \end{aligned}$$

Using these expressions we obtain

$$\begin{aligned}\widetilde{K}_3(l_{2p}) = \frac{(1+E_2)\varepsilon'}{\lambda_2}\widetilde{G}^{(\pm)}_{n'}(l_{2p})\Bigg[&(2\gamma_2+1)\left(\frac{1}{2}-\frac{\gamma_2+2}{E_2}\right)\\ &\times\left\{n'J_{n'-1}(\tilde{\varrho}_2)-(\kappa'\mp N_{n'\kappa'})J_{n'}(\tilde{\varrho}_2)\right\}\\ &+\frac{\lambda_2(\gamma_2+2)}{\lambda' E_2}\left\{n'J_{n'-1}(\tilde{\varrho}_2+1)-(\kappa'\mp N_{n'\kappa'})J_{n'}(\tilde{\varrho}_2+1)\right\}\\ &-\left(\frac{E_2+\gamma_2+2}{4E_2(\gamma_2+1)}\right)\left(\frac{\lambda_2}{\lambda'}\right)^2\left\{n'J_{n'-1}(\tilde{\varrho}_2+2)-(\kappa'\mp N_{n'\kappa'})J_{n'}(\tilde{\varrho}_2+2)\right\}\Bigg],\end{aligned} \tag{H.14}$$

where we defined

$$\begin{aligned}\widetilde{G}^{(\pm)}_{n'}(l_{2p}) = &\frac{k^{l_{2p}}}{2\Gamma(2\gamma'+1)}\left(\frac{\lambda_2}{\lambda'}\right)^{\gamma_2+1}\\ &\times\sqrt{\frac{\mathcal{Z}(\gamma_2+1)E_2\Gamma(n'+2\gamma'+1)}{(1+E_2)(4\gamma_2+5)(E_2+\gamma_2+2)\Gamma(2\gamma_2+2)\varepsilon' N_{n'\kappa'}(N_{n'\kappa'}\mp\kappa')n'!}},\end{aligned} \tag{H.15}$$

and

$$\begin{aligned}\widetilde{K}_4(l_{2p}) = \widetilde{G}^{(\pm)}_{n'}(l_{2p})\Bigg[&(2\gamma_2+1)\left(\frac{3}{2}+\frac{\gamma_2+2}{E_2}\right)\\ &\times\left\{n'J_{n'-1}(\tilde{\varrho}_2)+(\kappa'\mp N_{n'\kappa'})J_{n'}(\tilde{\varrho}_2)\right\}\\ &-\frac{\lambda_2(2E_2+\gamma_2+2)}{\lambda' E_2}\left\{n'J_{n'-1}(\tilde{\varrho}_2+1)+(\kappa'\mp N_{n'\kappa'})J_{n'}(\tilde{\varrho}_2+1)\right\}\\ &+\left(\frac{E_2+\gamma_2+2}{4E_2(\gamma_2+1)}\right)\left(\frac{\lambda_2}{\lambda'}\right)^2\left\{n'J_{n'-1}(\tilde{\varrho}_2+2)+(\kappa'\mp N_{n'\kappa'})J_{n'}(\tilde{\varrho}_2+2)\right\}\Bigg].\end{aligned} \tag{H.16}$$

Transition $|1\ ^2S\rangle \to |3\ ^2D_{3/2}\rangle$

The formulae for the $|3\ ^2D_{3/2}\rangle$ excited state, with the quantum numbers $n_2 = 1,\ j_2 = 3/2,\ l_2 = 2,\ m_2 = \pm 1/2, \pm 3/2,\ \epsilon_2 = 1,\ \kappa_2 = 2$, are

$$\begin{aligned}E_2 = (\gamma_2+1)/\sqrt{2\gamma_2+5},\ \lambda_2 = \mathcal{Z}/\sqrt{2\gamma_2+5},\ \gamma_2 = \sqrt{4-\mathcal{Z}^2},\\ \Psi_{1,2,m_2}(\boldsymbol{r}) = \frac{1}{r}\begin{pmatrix} P_{1,2}(2\lambda_2 r)\Omega_{2,m_2}(\hat{\boldsymbol{r}}) \\ \mathrm{i}Q_{1,2}(2\lambda_2 r)\Omega_{-2,m_2}(\hat{\boldsymbol{r}})\end{pmatrix},\end{aligned}$$

where the radial components are given by

$$P_{1,2}(2\lambda_2 r) = \sqrt{\frac{\mathcal{Z}E_2(1+2\gamma_2)(1+E_2)}{2\Gamma(1+2\gamma_2)(2\gamma_2+5)(\gamma_2-2E_2+1)}}\,(2\lambda_2 r)^{\gamma_2}\exp(-\lambda_2 r)$$
$$\times\left[(3-\frac{\gamma_2+1}{E_2})+\frac{2\mathcal{Z}}{(2\gamma_2+1)}(1-\frac{2E_2}{(\gamma_2+1)})r\right],$$
$$Q_{1,2}(2\lambda_2 r) = \sqrt{\frac{\mathcal{Z}E_2(1+2\gamma_2)(1-E_2)}{2\Gamma(1+2\gamma_2)(2\gamma_2+5)(\gamma_2-2E_2+1)}}\,(2\lambda_2 r)^{\gamma_2}\exp(-\lambda_2 r)$$
$$\times\left[(-1+\frac{\gamma_2+1}{E_2})-\frac{2\mathcal{Z}}{(2\gamma_2+1)}(1-\frac{2E_2}{(\gamma_2+1)})r\right],$$

From these expressions we easily derive

$$\widetilde{K}_3(l_{2p}) = \frac{(1+E_2)\varepsilon'}{\lambda_2}\widetilde{G}^{(\pm)}_{n'}(l_{2p})\left[\left(3-\frac{\gamma_2+1}{E_2}\right)\right.$$
$$\times\left\{n'J_{n'-1}(\tilde{\varrho}_2)-(\kappa'\mp N_{n'\kappa'})J_{n'}(\tilde{\varrho}_2)\right\}$$
$$\left.+\left(\frac{\lambda_2(\gamma_2-2E_2+1)}{\lambda' E_2(2\gamma_2+1)}\right)\left\{n'J_{n'-1}(\tilde{\varrho}_2+1)-(\kappa'\mp N_{n'\kappa'})J_{n'}(\tilde{\varrho}_2+1)\right\}\right], \tag{H.17}$$

where we have set

$$\widetilde{G}^{(\pm)}_{n'}(l_{2p}) = \frac{k^{l_{2p}}}{4\Gamma(2\gamma'+1)}\left(\frac{\lambda_2}{\lambda'}\right)^{\gamma_2+1}$$
$$\times\sqrt{\frac{\mathcal{Z}(2\gamma_2+1)E_2\Gamma(n'+2\gamma'+1)}{(1+E_2)(2\gamma_2+5)(\gamma_2-2E_2+1)\Gamma(2\gamma_2+1)\varepsilon' N_{n'\kappa'}(N_{n'\kappa'}\mp\kappa')n'!}}, \tag{H.18}$$

and

$$\widetilde{K}_4(l_{2p}) = \widetilde{G}^{(\pm)}_{n'}(l_{2p})\left[\left(-1+\frac{\gamma_2+1}{E_2}\right)\left\{n'J_{n'-1}(\tilde{\varrho}_2)+(\kappa'\mp N_{n'\kappa'})J_{n'}(\tilde{\varrho}_2)\right\}\right.$$
$$\left.-\left(\frac{\lambda_2(\gamma_2-2E_2+1)}{\lambda' E_2(2\gamma_2+1)}\right)\left\{n'J_{n'-1}(\tilde{\varrho}_2+1)+(\kappa'\mp N_{n'\kappa'})J_{n'}(\tilde{\varrho}_2+1)\right\}\right]. \tag{H.19}$$

Transition $|1\ ^2S\rangle \to |3\ ^2D_{5/2}\rangle$

The formulae for the $|3\ ^2D_{5/2}\rangle$ excited state, with the quantum numbers $n_2 = 0,\ j_2 = 5/2,\ l_2 = 2,\ m_2 = \pm 1/2, \pm 3/2, \pm 5/2,\ \epsilon_2 = -1,\ \kappa_2 = -3$, are

$$E_2 = \gamma_2/3,\ \ \lambda_2 = \mathcal{Z}/3,\ \ \gamma_2 = \sqrt{9-\mathcal{Z}^2},$$
$$\Psi_{0,-3,m_2}(\boldsymbol{r}) = \frac{1}{r}\begin{pmatrix} P_{0,-3}(2\lambda_2 r)\Omega_{-3,m_2}(\hat{\boldsymbol{r}}) \\ \mathrm{i}Q_{0,-3}(2\lambda_2 r)\Omega_{3,m_2}(\hat{\boldsymbol{r}}) \end{pmatrix},$$

where the radial components are given by

$$P_{0,-3}(2\lambda_2 r) = -\sqrt{\frac{\mathcal{Z}(3+\gamma_2)}{9\Gamma(1+2\gamma_2)}}\,(2\mathcal{Z}r/3)^{\gamma_2}\exp\left(-\mathcal{Z}r/3\right),$$

$$Q_{0,-3}(2\lambda_2 r) = \sqrt{\frac{\mathcal{Z}(3-\gamma_2)}{9\Gamma(1+2\gamma_2)}}\,(2\mathcal{Z}r/3)^{\gamma_2}\exp\left(-\mathcal{Z}r/3\right).$$

From these expressions one deduces

$$\widetilde{K}_3(l_{2p}) = -\frac{(1+E_2)\varepsilon'}{\lambda_2}\widetilde{G}^{(\pm)}_{n'}(l_{2p})\left[n' J_{n'-1}(\tilde{\varrho}_2) - (\kappa' \mp N_{n'\kappa'})J_{n'}(\tilde{\varrho}_2)\right], \quad \text{(H.20)}$$

where

$$G^{(\pm)}_{n'}(l_{2p}) = \frac{k^{l_{2p}}}{2\Gamma(2\gamma'+1)}\left(\frac{\lambda_2}{\lambda'}\right)^{\gamma_2+1} \times \sqrt{\frac{\mathcal{Z}\Gamma(n'+2\gamma'+1)}{2(\gamma_2+3)\Gamma(2\gamma_2+1)\varepsilon' N_{n'\kappa'}(N_{n'\kappa'} \mp \kappa')n'!}}, \quad \text{(H.21)}$$

and

$$\widetilde{K}_4(l_{2p}) = \widetilde{G}^{(\pm)}_{n'}(l_{2p})\left[n' J_{n'-1}(\tilde{\varrho}_2) + (\kappa' \mp N_{n'\kappa'})J_{n'}(\tilde{\varrho}_2)\right]. \quad \text{(H.22)}$$

H.2 Radial integrals of the second-order $K_i(l), i = 1, 2, 3, 4$

We turn now to the calculation of the radial integrals K_1,K_2, K_3, and K_4.

Transition $|1\ ^2S\rangle \rightarrow |2\ ^2S\rangle$

We begin with the integrals

$$K_1(l_{1p}) = K_2(l_{1p}) = \int_0^\infty \mathrm{d}r\ r^2 S_{n'}(2\lambda' r)\ j_{l_{1p}}(\omega r)\Phi_{n_1\epsilon_1}(r). \quad \text{(H.23)}$$

On substituting the Sturmian function $S_{n'}(2\lambda' r)$ and the ground state function $\Phi_{n_1\epsilon_1}(r)$ inferred from equation (7.77)

$$\zeta_1 = \gamma_1,\ \ \tilde{\beta}_1 = -\mathcal{Z}/(1+\gamma_1),\ \ \Phi_{0,1/2,0,m_1}(\boldsymbol{r}) = \Phi_{0,-1}(r)\begin{pmatrix} \Omega_{1/2,0,m_1}(\hat{\boldsymbol{r}}) \\ \mathrm{i}\tilde{\beta}_1\Omega_{1/2,1,m_1}(\hat{\boldsymbol{r}}) \end{pmatrix},$$

where the radial part of the function is given by

$$\Phi_{0,-1}(r) = \sqrt{\frac{(2\mathcal{Z})^3(1+\gamma_1)}{2\gamma_1\Gamma(1+2\gamma_1)}}\,(2\mathcal{Z}r)^{\gamma_1-1}\exp\left(-\mathcal{Z}r\right),$$

we find that

$$K_1(l_{1p}) = K_2(l_{1p}) = G_{n'}(l_{1p}) J_{n'}(\tilde{\varrho}_1), \tag{H.24}$$

$$G_{n'}(l_{1p}) = \frac{k^{l_{1p}}}{4\gamma_1 \lambda' \Gamma(2\zeta')} \left(\frac{\lambda_1}{\lambda'}\right)^{\zeta_1} \sqrt{\frac{2(\gamma_1+1)\Gamma(n'+2\zeta')}{n'!\Gamma(2\zeta_1)}}, \tag{H.25}$$

$$\varrho_1 = \zeta_1 + \zeta'. \tag{H.26}$$

In the calculation of the radial integrals

$$K_3(l_{2p}) = \int_0^\infty \mathrm{d}r \; r^2 \Phi_{n_2\epsilon_2}(r) \;\; j_{l_{2p}}(\omega r) g_d(r), \tag{H.27}$$

$$K_4(l_{2p}) = \tilde{\beta}_2 \int_0^\infty \mathrm{d}r \; r^2 \Phi_{n_2\epsilon_2}(r) \;\; j_{l_{2p}}(\omega r) g_u(r), \tag{H.28}$$

new type of integrals actually occurs, which can be treated analogously to equation (H.24). From the first excited state

$$\zeta_2 = \gamma_2, \;\; \tilde{\beta}_2 = -\mathcal{Z}/(1+\gamma_2), \;\; \Phi_{1,1/2,0,m_2}(\boldsymbol{r}) = \Phi_{1,-1}(r) \begin{pmatrix} \Omega_{1/2,0,m_2}(\hat{\boldsymbol{r}}) \\ \mathrm{i}\tilde{\beta}_2 \Omega_{1/2,1,m_2}(\hat{\boldsymbol{r}}) \end{pmatrix},$$

where the radial part of the function is given by

$$\Phi_{1,-1}(r) = \sqrt{\frac{\mathcal{Z}(1+E_2)(1-E_2)}{E_2\gamma_2\Gamma(1+2\gamma_2)}} \left(\frac{\mathcal{Z}r}{E_2}\right)^{\gamma_2-1} \exp\left(-\mathcal{Z}r/2E_2\right) \times \left[(2E_2+1)(2E_2-1) - 1 - \mathcal{Z}r/E_2\right],$$

and owing to what precedes, we straightforward obtain explicit expressions

$$K_3(l_{2p}) = \mathcal{F}_{n'} \left[\left(2q_1\zeta_2 - q_2\frac{\lambda_2}{\lambda'}\right) J_{n'}(\tilde{\varrho}_2) - q_1 \frac{\lambda_2}{\lambda'} J_{n'}(\tilde{\varrho}_2 + 1) + 2q_2\zeta_2 J_{n'}(\tilde{\varrho}_2 - 1) - (n' + 2\zeta') \left(2\zeta_2 J_{n'+1}(\tilde{\varrho}_2 - 1) - \frac{\lambda_2}{\lambda'} J_{n'+1}(\tilde{\varrho}_2)\right)\right], \tag{H.29}$$

where we have set

$$\mathcal{F}_{n'} = \frac{k^{l_{2p}}(\kappa' + \epsilon'\gamma')}{4\epsilon'\lambda'\gamma'(n' - \eta' + \zeta')\Gamma(2\zeta')} \left(\frac{\lambda_2}{\lambda'}\right)^{\zeta_2} \sqrt{\frac{\mathcal{Z}\lambda_2\Gamma(n'+2\zeta')}{2\gamma_2\Gamma(2\zeta_2+1)n'!}}, \tag{H.30}$$

$$q_1 = -\frac{1}{2}\left(1 + \frac{E'(\kappa' - \epsilon'\gamma')}{\eta'(1+E')}\right) \qquad q_2 = n' + \eta' - \epsilon'\gamma' \qquad \varrho_2 = \zeta_2 + \zeta'. \tag{H.31}$$

$$K_4(l_{2p}) = \tilde{\beta}_2 \frac{\mathcal{Z}}{\kappa' + \epsilon'\gamma'} \mathcal{F}_{n'} \left[\left(2\tilde{q}_1\zeta_2 - q_2 \frac{\lambda_2}{\lambda'} \right) J_{n'}(\tilde{\varrho}_2) - \tilde{q}_1 \frac{\lambda_2}{\lambda'} J_{n'}(\tilde{\varrho}_2 + 1) \right.$$
$$\left. + 2q_2\zeta_2 J_{n'}(\tilde{\varrho}_2 - 1) - (n' + 2\zeta') \left(2\zeta_2 J_{n'+1}(\tilde{\varrho}_2 - 1) - \frac{\lambda_2}{\lambda'} J_{n'+1}(\tilde{\varrho}_2) \right) \right], \tag{H.32}$$

where we defined

$$\tilde{q}_1 = -\frac{1}{2} \left(1 + \frac{E'(\kappa' + \epsilon'\gamma')}{\eta'(1 - E')} \right). \tag{H.33}$$

In the same way, we obtain after some manipulations the following results.

Transition $|1\ ^2S\rangle \to |3\ ^2S\rangle$

The second excited state

$$\zeta_2 = \gamma_2, \ \ \tilde{\beta}_2 = -\mathcal{Z}/(1 + \gamma_2), \ \ \Phi_{2,1/2,0,m_2}(\boldsymbol{r}) = \Phi_{2,-1}(r) \begin{pmatrix} \Omega_{1/2,0,m_2}(\hat{\boldsymbol{r}}) \\ \mathrm{i}\tilde{\beta}_2 \Omega_{1/2,1,m_2}(\hat{\boldsymbol{r}}) \end{pmatrix},$$

with the radial component

$$\Phi_{2,-1}(r) = \sqrt{\frac{\mathcal{Z}E_2(\gamma_2 + 1)}{\gamma_2\Gamma(2 + 2\gamma_2)}} (2\lambda_2)^{\gamma_2} r^{\gamma_2 - 1} \exp(-\lambda_2 r)$$
$$\times \left[\frac{\gamma_2(2\gamma_2 + 1)}{(\gamma_2 + 2)} - \frac{2\mathcal{Z}E_2(2\gamma_2 + 1)}{(\gamma_2 + 2)} r + \frac{2(1 - E_2^2)}{(\gamma_2 + 2)} r^2 \right],$$

respectively yields

$$K_3(l_{2p}) = \mathcal{F}_{n'} \left[(2\zeta_2 + 1) \left(q_1\zeta_2 - q_2 \frac{\lambda_2}{\lambda'} \right) J_{n'}(\tilde{\varrho}_2) \right.$$
$$- \frac{\lambda_2}{\lambda'} \left(q_1(2\zeta_2 + 1) - q_2 \frac{\lambda_2}{2\lambda'} \right) J_{n'}(\tilde{\varrho}_2 + 1)$$
$$+ \frac{1}{2} q_1 \left(\frac{\lambda_2}{\lambda'} \right)^2 J_{n'}(\tilde{\varrho}_2 + 2) + q_2\zeta_2(2\zeta_2 + 1) J_{n'}(\tilde{\varrho}_2 - 1)$$
$$- (n' + 2\zeta') \left(\zeta_2(2\zeta_2 + 1) J_{n'+1}(\tilde{\varrho}_2 - 1) - (2\zeta_2 + 1) \frac{\lambda_2}{\lambda'} J_{n'+1}(\tilde{\varrho}_2) \right.$$
$$\left. \left. + \frac{1}{2} \left(\frac{\lambda_2}{\lambda'} \right)^2 J_{n'+1}(\tilde{\varrho}_2 + 1) \right) \right], \tag{H.34}$$

where

$$\mathcal{F}_{n'} = \frac{k^{l_{2p}}(\kappa' + \epsilon'\gamma')}{4\epsilon'\lambda'\gamma'(n' - \eta' + \zeta')\Gamma(2\zeta')} \left(\frac{\lambda_2}{\lambda'} \right)^{\zeta_2} \sqrt{\frac{\mathcal{Z}\lambda_2(\gamma_2 + 1)\Gamma(n' + 2\zeta')}{\gamma_2(\gamma_2 + 2)\Gamma(2\zeta_2 + 2)n'!}}. \tag{H.35}$$

$$
\begin{aligned}
K_4(l_{2p}) = \tilde{\beta}_2 \frac{\mathcal{Z}}{\kappa' + \epsilon'\gamma'} \mathcal{F}_{n'} \Bigg[& (2\zeta_2 + 1) \left(\tilde{q}_1 \zeta_2 - q_2 \frac{\lambda_2}{\lambda'} \right) J_{n'}(\tilde{\varrho}_2) \\
& - \frac{\lambda_2}{\lambda'} \left(\tilde{q}_1 (2\zeta_2 + 1) - q_2 \frac{\lambda_2}{2\lambda'} \right) J_{n'}(\tilde{\varrho}_2 + 1) \\
& + \frac{1}{2} \tilde{q}_1 \left(\frac{\lambda_2}{\lambda'} \right)^2 J_{n'}(\tilde{\varrho}_2 + 2) + q_2 \zeta_2 (2\zeta_2 + 1) J_{n'}(\tilde{\varrho}_2 - 1) \\
& - (n' + 2\zeta') \Bigg(\zeta_2 (2\zeta_2 + 1) J_{n'+1}(\tilde{\varrho}_2 - 1) - (2\zeta_2 + 1) \frac{\lambda_2}{\lambda'} J_{n'+1}(\tilde{\varrho}_2) \\
& + \frac{1}{2} \left(\frac{\lambda_2}{\lambda'} \right)^2 J_{n'+1}(\tilde{\varrho}_2 + 1) \Bigg) \Bigg] .
\end{aligned} \tag{H.36}
$$

Transition $|1\ ^2S\rangle \rightarrow |3\ ^2D_{3/2}\rangle$

Here the second excited state

$$
\zeta_2 = 1 + \gamma_2, \ \ \tilde{\beta}_2 = \mathcal{Z}/(2 + \gamma_2), \ \ \Phi_{1,3/2,2,m_2}(\boldsymbol{r}) = \Phi_{1,+1}(r) \begin{pmatrix} \Omega_{3/2,2,m_2}(\hat{\boldsymbol{r}}) \\ \mathrm{i}\tilde{\beta}_2 \Omega_{3/2,1,m_2}(\hat{\boldsymbol{r}}) \end{pmatrix},
$$

where

$$
\Phi_{1,+1}(r) = \sqrt{\frac{\mathcal{Z} E_2 (\gamma_2 + 2)}{2\gamma_2 (\gamma_2 + 1)^2 \Gamma(2 + 2\gamma_2)}} \, (2\lambda_2)^{\gamma_2 + 1} \, r^{\gamma_2} \exp(-\lambda_2 r) ,
$$

is used to obtain the following results

$$
K_3(l_{2p}) = \mathcal{F}_{n'} \left[q_1 J_{n'}(\tilde{\varrho}_2) + q_2 J_{n'}(\tilde{\varrho}_2 - 1) - (n' + 2\zeta') J_{n'+1}(\tilde{\varrho}_2 - 1) \right] , \tag{H.37}
$$

where we defined

$$
\mathcal{F}_{n'} = \frac{k^{l_{2p}} (\kappa' + \epsilon'\gamma')}{4\epsilon'\lambda'\gamma' (n' - \eta' + \zeta') \Gamma(2\zeta')} \left(\frac{\lambda_2}{\lambda'} \right)^{\zeta_2} \sqrt{\frac{\mathcal{Z}\lambda_2 (\gamma_2 + 2) \Gamma(n' + 2\zeta')}{2\gamma_2 (\gamma_2 + 1) \Gamma(2\zeta_2) n'!}} . \tag{H.38}
$$

$$
K_4(l_{2p}) = \tilde{\beta}_2 \frac{\mathcal{Z}}{\kappa' + \epsilon'\gamma'} \mathcal{F}_{n'} \left[\tilde{q}_1 J_{n'}(\tilde{\varrho}_2) + q_2 J_{n'}(\tilde{\varrho}_2 - 1) - (n' + 2\zeta') J_{n'+1}(\tilde{\varrho}_2 - 1) \right] . \tag{H.39}
$$

Transition $|1\ ^2S\rangle \rightarrow |3\ ^2D_{5/2}\rangle$

Given the second excited state

$$
\zeta_2 = \gamma_2, \ \ \tilde{\beta}_2 = -\mathcal{Z}/(3 + \gamma_2), \ \ \Phi_{0,5/2,2,m_2}(\boldsymbol{r}) = \Phi_{0,-1}(r) \begin{pmatrix} \Omega_{5/2,2,m_2}(\hat{\boldsymbol{r}}) \\ \mathrm{i}\tilde{\beta}_2 \Omega_{5/2,3,m_2}(\hat{\boldsymbol{r}}) \end{pmatrix},
$$

where

$$\Phi_{0,-1}(r) = \sqrt{\frac{\mathcal{Z}(\gamma_2+3)}{3\gamma_2\Gamma(1+2\gamma_2)}}\,(2\mathcal{Z}/3)^{\gamma_2}\,r^{\gamma_2-1}\exp\left(-\mathcal{Z}r/3\right),$$

one easily obtains

$$K_3(l_{2p}) = \mathcal{F}_{n'}\left[q_1 J_{n'}(\tilde{\varrho}_2) + q_2 J_{n'}(\tilde{\varrho}_2-1) - (n'+2\zeta')J_{n'+1}(\tilde{\varrho}_2-1)\right], \quad \text{(H.40)}$$

where we have

$$\mathcal{F}_{n'} = \frac{k^{l_{2p}}(\kappa'+\epsilon'\gamma')}{4\epsilon'\lambda'\gamma'(n'-\eta'+\zeta')\Gamma(2\zeta')}\left(\frac{\lambda_2}{\lambda'}\right)^{\zeta_2}\sqrt{\frac{\mathcal{Z}\lambda_2(\gamma_2+3)\Gamma(n'+2\zeta')}{\gamma_2\Gamma(2\zeta_2+1)n'!}}, \quad \text{(H.41)}$$

and finally

$$K_4(l_{2p}) = \tilde{\beta}_2\frac{\mathcal{Z}}{\kappa'+\epsilon'\gamma'}\mathcal{F}_{n'}\left[\tilde{q}_1 J_{n'}(\tilde{\varrho}_2) + q_2 J_{n'}(\tilde{\varrho}_2-1) - (n'+2\zeta')J_{n'+1}(\tilde{\varrho}_2-1)\right]. \quad \text{(H.42)}$$

Faculté des Sciences
Institut de la Matière Condensée et des Nanosciences
Pôle Nanoscopic Physics

Chemin du Cyclotron 2, 1348 Louvain-la-Neuve, Belgique
Tél. : +32 (0) 10 47 32 45 – Fax : +32 (0) 10 47 24 31
E-mail : hugues.tetchou@uclouvain.be – htetchou@yahoo.com
http://www.pamo.ucl.ac.be

Recent calculations of ionization rate based on the numerical solution of the time-dependent Schrödinger equation (TDSE) in configuration space gave results in disagreement with the ionization rate obtained under the strong field approximation(SFA), is to say, assuming that the ionization is by tunneling. Moreover, recent experimental results, which clearly show among other things, (a) the presence of resonant structures in the region of low energy spectrum of emitted electrons and (b) interference figures for the distribution of moments of electrons emitted cannot be explained in the context of the SFA. These findings reinforce the idea that the electrons, at least those of low energies, are emitted by another process than the tunnel effect. Under these conditions, the influence of the Coulomb potential compared to the electric field remains high even in the strong field limit. To analyze the role of the Coulomb potential, we developed a new mathematical model that goes beyond the SFA as well as the efficient numerical codes that allow obtaining relevant information on the role of atomic structure in the dynamics of ionization.

Using Sturmian expansions of the Dirac-Coulomb Green's functions derived by R. Szmytkowski (J. Phys. B: At. Mol. Opt. Phys. **30**, 825 (1997), fully relativistic treatment) and us (quasirelativistic approach), we have derived in a rigorous way the explicit expressions of the two-photon absorption, Rayleigh and Raman scattering probability amplitudes that take into account both relativistic and retardation effects. A distinctive feature of our tensor treatment is that the expressions derived are quite general and could be applied to any multipole of the two-photon bound-bound transitions. An illustration of our method is undertaken by computing the two-photon absorption transition rates from the ground state towards the excited states of L and M shells for the lighter elements to the heavier ones. A comparison is made also with the quasirelativistic treatment. The numerical results obtained enable us to draw inferences as to the improvements of our method.

H. M. TETCHOU NGANSO holds a BS in Physics and a DEA in Atomic Physics from the University of Yaounde I, Cameroon. Through a scholarship STEP (Sandwich Training Educational Programme), ICTP (The Abdus Salam International Centre for Theoretical Physics, Trieste, Italy) - IAEA (International Atomic Energy Agency, Vienna, Austria) he carried out this thesis under the auspices of a joint supervision between the Université Catholique de Louvain and the University of Douala.